



**MONASH** University

**Prostate Cancer: Targeting for Precision Radiotherapy**

**Daryl Adrian LIM JOON**

**Bachelor of Medicine & Bachelor of Surgery**

**Diploma of the Royal Australian and New Zealand College of Radiologists**

**Fellow of the Royal Australian and New Zealand College of Radiologists**

**(Faculty of Radiation Oncology)**

A thesis submitted for the degree of Doctor of Philosophy at

Monash University in 2021

Faculty of Medicine, Nursing and Health Sciences

## **Copyright notice**

© The author (2021). Except as provided in the *Copyright Act 1968*, this thesis may not be reproduced in any form without the written permission of the author.

I certify that I have made all reasonable efforts to secure copyright permissions for third-party content included in this thesis and have not knowingly added copyright content to my work without the owner's permission.

## **Conflict of interest**

I, or any of the authors, have no actual or potential conflicts of interest arising from any studies undertaken that contribute to this thesis.

# CONTENTS

---

<b>List of Figures</b> .....	<b>vi</b>
<b>List of Tables</b> .....	<b>viii</b>
<b>Abstract</b> .....	<b>x</b>
<b>Declaration</b> .....	<b>xiii</b>
<b>Publications Arising from the PhD</b> .....	<b>xiv</b>
<b>Other Publications During Enrolment</b> .....	<b>xv</b>
<b>Thesis Including Published Works Declaration</b> .....	<b>xxi</b>
<b>COVID-19 Disclosure</b> .....	<b>xxix</b>
<b>Acknowledgements</b> .....	<b>xxx</b>
<b>Abbreviations</b> .....	<b>xxxii</b>
<b>Chapter 1 Introduction</b> .....	<b>1</b>
1.1 Epidemiology .....	1
1.2 Aetiology and Risk Factors.....	2
1.3 The Function of the Prostate Gland .....	5
1.4 Anatomy .....	6
1.5 Prostate Cancer Histopathology.....	13
1.6 Clinical Presentation .....	15
1.7 Staging and Risk Categorisation .....	16
1.8 Treatment with Curative Intent.....	30
1.9 Treatment of Metastatic Prostate Cancer.....	43
1.10 Purpose of the Thesis .....	62
<b>Chapter 2 Literature Review</b> .....	<b>66</b>
2.1 Precision Radiotherapy.....	66
2.2 High-Risk Prostate Cancer .....	67
2.3 Prostate Dose Escalation .....	70
2.4 Radiotherapy Toxicity .....	71
2.5 Intensity-Modulated Radiotherapy and Dose Escalation.....	73
2.6 Hypofractionation.....	80
2.7 Post-Prostatectomy Radiotherapy .....	88
2.8 Multi-Modality Imaging Techniques For Radiotherapy .....	90

2.9	Image-Guided Radiotherapy .....	97
2.10	Prostate Fiducial Markers.....	101
2.11	Rectal Spacers.....	108
2.12	Conclusion .....	112
<b>Chapter 3 Prostate Cancer Post-Prostatectomy Radiotherapy: CT vs MRI for</b>		
<b>Vesicourethral Anastomosis Target Delineation .....</b>		
		<b>114</b>
3.1	Preface.....	115
3.2	Context .....	116
3.3	Abstract.....	118
3.4	Introduction.....	119
3.5	Materials and Methods .....	120
3.6	Results.....	123
3.7	Discussion .....	128
3.8	Conclusion .....	132
<b>Chapter 4 Proximal Seminal Vesicle Displacement and Margins for Prostate Cancer</b>		
<b>Radiotherapy.....</b>		
		<b>133</b>
4.1	Preface.....	134
4.2	Context .....	135
4.3	Abstract.....	138
4.4	Introduction.....	139
4.5	Methods.....	140
4.6	Results.....	143
4.7	Discussion .....	150
4.8	Conclusion .....	154
<b>Chapter 5 A Phantom Study to Contrast and Compare Polymer and Gold Fiducial</b>		
<b>Markers in Radiotherapy Simulation Imaging.....</b>		
		<b>156</b>
5.1	Preface.....	157
5.2	Context .....	158
5.3	Abstract.....	159
5.4	Introduction.....	160
5.5	Materials and Methods .....	161
5.6	Results.....	168

5.7	Discussion .....	175
<b>Chapter 6 A Clinical Study Comparing Polymer and Gold Fiducials for Prostate Cancer</b>		
<b>Radiotherapy.....</b>		<b>179</b>
6.1	Preface.....	180
6.2	Context .....	180
6.3	Abstract.....	183
6.4	Introduction.....	185
6.5	Materials and Methods .....	186
6.6	Results.....	191
6.7	Discussion .....	201
6.8	Conclusion .....	204
<b>Chapter 7 Fiducial Markers: Can The Urologist Do Better? .....</b>		<b>205</b>
7.1	Preface.....	206
7.2	Context .....	207
7.3	Abstract.....	208
7.4	Introduction.....	209
7.5	Materials and Methods .....	210
7.6	Results.....	214
7.7	Discussion .....	216
7.8	Conclusions.....	220
<b>Chapter 8 Exploratory Models Comparing Lipiodol™/ ethiodized oil –Glue and Gold Fiducials for Post Prostatectomy &amp; Bladder Radiotherapy Image-Guidance .....</b>		<b>221</b>
8.1	Preface.....	222
8.2	Context .....	223
8.3	Abstract.....	225
8.4	Introduction.....	226
8.5	Materials and Methods .....	227
8.6	Results.....	233
8.7	Discussion .....	241
8.8	Conclusion .....	244
<b>Chapter 9 Thesis Discussion.....</b>		<b>245</b>
9.1	Introduction.....	245

9.2	Prostate Radiotherapy and Dose Escalation .....	245
9.3	Multi-Modality Imaging Techniques For Radiotherapy .....	251
9.4	Motion Management and Image-Guided Radiotherapy.....	254
9.5	Fiducial Markers for Prostate Cancer Image-Guided Radiotherapy .....	258
<b>Chapter 10 Conclusions and Future Directions .....</b>		<b>268</b>
<b>References.....</b>		<b>273</b>
<b>Appendices.....</b>		<b>325</b>
	Appendix A: Dissemination of Findings .....	325
	Appendix B: Paper Included in Chapter 3 (as published) .....	327
	Appendix C: Paper Included in Chapter 4 (as published) .....	332
	Appendix D: Paper Included in Chapter 7 (as published).....	341
	Appendix E: Paper Included in Chapter 8 (as published) .....	348

## LIST OF FIGURES

---

Figure 1.1	Sagittal view of prostate zonal anatomy.....	11
Figure 1.2	MRI of axial, sagittal and coronal views of prostate zonal anatomy .....	12
Figure 2.1	Cell survival curves of low and high alpha-beta ratio cells and the relative effect of fractionation .....	82
Figure 2.2	Transverse T2 weighted magnetic resonance imaging showing dominant intraprostatic lesion and extracapsular extension .....	92
Figure 3.1	Vesicourethral anastomosis z-axis coordinates for 34 patients: computed tomography (CT) vs magnetic resonance imaging (MRI).....	125
Figure 3.2	Differences between the ctVUA and mrVUA based on axial slices of 1.25mm thickness co-registered CT and MRI, respectively .....	126
Figure 3.3	Vector difference of mrVUA relative to ctVUA for each patient (i.e. ctVUA normalised to 0.0), illustrating the relationship to the recommended clinical target volume (CTV) (inferior) margins of 5mm, 8mm and 12mm.....	127
Figure 3.4	Multi-planar views of co-registered computed tomography (CT) and magnetic resonance imaging (MRI) scans of a single patient showing the mrVUA caudal to the ctVUA.....	129
Figure 4.1	Anterior-posterior image: mean correctional verification shifts with respect to bone and gold seed fiducials in prostate, right seminal vesicle and left seminal vesicle, relative to the isocentre .....	145
Figure 4.2	Left lateral image: mean correctional verification shifts with respect to bone and gold seed fiducials in prostate, right seminal vesicle and left seminal vesicle, relative to the isocentre .....	147
Figure 5.1	(a) Gold seeds, (b) Polymer seeds, (c) CT of gold seeds with the defined area for the greyscale histograms, (d) CT of polymer seeds with the defined area for the greyscale histograms, (e) MRI co-registered with CT of gold seeds, and (f) MRI co-registered with CT of polymer seeds .....	162
Figure 5.2	(a) Perspex box for the phantom with rigid foam plate to guide needles with gold seeds for reproducibility, (b) Phantom contained within Perspex box .....	163
Figure 5.3	(a) Line profile of average relative pixel grey values along a 50mm horizontal line centred on each fiducial marker on CT, for polymer and gold, (b) CT histogram of	

average relative pixel grey values within a 50x50mm square centred on each fiducial marker on CT, for polymer and gold .....	169
Figure 5.4 Area greyscale “terrain” of a 50x50mm square centred on (a) Single gold seed, (b) Single polymer seed, (c) Two adjacent gold seeds, and (d) Two adjacent polymer seeds, that provides an visual overview of the analysis .....	172
Figure 5.5 (a) Line profile of average relative pixel grey values along a 20mm line centred on each fiducial marker on MRI, polymer and gold, (b) MRI histogram of average relative pixel grey values within a 50x50mm square centred on each fiducial marker, polymer and gold.....	174
Figure 6.1 Comparison of visibility and artefact for gold and polymer fiducials on CT and MRI.....	197
Figure 6.2 Boxplots showing the distribution of percentile ranges in the Hounsfield units for the polymer and gold groups .....	199
Figure 6.3 Boxplots illustrating the distribution of the proportion of voxel counts within the defined Hounsfield unit normal tissue ranges for the polymer and gold groups .....	201
Figure 7.1 Endoscopic ex vivo submucosal glue fiducial injection of fluid-filled porcine bladder.....	212
Figure 7.2 Contrast/glue injection sites within the porcine bladder .....	212
Figure 7.3 Verification of Lipiodol™ and glue fiducial marker on computed tomography (CT) and cone beam computed tomography (CBCT) .....	214
Figure 8.1 Porcine model: pig’s bladder and pelvis in two-part foam immobilisation.....	229
Figure 8.2 Phantom model artefact analysis: example of histogram and cumulative percentage distribution of voxel count and calculated percentile range by computed tomography (CT) number Hounsfield unit (HU) for wax control .....	233
Figure 8.3 Phantom model: computed tomography scan of phantom showing A) Wax control – normal tissue density but less dense than the phantom, B) Gold fiducial and artefact, C) Small LC fiducial, and D) Small LM fiducial.....	235
Figure 8.4 Phantom model artefact analysis: average histograms (frequency distribution) of voxel count by CT number Hounsfield Unit (HU) for a 2cm sphere minus the fiducial volume illustrating A) Control (2cm phantom sphere alone), control (wax) and gold fiducial; B) Gold fiducial, small LC and small LM; and C) Gold fiducial, large LC and large LM, i.e. three histograms in each panel.....	240

## LIST OF TABLES

---

Table 1.1	Evolving indications for prostate cancer biomarkers.....	22
Table 2.1	The American Joint Committee on Cancer (AJCC) TNM staging system (2018) ..	68
Table 2.2	D`Amico [435] and National Comprehensive Cancer Network (NCCN) [442] prostate cancer risk categorisation.....	69
Table 2.3	ICRU recommended target and organ-at-risk volumes .....	74
Table 2.4	ICRU 83 intensity-modulated radiotherapy dose-volume histogram recommendations .....	75
Table 3.1	Prostatectomy pathological characteristics: T stage, Gleason score and margin status.....	124
Table 4.1	Planning target volume margin calculation based on prostate and seminal vesicle shifts .....	149
Table 5.1	A statistical comparison of the relative greyscale histograms (where the phantom normal tissue greyscale was normalised to 1) of the polymer versus gold fiducials, generated from a 50mm square centred on the fiducial for CT and MRI imaging.....	170
Table 5.2	Comparison of the mean (SD) of the CNR, SNR and AI of the polymer and gold fiducials in CT and MRI imaging .....	171
Table 6.1	Patient characteristics across the two groups .....	192
Table 6.2	MRI, CT and CBCT fiducial visibility assessments .....	193
Table 6.3	2D kilovoltage (kV) fiducial visibility assessments .....	195
Table 7.1	Injection visibility of contrast/glue markers with multimodal imaging.....	216
Table 7.2	Current published series investigating Lipiodol™ as a marker for image-guided radiotherapy.....	217
Table 8.1	Phantom model: comparison of the fiducial and controls in terms of volume, voxel number, and CT number (HU) characteristics .....	236
Table 8.2	Phantom model: artefact analysis – mean and standard deviations (SD) of percentile ranges of the CT number (HU) versus voxels count histograms and proportion of voxels within normal tissue CT number range for 2cm spheres surrounding the fiducial.....	238



## ABSTRACT

---

This thesis investigates techniques for precision prostate cancer radiotherapy. The initial developments in prostate radiotherapy dose escalation involved creating conformal dose distributions around the prostate. Further accuracy required improved design and targeting, as precision depends on the weakest link in the radiotherapy chain. The thesis focuses on improving image guidance by using multi-modality imaging to design the target, better understanding of target motion and subsequent margins, and utilising fiducials for precise radiotherapy delivery. Chapter 1 provides a comprehensive overview of prostate cancer and its treatment to provide a background for the radiotherapy management. This leads to Chapter 2 that reviews the rationale for precision radiotherapy and the technical aspects in the design and delivery of modern dose escalated intensity modulated radiotherapy (IMRT) with image guidance radiotherapy (IGRT)

Chapter 3 examined the use of MRI in combination with the simulation CT to define the vesicourethral anastomosis (VUA), the commonest recurrence site in post-prostatectomy radiotherapy. Guidelines acknowledge that CT is most often used for VUA identification; however, they admit that MRI has superior soft tissue contrast but has not been validated. The study illustrated that the MRI-defined VUA is most often caudal to the CT-defined VUA. It validated the use of MRI as part of the multi-modality imaging for target delineation in post-prostatectomy radiotherapy.

Patients with locally advanced prostate cancer have a high risk of seminal vesical involvement. Guidelines recommend that proximal seminal vesicles be included in the clinical target volume. While verification is performed by aligning to the prostate, the seminal vesicles can move relative to the prostate. Chapter 4 used fiducials inserted into the

prostate and proximal seminal vesicles to track their displacement. The study confirmed that seminal vesicles move relative to the prostate and proposed that greater margins are required for the seminal vesicles.

Chapters 5 and 6 compared polymer fiducials to the standard gold for prostate cancer radiation. Our preliminary investigation using a purpose-built MRI and CT tissue-equivalent phantom found that while the polymer fiducials have a lower contrast than gold, they were well seen on CT and MRI with far less artefact. This led to a clinical study in which polymer fiducials were compared to gold for verification using kilovoltage, planar imaging and cone beam CT radiotherapy. The study illustrated that polymer fiducials have good visibility and minimal artefact compared to gold on CT. However, neither were well seen on MRI because of tissue heterogeneity. The polymer fiducials, unlike gold, could not be visualised on kV planar imaging.

The final two chapters compare a liquid glue fiducial to gold in a porcine bladder model and a tissue-equivalent phantom. Chapter 7 describes the successful cystoscopic insertion of the glue fiducials into a water-filled ex vivo porcine bladder to simulate the use in post prostatectomy or bladder radiotherapy. Chapter 8 compared the imaging characteristics of the glue fiducials relative to gold in both models. The studies showed that the glue fiducials could be well visualised on CT, CBCT and kV planar imaging. Although contrast was lower, they produced less artefact than gold.

The thesis follows the theme of and processes for improving precision radiotherapy for prostate cancer. It aims to show that modern multi-modality imaging, including MRI, CT and CBCT with new fiducials, can improve target definition and verification of prostate

radiotherapy. These incremental technical gains in precision are aimed at improving the outcome of patients with locally advanced prostate cancer undergoing radiotherapy.

## DECLARATION

---

This thesis is an original work of my research and contains no material which has been accepted for the award of any other degree or diploma at any university or equivalent institution and that, to the best of my knowledge and belief, this thesis contains no material previously published or written by another person, except where due reference is made in the text of the thesis.

Signature:

Print Name: Daryl Lim Joon

Date:

## PUBLICATIONS ARISING FROM THE PHD

---

### ACCEPTED FOR PUBLICATION

1. **Lim Joon D**, Lim A, Schneider M, Hiew C-Y, Lawrentschuk N, Sengupta S, Foroudi F, Jenkins T, Angus D, Wada M, Chao M, Khoo V. Prostate cancer post-prostatectomy radiotherapy: CT vs MRI for vesico-urethral anastomosis target delineation. *Radiother Oncol*. 2017;125(1):113–7. <https://doi.org/10.1016/j.radonc.2017.08.031>
2. Duncan C, **Joon DL**, Lawrentschuk N, Jenkins T, Schneider M, Khoo V, Chao M, Lawlor M, O’Meara R, Berry C, Viotto A, Brown K, Wada M, Foroudi F, Sengupta S. Fiducial markers: can the urologist do better? *World J Urol*. 2019;37(7):1281–7. <https://doi.org/10.1007/s00345-018-2515-0>
3. **Lim Joon D**, Chao M, Piccolo A, Schneider M, Anderson N, Handley M, Benci M, Ong WL, Daly K, Morrell R, Wan K, Lawrentschuk N, Foroudi F, Jenkins T, Angus D, Wada M, Sengupta S, Khoo V. Proximal seminal vesicle displacement and margins for prostate cancer radiotherapy. *J Med Radiat Sci*, 2021: Online ahead of print. <https://doi.org/10.1002/jmrs.457>
4. **Lim Joon D**, Berlangieri A, Harris B, Tacey M, O’Meara R, Pitt B, Viotto A, Brown K, Schneider M, Lawrentschuk N, Sengupta S, Berry C, Jenkins T, Chao M, Wada M, Foroudi F, Khoo V. Exploratory models comparing ethiodized oil–glue and gold fiducials for bladder radiotherapy image-guidance. *Phys Imaging Radiat Oncol*. 2021;17(2021):77–83. <https://doi.org/10.1016/j.phro.2021.01.008>

### SUBMITTED FOR PUBLICATION

1. **Lim Joon D**, Smith D, Tacey M, Schneider M, Harris B, Ong WL, Foroudi F, Jenkins T, Wada M, Chao M, Rykers K, Khoo V. A phantom study to contrast and compare polymer and gold fiducial markers in radiotherapy simulation imaging. Submitted to *Scientific Reports*, 2021.

2. **Lim Joon D**, Berry C, Harris B, Tacey M, Smith D, Schneider M, Hall M, Lawrentschuk N, Sengupta S, Chao M, Foroudi F, Jenkins T, Angus A, Wada M, Khoo V. A clinical study comparing polymer and gold fiducials for prostate cancer radiotherapy. Submitted to *Technology in Cancer Research & Treatment*, 2021.

## OTHER PUBLICATIONS DURING ENROLMENT

---

1. Chang JH, **Lim Joon D**, Lee ST, Gong SJ, Anderson NJ, Scott AM, Davis ID, Clouston D, Bolton D, Hamilton CS, Khoo V. Intensity modulated radiation therapy dose painting for localised prostate cancer using  $^{11}\text{C}$ -choline positron emission tomography scans. *Int J Radiat Oncol Biol Phys.* 2012;83(5):e691–6.  
<https://doi.org/10.1016/j.ijrobp.2012.01.087>
2. Davis ID, Lee ST, Shanker L, Clouston D, Bolton DM, Angus D, Webb D, Lawrentschuk N, Woon DT, Esler S, **Lim Joon D**, Chang J, O’Sullivan R, Pathmaraj K, Tochon-Danguy H, O’Keefe GJ, Scott AM.  $^{11}\text{C}$ -choline PET scanning is more accurate than biopsy in assessment of localized prostate cancer planned for radical prostatectomy. *J Clin Oncol.* 2012;30(5 Suppl):182.  
[https://doi.org/10.1200/jco.2012.30.5\\_suppl.182](https://doi.org/10.1200/jco.2012.30.5_suppl.182)
3. Senthil S, Gill SS, Haworth A, Kron T, Cramb J, Rolfo A, Thomas J, Duchesne GM, Hamilton CH, **Joon DL**, Bowden P, Foroudi F. Benchmarking dosimetric quality assessment of prostate intensity-modulated radiotherapy. *Int J Radiat Oncol Biol Phys.* 2012;82(2):998–1005. <https://doi.org/10.1016/j.ijrobp.2010.12.016>
4. Chang JH, Wada M, Anderson NJ, **Lim Joon D**, Lee ST, Gong SJ, Gunawardana DH, Sachinidis J, O’Keefe G, Gan HK, Khoo V, Scott AM. Hypoxia-targeted radiotherapy dose painting for head and neck cancer using  $^{18}\text{F}$ -FMISO PET: a biological modeling study. *Acta Oncol.* 2013;52(8):1723–9.  
<https://doi.org/10.3109/0284186x.2012.759273>
5. Cheung AS, Pattison D, Bretherton I, Hoermann R, **Lim Joon D**, Ho E, Jenkins T, Hamilton EJ, Bate K, Chan I, Zajac JD, Grossmann M. Cardiovascular risk and bone loss

- in men undergoing androgen deprivation therapy for non-metastatic prostate cancer: implementation of standardised management guidelines. *Andrology*. 2013;1(4):583–9. <https://doi.org/10.1111/j.2047-2927.2013.00093.x>
6. Anderson NJ, Wada M, Schneider-Kolsky M, Rolfo M, **Lim Joon D**, Khoo V. Dose-volume response in acute dysphagia toxicity: validating QUANTEC recommendations into clinical practice for head and neck radiotherapy. *Acta Oncol*. 2014;53(10):1305–11. <https://doi.org/10.3109/0284186x.2014.933874>
  7. Chang JH, **Lim Joon D**, Lee ST, Hiew CY, Esler S, Gong SJ, Wada M, Clouston D, O’Sullivan R, Goh YP, Tochon-Danguy H, Chan JG, Bolton D, Scott AM, Khoo V, Davis ID. Diffusion-weighted MRI, <sup>11</sup>C-choline PET and <sup>18</sup>F-fluorodeoxyglucose PET for predicting the Gleason score in prostate carcinoma. *Eur Radiol*. 2014;24(3):715–22. <https://doi.org/10.1007/s00330-013-3045-1>
  8. Chang JH, **Lim Joon D**, Nguyen BT, Hiew CY, Esler S, Angus D, Chao M, Wada M, Quong G, Khoo V. MRI scans significantly change target coverage decisions in radical radiotherapy for prostate cancer. *J Med Imaging Radiat Oncol*. 2014;58(2):237–43. <https://doi.org/10.1111/1754-9485.12107>
  9. Chang JH, **Lim Joon D**, Davis ID, Lee ST, Hiew CY, Esler S, Gong SJ, Wada M, Clouston D, O’Sullivan R, Goh YP, Bolton D, Scott AM, Khoo V. Comparison of [<sup>11</sup>C]choline positron emission tomography with T2- and diffusion-weighted magnetic resonance imaging for delineating malignant intraprostatic lesions. *Int J Radiat Oncol Biol Phys*. 2015;92(2):438–45. <https://doi.org/10.1016/j.ijrobp.2015.02.004>
  10. Chandran S, Vaughan R, Jacob A, Hamilton C, **Lim Joon D**, Lim K, Tog C, Bhatia K, Aly A, Sweeney T, Efthymiou M. A novel endoscopic marker for radiological localisation and image-guided radiotherapy in esophageal and gastric cancers (with video). *Gastrointest Endosc*. 2016;83(2):309–17. <https://doi.org/10.1016/j.gie.2015.06.042>

11. Chang JH, Gehrke C, Prabhakar R, Gill S, Wada M, **Lim Joon D**, Khoo V. RADBIOMOD: A simple program for utilising biological modelling in radiotherapy plan evaluation. *Phys Med*. 2016;32(1):248–54. <https://doi.org/10.1016/j.ejmp.2015.10.091>
12. Cheung AS, Hoermann R, Dupuis P, **Lim Joon D**, Zajac JD, Grossmann M. Relationships between insulin resistance and frailty with body composition and testosterone in men undergoing androgen deprivation therapy for prostate cancer. *Eur J Endocrinol*. 2016;175(3):229–37. <https://doi.org/10.1530/eje-16-0200>
13. Cheung AS, de Rooy C, Hoermann R, **Lim Joon D**, Zajac JD, Grossmann M. Quality of life decrements in men with prostate cancer undergoing androgen deprivation therapy. *Clin Endocrinol (Oxf)*. 2017;86(3):388–94. <https://doi.org/10.1111/cen.13249>
14. Cheung AS, Gray H, Schache AG, Hoermann R, **Lim Joon D**, Zajac JD, Pandy MG, Grossmann M. Androgen deprivation causes selective deficits in the biomechanical leg muscle function of men during walking: a prospective case-control study. *J Cachexia Sarcopenia Muscle*. 2017;8(1):102–12. <https://doi.org/10.1002/jcsm.12133>
15. White R, Foroudi F, Sia J, Marr MA, **Lim Joon D**. Reduced dose to small bowel with the prone position and a belly board versus the supine position in neoadjuvant 3D conformal radiotherapy for rectal adenocarcinoma. *J Med Radiat Sci*. 2017;64(2):120–4. <https://doi.org/10.1002/jmrs.187>
16. Anderson NJ, Jackson JE, Smith JG, Wada M, Schneider M, Poulsen M, Rolfo M, Fahandej M, Gan H, **Lim Joon D**, Khoo V. Pretreatment risk stratification of feeding tube use in patients treated with intensity-modulated radiotherapy for head and neck cancer. *Head Neck*. 2018;40(10):2181–92. <https://doi.org/10.1002/hed.25316>
17. Chao M, Ho H, Chan Y, Tan A, Pham T, Bolton D, Troy A, Temelcos C, Sengupta S, McMillan K, Cham CW, Liu M, Ding W, Subramanian B, Wasiak J, **Lim Joon D**, Spencer S, Lawrentschuk N. Prospective analysis of hydrogel spacer for patients with

- prostate cancer undergoing radiotherapy. *BJU Int.* 2018;122(3):427–33.  
<https://doi.org/10.1111/bju.14192>
18. Chao M, Spencer S, Guerrieri M, Ding W, Goharian M, Ho H, Ng M, Healey D, Tan A, Cham C, **Lim Joon D**, Lawrentschuk N, Travis D, Sengupta S, Chan Y, Troy A, Pham T, Clarke D, Liodakis P, Bolton D. A single institution analysis of low-dose-rate brachytherapy: 5-year reported survival and late toxicity outcomes. *J Contemp Brachytherapy.* 2018;10(2):155–61. <https://doi.org/10.5114/icb.2018.75600>
  19. Berghen C, Albersen M, Blanchard P, Bossi A, Briganti A, Cozzarini C, Decaestecker K, Fonteyne V, Haustermans K, Joniau S, **Lim Joon D**, Khoo V, Nguyen PL, Ost P, Villeirs G, Vulsteke C, Zietman A, De Meerleer G. Readdressing the rationale of irradiation in stage I seminoma guidelines: a critical essay. *BJU Int.* 2019;124(1):35–9. <https://doi.org/10.1111/bju.14686>
  20. Chao M, Bolton D, **Lim Joon D**, Chan Y, Lawrentschuk N, Ho H, Spencer S, Wasiak J, Guerrieri M, Ow D, Troy A, Pham T, Sengupta S, Tan A, McMillan K, Koufogiannis G, Foroudi F, Ng M, Khoo V. High dose rate brachytherapy boost for prostate cancer: biochemical control and the impact of transurethral resection of the prostate and hydrogel spacer insertion on toxicity outcomes. *J Med Imaging Radiat Oncol.* 2019;63(3):415–21. <https://doi.org/10.1111/1754-9485.12882>
  21. Chao M, **Lim Joon D**, Khoo V, Spencer S, Ho H, Guerrieri M, Foroudi F, Bolton D. Combined low dose rate brachytherapy and external beam radiation therapy for intermediate-risk prostate cancer. *J Med Imaging Radiat Sci.* 2019;50(1):82–6. <https://doi.org/10.1016/j.jmir.2018.09.010>
  22. Chao M, **Lim Joon D**, Khoo V, Lawrentschuk N, Ho H, Spencer S, Chan Y, Tan A, Pham T, Sengupta S, McMillan K, Liu M, Koufogiannis G, Cham CW, Foroudi F, Bolton D. The use of hydrogel spacer in men undergoing high-dose prostate cancer radiotherapy: results of a prospective phase 2 clinical trial. *World J Urol.* 2019;37(6):1111–6. <https://doi.org/10.1007/s00345-018-2502-5>

23. Duncan C, Zamir E, Teh J, **Lim Joon D**, Liodakis P. A blind spot in urology: prostate cancer associated retinopathy. *Urol Case Rep.* 2019;24:100872.  
<https://doi.org/10.1016/j.eucr.2019.100872>
24. Jackson JE, Anderson NJ, Rolfo M, Wada M, Schneider M, Poulsen M, Fahandej M, Huynh A, Lee ST, **Lim Joon D**, Khoo V. <sup>18</sup>F-FDG metabolic tumor volume: association with short- and long-term feeding tube use in head and neck IMRT. *Dysphagia.* 2019;34(3):341–9. <https://doi.org/10.1007/s00455-018-9946-z>
25. **Lim Joon D**, Foroudi F, Wasiak J, Schneider M, Chao M, Jenkins T, Khoo V. The collaborative management of late urological complications after radiation therapy. *BJU Int.* 2019;123 Suppl 5:8–9. <https://doi.org/10.1111/bju.14679>
26. Ong WL, Koh TL, **Lim Joon D**, Chao M, Farrugia B, Lau E, Khoo V, Lawrentschuk N, Bolton D, Foroudi F. Prostate-specific membrane antigen-positron emission tomography/computed tomography (PSMA-PET/CT)-guided stereotactic ablative body radiotherapy for oligometastatic prostate cancer: a single-institution experience and review of the published literature. *BJU Int.* 2019;124 Suppl 1:19–30.  
<https://doi.org/10.1111/bju.14886>
27. Abbouchie H, Chao M, Tacey M, **Lim Joon D**, Ho H, Guerrieri M, Ng M, Foroudi F. Vertebral fractures following stereotactic body radiotherapy for spine oligometastases: a multi-institutional analysis of patient outcomes. *Clin Oncol (R Coll Radiol).* 2020;32(7):433–41. <https://doi.org/10.1016/j.clon.2020.02.030>
28. Abbouchie H, Chao M, Tacey M, **Lim Joon D**, Ho H, Guerrieri M, Ng M, Foroudi F. Vertebral fractures following stereotactic body radiotherapy for spine metastases. *J Med Imaging Radiat Oncol.* 2020;64(2):293–302. <https://doi.org/10.1111/1754-9485.13010>
29. Cheung AS, Gray HA, Schache AG, Hoermann R, Bicknell J, **Lim Joon D**, Zajac JD, Pandy MG, Grossmann M. Biomechanical leg muscle function during stair ambulation

- in men receiving androgen deprivation therapy. *J Gerontol A Biol Sci Med Sci*. 2020;75(9):1715–22. <https://doi.org/10.1093/gerona/glz169>
30. Cheung AS, Hoermann R, Ghasem-Zadeh A, Tinson AJ, Ly V, Milevski SV, **Lim Joon D**, Zajac JD, Seeman E, Grossmann M. Differing effects of zoledronic acid on bone microarchitecture and bone mineral density in men receiving androgen deprivation therapy: a randomized controlled trial. *J Bone Miner Res*. 2020;35(10):1871–80. <https://doi.org/10.1002/jbmr.4106>
31. Jackson JE, Anderson NJ, Wada M, Schneider M, Poulsen M, Rolfo M, Fahandej M, Gan H, **Lim Joon D**, Khoo V. Clinical and dosimetric risk stratification for patients at high-risk of feeding tube use during definitive IMRT for head and neck cancer. *Tech Innov Patient Support Radiat Oncol*. 2020;14:1–10. <https://doi.org/10.1016/j.tipsro.2020.01.003>
32. Wilson C, Moseshvili E, Tacey M, Quin I, Lawrentschuk N, Bolton D, **Lim Joon D**, Chao M, Dunshea T, Kron T, Foroudi F. Assessment of intrafraction motion of the urinary bladder using magnetic resonance imaging (cineMRI). *Clin Oncol (R Coll Radiol)*. 2020;32(2):101–9. <https://doi.org/10.1016/j.clon.2019.09.056>

## THESIS INCLUDING PUBLISHED WORKS DECLARATION

---

I hereby declare that this thesis contains no material which has been accepted for the award of any other degree or diploma at any university or equivalent institution and that, to the best of my knowledge and belief, this thesis contains no material previously published or written by another person, except where due reference is made in the text of the thesis.

This thesis includes six original papers i.e., four published in peer-reviewed journals and two submitted for publication. The core theme of the thesis is the investigation of precision radiotherapy for prostate cancer. There was a detailed focus on imaging and the use and development of fiducials to study seminal vesical motion and for the accurate delivery of prostate radiotherapy. The ideas, development and writing of all the papers in the thesis were the principal responsibility of myself, the student, working within the Faculty of Medicine, Nursing and Health Sciences under the supervision of Professor Michal Schneider; and at the Royal Marsden Hospital (London, UK) under the supervision of Associate Professor Vincent Khoo.

(The inclusion of co-authors reflects the fact that the work came from active collaboration between researchers with complementary and technical skillsets and acknowledges input into multidisciplinary team-based research.)

In the case of Chapters 3, 4, 5, 6, 7 and 8, my contribution to the work involved the following:

<b>Thesis chapter</b>	<b>Publication title</b>	<b>Status</b> (published, in press, accepted or returned for revision, submitted)	<b>Nature and % of student contribution</b>	<b>Co-author names</b> <b>Nature and % Co-author's contribution</b>	<b>Co-authors, Monash student Y/N</b>
<b>3</b>	Prostate Cancer Post-Prostatectomy Radiotherapy: CT vs MRI for Vesico-Urethral Anastomosis Target Delineation	Published	65%. Concept and data collection and analysis and interpretation and manuscript	<ol style="list-style-type: none"> <li>1. Adeline Lim, input into concept, data collection, manuscript 6%</li> <li>2. Michal Schneider, input into manuscript 5%</li> <li>3. Chee-Yan Hiew, input into data collection 2%</li> <li>4. Nathan Lawrentschuk, input into manuscript 2%</li> <li>5. Shomik Sengupta, input into manuscript 2%</li> <li>6. Farshad Foroudi, input into manuscript 2%</li> <li>7. Trish Jenkins, input into manuscript 4%</li> <li>8. David Angus, input into Data collection 2%</li> <li>9. Morikatsu Wada, input into manuscript 2%</li> <li>10. Michael Chao, input into manuscript 3%</li> <li>11. Vincent Khoo, input into manuscript 5%</li> </ol>	No  No  No  No  No  No  No  No

4	Proximal Seminal Vesicle Displacement and Margins for Prostate Cancer Radiotherapy	Published	70%. Concept and data collection and analysis and interpretation and manuscript	<ol style="list-style-type: none"> <li>1. Michael Chao, input into manuscript 3%</li> <li>2. Angelina Piccolo, input into data collection, analysis, Interpretation 4%</li> <li>3. Michal Schneider, input into manuscript 3%</li> <li>4. Nigel Anderson, input into manuscript 1%</li> <li>5. Monica Handley, input into data collection 2%</li> <li>6. Margaret Benci, input into data collection 1%</li> <li>7. Wee Loon Ong, input into manuscript 1%</li> <li>8. Karen Daly, input into data collection 1%</li> <li>9. Rebecca Morrell, input into data collection 2%</li> <li>10. Kenneth Wan, input into Data collection 1%</li> <li>11. Nathan Lawrentschuk, input into data collection 2%</li> <li>12. Farshad Foroudi, input into manuscript 1%</li> <li>13. Trish Jenkins, input into data collection, manuscript 1%</li> <li>14. David Angus, input into data collection 1%</li> <li>15. Morikatsu Wada, input into manuscript 1%</li> <li>16. Shomik Sengupta, input into data collection 2%</li> <li>17. Vincent Khoo, input into concept, manuscript 3%</li> </ol>	<p>No</p>
---	--	-----------	---	---	---

5	A Phantom Study to Contrast and Compare Polymer and Gold Fiducial Markers in Radiotherapy Simulation Imaging	Submitted Under review	65%. Concept and Data collection and Analysis and Interpretation and Manuscript	1. Drew Smith, input into concept, data collection, analysis, interpretation 7%	Yes
				2. Mark Tacey, input into analysis 5%	No
				3. Michal Schneider, input into manuscript interpretation 4%	No
				4. Benjamin Harris, input into analysis, interpretation, manuscript 5%	No
				5. Wee Loon Ong, input into manuscript 1%	No
				6. Farshad Foroudi, input into manuscript 1%	No
				7. Trish Jenkins, input into manuscript 3%	No
				8. Morikatsu Wada, input into manuscript 2%	No
				9. Michael Chao, input into manuscript 2%	No
				10. Kym Rykers, input into manuscript 1%	No
				11. Vincent Khoo, input into manuscript 4%	No

6	A Clinical Study Comparing Polymer and Gold Fiducials for Prostate Cancer Radiotherapy	Submitted Under review	65%. Concept and Data collection and Analysis and Interpretation and Manuscript	<ol style="list-style-type: none"> <li>1. Colleen Berry, input into data collection, interpretation, manuscript 6%</li> <li>2. Benjamin Harris, input into data collection, analysis, interpretation 5%</li> <li>3. Mark Tacey, input into analysis, interpretation 5%</li> <li>4. Drew Smith, input into concept, data collection 1%</li> <li>5. Nathan Lawrentschuk, input into data collection 2%</li> <li>6. Shomik Sengupta, input into data collection 2%</li> <li>7. Michal Schneider, input into manuscript 3%</li> <li>8. Megan Hall, input into data collection 2%</li> <li>9. Michael Chao, input into manuscript 1%</li> <li>10. Farshad Foroudi, input into manuscript 1%</li> <li>11. Trish Jenkins, input into manuscript 2%</li> <li>12. David Angus, input into data collection 1%</li> <li>13. Morikatsu Wada, input into manuscript 1%</li> <li>14. Vincent Khoo, input into manuscript 3%</li> </ol>	<p>No</p> <p>No</p> <p>No</p> <p>Yes</p> <p>No</p>
---	--	------------------------	---	--	--

7	Fiducial Markers: Can The Urologist Do Better?	Published	60%. Concept and Data collection and Analysis and Interpretation and Manuscript	<ol style="list-style-type: none"> <li>1. Catriona Duncan, input into manuscript, analysis, interpretation 5%</li> <li>2. Nathan Lawrentschuk, input into concept, design, data collection 5%</li> <li>3. Trish Jenkins, input into manuscript input, data collection 3%</li> <li>4. Michal Schneider, input into manuscript 2%</li> <li>5. Vincent Khoo, input into manuscript 2%</li> <li>6. Michael Chao, input into manuscript 1%</li> <li>7. Marita Lawlor, input into data collection 1%</li> <li>8. Rachel O'Meara, input into data collection, interpretation 4%</li> <li>9. Colleen Berry, input into data collection, analysis, interpretation 3%</li> <li>10. Angela Viotto, input into data collection 4%</li> <li>11. Kerryn Brown, input into data collection 3%</li> <li>12. Morikatsu Wada, input into manuscript 1%</li> <li>13. Farshad Foroudi, input into manuscript 1%</li> <li>14. Shomik Sengupta, input into concept, design, data collection 5%</li> </ol>	<p>No</p>
---	---	-----------	---	---	---

8	Exploratory Models Comparing Ethiodized Oil–Glue and Gold Fiducials for Bladder Radiotherapy Image-Guidance	Published	70%. Concept and design and Data collection and Analysis and Interpretation and Manuscript	<ol style="list-style-type: none"> <li>1. Alexandra Berlangieri, input into data collection, analysis 4%</li> <li>2. Benjamin Harris, input into concept, analysis, interpretation 3%</li> <li>3. Mark Tacey, input into analysis, interpretation 3%</li> <li>4. Rachel O’Meara, input into data collection 1%</li> <li>5. Brent Pitt, input into concept, design, data collection 3%</li> <li>6. Angela Viotto, input into data collection 1%</li> <li>7. Kerryn Brown, input into data collection 1%</li> <li>8. Michal Schneider, input into manuscript 2 %</li> <li>9. Nathan Lawrentschuk, input into data collection 1%</li> <li>10. Shomik Sengupta, input into data collection 1%</li> <li>11. Colleen Berry, input into data collection 2%</li> <li>12. Trish Jenkins, input into manuscript 2%</li> <li>13. Michael Chao, input into manuscript 1%</li> <li>14. Morikatsu Wada, input into manuscript 1%</li> <li>15. Farshad Foroudi, input into manuscript 1%</li> <li>16. Vincent Khoo, input into manuscript 3%</li> </ol>	<p>No</p>
---	---	-----------	--	--	---

I have renumbered sections of submitted or published papers in order to generate a consistent presentation within the thesis.

**Student name:** Daryl Lim Joon

**Student signature:**

**Date:**

I hereby certify that the above declaration correctly reflects the nature and extent of the student's and co-authors' contributions to this work. In instances where I am not the responsible author, I have consulted with the responsible author to agree on the respective contributions of the authors.

**Main Supervisor name:** Michal Schneider

**Main Supervisor signature:**

**Date:**

## COVID-19 DISCLOSURE

---

There has been a 3-month delay with the final PhD submission due to an increase in my clinical and hospital work, in addition to the slow logistics of many aspects of the research, publications and daily work that has resulted from the COVID-19 pandemic. Research has also been delayed by the pandemic, as online communication and interactions between the collaborators, supervisors and journals have been more complex and consequently prolonged over 2020.

## ACKNOWLEDGEMENTS

---

An enormous amount of dedicated time is required for the compilation of any PhD thesis, which requires support and guidance from both an academic and social perspective. The acknowledgement of these individuals is as important as the thesis itself. With their support, the many hours bring an enjoyment and fulfillment with the completion of the body of work.

I would like to sincerely thank my supervisors. Professor Michal Schneider has supplied a wealth of experience and wisdom, particularly in the areas of design and logistics. Together with her sincere and friendly personality, she has been delightful to work with. Associate Professor Vincent Khoo has been critical to the thesis concepts and publications. His mountain of radiation oncology expertise and unsurpassable knowledge of radiotherapy academic and scientific processes has greatly augmented the thesis and publications. He was often the final arbitrator in difficult situations and was never wrong. Professional editor Donna Armstrong provided much valued assistance with meticulous proofreading and formatting.

I would also like to acknowledge the support from other members of the multidisciplinary team within the Olivia Newton-John Cancer and Wellness and Research Centre at Austin Health Radiation Oncology, including the radiation therapists (in particular Drew Smith, Alexandra Berlangieri, Brent Pitt and Colleen Berry), radiation oncologists (including Morikatsu Wada, Farshad Foroudi, Michael Chao and Adeline Lim), physicists (importantly Ben Harris and Kym Rykers), statisticians (including Mark Tacey and Jenny Smith), data and project manager (Trish Jenkins), and urologists (notably Shomik Sengupta, Nathan Lauwrentschuk and David Angus).

I would importantly like to thank and acknowledge my family – my children Kianan, Tiernan and Kyan, and of course my loving wife and amazing cook, Linh.

## ABBREVIATIONS

---

3DCRT	3D conformal radiotherapy
4K	Four kallikrein score
4K	Kallikrein score
ADT	Androgen deprivation therapy
ANOVA	Analysis of variance
AP	Anterior-posterior
ART	Adjuvant radiotherapy
CBCT	Cone beam Computed tomography
CI	Confidence interval
CT	Computed tomography
ctCTV	Computed tomography -defined CTV
CTV	Clinical target volume
ctVUA	Computed tomography vesicourethral anastomosis
DIL	Dominant intra-prostatic lesion
DRE	Digital rectal examination
DVH	Dose-volume histogram
DW-MRI	Diffusion-weighted MRI
EBRT	External beam radiotherapy
ETS-ERG	
FDG	Erythroblast transformation-specific-related genes
GI	Fluorodeoxyglucose
GTV	Gastrointestinal
GU	Gross tumour volume
HR	Genitourinary
HU	Hazard ratio
IGRT	Hounsfield unit
IMRT	Image-guided radiotherapy
IQR	Intensity-modulated radiotherapy
kV	Interquartile range

LR	Kilovoltage
LSV	Left-right
LUTs	Left seminal vesicle
mCRPC	Lower urinary tract symptoms
mHSPC	Metastatic castration-resistant prostate cancer
mpMRI	Metastatic hormone-sensitive prostate cancer
MRgRT	Multi-parametric magnetic resonance imaging
MRI	Magnetic resonance image guided radiation therapy
mrVUA	Magnetic resonance imaging
MV	Magnetic resonance imaging vesicourethral anastomosis
OAR	Megavoltage
PARP	Organ at risk
PCA3	Poly (ADP-ribose) polymerase
PET	Prostate cancer antigen 3 mRNA
PHI	Positron emission tomography
PI-RADS	Prostate Health Index
PPRT	Prostate Imaging Reporting and Data System
PrSV	Post-prostatectomy radiotherapy
PSA	Proximal seminal vesicles
PSMA	Prostate-specific antigen
PTV	Prostate-specific membrane antigen
QUANTEC	Planning target volume
RCT	Quantitative Analyses of Normal Tissue Effects in the Clinic
RSV	Randomised controlled trial
RTOG	Right seminal vesicle
SABR	Radiation Therapy Oncology Group
SBRT	Stereotactic ablative body radiotherapy
SD	Stereotactic body radiotherapy
SI	Standard deviation
SPCG	Superior-inferior
SRT	Swedish Prostate Cancer Group

SVI	Salvage radiotherapy
TRUS	Seminal vesicle invasion
UK	Transrectal ultrasound-guided
USA	United Kingdom
VMAT	United States of America
VUA	Volumetric modulated arc therapy
	Vesicourethral anastomosis

# Chapter 1 INTRODUCTION

---

This introductory chapter is a comprehensive overview of prostate cancer to provide a background and perspective for the technical aspects of prostate radiotherapy that is reviewed in Chapter 2.

The final update was performed in December 2020.

## 1.1 EPIDEMIOLOGY

It is estimated that, worldwide, over 1 million men are diagnosed with prostate cancer each year; this equates to about 15% of cancers diagnosed in men [1]. The majority, 70%, occur in developed countries, but there is 25 times variation in incidence between countries [1]. The highest rates are seen in Australia, New Zealand, North America and Western and Northern Europe. However, some less developed regions also have high rates, including Southern Africa and South America [2]. The lowest rates are seen in Central and Southeast Asia [3]. Prostate cancer is the fifth leading cause of all cancer deaths worldwide. Death from prostate cancer is more common in less developed regions. The mortality is high in Black populations, intermediate in North America and Oceania, and low in Asia [2].

Among Australian men, prostate cancer is the most common cancer (excluding skin cancer) and the second commonest cause of cancer-related deaths. An Australian Government publication reported that 21,808 new cases were reported in 2009. This represented an increase from 79 new cases per 100,000 males in 1982 to 194 per 100,000 in 2009. The mortality rates are decreasing but still represented 3,294 deaths (or 31 deaths per 100,000) in 2011. Prostate cancer is the fourth leading cause of all deaths among Australian males [4].

## 1.2 AETIOLOGY AND RISK FACTORS

The aetiology of prostate cancer is uncertain, but three reasonably well-defined risk factors include increasing age, ethnicity, and heredity or family history [2]. The risk of developing prostate cancer increases with age. It is rare before 40 years and uncommon before 50 years of age. The incidence generally peaks in the late 60s to 70s. The incidence rate at 65 years of age is approximately 60% [2]. The median age of men with prostate cancer in Australia is 69 years, and by 85 years, 1 in 5–9 men will be diagnosed with prostate cancer [4].

The evidence for a genetic factor in prostate cancer is based on family history and ethnic background. Familial studies have shown a two-fold risk if one first-degree relative has prostate cancer. True hereditary prostate cancer represents about 5–9% of patients.

Hereditary prostate cancer was explicitly defined and based on families meeting at least one of the following criteria: 1) prostate cancer in three or more first-degree relatives; 2) prostate cancer in three successive generations of the maternal or paternal lineages; or 3) two first-degree relatives affected at age  $\leq 55$  years [5]. In summary, this means three or more affected relatives, or at least two relatives diagnosed with early-onset prostate cancer, before the age of 55 [6].

Ethnicity has also been shown to affect the incidence of prostate cancer. It is thought to be related to genetic factors, although other factors such as diet may also be a factor. A UK study showed that Black men are roughly at twice the risk of diagnosis and death as white men, who are, in turn, at nearly twice the risk of diagnosis and death compared to Asian men [7]. The risk of dying – one in three – was similar in all ethnic groups. This rate contrasts

with studies in the USA that show a higher risk of death in Black men once diagnosed [8]. It is uncertain whether this is related to socio-economic differences or difference in biology.

Genetic studies have shown that no single gene is responsible for prostate cancer, although many genes have now been implicated [9]. Genome-wide association studies, including a meta-analysis, have identified 100 common loci contributing to prostate cancer [10]. Several notable genetic mutations have been related with a higher risk of developing prostate cancer, including *BRCA1/BRCA2* gene mutations, homeobox B13 (*HOXB13*) gene mutations and Lynch syndrome (also known as hereditary non-polyposis colorectal cancer; mutations of *MSH2* and *MLH1*) [11]. *P53* mutations in primary prostate cancer are rare but are more frequently seen in metastatic disease and, thus, are associated with a poor prognostic finding [12]. Many other single nucleotide polymorphisms and genes that mainly promote cancer cell growth have been linked to an increased prostate cancer risk. These include, various androgen and vitamin D receptors, hereditary prostate cancer gene 1 (*HPC1*), *HPC2*, hereditary prostate cancer, X-linked (*HPCX*), carcinoma prostate brain (*CAPB*), post-meiotic segregation increased 2 (*PMS2*), checkpoint kinase 2 (*CHEK2*), nibrin (*NBN*), *BRCA1*-interacting protein C-terminal helicase 1 (*BRIP1*), ataxia telangiectasia mutated (*ATM*) and the *TMPRSS2-ETS* gene family (*TMPRSS2-ERG* and *TMPRSS2-ETV1/4*) [9, 11, 13, 14].

Prostate cancer was previously considered to be mainly sporadic, with the gene mutations being acquired mutations (somatic), developing during a man's life, rather than being inherited (germline) [15]. However, it is now estimated that heritability, or the proportion of prostate cancer attributed to germline genetics, is about 58% [16].

A Western diet [17], comprising a diet high in animal fat and low in vegetables, has been inconsistently and weakly associated with prostate cancer. Other dietary factors that have been weakly associated with prostate cancer or aggressive prostate cancer include high alcohol and total alcohol abstinence, high intake of dairy products, fried foods and saturated fats, red or processed meat, low and high vitamin D, and high nail selenium (long-term exposure) [18-26]. Factors that may weakly reduce the risk include fish and vegetarian diets, lycopene, and phytoestrogens [27-29]. Metabolic syndrome is also weakly associated with prostate cancer. In a meta-analysis of metabolic syndrome that included high body mass index, dyslipidaemia, glycaemia, high triglycerides and low high-density lipoprotein cholesterol, only hypertension and waist circumference (>102cm) were associated with a greater risk of prostate cancer, by 15% and 56% respectively [30].

Medications are also thought to have a role in prostate cancer. Epidemiologic studies and multiple meta-analyses have investigated the potential protective properties of aspirin in prostate cancer. However, while it appears that aspirin confers a benefit, its use remains controversial [31-40].

Meta-analyses and systematic reviews have inferred that 5-alpha-reductase inhibitors (5-ARIs) may reduce the risk of developing prostate cancer [41-44]. A review of 15 randomised controlled trials (RCTs) noted that men who were regularly screened for prostate-specific antigen (PSA) for early detection of prostate cancer might benefit from 7 years of 5-ARIs by prostate cancer being prevented [41]. However, there is a potential risk that if they do develop prostate cancer, it may be high-risk disease [41, 44]. There appears to be no significant overall survival benefit with the use of 5-ARIs [45].

Statins have also been studied in multiple prospective studies to investigate a possible protective effect, but studies have shown conflicting results [46]. A meta-analysis and results of the REDUCE study did not confirm the preventive effect of statins on prostate cancer risk [47]. Other studies have reported that statins reduce the risk of advanced prostate cancer [46, 48-52] and possibly lethal prostate cancer [53]. Statins may improve survival when used with androgen deprivation therapy (ADT) in advanced prostate cancer [48].

The diabetic medication metformin has been investigated for its association with prostate cancer. It is not associated with an increased risk of prostate cancer and may have a preventive effect [54, 55].

While testosterone promotes the progression of prostate cancer, testosterone replacement in hypogonadal men has not been shown to increase the risk of prostate cancer [56, 57].

Other associations and environmental factors are associated with prostate cancer, but a direct causative link is uncertain. Environmental carcinogens, such as Agent Orange, have been associated with a high incidence, higher grade and higher stage of prostate cancer. Balding, gonorrhoea, night-shift work, cigarette smoking and cadmium exposure have been associated with an increased risk. Ultraviolet radiation exposure, circumcision and high ejaculatory frequency have been associated with a lower prostate cancer risk [58].

### **1.3 THE FUNCTION OF THE PROSTATE GLAND**

The sperm, produced in the testes, enters the prostate's upper portion through the vas deferens via the seminal vesicles. Sperm and fluid from the seminal vesicles then mix with secretions emitted from the prostate to form the seminal fluid that is expelled at the time of

ejaculation [59]. Seminal fluid is a thin, milky, alkaline liquid rich in spermine, phospholipids, cholesterol, fibrinogenase, citric acid, fibrinolysin, zinc, and acid phosphatase and other proteins. The prostate contributes 20–30% of the volume of the seminal fluid.

The prostatic secretions are alkaline and neutralise the acidity in the vagina and thus protect the sperm from denaturation. During ejaculation, the smooth muscle surrounding the small glands of the prostate contracts. This squeezes the secretions into the prostatic urethra, where it is mixed with the seminal fluid.

The prostate also plays a part in urethral sphincter function as an internal sphincter; it supports the function of the external urethral sphincter in maintaining urinary control and is, therefore, one of the reasons that men rarely have urinary stress incontinence. The internal sphincter also plays a vital role during ejaculation, as it contracts during ejaculation and blocks the ejaculate from passing to the bladder.

#### **1.4 ANATOMY**

The prostate is conical or pyramid-shaped, with its base surrounding the bladder neck outlet superiorly and its apex abutting the urogenital diaphragm inferiorly. This inverted pyramid envelops the prostatic urethra and ejaculatory ducts. The ejaculatory ducts connect to the seminal vesicles, which are attached to the posterolateral prostate. The prostate is surrounded by a “true” capsule which is a thin layer of connective tissue around the periphery, although it is usually deficient inferiorly at the apex. Outside this is a “false” capsule, which is a condensation of the pelvic fascia. A prostatic plexus of veins lies between the two capsules.

The normal prostate gland weighs about 20g in the young adult male and measures approximately 3.8 x 2.5 x 3.2cm with a volume of 25cc. However, the prostate generally enlarges with age due to benign prostate hyperplasia. Anatomically, the prostate has been described as consisting of five lobes: anterior and posterior lobes, two lateral lobes, and one median lobe. This has mainly been replaced by a zonal anatomical description [59].

#### 1.4.1 Prostate zones

McNeal (1981) described the anatomic zones based on biological and histological concepts [60]. The prostate is divided into five histological zones: the non-glandular anterior fibromuscular layer and four glandular components. The four glandular zones consist of the peripheral zone, central zone, transition zone and the periurethral glandular tissue. These make up 70%, 25%, 5% and <1% of the prostate's glandular tissue, respectively. Each zone originates from the prostatic urethra and has specific architectural features. The peripheral zone forms the rim of tissue surrounding the posterolateral and inferior aspect of the prostate. Its glandular ducts open into the prostatic urethra distal to the verumontanum. In the younger man, this rim is well defined and relatively thick, but it can often atrophy with age and be compressed by benign prostatic hypertrophy of the transition zone. Most cancers arise in the peripheral zone. The central zone is wedge-shaped and surrounded by the peripheral zone laterally and inferiorly. With age, it is often compressed by hypertrophy of the transition zone, forming a pseudo-capsule. Malignancy uncommonly arises from the central zone. The transition zone consists of two lobes of glandular tissue lateral to the urethra in the fibromuscular components of the pre-prostatic sphincter. The transition zone enlarges with age being the most typical site of benign prostatic hypertrophy. The periurethral zone consists of small ducts and acini along the urethra and periprostatic

sphincter. The anterior fibromuscular layer covers the convex anterior surface of the prostate. The apical portion of this area is rich in striated muscle and blends into the gland and the pelvic diaphragm muscle.

#### 1.4.2 Urethra

The male urethra is approximately 18 to 20cm long and can be divided into the posterior and anterior urethra. The posterior urethra consists of the prostatic and membranous urethra.

The prostatic urethra is about 3.5cm in length. It traverses the prostate gland from the bladder neck outlet to the apex where it is continuous with the membranous urethra in the urogenital diaphragm. At the verumontanum level, midway between the prostatic base and apex, the urethra curves 35 degrees antero-caudally towards the bladder neck. The verumontanum is where the urethral crest (the longitudinal ridge of smooth muscle on the posterior wall) widens and protrudes into the urethra. The verumontanum has a saccular depression called the prostatic utricle. The paired ejaculatory ducts enter the posterior urethra slightly distal and lateral to the utricle, adjacent to the verumontanum. The prostatic urethra ends at the urogenital diaphragm, which is composed of transversely oriented muscle covered by a superior and inferior fascia.

The membranous urethra is approximately 1 to 1.5cm long and traverses through the urogenital diaphragm. The urogenital diaphragm contains the transverse perinei muscle, external urethral sphincter and a Cowper's gland on each side of the diaphragm.

The anterior urethra includes the bulbous and the penile urethra. The bulbous urethra extends from the inferior urogenital diaphragm to the penoscrotal junction. The penile urethra extends from the penoscrotal junction, through the corpus spongiosum, and

terminates at the external meatus. Before terminating at the glans penis, it forms the fossa navicularis, a mildly widened portion of the urethra, 1 to 1.5cm in length.

#### 1.4.3 Seminal vesicles

Seminal vesicles are paired thin-walled grapelike or lobulated sacs, about 3 to 5cm long and 1cm in diameter, situated posterolateral to the prostate, between the bladder and rectum. They are separated from the rectum by Denonvilliers' fascia. They produce 60% of the ejaculate fluid. The seminal vesicle ducts join at the caudal tip with the vas deferens to form the ejaculatory ducts. The ejaculatory ducts traverse the central prostate zone to open in the posterior urethra at the verumontanum, on either side of the utricle [61].

#### 1.4.4 Anatomical Relationships

Superiorly, the prostate's base is continuous with the neck of the bladder and internal urethral sphincter muscles. Inferiorly, the apex lies on the superior aspect of the urogenital diaphragm, the bulbourethral glands of Cowper and rectovesical space. The urethra leaves the prostate just above the apex on its anterior surface. Anterior to the anterior fibrous muscular layer of the prostate is the retropubic space of Retzius, venous plexus of Santorini and the pubic symphysis. Posteriorly, the prostate is related to the seminal vesicles, and rectovesical fascia of Denonvilliers that overlies the rectal ampulla. Along the inferolateral prostate, the surface is the pubourethralis portions of the levator ani muscle.

#### 1.4.5 Lymphatic drainage

The prostate's primary lymphatic drainage is to the periprostatic lymphatic plexus and the obturator nodes (external iliac), and superior to the internal iliac systems. Further lymphatic

drainage is laterally to the external iliac system, and posteriorly to the presacral lymph nodes adjacent first to third sacral segments (S1-S3) and then to the para-aortic lymphatic system

#### 1.4.6 Blood supply

Arterial supply is provided by branches of the inferior vesical and middle rectal arteries.

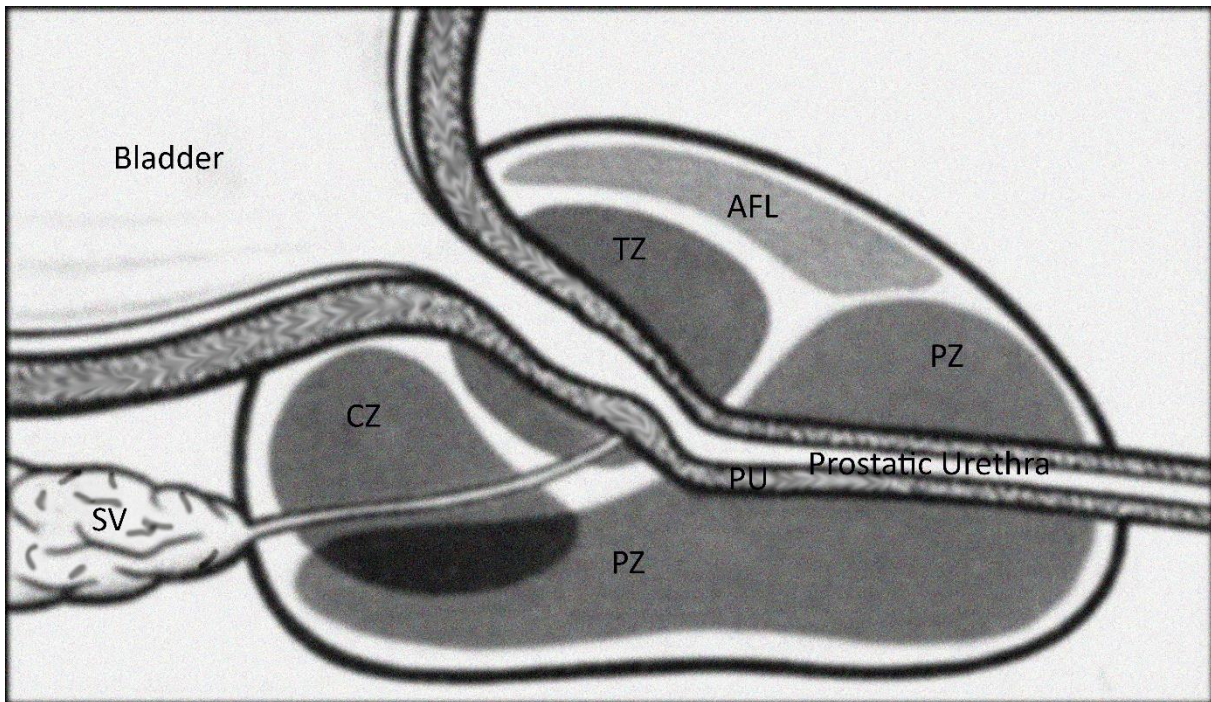
Venous drainage is by way of small veins that form a prostatic venous plexus, lying outside the prostate capsule. In addition to small prostatic veins, the plexus of Santorini also receives the deep dorsal vein of the penis and numerous vesical veins. The plexus drains into the internal iliac veins.

#### 1.4.7 Nerve supply

The prostate's nerve supply arises from the pelvic plexus formed by the parasympathetic, visceral, efferent and preganglionic fibres from the sacral levels S2 to S4, and the sympathetic fibres from the lumbar levels L1 to L2. Consequently, the inferior hypogastric plexus supplies the nerve fibres to innervate the prostate. Sympathetic stimulation causes smooth muscles to contract and thus squeezes the secretions out of the prostate during ejaculation.

#### 1.4.8 Appearance on magnetic resonance imaging

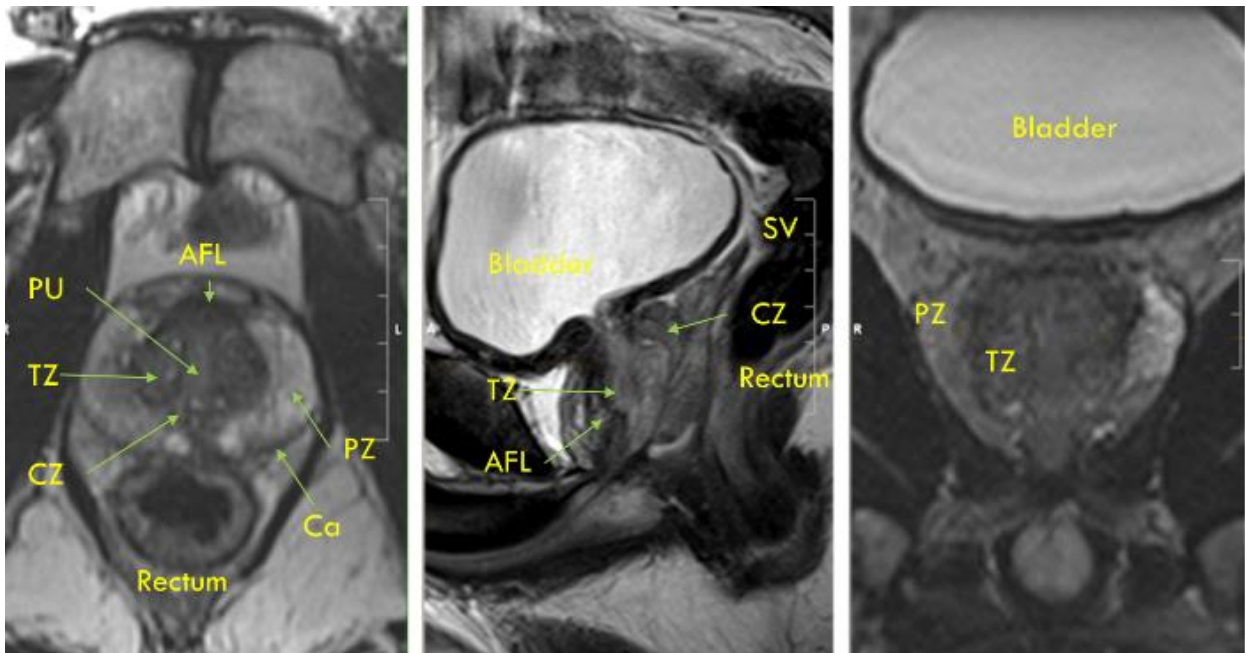
The zonal anatomy of the prostate, including the peripheral zone, central zone, transition zone and the anterior fibromuscular layer, are best visualised on T2-weighted magnetic resonance imaging (MRI) [61-65] (see Figures 1.1 and 1.2).



AFL = anterior fibromuscular layer, CZ = central zone, PU = periurethral tissue, PZ = peripheral zone, SV = seminal vesicles, TZ = transition zone

Source: Austin Health

Figure 1.1 Sagittal view of prostate zonal anatomy



AFL = anterior fibromuscular layer, Ca = prostate capsule, CZ = central zone, PU = periurethral zone, PZ = peripheral zone, SV = seminal vesicles, TZ = transition zone

Source: Austin Health

Figure 1.2 MRI of axial, sagittal and coronal views of prostate zonal anatomy

The anterior fibromuscular stroma contains no glandular tissue and thus is hypointense or dark on T2-weighted MRI, and is contiguous with the bladder neck. The peripheral zones are hyperintense, forming the posterolateral and inferior parts of the prostate. They are incompletely surrounded by a thin line of the hypointense capsule that is most often deficient inferiorly at the apex. The transition zone has a low signal in young men, but with age is most often heterogeneous, with an increasing chaotic pattern of low and high signal that can be asymmetrical as benign prostatic hypertrophy progresses.

On T2-weighted MRI, the central zone is generally a homogeneous low signal intensity (dark) that symmetrically surrounds the ejaculatory ducts from the prostatic base to the verumontanum, which usually has a high T2 signal. With age, benign prostatic hypertrophy compresses the central zone to a thin hypointense rim of the pseudo-capsule. The seminal

vesicles are paired grapelike pouches filled with fluid and thus exhibit a high signal intensity. The associated ejaculatory duct appears as a low-T2-signal, thick muscular structure that traverses the central zone to the verumontanum.

The distal prostatic urethra is seen as a central hyperintense inverted “U” with a hypointense rim of periurethral tissue. However, the proximal urethra, having a similar intensity to the surrounding prostate, often cannot be defined in the mid-gland until the bladder outlet. The membranous urethra can be seen on axial T2-weighted images as a low-signal-intensity ring surrounding the high-signal-intensity epithelial surface. The bulbous urethra traverses the root of the penis. It is a lower-signal-intensity tubular structure in the midline, within the bulb of the corpus spongiosum. Sagittal and coronal T2-weighted images may show the course of the anterior and posterior urethra. The distal penile urethra is often not seen on MR images.

## **1.5 PROSTATE CANCER HISTOPATHOLOGY**

The vast majority (more than 90%) of prostate cancer cases are adenocarcinomas of the prostate [66]. In contrast, sarcomas of the prostate are rare and account for only 0.1% to 0.2% of all malignant prostatic tumours, and are generally aggressive cancers. The most common prostate adult sarcomas are rhabdomyosarcomas and leiomyosarcomas [66-68]. Primary urothelial carcinoma of the prostate without bladder involvement accounts for 1% to 4% of all prostate carcinomas [69, 70]. Primary lymphoma of the prostate is rare, being less common than secondary lymphoma infiltration [71, 72].

There are uncommon subtypes of prostate adenocarcinoma. Mucinous adenocarcinoma of the prostate gland is one of the least common morphologic variants. It behaves like non-

mucinous prostate carcinomas, having a propensity to develop bone metastases with advanced disease [73]. Neuroendocrine differentiation is evident in a large proportion of prostate adenocarcinomas; almost half show neuroendocrine differentiation with immunohistochemistry evaluation using multiple neuroendocrine markers [74, 75]. The proportion appears to increase following the use of hormone therapy [76]. Small cell carcinomas of the prostate behave similarly to small cell carcinomas of the lung and have an inferior prognosis [77-79]. Between 0.4% and 0.8% of prostatic adenocarcinomas arise from prostatic ducts with most defined as intraductal adenocarcinomas. Intraductal carcinomas often present in an advanced stage and have an aggressive clinical course with poor response to therapy and poor prognosis [80-85].

The Gleason score is the most widely accepted method of scoring prostate cancer histopathology [86]. It was originally based on five Gleason patterns ranging from least to most aggressive on a scale of 1 to 5. The Gleason score was derived from the most extensive (primary) pattern, plus the second most common (secondary) pattern if two patterns are present. If only one pattern is present, the Gleason pattern value is doubled to yield the Gleason score. The Gleason systems have undergone many updates by the International Society of Urological Pathology (ISUP), leading to the modified Gleason score [87-89]. Nowadays, Gleason patterns 1 and 2 are rarely scored as they are regarded as reflecting benign disease. More aggressive patterns such as ductal and small cell are now graded as Pattern 4 and 5, respectively. The modified Gleason score also includes a tertiary pattern if there is a small component of aggressive cancer such as Pattern 5.

Further attempts have been made to better correlate the Gleason scoring system with prognosis. The 2014 ISUP Gleason Grading Conference proposed a five-grade system [88,

90]. This system was accepted by the World Health Organization in 2016 and the College of American Pathologists in 2018. It consists of the following five ISUP Grade Groups:

1. Grade Group 1 (Gleason score 3+3 = 6): only individual discrete well-formed glands
2. Grade Group 2 (Gleason score 3+4 = 7): predominantly well-formed glands with a lesser component of poorly formed/fused/cribriform glands
3. Grade Group 3 (Gleason score 4+3 = 7): predominantly poorly formed, fused, cribriform glands with a lesser component of well-formed glands
4. Grade Group 4 (Gleason score 8): only poorly formed, fused glands; or predominantly well-formed glands and lesser component lacking glands; or predominantly lacking glands and a lesser component of well-formed glands
5. Grade Group 5 (Gleason scores 9 and 10): lacking gland formation (or with necrosis), with or without poorly formed/fused/cribriform glands

## 1.6 CLINICAL PRESENTATION

Approximately 30% of men with prostate cancer are asymptomatic at diagnosis [91]. Early-stage prostate cancer is most often detected because of a raised PSA or less frequently an abnormal digital rectal examination (DRE). Most prostate cancers are located in the prostate gland's peripheral zone and may be evident as a nodule on DRE. Approximately 18% of prostate cancers are detected by DRE alone, but DRE by itself has a low detection rate of 3.2% [92, 93]. Abnormal DRE findings warrant a PSA test and prostate biopsy as DRE alone has a positive predictive value of 10% even with a normal PSA [94].

Symptoms may appear when cancer invades the urethra and obstructs the urinary flow, i.e., lower urinary tract symptoms. These include difficulty initiating urine flow, hesitancy, poor stream and terminal dribbling [95, 96], although these symptoms are more frequently associated with benign prostatic hypertrophy. Other less common symptoms include

haematuria and haemospermia. In severe obstruction, acute or chronic urinary retention can result in renal failure. Uncommonly nowadays in the PSA era, locally advanced prostate cancer can obstruct the rectum.

In advanced or metastatic disease, patients may complain of bone pain, mainly in the axial skeleton, e.g., back pain due to vertebral metastasis in association with fatigue or lethargy. If the metastatic disease invades or compresses the spinal cord or cauda equina, patients can develop neurological signs.

Progressive spinal metastases can lead to spinal cord compression or cauda equina syndrome. Typical symptoms are back pain associated with lower limb weakness, paraesthesia, perineal/saddle anaesthesia, and urinary and faecal incontinence. This clinical situation requires urgent assessment, with MRI for diagnosis, and treatment with steroids, radiotherapy and/or decompressive surgery. Extensive involvement of lymph nodes can result in lymphoedema of the pelvis and lower limbs. Visceral metastases most often occur late in the course of advanced metastatic prostate cancer, when the cancer is undifferentiated and classified as metastatic castrate-resistant prostate cancer (mCRPC).

## **1.7 STAGING AND RISK CATEGORISATION**

### **1.7.1 Digital rectal examination**

DRE is a standard part of clinical examination to evaluate male lower urinary tract symptoms, but its utility for the initial detection of cancer is limited because of its relatively low sensitivity and specificity in a screened population. Most patients detected with prostate cancer during the screening PSA program have normal DRE. By itself, DRE has a low cancer detection rate of 3.2% [92, 93]. An abnormal DRE has a positive predictive value of 42.3% for

prostate cancer, and a normal DRE has a negative predictive value of 84.2%. Therefore, palpation of irregularity or nodule during DRE remains an indication for prostate biopsy regardless of the level of PSA [97], and is of prognostic importance when prostate cancer is diagnosed as it is more likely to detect clinically significant cancers with extra-prostatic extension or seminal vesicle invasion [98].

### 1.7.2 Prostate-specific antigen and prostate cancer biomarkers

#### *Blood-based biomarkers*

PSA, or kallikrein-3 (KLK3), is a glycoprotein enzyme encoded in humans by the *KLK3* gene. PSA is present in the blood in multiple isoforms, some being more cancer-specific than others. PSA is relatively organ-specific, but elevations in serum PSA levels are not cancer-specific. PSA is secreted by the prostate gland into the prostatic ducts. Usually, only low levels of PSA enter the bloodstream. However, pathological processes such as benign prostatic hypertrophy, prostatitis and malignancy disrupt the prostate blood barrier and allow increasing levels of PSA to enter the bloodstream [99].

A PSA level greater than 4.0ng/mL is generally regarded as abnormal. It has a sensitivity of 21–44% and specificity of 91–92% for detection of prostate cancer. With a 3.0ng/mL threshold, the sensitivity increases to above 32%, but the specificity decreases to 85% [100, 101]. The positive predictive value for a PSA level >4.0ng/mL is approximately 30% [92], and the negative predictive value for a PSA value <4.0ng/mL is 85% [102]. However, some forms of prostate cancer, including aggressive cancers, can present with a low PSA [103, 104].

Modifications of PSA measurement such as PSA density and PSA kinetics have been developed to improve its specificity. The PSA density is the PSA level divided by the prostate

volume determined by transrectal ultrasound. Lower densities are more indicative of benign prostatic hypertrophy, whereas higher densities imply a greater probability of a significant cancer. PSA velocity (PSAV) is the increase in PSA over time (ng/mL/year), and PSA doubling time (PSA-DT) is the exponential increase in PSA measured against previous values. A rapid PSAV and PSA-DT indicate more aggressive disease or an increased likelihood of metastatic disease. They may have a role in prognosis but are of limited diagnostic use [105]. The free/total (f/t) PSA ratio may be used to differentiate benign prostatic hypertrophy from prostate cancer, particularly in the PSA grey zone range of 4.0–10.0ng/mL [106, 107]. The lower the f/t PSA ratio, the greater the probability of prostate cancer. Recommended thresholds have ranged from 0.14 to 0.25. However, a meta-analysis concluded that f/t PSA ratio had low sensitivity and specificity and should only be used in conjunction with other diagnostic tools [108].

Human kallikrein 2 (hK2) is closely related to PSA, being a serine protease belonging to the kallikrein family. Studies have used a panel of markers including hK2, such as the FDA-approved Prostate Health Index (PHI), to guide biopsy decisions.

Blood-based prostate biomarkers such as the PHI and four kallikrein score (4K) are forms of PSA testing that measure a range of kallikreins in serum and plasma. Their primary use has been to reduce the number of unnecessary repeat biopsies in previously biopsy-negative men by increasing the specificity of PSA testing and indicating a greater risk of a clinically significant cancer [109-112]. The PHI is calculated from the combination of free and total PSA and the PSA isoform p2PSA. Studies have shown that the PHI can improve high-risk prostate cancer detection and is associated with prostate cancer aggressiveness [113-116]. The 4K score measures free, intact and total PSA and kallikrein-like peptidase 2 (hK2). It also

accounts for clinical information, such as age, DRE and prior biopsy results. A meta-analysis noted that the 4K score is associated with an improvement in predicting biopsy-confirmed prostate cancer while avoiding 48–56% of repeat prostate biopsies [117]. It has also shown that it can improve the discrimination of high-grade cancer [118]. A comparison of PHI and 4K has shown that they have similar performance [119].

### *Urine-based biomarkers*

Prostate cancer antigen 3 mRNA (PCA3) is overexpressed in 95% of prostate cancers. The PCA3 gene is located on chromosome 9q21-22 [120]. PCA3 is detectable in urine as a prostate cancer-specific biomarker, using the commercially available test, ProgenSA. PCA3 is used with PSA to estimate whether the risk of prostate cancer warrants repeat biopsies for men with previous negative biopsies, particularly when PSA levels are persistently elevated in the intermediate range [121, 122]. PCA3 does not, however, appear to improve on PHI in predicting cancer on initial or repeat biopsies [123, 124].

Another urine-based mRNA biomarker is SelectMDX, which tests for the presence of *HOXC6* and *DLX1* mRNA. These are included in the SelectMDX score, which uses an algorithm that also includes total PSA, PSA density, DRE, age and family history [125]. It provides a risk of prostate cancer and the presence of high-risk disease and thus could assist in avoiding unnecessary biopsies [125, 126].

Gene rearrangements have been described in multiple cancers and can be measured in urine. The *TMPRSS2-ERG* fusion gene, comprising the androgen-responsive gene *TMPRSS2* and erythroblast transformation-specific (ETS)-related gene (ERG), was observed in 40–80% of prostate cancers [127]. Both genes are located on chromosome 21. A recent meta-

analysis showed that *TMPRSS2-ERG* overexpression is associated with tumour stage, but not with disease recurrence or mortality in men treated with radical prostatectomy [128].

The Mi-Prostate Score (MiPS) combines the prognostic significance of urine *TMPRSS2-ERG* and urine PCA3 with serum PSA to generate a prostate cancer risk assessment score [126].

MiPS is superior to PSA alone in predicting biopsy-confirmed prostate cancer and high-grade disease [129] and may reduce the number of biopsies required [130].

### *Tissue-based biomarkers*

A number of tissue-based biomarkers that test for multiple molecular species, notably mRNA, have been developed to determine prostate cancer aggressiveness and prognosis, thereby aiding in clinical decisions (Table 1.1).

ConfirmMDx is a tissue-based epigenetic test. The ConfirmMDx test quantifies the methylation level of promoter regions of three genes, Ras association (*RASSF1*), glutathione s-transferase Pi1 (*GSTP1*) and adenomatous polyposis coli (*APC*), in benign prostatic tissue. It helps distinguish a true-negative biopsy from possible occult cancer and may help avoid repeat biopsies [126, 131, 132].

Prolaris is a commercially available biomarker. It calculates a cell cycle progression score by analysing 31 cell cycle progression transcripts [133]. It has been shown to be of prognostic value by predicting outcome following treatment with prostatectomy and radiotherapy, and in surveillance populations. It thereby may indicate the utility of the treatment modality [134-136].

The Decipher® test measures the RNA expression of 22 marker genes, including non-coding and intronic sequences to produce a genetic signature [126]. Decipher signature has been validated to be of prognostic value for prostate cancer–specific mortality [137, 138]. It predicts for systemic progression and development of metastatic disease following prostatectomy, and for the benefit of post-prostatectomy radiotherapy in high-risk patients [139-142]. Decipher is commercially available as a prognostic tool to assist in clinical decision-making.

The Oncotype D® X Genomic Prostate Score (GPS) is a genomic tissue-based test of 12 genes relating to prostate cancer progression and housekeeping genes for normalisation [143]. The prognostic value has been shown in the pre-operative biopsy diagnosis of low- to intermediate-risk cancer. GPS can predict high-grade adverse pathology, high-stage disease and biochemical relapse in men with low- or low-intermediate-risk prostate cancer [126, 144]. Following these promising results, it has been made available commercially.

ProMark® is a quantitative proteomics-based test that measures eight proteins (DERL1, CUL2, SMAD4, PDSS2, HSPA9, FUS, pS6 and YBOX1) [145]. It predicts potential aggressiveness in Gleason 3+3 and 3+4, or very low, low- and low-intermediate-risk prostate cancer [126]. Early validation studies suggest it can separate favourable from unfavourable pathology and Gleason score 6 from non–Gleason score 6 [146].

Recently, several biomarkers have been proposed for predicting response to therapy. These include AR-V7, measured in circulating tumour cells for predicting enzalutamide and abiraterone resistance; mutant *BRCA1/2* from prostate tissue for predicting response to a poly [ADP–ribose] polymerase (PARP) inhibitor, olaparib; the PORTOS test in prostate tissue

for predicting response to radiotherapy; and circulating tumour DNA for predicting resistance to enzalutamide in castrate-resistant prostate cancer [121, 147].

The studies of biological markers appear promising and may greatly assist in the management of prostate cancer [121, 147, 148]. However, while some tests are available, they are expensive. Further rigorous prospective validation data and comparisons with standard tools are required before such markers can be adopted in routine clinical practice [126, 143].

Table 1.1 Evolving indications for prostate cancer biomarkers

Indication	Biomarker
Need for initial biopsy	<ol style="list-style-type: none"> <li>1. Prostate Health Index (PHI)</li> <li>2. SelectMDx</li> <li>3. Four kallikrein score (4K)</li> <li>4. Mi-Prostate Score (MiPS)</li> </ol>
Need for repeat biopsy	<ol style="list-style-type: none"> <li>1. Prostate cancer antigen 3 mRNA (PCA3)</li> <li>2. Confirm Dx</li> <li>3. 4K</li> <li>4. MiPS</li> </ol>
Active surveillance vs intervention/treatment	<ol style="list-style-type: none"> <li>1. Oncotype DX</li> <li>2. Promark</li> <li>3. Prolaris</li> <li>4. Decipher</li> </ol>
Post-prostatectomy observation vs adjuvant treatment	<ol style="list-style-type: none"> <li>1. Prolaris</li> <li>2. Decipher</li> </ol>

### 1.7.3 Transperineal vs transrectal biopsy

Biopsy remains the clinical cornerstone for the diagnosis of prostate cancer. Historically, transrectal ultrasound-guided (TRUS) biopsy with a 12-core extended sextant was recommended by guidelines as it was regarded as sufficiently accurate, with only 15–31% of

patients requiring repeated biopsies to make the diagnosis [100, 149]. Repeat biopsies are typically due to sampling errors, especially with anterior and apical tumours [150]. It also has been noted that the Gleason grading from TRUS biopsies was not consistent with prostatectomy specimens in up to 31.5% cases [151], and, in another study, was upgraded in 33.2% to 50% of cases [152-154]. TRUS biopsies have generally been regarded as being safe with an antibiotic cover. Complications such as bleeding and infection occur in approximately 6% of cases, with haemospermia being the most common complication (37.4% of cases). Severe complications, such as abscess formation and gram-negative septicaemia, occur in less than 1% of cases [105, 153].

Transperineal template biopsy (TPB) has been increasingly utilised because of its improved diagnostic accuracy and lower complication rate [154]. It has been estimated that about 30% of patients are diagnosed with prostate cancer with a TPB after an initial negative TRUS biopsy. Transperineal biopsies enable the procedure to utilise a greater number of cores, including saturation biopsies of up to 50 cores, to increase the detection rate. Severe complication rates, including prostatic abscess and septicaemia, are lower with TPB than TRUS [154].

To further improve biopsy diagnostic accuracy, multi-parametric MRI (mpMRI) guidance has been used to perform targeted biopsy [155, 156]. The mpMRI comprises sequences including T2-weighted and diffusion-weighted imaging with or without dynamic contrast-enhanced MRI. The interpretation of results has been standardised by the Prostate Imaging Reporting and Data System (PI-RADS) [157-159]. The PI-RADS categorises prostate lesions based on the likelihood of cancer according to a five-point scale: PI-RADS 1 – clinically significant cancer is highly unlikely to be present; PI-RADS 2 – clinically significant cancer is unlikely to be

present; PI-RADS 3 – the presence of clinically significant cancer is equivocal; PI-RADS 4 – clinically significant cancer is likely to be present; and PI-RADS 5 – clinically significant cancer is highly likely to be present.

MRI can be used in several ways, including in-bore biopsies, cognitive MRI ultrasound fusion, or device- or software-mediated MRI ultrasound fusion [160]. MRI in-bore biopsies require significant magnet time and are costly, so their utilisation has been limited to dedicated centres. Cognitive fusion is logistically easier, and the detection rate is similar to device-mediated fusion [160, 161]. A meta-analysis has illustrated that mpMRI fusion biopsies improve the diagnosis of significant cancer and decrease the detection of indolent cancers [162, 163]. It has a sensitivity of 80–95% [164].

Three recent and important trials have elucidated the use of mpMRI-guided biopsy: PROMIS [150], randomised PRECISION [165] and the 4M Study [149]. They have confirmed that the use of mpMRI-guided biopsies increases the likelihood of a clinically significant cancer being identified, reduces over detection of clinically indolent insignificant cancers, and results in fewer biopsies being required. The use of MRI before biopsy and MRI-targeted biopsy was superior to standard transrectal ultrasonography-guided biopsy in men at clinical risk for prostate cancer who had not undergone biopsy previously [150, 165]. It has also been proposed that mpMRI-targeted biopsy could omit the need for systematic sampling to reduce the diagnosis of low-risk disease and thereby decrease the potential treatment harm to patients [166].

MpMRI-guided TPB is increasingly being considered the primary pathological diagnostic tool in prostate cancer and is increasingly used in Australia.

#### 1.7.4 Computed tomography

Pelvic computed tomography (CT) is regarded as the standard investigation for the assessment of lymph node involvement in intermediate- and high-risk prostate cancer [154, 167]. The risk of lymph node metastases is based on site, number, shape, lymph node architecture and size, mainly a diameter greater than 8–12mm in the short axis [168-170]. According to diameter, the sensitivity is relatively low, with a median of 0.42, as CT cannot detect microscopic nodal involvement; however, its specificity is relatively high at 0.82 [154, 169]. CT with positron emission tomography (PET), particularly prostate-specific membrane antigen (PSMA) PET, has been used to improve the performance of CT [154].

#### 1.7.5 Technetium bone scan

Technetium bone scan is regarded as the standard investigation for bone metastases in high-risk and symptomatic prostate cancer [167]. It has a sensitivity of 79% and a specificity of 82% [167, 171]. However, technetium scintigraphy performs poorly with PSA values <20ng/mL [172]. Its performance may be improved with single-photon emission computed tomography (SPECT); however, more recently, whole-body MRI and sodium fluoride (NaF) PET have been proposed as alternatives to bone scan [167, 172, 173].

#### 1.7.6 Magnetic resonance imaging

While mpMRI is important for targeted biopsies and radiotherapy planning [174], its utility for local staging before surgery is debatable. MRI has relatively low sensitivity in detecting extracapsular extension as it will not detect microscopic capsular invasion. Therefore, it is not generally recommended for low-risk prostate cancer patients. However, in intermediate-

and high-risk disease, a meta-analysis has shown a sensitivity of 71% and specificity of 82% for extraprostatic extension and seminal vesicle invasion [175].

Whole-body MRI is an appealing modality for prostate cancer staging because of its high soft tissue contrast and anatomical detail. It can image bone marrow, nodal and soft tissue metastases, in addition to the locoregional disease, in a single scan session. It allows for combining sequences such as T1-weighted, T2-weighted and diffusion-weighted scans, providing not only morphological but also structural and functional information [176]. A meta-analysis of whole-body MRI found that MRI outperformed bone scan in the staging of bone metastases in high-risk prostate cancer, and offered anatomical and structural information [171]. However, it may be less sensitive than PET for bone metastasis and lymph node staging [177-179].

#### 1.7.7 Positron emission tomography

PET has been shown to have an increasing role in the diagnosis and staging of prostate cancer. It has also been utilised for the targeting of biopsy, radiotherapy planning and response assessment [180-182].

<sup>18</sup>F-FDG (fluorodeoxyglucose) PET/CT is widely used in cancer imaging, but it appears to have low sensitivity and limited activity in prostate adenocarcinoma diagnosis and staging because of the low metabolic activity of prostate [176, 183]. However, it appears to be more useful in staging aggressive high-grade and high Gleason score cancers, including small cell/neuroendocrine tumours and metastatic medical castration-resistant prostate cancer [171, 184].

Choline PET/CT, using either  $^{11}\text{C}$ - or  $^{18}\text{F}$ -labelled choline, has been utilised in a limited number of centres for the assessment of prostate cancer.  $^{11}\text{C}$  has the advantage of lower urinary excretion compared to  $^{18}\text{F}$ , but the shorter half-life necessitates a local cyclotron. Due to its low sensitivity in the diagnosis and initial staging of prostate cancer, the role for choline PET/CT appears limited. While some studies have shown choline PET/CT to be useful in detecting intra-prostatic lesions for radiotherapy planning, and in combination with multi-modality imaging for correlation with the Gleason score [185-187], other studies have been conflicting [188, 189]. Choline PET/CT appears more useful for evaluating lymph node metastases or recurrence outside the pelvis in the setting of a PSA recurrence after local therapy. A recent review reported an improvement with choline PET/CT compared to anatomical imaging for metastatic lymph node detection, with pooled positive predictive values ranging between 75% and 85.8% [190]. However, comparison of choline PET/CT with PSMA PET shows that PSMA PET has a higher sensitivity than  $^{11}\text{C}$ -choline or  $^{18}\text{F}$ -fluciclovine PET/CT imaging, along with higher levels of specificity [191].

PSMA PET is rapidly emerging as an important investigative tool for prostate cancer diagnosis, staging and response assessment due to its excellent sensitivity and specificity compared to other available imaging [192]. PSMA is a promising imaging and therapeutic target because of its preferential overexpression by most prostate cancer cells, its correlation with tumour grade, low presence in the bloodstream and sufficient retention. A meta-analysis of 15 studies showed that PSMA PET had a large impact on management in prostate cancer patients, with greater PET positivity associated with a higher proportion of changes in management [193].

While mpMRI is increasingly utilised for the diagnosis and local staging of prostate cancer, studies have indicated that its performance in targeting biopsies and the staging of extracapsular extension and seminal vesicle invasion may be improved with PSMA PET [194, 195].

PSMA has an increasing role in assessing lymph node metastases, both for staging and for PSA relapse following treatment. Traditionally, CT has been used clinically, with a sensitivity of 42% and specificity of 82%; more recently, mpMRI, with sensitivity of 39% and specificity of 82%, has also been used [169]. A number of studies have illustrated the improved accuracy and detection of PSMA PET overall, but especially with smaller lymph nodes apparently uninvolved on standard imaging [196-198]. A recent prospective study of pre-operative staging with <sup>68</sup>Ga-PSMA-11 PET/MRI found a good sensitivity (68.8%), excellent specificity (100%) and high accuracy (93%) for detection of lymph node metastases [196].

PSMA PET also has a role in detecting recurrent disease, particularly after treatment with prostatectomy, radiotherapy or both [199]. In a large prospective study, PSMA PET could localise the recurrent prostate cancer in 75% of cases. The detection rates were significantly increased with higher levels of PSA [200]. Similar results have been confirmed in multiple meta-analyses [201]. However, existing studies are heterogeneous and limited by retrospective design, publication bias and limited reference standards. Therefore, the results need to be confirmed in prospective clinical trials [202].

PSMA PET's ability to accurately stage high-risk localised and metastatic prostate cancer is further highlighted by a systematic review of 37 articles involving 4,790 patients [203]. The review confirmed the increase in the percentage of positive scans with increasing PSA. For

PSA categories 0–0.19, 0.2–0.49, 0.5–0.99, 1–1.99 and  $\geq 2$ ng/mL, the percentages of positive scans were 33%, 45%, 59%, 75% and 95%, respectively. The review showed that PSMA PET had a high sensitivity (75%) and excellent specificity (99%) on a per-node analysis. It concluded that PSMA PET improved the detection of metastases with PSA recurrence, particularly at low PSA levels where most other imaging fails [203].

PSMA PET, however, is not without its caveats. False positives may occur due to physiologic uptake in normal tissue, such as the kidney, gut, breast, brain, adrenal, ovary, salivary gland, celiac ganglion, small intestine and reactive lymph nodes. Additionally, other benign and malignant tumours, such as non-small-cell lung carcinoma, neuroendocrine tumours, renal cell carcinomas and Paget's disease of the bone, can show PSMA activity [204-206].

False negatives can also occur with PSMA PET as it has a low sensitivity for nodal disease at  $< 4$ mm, and nodes cannot often be detected at  $< 2$ mm. Notably, 5–10% of prostate cancers do not express PSMA, although some of these are the small cell neuroendocrine or de-differentiated prostate cancers that are FDG avid [197, 206, 207].

$^{18}\text{F}$ -NaF PET/CT has been increasingly utilised in cancer patients as a more sensitive alternative to the other methods, including technetium bone scan, for detecting bone metastases [208, 209]. Previous meta-analyses have illustrated this improved performance in various cancers, including prostate cancer [210, 211]. The improved performance is essential for high-risk prostate cancer as it has a propensity to metastasise to bone, which can be a major cause of morbidity. A meta-analysis of 14 studies published in 2019 systematically analysed NaF PET in prostate cancer [212]. The authors concluded that NaF PET had an excellent diagnostic performance for staging and restaging of bone

metastases in prostate cancer. Its performance was superior to technetium bone scintigraphy and SPECT, and comparable to diffusion-weighted MRI. Comparisons of NaF PET and PSMA PET in the detection of bone metastases have been conflicting. A recent pooled analysis in prostate cancer showed that PSMA PET had the highest per-patient sensitivity, but NaF PET/CT had the highest sensitivity per lesion. PSMA PET/CT and NaF PET/CT were equivalent to or outperformed MRI and choline PET/CT, whereas bone scan was the least effective [213].

## **1.8 TREATMENT WITH CURATIVE INTENT**

### **1.8.1 Active surveillance**

Active surveillance is the active monitoring of low-risk or low-intermediate-risk prostate cancer. Intervention with treatment with curative intent is only instituted if there is disease progression [214]. The aim is to avoid unnecessary treatment-related toxicities in men whose cancer is unlikely to progress in their lifetime.

For men diagnosed with prostate cancer, approximately 50% will have low-risk disease, typically a Gleason score of 6 or, more recently, Grade Group 1 [215-217]. Many of these will be indolent tumours that remain clinically insignificant for many years, possibly for the remainder of the man's life. There is a discordance between prostate cancer prevalence and the risk of mortality from prostate cancer [217]. Autopsy studies of men have shown that many harbour prostate cancer that has remained asymptomatic and not metastasised. Molecular genetic testing has also illustrated that Gleason pattern 3 cancers, unlike Gleason pattern 4 cancer, often do not have the genetic or molecular aberrations associated with cancer progression and metastases [217, 218]. This is clinically evident in that only a small

proportion of men with Gleason pattern 6 cancer will have metastases; one study estimated this proportion to be 0.2% at 20 years [218]. Studies have shown that most patients with low-risk disease will not benefit from radical treatment and that active surveillance may be a more reasonable option in these men.

The Swedish Prostate Cancer Group-4 (SPCG-4) study randomly assigned men with localised prostate cancer to radical prostatectomy or watchful waiting. Patients were recruited over 10 years, from 1989 to 1999, and followed until 2012. Watchful waiting consisted of no immediate treatment or active monitoring, except a transurethral resection of the prostate (TURP) if required, which was in contrast to contemporary active surveillance protocols. The SPCG-4 study found that men with localised prostate cancer benefited from prostatectomy compared with watchful waiting [219]. They noted that the number needed to treat to prevent one death was eight. The greatest benefit was seen in men younger than 65 years with intermediate-risk prostate cancer, although prostatectomy was associated with a reduced risk of metastases in older men.

The Prostate Intervention versus Observation Trial (PIVOT), which randomised 731 men with localised prostate cancer (mainly low risk and intermediate risk) to observation versus radical prostatectomy from 1994 to 2002, provides randomised evidence supporting active surveillance [220]. The authors reported an updated series with nearly 20 years of follow-up and confirmed no difference in all-cause or prostate cancer-specific mortality. Treatment was associated with an increased frequency of adverse events but a lower frequency of treatment for disease progression.

Similarly, the ProtecT trial randomised 1,643 men with localised prostate cancer to undergo active monitoring, radiotherapy or surgery from 1999 to 2009 [221]. Approximately 80% of the patients in this study were considered low risk. A recent update of 10-year mortality, disease progression and side effects of the study reported a low incidence of prostate cancer mortality. With no difference between the treatment groups, 95% of patients with low- and intermediate-risk prostate cancer did not die of prostate cancer. There was a trend towards increasing prostate cancer deaths and an increase in progression and metastatic disease with active monitoring. However, the increased patient-reported harms due to treatment, in part, balanced the adverse prostate cancer effects [222].

Clinical evidence supporting active surveillance for intermediate-risk patients comes from prospective institutional cohorts. Cooperberg et al. reported data comparing intermediate- and low-risk patients who underwent active surveillance [223]. After 4 years of follow-up, the study found no difference in the rate of cancer progression or the proportion of men undergoing treatment between the two groups [223]. In contrast, a previous report from the University of Toronto showed an increased risk of late metastasis in men with intermediate-risk prostate cancer who chose active surveillance [224]. Men with Gleason 7 prostate cancer primarily drove this relationship. However, these men were selected and monitored by clinical and pathologic criteria only and perhaps underwent serial biopsy too infrequently for their level of risk. A systematic review of active surveillance in intermediate-risk prostate cancer showed a higher risk of prostate-directed treatment and metastatic disease [225].

Patients with Gleason 6 cancers and Gleason 3+4 with a low percentage of pattern 4 are considered active surveillance candidates. Patients are followed with serial PSA and rectal examinations, and repeat biopsies. The American Society of Clinical Oncology encourages

the following testing schedule for active surveillance: a PSA test every 3 to 6 months, a DRE at least once every year, another prostate biopsy within 6 to 12 months, then a biopsy at least every 2 to 5 years [226]. However, increasingly, mpMRI and biomarkers are being used as an important part of the selection and follow-up of such patients [121, 126, 227, 228]. Guidelines for patient selection and management are now well established [226, 229-232].

## 1.8.2 Surgery

### *Radical prostatectomy vs robotic (including laparoscopic) prostatectomy*

Historically, radical prostatectomy, more typically via a retropubic approach, has been the standard treatment of localised prostate cancer. Typically, this has been utilised in patients with low- and intermediate-risk prostate cancer who had a life expectancy of 10 years. Many of these patients are now entered into an active surveillance program. Prostatectomy is now considered in the younger patient with high-risk disease, and even in patients with pelvic lymph node metastases, as part of a multi-modality treatment [233].

Surgery can provide good long-term oncological outcomes in selected high-risk patients, either alone or with post-operative radiotherapy +/- adjuvant ADT [234]. A recent meta-analysis also suggests that prostatectomy may prolong survival in high-risk prostate patients at the expense of poorer urinary and sexual function [235]. It indicated that cancer-specific survival might be further improved in combination with radiotherapy. However, careful patient selection was considered necessary [235].

Increasingly, laparoscopic or robot-assisted prostatectomy has been used in prostate cancer. It has some advantages in terms of shortened hospitalisation and earlier return to work.

However, randomised studies between open and robotic prostatectomy did not show a benefit in functional or oncologic outcome [236, 237].

### *Lymph node dissection*

Pelvic lymph node dissection, including extended pelvic lymph node dissection in men with intermediate- and high-risk prostate cancer undergoing prostatectomy, is controversial. European Association of Urology (EAU) guidelines suggest it should be considered if the lymph node risk is greater than 5%, while National Comprehensive Cancer Network (NCCN) guidelines suggest consideration if the risk is greater than 2%. [233, 238]. However, there is no level 1 evidence supporting the implementation of lymph node dissection, and systematic reviews have not shown an improved outcome, including survival [239]. The utilisation of lymph node dissection is mainly based on institutional studies indicating long-term survival in patients with lymph node metastases who have undergone lymph node dissection [240, 241]. However, other studies have failed to improve outcomes and highlight the possible side effects of pelvic lymph node dissection [242]. Its role appears to be mainly prognostic and staging, to direct post-prostatectomy therapy [239].

### 1.8.3 Radiotherapy

Primary radiotherapy with curative intent is a well-established treatment for prostate cancer. Depending on the clinical situation, it can be delivered using a number of techniques including external beam radiotherapy (EBRT), EBRT with a high-dose-rate brachytherapy boost and low-dose-rate brachytherapy monotherapy.

EBRT is the most widely utilised form of prostate radiotherapy, and recent randomised studies have confirmed its utility in the modern setting. Two randomised studies comparing

radiotherapy plus adjuvant hormone therapy versus hormone therapy alone have shown an improved outcome for the combination [243, 244]. Widmark et al. randomised 875 patients with locally advanced or high-risk prostate cancer to radiotherapy and ADT (neoadjuvant and continuous) versus continuous ADT alone [243]. The addition of local radiotherapy to endocrine treatment halved the 10-year prostate cancer-specific mortality. It substantially decreased overall mortality with an acceptable risk of side effects compared with endocrine treatment alone. In another study, Warde et al. randomised 1,057 high-risk prostate cancer patients to androgen deprivation with or without radiotherapy. In the radiotherapy arm, the patients had a significantly higher 7-year overall survival of 74% versus 66% for the androgen deprivation alone arm ( $p=0.033$ ). The trial showed a clear overall survival benefit for radiotherapy with androgen deprivation in a locally advanced or high-risk prostate cancer patient population [244].

The STAMPEDE study has further supplied prospective non-randomised data that support local radiotherapy for locally advanced prostate cancer with or without pelvic node metastases [245]. The study found that failure-free survival outcomes of nonmetastatic, high-risk prostate cancer patients with newly diagnosed disease were increased by radiotherapy to the prostate with or without pelvic radiotherapy, compared to the standard of care, ADT alone. The improved outcome was confirmed for patients both with and without nodal involvement. The study authors concluded that the data, together with previous studies, supported the routine use of radiotherapy in patients with node-positive nonmetastatic prostate cancer.

The ProtecT study randomised 1,633 patients with mainly low- or intermediate-risk prostate cancer to active monitoring, surgery or radiotherapy [246]. At a median of 10 years follow-

up, there was low mortality with no differences between treatment groups. Notably, both surgery and radiotherapy were associated with a lower incidence of progression, metastasis and possibly dying from prostate cancer, but there was no difference between prostatectomy and radiation [222, 246]. In a separate report on patient-reported outcomes, surgery had the greatest negative impact on urinary and sexual outcomes, whereas radiotherapy had the greatest impact on bowel function [246]. There were no significant differences observed among the groups in measures of anxiety, depression, or general health-related or cancer-related quality of life. The study illustrated that radiotherapy is a reasonable alternative to surgery. It is most often recommended in the older patient and/or men with more advanced disease.

Treatment outcomes, including biochemical control and lower toxicity for radiotherapy, have improved with the utilisation of intensity-modulated radiotherapy and image-guidance techniques. In addition, recently, four large prospective RCTs have demonstrated that EBRT delivered to the prostate using moderate hypofractionation (2.4 to 3.4Gy per fraction) provides similar early prostate cancer control and similar toxicity to EBRT delivered using conventional fractionation (1.8 to 2.0Gy per day) [247, 248], increasing the convenience of radiotherapy by reducing overall treatment times of approximately 8–9 weeks to 4–6 weeks.

EBRT with high-dose-rate brachytherapy boost is associated with lower rates of biochemical failure in retrospective and phase 2 studies [249, 250]. A recent phase 3 study, ASCENDE-RT, has confirmed the improvements with a brachytherapy boost and thus increased radiation dose [251]. This study randomised 398 intermediate- and high-risk prostate cancer patients to pelvic radiotherapy to 46Gy plus an EBRT boost to 78Gy or a brachytherapy boost. The men randomised to external beam boost were significantly more likely to experience

biochemical failure. However, the brachytherapy boost showed no survival benefit, a significant increase in acute and late genitourinary morbidity, and a non-significant trend for worse gastrointestinal morbidity [252]. There was a significantly greater decline in mean health-related quality of life for the brachytherapy boost on physical and urinary function scales.

Low-dose-rate brachytherapy alone is a well-established prostate cancer treatment, particularly for the low-risk disease [253]. It is seen as an alternative to surgery and has similar outcomes to both surgery [254] and EBRT. It has been shown to have less rectal toxicity and better preservation of erectile function, but at the expense of slightly greater urethral side effects [254-256].

### *Pelvic nodal radiotherapy*

There is no level 1 evidence that prophylactic whole pelvic nodal irradiation improves survival in patients who undergo radiotherapy for prostate cancer. However, it is considered an acceptable option for men who have a high risk of nodal involvement. The risk may be estimated using widely available tools such as Partin tables [257] and the Roach's formula [258]. Typically, whole pelvic nodal irradiation is recommended if the risk of nodal involvement is greater than 15%. Guidelines recommend covering the lymphatic drainage that includes the external and internal iliac lymph node regions to the common iliac bifurcation, and the presacral lymph nodes [259, 260].

The indirect evidence supporting pelvic lymph node irradiation is mainly based on multi-centre randomised trials that showed an advantage for radiotherapy including pelvic nodal radiation combined with ADT, and institutional studies of whole pelvic radiotherapy in locally

advanced disease [261-264]. The evidence includes the Radiation Therapy Oncology Group (RTOG) 9413 study. This study of intermediate- and high-risk localised prostate cancer has been interpreted as showing that the combination of neoadjuvant hormonal therapy plus whole pelvic radiotherapy improved progression-free survival, compared to neoadjuvant therapy plus prostate-only radiotherapy [261].

However, the two randomised studies that directly compared prostate plus prophylactic pelvic nodal radiotherapy to prostate radiotherapy alone (RTOG 9413 and GETUG) have not shown a statistically significant overall survival difference [261, 265]. Indeed, the GETUG 01 study did not show an improvement in progression-free survival, although both studies had methodological caveats. Furthermore, a large database analysis also failed to show a survival benefit for whole pelvic radiotherapy [266].

Whole pelvic radiotherapy for positive pelvic nodes is also a controversial topic, although it is considered an option in major guidelines [267]. There is no randomised evidence supporting its implementation. However, a large population database study [268] and a systematic review [269] have suggested there may be a survival benefit.

#### *Prostate radiotherapy with adjuvant androgen deprivation therapy*

Multiple randomised studies have investigated various durations of ADT with radiotherapy versus radiotherapy alone. Systematic reviews summarising the data showed that combining EBRT with hormone therapy resulted in a significant relapse-free and overall survival advantage when compared to EBRT alone [270, 271]. The trials have shown that this advantage is mainly in intermediate- and high-risk prostate cancer patients. Generally, the longer ADT arms have performed better than the shorter durations in high-risk prostate

cancer [272]. However, a 2018 randomised study has further elucidated ADT's optimal duration by investigating the two most widely used durations of 36 months and 18 months [273]. The study randomised 630 patients with localised high-risk prostate cancer treated with radiotherapy to either 36 months or 18 months of ADT. Results showed that 36 months was not superior to 18 months ( $p=0.07$ ) in terms of 5-year survival. However, the quality of life was significantly worse with the longer ADT course ( $p<0.001$ ) [273].

#### *Local prostate radiotherapy with adjuvant chemotherapy*

Adjuvant docetaxel in high-risk prostate cancer patients receiving radiotherapy has also been investigated. The RTOG 0521 trial randomised 612 patients, of which 563 were evaluable after a median follow-up of 5.7 years [274]. The study found that docetaxel with radiotherapy and ADT in high-risk prostate cancer patients improved the overall survival, disease-free survival and rate of distant metastases, suggesting a possible role for this treatment in these patients. The randomised GETUG-12 study (413 patients) showed that docetaxel-based chemotherapy improved relapse-free survival in patients with high-risk localised prostate cancer, but has not yet established a benefit for metastasis-free survival and overall survival [275]. Another randomised study that included adjuvant docetaxel with radiotherapy, the SPCG-13 study (376 patients), did not show a significant improvement in the primary endpoints of metastases-free survival or biochemical disease-free survival [276]. In addition, an earlier RTOG trial (9902) that randomised patients with high-risk prostate cancer to radiotherapy and ADT with or without paclitaxel, estramustine and etoposide closed early because of an excess in thromboembolic events [277]. After a median follow-up of 9.2 years, there was no difference in biochemical recurrence, local or metastatic progression, disease-free survival or overall survival between treatments with and without

adjuvant chemotherapy [277]. While adjuvant docetaxel with radiotherapy and ADT is a consideration in high-risk prostate cancer patients, its role is yet to be fully elucidated.

### *Post-prostatectomy adjuvant vs salvage radiotherapy*

Three randomised trials have investigated adjuvant radiotherapy (ART) following prostatectomy for prostate cancer patients who had positive surgical margins and/or extracapsular extension and, therefore, an increased risk of local recurrence [278-283]. All showed an improvement in freedom from PSA progression. A subsequent meta-analysis confirmed a significant improvement in biochemical progression-free survival, but there were no significant overall survival differences [284]. Subsequently, the SWOG 8794 study was updated with longer follow-up of 10 years, and showed a significant improvement in overall survival and metastasis-free survival [281]. However, use of ART has been declining because of some statistical concerns with the studies, particularly the SWOG study, and because approximately one-third of patients would undergo radiotherapy without any benefit but would risk toxicity.

Salvage radiotherapy (SRT), radiotherapy instituted following a PSA rise post prostatectomy, has often been used as an alternative to ART to avoid overtreatment. Its utilisation has been predicated on large retrospective reviews. The most notable of these was done by Stephenson et al. [285, 286]. The analysis included 501 patients treated with SRT and showed a 4-year progression-free survival of 45%. The significant risk factors for progression in the multivariate analysis were seminal vesicle invasion, negative surgical margins, Gleason score  $\geq 8$ , PSA doubling in  $<10$  months and PSA  $>2\text{ng/mL}$  pre-radiotherapy (i.e., predictors of metastatic disease). Those with no risk factors had a 4-year progression-free survival of 80%, whereas for those in the worst prognostic group it was 20%.

The controversy regarding ART versus SRT has recently been resolved following a presentation of three randomised trials – RADICALS (ISRCTN40814031), GETUG-AFU 17 (NCT00667069) and RAVES (NCT00860652) – and a subsequent planned meta-analysis by the ARTISTIC collaboration [287, 288]. The analysis included 1,074 patients randomised to ART and 1,077 randomised to SRT with a median follow-up that ranged from 47 to 61 months across the trials. The preliminary pooled analysis shows no evidence that relapse-free survival is improved with ART compared to SRT (hazard ratio [HR] 1.09, 95% confidence interval [CI] 0.86–1.39,  $p=0.47$ ). The result translates to a potential absolute difference of 1% at 5 years favouring SRT (95% CI: 2% in favour of ART to 4% in favour of SRT) [288]. The level 1 evidence is now consistent with the clinical implementation of SRT for PSA relapse post prostatectomy.

Whole pelvic nodal radiotherapy with post-operative prostate bed radiotherapy is a controversial area. It has been frequently used in men with a high risk of nodal metastases, most often following a PSA relapse. There are no randomised studies that support its use. However, preliminary results from an interim analysis of the NRG Oncology/RTOG 0534 SPORRT study have indicated that prostate bed radiotherapy plus pelvic lymph node radiotherapy plus short-term hormone therapy has superior freedom from disease-free progression at 5 years compared to prostate bed radiotherapy alone or prostate bed radiotherapy and hormone therapy.

#### *Post-prostatectomy salvage radiotherapy with androgen deprivation therapy*

While level 1 evidence supports adjuvant androgen deprivation with radiotherapy for high-risk (intact) prostate cancer, the use of adjuvant androgen deprivation with post-prostatectomy radiotherapy has also been controversial. Two recent randomised studies

(RTOG 9601 and GETUG-AFU 16) showing an improvement in outcome have elucidated the issue [289, 290].

The GETUG study included 743 patients: 374 were randomised to radiotherapy alone and 369 to radiotherapy plus goserelin for 6 months [289]. The updated study showed a 120-month progression-free survival of 64% (95% CI 58%–69%) for patients treated with radiotherapy plus goserelin, and 49% (95% CI 43%–54%) for patients treated with radiotherapy alone (HR 0.54, 95% CI 0.43–0.68; stratified log-rank test  $p < 0.0001$ ), indicating an advantage for the addition of short-course ADT [289].

The RTOG 9601 study randomly assigned 760 post-prostatectomy patients with a PSA relapse with positive surgical margins or extracapsular extension to bicalutamide plus SRT (384 patients) or SRT plus placebo (376 patients) [290]. The overall survival was improved at 12 years – 76.3% in the bicalutamide group versus 71.3% in the placebo group (HR for death 0.77, 95% CI 0.59–0.99,  $p = 0.04$ ). The 12-year incidence of death from prostate cancer was better in the bicalutamide group at 5.8% compared with 13.4% in the placebo group ( $p < 0.001$ ). The incidence of metastatic prostate cancer was significantly better at 12 years: 14.5% in the bicalutamide group and 23.0% in the placebo group ( $p = 0.005$ ) [290]. Thus, the outcomes were better with the addition of bicalutamide to SRT.

SRT combined with short-term androgen suppression significantly reduced risk of biochemical or clinical progression and death compared with SRT alone. The unresolved issues for future trials are whether an antiandrogen or luteinising hormone-releasing hormone (LHRH) agonists should be used, and for what duration.

### *Post-prostatectomy radiotherapy with chemotherapy*

There have been two phase 3 trials of adjuvant docetaxel systemic therapy to reduce the recurrence rates in high-risk patients following prostatectomy: the SPCG-12 trial [291] and the VA Cooperative Studies Group Study [292]. The SPCG-12 trial randomised 459 patients, to prostatectomy and chemotherapy versus prostatectomy alone but there was no significant difference in biochemical recurrence or median survival [291]. The VA Cooperative Studies Group Study #553 similarly randomised 298 high-risk patients before it was closed due to slow accrual. After a median follow-up of 62.4 months, there was no significant difference in median time to progression in the patients accrued. However, subgroup analysis did show a benefit for docetaxel for African American men with at least pT3b disease (i.e., very high-risk prostate cancer) [292].

## **1.9 TREATMENT OF METASTATIC PROSTATE CANCER**

Management of metastatic prostate cancer aims to prolong survival and, importantly, control symptoms and minimise complications while maintaining quality of life. Metastatic prostate cancer can have a wide range of manifestations. These can extend from an elevated PSA without imaged disease, to oligometastatic prostate cancer with fewer than five metastases, to widespread lymph node or bone metastases, to involvement of viscera such as lung, liver and even brain in the very advanced stages. Most patients with metastatic prostate cancer initially have a disease that is dependent on androgens or testosterone for growth and spread.

### 1.9.1 Watchful waiting

Watchful waiting is most often utilised for elderly patients with prostate cancer. Watchful waiting is particularly applicable if they have low-risk disease, as their risk of progression and need for treatment is low. It also applies to patients with multiple comorbidities and a short life expectancy, usually less than 5 years. Unlike active surveillance, investigation and intervention are performed only if the patient is likely symptomatic from his prostate cancer, either locoregional or metastatic disease.

Interestingly, the SPCG-4 trial that randomised men with localised prostate cancer to prostatectomy versus watchful waiting reported their results after 29-years of follow-up [293]. The authors concluded that men with clinically detected localised prostate cancer with long life expectancy benefited from radical prostatectomy, with a mean of 2.9 years of life gained compared to watchful waiting. A high Gleason score and extracapsular extension were highly predictive of death from prostate cancer. The study has a number of caveats including significant changes in diagnosis and treatment over the 29 years. However, the findings do highlight that the patient with a long-life expectancy or more advanced disease are often not good candidates for watchful waiting.

### 1.9.2 Androgen deprivation therapy

Testicular androgen suppression has been the standard therapy for patients with symptomatic metastatic disease since the original reports of Huggins et al. many years ago [294]. Initial systemic treatment for metastatic prostate cancer is ADT. Androgen deprivation can be achieved with surgical (bilateral orchidectomy) or medical castration. Surgical castration is a cost-effective and straightforward method that achieves a rapid

decline of testosterone to castrate levels. However, it is permanent, and there are often psychological barriers to bilateral orchidectomy. Thus, many men prefer to pursue the medical option.

#### *Luteinizing hormone agonist (LHRH) agonists*

The most common method of achieving medical castration is the use of gonadotropin-releasing hormone (GnRH) or luteinizing hormone agonist (LHRH) agonists [295]. Typically, these include goserelin, triptorelin and leuprorelin. The mechanism of action is identical, but there are differences in delivery, pharmacokinetics and duration of action [296]. These agents bind to the pituitary receptor and produce initial stimulation, resulting in a transitory increase in testosterone and a flare of prostate cancer symptoms. The flare can be prevented with the use of an antiandrogen. Following this initial stimulation, GnRH agonists suppress GnRH, and testosterone synthesis by the testicles falls to castrate levels. GnRH agonists are delivered as subcutaneous or intramuscular injections [297]. The duration of action is up to 6 months, depending on the formulation. Therefore, they are a generally convenient and compliant treatment for metastatic prostate cancer.

#### *GnRH antagonist*

The alternative to the agonist is a GnRH antagonist. There is only one that is commercially available, degarelix. It is non-inferior to leuprolide in randomised studies [298, 299].

Degarelix has a quicker onset of action and does not produce a flare like GnRH agonists.

However, it is only available as a 1-month depot injection, making it less convenient. It has also been suggested that degarelix may improve International Prostate Symptom Scores (IPSS) [300] and reduce cardiovascular deaths when compared to GnRH agonists [301]. A

comparison study of degarelix and GnRH agonists showed a reduced incidence of joint, musculoskeletal and urinary tract adverse events [301]. GnRH antagonist is preferred over agonists initially in particular clinical situations where a rapid onset of action is desired, and flare is best avoided, such as in patients with spinal cord compression, impending urinary retention or severe bone pain.

### *Continuous versus intermittent androgen blockade*

Intermittent ADT aims to limit the toxicity associated with continuous ADT. Side effects of ADT due to castrate levels of serum testosterone may be lessened if testosterone levels are allowed to return to normal once patients have responded. ADT is then re-initiated once the disease progresses, at either a clinical or PSA threshold.

Intermittent ADT appears to be an appropriate strategy for men having a PSA relapse alone, with no apparent disease clinically or on imaging. A non-inferiority phase 3 study [302] was performed that randomised 1,386 patients with rising PSAs at least 1 year after primary or salvage radiotherapy for localised prostate cancer to either continuous or intermittent ADT. After a median follow-up of 6.9 years, intermittent ADT was non-inferior to continuous ADT according to the trial definition of overall survival at 7 years. Quality of life was better with intermittent ADT.

The role of intermittent ADT in those patients with overt metastatic disease is individualised. Hussain et al. [303] performed a non-inferiority phase 3 trial of intermittent versus continuous ADT. The study randomised 1,535 patients with newly diagnosed metastatic prostate cancer, in whom the PSA declined to <4ng/mL following ADT. The median survival was found to be 5.8 years in the continuous ADT group and 5.1 years in the intermittent ADT

group (HR for death with intermittent ADT 1.10, 90% CI 0.99–1.23). The trial was regarded as statistically inconclusive as the confidence interval for median survival exceeded the upper boundary for non-inferiority. There were too few events to rule out the inferiority of intermittent therapy. There was, however, less erectile dysfunction and better mental health in the short term with intermittent ADT. Intermittent ADT was not generally recommended for patients with clinically apparent metastatic disease, as this trial indicated a trend toward inferiority. However, as intermittent ADT was associated with a better quality of life in the short term, it remains an option for men willing to accept a potentially shorter survival.

In addition, a meta-analysis of intermittent versus continuous ADT found that it was non-inferior concerning disease progression, cancer-specific survival and overall survival, although the issue remains controversial [304]. Besides, many men do not achieve objective testosterone recovery during therapy.

#### *Early versus delayed Androgen Deprivation Therapy*

While ADT has been the standard treatment for PSA relapse following definitive or salvage radiotherapy for high-risk prostate cancer, the timing of the ADT has been controversial. Immediate ADT is instituted upon PSA relapse, whereas delayed ADT is started either with the onset of symptoms or detection of progressive disease with imaging. Studies of early versus delayed ADT [305-308] including a randomised study [309] have generally shown a benefit in terms of overall survival [309] and prostate cancer-specific mortality with early ADT [305, 308]. However, there have been concerns regarding an increase in non-prostate cancer mortality [308] and the detrimental effects on quality of life. Additionally, some studies, such as a retrospective study of immediate versus delayed ADT after PSA relapse following prostatectomy or radiotherapy, have found no survival advantage for immediate

ADT [310]. A meta-analysis suggested that ADT for relapse after primary curative therapy should be reserved for patients at highest risk of progression and with a long life expectancy. The potential benefits of ADT should be balanced against the associated risk of harm [311].

### *Total androgen blockade*

Total androgen blockade uses a GnRH agonist, typically in combination with a first-generation antiandrogen to prevent the flare phenomenon. However, the long-term addition of a nonsteroidal antiandrogen (NSAA) to standard ADT was an attempt to improve the outcome of metastatic prostate treated with ADT [312]. However, while some meta-analyses have shown a benefit [312, 313], the general opinion is that there is a minimal survival benefit, and increased toxicity and cost [314-316].

### *Antiandrogens*

First-generation antiandrogens, including flutamide and bicalutamide, and strategies such as antiandrogen withdrawal have been widely utilised following disease progression. They are used with GnRH agonists, and before introducing docetaxel and novel agents. These androgen manipulations have resulted in a PSA decline in approximately 20% to 60% of patients in some studies. However, there is no survival benefit [317, 318].

Phase 2 studies have demonstrated that second-generation antiandrogens offer much greater PSA responses and progression-free survival than first-generation antiandrogens [319, 320]. However, first-generation antiandrogens remain in use as they can delay the need for the newer and more expensive agents if the patient has a good response.

*Enzalutamide*

Enzalutamide is a potent second-generation antiandrogen with three sites of action: androgen receptor binding and inhibition, inhibition of nuclear translocation of the androgen receptor, and inhibition of the androgen receptor's association with the nuclear DNA [321].

The randomised phase 2 TERRAIN [322] and STRIVE [319] trials showed survival benefits for enzalutamide in comparison with bicalutamide in the non-metastatic castrate-resistant prostate cancer or asymptomatic/minimally symptomatic mCRPC setting [320].

Large phase 3 trials (including AFFIRM, PREVAIL and PROSPER) have shown that enzalutamide has significant anti-tumour activity with improved overall survival in both the pre-and post-chemotherapy settings, including metastatic and nonmetastatic mCRPC [323-325].

Recent randomised phase 3 studies, including ENZAMET and ARCHES, which utilise enzalutamide in hormone-sensitive prostate cancer, have also shown improvements in progression-free survival and overall survival with the maintenance of quality of life [326-328].

*Abiraterone*

Abiraterone acetate is an inhibitor of CYP17A1 and targets both 17 $\alpha$ -hydroxylase and 17,20-lyase activities, thereby inhibiting androgen biosynthesis in the tumour as well as the testes and adrenal glands. Concurrent administration of low-dose prednisone with abiraterone is required to prevent hypertension, hypokalaemia and fluid retention resulting from adrenocorticotrophic-generated mineralocorticoid excess [329].

The final analysis of the large randomised trial COU-AA-301 showed that abiraterone prolonged overall survival in docetaxel-treated men with mCRPC compared with placebo [330]. Abiraterone also significantly improved all secondary endpoints, including the time to PSA progression, progression-free survival and PSA response rate.

In asymptomatic or mildly symptomatic mCRPC patients not treated with chemotherapy, abiraterone improved radiographic progression-free survival and delayed clinical decline and initiation of chemotherapy compared with placebo in the randomised COU-AA-302 trial [331, 332]. In the final overall analysis at a median follow-up of 49.2 months, median overall survival was significantly longer in the abiraterone acetate group than in the placebo group [333].

Results from the STAMPEDE [334] and LATITUDE [335] trials showed increased overall survival in men with locally advanced or hormone-sensitive metastatic prostate cancer with the addition of abiraterone to ADT [334, 335]. These results were further consolidated by a meta-analysis of abiraterone in hormone-sensitive prostate cancer [336], which also concluded that the toxicity was acceptable [337].

### 1.9.3 Palliative radiotherapy

EBRT is an efficacious treatment for painful bony metastases, especially if the pain is not controlled with analgesia. It provides palliation in 60–70% of patients, with 30–40% having complete relief of the symptoms. EBRT, sometimes combined with surgery, has also been an effective treatment for spinal cord compression due to metastatic prostate cancer [338, 339]. Two randomised studies of palliative radiotherapy doses for spinal cord compression have shown no significant differences between selected doses [340, 341]. However, neither

study provided details pertaining to modern radiotherapy, including technique, and thus the delivered dose is uncertain. There is increasing interest in using stereotactic ablative body radiotherapy (SABR) with minimally invasive surgery for metastatic spinal cord involvement to improve outcomes.

#### 1.9.4 Radiotherapy for oligometastatic Prostate Cancer:

##### *Stereotactic ablative body metastasis directed therapy*

Prostate cancer patients with a low volume of metastatic disease have better outcomes than those with high volume disease [342]. Large population analyses have shown that the number and site of metastases impacts survival. Lymph metastases alone have the best prognosis, bone metastases intermediate and visceral metastases have the most inferior survival [343, 344]. There has been increasing interest in more aggressive treatment in patients with low volume metastatic disease, particularly oligometastatic disease [345]. While there is no consensus, the term oligometastatic disease has been generally defined in trials as three or five metastases.

Recent reviews of stereotactic metastasis directed radiotherapy for oligometastatic prostate cancer have reported excellent control rates of 82-100% at two years [346, 347]. The control rates appear to be dose-dependent [348, 349], but significantly higher local control rates are observed with BED>100Gy [348]. It was noted that 25-38% of patients progress but remain amenable to further stereotactic ablative radiotherapy and that 67% lymph node relapses occurred out of field [346]. All published series found the toxicity low and generally limited to gastrointestinal side effects [346]. The outcomes from the studies analysed were median ADT free survival 15.6-39.7 months and median progression-free survival of 40-72% at one

year and 35-45% at two years [346]. SABR for oligometastatic prostate cancer appears efficacious and safe.

POPSTAR was a single-arm study of SABR for oligometastatic prostate cancer to determine safety and feasibility[350]. It accrued 33 patients that received single 20 Gy fraction SABR to 50 metastases with a 2-year follow-up. It found that SABR was feasible with low morbidity while maintaining QOL. Over a third of patients did not progress and were free from ADT at two years.

The STOMP phase 2 study randomised 62 patients with oligometastatic prostate cancer to either surveillance or metastasis directed therapy with the primary endpoint being androgen deprivation therapy free survival [351]. At a median follow-up of 3 years, the ADT free survival was significantly longer for the MDT arm (21 months, 80% CI 14–29 months) versus the surveillance group (13 months, 80% CI 12–17 months). Quality of life remained similar, and toxicity was mild.

The SABR-COMET trial, a phase 2 study, randomised 99 patients with oligometastatic cancer (up to five metastases), including breast, colon, lung and prostate cancer patients, to standard palliative care or SABR [352]. After a median follow-up of 25–26 months, the median survival was significantly improved in the SABR group (median survival of 41 months, 95% CI 26 months–not reached) compared to the control group (28 months, 95% CI 19–33 months) with HR=0.57, p=0.090. Median progression-free survival was 12 months for the SABR group versus 6 months for the control group (HR=0.47, p=0.0012). However, there were three treatment-related deaths.

The phase 2 Oriole clinical trial [353] randomised 54 men with oligometastatic (one to three metastases) hormone-sensitive prostate cancer to SABR versus observation. The study showed a significant improvement in progression-free survival at 6 months for the SABR arm. Local control was excellent at 98.9%. PSMA PET was performed on all patients but blinded to the investigative team. Therefore, SABR was directed only at metastases visualised on conventional imaging, meaning that a proportion of the metastases detected by PSMA only were not treated. The trial showed a significant advantage in progression-free survival and distant metastasis-free survival in men who received SABR to all PSMA-detected lesions. This underlined the importance of PSMA PET in the treatment of all detected lesions. The study also illustrated an immune response in terms of enhanced differential clonotype expansion (i.e., clusters of similar expanded T-cell receptors) in only patients receiving SABR. The immune response to SABR is an interesting finding, but future studies are required to assess this result's impact and utility.

#### *Prostate radiotherapy in metastatic hormone-sensitive prostate cancer*

In the early stages of metastatic hormone-sensitive prostate cancer (mHSPC), the prostate primary most often represents the site of greatest cancer clonogen number. It has been argued that by controlling the primary site the outcome may be improved [354], as shown in database studies [355].

The concept of radiotherapy to the prostate primary in the setting of mHSPC has been tested in three randomised studies and recently reviewed by a prospective, planned STOPCAP systematic review and meta-analysis [356]. This review included the completed STAMPEDE studies [357] and HORRAD study [358], as well as the ongoing PEACE trials [356]. It compared prostate radiotherapy and ADT versus ADT alone from the STAMPEDE A1 (1,694

patients), HORRAD (432 patients) and PEACE 1A1 (234 patients) studies. It also compared prostate radiotherapy plus ADT plus other agents from the STAMPEDE study and remaining PEACE studies that included the other agents – abiraterone or docetaxel. Overall, the review found no significant improvement in overall survival or progression-free survival by adding prostate radiotherapy to ADT. However, it did find a highly significant benefit of prostate radiotherapy in biochemical progression-free and failure-free survival. Toxicity results were based on the STAMPEDE study that reported 4% severe acute bladder toxicity, 1% severe acute bowel toxicity and 4% severe late side effects. Similar overall results were found with the STAMPEDE docetaxel study. Importantly, the review authors noted that prostate radiotherapy's impact on survival varied with the number of bone metastases. The benefit was mainly seen with fewer than five metastases; there was no benefit in men with five or more bone metastases. The recommendation of the review authors was that the addition of local prostate radiotherapy to ADT should be considered in men with metastatic hormone sensitive prostate cancer (mCSPC) who have four or fewer bone metastases.

#### 1.9.5 Chemotherapy for metastatic castration-resistant prostate cancer

Before docetaxel, prostate cancer chemotherapy was mainly limited to mitoxantrone which had a symptomatic effect but no survival benefit. In 2004, two phase 3 trials of mCRPC patients were reported: TAX 327 that randomised docetaxel versus mitoxantrone [359], and SWOG 9916 that randomised docetaxel plus estramustine versus mitoxantrone [360]. Both studies showed a significant median survival benefit for the docetaxel arm. The survival benefit of TAX 327 was confirmed in later studies that showed a significant reduction in pain and improvement in quality of life for mCRPC patients [361-363]. Subsequently, docetaxel is well established as first-line chemotherapy for metastatic castrate-resistant prostate cancer.

Cabazitaxel, a synthetic taxane, is an effective treatment in mCRPC patients who have progressed while on docetaxel. The TROPIC phase 3 trial randomised 800 men who had progressed on docetaxel to cabazitaxel plus prednisolone versus mitoxantrone plus prednisolone [364]. The study showed an advantage for cabazitaxel, with an HR for death of 0.70 (95% CI 0.59–0.83,  $p < 0.0001$ ) and 2.4-month median survival advantage. Cabazitaxel is now considered second-line chemotherapy for mCRPC patients.

#### 1.9.6 Chemotherapy for metastatic castration-sensitive prostate cancer

Following the successful introduction of docetaxel as treatment of mCRPC, trials commenced in earlier-staged disease, mCSPC.

Three randomised studies of docetaxel with ADT versus ADT alone have been completed: the GETUG-AFU 15 [365, 366], ECOG-CHAARTED [367] and a STAMPEDE study [368]. These studies showed a benefit for docetaxel with ADT in mCSPC, in terms of progression-free survival in all three studies and overall survival in the CHAARTED and STAMPEDE studies [369]. Patients with high-volume metastatic disease appeared to obtain the most improvement [366, 367], although this remains controversial [370, 371]. A subsequent meta-analysis confirmed that docetaxel with ADT in mCSPC significantly improved failure-free survival, absolute 4-year failure and, notably, overall survival [372].

#### 1.9.7 Bone agents

##### *Bisphosphonates and denosumab*

Bisphosphonates are degradation-resistant structural analogues of pyrophosphates that bind avidly to the bone and are ingested by osteoclasts during bone resorption. The bisphosphonate inhibits osteoclast-mediated bone resorption. Bisphosphonates have been

used for patients with extensive prostate bony metastases to decrease skeletal-related events and possibly palliate pain, but do not have any impact on overall survival [373, 374].

Denosumab is a monoclonal antibody that specifically binds to the receptor activator of nuclear factor kappa B (RANK) ligand, preventing the binding of the RANK ligand to RANK. This binding inhibits osteoclast formation, function and survival, and decreases bone resorption resulting in increased bone density. It has been shown in multiple systematic reviews to be better than bisphosphonates in reducing skeletal-related events [375-378].

### *Radioisotopes including radium*

Radioisotopes such as samarium-153 [379, 380] and strontium-89 [381, 382] have been used as monotherapy, or in combination with chemotherapy, in the treatment of prostate cancer bone metastases [383, 384]. They have been used for bone palliation, especially in men with extensive osseous metastatic disease, although they do not improve overall survival [385]. These isotopes are beta emitters and can cause marrow toxicity, resulting in transfusion dependence or infection risk. Radium-223 is an alpha-emitter and calcium mimetic that binds to the microenvironment of sclerotic metastases. The alpha radiation particles have a much shorter range than the beta emitters and, consequently a lower risk of haematologic toxicity. The phase 3 ALSYMPCA (Alpharadin in Symptomatic Prostate Cancer Patients) trial randomised patients who had previous docetaxel or were ineligible for docetaxel to radium-223 treatment or placebo [386]. The trial showed a significant improvement in overall survival (14.9 vs 11.3 months) with radium-223 treatment. A recent update confirmed these results and showed a reduced hospital stay, reduced time to skeletal-related events and improved quality of life [387]. Notably, the toxicity rates were lower in the radium-223 arm than in the placebo arm [386, 388]. A meta-analysis of radium-223 has confirmed the

improvement in overall survival [389]. The follow-up phase 3 ERA 223 study investigated radium-223 with or without the addition of abiraterone acetate. This study was unblinded and halted early because higher death rates and fractures were observed in the combination arm [390]. Radium-223 is useful for bone palliation, but is dose-dependent [391]. However, the PSA response rate after radium treatment appears low [392].

### 1.9.8 Immunotherapy

#### *Vaccine: Sipuleucel-T*

Sipuleucel-T is the only approved immunotherapy for prostate cancer, notably for the treatment of asymptomatic or minimally symptomatic mCRPC. It is a dendritic cell vaccine that is prepared from the patient's harvested peripheral blood mononuclear cells. It is composed of autologous antigen-presenting cells cultured with a fusion protein, PA2024, which consists of prostatic acid phosphatase linked to granulocyte–macrophage colony-stimulating factor. These antigen-pulsed antigen-presenting cells are infused back into the original patient and produce an anti-tumour immune response [393-395].

Three completed phase 3 trials have confirmed the efficacy of this Sipuleucel-T. The D9901 [394], D9902A [396] and D9902B trials [393], in addition to the randomised phase 2 crossover study APC8015F [397], have shown significant improvement in median survival. The D9902B (IMPACT – Immunotherapy for Prostate Adenocarcinoma Treatment) phase 3 study was designed with overall survival as the primary endpoint. The study randomised 512 patients and confirmed a survival benefit of 4.1 months (median overall survival 25.8 vs 21.7 months). Time to progression was similar in both arms [393]. A recent study has also shown a stabilisation of PSA in select mCRPC patients that may indicate a delay in progression [398].

However, routine clinical use of Sipuleucel-T has not been available because of logistics and cost, and further trials are required to investigate the optimal sequence with other therapies [399].

#### *PARP inhibition: Olaparib*

PARP inhibition has been investigated for cancers that have underlying *BRCA1/2* or other germline DNA damage repair defects, such as breast and ovarian cancers. Recent studies have demonstrated these germline defects occur in men with advanced prostate cancer [400, 401] and mCRPC [402], suggesting that PARP inhibition is a potential therapy for prostate cancer [401]. The phase 2 TOPARP-A trial showed a 33% response rate to the PARP inhibitor olaparib in heavily pre-treated mCRPC patients [403]. Fourteen of the 16 patients with homologous deletions or deleterious mutations in DNA damage repair genes responded to olaparib. Overall, biomarker-positive patients experienced superior median progression-free survival (9.8 vs 2.7 months) and median overall survival (13.8 vs 7.5 months).

#### *Immune checkpoint inhibitor: Pembrolizumab*

Immune checkpoints are a normal part of the immune system that control the immune response so that normal cells are not attacked. Immune checkpoints engage when immune checkpoint proteins on the surface of T cells recognise and bind to partner proteins on other cells. This binding turns off the T cells. In cancers, this can prevent the immune system from destroying the cancer [404].

Immune checkpoint inhibitors block checkpoint proteins from binding with their partner proteins on neoplastic cells, allowing the T cells to kill cancer cells. These immunotherapy agents include CTLA-4, ipilimumab, and PD-1 or its partner protein PD-L1 (nivolumab and

pembrolizumab) [404]. They have therapeutic action in a number of solid tumours, but activity and response rates in prostate cancer are limited [405-407]

However, it has been proposed that immune checkpoint inhibitors, including pembrolizumab, may be a therapeutic consideration for a small subset of mCRPC patients [408]. Approximately 2–12% of prostate cancers harbour microsatellite instability, a marker of DNA mismatch repair and a hypermutated state [402, 404]. The high response rate in tumours with mismatch-repair deficiency has been observed with pembrolizumab, regardless of the primary site [409]. In the phase 2 KEYNOTE-199 study, pembrolizumab has shown anti-tumour activity, durable responses and encouraging survival estimates with acceptable toxicity in mCRPC patients with mainly bone metastases [410].

### 1.9.9 Palliative surgery

Palliative surgery may be required for specific clinical situations. This is often an emergency or urgent situation such as the fracture of a long bone, spinal cord compression or urinary retention. Surgery is also indicated for ongoing symptoms in a relatively young patient with few comorbidities or a disease with a long natural history. Bilateral orchidectomy can be an alternative to medical castration, particularly in patients with symptomatic widespread metastatic prostatic cancer, and who do not want to have regular injections.

Transurethral resection of the prostate (TURP) may be required, typically in the mCRPC patient with lower urinary tract symptoms or urinary retention. Palliative TURP for mCRPC is reasonably safe, but side effects are higher than for a conventional TURP [411]. More radical procedures may be contemplated in the young mCRPC patient with good performance status and reasonable life expectancy. Patients with local progression with infiltration of the

pelvic floor, bladder neck and trigone, or symptomatic involvement of the rectum, can have an extremely poor life quality due to local symptoms. Thus, aggressive but palliative surgery may be considered on an individual basis. Typical procedures include cystoprostatectomy with urinary diversions, and anterior and posterior exenteration [412].

Like prostate radiotherapy in mHSPC, retrospective reports including large database analysis suggest that, in selected patients with mHSPC, prostatectomy is associated with improved oncological outcomes and better overall survival, cancer-specific survival and prostate cancer-free survival [413-417]. Several randomised prospective studies are investigating the role of prostatectomy in patients with metastatic disease, including TroMBOne [418], SWOG S1802 (<https://clinicaltrials.gov/show/NCT03678025>) and g-RAMMP (<https://clinicaltrials.gov/show/NCT02454543>).

Prostate cancer has the highest incidence of bone metastases of any solid tumour. A recent large database analysis showed an incidence of 18.0% at 1 year, 20.4% at 2 years, 24.5% at 5 years and 29% at 10 years [419]. The most frequent sites are the spine, pelvis and long bones. Internal fixation or joint replacement surgery may be required to prevent or repair pathological fractures of long bones. The palliative surgery goals for bone metastases are the control of pain, preservation or restoration of neurologic function, and mechanical stability in appropriately selected patients [420-422]. A recent systematic review of the surgical management of bone metastases showed adequate pain relief, and maintenance of or improved function following surgery. However, the authors did note a relatively high perioperative complication rate and perioperative mortality [423].

Indications for spinal surgery include the progression of disease that is not responding to standard treatments including radiotherapy; spinal instability including pathological fracture; progressive deformity; neural (spinal cord, cauda equina, nerve or nerve root) compression, especially if it is causing a neurological deficit; or a mechanical issue such as a bone fragment. Typical spinal surgeries include limited decompression, such as a laminectomy; wide tumour excisions, including vertebrectomy; and internal stabilisation [424].

Increasingly minimally invasive spinal surgery is being utilised with the aim of reducing morbidity and avoiding delays for radiotherapy and chemotherapy [425]. The goals of minimally invasive surgery include critical neural structure decompression (spinal cord and cauda equina) and maintenance of spine stability, and reduction of the morbidity of major open spine surgery. Typical applications of minimally invasive surgery include percutaneous vertebroplasty, percutaneous kyphoplasty, radiofrequency ablations, cryoablations and transarterial embolisations [426].

Minimally invasive surgery is increasingly utilised, often in association with stereotactic radiotherapy, when there is spinal cord compression [425]. Typically, separation surgery is used to do a minimal resection of the tumour with the separation of cancer from the spinal cord. The residual tumour is then treated with SABR to minimise the morbidity from surgery and avoid exceeding spinal cord radiation tolerances. Surgical decompression followed by radiotherapy has been shown to improve local control rates compared to radiotherapy alone [338, 427], as well as improving motor function [428].

### 1.10 PURPOSE OF THE THESIS

Precision radiotherapy for prostate cancer requires an accurately designed target volume for the prostate and prostate cancer, that is ideally aligned perfectly during the verification and treatment process. Precision is dependent on the weakest link in the radiotherapy planning and treatment chain. Accuracy is accomplished with increasingly sophisticated techniques of multi-modality imaging and targeting systems known as image-guided radiotherapy.

Therefore, the thesis's overarching purpose is to investigate improvements in image guidance through imaging for target volume design and delineation, study the target motion and resultant margins, and assess fiducial markers for precise targeting of prostate radiotherapy.

Chapters are arranged in accordance with the radiotherapy and research processes. The initial step of the radiotherapy process is image acquisition, and therefore Chapter 3 investigates the use of MRI with CT to improve the accuracy of target delineation. The next chapter utilises standard gold fiducials to assess prostate and seminal vesicle motion while delivering the radiotherapy and calculates the appropriate margins. The following chapters consider alternative commercially available polymer fiducials, as the artefact from standard gold fiducials can interfere with accurate contouring and verification. The final chapter investigates the development of an in-house novel liquid fiducial with unique properties.

The thesis has four aims. The relationship of the thesis studies and chapters to these aims is as follows.

**Aim 1.** *To study the impact of multi-modality imaging, including MRI, on target delineation.*

The initial study examined the use of MRI in combination with the simulation CT in the

identification and definition of the vesicourethral anastomosis (VUA), the principal target in post-prostatectomy radiotherapy. The study aimed to analyse the spatial differences between MRI and CT in the localisation of the VUA, and subsequently to assess the MRI-based VUA relative to the CT-based clinical target volume margins recommended by the published guidelines. This aim is addressed in Chapter 3.

**Aim 2.** *To analyse motion and margins using gold fiducials.* Chapter 3 studied initial phases of radiotherapy planning in terms of target definition; the next chapter explores target motion during a course of prostate radiotherapy. Chapter 4 therefore analyses inter-fraction displacement and margins utilising gold fiducials and daily online image guidance. The seminal vesicles form part of the radiotherapy treatment target of locally advanced prostate cancer but can move relative to the prostate. This study used gold fiducials in both the prostate and proximal seminal vesicles to minimise observer variation and more accurately track seminal vesicle displacement through the entire course of radiotherapy. Thus, the specific aims of Chapter 4 were to quantify the proximal seminal vesicle displacement relative to the prostate, and calculate appropriate margins for the planning target volume, minimising the risk of geometric miss or under-dosage.

**Aim 3.** *To contrast and compare polymer fiducials to gold fiducials for prostate radiotherapy.* While gold fiducials are regarded as the standard fiducial in radiotherapy and were used in the Chapter 4 study of motion, they produce a significant artefact that can interfere with target delineation on CT and verification with cone beam CT. Chapters 5 and 6 thus investigate a newer commercially available polymer fiducial and compare it to gold. Before implementing the polymer fiducial in a patient population, we decided to perform a phantom study to understand its imaging characteristics better. A purpose-built phantom

that was tissue-equivalent for both CT and MRI was constructed. The phantom study in Chapter 5 aimed to assess the visibility of the polymer fiducial and characterize the artefacts so as to compare to the standard gold markers on CT and MRI simulation images. Following the phantom project results, a study was initiated in a cohort of patients with locally advanced prostate cancer. Chapter 6 aims to compare polymer fiducials to the standard gold fiducials using clinical radiotherapy protocols (CT, MRI, cone beam CT and kilovoltage [kV] planar imaging) to assess the visibility and relative CT artefact production in a population of prostate cancer patients.

**Aim 4.** *To develop a novel liquid glue fiducial and assess its deliverability and visibility.* The initial thesis studies utilised the standard gold fiducials and then compared their imaging characteristics to a newer polymer fiducial. The next step was to develop a novel liquid glue fiducial that could be utilised in prostate and post-prostatectomy bladder radiotherapy. The first study of glue fiducials was a technical study of deliverability. As the tissue glue polymerises in water, we decided to simulate the clinical situation of fiducial insertion into the bladder base for post-prostatectomy radiotherapy. Therefore, Chapter 7 aimed to test the technical and procedural aspects of combining and delivering liquid contrast agents with several types of tissue glues in a porcine bladder (water-filled) model, to create multiple reproducible discrete glue fiducial markers that could be visualised with standard radiotherapy imaging. The technical deliverability of the fiducial is an essential first step, but it is vital to consider the glue fiducial's verification performance. Therefore, the aim of the final study was to characterise the Lipiodol™-glue fiducials in terms of their visibility and artefact production with conventional radiotherapy imaging, and compare them to the

standard gold fiducial in the porcine bladder model and the more-reproducible tissue-equivalent phantom. This study is elucidated in Chapter 8.

## Chapter 2 LITERATURE REVIEW

---

The initial thesis radiotherapy technical literature review was performed in 2015. It has been updated continuously throughout the course of my candidature, with the final update conducted in December 2020.

### 2.1 PRECISION RADIOTHERAPY

Prostate cancer is the most common cancer among Australian men (excluding skin cancer) and the second commonest cause of cancer-related deaths. Approximately 10–20% of patients diagnosed with prostate cancer will have locally advanced disease. Uncontrolled prostate cancer can have a variable but complicated natural history. Inadequately treated cases can result in a prolonged period of disease-related morbidity that will significantly impact patients' quality of life. Many patients with locally advanced disease can still be cured.

Historically, androgen deprivation therapy (ADT) alone was often used to palliate locally advanced disease. Recent randomised controlled trials (RCTs) that compared the addition of radiotherapy to ADT versus ADT alone have reported an overall survival advantage for the combination [243, 429]. Thus, radiotherapy with ADT can prolong and maintain patients' quality of life and is a cost-effective method of avoiding the need for prolonged palliative care.

RCTs have shown significant improvements in locally advanced prostate cancer outcomes using higher radiation doses [430] and adjuvant ADT [271, 431-433]. The therapeutic ratio may be further improved by using precision radiotherapy techniques, including intensity-

modulated radiotherapy (IMRT), and imaging techniques such as multi-modality imaging and image-guided radiotherapy (IGRT). These methods can further exploit the dose-response and escalate the dose in potential radio-resistant regions within the prostate gland, such as the dominant intra-prostatic lesion (DIL).

## 2.2 HIGH-RISK PROSTATE CANCER

The primary use of external beam radiotherapy (EBRT) has been in the treatment of locally advanced or, as more recently defined, high-risk prostate cancer. Locally advanced disease has, in the past, been inconsistently defined. The TNM (tumour [T], node [N] and metastasis [M]) system (Table 2.1) has been used to define locally advanced disease, but it does not include important prognostic parameters such as the Gleason score or prostate-specific antigen (PSA). Subsequently, there have been attempts to improve prostate cancer risk categorisation [434]. Notably, D'Amico was the first to propose a risk categorisation system based on PSA failure. This system defined high risk as T stage  $\geq T2c$ , Gleason score  $\leq 8$  or PSA  $>20\text{ng/mL}$  [435] (Table 2.2). The National Comprehensive Cancer Network (NCCN) recently proposed an increasingly accepted standard of risk classification. It defines "high risk" as T stage T3a, Gleason score  $\geq 8$  or PSA  $\geq 20\text{ng/mL}$ , and "very high risk" as T3b or T4 disease [436] (Table 2.2). Other classifications have been proposed that use additional survival data [437], the proportion of biopsy cores involved [438, 439] or sophisticated nomograms such as Kattan's nomogram [440, 441] in an attempt to improve the categorisation. Patients with locally recurrent disease are generally regarded as high risk.

Table 2.1 The American Joint Committee on Cancer (AJCC) TNM staging system (2018)

<b>Stage</b>	<b>Definition</b>
<b>T</b>	<b>Primary tumour</b>
TX	Primary tumour cannot be assessed TO No evidence of primary tumour
T1	Clinically inapparent tumour neither palpable nor visible by imaging
T1a	Tumour incidental histologic finding in <5% of tissue resected
T1b	Tumour incidental histologic finding in >5% of tissue resected
T1c	Tumour identified by needle biopsy (e.g. because of elevated prostate-specific antigen)
T2	Tumour confined within prostate
T2a	Tumour involves one-half of one lobe or less
T2b	Tumour involves more than one-half of one lobe but not both lobes
T2c	Tumour involves both lobes
T3	Tumour extends through the prostate capsule
T3a	Extracapsular extension (unilateral or bilateral)
T3b	Tumour invades seminal vesicle(s)
T4	Tumour is fixed or invades adjacent structures other than seminal vesicles such as external sphincter, rectum, bladder, levator muscles, and/or pelvic wall
<b>N</b>	<b>Regional lymph nodes</b>
NX	Regional lymph nodes were not assessed
NO	Katan's regional lymph node metastasis
N1	Metastasis in regional lymph node(s)
<b>M</b>	<b>Distant metastasis</b>
MO	No distant metastasis
M1	Distant metastasis
M1a	Non-regional lymph node(s)
M1b	Bone(s)
M1c	Other site(s) with or without bone disease

Table 2.2 D'Amico [435] and National Comprehensive Cancer Network (NCCN) [442]  
prostate cancer risk categorisation

<b>Risk category</b>	<b>Risk criteria</b>
<b>Very low</b>	Has all of the following: T1c stage Grade Group 1 Prostate-specific antigen (PSA) of less than 10ng/mL Cancer in 1 to 2 biopsy cores with no more than half showing cancer PSA density of less than 0.15ng/mL/g
<b>Low</b>	Has all of the following: T1 to T2a stage Grade Group 1 PSA of less than 10ng/mL
<b>Intermediate</b>	Has all of the following: No high-risk group features No very-high-risk group features 1 or more of the following intermediate risk factors: T2b or T2c stage Grade Group 2 or 3 PSA of 10 to 20ng/mL
<b>Favourable intermediate</b>	Has all of the following: 1 intermediate risk factor Grade Group 1 or 2 Less than half of biopsy cores show cancer
<b>Unfavourable Intermediate</b>	Has all of the following: 2 or more intermediate risk factors Grade Group 3 More than half of biopsy cores show cancer
<b>High</b>	Has one of the following: T3a stage Grade Group 4 Grade Group 5 PSA of more than 20ng/mL
<b>Very high</b>	Has one of the following: T3b to T4 stage Primary Gleason pattern 5 More than 4 biopsy cores with Grade Group 4 or 5

### 2.3 PROSTATE DOSE ESCALATION

The Patterns of Care study [443, 444] showed that prostate cancer has a radiation dose-response, that is, the higher the dose, the greater the probability of cure. However, it also demonstrated that older conventional techniques employing doses greater than 60–64Gy increased rectal toxicity. Technical improvements in radiotherapy, initially 3D conformal radiotherapy (3DCRT), were developed to reduce the rectal dose. Dearnaley et al. published the first randomised study that illustrated that 3DCRT led to a 50% reduction in late rectal toxicity when compared to conventional techniques to the same dose of 64Gy [445].

The use of 3DCRT has led to four RCTs of external beam photons [446-449] that showed significantly improved biochemical PSA control rates in men treated in the dose-escalated arms. The low-dose arms varied in dose from 64 to 70Gy while the high-dose arms used 74–80Gy. The long-term median follow-up of these studies at 5–10 years has been reported. All confirmed the advantage of the high-dose arms in terms of biochemical relapse, and two also showed an improvement in clinical relapse. However, this did not translate into a survival advantage. The standard doses now delivered for locally advanced prostate cancer range from 74 to 78Gy. Also, despite the improved radiotherapy technique, dose escalation over 70Gy led to a near doubling of late bowel side effects as 3DCRT was unable to avoid excessive dose to the adjacent rectum altogether. The reported genitourinary (GU) toxicity was similar in both arms.

Viani et al. have performed two meta-analyses of prostate dose escalation in 2009 [430] and 2012 [450]. The first involved studies using various radiotherapy methods including photon (conventional and 3DCRT) or proton therapy, and brachytherapy. The analysis showed a

highly significant improvement in the high-dose group's biochemical failure in all risk groups after a 5-year median follow-up. There was a linear relationship between biochemical control and dose (i.e. 1.8% for every 1Gy). The results showed no difference in overall or prostate cancer-specific mortality. There was significantly higher late grade >2 gastrointestinal (GI) toxicity, but no difference in GU side effects in the high-dose group. The second analysis concentrated on the five randomised trials that mainly used photon 3DCRT, with only one study using conventional photons before a conformal boost and another using a proton boost. This analysis was the first to show that conformal radiotherapy dose escalation was superior to conventional doses in preventing biochemical or clinical failure and prostate cancer-specific death at both 5 and 10 years. However, there was no difference in overall survival.

#### **2.4 RADIOTHERAPY TOXICITY**

Rectal toxicity has been the dose-limiting parameter in prostate cancer dose escalation. The increase in rectal toxicity with dose escalation resulted in more detailed studies that confirmed the dose-volume relationship [451, 452]. Jackson et al. analysed a subset of 262 patients treated to minimum target doses of 70.2 and 75.6Gy [451]. Patients were classified into two groups: patients with Grade 2+ rectal bleeding – bleeders; and patients with Grade ≤1 rectal bleeding – non-bleeders. The authors analysed the radiotherapy plans and generated average rectal dose-volume histograms (DVH) for each group. They showed that the area under the DVH curve for the bleeders' rectal wall was significantly higher than for the non-bleeders. Rectal bleeding correlated with the volume of rectum wall exposed to 46Gy. There was a borderline significant correlation with the percent rectal wall exposed to

71Gy in the 70.2Gy group. The results were utilised in the development of their dose-escalation studies including IMRT.

Subsequently, numerous studies have investigated the dose-volume relationship of the organs at risk in prostate radiotherapy. The Quantitative Analyses of Normal Tissue Effects in the Clinic (QUANTEC) group [453] attempts to summarise available 3D dose-volume/outcome data across a range of normal tissues and organs at risk. For rectal injury, they plotted percent rectal volume against linear-quadratic equivalent in 2Gy fractions (assuming alpha-beta ratio  $[\alpha/\beta] = 3$ ) for Grade 2+ rectal toxicity from the available 10 prostate cancer studies [454]. They found that the volume of rectum receiving  $\geq 60$ Gy was consistently and significantly associated with Grade 2+ rectal toxicity or rectal bleeding; rectal volumes receiving  $\leq 45$ Gy were not significantly associated with rectal toxicity. Intermediate doses produced mixed results. They also noted that the DVH curves from multiple centres converged at doses  $> 70$ Gy and volumes  $< 20\%$ . They recommended dose constraints for the rectum of  $V_{50\text{Gy}} < 50\%$ ,  $V_{60\text{Gy}} < 35\%$ ,  $V_{65\text{Gy}} < 24\%$ ,  $V_{70\text{Gy}} < 20\%$  and  $V_{75\text{Gy}} < 15\%$ . These constraints should limit Grade 2+ late rectal toxicity to  $< 15\%$  and grade 3+ to  $< 10\%$  for prescriptions up to 79.2Gy in standard 1.8–2Gy fractions. However, QUANTEC cautioned that these constraints have yet to be validated, and thus clinicians should strive to minimise  $V_{70}$  and  $V_{75}$  to below the recommended constraints. It was highlighted that most of the data was from 3DCRT.

QUANTEC also noted that prostate IMRT often leads to a much lower volume of the rectum receiving intermediate to high doses. As intermediate doses often correlated to the specific 3D techniques used, the rectal volumes exposed to these doses were often correlated to biologically relevant high-dose volumes. Thus, if intermediate- and high-dose volumes have

biological significance, then a reduction of rectal volumes to the 45–60Gy range by IMRT may become more critical, as this surrounding rectal tissue may be necessary to heal the rectum that receives higher doses.

QUANTEC also analysed the dose-volume data for the bladder, the other major organ at risk in prostate radiotherapy [455]. However, they did emphasise that there were no studies that comprehensively reported the 3D bladder dosimetry concerning toxicity. Most studies found no dose-volume relationship with regard to late GU toxicity and, therefore, the issue of bladder toxicity with prostate radiation has not been resolved. Dose constraints have been used for prostate radiotherapy; however, these are not based on toxicity data but instead used to control and limit the dose in the planning process. QUANTEC recommended clinicians might consider the Radiation Therapy Oncology Group (RTOG) 0415 bladder constraints for solid bladder (i.e.  $V_{>80\text{Gy}} < 25\%$ ,  $V_{>75\text{Gy}} < 35\%$  and  $V_{>65\text{Gy}} < 50\%$ ).

## **2.5 INTENSITY-MODULATED RADIOTHERAPY AND DOSE ESCALATION**

After 3DCRT, IMRT was the next major technical refinement in radiotherapy technique. IMRT uses sophisticated iterative algorithms to modulate and filter the delivered radiation with the motion of a multi-leaf collimator's tungsten leaves. The dose conforms more intricately to the shape of the target. Notably, IMRT, unlike 3DCRT, can better conform to the concave shape of the interface between the prostate target and the rectum, further minimising the dose to the rectum.

The International Commission on Radiation Units and Measurements (ICRU) has published a series of important documents that include technical definitions of target and organ-at-risk

volumes for the design and dosimetric description of 3DCRT and IMRT [456, 457]. The more commonly utilised volumes are included in Table 2.3.

Table 2.3 ICRU recommended target and organ-at-risk volumes

<b>Volume</b>	<b>Definition</b>
Gross tumour volume (GTV)	The visible tumour as defined clinically, e.g. GTV (clin), or by imaging, e.g. GTV-T (MRI)
Clinical target volume (CTV)	Accounts for the probability of microscopic spread from the GTV either by direct infiltration (CTV-T) or by lymphatic spread (CTV-N) that warrants radiotherapy treatment
Planning target volume (PTV)	A “safety margin” around the GTV/CTV for uncertainties including set-up errors (set-up margin, SM) and organ motion (internal margin, IM)
Organ at risk (OAR)	Critical dose-limiting normal tissue structures
Planning organ-at-risk volume (PRV)	A “safety margin” around the OAR for uncertainties including set-up errors and organ motion
Treated volume (TV)	Proposed as the volume enclosed by the prescribed dose (D98% proposed) and may be different from the PTV. It was defined as the volume of tissue enclosed by a specific isodose envelope appropriate to achieve tumour eradication or palliation-within the bounds of acceptable complications.
Remaining volume at risk (RVR)	Defined as all tissues that could be potentially irradiated to take into account the risk of late effects such as carcinogenesis. Thus, the RVR was defined as the imaged volume in the external contour of the patient, excluding any delineated OAR and the CTV(s).

ICRU = International Commission on Radiation Units and Measurements, MRI = magnetic resonance imaging

While the ICRU 50 report and its supplement (ICRU 62) [456, 457] set out an underlying philosophy for prescribing, recording and reporting radiotherapy, the ICRU 83 report more fully addressed issues related to IMRT, in particular, those relating to DVH values [458].

These guidelines include but are not limited to the important recommendations shown in

Table 2.4.

Table 2.4 ICRU 83 intensity-modulated radiotherapy dose-volume histogram recommendations

Definition	Description
Near minimum and near maximum dose	It was recommended that a near maximum (D2%) and near minimum covering isodose (D98%) should be reported rather than a maximum and minimum (D100%) isodose. The rationale is that the minimum and maximum can be in a high-dose gradient typical of IMRT, making it highly sensitive to the resolution of the calculation, and accuracy of CTV or PTV determination.
Reported dose	While the ICRU did not recommend a particular definition for a prescription dose, it was noted that the median dose (D50%) or mean dose (Dmean) would be a good representation of a typically reported dose.
Organ-at-risk dose	Most organs at risk are not clearly serial or parallel, and thus it was recommended that Dmean, D2% and VD (volume that receives at least a dose [D] in Gray) specifications should be reported, preferably for the whole organ when possible. For serial organs at risk, the near maximum, i.e. D2%, is the more important.
Dosimetric comparison	To more fully define and compare dose distributions, it was recommended that measures of dose homogeneity and dose conformity be reported.

CTV = clinical target volume, ICRU = International Commission on Radiation Units and Measurements, IMRT = intensity-modulated radiotherapy, PTV = planning target volume

RCTs have shown that the optimal dose for prostate radiation is at least 74–78Gy, and there is evidence that even higher doses may be required for high-risk disease as noted below.

Numerous planning studies have shown that IMRT improves conformity of the dose distribution around the planning target volume (PTV), and reduces the rectal and other organs-at-risk doses compared with 3DCRT [459-462]. Therefore, IMRT appears to be the most appropriate method to deliver these higher doses.

Eade et al. studied a large cohort of 1,530 patients with prostate cancer treated with 3DCRT [463]. The cohort was divided into four dose groups: <70Gy, 70–74.9Gy, 75–79.9Gy and ≥80Gy. Radiotherapy dose was found to be a significant factor for freedom from biochemical

failure. The dose-response curves suggested a benefit beyond 80Gy, with a 2.2% gain in long-term freedom from biochemical failure for every 1Gy. A radiotherapy dose-response for distant metastases was also found – an 8% reduction in risk of distant metastases for each 1Gy delivered. The improved freedom from distant metastases with dose appeared to translate into a survival advantage at 10 years. The authors concluded that image guidance

The Memorial Sloan Kettering Cancer Center (MSKCC) has executed an extensive serial non-randomised prostate dose-escalation program using initially 3DCRT and then IMRT. During their transition from 3DCRT to IMRT, they were one of the first groups to illustrate the advantages of IMRT. In 2000, Zelefsky et al. reported a cohort of patients treated to 81Gy during this transition: 61 patients with 3DCRT and 171 with IMRT [464]. They showed a greater proportion of the clinical target volume (CTV) received the prescribed dose with IMRT. Toxicity was found to be dose-dependent, with IMRT reducing the dose to the rectal and bladder walls. The dose reduction translated into a highly significant decrease in rectal bleeding rates. Further analysis showed an improvement in biochemical outcome with increasing dose, notably in the intermediate- and high-risk groups [465], which translated to a significant decrease in risk of distant metastases [466].

The NRG Oncology RTOG 0126 clinical trial of radiation dose escalation randomised 1,532 patients to either 79.2Gy or 70.2Gy using 3DCRT or IMRT [467]. Approximately 33–34% of patients in both arms received IMRT. The rate of late Grade 2+ GI toxicity was significantly higher in the 79.2Gy arm compared to the 70.2Gy arm (21% vs 15%,  $p=0.006$ ). A preliminary analysis of toxicity was conducted comparing 3DCRT versus IMRT for the high-dose 79.2Gy arm [468]. The median rectal V70 was 18.2% for the IMRT arm compared to 21.7% for the 3DCRT arm. The rate of acute Grade 2+ GI and GU toxicity was 9.7% for the IMRT arm

compared to 15.1% for the 3DCRT arm ( $p=0.042$ ). At 3 years of follow-up, the rate of late Grade 2+ GI toxicity was significantly reduced in the IMRT arm compared to the 3DCRT arm (15.1% vs 22%,  $p=0.039$ ).

Some centres are now reporting long-term follow-up, approaching 10 years, of their prostate IMRT patients. MSKCC has separately analysed and reported 10-year outcomes in 170 patients treated with high-dose IMRT (81Gy) [469]. The 10-year actuarial PSA relapse-free survival rates were 81% for the low-risk group, 78% for the intermediate-risk group and 62% for the high-risk group. The 10-year distant metastases-free rates were 100%, 94% and 90%, respectively, and cause-specific mortality rates were 0%, 3% and 14%, respectively. The 10-year likelihood of developing late Grade 2 and 3 GU toxicity was 11% and 5%, respectively, and the likelihood of developing late Grade 2 and 3 late GI toxicity was 2% and 1%, respectively. No Grade 4 toxicities were observed.

Another study with a median follow-up of 10 years was published by Vora et al. and included 302 patients [470]. The median dose delivered was 75.6Gy (range 70.2–77.4). Local and distant recurrence rates were 5% and 8.6%, respectively. The biochemical control rates were 77.4% for low risk, 69.6% for intermediate risk and 53.3% for high risk. At last follow-up, no patients had persistent Grade 3+ GI toxicity, and 0.7% had persistent Grade 3+ GU toxicity. The high-risk group was noted to have a higher rate of distant metastases. These findings indicate that IMRT is associated with good long-term tumour control and low rates of severe toxicity in patients with localised prostate cancer.

The use of ultra-high-dose IMRT using doses greater than 86Gy has also been reported [471, 472]. The MSKCC performed a retrospective comparison of biochemical outcomes using

ultra-high-dose IMRT (86.4Gy in 1.8Gy fraction sizes) versus high-dose-rate brachytherapy with IMRT [471]. The 5-year PSA relapse-free survival rates were 98% versus 100%, respectively, ( $p=0.71$ ) for the low-risk disease group, 84% versus 98% ( $p<0.001$ ) for the intermediate-risk group, and 71% versus 93% ( $p=0.23$ ) for the high-risk group. The 7-year late toxicity rates for ultra-high dose IMRT versus high-dose-rate brachytherapy with IMRT were 4.6% versus 4.1% ( $p=0.89$ ) for Grade 2 GI toxicity, 0.4% versus 1.4% ( $p=0.36$ ) for Grade 3 GI toxicity, 19.4% versus 21.2% ( $p=0.14$ ) for Grade 2 GU toxicity, and 3.1% versus 1.4% ( $p=0.74$ ) for Grade 3 GU toxicity. Petrongari et al. published a prospective phase 2 study that treated 39 intermediate-risk prostate cancer patients with ultra-high-dose IMRT of 86Gy using standard fractionation [472]. After a median follow-up of 71 months, the 5-year freedom from biochemical failure was 87%. The incidence of late Grade 2, Grade 3 and Grade 4 GI toxicity was 18%, 2.5% and 2.5%, respectively. The incidence of late Grade 2 and Grade 3 GU toxicity was 5% and 8%, respectively.

While there are numerous single-institution studies with long-term follow-up of prostate IMRT, there have been no randomised studies of IMRT versus 3DCRT. The RCTs of prostate dose escalation mainly utilised 3DCRT, and illustrated the improved outcome but at the expense of an increase in GI toxicity. The dosimetric planning studies of IMRT versus 3DCRT showed a reduction in rectal doses that translated, in non-randomised studies, to a significant reduction in rectal toxicity. The reduced toxicity resulted in a rapid change in equipoise, making the randomised comparison of 3DCRT versus IMRT unpalatable. An analysis of the US-based SEER (Surveillance, Epidemiology and End Results) database that identified 52,290 men with nonmetastatic prostate cancer from 2000 to 2007 showed that IMRT had replaced 3DCRT as the primary treatment with external beam radiation [473].

A systematic review comparing IMRT and 3DCRT for prostate cancer was published in 2012 [474]. After an extensive literature search, the authors selected 11 articles, including 4,559 patients, nine retrospective cohort studies and two RCTs [468, 475]. The RCTs were randomised studies of dose escalation. Patients were treated with 3DCRT or IMRT; however, patients were not randomised between the two modalities. The review authors concluded that there was either no difference between 3DCRT and IMRT or, as shown in many studies, a superiority for IMRT in terms of outcomes, and acute and late GI and GU toxicity in the setting of dose escalation above 70Gy. They recommended IMRT rather than 3DCRT for radical prostate radiotherapy with doses over 70Gy. A subsequent economic analysis (based on this systematic review data) demonstrated that, for radical radiation treatment (>70Gy) of prostate cancer, IMRT seems to be cost-effective when compared with an equivalent dose of 3DCRT from the perspective of the Canadian healthcare system for 2009 [476].

The next development in IMRT is volumetric modulated arc therapy (VMAT), most often utilising flattening filter-free linear accelerators (linacs). Planning studies are increasingly illustrating improved dosimetric quality with improved target coverage and better rectal sparing with VMAT [477, 478]. The treatment delivery is more efficient, and the treatment time is much shorter [479, 480]. The shortened treatment time most likely will result in a more precise delivery as patient and organ movement is less likely to degrade the delivered dosimetry.

In conclusion, dose-escalated IMRT to doses of at least 74–78Gy has become the treatment of choice of locally advanced prostate cancer because large-scale studies with long-term results have shown that it is at least as effective as 3DCRT, reduces toxicity and is cost-effective. With the rapid development of technology (e.g. VMAT), planning and delivery are

increasingly quicker and more efficient than older technologies, making it possible to deliver even higher doses safely. However, although we have seen a reduction in late Grade 2+ GI toxicity from 15.1% to 9.7% and in late Grade 2+ GU toxicity from 11% to 5%, further dose escalation with IMRT has seen an increase in both GI and GU toxicity.

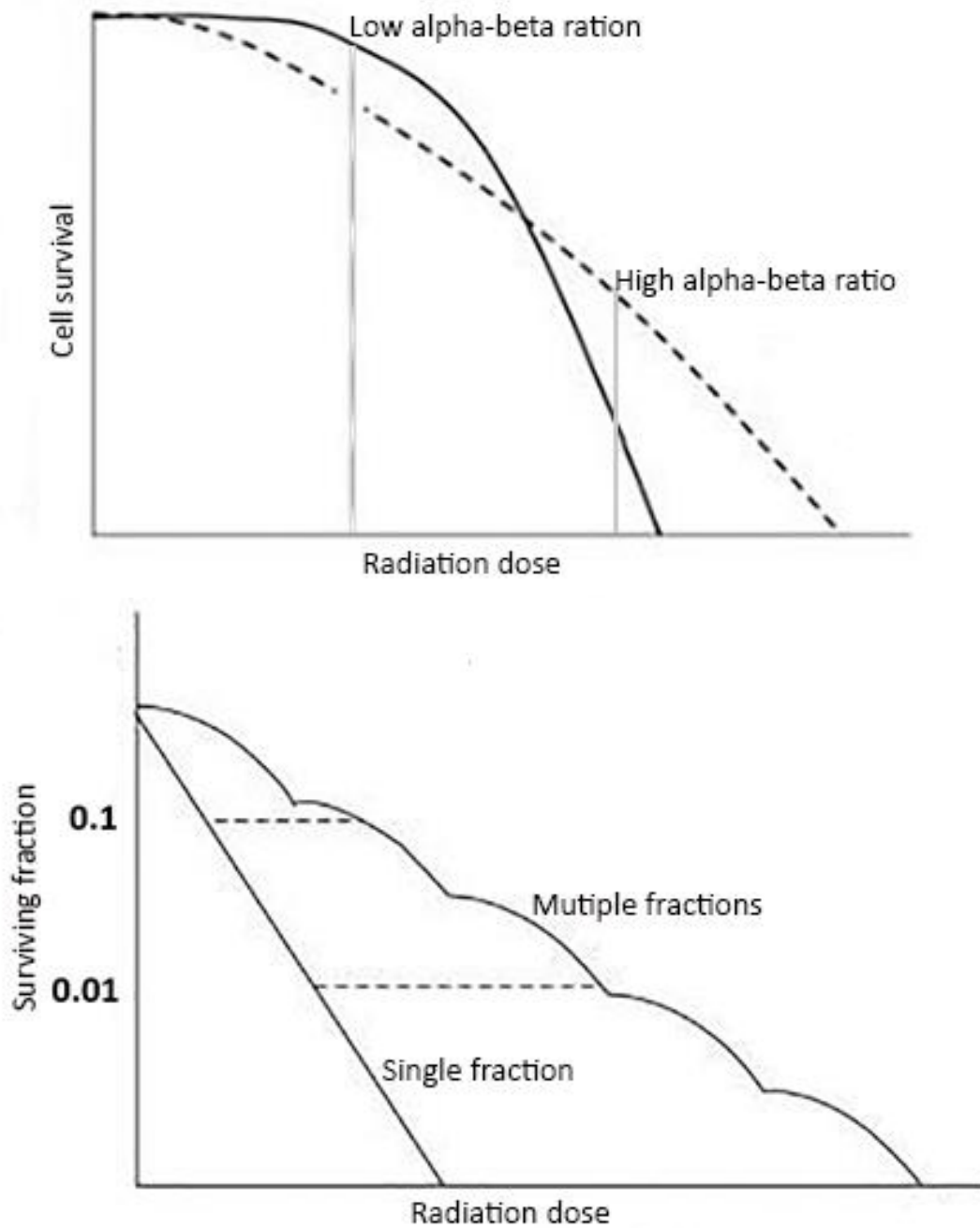
## 2.6 HYPOFRACTIONATION

The biological rationale for hypofractionated radiation for prostate cancer is predicated on prostate cancer having a low alpha-beta ratio. The linear-quadratic model (surviving fraction =  $e^{-\alpha D - \beta D^2}$ ) fits radiation survival data to a continuously bending curve, where D is dose and  $\alpha$  (alpha) and  $\beta$  (beta) are constants describing radiation sensitivity [481, 482] (Figure 2.1). Alpha is the linear component of cell killing kinetics, representing “single-hit” killing, which dominates the radiation response at low doses. Beta is the quadratic component, representing “multiple-hit” killing, which causes the curve to bend as the dose increases. The ratio of alpha to beta is the dose at which the linear and quadratic components of cell killing are equal. The more linear the cell killing response at low radiation doses, the higher is the value of alpha, and the greater is the radiosensitivity of the cells. The beta or quadratic component of the response, relating to the curve or shoulder of the curve, is particularly significant if a dose is broken up into many small exposures or fractions (Figure 2.1). If cells are allowed sufficient time to recover after irradiation (6–24 hours), sublethal damage from the initial exposure will be fully repaired, and cells will respond to the next exposure as if they had not previously been irradiated, repeating the “shouldered” part of the curve. This shoulder leads to increases in cell survival by reducing the magnitude of the quadratic contribution to cell killing. This sparing is low for cell lines with a high alpha-beta ratio,

where single-hit killing dominates, while cells with a low alpha-beta ratio experience significant sparing.

Theoretically, cell killing relates to death from the alpha component or single-hit events (i.e. lethal damage caused by a single incident particle), while the beta component, or multiple-hit cell death, results from the interaction of damage from different radiation tracks, which scales in proportion to the square of the dose but can be repaired at a lower dose per fraction (i.e. sublethal damage repair).

Thus, the linear-quadratic model with its alpha and beta values can be used to describe the curvature of cell killing in relationship to radiotherapy dose, both for tumour control and normal tissue complications. Tissues with a low alpha-beta ratio are relatively resistant to low doses compared to tissues with a high alpha-beta ratio. Thus, early-responding tissues and rapidly proliferating tumours have a high alpha-beta ratio of more than 10Gy, and late-responding tissues or slowly proliferating tumours have a low alpha-beta ratio of around 3–5Gy. Most tumours have a high alpha-beta ratio and can be reasonably treated with conventionally fractionated radiotherapy (using fraction sizes of 1.8–2Gy). Nevertheless, some tumours such as melanoma, sarcoma, renal cell carcinoma and notably prostate cancer, have a low alpha-beta ratio, and therefore hypofractionation (using fraction sizes >2Gy) may improve the therapeutic ratio of EBRT by minimising sublethal damage repair [483].



Source: Austin Health

Figure 2.1 Cell survival curves of low and high alpha-beta ratio cells and the relative effect of fractionation

### 2.6.1 Moderate hypofractionation

Brenner and Hall were the first to report that prostate cancer may have a low alpha-beta ratio of 1.5Gy [484]. This low ratio was supported by additional studies [485-487], resulting in proposals for the investigation of hypofractionation in prostate cancer [484, 488-490]. A meta-analysis of clinical data supported the concept that prostate cancer had a low alpha-beta ratio [491]. The caveat to the analysis was that a single study mostly drove the low alpha-beta ratio and, if excluded, an alpha-beta ratio of >4Gy may be possible.

This recognition that prostate cancer has a low alpha-beta ratio has resulted in several large scale RCTs that have demonstrated the non-inferiority of moderate hypofractionation (fraction size 2.4–3.4Gy) compared to standard fractionation, with similar disease control and late toxicity at 5 years (see Table 2.5).

Table 2.5 Characteristics and Results of Prostate cancer hypofractionated radiotherapy randomised controlled trials

Trial	Standard fractionation	Hypofractionation	Number of patients	Median age (years)	Risk group	ADT	Median follow-up	5-year biochemical failure free survival	Overall survival	Acute toxicity	Late toxicity
<b>RTOG 0415</b>	73.8Gy/41Fx/1.8GPF 8–9 weeks	70Gy/28Fx/2.5GPF 6 weeks	1,115	67	Low	No	5.9 years	Not inferior	Not inferior	Not significant	Increase Grade 2 GI&GU toxicity
<b>CHHiP</b>	74Gy/37Fx/2GPF 7–8 weeks	60Gy/20Fx/3GPF 4 weeks	3,216	69	Low 13% Intermediate 73% High 12%	24 weeks	62.4 months (5.2 years)	Not inferior	Not inferior	Not significant	Not significant
		57Gy/19Fx/3GPF 4 weeks						NOT inferior (i.e. Inferior)	Not inferior	Not significant	Not significant
<b>PROFIT</b>	78Gy/39Fx/2GPF 8 weeks	60Gy/20Fx/3GPF 8 weeks	1,206	71	Intermediate	12 weeks	6 years	Not Inferior	Not inferior	Not significant	Not significant

ADT = androgen deprivation therapy, Fx = fractions, GI = gastrointestinal, GPF = gray per fraction, GU = genitourinary, Gy = gray

In the CHHiP trial, 3,216 patients with predominantly low- to intermediate-risk prostate cancer were randomised to ADT and IMRT using a conventional fractionation schedule (74Gy in 2Gy fractions) or one of two hypofractionated schedules (60Gy or 57Gy in 3Gy fractions) [492]. With a median follow-up of 5.2 years, the 60Gy arm was non-inferior to the 74Gy arm for biochemical failure-free survival and late toxicity (see Table 2.5). However, the 57Gy arm was found to be inferior, illustrating a rapid dose-response.

In the PROFIT trial, 1,206 patients with intermediate-risk prostate cancer were randomised to conventional (78Gy in 2Gy fractions) or hypofractionated (60Gy in 3Gy fractions) IMRT [493]. With a median follow-up of 6 years, the 60Gy arm was non-inferior with respect to biochemical failure, clinical failure, disease-free survival and late toxicity (see Table 2.5).

The NRG/RTOG 0415 trial randomised 1,115 patients with low-risk prostate cancer to conventional (73.8Gy in 1.8Gy fractions) or hypofractionated (70Gy in 2.5Gy fractions) 3DCRT or IMRT [494]. With a median follow-up of 5.9 years, the 70Gy arm was non-inferior with respect to biochemical disease-free survival. However, a small statistically significant increase in late Grade 2 GI and GU toxicity was observed in the hypofractionated arm (see Table 2.5).

An attempt at dose-escalating the hypofractionated arm was made in the HYPRO superiority trial, but this led to an increase in GI and GU toxicity [495, 496]. In the HYPRO trial, 804 patients with intermediate- and high-risk prostate cancer were randomised to conventional fractionation (78Gy in 2Gy fractions), or dose-escalated hypofractionated (64.6 Gy in 3.4Gy fractions) IMRT [497]. After a median follow up of 60 months, the 5-year relapse-free survival was 77.1% for the conventional arm compared to 80.5% for the dose-escalated

hypofractionation arm ( $p=0.36$ ). The 3-year incidence of late Grade 2+ GI and GU toxicity was 17.7% and 39%, respectively, for the 78Gy arm compared to 21.9% and 41.3%, respectively, for the 64.6Gy arm. Non-inferiority could not be confirmed, and the dose escalation did not improve 7-year relapse survival [498]. However, cumulative late Grade 3+ GU toxicity was significantly higher in the 64.6Gy arm (19% vs 12.9%,  $p=0.021$ ).

In summary, four large prospective RCTs that enrolled over 6,000 patients, as well as additional single-institution RCTs, demonstrate that EBRT delivered to the prostate using moderate hypofractionation (2.4 to 3.4Gy per fraction) provides similar early prostate cancer control and similar toxicity to EBRT delivered using conventional fractionation (1.80 to 2.0Gy per day) [247]. It should be acknowledged that most of the patients in these trials had low- and intermediate-risk prostate cancer. It remains uncertain whether high-risk prostate cancer has a low alpha-beta ratio and whether hypofractionation would be appropriate.

Therefore, moderate hypofractionation should be offered to low- to intermediate-risk prostate cancer patients who choose EBRT for the treatment of prostate cancer [247, 248, 499]. Moderate hypofractionation (60Gy) is non-inferior to conventional EBRT (78–80Gy) and has advantages in terms of patient convenience and resource utilisation. However, attempts at further dose escalation have not improved biochemical control, and have similar late GI toxicity rates but an increase in late severe GU toxicity.

### 2.6.2 Ultra-hypofractionation

More extreme hypofractionation schedules are currently being explored. Ultra-hypofractionation (fraction size of  $>5$ Gy) is delivered with stereotactic body radiotherapy (SBRT). Multiple single-centre prospective studies treating patients with predominantly low-

risk prostate cancer with SBRT to doses of 35–36.25Gy in 7–7.25Gy fraction sizes have shown excellent biochemical progression-free survival of 95–98% for low-risk and 90.7% for intermediate-risk prostate cancer after at least 44 months of follow-up [500-503]. The incidence of late Grade 2 and 3+ GI toxicity ranged from 2 to 12% and 0 to 5%, respectively. Late Grade 2 and 3+ GU toxicity incidence ranged from 4 to 17% and 0 to 2.5%, respectively.

A phase 1/2 study of ultra-hypofractionated dose escalation in SBRT for localised prostate cancer (in 91 patients) has been performed with 45, 47.5 and 50Gy in 5 fractions [504]. At the highest dose level of 50Gy, the overall incidence of late Grade 2, 3 and 4 toxicity was 24.6%, 4.9% and 3.3%, respectively. Notably, at this dose level, 6.6% of patients developed high-grade rectal toxicity and five of these patients required a colostomy. Grade 3+ late rectal side effects correlated with the volume of rectal wall receiving 50Gy being  $>3\text{cm}^3$  and  $>35\%$  circumference of the rectal wall receiving 39Gy. Grade 2+ acute rectal toxicity was significantly correlated with treatment of  $>50\%$  of the rectal wall circumference to 24Gy. Thus, caution was advised with high-dose SBRT to the prostate because of its proximity to the bowel, and the need for appropriate dose constraints was emphasised.

The Scandinavian HYPRO-RT-PC non-inferiority phase 3 trial randomised 1,200 patients to conventional IMRT (78Gy in 2Gy fractions) or an accelerated, hypofractionated SBRT arm of 42.7Gy in 6.1Gy fractions [505]. No difference in late toxicity has been reported at 2 years. After a median follow-up of 5 years, the reported failure-free survival following ultra-hypofractionated radiotherapy is non-inferior to conventionally fractionated radiotherapy for intermediate- to high-risk prostate cancer. There were more severe early side effects with the ultra-hypofractionated schedule, but late side effects were similar.

The Prostate Advances in Comparative Evidence (PACE) non-inferiority study will randomise patients to conventional IMRT (62Gy in 3.1Gy fractions) or a hypofractionated SBRT arm of 36.25Gy in 7.25Gy fractions; this study is still in progress. There are also ongoing trials using one or two fractions of ultra-hypofractionated stereotactic ablative body radiotherapy (SABR) for prostate cancer, including the ONE-SHOT trial (NCT03294889) [506], the PROSINT-IGRT phase 2 trial (NCT02570919) [507], the NCT04004312 trial [508], and the 2STAR phase 2 study [509].

The evidence for ultra-hypofractionation consists of a single phase 3 study, and prospective single-arm trials and meta-analysis [510] with limited follow-up. The recommendation for prostate ultra-hypofractionation in the guideline from the American Society for Radiation Oncology, American Society of Clinical Oncology and American Urological Association (ASTRO-ASCO-AUA) guideline recommendation for prostate ultra-hypofractionation is conditional, as the evidence is immature and there is uncertainty regarding the risk-to-benefit ratio [248, 504]. The guideline does not recommend dose-escalated ultra-hypofractionation, and, thus, it is generally regarded as an investigational technique.

## **2.7 POST-PROSTATECTOMY RADIOTHERAPY**

The role of dose escalation and IMRT in the post-prostatectomy setting for PSA salvage is less well documented. Some have suggested that the dose-response relationship is similar for salvage and definitive primary EBRT [511]. Two analyses [512, 513] have suggested that a strong dose-response relationship exists, and concluded that it is appropriate to consider doses above 66.6Gy for post-prostatectomy radiotherapy (PPRT). A recent review by Ohri et al. [514] estimated a potential 2.5% gain in PSA control per 1Gy. The American Society for

Therapeutic Radiology and Oncology Consensus Panel has suggested that “the highest dose of radiation therapy that can be given without morbidity is justifiable” [515].

The proximity of the rectum to the prostatic bed means that dose escalation for PPRT can be associated with increased rectal toxicities. When conventional radiotherapy techniques are used, it is estimated that dose escalation above 72Gy would result in an unacceptably high rate (20%) of Grade 3 toxicity [514]. Ohri et al. reported that late GI toxicity in PPRT increased by 1.2% per gray [514]. Consequently, the European Association of Urology (EAU) guidelines still recommend only 64–66Gy, which is reasonable for conventional or 3DCRT techniques [516]. However, a recent survey among physicians in the USA revealed that 55% of them deliver doses of at least 70Gy and 91% use IMRT [517]. A number of studies have concluded that high-dose salvage EBRT is safe mainly when IMRT technique is used, and that the 5-year PSA relapse-free survival is greater than 70% in patients with pre-treatment PSA <0.5ng/mL [518, 519]. Goenka et al. reported late Grade 2+ GU and GI toxicities of 16.8% and 1.9%, respectively, for their IMRT cohort receiving >70Gy [520]. Ost et al. delivered higher PPRT doses with a median of 74Gy, and reported late Grade 2+ GU and GI toxicities of 22% and 8%, respectively [521].

Furthermore, there is emerging evidence that supports the concept that higher doses may improve outcomes. Cozzarini et al. reported an improved 5-year biochemical relapse-free survival (83% vs 71%) and disease-free survival (94% vs 88%), for dose-escalated PPRT to >70.2Gy compared to <70.2Gy [522]. A systematic review by King et al. suggested that the dose-response curve approximates a sigmoidal curve for PPRT. It appeared to parallel that for definitive radiotherapy for localised disease, with a dose of 70Gy achieving 58.6% biochemical relapse-free survival versus 38.5% for 60Gy [523]. The estimated proportional

gain in biochemical relapse-free survival was 2% per incremental Gy. The ongoing phase 3 Swiss Group Clinical Research 09/10 trial will randomise patients without macroscopic disease to either 64Gy or 70Gy, and may provide a further understanding of dose escalation in the salvage setting [524]. In the presence of macroscopic disease, it is recommended that dose-escalated PPRT is utilised while taking into account the organs at risk [518].

## **2.8 MULTI-MODALITY IMAGING TECHNIQUES FOR RADIOTHERAPY**

IMRT and VMAT allow for the creation of very conformal radiotherapy dose distributions. However, radiotherapy is a process, and therefore each step in the process must be optimised to achieve the precise delivery of the IMRT to the target. Consequently, accurate design of the target that the IMRT dose distributions can be shaped around, and precise alignment with the patient and target, are required. Newer imaging methods are being employed to achieve this:

- multi-modality imaging for the design and assessment of the target(s)
- IGRT for accurate alignment and verification of the delivery.

### **2.8.1 Magnetic resonance imaging**

Following the advent of 3DCRT, the CT scan has formed the basis of radiotherapy planning. CT is an excellent template for IMRT. Once it is appropriately calibrated, a planning CT is geometrically correct, and the Hounsfield numbers are directly related to electron density. This allows for heterogeneity corrections and accurate radiotherapy dose calculation. CT scans can be performed rapidly at high resolutions, limiting the movement artefact.

However, for prostate radiotherapy, CT does not have sufficient soft tissue contrast to accurately separate the prostate from surrounding tissues such as muscle and vessels, and it

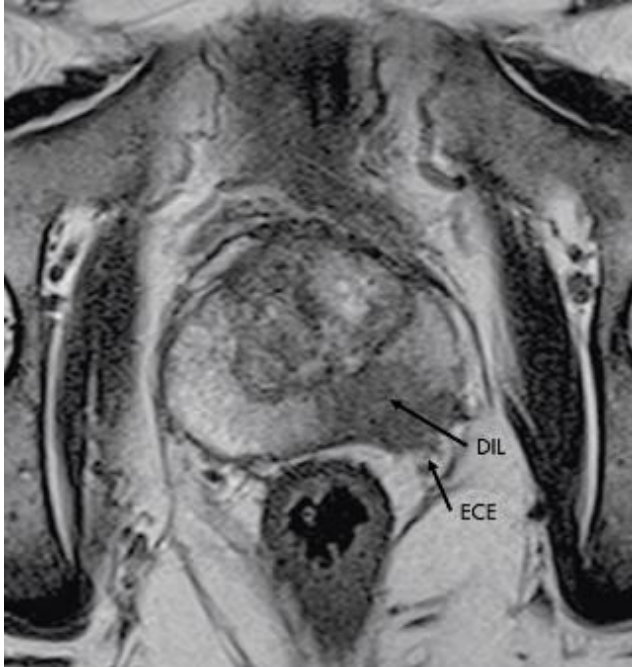
is unable to define the structure of the prostate, including the zonal anatomy. It is generally not possible to delineate the tumour within the prostate, including the dominant intraprostatic lesion (DIL), or the extent of the tumour, such as extracapsular extension or seminal vesicle invasion [174, 525].

MRI is increasingly used in oncology for staging, assessing tumour response and treatment planning in radiotherapy. MRI can enhance the radiotherapy treatment planning process by providing an excellent characterisation of soft tissues compared with CT. MRI, together with the developments of dynamic contrast-enhanced MRI and diffusion MRI (multi-parametric MRI; mpMRI), can better characterise the morphology and functional aspects of tissue and tumour regions. These MRI developments permit treatment individualisation, dose-escalation strategies and, in the future, IGRT.

MRI is an important tool in prostate radiotherapy for defining the prostate and the tumour within the prostate [526]. It is superior to digital rectal examination and transrectal ultrasound-guided (TRUS) biopsy for staging and localising prostate cancer [527]. It can visualise the normal anatomy, including the zonal anatomy, capsule, seminal vesicles and surrounding structures [525]. Prostate volumes defined on MRI are significantly smaller than CT because less normal tissue is included [528-530]. MRI improves the uncertainty in contouring, particularly at the apex and base of the prostate, and therefore reduces inter-observer and intra-observer variation [526, 531-533] and the dose to normal tissue [534].

MRI can define the DIL, which is the most common local recurrence site [535, 536] (see Figure 2.2). Furthermore, it can determine the pathological extent of the tumour, having a high specificity for extracapsular extension and seminal vesicle invasion that can be difficult

to define clinically or on CT, ensuring that these target components are appropriately treated [174, 537].



DIL = dominant intra-prostatic lesion, ECE = extracapsular extension

Source: Austin Health

Figure 2.2 Transverse T2 weighted magnetic resonance imaging showing dominant intra-prostatic lesion and extracapsular extension

Prostate cancer is typically seen on T2-weighted MRI as a hypointense lesion within the peripheral zone's hyperintense glandular tissue. In the central zone, which can show a mixed hypointense and hyperintense pattern due to benign prostatic hypertrophy, prostate cancer can appear as a severely hypointense lesion that is referred to as the charcoal sign.

Aggressive cancers tend to have more hypointense signal with increasing Gleason score [538].

### 2.8.2 Functional imaging and dominant intra-prostatic lesion

While dose-escalated radiotherapy (with ADT) produces favourable outcomes in most patients, disease failure, including local recurrence, remains an issue in up to 20% of patients [539]. Recent studies suggest that the majority of these local failures occur at the site of the original tumour, that is, the DIL defined on T2-weighted MRI [536, 540]. It is presumed that this results from the higher probability of radiation-resistant clones being present at the site of highest clonogen or cancer cell number [535]. As prostate cancer has been shown to have a radiotherapy dose-response, it is presumed that local control could be improved by increasing the dose to this region [541]. Several planning studies have demonstrated the feasibility of using a simultaneous integrated boost (SIB) to very high doses while providing adequate rectal sparing, such as maintaining a DIL to rectal distance of >4.2mm [542]. There have been only a few studies that have reported early outcomes of SIB IMRT techniques. [543-545]. However, it is hoped that better local control may prevent seeding or re-seeding distant disease [546] and subsequently lead to improved survival [281].

The effectiveness of escalated radiation doses to DILs is currently partly limited by conventional imaging's ability to identify the DIL reliably [174, 537]. The definition and assessment of the DIL have mainly been performed on T2-weighted MRI. However, there is increasing evidence that functional imaging, including diffusion-weighted MRI (DW-MRI) [187, 547-550], dynamic contrast-enhanced MRI [547-549, 551] and positron emission tomography (PET) [187, 543], can more reliably identify the DIL. Magnetic resonance spectroscopy has also been used in the past, but its importance appears to be diminishing as newer imaging techniques become available.

DW-MRI depicts differences in the diffusion of water molecules due to Brownian motion. High cell densities, for example, in cancer, intracellular oedema and fibrotic stroma, can restrict water diffusion. In prostate cancer, normal glandular architecture is disrupted and replaced by a high density of aggregated cancer cells and fibrotic stroma. These changes inhibit the movement of water molecules with resultant restriction of diffusion, which is measured as a reduction of apparent diffusion coefficient (ADC) values in the cancer tissue. Prostate cancers usually exhibit reduced ADC values and high signal intensity in a high b-value DW-MRI. Investigators have found that DW-MRI is better than T2-weighted imaging in detecting prostate cancer and differentiating it from benign tissue [552-555]. Moreover, DW-MRI may be able to discern prostate cancer's aggressiveness by differentiating low-risk from the high-risk disease [552]. Changes detected by DW-MRI may characterise the response to treatment such as ADT [556].

Dynamic contrast-enhanced MRI visualises the blood flow characteristics due to the vascularisation of the prostate and the neo-angiogenesis of prostate cancer [557]. It measures the change in T1-weighted signal intensity with time (i.e. SI-t curves) following administration of the gadolinium contrast. The resultant SI-t curve will show a rise or wash-in, and then a fall or wash-out. Qualitative and quantitative analysis can characterise prostate cancer from normal prostate tissue. Typically, prostate cancers show a steeper wash-in slope, higher peak enhancement and steeper wash-out compared to normal prostate tissue. Combined with T1 and T2 imaging, dynamic contrast-enhanced MRI is reported as having better accuracy than conventional MRI.

Increasingly a multi-parametric approach (mpMRI) using T2-weighted MRI, diffusion-weighted MRI and dynamic contrast-enhanced MRI is being used to improve the diagnostic

accuracy of defining prostate cancer, by combining the morphological and functional components of MRI. The European Society of Urogenital Radiology (ESUR) has published guidelines for the structured reporting of mpMRI, called the Prostate Imaging Reporting and Data System (PI-RADS) [558]. This system is used to generate a final overall PI-RADS score (1–5) that reflects the likelihood of a significant aggressive prostate cancer. It is presently being utilised most often for guiding biopsy and monitoring active surveillance.

PET is an imaging technique that provides in vivo measurements in absolute units of a radioactive tracer. The radioactive tracer can be labelled with short-lived radioisotopes of the natural elements of the body's biochemical constituents. Thus, PET provides the ability to detect and quantitate physiologic and receptor processes in the body, particularly cancer cells. FDG (fluorodeoxyglucose) PET is the most widely utilised PET in oncology. However, its performance is suboptimal with prostate cancer because of the low metabolism and urinary excretion of FDG that mask the prostate uptake [559]. Newer tracers such as  $^{11}\text{C}$ -choline,  $^{18}\text{F}$ -choline [560],  $^{11}\text{C}$ -acetate [561] and prostate-specific membrane antigen (PSMA) [562, 563] are increasingly being used in the management of prostate cancer, including radiotherapy [564].

Previously, choline-based PET has been the most utilised PET method for assessing primary prostate cancer. Choline is an essential component of the cell membrane [565], which is taken up into cells and phosphorylated by choline kinase to phosphatidylcholine and integrated into cell membrane phospholipids.  $^{11}\text{C}$ -choline is a radiotracer based on choline. Prostate cancer cells show increased transport and increased expression of choline kinase compared with normal cells, providing the rationale for the use of  $^{11}\text{C}$ -choline as a radiotracer in prostate cancer.  $^{11}\text{C}$ -choline, unlike FDG, has minimal urine excretion and thus

improves the visualisation of prostate cancer. It also has impressive sensitivity for primary and metastatic prostate cancer and excellent specificity of 81%. It is superior to FDG and magnetic resonance spectroscopy. <sup>11</sup>C-choline PET has shown particular promise for identifying the DIL [188, 566-570]. Pathological correlation studies have suggested that <sup>11</sup>C-choline PET standardized uptake value (SUV) 60% provides the most accurate DIL definition [185], and may assist in defining the most aggressive tumours [571] with the highest Gleason score [187]. This DIL would be a very suitable target for further radiotherapy dose escalation [181].

PSMA PET staging shows high sensitivity and excellent specificity in detecting the primary within the prostate, and for nodal and metastatic disease [194, 195, 203, 572], although this is dependent on the PSA level. PSMA PET's accuracy and resolution have resulted in its increasing use for staging advanced prostate cancer [178, 573, 574]. PSMA PET is also a useful tool for radiotherapy planning, including location of the DIL, and of recurrent disease and lymph node metastases post prostatectomy [575-578]. A study showed that PSMA PET resulted in salvage radiotherapy modifications in 59% of patients compared to CT alone [579]. Other studies have shown a similar impact of PSMA PET; it altered treatment decisions in 26–33% of primary treated patients [580, 581], and 42–61% of salvage radiotherapy patients [581, 582]. PSMA PET may also assist in the assessment of response following radiotherapy. Zamboglou et al. showed PET or MRI detected a local recurrence in 27% of patients. The dose distribution in the DIL defined by PSMA PET/CT or MRI or both was an independent risk factor for biochemical recurrence [583].

While functional imaging techniques such as DW-MRI, dynamic contrast-enhanced MRI, <sup>11</sup>C-choline PET and PSMA PET can distinguish aggressive prostate cancer, they still suffer

from low resolution. The low resolution can be partly overcome by co-registering or fusing the images with high-resolution T2-weighted MRI and CT to improve the DIL delineation.

In conclusion, while CT gives an excellent geometric and dosimetric representation of the patient, it does not have sufficient soft tissue contrast to accurately define the prostate, the DIL or tumour extent. Increasingly, multi-modality imaging, including functional imaging, plays a complementary role in accurately and precisely defining the targets in prostate cancer radiotherapy. Following the development of MRI linacs, MRI will increasingly play a pivotal role in radiotherapy alongside CT.

## **2.9 IMAGE-GUIDED RADIOTHERAPY**

Multi-modality imaging allows for an increasingly precise definition of the shape and function of the cancer target. IMRT or VMAT can intricately shape a tight conformal radiation dose distribution around these targets. As the last step in the radiotherapy chain of events, the precise delivery of the radiation takes on paramount importance; the patient and particularly the cancer targets need to be accurately aligned with the radiotherapy dose distribution. Increasingly, imaging techniques such as IGRT are being utilised daily to align and monitor the patient and target.

### **2.9.1 Prostate and prostate bed motion**

Prostate motion can occur between daily radiotherapy treatments and is defined as inter-fractional motion. Motion during the delivery of a radiotherapy fraction is known as intra-fractional motion. The motion is secondary to physiological changes, including changes in bladder volume, rectal distension, levator contractions and respiration [584]. Motion is greater in the anterior-posterior (AP) and superior-inferior (SI) axes, compared to the left-

right (LR) axis. An analysis of prostate motion reported an inter-fractional standard deviation of 1–2mm in the LR axis and 2–4mm in both the AP and SI axes [585]. However, even greater motion has been reported with one study, with the prostate moving 7.2mm posteriorly, 9.2mm anteriorly, 6.8mm inferiorly and 12.9mm superiorly [586]. Intra-fractional motion is smaller, ranging between 0.86mm and 1.8mm in all directional axes [587]. However, intra-fractional displacement of greater than 2mm occurred in 14% of fractions has been reported [588].

The efficacy of radiation therapy is based on the precise delivery of treatment to the target. Historically, pelvic bones were used for alignment and verification for prostate radiotherapy. However, the prostate can move relative to bony pelvis. Therefore, modern prostate radiotherapy uses daily online verification with gold fiducials inserted into the prostate to ensure treatments are accurately aligned. The differences in fiducial position are measured prior to radiation delivery, and if necessary, the treatment couch is repositioned (known as “couch shift”) to match the intended position. Up to 90% of treatment fractions require such a treatment shift correction when using fiducial localisation [589].

The prostate bed is the main target in PPRT. The prostate bed is not rigid and can be divided into two halves: the superior and inferior prostate bed. The superior prostate bed can move independently of the inferior prostate bed due to the proximity of the rectum and bladder [590]. The inferior prostate bed includes the vesicourethral anastomosis (VUA) and adjacent periurethral tissue. The majority of post-prostatectomy recurrences (70%) occur in the inferior prostate bed, which therefore needs to be targeted precisely [591-596]. The superior prostate bed is the second most common recurrence site after the VUA. The superior

prostate bed includes the posterior bladder wall with retrovesical space, and the seminal vesicle remnant extending to the cut end of the vas deferens.

With contemporary radiotherapy, cone beam CT (CBCT) can identify the superior prostate bed using the bladder/rectum interface. Therefore, the utility of fiducial markers to delineate the superior prostate bed is less important. However, CBCT cannot visualise the VUA or inferior prostate bed accurately because of insufficient soft tissue contrast relative to surrounding tissues, making the use of fiducial markers more critical. Also, the predominant displacement seen in the superior prostate bed is an anterior-posterior rotation which is very difficult to correct. Most treatment couches cannot tilt or only possess a limited range of rotation [590].

The use of fiducial markers and surgical clips placed in the prostate bed for PPRT is uncommon but has been reported in the literature [585, 590, 597-604]. Reasons proposed for lack of use of fiducials include the prostate bed's deformability [603], the ability to use the existing surgical clips as fiducials [604], availability of alternative localisation techniques such as in-room CBCT for image guidance radiotherapy [603]. There is also an infection risk and fistula, if the fiducials are inserted via the rectum [605].

Surgical clips do have the advantage of being non-invasive. However, some studies have found them difficult to match because of the varying number and asymmetric shape [601, 602]. The use of gold seeds is more reliable as they are easily identifiable, stable and representative of the prostate bed [585, 601, 602].

An analysis of prostate bed motion by Alander et al., who used a combination of gold seed fiducial markers and CBCT, reported inter-fractional standard deviation of 1.4mm in the LR axis, and 5.9mm in both the AP and SI axes [601]. Huang et al. used a combination of surgical clips and CBCT, and reported inter-fractional standard deviation of 2.8mm in the LR axis, 3.9mm in the SI axis and 4.3mm in the AP axis [599]. These shifts are not dissimilar to motion seen with an intact prostate. Therefore, fiducial marker utilisation for PPRT is being contemplated, particularly for dose escalation.

### 2.9.2 Seminal vesicle motion

The incidence of seminal vesicle invasion at presentation is 7–24% [606, 607], although the incidence is decreasing, most likely due to earlier detection by PSA testing. For prostate radiotherapy, seminal vesicle invasion risk is often calculated using either Partin tables [608] or Roach's formulae [258]. However, it is generally agreed that seminal vesicles should be included in the CTV in all high-risk prostate cancer patients. Parker et al. showed that if the seminal vesicles are not included, the proximal half of the seminal vesicles will receive some dose but it would generally be regarded as inadequate dosimetric coverage [609].

The proportion of seminal vesicles that should be included in the CTV is mainly based on pathological analysis of prostatectomy specimens. Most studies, including the largest and often-quoted review of 344 prostatectomy specimens, suggest that the pattern of spread is generally continuous and usually (90%) contained in the proximal half [610-612]. It should be noted that these were surgical studies and contained very few patients with T3 disease. Other studies have suggested that seminal vesicle invasion extending to the tip occurs in 40–58% of patients [613, 614]. Notably, one such study did have 16% of T3 patients, which may be more indicative of radiotherapy patients in practice [613]. While clinical guidelines state

that either the proximal half or the proximal 1–2cm of seminal vesicles [615, 616] should be included in the CTV, patients with high-risk disease referred for radiotherapy may have more extensive seminal vesicle invasion than surgical studies would suggest.

Investigations of seminal vesicle motion have varied in the patient number, the number of scans, methodology (prostate centroid or fiducial seeds), and margin calculation. The movements, both systematic and random from 1.1 to 1.9mm laterally, 2.8 to 7.3mm anterior to posterior, and 2.2 to 3.6mm superior to inferior, while random movements varied from 0.4 to 1.4mm laterally, 1.2 to 3.1mm anterior to posterior, and 0.06 to 2.1mm superior to inferior [617-620]. The CTV to PTV margins ranged from 4.5mm to 15mm [617-624]. Seminal vesicle displacement mainly occurs in the anterior-posterior direction and is mostly a result of changes in the rectal filling. Bladder filling appears to have a weak correlation with seminal vesicle motion [617, 619]. The differences in the studies are partly due to methodology, but observer error may also have contributed.

It is clear that seminal vesicle displacement is greater than and sometimes independent of the prostate motion, particularly in the anterior to posterior and inferior to superior directions. Consequently, most studies recommend greater margins for seminal vesicles to achieve an adequate dose. This is most likely of more importance in high-risk patients when the seminal vesicles are more likely to be involved. At least the proximal half of the seminal vesicles should be treated, if not the entire seminal vesicle with adequate margin.

## **2.10 PROSTATE FIDUCIAL MARKERS**

Historically, positional verification was based on the alignment of pelvic bones on orthogonal X-ray film images. The use of film required time for them to be processed and developed.

Because film verification was time-consuming, it was performed weekly after treatment and assessed offline. With the advent of rapid digital imaging, such as electronic portal imaging, verification was increasingly performed daily before treatment and assessed online.

However, because the prostate can move relative to the pelvic bones, this method was considered inaccurate for dose-escalated IMRT for prostate cancer [589, 625-627].

The utilisation of biologically inert radiopaque fiducial markers is regarded as a more precise method of prostate target localisation and has rapidly gained acceptance. Gold seeds are the most commonly used fiducial. Crook et al. were the first to report that fiducial markers provide a very accurate method for localising the prostate during radiotherapy [628]. The use of fiducials in the prostate gland is ideal. They can be implanted with little risk of migration, can easily be visualised in the treatment room, and the prostate shape rarely changes significantly during radiation therapy. Typically, three fiducials are inserted into the prostate, at the apex, mid-gland and base, for better accuracy and reproducibility of prostate alignment. Use of three fiducials also reduces localisation uncertainty due to migration of the fiducials in the organ [625, 629]. Fiducials have been used infrequently in the post-prostatectomy setting as the prostate bed is subject to deformation [603], the drop-out rate and migration of fiducials are higher when inserted into the bladder compare to the prostate [630], and there is a risk of infection and even fistula, particularly if fiducials are inserted transrectally [631, 632].

Gold seeds, however, can cause artefacts on CT imaging, such as distortion or so-called metal artefact and change in target density. The distorted CT image can also result in inaccurate delivery if not accounted for [633]. The artefacts can also hide anatomical detail that could lead to inaccurate contouring, particularly at the prostate's apex.

The ideal fiducial marker is easy to deliver with good visibility, minimal distortion in CT imaging, minimal dose perturbation, biocompatibility with soft tissue and negligible migration [634]. Several new fiducial markers have been developed to produce less distortion with CT imaging. Visicoil™ uses helical coils of gold to reduce the relative thickness of the fiducial and decrease the equivalent density, thus reducing image artefact [635]. Others use a mixture of low-density biocompatible materials and gold particles [634]. Other alternatives are to use radiopaque materials with lower Z numbers such as stainless steel; titanium [636]; and carbon, ceramic or polymer materials [625, 637].

#### 2.10.1 Fiducial construction

Fiducials for prostate cancer are inert, constructed of readily available material, relatively inexpensive and visualised for treatment verification. The fiducials are most frequently made from gold, 0.5–1.5mm in diameter, cylindrical and 2–5mm in length. Some fiducials are knurled to decrease the risk of migration. In contrast, others are either star-shaped in cross-section (Goldlock™, Beampoint, Sweden) or are folded (Gold Anchors™, Naslund Medical AB, Vassvagen, Sweden). To improve MRI visualisation, markers may contain some steel (PolyMark™, CIVCO, USA).

TraceIT™ (Augmenix, Waltham, MA, USA) is a liquid fiducial marker composed of polyethylene glycol (PEG) hydrogel with 1% bound iodine. It is injected as a particulate material and is absorbed by the body within 7 months. It is visible on MRI, ultrasound, CT and CBCT, with no artefact seen on CT. Higher-tech fiducials include electromagnetic transponders (Calypso Medical Technologies, Seattle, USA) which transmit radiofrequency waves. These require a unique localisation and tracking system that can track prostate motion during delivery of the radiotherapy fraction [638]. However, Calypso transponders

can distort MRI planning images, and the system is expensive to implement [639]. Navotek is a radioactive emitting fiducial, but it is also costly with additional concerns regarding its radioactivity [640].

### 2.10.2 Fiducial insertion

The technique of implanting prostate fiducials has been well described [641, 642]. Fiducials can be inserted under local or general anaesthetic. Insertion should be performed at least a few days, preferably 1 week, before the planning CT scan to allow for any oedema or haemorrhage to settle.

During the insertion procedure, patients are positioned in the left lateral or lithotomy position, and a lubricated transrectal ultrasound is inserted into the rectum. The prostate is fully visualised in the axial and sagittal planes and the position for fiducials determined. Needles are used to deploy the gold seeds transrectally or, more recently, transperineally. The transperineal approach has a lower risk of infection and rectal bleeding (similar to transperineal prostate biopsies). Moman et al. reported on 914 patients having gold fiducials implanted; of the 402 patients undergoing transrectal insertion, two patients developed urosepsis, while there were no episodes of urosepsis among 512 patients having transperineal implantation [643]. Igdem et al. assessed pain scores among outpatients following TRUS implants without local anaesthesia; they reported low mean pain scores and 87% of patients reported comparable or less pain than the diagnostic biopsy [644].

The insertion of fiducials for PPRT is most often performed using the transperineal approach to minimise infection risk. The patient is positioned in the dorsal lithotomy position with an indwelling catheter (IDC) inserted into the bladder. A transrectal ultrasound is used to

visualise the bladder, urethra and prostate bed. Traction on the IDC balloon positions it at the bladder neck, just above the primary target, the VUA. The fiducials are inserted using a brachytherapy grid and stepper around the VUA.

Severe complications from fiducial insertion are rare. Moderate complications include pain and fever in 6.2% of men and minor voiding problems in 1.9% [645]. Minor complications consist of haematuria and haemospermia (18.5%), and rectal bleeding (9.1%).

### 2.10.3 Fiducial position

It is generally recommended that three fiducials be inserted. This allows for triangulation, permits multi-planar positioning of the prostate, enables fiducial migration to be assessed, and allows for some redundancy when a fiducial is lost [625, 629]. However, marker loss during radiotherapy is uncommon and is reported at 1.4% [646]. The lost fiducials are usually passed via the rectum but occasionally some embolise to the lung. When inserted at the prostate apex and base, two fiducials are nearly as effective as three for prostate radiotherapy alignment [585, 629]. Typically, the three fiducials are positioned at the prostate base, mid zone and apex, preferably in an alternating right-left pattern but avoiding the urethra. Ideally, they are spaced approximately 1cm apart.

For PPRT, the VUA in the lower prostate bed is delineated by two to three markers inserted into the retrovesical tissue adjacent to the VUA. Two fiducials are reported to be effective [647]. This does not allow the calculation of rotational errors, but this is small at the VUA, and rotational corrections do not greatly improve translational shifts [647]. Fiducials can also be inserted into the retrovesical tissue or into the posterior bladder wall to delineate the upper prostate bed [631].

#### 2.10.4 Fiducials and image guidance

Radiotherapy verification using fiducial markers most frequently utilises image guidance with CBCT or kV orthogonal planar imaging. Previous methods used MV imaging, including MV electronic portal orthogonal planar imaging and MV CT. Moseley et al. had shown a highly significant correlation of isocentre shifts between MV, kV and CBCT fiducials [648]. However, CBCT and MRI volumetric imaging provide information about the organs at risk, such as bladder filling and rectal distension. The Calypso image guidance system has been an innovative method that can track prostate motion during treatment (i.e. intra-fraction motion). However, it does not provide information about the organs at risk [649].

Comparison studies of the use of IGRT/fiducial markers with IMRT versus non-IGRT treatments have generally shown a decrease in late GI and/or GU toxicity [650-652], and in one study there was an improvement in clinical outcome [650]. The difference in toxicity can be attributed to the combination of the IMRT technique with reduced dose to organs at risk, daily image guidance and margin reduction

While the first studies that showed an improvement in outcome utilized weekly fiducial orthogonal planar imaging match, daily online CBCT fiducial verification should result in similar, if not better, results. Some studies of CBCT have shown similar verification shifts to fiducial based planar imaging [653]. Contemporary online CBCT is likely to be more accurate as it enables the daily assessment of fiducials as well as rectal and bladder filling.

Soft tissue matching cone-beam CT (CBCT) has been considered an alternative to fiducials as it avoids the surgical intervention, albeit minor, for the insertion. However, it has been suggested that fiducial based matching of CBCT may be more accurate than soft tissue-based

CBCT matching while still providing the assessment of soft tissue and organs at risk assessment. Shi et al. concluded that CBCT with soft-tissue-based automatic corrections is not as accurate compared to alignment to fiducial markers for prostate IGRT [654].

The online assessment of a 3D soft tissue match on CBCT can be complex, prolonging the verification to treatment time. This prolongation can lead to patient and or organ motion due to bowel gas or bladder filling, resulting in inaccurate radiotherapy delivery.

The prostate is challenging to define on CT because it has a similar HU value and contrast to surrounding tissues. Prostate soft tissue verification assessment of CBCT is even more difficult due to its poorer image quality resulting from its cone-beam geometry and prolonged acquisition time, making it more prone to artifacts and scatter than conventional CT. The resultant images have a diminished signal to noise ratio, contrast to noise ratio, and often greater artefact from bowel gas [655]. The inferior image quality of CBCT contributes to a significantly worse interobserver variability with CBCT soft tissue matching compared with fiducial matching [656]. Matching to the prostate base adjacent to the bladder is easier, but one cannot accurately assess rotations and translations resulting from prostate distortion. Studies of inter-observer variability have highlighted the difficulty distinguishing the soft-tissue prostate from adjacent structures, particularly at the base and apex, due to similar densities [657, 658].

Furthermore, radiation therapists require greater training to perform soft tissue matching to assess translations and complex rotations on grainy images subject to artefact production

[659]. Whereas fiducial imaging, including CBCT, has similar or better accuracy but requires less daily physician input and is less time-consuming [660].

Fiducial matching with daily online CBCT provides an efficient workflow with accurate prostate targeting while maintaining appropriate soft tissue and organ at risk assessment. However, with continued improvements in the matching algorithms and artificial intelligence, fiducial markers may eventually be supplanted. Furthermore, the increasing use of MRI linacs (MRL) that can better visualize the prostate gland and the tumour will enhance the accuracy of soft tissue verification due to its better soft-tissue contrast [659]. However, MRL workflow can be arduous, and MRI-visible fiducials may still improve workflow efficiency, but this is yet fully explored.

### **2.11 RECTAL SPACERS**

The rectum has been the limiting organ at risk in prostate cancer radiotherapy. Rectal filling can change the prostate position, leading to inaccurate dose delivery with worse cancer outcomes and increased rectal toxicity [661-663]. Initial attempts to minimise rectal filling that have been shown to diminish prostate motion include low-residue diet, laxatives, emptying rectal gas before radiotherapy, enemas and suppositories [664-666].

Endorectal balloons have been used to provide a constant rectal volume that can immobilise the prostate and decrease the volume of rectum irradiated [667]. Endorectal balloons are associated with lower rates of rectal mucosa changes than standard prostate radiotherapy, which results in less rectal toxicity [668]. They reduce the radiation dose to most of the

rectum, but the anterior rectal wall remains adjacent to the prostate and receives relatively high doses.

Rectal spacers have been investigated to reduce the radiation dose to the rectum, including the anterior rectal wall. Spacers are inserted into the perirectal space between the prostate and Denonvillier's fascia, anterior to the rectal wall [669], thereby displacing the rectum posteriorly away from the prostate. Prada et al. first described the use of a biodegradable spacer gel to provide temporary separation of the prostate and rectum for prostate radiotherapy [670]. The role of rectal spacers in reducing toxicity from prostate radiotherapy is increasing. Therefore, spacers may enable increasing dose escalation [671], safer hypofractionation [669] and prostate re-irradiation [672].

Spacers used in prostate cancer radiotherapy should remain stable in size during treatment and eventually degrade after the completion of the prostate radiotherapy. The materials used for spacers include blood (blood patch) [673], hyaluronic acid [669], collagen [674], synthetic hydrogels [675] (SpaceOAR™, Augmenix, Waltham, MA, USA) and biodegradable (poly [L-lactide-co-caprolactone]) balloons [676, 677]. SpaceOAR™ (Augmenix, Waltham, MA, USA) is the most commonly used and studied spacer. It consists of a commercially available synthetic PEG-based hydrogel. SpaceOAR has a low allergic rate, distributes well in the perirectal space, remains stable during the course of radiotherapy, and is absorbed by 6 months and excreted by the kidneys [675, 678].

The insertion technique for SpaceOAR™ hydrogel injection was first described by Hatiboglu et al. [679]. The patient is anaesthetised or sedated and placed in the lithotomy position. Antibiotic prophylaxis is recommended to reduce the risk of infection. The prostate and

rectum are visualised using a transrectal ultrasound probe to guide an 18G needle transperineally, posterior to Denonvilliers' (rectoprostatic) fascia into the anterior perirectal fat. Hydro-dissection of the tissue planes is performed with sterile saline. Then the hydrogel mixture is injected into this hydro-dissected space, where it subsequently polymerises.

Complications from spacer insertions are uncommon. They include infection, allergic reactions, injection site reactions such as bleeding and pain, urinary retention, rectal pressure, constipation, and inadvertent injection into the prostate or rectum. Rare major complications include acute pulmonary embolism, severe anaphylaxis, prostatic abscess and sepsis, purulent perineal drainage, rectal wall erosion, and rectourethral fistula [680].

Spacers may be relatively contraindicated in patients with a high risk of adhesions in the perirectal space, including those with inflammatory bowel disease, chronic prostatitis and perianal disease [671].

Multiple retrospective and phase 2 studies have analysed rectal spacers. They have generally shown that a prostate–rectal separation of 9–14mm is achieved [671, 674]. The use of spacers has resulted in lower rectal doses and reduced toxicity with improved rectal quality of life [605, 674, 678, 681-684].

The first phase 3 study of hydrogel spacers was reported by Mariados et al. [685] and then updated by Hamstra et al. [686]. It was a multi-institutional study that randomised 222 men with low- to intermediate-risk prostate cancer to hydrogel spacer or the control arm in a 2:1 ratio. Fiducial markers were placed at the same time as the spacer insertion for image guidance. The trial confirmed the initial phase 2 studies, showing that the spacer was well tolerated, and easily and successfully inserted into approximately 99% of patients without

major complication. Overall, there was no difference in acute rectal toxicity between the spacer and control arms. However, there was a significant increase in the perirectal space and reduced rectal radiation doses in the spacer arm. The trial also showed a significant improvement in late rectal toxicity and its severity, and a better bowel quality of life in the spacer group. The decline in urinary and sexual quality of life was worse in the control group. The conclusion was that the spacer was a safe and effective tool for reducing radiation rectal toxicity and improving quality of life [685-687].

The investigation of spacers in the PPRT setting is limited [688-692]. The insertion of a spacer in post-prostatectomy patients can be challenging as the tissue planes are disrupted during surgery. There is also a concern that tumour cells could be displaced posteriorly by the spacer, leading to a geographic radiotherapy miss. However, the anterior rectal wall is not a common site of local recurrence following radical prostatectomy [591-594, 693, 694], suggesting that spacers have a potential role at least in patients with macroscopic local recurrence. Earlier studies using TRUS biopsies to identify the recurrence site following prostatectomy showed that the peri-anastomotic site or VUA was the most common site, with an incidence in the range of 60% [591-593]. Later MRI studies of post-prostatectomy PSA relapses have confirmed that local recurrences occur mainly in the VUA region, followed by the retro-vesicle space and seminal vesicles [594, 693, 694]. Therefore, it is essential that patients be carefully selected for the use of rectal spacers, and that a macroscopic local recurrence does not involve the anterior rectal wall [690].

Lehrich et al. performed a retrospective review of 21 post-prostatectomy patients undergoing post-operative adjuvant or salvage IMRT to a dose of greater than 72Gy and who had a PEG hydrogel rectal spacer inserted [689]. The patients did not have an imaged local

recurrence. This study showed that using a rectal spacer did not appear to compromise biochemical relapse-free survival or rectal toxicity. Following dose-escalated post-operative radiotherapy with a rectal spacer, the acute and late GI toxicity rates were low. The relapse-free survival was high compared to both historical controls and toxicity grades previously reported in the literature.

In conclusion, studies have shown that spacers increase the separation of prostate and rectum with significant dosimetric rectal sparing effects. The rectal sparing has resulted in at least a reduction of late rectal toxicity. Spacers are generally safe and easy to deliver with low complication rates. However, image guidance remains essential. Even though posterior prostate displacements are reduced with spacers, prostate motion during a course of radiotherapy is still an important factor in the delivery [675]. The use of spacers in the post-prostatectomy setting shows some promise but has not yet been subject to rigorous analysis. Spacers are likely to be critical with further dose escalation or hypofractionated prostate radiotherapy, particularly ultra-hypofractionated or SABR techniques, but studies are not completed [669].

## **2.12 CONCLUSION**

Radiotherapy dose escalation for high-risk prostate cancer has progressed from 3DCRT to IMRT, resulting in a steady improvement in dosimetry and outcomes. The dose conformity and efficiency are further improved with the VMAT form of intensity modulation. Therefore, it is increasingly important that the target cancer is appropriately identified and defined with multi-modality imaging, incorporating high-resolution morphological and functional scans. The precision of delivery also becomes paramount, requiring the appropriate utilisation of

IGRT techniques. Together with fiducials and spacers, these imaging techniques greatly add to the accuracy and safety of prostate radiotherapy.

## Chapter 3 PROSTATE CANCER POST-PROSTATECTOMY RADIOTHERAPY: CT VS MRI FOR VESICourethRAL ANASTOMOSIS TARGET DELINEATION

---

Daryl Lim Joon<sup>a</sup>, Adeline Lim<sup>a</sup>, Michal Schneider<sup>b</sup>, Chee-Yan Hiew<sup>a</sup>, Nathan Lawrentschuk<sup>a</sup>,  
Shomik Sengupta<sup>a</sup>, Farshad Foroudi<sup>a</sup>, Trish Jenkins<sup>a</sup>, David Angus<sup>a</sup>, Morikatsu Wada<sup>a</sup>, Michael  
Chao<sup>a</sup>, Vincent Khoo<sup>c</sup>

<sup>a</sup> Department of Radiation Oncology, Olivia Newton-John Cancer Wellness and Research  
Centre, Austin Health, Heidelberg, Australia

<sup>b</sup> Department of Medical Imaging and Radiation Sciences, Monash University, Clayton,  
Australia

<sup>c</sup> Royal Marsden Hospital, London, UK

Published: Lim Joon D, Lim A, Schneider M, Hiew C-Y, Lawrentschuk N, Sengupta S, Foroudi  
F, Jenkins T, Angus D, Wada M, Chao M, Khoo V. Prostate cancer post-prostatectomy  
radiotherapy: CT vs MRI for vesico-urethral anastomosis target delineation. *Radiother Oncol.*  
2017;125(1):113–117. <https://doi.org/10.1016/j.radonc.2017.08.031>

### 3.1 PREFACE

Chapter 3 represents a manuscript that was peer-reviewed and subsequently published in *Radiotherapy and Oncology* in 2017 (see full reference above).

The first important step in precision radiotherapy is computed tomography (CT) simulation and image acquisition. Target definition is vital for accurate conformal radiotherapy planning and subsequent treatment delivery. An error in target definition will be propagated throughout the radiotherapy course, potentially leading to a geographic miss. Therefore, the first investigative chapter of this thesis explores the use of co-registered magnetic resonance imaging (MRI) to define the target more accurately.

Post-prostatectomy radiotherapy (PPRT), either adjuvant or salvage, is an effective modality in the treatment of prostate cancer. The clinical target volume (CTV) includes the surgical bed (i.e. the prostate fossa and seminal vesicle bed), as this represents the most common sites of local recurrence. The specific anatomical sites include the vesicourethral anastomosis (VUA); bladder base, including bladder suture line; retrovesical space; and seminal vesicle bed to the cut end of the vas deferens.

Notably, the most common site of recurrence is the VUA. Therefore, the VUA must be accurately identified to ensure adequate dosimetric coverage. Radiotherapy protocols stress the importance of including the VUA in the CTV. Present guidelines recommend adding an inferior margin to the VUA to allow for microscopic extension beyond the VUA. The Radiation Therapy Oncology Group (RTOG) guidelines recommend an 8–12mm inferior margin, whereas the Australasian Faculty of Radiation Oncology Genito-Urinary Group (FROGG) guidelines suggest 5–6mm.

The hypothesis is that standard radiotherapy planning CT does not define the most common recurrence site, the VUA, as accurately as T2-weighted MRI. The aim of this study was to analyse the spatial differences between MRI and CT in the localisation of the VUA, and assess and validate guideline recommendations for the CT-defined VUA CTV margins in comparison to an MRI-defined VUA.

### **3.2 CONTEXT**

International guidelines have suggested that MRI be the gold standard for identifying the most common site of recurrence, the VUA, for PPRT. However, prior to this study, there was only indirect evidence to support this recommendation. This published study validates and confirms the guideline recommendation that a T2-weighted MRI is more precise than CT in identifying the VUA for precision post-prostatectomy radiotherapy. Future studies on the clinical impact of MRI on tumour control and normal tissues toxicity are warranted, particular as radiotherapy embraces MRI simulators and MRI linacs.

CTV margins account for the microscopic extension of the gross tumour. Therefore, CTV margins are based on pathology studies of microscopic extension and data pertaining to clinical and imaging recurrence patterns. The CTV margins for post-prostatectomy radiotherapy depend on the accuracy of the VUA definition. The 5-12mm margins recommended by the guidelines may be insufficient if the VUA is not well defined. PTV margins are margins beyond the CTV to compensate mainly for setup uncertainty and inter and intra-fraction motion. They may also account for delineation errors, including the definition of the VUA. If the CTV is defined using CT imaging, it may require additional margins to account for delineation error. If MRI is used to assist with the VUA delineation,

the PTV may be reduced if one initially incorporated a delineation error margin. However, PTV margins are department dependent. Therefore, appropriate considerations and clinical study are required. Further reductions in margins to reduce toxicity would need to be appropriately addressed in prospective studies.

### 3.3 ABSTRACT

**Background:** The VUA is critical to the CTV in post-prostatectomy radiotherapy (PPRT), as it is the commonest site of recurrence. Typically, VUA localisation is performed on a CT alone but guidelines recommend MRI.

**Objective:** Evaluate the VUA spatial differences between CT (ctVUA) and MRI (mrVUA). Analyse its impact on the CT-defined CTV (ctCTV) as recommended by published guidelines.

**Materials and methods:** We identified 34 patients with a co-registered simulation CT and T2-weighted MRI. The VUA was located on CT and MRI while blinded to the opposing scan. The differences were analysed using the Wilcoxon signed-ranks test. The mrVUA coverage was investigated using three ctCTV margins of 5mm, 8mm and 12mm.

**Results:** Median age was 63 years with 59% having pT3a disease and median Gleason score of 7. The mrVUA was coincident with the ctVUA in 12% and inferior in 88%. Median difference was 5mm (0–10mm) ( $p < 0.0001$ ). Only a ctCTV margin of 12mm would have encompassed all mrVUAs. A ctCTV margin of 8mm and 5mm resulted in 12% and 38% of cases, respectively, where the VUA was excluded from the ctCTV.

**Conclusions:** MRI is important for the accurate delineation of VUA for PPRT.

### 3.4 INTRODUCTION

Prostate cancer post-prostatectomy radiotherapy (PPRT) is used as adjuvant treatment for men at high risk of relapse or for the salvage of men who have suffered biochemical prostate-specific antigen (PSA) relapse or clinical recurrence [280, 282, 286, 695-697]. However, up to one-third of adjuvant patients and two-thirds of salvage cases will further relapse following PPRT [698].

Initial investigations to define the site of local recurrence following PSA relapse post prostatectomy used transrectal ultrasound-guided biopsy alone. They showed that the perianastomotic site, or VUA, was the most common site of recurrence with the incidence ranging from 56% to 66% [591-593].

It is therefore essential that the VUA be accurately identified prior to PPRT to ensure adequate dosimetric coverage. Precision targeted radiotherapy with intensity-modulated radiotherapy (IMRT) and image-guided radiotherapy (IGRT) in prostate cancer has been shown to be important for both disease outcome and minimisation of toxicity [650-652]. International guidelines and protocols stress the importance of the VUA [699-702], suggesting that it is critical to the definition of the radiotherapy clinical target volume (CTV), that is, the volume at high risk of containing residual microscopic disease.

The guidelines recommend that axial CT slices should be used when identifying the VUA [699-702]. They acknowledge that the VUA may be more accurately identified on MRI, as the gold standard reference [702], because of its superior soft tissue contrast. However, they concede that the utility of MRI has not been fully evaluated [700, 702].

The guidelines also recommend an additional caudal CTV margin from the VUA to allow for microscopic extension [699-702]. The suggested geometric margins range from 5mm to 12mm. However, unless the VUA is accurately delineated, this margin for microscopic disease extension may be compromised and consequently under-dosed.

The purpose of the study was to evaluate the utility of MRI in the accurate identification of the VUA and the impact on the CTV for PPRT relative to the recommended guidelines.

Therefore, the aims of this study are:

- 1) To analyse the spatial differences between MRI and CT in the localisation of the VUA.
- 2) To assess the mrVUA relative to the CT-based CTV margins (ctCTV) recommended by the published guidelines.

### **3.5 MATERIALS AND METHODS**

The investigation was approved as a retrospective analysis by the institutional ethics committee. The study cohort consisted of 34 eligible consecutive prostate cancer patients previously treated with post-prostatectomy IMRT/IGRT between December 2011 and October 2013 with uniform CT slice thickness.

#### **3.5.1 Simulation and imaging**

A bladder and bowel protocol was adopted to standardize the organ at risk filling. The purpose was to minimize the impact of bladder and bowel filling on the VUA position and maintain consistency with standard radiotherapy protocols. Patients were instructed to empty their bowels before the scans using an enema. In addition, they emptied their bladder and drank 500mls of water before the scans. The aim was to have an empty bowel and comfortably full bladder.

Patients were positioned supine with an individualised foam Alpha cradle placed on an indexed pelvic board with foot stocks. CT simulation (non-contrast) was performed on a General Electric Radiation Therapy Lightspeed Widebore® helical scanner (General Electric Healthcare, Buckinghamshire, UK) with a resolution of 512x512, pitch 0.75, no gap and a slice thickness of 1.25mm. The CT origin (z-axis 0) was centred and tattooed 5cm superior to base of penis.

The planning MRI was performed on a 1.5 T Siemens Magneto Avanto Syngo MR B17® (Siemens Healthcare, Erlangen, Germany). The MRI sequence utilised for this study was a high-resolution 3D T2-weighted scan with a voxel size of 1mm. This was reformatted in the axial plane and imported into CMS Focal Sim® (Elekta, Stockholm, Sweden) and co-registered with the simulation CT.

### 3.5.2 Vesicourethral anastomosis identification and analysis

Following a prostatectomy, the bladder is anastomosed to the proximal membranous urethra [703-705]. The membranous urethra is normally closed by the external sphincter, both being contained within the urogenital diaphragm. Consequently it does not contain urine. Therefore, as the guidelines recommend, the VUA was defined on the axial slice just inferior to the last slice where urine is visible, as the urine defines the bladder on both CT and MRI [699, 701, 702]. This was confirmed on multi-planar views. Furthermore, on T2-weighted MRI, the VUA can be more precisely defined due to ability to visualise the low signal elliptic cylindrical wall of the VUA and proximal membranous urethra in contrast to the very bright signal of urine in the bladder [706].

The CT and MRI were co-registered initially using the entire pelvic bones but then refined to the region of interest that encompasses the urogenital diaphragm and VUA, that is, the bones of the ischiopubic ramus and coccyx.

The department regards the gold standard for delineation of the CTV to be the MRI for the soft tissue components not well visualised on CT, that is, the VUA, membranous urethra and urogenital diaphragm (5–10mm), and, posteriorly, the meso-rectal fascia. The CT is used to define the posterior pubis, obturator internus and bladder components of the CTV as these are well seen on CT.

Following co-registration of the CT and MRI, the treating radiation oncologist delineated the ctVUA on the CT while blinded to the MRI. At a later date, the same radiation oncologist defined the mrVUA on the co-registered MRI while blinded to the CT. All VUAs were reviewed and adjusted by the study radiation oncologist and radiologist, both of whom specialised in urology.

The superior-inferior (z-axis) coordinate, that is, the vertical distance from the CT origin, was recorded for both the ctVUA and mrVUA. The differences between these VUAs were calculated.

### 3.5.3 Clinical target volume analysis

Published guidelines recommend adding an inferior margin to the VUA to allow for microscopic extension beyond the VUA [699-702]. The RTOG guidelines recommend 8–12mm [699], Princess Margaret Hospital (PMH) recommend 8mm [702], whereas the FROGG guidelines suggest 5–6mm [701]. The remaining guideline from the EORTC recommends that

the relevant CTV include “Centrally: the urethra-vesical anastomosis” and “Caudally: including the apex (15mm cranially from the penile bulb)” with a 5mm margin for high-risk areas including microscopic extension, incompletely resected extracapsular extension and involved margins [700].

#### 3.5.4 Statistics

The differences (ctVUA – mrVUA) were calculated for each patient. As the differences relate to the CT discrete slice thickness, the median value and range was calculated. A p-value of <0.05 was afforded statistical significance between the median differences of the ctVUA and mrVUA using the two-tailed Wilcoxon signed-ranks test for paired samples. The mean difference for the patient population was also calculated to compare with the literature. The statistical analysis was performed using Microsoft® Excel (Microsoft®, Redfern, USA) and Graphpad Prism™ Version 6.07 (Graphpad®, California, USA).

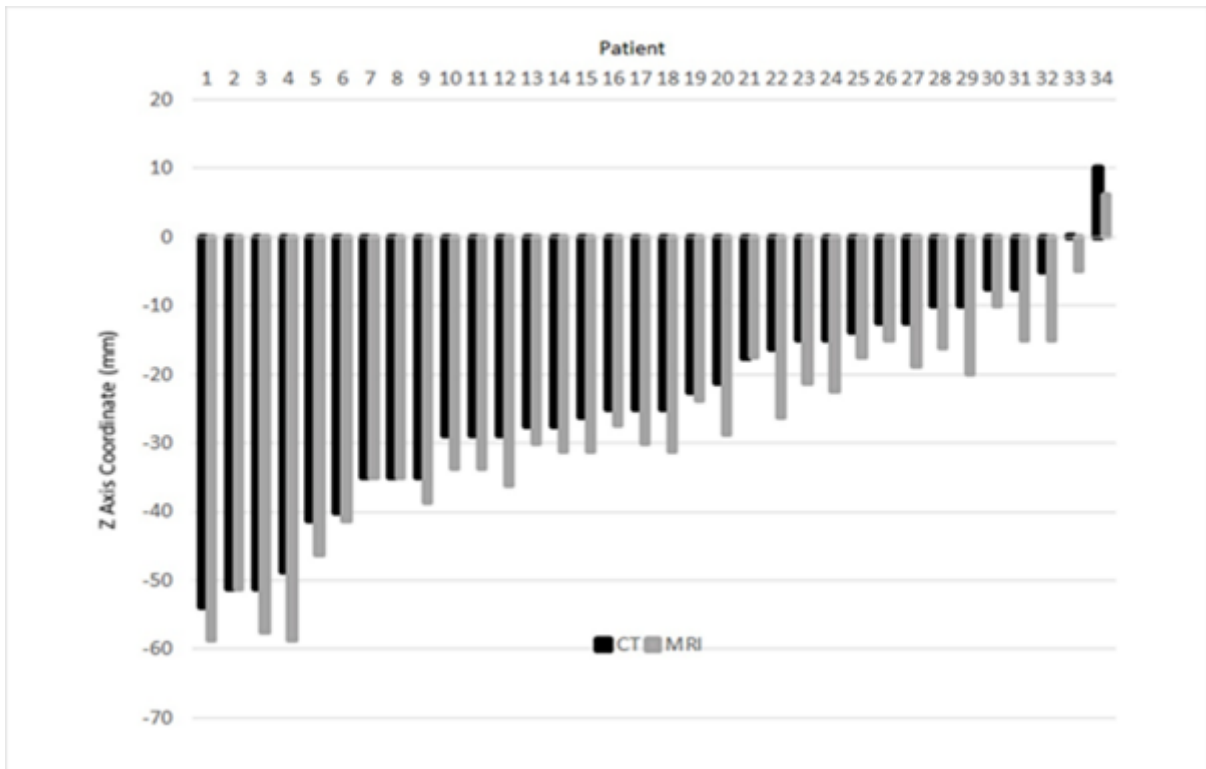
### 3.6 RESULTS

The study cohort consisted of 34 patients with a median age of 63 years (range 52–72 years). Nine patients (26%) received adjuvant PPRT to a mean dose of 66Gy and the remaining 25 (74%) received salvage PPRT for PSA relapse to a mean dose of 70Gy. The majority had locally advanced disease, with almost 60% having extracapsular extension (pT3a), while the median Gleason score was 7. The apical margin was involved in 14 of the 21 patients (56%) with positive surgical margins (Table 3.1).

Table 3.1 Prostatectomy pathological characteristics: T stage, Gleason score and margin status

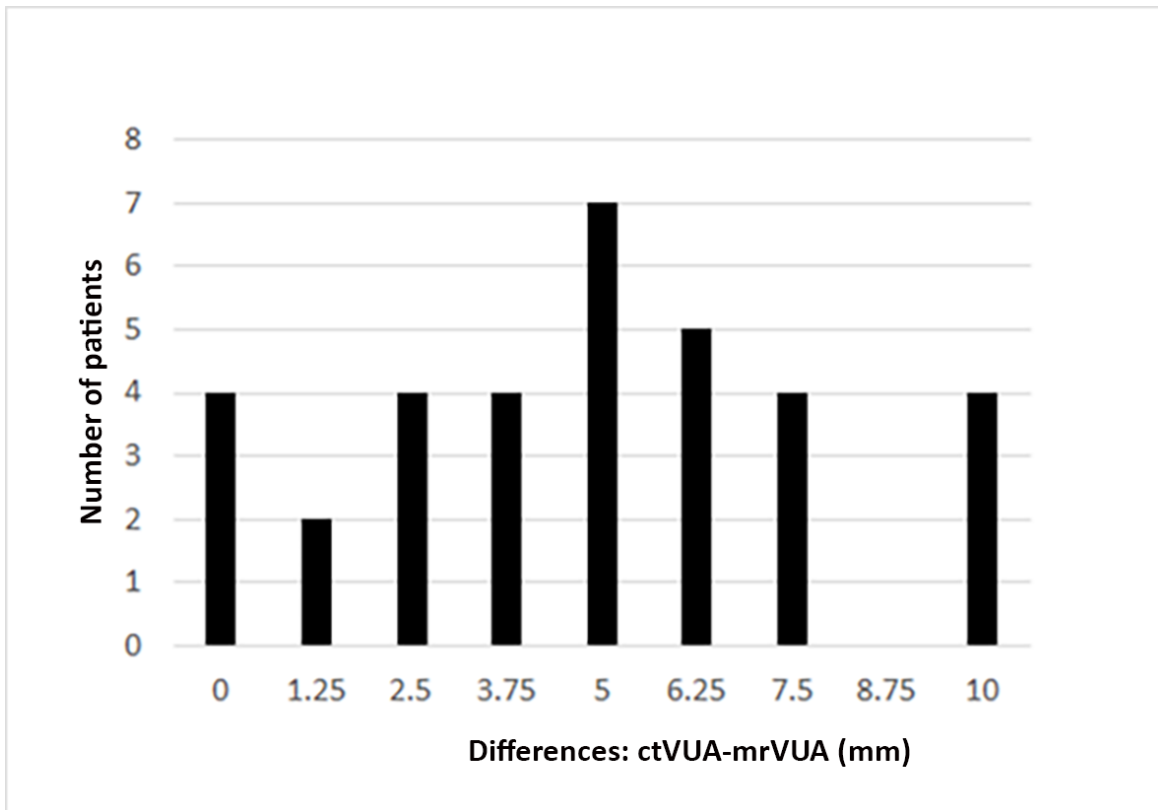
Characteristic	Patients (n=34)	%
<b>T Stage</b>		
2a	2	5.9%
2b	3	8.8%
2c	5	14.7%
3a	20	58.8%
3b	4	11.8%
<b>Gleason score</b>		
7	25	73.5%
8	2	5.9%
9	7	20.6%
<b>Surgical margins</b>		
Positive	21	61.8%
Negative	13	38.2%

In 30 patients (88%) the vector difference between the mrVUA and ctVUA was caudal ( $p < 0.0001$ ). The ctVUA and mrVUA were coincident in four patients (12%). The median difference was 5mm, with a range of 0 to 10mm. The mean difference was 4.82mm with a standard deviation (SD) of 2.97mm (Figure 3.1). Notably, there were four patients (12%) with a mrVUA that was 10mm inferior to the ctVUA (Figure 3.2).



Source: Austin Health

Figure 3.1 Vesicourethral anastomosis z-axis coordinates for 34 patients: computed tomography (CT) vs magnetic resonance imaging (MRI). Z-axis origin (0) is centred and tattooed 5cm superior to base of penis.

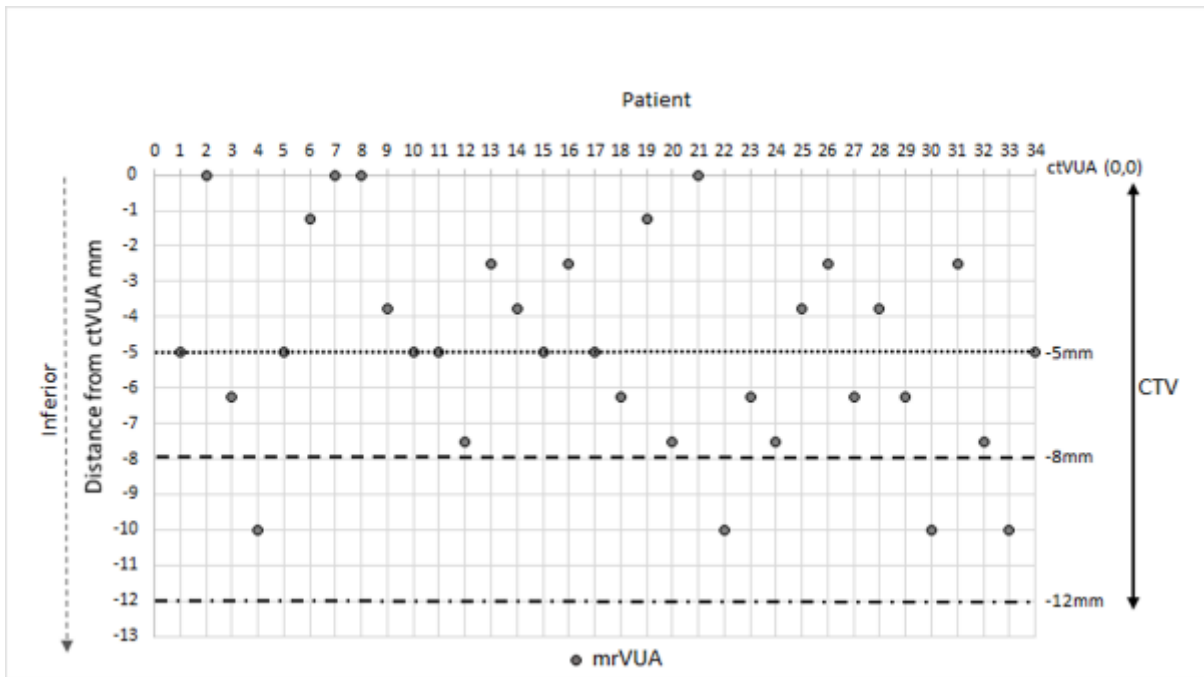


CT = computed tomography, ctVUA = computed tomography vesicourethral anastomosis, MRI = magnetic resonance imaging, mrVUA = magnetic resonance imaging vesicourethral anastomosis

Source: Austin Health

Figure 3.2 Differences between the ctVUA and mrVUA based on axial slices of 1.25mm thickness co-registered CT and MRI, respectively

Comparison of the differences between mrVUA and ctVUA with recommended guidelines for CTV margins are shown in Figure 3.3. The mrVUA was encompassed by the ctCTV in all patients when a margin of 12mm was used. For the 8mm and 5mm margins, the mrVUA was included within the CTV in 30 (88%) and 21 (62%) patients, respectively. Four patients (12%) would have had correct CTV margins as the ctVUA and mrVUA were coincident.



ctVUA = computed tomography vesicourethral anastomosis, mrVUA = magnetic resonance imaging vesicourethral anastomosis

Source: Austin Health

Figure 3.3 Vector difference of mrVUA relative to ctVUA for each patient (i.e. ctVUA normalised to 0.0), illustrating the relationship to the recommended clinical target volume (CTV) (inferior) margins of 5mm, 8mm and 12mm

The median (range) mrVUA to ctCTV distance in those patients whose mrVUA was included within the ctCTV was 7mm (2–12mm), 3mm (0.5–8mm) and 2.5mm (1.25–5mm) for the margins of 12mm, 8mm and 5mm, respectively.

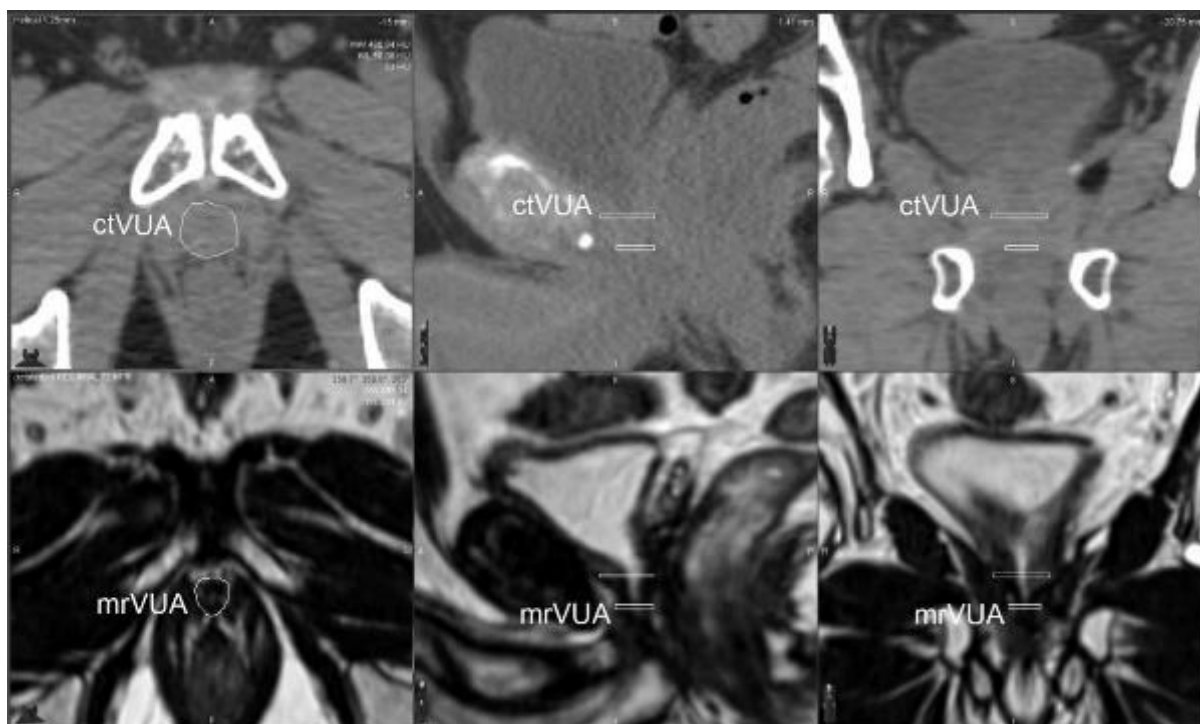
The mrVUA was caudal and excluded from the ctCTV when using a margin of 8mm and 5mm, in four (12%) and 13 (38%) patients, respectively. The median distance of the mrVUA from the inferior margin of the ctCTV was 2mm (range 2mm) for the 8mm margin and 2.5mm (1.25–5mm) for the 5mm margin.

### 3.7 DISCUSSION

This study validates the international recommendation for MRI to optimally define the VUA in PPRT, particularly when using non-contrast simulation CT. The MRI-defined VUA is more likely to be a truer definition of the VUA because of MRI's markedly better soft tissue contrast. In most patients, the mrVUA was caudal to the ctVUA. Consequently, the recommended CTV margin was reduced in the majority of patients with the mrVUA compared to ctVUA. Notably, the mrVUA was excluded entirely from the CTV in up to 38% of patients, depending on the CTV margin used.

Compared to CT, MRI improves the target volume delineation in radiotherapy for an intact prostate [174, 525, 707]. The present study has similarly confirmed its utility in the post-prostatectomy setting. A non-contrast simulation CT alone only accurately identified the VUA in 12% of patients. Precisely identifying the last CT slice with visible urine can be difficult as it is often a small dot with a greyscale contrast that approaches that of the bladder neck and VUA. In comparison, in T2-weighted MRI, the urine is contrastingly bright compared to the surrounding tissue (Figure 3.4).

MRI, and more recently multi-parametric MRI (mpMRI), has been used to define the site of recurrence that would be suitable for biopsy confirmation and salvage radiotherapy [693, 708]. Most MRI studies agree with earlier ultrasound studies that the peri-anastomotic site was the most frequent site of recurrence with an incidence range between 52% and 100% [591, 592, 693, 708, 709].



ctVUA = computed tomography vesicourethral anastomosis, mrVUA = magnetic resonance imaging vesicourethral anastomosis

Source: Austin Health

Figure 3.4 Multi-planar views of co-registered computed tomography (CT) and magnetic resonance imaging (MRI) scans of a single patient showing the mrVUA caudal to the ctVUA

Two contemporary studies, one using MRI [708] and another mpMRI [693], found that the local recurrence occurred at the VUA in 76% and 70% of patients, respectively. Interestingly, in both studies there were no differences in pathological or clinical variables between the sites of recurrence. Notably, the tumour site and location of the positive surgical margins did not correlate statistically with the site of local recurrence [708].

PMH performed a comprehensive study to derive a consensus definition of the anatomic boundaries of the CTV for PPRT [702]. This included an analysis of 12 patients for the critical VUA localisation. They compared CT images with a slice thickness of 2mm to reference MRI images with a slice thickness of 3mm. This study found that the mean ( $\pm$ SD) uncertainty in

identifying the VUA using CT was 1.8mm ( $\pm 2.5$ ). The present study found a larger mean uncertainty when comparing CT to MRI of 4.82mm ( $\pm 2.97$ ). The differences may be a result of the thicker slice images, particularly the MRI, and limited patient numbers in the PMH study.

The CTV incorporates the most common sites of local recurrence, that is, the surgical, prostatic and seminal vesicle beds [591, 592, 709]. This is represented anatomically by the VUA; the bladder base, including the posterior bladder suture line; the retrovesical space; and the seminal vesicle bed to the cut end of the vas deferens [699-702, 708]. The increasing utilisation of IMRT in PPRT permits greater dosimetric conformity around the CTV.

Therefore, the correct CTV definition becomes increasingly important in the optimisation of local control and the minimisation of toxicity. Additionally, it may allow dose escalation to high-risk regions to further improve local control [523].

The various guidelines recommend that a CTV margin should be applied to the VUA to allow for microscopic extension inferiorly that may occur with apical involvement or surgical manipulation [699-702]. The present study showed that even if the maximum recommended margin of 12mm is applied to the ctVUA, there will still be eight patients (24%) that will have less than the minimum recommended margin of 5mm. If a non-contrast CT alone is used, then an appropriately larger planning target volume (PTV) or margin needs to be considered to compensate for these uncertainties.

A contrast CT is likely to produce similar results to MRI although it was not investigated in the present study. We have routinely used a non-contrast CT plus MRI, rather than a contrast CT, as the large volume of bladder contrast may lead to dosimetric perturbations

necessitating co-registration with a non-contrast CT or, alternatively, applying density corrections. The other major caveat is that contrast CT could not be used in patients with contrast allergies.

The commonest positive surgical margin is at the prostatic apex. This is a consequence of anatomical factors including the broad extent of the dorsal venous plexus, the prostatic location under the pubic bone, the proximity of the urethral sphincter and neurovascular bundle, and the absence of a complete capsule [710, 711]. In the present study, the apical margin was the most common positive surgical margin, occurring in 71% of patients. Two of the guidelines recommend an additional margin if the apex is involved; the EORTC recommends an additional 5mm [700] and the RTOG recommends extending to the genitourinary diaphragm [699]. This additional margin would reduce the dosimetric impact of an inaccurate VUA identification.

Contouring guidelines recommend the superior aspect of the penile bulb as an alternative anatomical marker of the inferior CTV margin. This can be used if the VUA is difficult to identify [699, 701]. It ensures that the VUA is encompassed. However, it would increase the penile bulb dose, increasing the risk of erectile dysfunction [712]. QUANTEC (the Quantitative Analyses of Normal Tissue Effects in the Clinic group) recommends keeping the mean dose to 95% of the penile bulb volume to <50Gy and limiting the penile bulb dose to  $D_{95} < 50\text{Gy}$  and  $D_{70} < 70\text{Gy}$  to minimise the risk of erectile dysfunction [712]. This may be difficult to achieve, particularly with dose escalation, as the CTV would be immediately adjacent to the penile bulb and the PTV expansion would overlap this organ at risk.

Limitations of the study include co-registration uncertainty, deformation, inter-observer and intra-observer variation, optimisation of window levels and the effect of training. In addition, the VUA location may vary because of internal organ motion secondary to bladder filling. A recent study investigating the prostate bed motion during treatment showed an internal organ motion up to 18mm in the superior-inferior direction [590]. The other important use of MRI, notably mpMRI, is the identification of local recurrences. Notably, MRI with prostate-specific membrane antigen (PSMA) PET improves the detection of prostate cancer and may better select patients for salvage radiotherapy by detecting the local recurrence and excluding patients with metastatic disease [713-715]. Higher doses of radiotherapy targeting visible local recurrences may be required to optimise local control [523].

### **3.8 CONCLUSION**

The present study validates the recommendation that a T2-weighted MRI is critical to accurately delineate the VUA for PPRT. If an MRI is not available or is contraindicated, a contrast CT may be an alternative or the PTV margins could be increased to compensate for the delineation uncertainty.

### **Acknowledgements**

Ms Jenny Smith for statistical advice.

## Chapter 4 PROXIMAL SEMINAL VESICLE DISPLACEMENT AND MARGINS FOR PROSTATE CANCER RADIOTHERAPY

---

Daryl Lim Joon<sup>a</sup>, Michael Chao<sup>a</sup>, Angelina Piccolo<sup>a</sup>, Michal Schneider<sup>b</sup>, Nigel Anderson<sup>a</sup>,  
Monica Handley<sup>a</sup>, Margaret Benci<sup>a</sup>, Wee Loon Ong<sup>a</sup>, Karen Daly<sup>a</sup>, Rebecca Morrell<sup>a</sup>, Kenneth  
Wan<sup>a</sup>, Nathan Lawrentschuk<sup>c</sup>, Farshad Foroudi<sup>a</sup>, Trish Jenkins<sup>a</sup>, David Angus<sup>c</sup>, Morikatsu  
Wada<sup>a</sup>, Shomik Sengupta<sup>c</sup>, Vincent Khoo<sup>a,b,d</sup>

<sup>a</sup> Department of Radiation Oncology, Olivia Newton-John Cancer Wellness and Research Centre, Austin Health, Heidelberg, Australia

<sup>b</sup> Department of Medical Imaging and Radiation Sciences, Monash University, Clayton, Australia

<sup>c</sup> Department of Urology, Austin Health, Heidelberg, Australia

<sup>d</sup> Royal Marsden NHS Foundation Trust, London, UK

Published: Lim Joon D, Chao M, Piccolo A, Schneider M, Anderson N, Handley M, Benci M, Ong WL, Daly K, Morrell R, Wan K, Lawrentschuk N, Foroudi F, Jenkins T, Angus D, Wada M, Sengupta S, Khoo V. Proximal seminal vesicle displacement and margins for prostate cancer radiotherapy. J Med Radiat Sci, 2021: Online ahead of print.

<https://doi.org/10.1002/jmrs.457>

#### 4.1 PREFACE

Chapter 4 represents a manuscript that has been published in the *Journal of Medical Radiation Sciences* (JMRS) in 2020.

While the first investigative chapter explored the initial steps of computed tomography (CT) simulation and image acquisition in planning radiotherapy, this chapter focuses on the next major component of radiotherapy: treatment verification and delivery. It uses the standard gold seeds to study the motion of seminal vesicles relative to the prostate during the entire course of a dose-escalated radiotherapy course.

Randomised studies have shown that radiotherapy dose escalation in prostate cancer has improved patient outcomes. The first developments to minimise toxicity involved the planning of increasingly more conformal dose distributions, with 3D conformal radiotherapy and then intensity-modulated radiotherapy (IMRT). Further improvements were achieved with image-guided radiotherapy (IGRT), which allowed the conformal dose distributions to be more accurately delivered. IGRT for prostate cancer has mainly involved using gold fiducial markers, which allow for efficient and accurate targeting using daily online verification.

For patients undergoing radiotherapy for locally advanced or high-risk disease, IMRT plans aim to deliver a conformal dose to both the prostate and at least the proximal, if not the entire, seminal vesicles. However, daily online targeting is verified according to the fiducial markers in the prostate alone. A number of studies have shown that the seminal vesicles can move in relation to the prostate. This motion can lead to a residual uncertainty in the radiotherapy delivery to the seminal vesicles.

The study hypothesis was that seminal vesicle motion is more significant than and independent of prostate motion and, therefore, the clinical target volume (CTV) to planning target volume (PTV) margins needed for the seminal vesicle are greater than required for prostate IMRT. The aim of the project was to study the movement of the seminal vesicles relative to the prostate and bone.

## **4.2 CONTEXT**

This study included a novel method of using gold seed markers to precisely track proximal seminal vesicle motion relative to the prostate during radiotherapy. This method is subject to less uncertainty in terms of inter-observer and intra-observer error than previous methods such as contouring prostate and seminal vesicle volumes. The study illustrated the seminal vesicle margins required for radiotherapy and contrasted them relative to prostate margins. For the first time, we were able to discern differential motion of the right and left seminal vesicles because of the study's statistical power.

As the study investigated clinical margins, it used a clinically relevant methodology by defining the prostate according to radiotherapy verification practices, i.e. three gold fiducials to define the prostate and a fiducial to define the proximal SV on a planning CT in accordance to major radiotherapy guidelines. The subsequent margins, therefore, have greater relevance to the verification method presently used in radiotherapy as they account for translations, rotation and distortion. A pure anatomical study of the SV motion relative to the prostate could use anatomical parameters, but this would ideally be done on MRI, where the components are well visualized.

The seminal vesicles (SV) are attached to the prostate, where its excretory duct joins the vas deferens to form the ejaculatory duct. The ejaculatory ducts traverse the central prostate zone to open in the posterior urethra at the verumontanum, on either side of the utricle. Thus, the SVs are attached to the posterior prostate as the ejaculatory duct enters the prostate, most likely the pivot point of the SVs. However, the SV's more flexible glandular more easily distorted component is attached to the posterior prostate along a variable length. This attachment of the ejaculatory duct and SV to the prostate is poorly defined on CT, as they have similar HU and greyscale values. The attachment is not seen on orthogonal planar imaging. An anatomical study of SV motion is more relevant to future MR based linacs, where the anatomy and appropriate MR based margins can be better defined.

Precision is vital in the outcome of prostate cancer treated with radiotherapy. The differences in PTV margins to account for the motion of the SV compared to the prostate ranged from 0.3 to 4.9mm. The departmental PTV margins to allow for all uncertainties during the study was 10mm. Thus, these differences are almost 50% of our total margins. Studies of rectal motion and some studies of margin reductions in prostate cancer have shown poorer outcome [663]. Thus, the margins noted in this study would appear to be clinically relevant. Specific clinical studies are required to confirm this proposal. However, clinical prostate investigations have already illustrated that millimetre margin differences not dissimilar to those in the present work can impact the outcome [716]. The Dutch randomized dose-escalation trial showed that with margins of 10mm for the first 68Gy and 0-5mm for the 10Gy boost that a large rectal volume resulted in a significantly decreased tumour control in patients with a risk of SV involvement greater than 25% and at risk of geometric miss [661]. Engels et al. [5] found that IGRT with 3–5 mm margins was associated

with a poorer biochemical progression-free survival in patients treated with conformal arc therapy compared to non-IGRT and 6–10 mm margins [717]. The margins used in this cohort were based on weekly verification and thus larger than the calculated margins in this study. The data was used to adjust both the prostate and seminal vesicle margins for daily online verification where the seminal vesicle margins were greater.

### 4.3 ABSTRACT

**Introduction:** Guidelines recommend that the proximal seminal vesicles (PrSV) should be included in the CTV for locally advanced prostate cancer patients undergoing radiotherapy. Verification and margins for the prostate may not necessarily account for PrSV displacement. The purpose of this study was to determine the inter-fraction displacement of the PrSV relative to the prostate during radiotherapy.

**Method:** Fiducials were inserted into the prostate, and right and left PrSV (RSV and LSV) in 30 prostate cancer patients. Correctional shifts for the prostate, right and left PrSV and pelvic bones were determined from each patient's 39 daily orthogonal portal images relative to reference, digitally reconstructed radiographs.

**Results:** There was a significant displacement of the RSV relative to the prostate in all directions: on average 0.38mm (95% confidence interval [CI] 0.26–0.50) to the left, 0.80–0.81mm (95% CI 0.68–0.93) superiorly and 1.51mm (95% CI 1.36–1.65) posteriorly. The LSV was significantly displaced superiorly to the prostate by 1.09–1.13 mm (95% CI 0.97–1.25) and posteriorly by 1.81mm (95% CI 1.67–1.96), but not laterally (mean 0.06mm, 95% CI –0.06 to 0.18). The calculated PTV margins (left-right, superior-inferior, posterior-anterior) were 4.9, 5.3–5.6 and 4.8mm for the prostate, 5.2, 7.1–8.0 and 9.7mm for the RSV, and 7.2, 7.5–7.6 and 8.6mm for the LSV.

**Conclusion:** There is a significant displacement of the PrSV relative to the prostate during radiotherapy. Greater margins are recommended for the PrSV compared to the prostate.

#### 4.4 INTRODUCTION

Seminal vesicle invasion (SVI) is detected in 7–24% of prostate cancer patients at presentation [718]. It is an important poor prognostic factor, indicative of aggressive disease with a high risk of metastases [718]. However, it is not uniformly fatal [719]. Radiotherapy studies have shown an improvement for high-risk disease, including SVI, with dose escalation [450] or androgen deprivation therapy [720]. The SWOG 8794 subset analysis of post-prostatectomy patients with SVI showed that adjuvant radiotherapy led to a significantly improved recurrence-free survival and a trend to better overall survival [721].

The risk for SVI in prostate cancer can be estimated using either Partin tables or Roach's formulae [613]. It is generally recommended that the seminal vesicles be included in the CTV for intermediate- to high- and very high-risk categories [214, 613]. Inclusion of the seminal vesicles in the CTV is important so that they receive an adequate dose [609].

Daily online targeting is verified according to the prostate position and does not necessarily account for seminal vesicle displacement. Studies have illustrated that the seminal vesicles can move in relation to the prostate [617-620, 622, 722, 723]. Most analysed the motion of the whole seminal vesicle to the tip. However, prostatectomy pathological analysis has shown that the SVI rarely extends beyond the proximal 2.0–2.5cm [724]. Guidelines recommend that only the proximal 1–2cm seminal vesicles (PrSV) should be included in the CTV [724]. Measures of the whole seminal vesicle motion and margins may not accurately reflect the PrSV.

The present study has minimised observer uncertainties by inserting gold fiducial markers into both the prostate and PrSV. This exploratory study aimed to quantify the inter-fraction

PrSV displacement relative to the prostate and evaluate the related PTV margins of the PrSV as recommended in clinical guidelines.

## **4.5 METHODS**

### **4.5.1 Study cohort**

This study was approved by our institutional Human Research and Ethics Committee. The overriding eligibility criteria were men with locally advanced prostate cancer [214], where the inclusion of the seminal vesicles in the radiotherapy volume was indicated. Patients were recruited prospectively after signing informed consent. The planned sample size of 25 men was considered sufficient to estimate margins. Some patients were excluded because of incorrectly placed fiducials, and therefore the protocol was amended and approved by ethics to increase the patient accrual number.

### **4.5.2 Gold seed insertion technique**

The Northwest Medical Physics Equipment (NMPE)<sup>®</sup> Soft Tissue Marker Kit (P/N 887-825) was utilised. Three 3mm x 1.2mm gold fiducials were inserted by a single experienced urologist under sedation and antibiotic prophylaxis using transrectal ultrasound guidance. The seminal vesicle fiducials were inserted to define the proximal 2cm of the seminal vesicles and confirmed at CT simulation. The five fiducials were positioned as follows: Seed 1 on right prostate base, Seed 2 on left prostate mid-gland, Seed 3 on the right prostate apex, Seed 4 on the right seminal vesicle (RSV), and Seed 5 on the left seminal vesicle (LSV).

#### 4.5.3 Image acquisition

CT simulation was performed on a General Electric Radiation Therapy Lightspeed Widebore® helical scanner (General Electric Healthcare, Buckinghamshire, UK) with a resolution of 512x512 pixels, pitch 0.75, no gap and a slice thickness of 1.25mm, 2 weeks following fiducial insertion. Patients were positioned supine with a custom foam Alpha cradle placed on an indexed pelvic board with foot stocks. A standard bladder and bowel protocol was used to have a comfortably full bladder and empty rectum (Microlax® enema). Orthogonal digitally reconstructed radiographs (DRRs) were generated from the CT and used as the reference images for verification. All patients were treated to a total dose of 78Gy in 39 fractions using the departmental IMRT protocol on an Elekta® Synergy linear accelerator (Elekta, Stockholm, Sweden). Daily pre-treatment orthogonal electronic megavoltage (MV) portal verification images were performed for each of the 39 fractions, that is, an anterior-posterior image (API) and left lateral image (LLI) with a resolution of 512x512 pixels.

#### 4.5.4 Image verification

The correctional shifts are calculated relative to the isocentre of the linear accelerator. The patient is positioned on the treatment couch. The couch is moved to align the patient to the machine isocentre by aligning the pre-determined patient tattoos with the orthogonal laser coordinate system. Image verification then determines if further fine-tuning of the couch position is required. This final position becomes the relative zero point for the shifts. The relative movement of the proximal SV to the prostate is calculated from the directional difference between the proximal SV shift and the prostate shift.

Two trained observers (radiation therapists) independently matched the daily verification images with the reference DRRs using Elekta iView® software (Elekta, Stockholm, Sweden) using four different marker matching methods relative to the initial set-up. The four matching methods were: prostate three seeds (prostate), RSV seed, LSV seed, and pelvic bones (bone) for historical comparison. The observers were blinded to the other observer's matches. The correctional shifts were recorded for each of the four different marker matches in millimetres for the two images **relative to the isocentre**:

1) Lateral left-right (LR) and superior-inferior (SI) correctional shifts for the API

2) Anterior-posterior (AP) and SI shifts for the LLI.

#### 4.5.5 Statistical methods

The statistician independently checked all the data for data entry errors by comparison with the original handwritten records. No genuine outliers were excluded.

To compare the fiducials, analysis of variance (ANOVA) was performed on the API and LLI separately, adjusting for patients, fractions within patients, and observers. If the ANOVA showed significant differences between fiducials ( $p < 0.05$ ), their means were compared using t-tests based on the ANOVA standard error of the difference. As there were no pre-specified hypotheses and six possible pairwise comparisons between the four fiducials, the least significant difference between the means at the 5% level ( $LSD_{0.05}$ ) was adjusted for the number of non-significant comparisons, if any, using the Hochberg-Benjamini modification of the Bonferroni correction to maintain the overall probability of a false positive conclusion (type 1 error) at less than 0.05 [725]. Ninety-five per cent confidence intervals (CI) for differences between means were calculated as the difference  $\pm LSD_{0.05}$ .

To assess the adequacy of PTV margins, the means and standard deviations (SD) for each patient over 39 fractions and two observers were calculated. We then derived the overall mean (group systematic error), the SD of the means (systematic error,  $\Sigma$ ) and the root mean square of the SD (random error,  $\sigma$ ). The margins were calculated according to the formula:  $\text{margin} = 2.5\Sigma + 0.7\sigma$  [726]. The PTV margins calculated from the inter-fraction displacements take into account uncertainties including set-up, delineation/verification and inter-fraction motion. The formula does not account for the overall mean shift (group systematic error) of the seminal vesicles relative to the prostate. GenStat<sup>®</sup> statistical software, version 18.1 (VSNi, Hertfordshire, UK), was used for the analysis.

## 4.6 RESULTS

### 4.6.1 Baseline characteristics of the study cohort

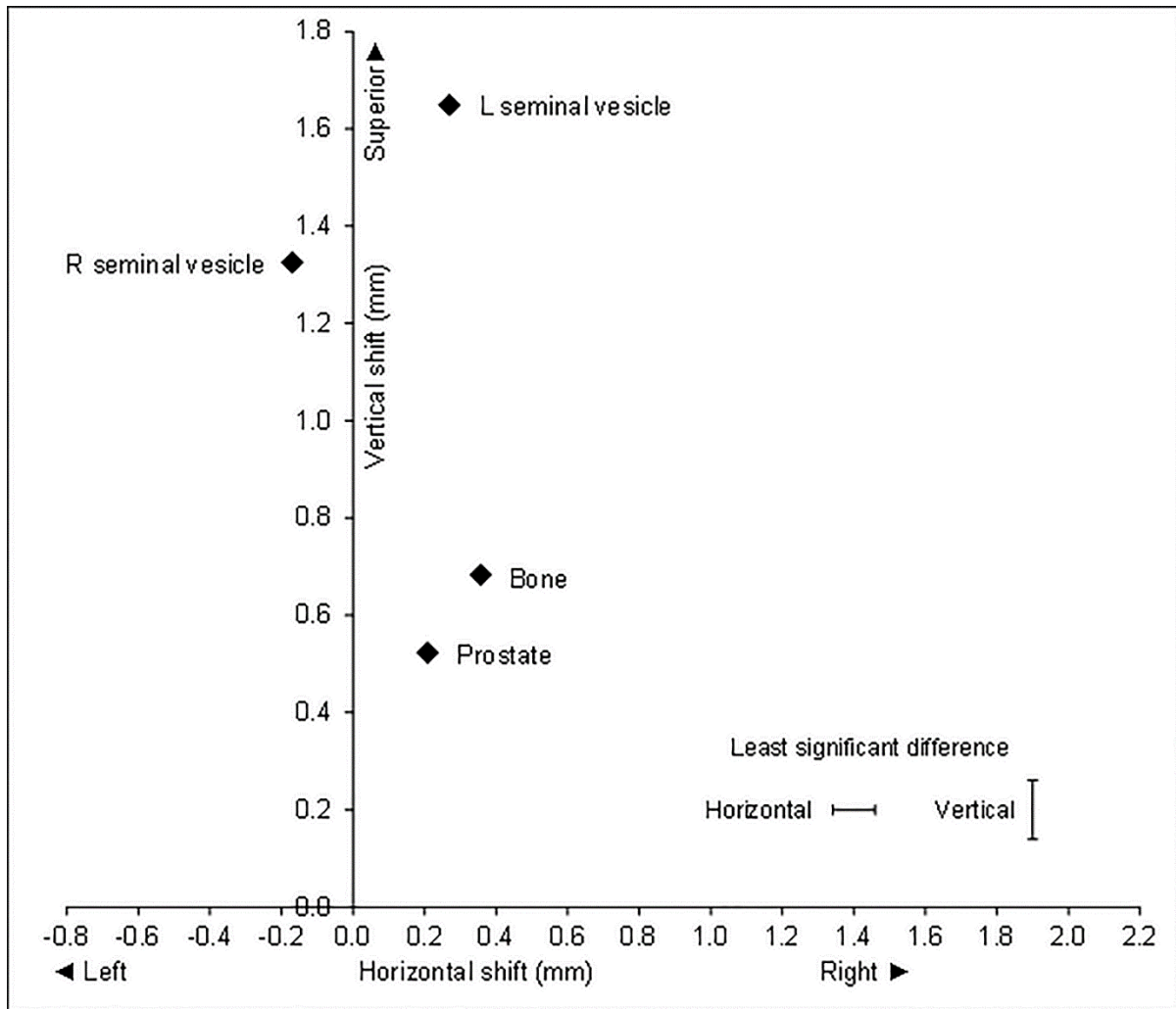
The patients were accrued over 3 years from 7 August 2006 to 15 May 2009. Forty-three patients were enrolled, but 13 were excluded from analysis because at least one seed was incorrectly placed, that is, missing, not within the prostate or not in the PrSV (eight); had migrated (one); or images were unclear or lost due to power failure (four). The final cohort consisted of 30 men with locally advanced prostate cancer: two patients (7%) with National Comprehensive Cancer Network (NCCN) [214] very high risk, 13 (43%) with high-risk and 15 (50%) with intermediate-risk prostate cancer. The mean age was 69 years (SD 6.3, range 55–77). The mean PSA was 12 (SD 10.3, range 0.4–54.2). T stages were T1c (n=10), T2 (n=10) and T3 (n=10). All but three had Gleason scores  $\geq 7$ .

The total dataset potentially consisted of 18,720 shifts in two dimensions (30 patients x 39 fractions x 2 images x 2 observers x 4 marker sites). Of these, 190 shifts (1%) were

missing. The reasons were image problems – image not taken, lost or poor quality (132 shifts or 0.7%) – or observer errors, for example, measured the wrong image or not appropriately recorded (58 shifts or 0.3%).

#### 4.6.2 Comparison of fiducials on the anterior-posterior image

The ANOVA on the shifts for the AP image showed there were highly significant differences between fiducials, both in the LR and SI directions ( $p < 0.001$ ,  $n = 9,250$ ) (Figure 4.1). Overall, the prostate, bone and LSV shifted to the right, and the RSV shifted to the left compared to the initial set-up. All fiducials shifted superiorly, with the LSV moving the most.



Source: Austin Health

Figure 4.1 Anterior-posterior image: mean correctional verification shifts with respect to bone and gold seed fiducials in prostate, right seminal vesicle and left seminal vesicle, **relative to the isocentre**

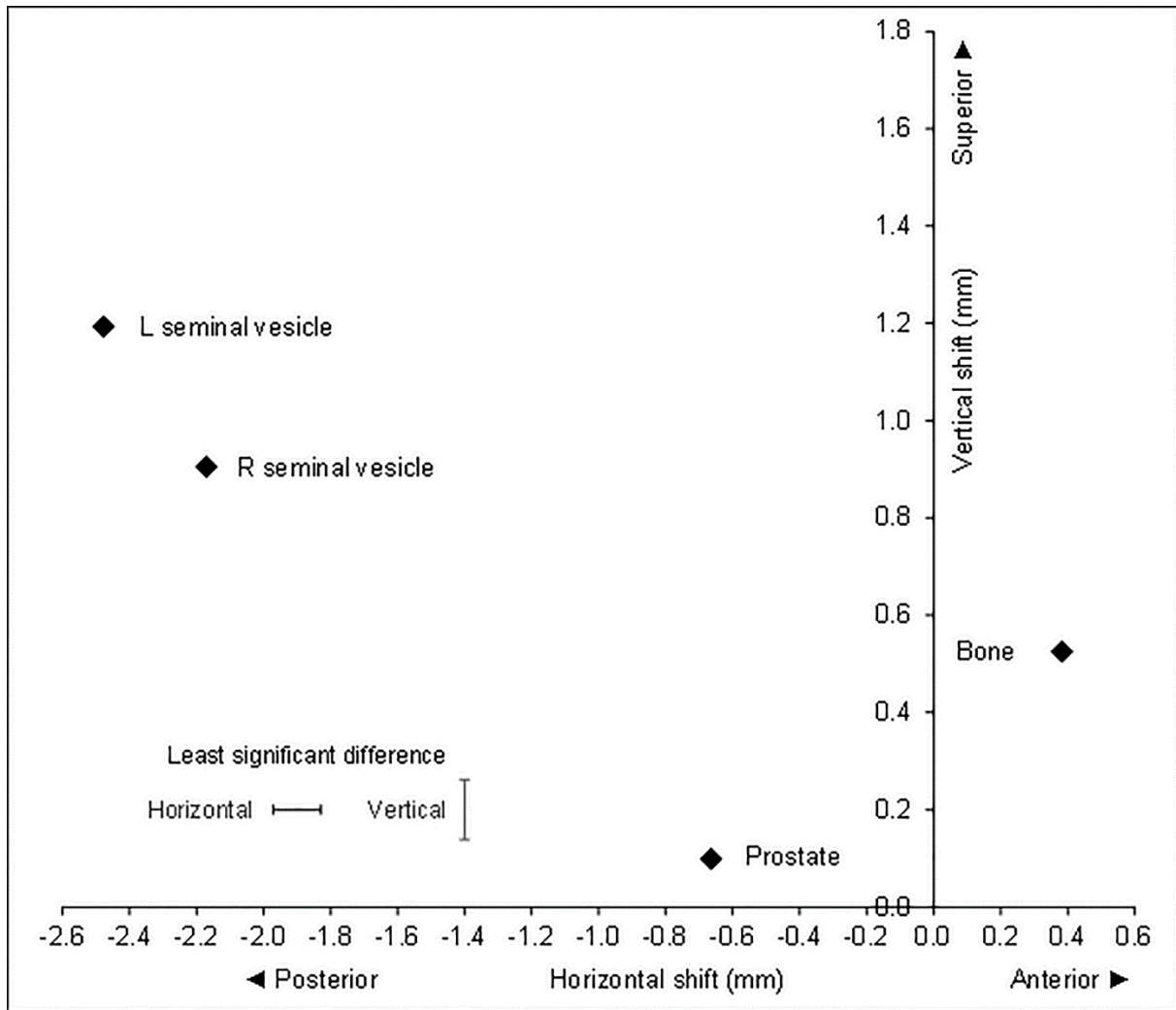
On average, the RSV and LSV correctional shifts were significantly greater than the prostate in the superior direction, and the RSV shifts were significantly more to the left than the prostate or the LSV. The mean shifts in millimetres for each verification method (LR, SI) were 0.21 and 0.52, respectively, for prostate; -0.17 and 1.33 for RSV; 0.27 and 1.65 for LSV; and 0.36 and 0.68 for bone. The standard errors of the difference between means for LR and SI directions were 0.050mm and 0.062mm, respectively. The least significant differences

( $p < 0.05$ ) were 0.12mm for the LR direction (adjusted for two non-significant comparisons) and 0.12mm for the SI direction (no adjustment required).

The displacement of the RSV relative to the prostate was 0.38mm to the left (95% CI 0.26–0.50) and 0.80mm superiorly (95% CI 0.68–0.92). The displacement of the LSV relative to the prostate was 0.06mm to the right (95% CI –0.06 to 0.18, not significant) and 1.13mm superiorly (95% CI 1.00–1.25). The mean shifts of the LSV and RSV were significantly different, with the LSV mean shift being superior to the RSV by 0.32mm (95% CI 0.20–0.44). Interestingly, the LSV mean shift was to the right and the RSV shift was to the left, indicating that both shifts were toward the midline, that is, they are closer together by 0.44mm (95% CI 0.32–0.56) (Figure 4.1).

#### 4.6.3 Comparison of fiducials on the left lateral image

The ANOVA showed that there were highly significant differences between the fiducials, both in the AP and SI directions ( $p < 0.001$ ,  $n = 9280$ ) (Figure 4.2). The prostate and both RSV and LSV shifted posteriorly, and the bone shifted anteriorly compared to the initial set-up. Both seminal vesicles and bone shifted superiorly, with the LSV moving the most.



Source: Austin Health

Figure 4.2 Left lateral image: mean correctional verification shifts with respect to bone and gold seed fiducials in prostate, right seminal vesicle and left seminal vesicle, **relative to the isocentre**

The mean shifts in millimetres for each verification method (AP, SI) were  $-0.66$  and  $0.10$ , respectively, for prostate;  $-2.17$  and  $0.91$  for RSV;  $-2.48$  and  $1.19$  for LSV; and  $0.38$  and  $0.53$  for bone. The standard errors of difference between means for the AP and SI directions were  $0.073\text{mm}$  and  $0.063\text{mm}$ , respectively. The least significant differences ( $p < 0.05$ ) were  $0.14\text{mm}$  and  $0.12\text{mm}$  for the AP and SI directions, respectively. All differences were significant ( $p < 0.05$ ), so no adjustments were required for the  $\text{LSD}_{0.05}$ .

The RSV and LSV correctional shifts in the AP and SI directions were significantly greater than the prostate. The displacement of the RSV relative to the prostate was 1.51mm (95% CI 1.36–1.65) posteriorly and 0.81mm (95% CI 0.68–0.93) superiorly. The displacement of the LSV relative to the prostate was 1.81mm (95% CI 1.67–1.96) posteriorly and 1.09mm (95% CI 0.97–1.22) superiorly. The mean shifts of LSV and RSV were significantly different, the LSV shift being greater than the RSV shift with a displacement of LSV relative to RSV of 0.31mm (95% CI 0.16–0.45) posteriorly and 0.29mm (95% CI 0.16–0.41) superiorly (Figure 4.2).

#### 4.6.4 Planning target volume margins

The CTV to PTV margins of the prostate and PrSV were calculated for both verification images for each axis (Table 4.1). The margins for the seminal vesicles are larger than for the prostate, except in the case of LR shifts for the RSV. The difference in margins between the RSV and prostate were LR 0.3mm, AP 4.9mm and SI 1.8–2.4mm. The differences between the LSV and prostate margins were LR 2.3mm, AP 3.9mm and SI 1.9–2.3mm.

Table 4.1 Planning target volume margin calculation based on prostate and seminal vesicle shifts

Anterior-posterior image								
Matched on	+ Right / - Left				+ Superior / - Inferior			
	Overall mean	SD mean	RMS SDs	Margin	Overall mean	SD mean	RMS SDs	Margin
		Systematic error	Random error			Systematic error	Random error	
	(M)	( $\Sigma$ )	( $\sigma$ )	(mm)	(M)	( $\Sigma$ )	( $\sigma$ )	(mm)
Prostate	0.21	1.354	2.162	4.90	0.53	1.315	2.900	5.32
RSV	-0.17	1.372	2.553	5.22	1.33	1.963	3.147	7.11
LSV	0.29	2.103	2.706	7.15	1.65	2.109	3.303	7.58
Bone	0.36	1.503	2.165	5.27	0.69	2.137	2.627	7.18
Left lateral image								
Matched on	+ Anterior / - Posterior				+ Superior / - Inferior			
	Overall mean	SD mean	RMS SDs	Margin	Overall mean	SD mean	RMS SDs	Margin
		Systematic error	Random error			Systematic error	Random error	
	(M)	( $\Sigma$ )	( $\sigma$ )	(mm)	(M)	( $\Sigma$ )	( $\sigma$ )	(mm)
Prostate	-0.66	1.110	2.843	4.77	0.10	1.450	2.780	5.57
RSV	-2.20	2.899	3.524	9.71	0.91	2.301	3.191	7.99
LSV	-2.48	2.426	3.685	8.65	1.20	2.098	3.244	7.52
Bone	0.38	2.159	2.439	7.10	0.53	2.270	2.533	7.45

LSV = left seminal vesicle, RSV = right seminal vesicle

Overall mean (M) = mean of the mean shifts for 30 patients = group systematic error; SD mean ( $\Sigma$ ) = standard deviation of the mean shifts for 30 patients = systematic error; root mean square (RMS) SDs ( $\sigma$ ) = square root of the mean of the squares of the standard deviations for 30 patients = random error; and PTV margin =  $2.5\Sigma + 0.7\sigma$ .

Source: Austin Health

## 4.7 DISCUSSION

This exploratory study specifically assessed the motion of the PrSV, rather than the entire seminal vesicles. Gold fiducials were used to define the prostate as well as the PrSV to approximate a point-to-point co-registration and minimise observer and verification error.

This study found significant displacement of the seminal vesicles relative to prostate verification using gold fiducials, and to bone match. We observed significant movement of the RSV relative to LSV. The LSV showed the greatest displacement. This can be expected as the displacement of the seminal vesicles is mainly due to rectal filling [617, 619], which is usually asymmetrical. The calculated margins for both seminal vesicles were greater than the prostate.

While it is recommended that the PrSV be included in the CTV, studies of seminal vesicle motion have investigated the entire seminal vesicles. They have confirmed that the seminal vesicles move relative to the prostate. The prostate was defined by three fiducials or contoured prostate centroid. The movements, both systematic and random, of the entire seminal vesicles, were reported to vary from 1.1 to 1.9mm and 0.4 to 1.4mm LR, 2.8 to 7.3mm and 1.2 to 3.1mm AP, and 2.2 to 3.6mm and 0.06 to 2.1mm SI, respectively. The PTV margins ranged from 4.5mm to 15mm [617-624].

The variation in seminal vesicle displacement measurements is likely due to differences in methodology in defining the prostate and seminal vesicles. Additionally, investigations of seminal vesicle motion have varied in the verification method, patient number and type and number of scans. Most investigations of seminal vesicle displacement have contoured the entire seminal vesicle length +/- prostate on multiple CTs. These studies are subject to a

greater observer variability as it is difficult to define the PrSV on CT or cone beam CT (CBCT). The PrSVs are attached to the posterior prostate over a varied length and are difficult to differentiate as they have similar Hounsfield unit and grey values. Therefore, defining the start of the seminal vesicle adjacent to the prostate and, subsequently, its length and position is subject to observer variation. The seminal vesicles are more easily defined on MRI as they are hyperintense on T2-weighted imaging compared to the prostate.

CT contouring studies of the prostate and seminal vesicles have illustrated this observer variation [727]. A report on the intra-physician variation for prostate contouring calculated a variation of 0.8, 1.1 and 1.5mm for the posterior, anterior and right-left directions, respectively, with an inter-observer standard deviation of 1.5, 1.4 and 2.0mm in the posterior, anterior and right-left directions, respectively [727]. For the seminal vesicles, they reported inter-observer variability of 1.5, 2.8 and 2.3mm in the posterior, anterior and lateral directions and intra-observer variability of 1.2, 1.2 and 1.5mm, respectively. The largest CT inter-observer variation appears to occur at the prostatic apex [728]. This ranged from 5.4 to 10.7mm [728]. Importantly, this observer variation is not dissimilar to and sometimes greater than the measure of the seminal vesicle displacements. The observer uncertainty may cloud the precise measurement and direction of the seminal vesicle motion.

Other investigators used greyscale matching techniques to calculate changes in seminal vesicle position relative to the prostate. A notable study compared entire seminal vesicle greyscale registration using CBCT, relative to prostate implanted fiducials [620]. They noted significant systematic and random seminal vesicle displacements of 1.6mm and 2.0mm in the LR direction and 2.8mm and 3.1mm in the AP direction, respectively. They did not find any difference between the RSV and LSV. These measurements are useful for entire seminal

vesicles as they are not subject to contouring errors and relate to a verification method that is used clinically. However, the measurements may be subject to registration errors, especially when dealing with issues such as seminal vesicle deformation.

Another interesting study quantified the PTV margins required to provide the adequate dosimetric margin of the entire seminal vesicle versus the proximal 1cm of the seminal vesicle. [729]. Twenty patients had three CT scans, and the contoured seminal vesicles were related to three intra-prostatic fiducials. They illustrated that the seminal vesicles move differentially from the prostate with a greater variation and distance. To ensure 95% coverage for 90% of patients, a margin of 8mm and 5mm was required for the entire seminal vesicle and PrSV, respectively. The PrSV margin was the same as the prostate margin. Conversely, our study found that the margin for the PrSV was greater than that of the prostate. The differences may have related to the different lengths of seminal vesicle used in this study (1cm versus 2cm in our study). Other causes may have related to observer variation with organ delineation and motion assessment technique.

MV imaging was selected for verification as the study protocol, and implementation occurred before and during a rapid departmental transition from MV to kV (kilovoltage) imaging and then CBCT. KV imaging affords better tissue contrast and CBCT provides volumetric imaging and rotational shifts. However, to maintain consistency with the initial patients it was decided to continue with MV as the gold fiducials were well visualised, only translational shifts were collected, and a well-performed prospective study by Moseley et al. had shown a highly significant correlation of isocentre shifts between MV, kV and CBCT fiducials [648]. Conversely, Gill et al. attributed a statistically significant smaller set-up error distribution with MV portal imaging compared to kV to the better image quality of kV [730].

The present study minimised observer uncertainty by using gold fiducials, multiple observers and all verification images. However, the impact of seminal vesicle deformation or seed migration was not assessed. CT quantification of seminal vesicle deformation analysis may be difficult as the PrSV origin is difficult to differentiate from the posterior prostate. Thus, it would be ambiguous as to whether the deformation, for example, shortening or lengthening, was occurring uniformly or differentially along its length. This could add to uncertainties in contouring and registration studies of seminal vesicle motion, whereas translational shifts of a fiducial defining the PrSV will at least, in part, reflect the deformation in the calculated margins. MRI may provide a more precise analysis of seminal vesicle motion and deformation.

Fiducials were inserted into the PrSVs under ultrasound guidance, and position confirmed at CT simulation. CT and CBCT may have detected gross fiducial migration. However, limited migration would be challenging to differentiate from seminal vesicle displacement or deformation. Reassuringly, most fiducial studies of prostate and other organs have shown only a very small proportion of fiducials migrate during radiotherapy, and the distance is small [731, 732]. Consequently, it is unlikely that fiducial migration would greatly affect the results.

In summary, a gold fiducial inserted into the SV defines a fixed anatomical segment of the PrSV. The subsequent shifts reflect motion and deformation that can be followed during the radiotherapy course. The major caveat is possible migration of the fiducial; however, studies of gold fiducials in prostate and other sites have suggested that this is infrequent. In comparison, contouring matching methodologies are subject to uncertainties in relation to prostate contouring, SV contouring or both, of approximately 1 to 10mm. These

methodologies can be affected by deformation and rotation as the different segments of the PrSV may be contoured even if it is the same length.

The clinical scenario of gross SVI, either clinically or on MRI, was not addressed. The radiotherapy volume should cover the extent of SVI on MRI and consideration to treat the entire seminal vesicle would seem appropriate with gross SVI. Margins may need to be greater to cover the entire seminal vesicle, although a recent study has shown that grossly involved seminal vesicle is less mobile [733].

Many of the caveats of this and previous studies of inter-fraction displacement, including migration, deformation and intra-fraction motion, would be addressed with MRI volumetric imaging that includes cine (4D) studies [734] and possibly MRI fiducials. An elegant study of intra-fraction seminal vesicle displacements that contoured the entire MRI on cine MRI showed that the seminal vesicle centroid moved significantly more than the prostate in the SI direction but not in the AP or LR directions [734]. The displacement increased with time until 10 minutes, after which it plateaued. The study authors concluded that the seminal vesicles required larger margins in the SI direction. Furthermore, more sophisticated solutions to PrSV inter-fraction and intra-fraction motion could be investigated with adaptive radiotherapy techniques to account for both position and shape.

#### **4.8 CONCLUSION**

The study confirms that PrSV displacement is greater than prostate displacement. While margin expansion is department-specific, this study has illustrated that larger inter-fraction margins for PrSV should be considered, but careful attention is required regarding the

organs at risk, notably the rectum, especially when considering hypofractionated radiotherapy.

## Chapter 5 A PHANTOM STUDY TO CONTRAST AND COMPARE POLYMER AND GOLD FIDUCIAL MARKERS IN RADIOTHERAPY SIMULATION IMAGING

---

Daryl Lim Joon<sup>a</sup>, Drew Smith<sup>a</sup>, Mark Tacey<sup>a</sup>, Michal Schneider<sup>b</sup>, Benjamin Harris<sup>a</sup>, Wee Loon Ong<sup>a</sup>, Farshad Foroudi<sup>a</sup>, Trish Jenkins<sup>a</sup>, Morikatsu Wada<sup>a</sup>, Michael Chao<sup>a</sup>, Kym Rykers<sup>a</sup>, Vincent Khoo<sup>a,c</sup>

<sup>a</sup> Department of Radiation Oncology, Olivia Newton-John Cancer Wellness and Research Centre, Austin Health, Heidelberg, Australia

<sup>b</sup> Department of Medical Imaging and Radiation Sciences, Monash University, Clayton, Australia

<sup>c</sup> Royal Marsden NHS Foundation Trust, London, UK

Submitted: Lim Joon D, Smith D, Tacey M, Schneider M, Harris B, Ong WL, Foroudi F, Jenkins T, Wada M, Chao M, Rykers K, Khoo V. A phantom study to contrast and compare polymer and gold fiducial markers in radiotherapy simulation imaging. Submitted to Scientific Reports, 2021.

## 5.1 PREFACE

Chapter 5 represents a manuscript that has been submitted for peer review to *Scientific Reports* in 2021 and is currently under review.

The preceding chapters concentrated on the major clinical radiotherapy processes in terms of radiotherapy planning using co-registered magnetic resonance imaging (MRI) to define the target more precisely and then radiotherapy treatment to deliver the radiation to the target more accurately. Standard gold seeds were used to track target motion during radiotherapy delivery. However, gold does have caveats, particularly computed tomography (CT) artefacts that can obscure vital anatomical structures. The next chapters explore a commercially available polymer fiducial as a viable alternative. The initial in vitro investigation studies the imaging characteristics of polymer fiducials for CT and MRI, as was utilised in Chapter 2, in a normal tissue–equivalent phantom.

Historically, positional verification was based on pelvic bone alignment, most often using orthogonal images using film. Film verification was time-consuming, so it was usually only done weekly after treatment. However, the prostate can move relative to the pelvic bones, and thus this method was considered insufficient for dose-escalated intensity-modulated radiotherapy (IMRT) for prostate cancer.

A more accurate prostate target localisation method includes biologically inert radiopaque fiducial markers, most commonly gold seed fiducials. Typically, three are inserted into the prostate. This use of image guidance with gold fiducials has improved the outcome and reduced toxicity of radiotherapy.

However, the downside of gold's high Z value is a substantial artefact from the scattering of X-rays that can reduce accurate fiducial definition. This can lead to imprecise image guidance, as well as obscuring prostate and normal tissue anatomy resulting in inaccurate target delineation. Alternative markers are available but are not well studied. Polymer fiducials have been considered as an alternative to gold because of their reduced artefact on X-ray imaging and improved visualisation on MRI, but they have only undergone general evaluation.

Two related studies have been completed for this thesis relating to the use of polymer seeds. This first study aims to evaluate the visibility and artefact of polymer fiducials compared to gold fiducials in radiotherapy CT and MRI.

## **5.2 CONTEXT**

The study investigated a new fiducial material, polymer. The study initially analysed the polymer fiducial's characteristics and compared them to the standard gold marker in a phantom, before implementing a more comprehensive clinical study in prostate cancer patients. The study developed a phantom that was greyscale tissue-equivalent in CT and MRI. An analytical tool was also designed to study the artefact and phantom greyscale in 2D. The study showed some advantages of the polymer fiducial in CT imaging in terms of less artefact than gold, and similar characteristics to gold on MRI; therefore, the patient investigation proceeded (Chapter 6).

### 5.3 ABSTRACT

**Aim:** To assess visibility and artefact characteristics of polymer fiducials compared to standard gold fiducials for radiotherapy computed tomography (CT) and magnetic resonance imaging (MRI) simulation.

**Materials and methods:** Three gold and three polymer fiducials were inserted into a CT and MRI tissue-equivalent phantom that approximated the prostate cancer radiotherapy configuration. The phantom and fiducials were imaged on CT and MRI. Images were assessed in terms of fiducial visibility and artefact. ImageJ software was employed to quantify the pixel greyscale of each fiducial and artefact. Fiducial greyscale histograms and profiles were generated for analysis. Objective measurements of the contrast-to-noise ratio (CNR), signal-to-noise ratio (SNR) and artefact index (AI) were calculated.

**Results:** The CT images showed that the gold fiducials are visually brighter, with greater contrast than the polymer. The higher peak values illustrate this in the line profiles. However, they produce bright radiating and dark shadowing artefacts. This is depicted by the greater width of line profiles and the disruption of phantom area profiles. Quantitatively, this results in greater percentile ranges of the histograms. Furthermore, for CT, gold had a higher CNR than polymer, relative to the phantom. However, the CNR and SNR were degraded by the artefact, as shown by the greater AI. Both fiducials were visible on MRI, and had similar histograms and profiles that were also reflected in comparable CNR, SNR and AI.

**Conclusion:** Polymer fiducials were well visualised in a phantom on CT and MRI and produced less artefact than the gold fiducials. Polymer markers could enhance the quality and accuracy of radiotherapy co-registration and planning but require clinical confirmation.

## 5.4 INTRODUCTION

The increasingly conformal dose distributions of IMRT and volumetric modulated arc therapy (VMAT) require a more precise target definition and treatment delivery to achieve an optimal therapeutic ratio. For contemporary prostate IMRT, the combination of fiducial alignment and soft tissue analysis is the most accurate and widely available image-guided radiotherapy (IGRT) method [735]. Importantly, IGRT with fiducial markers has been shown to improve treatment results [650].

In addition, MRI plays a vital role in prostate radiotherapy contouring and increasingly in terms of verification on MRI linacs. Fiducial markers have been employed to assist in the co-registration of CT and MRI [736]. MRI, particularly T2-weighted MRI, can better visualise the normal anatomy and the tumour within the prostate for radiotherapy contouring [174, 525, 526], thereby reducing inter-observer variation [737]. Thus, fiducials have potential CT and MRI roles for both image co-registration and X-ray-based verification, including electronic portal imaging devices (EPID) and cone beam CT, and MRI verification on MRI linacs.

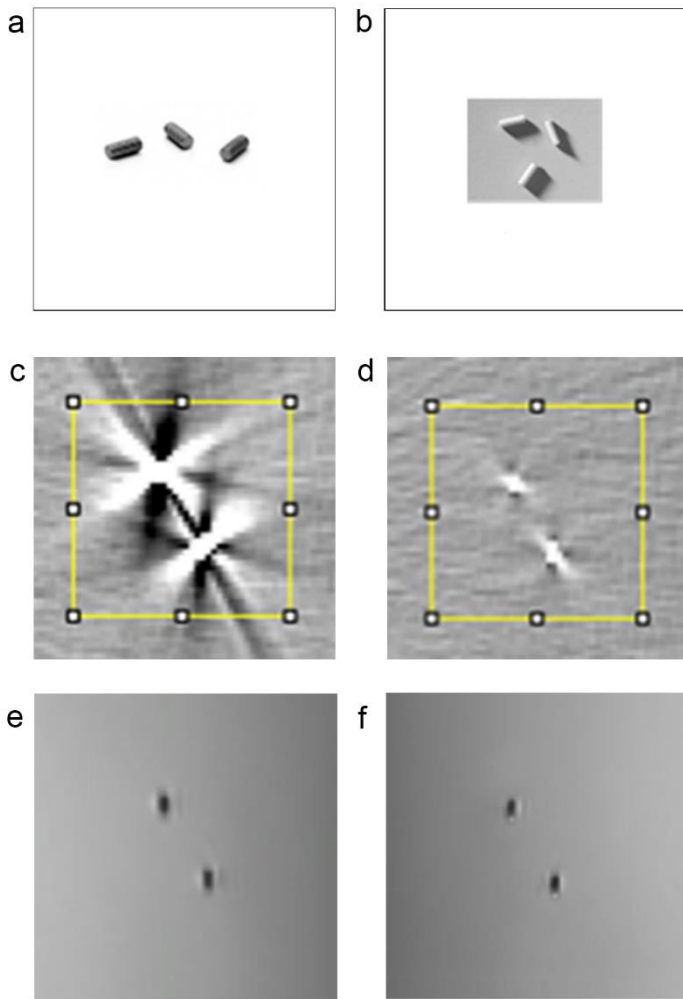
Gold fiducials are the most common fiducials used in prostate IMRT. Gold has a high Z value, making it radiopaque and highly visible with X-ray imaging. It is also safe to use with MRI and is biocompatible. However, the downside of the high Z value is a substantial artefact from the scattering of X-rays [625]. The artefact can interfere with accurate fiducial definition leading to imprecise image guidance [738]. It can also obscure adjacent prostate and normal tissue anatomy leading to inaccurate target delineation. Alternative fiducial markers are available but are not well studied [735].

Polymer fiducials (PolyMark™; CIVCO) have been promoted as an alternative to gold because of reduced artefact on X-ray imaging and improved MRI visualisation, but they have only undergone general evaluation [637, 738]. They are regarded as safe, as they are used clinically in multiple countries having passed appropriate regulatory standards. Hence, before considering polymer fiducials for prostate cancer clinical use, we investigated the polymer fiducials in a CT and MRI phantom study that approximated the prostate cancer scenario. The aim of the study was to assess the visibility and characterise the artefacts of the polymer fiducial compared to the standard gold fiducials on CT and MRI simulation images. If the results of this exploratory phantom study show a possible advantage for the polymer fiducials, then a clinical study using the methodological developments would be performed to assess whether they could replace the standard gold fiducials.

## **5.5 MATERIALS AND METHODS**

### **5.5.1 Fiducial markers**

Standard gold soft tissue fiducials measuring 0.9mm x 3mm and investigational PolyMark (polymer) fiducial markers measuring 1mm x 3mm (CIVCO Medical Solutions, Kalona, Iowa, USA) were utilised for the study (Figures 5.1a and 5.1b).



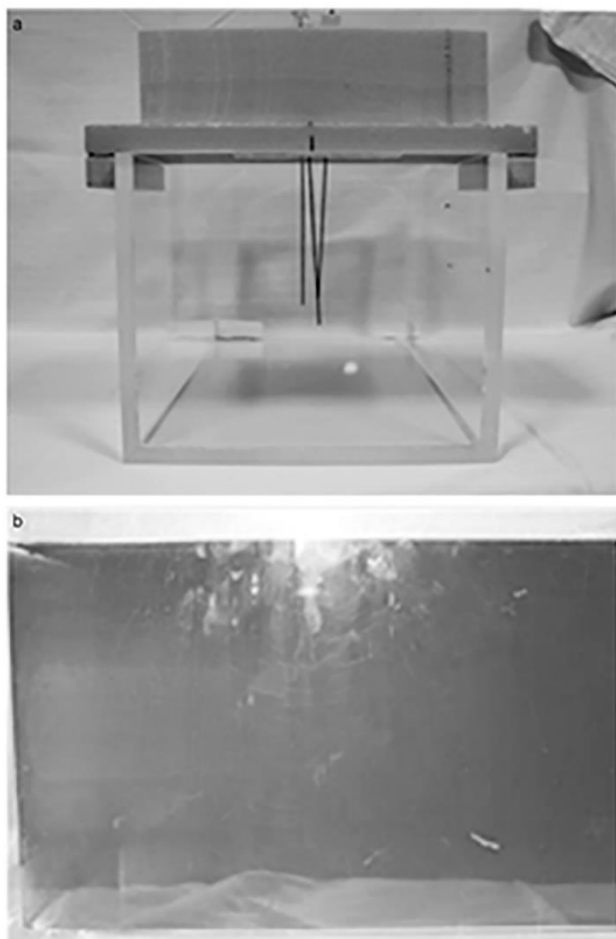
Source: Austin Health

Figure 5.1 (a) Gold seeds, (b) Polymer seeds, (c) CT of gold seeds with the defined area for the greyscale histograms, (d) CT of polymer seeds with the defined area for the greyscale histograms, (e) MRI co-registered with CT of gold seeds, and (f) MRI co-registered with CT of polymer seeds

### 5.5.2 Phantom

A purpose-built, in-house, uniform, gelatine-based phantom that was tissue-equivalent in both CT and MRI was constructed specifically for the study. A rectangular Perspex box, based on similar phantoms used for linear accelerator imaging quality assurance, was constructed to hold the phantom material (Figure 5.2a). It measured 330 x 230 x 190mm and was free

from metallic components. A high-density foam grid template was created to ensure reproducibility and avoid positional inaccuracy between the test groups (Figure 5.2a). This template positioned the gold and polymer fiducials precisely at either end of the phantom to simulate prostate cancer radiotherapy.



Source: Austin Health

Figure 5.2 (a) Perspex box for the phantom with rigid foam plate to guide needles with gold seeds for reproducibility, (b) Phantom contained within Perspex box

Following initial investigations, 200mL samples were produced using both 5% and 10% gelatine in addition to varying the diluent ratio of water to glycerol. Thus, three 5% gelatine

mixes and three 10% gelatine mixes were created, using water to glycerol ratios of 1:1, 2:1 and 3:1 for each. The six samples were then imaged on CT and MRI.

The 10% gelatine in water to glycerol ratio of 2:1 was selected for the study because of its superior appearance with respect to tissue equivalence on CT and MRI. A sufficient volume of the 10% gelatine mixed with the 2:1 water:glycerol solution was created and poured into the Perspex box (Figure 5.2b).

Once the mixture had set, the three gold and three polymer fiducial markers were placed within the phantom at mirrored positions using the template and native application apparatus needles (Sterile Placement Needle, 18GA ETW x 20cm, CIVCO Medical Solutions, Kalona, Iowa, USA). The three gold fiducials and three polymer fiducials were inserted at either end of the phantom around the phantom's long axis, 5cm from each short phantom side, and centred around the mid-depth for both fiducial sets. The positioning of the three fiducials approximated that used in prostate cancer. The gold and polymer fiducials were positioned far enough from the sides and each other, so they did not interact with the Perspex or other fiducial set.

The phantom containing the polymer and gold fiducials was then imaged on CT and MRI in a rapid sequence according to the parameters below. This ensured scanning parameters and the phantom were uniform for all fiducial measurements on CT and MRI, as the phantom can dry out, changing its physical characteristics and appearance with time. Alternative phantom material would be required to acquire measurements over a more prolonged time.

### 5.5.3 Imaging

The imaging parameters used for study CT and MRI are in accordance with those used for the clinical simulation for prostate cancer patients.

Simulation CT imaging was performed on a Lightspeed RT CT™ (GE®, Boston, Massachusetts, USA) with a 1.25mm slice width, helical, 0.75 pitch, no gap, 512x512 axial resolution, and a 650mm reconstruction diameter.

Simulation MRI was performed on a 1.5 T Magneto Avanto Syngo™ MR B17 (Siemens® Healthcare, Erlangen, Germany). The MRI sequence utilised for this study was a high-resolution 3D T2-weighted scan with a voxel size of 1mm, as it is used as the standard planning MRI scan at our centre.

### 5.5.4 Artefact measurement and analysis

Visual assessment, line and area measurements were analysed on DICOM transverse image files in a perpendicular plane corresponding to each fiducial marker's centre, that is, the three gold fiducials and three polymer fiducials.

ImageJ software (Rasband WS, ImageJ, US National Institutes of Health, Bethesda, Maryland, USA) was used to investigate and quantify the gold and polymer fiducials and image artefacts. It was used to assess the individual pixel greyscale values to generate line and surface profiles and histograms of greyscale for MRI and CT across a region of interest.

The line profiles graphically highlight the greyscale of the fiducials and artefacts within the phantom. The greyscale histogram plots mainly represent the phantom and display the phantom's disruption, which is mainly due to artefact as the fiducials only occupy a relatively

small number of pixels. The transverse CT and MRI images with the surface plots provide a visual comparison of the fiducials and the surrounding artefact terrain in the phantom, highlighting the artefact's interaction with multiple fiducials. This relatively simple and effective method was developed to illustrate the fiducials' similarities and differences in MRI and CT.

The horizontal line profile plots were generated by centring a 50mm and 20mm line over each of the three gold and three polymer fiducial markers on CT and MRI images, respectively. Longer lines were used with CT to incorporate the greater artefacts produced, particularly by the gold fiducials. The greyscale reading from each pixel along the line was measured for each fiducial and normalised relative to the average phantom grey value, that is, each pixel greyscale was divided by the average greyscale of the phantom material. Each pixel's average value for both the three gold and three polymer fiducials was then plotted on the final line plots. The line plots were used to illustrate the change in the greyscale relative to the distance across the phantom and fiducials. Line profile plots thus defined and highlighted the fiducial markers relative to the phantom.

Histograms and surface profiles were derived by centring a 50mm square region of interest (ROI) over each fiducial marker on the centre transverse slice for each respective seed. The raw greyscale pixel data for each fiducial was exported to Microsoft® Excel (Microsoft®, Redfern, USA) for analysis. The average value for each pixel for both gold and polymer was used for the histograms and plots.

The histograms show the distribution of pixel number having a particular greyscale value.

The pixel greyscale values were normalised relative to the background phantom grey value.

Most of the greyscale histogram represents the phantom as the fiducials occupy only a small number of pixels. A ratio of 1 represents the average phantom, whereas the spread of the histogram and slope relates to the artefact and its disruption of the phantom greyscale. The relative greyscale histograms were generated to highlight and contrast the artefact's effect on the more uniform phantom greyscale and indicate the amount of "true" greyscale phantom seen.

Descriptive statistics were prepared to compare the relative greyscale histograms for the polymer and gold fiducials for both the MRI and CT scans. Due to the non-normal distribution in the variation or range in voxel counts for the CT and MRI histograms, the relative grey values (artefact) attributable to each seed were measured as percentile ranges (1st to 99th, 5th to 95th, and interquartile range: 25th to 75th percentile).

To further quantify the fiducial visibility and artefact, objective measurements of the contrast-to-noise ratio (CNR), signal-to-noise ratio (SNR) and artefact index (AI) were calculated [739-741]. Two backgrounds were used to compare the contrast (CNR) and signal (SNR) for different fiducials: "Phantom", being distant from and not including the artefact; and the "ROI", being the 50mm square containing the artefact. The parameters were calculated for the three polymer fiducial and three gold fiducials. The means (standard deviation, SD) relate to the CT number for CT scans and greyscale for the MRI.

The CNR is an indicator of the relative image quality of the fiducial (i.e. visibility) being the ratio of contrast to noise. CNR equals the mean difference between the signal and the background divided by the background's standard deviation, that is,  $CNR = (\text{mean fiducial} - \text{mean background}) / (SD \text{ background})$ . The SNR compares the desired signal to the level of

background noise, or signal to noise. The SNR was calculated from the quotient of the mean signal of the background minus the fiducial and the SD, that is,  $SNR = (\text{background mean excluding fiducial}) / (\text{background SD excluding fiducial})$  <sup>[739, 740]</sup>. This provides a measure of the impact of the artefact on the image quality of the phantom surrounding the fiducial. Both background noise and metal artefacts can increase the SD. When considering SD as an expression of the metal artefacts (AI), the influence of the background (background SD) should be subtracted. Therefore, the AI was calculated as

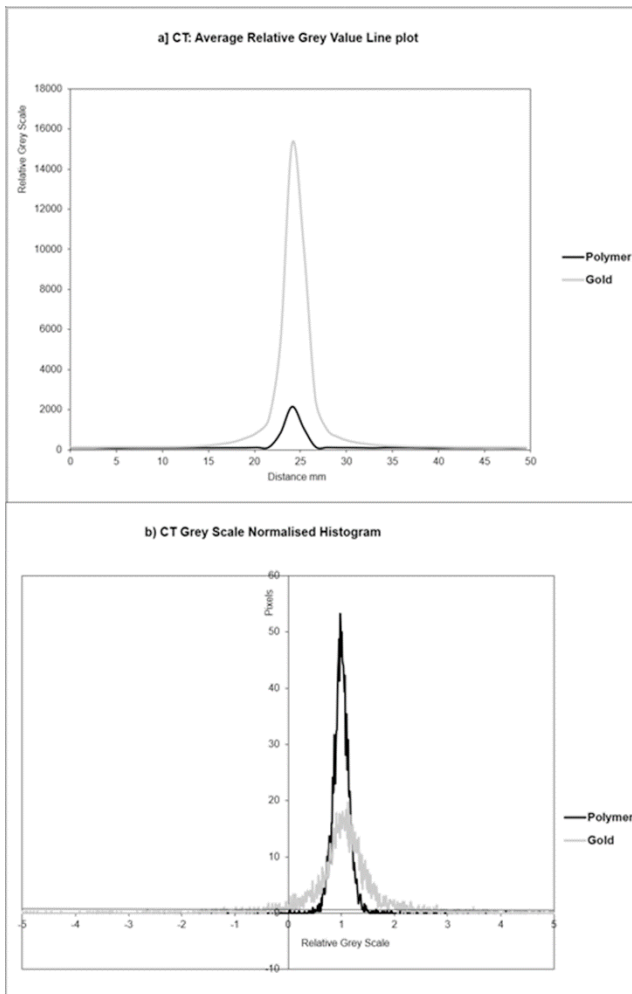
$$AI = \sqrt{(\text{ROI SD but excluding fiducial})^2 - (\text{Background SD excluding fiducial})^2}.$$

## 5.6 RESULTS

### 5.6.1 Computed tomography scan

The visual analysis showed that both the gold and polymer fiducials are bright and well seen on CT. However, the gold fiducials produce a greater amount of bright radiating and dark shadowing artefacts than the polymer seeds' relatively minor artefact (Figure 5.1c and 5.1d).

The CT horizontal greyscale line profile was generated through the fiducial centre (Figure 5.3a). The gold fiducials have a higher peak (15,279 in relative greyscale value) compared to polymer fiducials (2,168), indicating they are brighter, with greater contrast relative to the phantom and the polymer seed. The gold fiducials also exhibit a broader base indicating a greater spread of grey values, with an approximate relative greyscale range of 20mm compared to approximately 5mm for the polymer fiducials. Figure 5.3a is a graphical representation of the higher contrast and greater artefact of the gold fiducials compared to polymer fiducials.



Source: Austin Health

Figure 5.3 (a) Line profile of average relative pixel grey values along a 50mm horizontal line centred on each fiducial marker on CT, for polymer and gold, (b) CT histogram of average relative pixel grey values within a 50x50mm square centred on each fiducial marker on CT, for polymer and gold

The histogram of the normalised greyscale versus pixel number (Figure 5.3b) shows the effect of the fiducial and artefact on the phantom contained in the area of interest. The polymer histogram has a higher peak value around the centralised phantom grey value of 1, and the base was narrower (1st to 99th percentile: 0.6263 to 1.4848 for polymer fiducials compared to -3.6061 to 6.6970 for gold fiducials; Table 5.1; Figure 5.3b) showing that there is less spread of greyscale caused by the fiducial artefact and, to a lesser extent, the small

fiducial itself. The greater amount of the phantom greyscale being visible with the polymer fiducials is also illustrated by the smaller SD surrounding the mean values, and the narrower interquartile ranges surrounding the median and tighter percentile ranges (Table 5.1).

Table 5.1 A statistical comparison of the relative greyscale histograms (where the phantom normal tissue greyscale was normalised to 1) of the polymer versus gold fiducials, generated from a 50mm square centred on the fiducial for CT and MRI imaging. The mean (standard deviation; SD), median and percentile ranges highlight and contrast the artefact's effect on the more uniform phantom greyscale.

<b>Statistic</b>	<b>Polymer</b>	<b>Gold</b>
<b>CT</b>		
Mean (SD)	1.0645 (1.5304)	1.1311 (2.1159)
Median (interquartile range)	1 (0.9091 to 1.0909)	1 (0.7374 to 1.2727)
5th to 95th percentile	0.7475 to 1.2525	-0.3333 to 2.4343
1st to 99th percentile	0.6263 to 1.4848	-3.6061 to 6.6970
<b>MRI</b>		
Mean (SD)	1.0369 (0.0505)	1.0390 (0.0455)
Median (interquartile range)	1.0009 (0.9943 to 1.0075)	1.0004 (0.9949 to 1.0077)
5th to 95th percentile	0.9812 to 1.0163	0.9839 to 1.0169
1st to 99th percentile	0.9636 to 1.0339	0.9748 to 1.0315

CT = computed tomography, MRI = magnetic resonance imaging

The gold fiducials had a much higher CNR than the polymers relative to the phantom (Table 5.2). However, the greater contrast of gold was degraded by the artefact to a much greater extent than with the polymer when considering the CNR relative to the ROI that includes the artefact. SNR was similar for the gold and polymer fiducials relative to the phantom. However, the gold signal was degraded by a more considerable amount by the artefact in the ROI as it obscured the phantom signal. The much larger AI confirms the

increased artefact for the gold fiducial relative to the polymer, which degrades the contrast (increasing the CNR) and signal (increasing the SNR).

Table 5.2 Comparison of the mean (SD) of the CNR, SNR and AI of the polymer and gold fiducials in CT and MRI imaging. The means (SD) relate to the CT number for CT scans and greyscale for the MRI. CNR = contrast/noise = (fiducial mean – background mean) / (background SD). SNR = signal/noise = (background mean excluding fiducial) / (background SD excluding fiducial).

$$AI = \sqrt{(\text{ROI SD excluding fiducial})^2 - (\text{Background SD excluding fiducial})^2}.$$

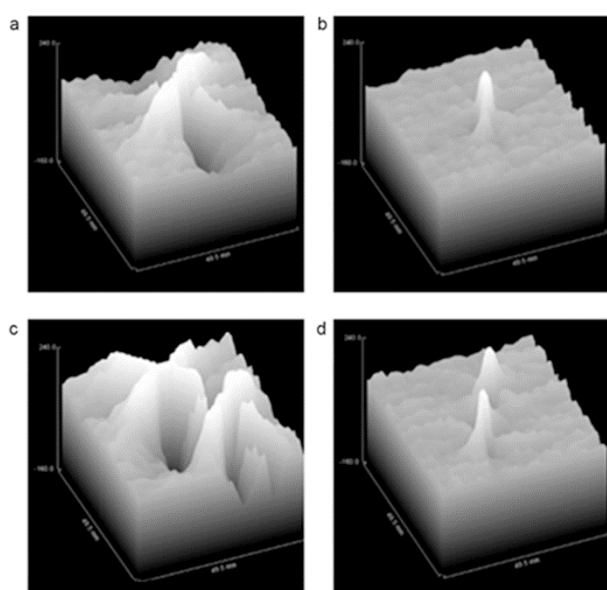
Two backgrounds were used for CNR and SNR: distant to the artefact for “Phantom”, and the 50mm square region of interest (ROI) containing the artefact for the “ROI”.

Statistic	Polymer Mean (SD)	Gold Mean (SD)
<b>CT</b>		
CNR (Phantom)	89.4 (25.4)	491.9 (24.7)
CNR (ROI)	54.2 (3)	30.1 (7.9)
SNR (Phantom)	103.5 (3.3)	97 (5.2)
SNR (ROI)	65.6 (15.3)	5.9 (1.3)
AI	13.7 (5.6)	191.6 (41.4)
<b>MRI</b>		
CNR (Phantom)	27.3 (5.1)	29.4 (4.4)
CNR (ROI)	21.2 (1.2)	24 (3.5)
SNR (Phantom)	70.2 (9.8)	106.9 (9.1)
SNR ROI)	52.8 (1.3)	85.4 (12.1)
AI	5.8 (0.9)	4.1 (1)

AI = artefact index , CNR = the contrast to noise ratio, CT = computed tomography, MRI = magnetic resonance imaging, SD= standard deviation, SNR = signal to noise ratio

Surface area greyscale profiles illustrated the fiducial’s impact on the surrounding phantom and demonstrated the interaction of multiple fiducials (Figure 5.4). The gold fiducial

produces a central peak but is surrounded by multiple irregular peaks and troughs of greyscale, representing the noisy artefacts around the fiducial (Figure 5.4a). The polymer fiducial produces a single well-defined peak with little perturbation of the surrounding gentle undulating terrain of the phantom greyscale (Figure 5.4b). This is further exemplified when two fiducials are in close proximity to each other, as would not uncommonly be seen in the clinical situation (Figures 5.4c and 5.4d).



Source: Austin Health

Figure 5.4 Area greyscale “terrain” of a 50x50mm square centred on (a) Single gold seed, (b) Single polymer seed, (c) Two adjacent gold seeds, and (d) Two adjacent polymer seeds, that provides an visual overview of the analysis

### 5.6.2 MRI scan

On MRI, the visual analysis showed that the gold and polymer fiducials have a similar appearance, being hypointense and thus dark on T2-weighted imaging relative to the phantom (Figures 5.1e and 5.1f). A mild uniform hyperintense area around the fiducials was

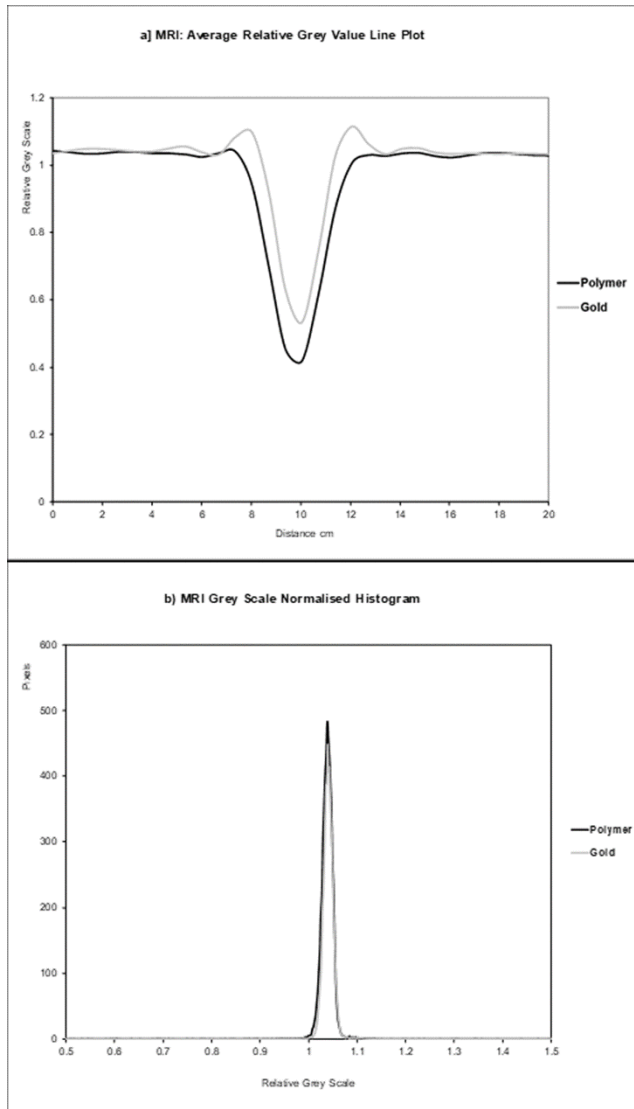
slightly more prominent with the gold fiducials. At one end of the polymer fiducials, a pronounced hyperintense area was due to the wax used to hold the fiducial in the needle. This was not present with the gold fiducial. The wax would usually be absorbed in vivo and thus would not be present on a clinical MRI.

A 20mm line profile was used with MRI because of the minimal artefacts from either fiducial (Figure 5.5a). The gold and polymer plots have a similar appearance. The main differences were that the polymer fiducials had a slightly darker greyscale trough than the gold fiducials (polymer relative greyscale value reaching a minimum of 0.4181 compared to 0.5328 for gold fiducials). Notably, there are small increases in the greyscale on either side of the peak base with the gold fiducials. This represents the small bright or hyperintense hue artefact around the fiducials, particularly the gold fiducials. The polymer fiducial's line profile appears slightly wider than the gold, but this may result from the polymer fiducial being slightly wider in diameter or a slight increase in dark artefact around the polymer fiducial.

The histogram of the MRI images shows that the polymer and gold fiducial plots are similar in appearance (Figure 5.5b). The polymer MRI normalised histograms show slightly wider percentile ranges (1st to 99th percentile: 0.9636 to 1.0339) when compared to the gold seeds (0.9748 to 1.0315), and a slightly larger standard deviation about the centralised mean value (0.0505 compared to 0.0455) (Table 5.1). The surface area profiles of both fiducials further showed the similarity between the two types of fiducial markers in that they produce minimal artefacts.

The gold and polymer fiducials' MRI CNR values show much smaller differences for MRI than CT relative to both phantom and ROI (Table 5.2). Gold has a higher SNR than polymer, but

the AI is almost equivalent. Thus, while gold has a higher signal than polymer, the contrast and artefact are similar to the polymer fiducials which is consistent with the visual appearance.



Source: Austin Health

Figure 5.5 (a) Line profile of average relative pixel grey values along a 20mm line centred on each fiducial marker on MRI, polymer and gold, (b) MRI histogram of average relative pixel grey values within a 50x50mm square centred on each fiducial marker, polymer and gold

## 5.7 DISCUSSION

The increasing precision of prostate radiotherapy requires a fiducial that can be visualised on multi-modality imaging with minimum artefacts. Therefore, to maintain consistency across imaging, a phantom was developed that was both CT and MRI tissue-equivalent. This is the first phantom to our knowledge with such dual properties. This phantom study has shown that polymer fiducials can be well seen on modern 3D imaging, such as MRI and CT. They produce fewer CT artefacts than the benchmark gold fiducials and appear at least equivalent to gold on MRI. This study further reinforces the findings in a recent prostate CT tissue-equivalent phantom study that included polymer fiducials, but provides further information by developing a phantom that was both CT and MRI tissue-equivalent [742].

The accuracy of MRI to planning CT co-registration may be improved with polymer fiducial matching as the fiducials are visible on CT and MRI. Use of polymer fiducials could also reduce interference from artefacts seen with gold that can conceal crucial soft tissue structures such as the prostate capsule, apex and dominant intra-prostatic lesion (DIL). The accurate co-registration of MRI and CT is essential as MRI-defined volumes are significantly smaller than CT because less normal tissue is included in target volumes [528-530]. Polymer fiducials reduce the contouring uncertainty, particularly at the prostate apex and base, and reduce the inter-observer and intra-observer variation [526, 531-533] and the dose to normal tissue [534]. MRI also better defines prostate cancer pathology, such as the DIL, extracapsular extension and seminal vesicle invasion. Metallic structures, such as gold, cause CT imaging anomalies, including distortion, metal artefacts and change in target density [633]. The distorted CT image can also result in inaccurate planning and delivery if not accounted for [633]. Polymer fiducials may minimise this problem.

Polymer fiducials may provide more accurate co-registration of cone beam CT to planning CT for treatment verification or IGRT. Comparison studies of IGRT/fiducial markers with IMRT versus non-IGRT treatments have shown a decrease in late gastrointestinal and genitourinary toxicity [650-652]. In one study, there was also an improvement in clinical outcome [650]. The toxicity difference can be attributed to the combination of the IMRT technique with a reduced dose to organs at risk, daily image guidance, and margin reduction that IGRT with fiducials safely permits.

The study's limitation is that the phantom was a uniform tissue density and a mobile size to provide an appropriate test environment. However, a human subject will have a greater thickness and heterogeneity, which may interfere with the fiducial visibility. Furthermore, the study did not analyse other markers available on the market. There are new fiducial markers that produce minimal distortion with CT imaging. Visicoil™ uses helical coils of gold to reduce the relative thickness and decrease the equivalent density, thus reducing image artefact [635]. Others use a mixture of low-density biocompatible materials and gold particles [634]. Additional alternatives utilise lower Z radiopaque materials such as stainless steel, titanium [636], and carbon or ceramic materials [625, 637].

Another limitation is that we did not have access to artefact suppression CT [633] during the investigation. While artefact suppression CT is becoming more common in clinical practice, it is not widespread in radiotherapy and not available for cone beam CT. Alternative MRI sequences were not used because of MRI time limitations in our centre. Investigations have shown that other MRI sequences such as T2\*2D and T2\*3D [743] and multi-parametric MRI with bTFE (balanced steady-state free precession sequence) [744] are better at visualising gold seeds. These sequences are not used commonly in radiotherapy, but their

implementation is being investigated with the recent advent of MRI simulators and MRI linacs in radiotherapy.

Nevertheless, these phantom results indicate that polymer fiducials may be more appropriate for X-ray-based imaging than the current standard gold markers. They are visualised as a discrete structure on CT and produce little to no image artefact. Given the CT visualisation improvements, combined with equivalent MRI visualisation and similar size and physical appearance, the polymer fiducial could improve radiotherapy treatment planning and localisation. However, they are more expensive than standard gold seeds.

The study was limited to the investigation of CT and MRI simulation images. The rationale was to focus on the major radiotherapy imaging tools and consider polymer fiducials to aid image co-registration. CT-based imaging, where the gold metallic artefact is an issue, forms the central part of contemporary radiotherapy in terms of geometry and dosimetry, whereas MRI has had a secondary function, being co-registered to CT. MRI's main function has been the identification of prostate anatomy and cancer pathology. However, it is becoming increasingly important as the primary modality of simulation and verification with the clinical introduction of MRI linacs [745, 746]. While the polymer fiducials have been approved for radiotherapy verification, future patient investigations are warranted to thoroughly test them against the standard gold fiducials across all modern verification modalities, including electronic portal imaging, cone beam CT and MRI. Notably, the polymer fiducials had less contrast than the gold fiducials, as evident from the CNR calculations. While gold fiducials are clearly seen for EPID or orthogonal kilovoltage (kV) verification, it is yet to be shown whether the polymer fiducials can be visualised with orthogonal matching, particularly lateral planar imaging, where pelvic bones could obscure the lower-contrast fiducials.

We have shown that polymer fiducials have good visibility and reduced artefacts compared to gold fiducials. The reduced CT artefact could enhance radiotherapy quality and accuracy by improving the visualisation of critical targets such as the prostate apex and allowing for more precise fiducial to fiducial verification, devoid of obscuring artefact. The polymer fiducials may have utility alongside the development of practice delivery protocols for MRI linacs for MRI linacs. However, the real value and cost-effectiveness of polymer fiducials in radiotherapy must be validated clinically before they can replace gold fiducial markers. A comparison of polymer and gold fiducials in prostate cancer patients is indicated based on these encouraging results.

### **Acknowledgements**

Leanne Elich and alphaXRT Pty Ltd, (Alexandria, NSW, Australia) for supplying the three polymer seeds.

## Chapter 6 A CLINICAL STUDY COMPARING POLYMER AND GOLD FIDUCIALS FOR PROSTATE CANCER RADIOTHERAPY

---

Daryl Lim Joon<sup>a</sup>, Colleen Berry<sup>a</sup>, Benjamin Harris<sup>a</sup>, Mark Tacey<sup>a</sup>, Drew Smith<sup>a</sup>, Nathan Lawrentschuk<sup>a</sup>, Shomik Sengupta<sup>a</sup>, Michal Schneider<sup>b</sup>, Megan Hall<sup>a</sup>, Michael Chao<sup>a</sup>, Farshad Foroudi<sup>a</sup>, Trish Jenkins<sup>a</sup>, David Angus<sup>a</sup>, Morikatsu Wada<sup>a</sup>, Vincent Khoo<sup>a,b,c</sup>

<sup>a</sup> Department of Radiation Oncology, Olivia Newton-John Cancer Wellness and Research Centre, Austin Health, Heidelberg, Australia

<sup>b</sup> Department of Medical Imaging and Radiation Sciences, Monash University, Clayton, Australia

<sup>c</sup> Royal Marsden NHS Foundation Trust, London, UK

Submitted: Lim Joon D, Berry C, Harris B, Tacey M, Smith D, Lawrentschuk N, Sengupta S, Schneider M, Hall M, Chao M, Foroudi F, Jenkins T, Angus A, Wada M, Khoo V. A clinical study comparing polymer and gold fiducials for prostate cancer radiotherapy. Submitted to Technology in Cancer Research & Treatment, 2021.

## 6.1 PREFACE

Chapter 6 represents a manuscript that has been submitted for peer review to *Technology in Cancer Research & Treatment* in 2021 and is currently under review.

As utilised in Chapter 4, three gold prostate fiducials have become the standard image-guidance method for prostate cancer radiotherapy as it has been shown to improve cancer-related and toxicity outcomes. Modern radiotherapy uses computed tomography (CT) simulation as a minimum and increasingly cone beam CT (CBCT) for daily online treatment verification. However, the high Z value of gold can lead to the substantial artefact on CT-based imaging, obscuring important anatomy of the targets and interfering with accurate verification. The previous chapter illustrated that polymer fiducials in a tissue-equivalent phantom compared favourably with gold as they were visible on CT and magnetic resonance imaging (MRI) and produced far less artefact. These results led to this prospective study comparing polymer and gold markers in patients with locally advanced prostate cancer.

Chapter 6 aims to compare and contrast polymer fiducials to the standard gold fiducials using clinical protocols for various radiotherapy imaging modalities to assess the visibility and relative artefact production in a population of prostate cancer patients.

## 6.2 CONTEXT

Chapter 5 was an exploratory phantom study to develop methodology and characterise polymer fiducials. Knowledge gained from this study was expanded to Chapter 6, which is one of the first clinical studies of polymer seeds in a prostate population.

The null hypothesis was that the polymer fiducials had the same visibility and artifacts as the gold and any differences are due to chance. The null hypothesis was rejected for visibility of polymers fiducials that were significantly inferior to the gold fiducials for CT and lateral KV. It was accepted for MRI, CBCT and APKV planar images where there were no significant differences in the visibility of the polymer and gold fiducials. The null hypothesis was also rejected for the artefact production on CT, whereby the polymer fiducials produced significantly less artefact than the gold fiducials.

Therefore the investigation showed that the polymer seeds were well seen on CT and CBCT imaging for clinical radiotherapy but produced less artefacts than gold. However, polymer fiducials were inferior to gold for orthogonal planar imaging, and, like gold, they were not well seen on T2-weighted MRI. The study provides essential information regarding the characteristics of polymer seeds for departments considering their deployment. Further clinical investigations of the impact on prostate contouring and verification would potentially enhance the understanding of their clinical utility and effect on patient outcomes. In addition, the 2D analytical methodology used in the previous study (Chapter 5) to investigate the artefact and fiducial characteristics were refined for analysis in 3D in Chapter 6.

The phantom model used in Chapter 5 was a uniform normal tissue similar to those used for radiotherapy quality assurance data collection. The phantom was used to minimize variables and explore the characteristics of polymer fiducials compared to gold in material that was normal tissue equivalent. However, prostates can have a varying heterogeneous greyscale, and thus, the fiducials are not well seen on patient MRIs. Therefore, phantoms are generally regarded as good representations of normal tissue but not necessarily a good representation of the variable human prostate of an older male. This chapter illustrated why the clinical

study is essential, as phantoms do not generally represent the variability seen in the human population. As with many investigations, it was considered very reasonable to start with an idealized model to learn from and obtain preliminary data before pursuing studies in humans.

### 6.3 ABSTRACT

**Purpose:** Image guidance with gold fiducials improves the outcome of prostate radiotherapy. However, gold produces artefact on computed tomography (CT) imaging, interfering with contouring and verification. The purpose was to compare polymer fiducials to the standard gold using clinical radiotherapy imaging modalities to assess the visibility and artefact in a prostate cancer patient population.

**Materials and methods:** The study cohort comprised 28 patients with locally advanced prostate cancer. Half had three polymer fiducials implanted into the prostate, while the remaining 14 had gold fiducials. Patients were imaged with CT, T2-weighted magnetic resonance imaging (MRI), cone beam CT (CBCT) and planar kilovoltage (kV) images. Fiducials were scored for visibility and assessed for CT artefact in the surrounding prostate tissue. The artefact was quantified from CT number, Hounsfield number (HU) histograms in terms of percentile ranges and proportion of voxels in HU normal tissue range of a 2cm sphere surrounding the fiducial.

**Results:** Gold and polymer fiducials were sufficiently visible for verification on CT and CBCT. The gold fiducials could be visualised well on kV planar imaging. However, the polymer markers were not suitable for verifying lateral kV imaging because pelvic bones obscured them. Neither polymer nor gold fiducials could be visualised on MRI. The polymer fiducial produced less artefact than gold on CT, having less voxel spread for the HU percentile ranges and a greater proportion of voxels in normal tissue range.

**Conclusion:** Polymer fiducials are a more suitable fiducial than gold for CT/CBCT in prostate cancer radiotherapy. They showed minimal artefact and good visibility in CT imaging.

However, they were not well seen on MRI or kV imaging, and thus are not suitable for co-registration or planar kV verification.

## 6.4 INTRODUCTION

Prostate cancer is one of the most commonly detected cancers in men and a leading cause of deaths [4]. Approximately 10–20% of patients diagnosed with prostate cancer will have locally advanced disease. Randomised studies have shown significant improvements in outcome for locally advanced prostate cancer using higher radiation doses [430, 446-449] and adjuvant androgen deprivation therapy [271, 431-433].

The therapeutic ratio is further improved with precision radiotherapy techniques such as intensity-modulated radiotherapy (IMRT) [474] and image-guided radiotherapy (IGRT) [650]. Modern IGRT methods for verification use daily online planar kilovoltage (kV) imaging and, more recently, cone beam computed tomography (CBCT). Both methods show good agreement; however, computed tomography (CT) provides additional information regarding the bladder and rectal filling [648].

Radiopaque fiducials for prostate target localisation are now widely used [589, 625-627]. Gold fiducials are the most used as they have a high Z value, making them radiopaque and highly visible with X-ray imaging. Gold fiducials, however, can cause artefacts on CT imaging that can interfere with contouring and verification. The ideal fiducial marker is easy to deliver, with good visibility, minimal distortion in CT imaging, minimal dose perturbation, biocompatibility with soft tissue and negligible migration [634]. Some suggest that a polymer marker may be a better fiducial.

The aims of the study were to compare polymer fiducials to the standard gold fiducials using clinical radiotherapy protocols to assess the visibility and relative CT artefact production in a population of prostate cancer patients.

## **6.5 MATERIALS AND METHODS**

The study was a prospective investigation that was approved by the hospital ethics committee. The study used identical standard clinical protocols for both fiducial types in terms of mode of insertion, simulation, treatment verification and image review to provide a valid clinical assessment of the polymer fiducials.

### **6.5.1 Patient accrual**

Patients with locally advanced prostate cancer with no contraindications to radiotherapy, magnetic resonance imaging (MRI) or fiducial insertion were invited to have polymer fiducial inserted as part of a prospective study. They were entered into the polymer fiducial group after signing the informed consent. Those patients who did not wish to participate were asked to join the comparator patient group, with the insertion of standard gold fiducials. They were entered into the comparator group after completion of the informed consent. The planned sample size of 14 men with polymer fiducials and 14 men with gold fiducials was considered sufficient for a technical analysis to account for differences seen in the phantom studies.

### **6.5.2 Fiducials**

PolyMark™ (polymer) fiducial markers measuring 1mm x 3mm and Gold Soft tissue markers measuring 0.9mm x 3mm (CIVCO Medical Solutions, Kalona, Iowa, USA) were used for the study. They were inserted into the peripheral prostate gland under sedation and antibiotic cover with transrectal ultrasound guidance. Three fiducials were implanted: one into the base, mid-gland and apex of the prostate.

### 6.5.3 Imaging simulation

Patients were positioned supine with an individualised foam Alpha cradle placed on an indexed pelvic board with foot stocks. Patients were scanned on Lightspeed RT CT™ (GE®, Boston, Massachusetts, USA), with 1.25mm slice width, helical, 0.75 pitch, no gap, 512x512 axial resolution, and 650mm reconstruction diameter.

The planning MRI was performed on a 1.5 T Magneto Avanto Syngo MR B17™ (Siemens® Healthcare, Erlangen, Germany). This study's MRI sequence was a high-resolution 3D T2-weighted scan with a voxel size of 1mm.

### 6.5.4 Treatment verification

Patients were treated on Elekta® linacs (Elekta®, Stockholm, Sweden), using IMRT to a dose of 78Gy in 39 fractions over 8 weeks. The departmental prostate verification protocol comprises daily pre-treatment, online CBCT. These were used to assess the visualisation of the polymer and gold fiducials on CBCT. The standard CBCT parameters consisted of 41cm diameter field of view (FOV), variable M10/M20 (scan length 12 or 24cm) depending on target size, 120 kV, 25 mA 40ms nominal per frame, 660 frames per scan (360 degrees rotation), 1mm voxel size, 2–3mm viewing slice resolution with an axial resolution of 512x512.

Patients also underwent weekly 2D orthogonal kV planar imaging: anterior-posterior (AP) and lateral as part of the imaging study. The Elekta® XVI (version 4.5+) kV imaging parameters were 120 kV, 25 (AP) or 32 (lateral) mA, and 40ms nominal per frame; and five frames averaged per image, 25.6x25.6cm imaging area and 0.25mm nominal pixel size (resolution 1024x1024).

### 6.5.5 Image assessment

The planning CT and MRI were transferred to MIM Maestro™ version 6.6.13 (Mim Software®, Cleveland, Ohio, USA) (MIM) as per clinical protocol for contouring. The visibility assessment and artefact analysis were performed in MIM.

All verification images were reviewed by the study radiation therapist, who routinely performs prostate radiotherapy verification and confirmed by the radiation oncologists. This was done to simulate the clinical situation and minimize observer variation. Subsequently, three representative CBCT and three pairs of kV planar images (AP and lateral) were selected for each patient for analysis – start, mid and end of treatment. The CBCT and kV planar images were transferred to Mosaicq™ (Elekta®, Stockholm, Sweden) as per the standard verification. The visibility assessment of CBCT and 2D kV images was performed in Mosaicq™ Image Review.

### 6.5.6 Fiducial visibility

To measure the fiducial visibility and minimise inter-observer variability, the study radiation therapist scored all the images.

3D imaging typically shows a single fiducial being visible on a single slice. Therefore, each seed was scored for visibility. The visibility was scored for simulation CT and MRI, and verification CBCT on a scale of 1 to 4 for each of the three fiducials – apex, mid-gland and base:

- 1) Clearly visible for verification
- 2) Visibility impaired but sufficient for verification
- 3) Visibility impaired but not sufficient for verification

4) Not visible and not sufficient for verification.

For 2D kV imaging, all three fiducials are visualised for verification simultaneously on each plane, that is, AP and lateral. Thus, the AP and lateral kV images were scored on the number of fiducials sufficiently visible for verification.

#### 6.5.7 Artefact analysis

A method was developed to analyse the artefact and seeds in a three-dimensional manner in the patient. A CT simulation represents the primary X-ray reference scan. Thus, artefact due to the fiducials was measured on the planning CT quantitatively using MIM's clinical imaging analysis tools.

The fiducials were initially manually contoured as for the standard verification. Then a 2cm diameter sphere was created around the contour centre. The fiducial, bone, physiological calcifications and rectal gas were subtracted from the sphere using the Boolean function to analyse the artefact's impact on normal tissue in this sphere. The voxel Hounsfield units (HU) for the sphere were then exported in bins of 5-HU each for analysis. The fiducials' characteristics were separately investigated as they produced very high HU signals compared to the artefacts.

These spheres of interest contained the normal prostate tissues and the 3D artefact of the relevant fiducial seed. MIM was used to create histogram plots of HU versus voxel count from the spheres. These histograms were used to assess the relative differences in HU variation surrounding each of the fiducial markers.

Most voxels within the sphere are normal prostate tissue density. The bright and dark artefact is seen as the voxel variation of HU outside the normal tissue range at the extreme high and low HU values, respectively, at the ends of the histogram.

Therefore, the greater spread of the histogram, the less normal tissue is represented as it is hidden by the high and low HU artefact from the fiducial. The spread of the histogram was analysed in terms of the percentile ranges in HU. This variation or range in voxel counts in the spherical contours that exclude the values attributable to each seed was measured by considering percentile ranges of 1st to 99th, 5th to 95th, 10th to 90th and interquartile range (25th to 75th). Hence, these analyses of the spheres focus on artefact production.

The normal tissue not hidden by the artefact was quantified by the proportion of voxels within normal tissue representative HU ranges of  $\pm 100$  HU and  $\pm 150$  HU. The greater the artefact, the less proportion of voxels were represented in this range.

#### 6.5.8 Statistical analysis

Descriptive statistics were prepared to illustrate the differences in patient characteristics, scan visibility, artefact variation and outcomes between the two fiducial marker types.

Frequencies and percentages were used to present results for categorical variables, with the Fisher's (exact) test used to test between groups. The mean  $\pm$  standard deviation (SD) or median and interquartile ranges (IQR) were used to present continuous variables, which were normally and non-normally distributed, respectively.

The percentile ranges and proportions were presented using median and IQRs and compared between the polymer and gold groups using the Mann-Whitney (rank-sum) test.

Adjustment for the clustering of up to three fiducials within each patient was considered using a mixed-effects model, with independent covariance structure.

Patient imaging data were collected as per standard processes and stored within password-protected systems. Data were collected and prepared in Microsoft® Excel (Microsoft®, Redfern, USA) and secured via password on a secure hospital server. Stata™ version 15.1 (StataCorp, College Station, Texas, USA) was used to conduct statistical analyses. A p-value of less than 0.05 was used to show statistical significance.

## **6.6 RESULTS**

### **6.6.1 Patient cohort**

Fourteen eligible patients with locally advanced prostate cancer were recruited to the polymer fiducial arm, and 14 patients were recruited to receive the standard gold fiducials. Table 6.1 provides a comparison of the demographic characteristics between the two groups. The gold fiducial patients were older than polymer patients ( $p=0.028$ ). Otherwise, there were no statistically significant differences between the two groups (Table 6.1). In relation to visibility, there was notably no significant difference in body mass index (BMI).

Table 6.1 Patient characteristics across the two groups

Factor	Gold	Polymer	<sup>c</sup> p-value
Number of patients	14	14	
Age (years), median ( <sup>b</sup> IQR)	77 (70, 78)	72 (68, 73)	0.028
<sup>a</sup> BMI, median ( <sup>b</sup> IQR)	26.2 (24.7, 31.4)	27.7 (27.0, 29.9)	0.44
Gleason score + total			0.79
3+4=7	4 (29%)	6 (43%)	
4+3=7	3 (21%)	2 (14%)	
3+5=8	0 (0%)	1 (7%)	
4+4=8	3 (21%)	3 (21%)	
4+5=9	2 (14%)	2 (14%)	
5+4=9	2 (14%)	0 (0%)	
Initial <sup>d</sup> PSA µg/L, median ( <sup>b</sup> IQR)	16.5 (9.9, 27.0)	15.5 (7.2, 22.0)	0.41
Initial T staging			0.87
T1c	2 (14%)	4 (29%)	
T2a	2 (14%)	2 (14%)	
T2b	0 (0%)	1 (7%)	
T2c	2 (14%)	3 (21%)	
T3	2 (14%)	1 (7%)	
T3a	4 (29%)	2 (14%)	
T3b	2 (14%)	1 (7%)	

<sup>a</sup> BMI = Body mass index, <sup>b</sup> IQR = interquartile range, <sup>c</sup> p<0.05 = statistical significance, <sup>d</sup>PSA = prostate specific antigen

### 6.6.2 Fiducial insertion

All the polymer and gold fiducial patients had three fiducials successfully inserted without incident. All fiducials were available for analysis. However, in the gold fiducial group, one CT dataset and the kV images of two patients, in addition to one polymer CT dataset, could not be restored for analysis because of data corruption (Tables 6.2 and 6.3).

## 6.6.3 Fiducial visibility

Visibility results for 3D imaging are shown in Tables 6.2 and 6.3.

Table 6.2 MRI, CT and CBCT fiducial visibility assessments

Fiducials and <sup>a</sup> visibility grade	MRI visibility			CT visibility			CBCT visibility		
	Gold	Polymer	<sup>c</sup> p-value	Gold	Polymer	<sup>c</sup> p-value	Gold	Polymer	<sup>c</sup> p-value
Number of patients	14	14		14	14		14	14	
<b>Apex fiducial</b>			1.00			<0.001			0.22
1	0	1 (7%)		1 (7%)	12 (86%)		14 (100%)	11 (79%)	
2	2 (14%)	1 (7%)		9 (64%)	2 (14%)		0	1 (7%)	
3	2 (14%)	2 (14%)		3 (21%)	0		0	2 (14%)	
4	10 (71%)	10 (71%)		0	0		0	0	
†Not restored	0	0		1 (7%)	0		0	0	
<b>Mid-gland fiducial</b>			1.00			<0.001			0.22
1	0	1 (7%)		1 (7%)	9 (64%)		14 (100%)	11 (79%)	
2	2 (14%)	1 (7%)		7 (50%)	5 (36%)		0	3 (21%)	
3	3 (21%)	2 (14%)		5 (36%)	0		0	0	
4	9 (64%)	10 (71%)		0	0		0	0	
†Not restored	0	0		1 (7%)	0		0	0	
<b>Base fiducial</b>			0.63			<0.001			0.098
1	0	2 (14%)		0	13 (93%)		14 (100%)	10 (71%)	
2	2 (14%)	1 (7%)		8 (57%)	1 (7%)		0	4 (29%)	
3	2 (14%)	2 (14%)		5 (36%)	0		0	0	
4	10 (71%)	9 (64%)		0	0		0	0	
<sup>b</sup> Not restored	0	0		1 (7%)	0		0	0	

CBCT = cone beam computed tomography, CT = computed tomography, MRI = magnetic resonance imaging

<sup>a</sup> Fiducials were scored for visibility, i.e.:

1. Clearly visible for verification
2. Visibility impaired but sufficient for verification

3. Visibility impaired but not sufficient for verification

4. Not visible and not sufficient for verification

<sup>b</sup> Not restored refers to images lost due to data corruption

<sup>c</sup>  $p < 0.05$  = statistical significance

Table 6.3 2D kilovoltage (kV) fiducial visibility assessments

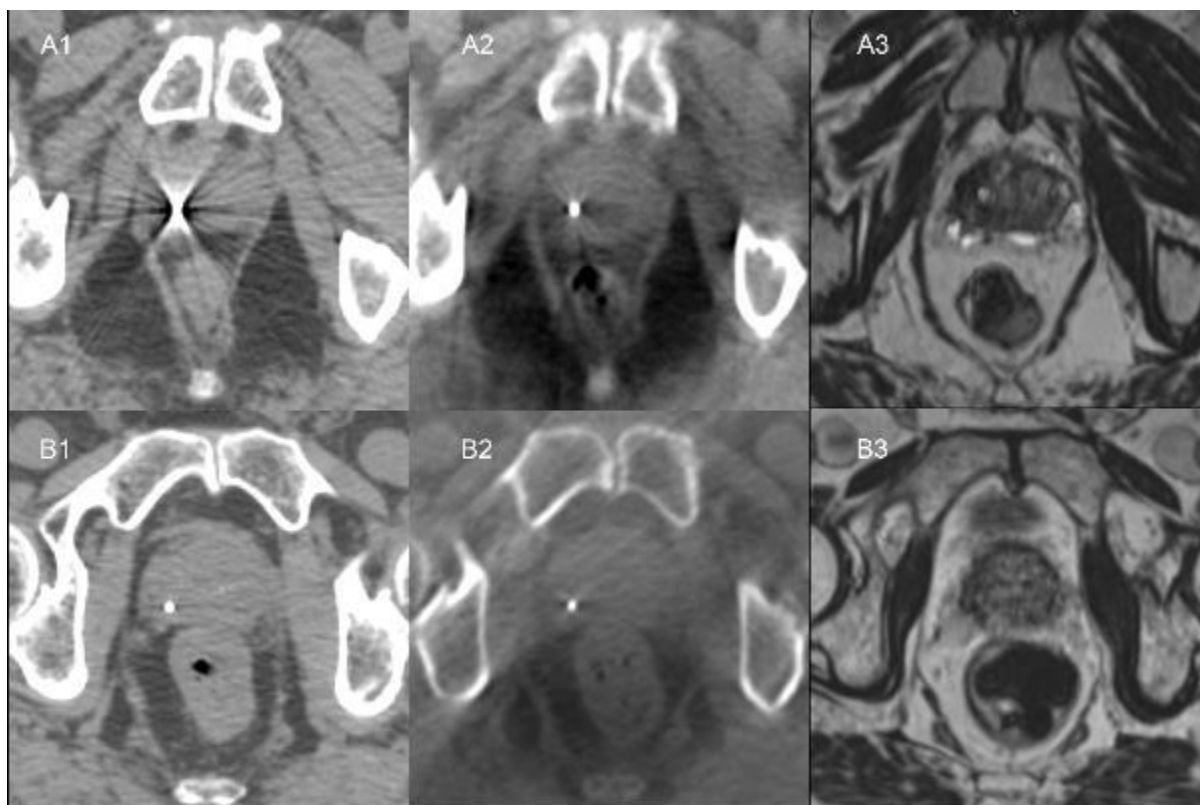
<b>kV type and number of fiducials visible</b>	<b>Gold</b>	<b>Polymer</b>	<b><sup>d</sup>p-value</b>
Number of patients	14	14	
<b><sup>a</sup>LATkV, start of radiotherapy</b>			<b>&lt;0.001</b>
No. fiducials visible			
0	2 (14%)	12 (86%)	
1	0	1 (7%)	
2	5 (36%)	0	
3	5 (36%)	0	
<sup>c</sup> Not restored	2 (14%)	1 (7%)	
<b><sup>a</sup>LATkV, mid-radiotherapy</b>			<b>&lt;0.001</b>
No. fiducials visible			
0	1 (7%)	14 (100%)	
1	2 (14%)	0	
2	4 (29%)	0	
3	5 (36%)	0	
<sup>c</sup> Not restored	2 (14%)	0	
<b><sup>a</sup>LATkV, end of radiotherapy</b>			<b>&lt;0.001</b>
No. fiducials visible			
0	1 (7%)	13 (93%)	
1	0	0	
2	6 (43%)	0	
3	5 (36%)	0	
<sup>c</sup> Not restored	2 (14%)	1 (7%)	
<b><sup>b</sup>APkV, start of radiotherapy</b>			<b>0.14</b>
No. fiducials visible			
0	0	0	
1	0	3 (21%)	
2	2 (14%)	3 (21%)	
3	10 (71%)	8 (57%)	
<sup>c</sup> Not restored	2 (14%)	0	

kV type and number of fiducials visible	Gold	Polymer	<sup>d</sup> p-value
<b><sup>b</sup>APkV, mid-radiotherapy</b>			0.65
No. fiducials visible			
0	0	1 (7%)	
1	0	1 (7%)	
2	2 (14%)	3 (21%)	
3	10 (71%)	9 (64%)	
<sup>c</sup> Not restored	2 (14%)	0	
<b><sup>b</sup>APkV, end of radiotherapy</b>			1.00
No. fiducials visible			
0	0	1 (7%)	
1	0	0	
2	2 (14%)	3 (21%)	
3	10 (71%)	9 (64%)	
<sup>c</sup> Not restored	2 (14%)	1 (7%)	

kV = kilovoltage imaging

<sup>a</sup> LATkV = lateral kV planar image, <sup>b</sup> APkV = anterior-posterior kV planar image, <sup>c</sup> Not restored refers to images lost due to data corruption, <sup>d</sup> p<0.05 = statistical significance

The gold fiducials were sufficiently visible with CT (Figure 6.1 A1) for verification in 71%, 57% and 57% of those positioned in the apex, mid-gland and base, respectively. However, the polymer fiducials scored significantly higher in terms of visibility with CT imaging (p<0.001) because of less artefact, being visible for verification in 100% of patients (Figure 6.1 B1).



CT = computed tomography, MRI = magnetic resonance imaging

Source: Austin Health

**Figure 6.1** Comparison of visibility and artefact for gold and polymer fiducials on CT and MRI. Patient A: A1) CT simulation with gold fiducial with associated artefact on CT. A2) Fiducial co-registered CBCT showing gold fiducial with little artefact. A3) Bone co-registered MRI where the gold fiducial was not visible. Patient B: B1) CT simulation showing polymer fiducial with minor artefact. B2) Fiducial co-registered CBCT with visible polymer fiducial with slight artefact. B3) Bone co-registered MRI where polymer fiducial was not visible.

Both the gold fiducials and polymer fiducials were well seen on CBCT, with no significant differences in visibility scores. However, all the gold fiducials (100%) were scored 1 (clearly visible for verification) compared to 71–79% of the polymer fiducials. The gold fiducials were well seen because of the gold having good contrast, and the artefact is less prominent with CBCT than CT (Figures 6.1 A2 and 6.1 B2).

The visibility of the gold and polymer fiducials for MRI was low (Figures 6.1 A3 and 6.1 B3). In 64–71% of the images, neither the gold nor the polymer fiducials could be seen on the MRI.

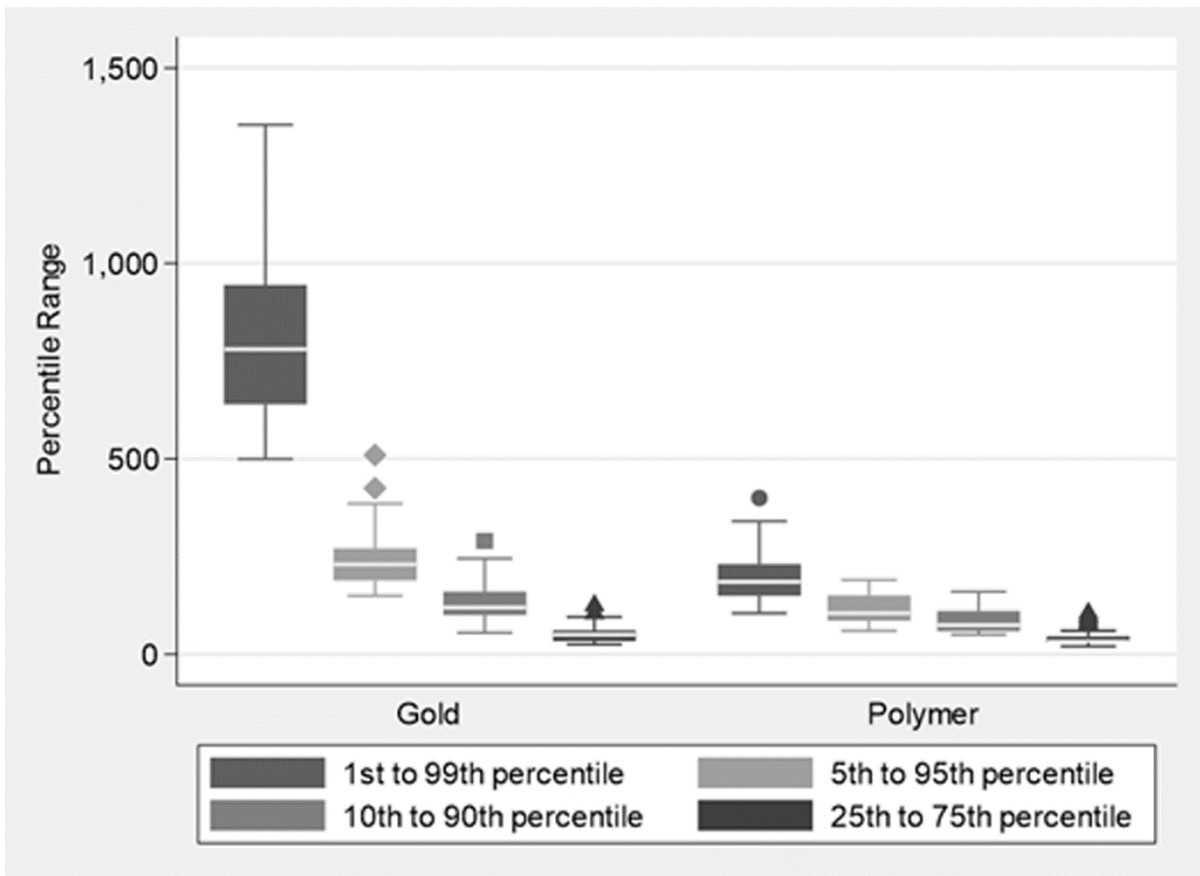
Gold markers were well visualised on kV imaging (Table 6.3). At least two of the gold fiducials were seen on 65–79% of the lateral kV images and 85% of the AP kV images. In contrast, only one polymer fiducial was visualised on lateral kV images across the three time points due to the overlying pelvic bones. Polymer fiducials were better seen on the AP kV images, with at least two fiducials visualised in 78–85% of the patient images.

#### 6.6.4 CT fiducial and artefact analysis

The fiducial contours had a small volume and low voxel count; consequently, only the maximum HU was considered as it is the most representative of the fiducial material. The polymer fiducial contours and gold fiducial contours had similar volume and voxel counts. The fiducial contours' median volume was 0.03cc (range 0.01 to 0.07cc) for the polymer compared to 0.03 cc (range 0.01 to 0.11 cc) for gold. The polymer group's voxel count had a median of 15 (range 5 to 34) voxels, similar to gold with a median of 15 (range 5 to 52) voxels. However, the maximum HU value for polymer was lower than gold, with a median of 2,603 (range 1,564 to 3,350) HU compared to 18,017 (range 3,025 to 23,635) HU for gold. The gold fiducials had a much higher HU contrast, that is, were brighter than polymer, on CT (Figures 6.1 A1 and 6.1 B1).

Box plots of the distribution of the percentile ranges (HU) (Figure 6.2) illustrate the range in voxel counts across the artefact spheres' HU range. It is a graphical representation of the relative width of the histogram. The plots showed a significantly lower median voxel count across the HU range for the polymer fiducials compared to gold fiducials. The median HU

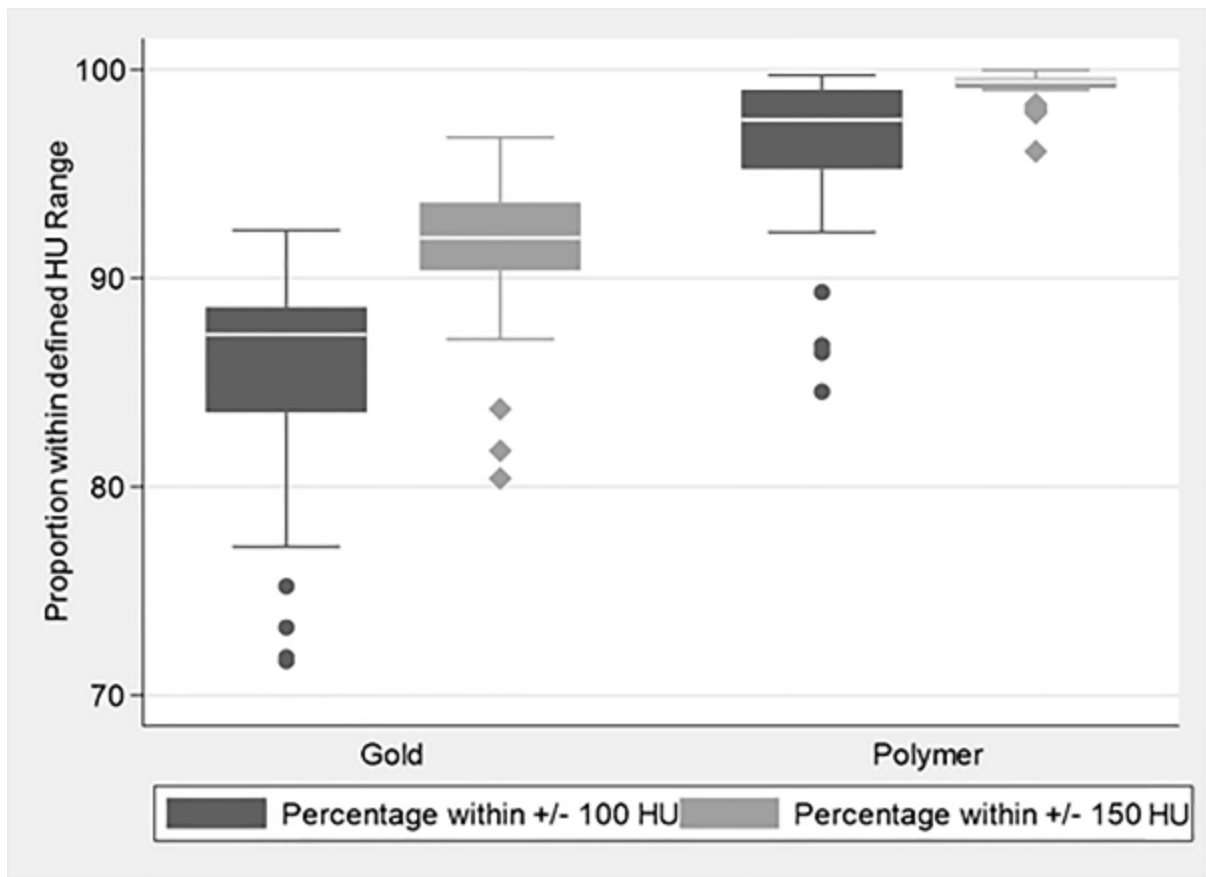
values (IQR) for polymer versus gold were 185 (150 to 230) versus 780 (640 to 945), respectively, ( $p < 0.001$ ) for the 1st to 99th percentile; 105 (85 to 150) versus 230 (190 to 270) ( $p < 0.001$ ) for the 5th to 95th percentile; 75 (60 to 110) versus 120 (100 to 160) ( $p < 0.001$ ) for the 10th to 90th percentile; and 33 (39 to 45) vs 50 (35 to 60) ( $p = 0.002$ ) for the 25th to 75th percentile (Figure 6.2). The polymer values show fewer voxels at the extreme HU artefact values and a narrower histogram than gold, suggesting that the polymer fiducials produced fewer artefacts on CT images.



Source: Austin Health

Figure 6.2 Boxplots showing the distribution of percentile ranges in the Hounsfield units for the polymer and gold groups

The proportion of voxel counts within the pre-defined HU normal tissue ranges of  $\pm 100$  HU and  $\pm 150$  HU (Figure 6.3) were also significantly higher for the polymer fiducials when compared to the gold fiducials (p-values  $< 0.001$ ), with a median (IQR) of 97.6% (95.23, 99.04) in the polymer group compared to 87.3% (83.56, 88.60) for the gold group when considering the  $\pm 100$  HU defined range, and 99.4% (99.12, 99.60) compared to 91.9% (90.39, 93.61) for the  $\pm 150$  HU range. These results show less prostate was obscured by artefact as a significantly greater proportion of prostate normal tissue was visualised for the polymer fiducials compared to gold. These statistically significant differences were maintained upon mixed-effects modelling, with the cluster effect of up to three fiducials per patient taken into account (all p-values  $< 0.001$ ).



Source: Austin Health

Figure 6.3 Boxplots illustrating the distribution of the proportion of voxel counts within the defined Hounsfield unit normal tissue ranges for the polymer and gold groups

## 6.7 DISCUSSION

The study is one of the first to examine and validate the use of polymer fiducials in a prostate cancer patient population. It found that while gold fiducials have a higher HU and are therefore brighter, they produce far more artefact than polymer fiducials on CT. The reduction in artefact around the polymer fiducials resulted in a greater volume of normal tissue being visualised as it was not obscured by high and low HU artefact seen with the gold. Both the polymer and gold fiducials were well seen on CBCT. However, the lower HU of the polymer fiducials than gold meant they could not be easily detected on lateral kV

imaging as the pelvic bones obscured them. Neither type of fiducials could be seen on MRI, in contrast to phantom studies [738], and were not useful for CT to T2 MRI co-registration.

The accurate localisation of the prostate is crucial for precise radiotherapy. Imaging can be used to localise the target and reduce uncertainty during treatment. IGRT can significantly minimise patient set-up uncertainties and achieve better conformal radiation therapy [747]. 3D multi-planar and multi-modality imaging is routinely used for contouring, but now 3D imaging is increasingly utilised for verification. Verification is mainly performed with CBCT, although MRI is being investigated [748].

IGRT historically used pelvic bony anatomy to provide patient alignment. However, the prostate can move relative to the pelvic bones, and thus bony alignment was considered insufficient for dose-escalated IMRT for prostate cancer [589, 625-627]. A more accurate prostate target localisation method uses biologically inert radiopaque fiducial markers, typically gold as it is well visualised on X-ray imaging. Typically, three fiducials are inserted into the prostate (apex, mid-gland and base) for better accuracy and reproducibility of prostate alignment. Three fiducials also reduce localisation uncertainty due to migration of the fiducials and deformation of the prostate [625, 629, 749].

Comparison studies of IMRT with IGRT using fiducial markers versus non-IGRT treatments have shown a decrease in late gastrointestinal and genitourinary toxicity [650-652] and, in one study, there was a significant improvement in prostate cancer outcome [650]. The toxicity difference can be attributed to the IMRT technique's combination with the reduced dose to organs at risk, daily image guidance and margin reduction that IGRT safely permits.

The shortcomings of gold fiducials are that they cause bright radiating and dark shadowing artefact on CT imaging, leading to a change in target and normal tissue density. The distorted CT image can also result in inaccurate delivery if not accounted for [633]. The artefact can also hide anatomical detail that could lead to inaccurate contouring. The obscuring of anatomical detail is most often an issue around the apex of the prostate. The artefact can also interfere with the efficiency and accuracy of verification. Polymer fiducials appear to alleviate these issues with CT.

The limitation of the study is that we only compared the polymer fiducials to the standard gold fiducials. Other new fiducial markers produce minimal distortion with CT imaging. Visicoill™ uses helical gold coils to reduce the relative thickness and decrease the equivalent density, thus lessening the image artefact [635]. Others use a mixture of low-density biocompatible materials and gold particles [634]. Other alternatives use lower Z radiopaque materials such as stainless steel, titanium [636], carbon or ceramic substances. [625, 637].

A further limitation of the study was that only the T2-weighted MRI was examined. Investigations have shown that other MRI sequences such as T2\*2D and T2\*3D [743] and multi-parametric MRI with bTFE (balanced steady-state free precession sequence) [744] are better at visualising gold fiducials. We have not investigated the optimisation of MRI sequences to visualise the polymer or gold fiducials better, as we wished to prioritise the most common sequence used for radiotherapy planning. Furthermore, we did not investigate artefact suppression CT [633] as it was not available at our centre at the time of the study.

## **6.8 CONCLUSION**

In conclusion, this patient study has shown that a polymer fiducial is a better fiducial for CT and CBCT in prostate cancer patients because of its minimal artefact and good visibility.

Polymer fiducials have minimal distortion with CT imaging, minimal dose perturbation and are biocompatible with soft tissue. However, they were not well seen on T2-weighted MRI or kV imaging, and are therefore not suitable for image co-registration or 2D planar kV verification.

## Chapter 7 FIDUCIAL MARKERS: CAN THE UROLOGIST DO BETTER?

---

Catriona Duncan<sup>a</sup>, Daryl Lim Joon<sup>b</sup>, Nathan Lawrentschuk<sup>a,c,d</sup>, Trish Jenkins<sup>b</sup>, Michal Schneider<sup>g</sup>, Vincent Khoo<sup>e</sup>, Michael Chao<sup>b</sup>, Marita Lawlor<sup>b</sup>, Rachel O’Meara<sup>b</sup>, Colleen Berry<sup>b</sup>, Angela Viotto<sup>b</sup>, Kerryn Brown<sup>b</sup>, Morikatsu Wada<sup>b,c</sup>, Farshad Foroudi<sup>b,c</sup>, Shomik Sengupta<sup>a,f</sup>

Catriona Duncan and Daryl Lim Joon contributed equally as first authors.

<sup>a1</sup> Department of Surgery, Austin Health, University of Melbourne, Melbourne, Australia

<sup>b2</sup> Department of Radiation Oncology, Olivia Newtown-John Cancer Centre, Austin Health, Melbourne, Australia

<sup>c3</sup> Olivia Newtown-John Cancer Research Institute, Austin Hospital, Melbourne, Australia

<sup>d4</sup> The Peter MacCallum Cancer Centre, Melbourne, Australia

<sup>e5</sup> Royal Marsden NHS Foundation Trust, London, UK

<sup>f6</sup> Eastern Health Clinical School, Monash University, Box Hill, Australia

<sup>g7</sup> Department of Medical Imaging and Radiation Sciences, Monash University, Clayton, Australia

Published: Duncan C, Joon DL, Lawrentschuk N, Jenkins T, Schneider M, Khoo V, Chao M, Lawlor M, O’Meara R, Berry C, Viotto A, Brown K, Wada M, Foroudi F, Sengupta S. Fiducial markers: can the urologist do better? *World J Urol.* 2019;37(7):1281–7.

<https://doi.org/10.1007/s00345-018-2515-0>

## 7.1 PREFACE

Chapter 7 represents a manuscript that has been published in the *World Journal of Urology* in 2019.

Previous chapters have investigated approaches to improving the precision of prostate cancer radiotherapy. Initial studies explored clinical perspectives of magnetic resonance imaging (MRI) to enhance target definition, and then seminal vesicle target motion and margins relative to the prostate using gold fiducials to further the accuracy of radiotherapy delivery. The subsequent chapters analysed a commercially available polymer fiducial – an alternative to gold – in an initial tissue-equivalent phantom study of computed tomography (CT) and MRI, and then in a prostate cancer patient population. The development of a 2D histogram analytical tool for the phantom study was further advanced to a 3D analysis in the clinical investigation. These studies showed that the polymer fiducials were well seen on CT and had less obscuring artefact than gold in the phantom and prostate cancer patient population. The final chapters will expand on fiducial enhancement and investigate the in-house development of a Lipiodol™ (ethiodised oil contrast agent) and tissue glue liquid fiducial.

Image-guided radiotherapy has been shown to improve the outcome of prostate radiotherapy, notably with prostate gold seed fiducials for primary prostate irradiation. However, in the post-prostatectomy setting, where the vesicourethral anastomosis and bladder base are the primary targets, fiducials have been used infrequently. Although gold seeds have been used, they can be difficult to insert post prostatectomy, can be expelled from the bladder and produce artefact on CT imaging. Lipiodol™ alone has been utilised for

radiotherapy bladder fiducials, but it can be technically challenging to inject as discrete fiducial markers as it can disperse widely, particularly in the post-prostatectomy setting. Lipiodol™ mixed with a tissue glue, Histoacryl™ (monomeric n-butyl-2-cyanoacrylate), has been used clinically in other sites. The tissue glue can prevent the dispersion of the Lipiodol™, but urine or saline could potentially result in premature setting of the glue.

The objective of this study was to investigate contrast agent/tissue glue mixtures as liquid bladder fiducials, with respect to deliverability and visualisation for radiotherapy verification. As water can cause the premature polymerisation of tissue glues, Chapter 7 details the procedural technique of delivering a Lipiodol™–tissue glue fiducial into an ex vivo water-filled porcine bladder.

## **7.2 CONTEXT**

This chapter is the first detailed description of the successful insertion of a discrete Lipiodol™–glue fiducial into an ex vivo water-filled porcine bladder model, while avoiding premature polymerisation of the tissue glue than can be caused by water-based solutions such as urine and blood. The model simulated the clinical and technical process of inserting fiducials for post-prostatectomy and bladder radiotherapy. The study showed that the glue fiducials could be delivered but the detailed characteristics were investigated in Chapter 8.

### 7.3 ABSTRACT

**Introduction:** Radiotherapy to the bladder has a risk of toxicity to pelvic structures, which can be reduced by using fiducial markers for targeting. Injectable contrast offers an alternative marker to gold seeds, which may fall out or exacerbate scarring. Combining a contrast agent with tissue glue can minimise dispersion through tissue, enhancing its utility. We evaluated combinations of contrast agents and tissue glue using porcine bladder, for feasibility and utility as fiducial markers to aid image-guided radiotherapy.

**Methods:** Different contrast agents (Lipiodol™ Ultra or Urografin™) were combined with different tissue glues (Histoacryl™, Tisseal™ or Glubran2™). The mixtures were endoscopically injected into porcine bladder submucosa to identify the area of interest with multiple fiducial markers. The porcine bladders were imaged within a phantom porcine pelvis using standard radiation therapy imaging modalities. The feasibility as an injectable fiducial marker and visibility of each fiducial marker on imaging were scored as binary outcomes by two proceduralists and two radiation therapists, respectively.

**Results:** Lipiodol™–glue combinations were successfully administered as multiple fiducials that were evident on computed tomography (CT) and cone beam CT (CBCT). Lipiodol™ with Histoacryl™ or Glubran2™ was visible on kilovoltage (kV) imaging. The Lipiodol™ Glubran2 combination was deemed subjectively easiest to use at delivery and a better fiducial on kV imaging.

**Conclusion:** This study demonstrates the feasibility of mixing contrast medium Lipiodol™ with Histoacryl™ or Glubran2™ tissue glue, which, injected endoscopically, provides discrete and visible fiducial markers to aid image-guided radiotherapy. Although promising, further study is required to assess the durability of these markers through a course of radiotherapy.

## 7.4 INTRODUCTION

Radiotherapy to the bladder is utilised in two common clinical situations. It is often used as adjuvant or salvage therapy following prostatectomy for the management of prostate cancer where the major radiotherapy targets include the vesicourethral anastomosis, posterior bladder and retrovesical space [516]. It is also used to treat muscle invasive bladder cancer following transurethral resection of bladder tumour (TURBT) in the context of bladder preservation, pre-radical surgery or if radical surgery is not suitable [58]. Efficacy of radiation therapy is directly related to the dose received by the tumour. Similarly, radiation toxicity is directly related to the dosing of normal adjacent tissues. Specifically, bladder toxicity is associated with significant morbidity and is directly related to the proportion of the bladder to receive high radiation doses [750]. As such, the aim of modern radiotherapy is to accurately target the area of malignancy to maximise treatment dose while minimising toxicity [751].

The use of fiducial markers in conjunction with image-guided radiotherapy (IGRT) allows for more accurate dose delivery of radiotherapy to the tumour or target, improving local control while reducing dose and thus toxicity to the normal bladder and bowel. The requirements of any fiducial marker are visibility on a given imaging modality for use in IGRT, availability and reasonable cost [735]. This concept has been clearly demonstrated with the use of gold fiducial markers and IGRT for radiotherapy to an intact prostate [650]. Several studies have demonstrated that fiducial markers improve targeting of the prostate over use of bony landmarks [735]. Fiducial markers have also been demonstrated to be better than surgical clips for use in IGRT post prostatectomy [602]. Solid fiducial markers are used in the bladder, but may be subject to migration, dislodgement or foreign body sequelae in the irradiated

post-operative field [630]. The degree of migration of solid fiducial markers unrelated to bladder volume change has been documented to be as little as 1mm over a course of treatment in a single patient [752] but needs further investigation and validation. Injectable contrast offers an alternative to potentially avoid these concerns [753]; however, dispersion of contrast through the bladder wall may impede its use [754].

A mixture of Lipiodol™ and cyanoacrylate tissue glue has been shown to be a safe and effective treatment of gastric and oesophageal varices [755]. Cyanoacrylate rapidly solidifies in the presence of weak bases such as water and blood. Lipiodol™ is an oily radiological contrast agent. The oil prevents the cyanoacrylate from polymerisation until it contacts water or blood in tissue. It also enables the operator to visualise the process on X-ray imaging. We have previously successfully used a mixture of Lipiodol™ and cyanoacrylate glue as a fiducial marker for oesophageal cancer [756]. However, the use of glue fiducials has never been described in a water-filled organ such as the bladder.

The aim of the study was to test the technical and procedural aspects of combining and delivering liquid contrast agents with several types of tissue glues in a porcine pelvis bladder model. The objective was to create multiple reproducible discrete glue fiducial markers that could be visualised with standard radiotherapy imaging.

## **7.5 MATERIALS AND METHODS**

Ethics approval was sought but not required according to the institutional Human Research and Ethics Committee, as this study was conducted in vitro on isolated porcine bladder.

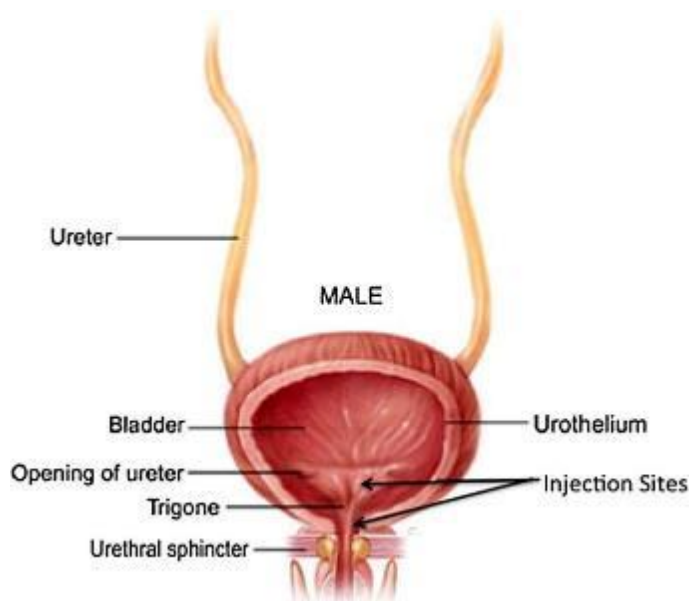
Six separate contrast–glue mixtures were tested by combining two contrast agents – Lipiodol™ Ultra liquid (esterised poppy seed oil, Aspen Medical) or Urografin™ 76% (amidotrizoate, Bayer Resources) – with three different tissue glues: Histoacryl™ (monomeric n-butyl-2-cyanoacrylate, B Braun), Glubran2™ (G-NB-2 NBCA-MS co-monomer, Baxter Healthcare) and Tisseal™ (fibrin sealant, Matrix Surgical), respectively, in a 1:1 ratio. For comparison, porcine bladders with no injection and single agent injection of Histoacryl™, Glubran2™ and Tisseal™ were used as controls. To create the mixtures, 1mL of contrast agent was drawn up in a 2mL syringe and 1mL of tissue glue was drawn up in a separate 1mL syringe. Mixing was performed using a luerlock connector by plunging the agents back and forth between the syringes. Once adequately combined, the mixtures were immediately used.

A 17fr rigid cystoscope was used to endoscopically inspect the isolated bladders and fill the bladder with occlusion of the bladder neck against the scope itself by manual pressure to maintain continence. Using a William's needle (Cook Medical, Australia), contrast/glue combinations were injected submucosally to raise a bleb of 0.1mL of mixture into the submucosal tissue (Figure 7.1). Injections were placed around the trigone to create discrete markers, to imitate marking out a small bladder tumour or the vesicourethral anastomosis following a prostatectomy, as demonstrated in Figure 7.2. Each individual mixture was tested in a separate bladder specimen.



Source: Austin Health

Figure 7.1 Endoscopic ex vivo submucosal glue fiducial injection of fluid-filled porcine bladder



Source: Austin Health

Figure 7.2 Contrast/glue injection sites within the porcine bladder

The contrast/glue combinations were assessed for technical feasibility with regards to mixing and injection procedures on a binary rating system by the investigators carrying out the injections (NL and SS). After the injection was completed, the cystoscope was removed from

the bladder with the needle kept beyond the scope to avoid occlusion of the working channel with the glue mixture. Once withdrawn from the bladder, the needle was disengaged from the cystoscope in a retrograde fashion (from the distal end) to protect the scope from the glue mixture passing through the working channel of the cystoscope.

The bladders were then placed in a detached porcine pelvis positioned to imitate a human in a supine position. This also approximates the tissue densities in a human pelvis undergoing radiotherapy image guidance. The porcine pelvis and contained bladder were then imaged using typical radiotherapy modalities, that is, cone beam computed tomography (CBCT), computed tomography (CT), and kilovoltage (kV) and megavoltage (MV) planar imaging (Figure 7.3). The images were evaluated for visibility of contrast markers. The basis of the fiducial marker utilisation during a course of radiotherapy is the accurate registration of the treatment images with the original planned images, so as to accurately deliver the radiation. This targeting and matching process is performed by trained radiation therapists or technicians. Therefore, if the markers were adequate to allow registration by the radiation technicians (consensus opinion of at least two investigators – RO, KB, ML) using standard imaging modalities for IGRT, the contrast–glue combination was considered to be visible on a binary rating system.



Source: Austin Health

Figure 7.3 Verification of Lipiodol™ and glue fiducial marker on computed tomography (CT) and cone beam computed tomography (CBCT)

## 7.6 RESULTS

### 7.6.1 Combining contrast with glue

Both contrast media were able to be mixed with the tissue glue in all combinations.

However, since Urografin set quite quickly when combined with the tissue glue, only limited time was available for injection to be carried out. Ease of mixing was also subjectively better with the Lipiodol™ Ultra when compared with the Urografin. The rate of polymerisation when Lipiodol™ Ultra was combined with Glubran2 was dependent on the ratio of the agents, with increased time to polymerisation as the proportion of Lipiodol™ Ultra was increased.

### 7.6.2 Injection of contrast–glue combination

Urografin combinations could only be injected once as a single marker due to the rapid polymerisation of the mixture, as Urografin is a water-soluble contrast medium.

Lipiodol™ combinations with Glubran2, Histoacryl and Tisseal could be easily injected repeatedly into the bladder submucosa, raising multiple small blebs. The combination of Lipiodol™ with Glubran2 was assessed as being technically easiest to inject as subjectively it required marginally less pressure.

### 7.6.3 Imaging of porcine bladders

All markers were assessed with several typical imaging modalities to determine whether the markers were adequately visible to allow registration, recorded as a binary outcome being visible or not visible. Urografin–glue combinations were each only able to produce a single fiducial that was visible on CT and CBCT, but not visible on kV or MV imaging.

Lipiodol™–tissue glue combinations were all able to deliver multiple fiducials that were adequately visualised on CT and CBCT. Lipiodol™ with either Histoacryl or Glubran2 produced visible fiducials on kV imaging. Subjectively, the Glubran2 combination created a better marker. The Lipiodol™ with Tisseal combination was not visible on imaging. No combination produced sufficient contrast with MV planar imaging. These results are summarised in Table 7.1.

Table 7.1 Injection visibility of contrast/glue markers with multimodal imaging

Contrast agent Glue agent	Urografin			Lipiodol™		
	Glubran2	Histoacryl	Tisseal	Glubran2	Histoacryl	Tisseal
Injection feasible	No	No	No	Yes	Yes	Yes
Visible	Yes <sup>a</sup>	Yes <sup>a</sup>	Yes <sup>a</sup>	Yes	Yes	No
Imaging method	CT, CBCT, kV	CT only	CT and CBCT	CT, CBCT, kV	CT, CBCT, kV	None

CBCT = cone beam computed tomography, CT = computed tomography, kV = kilovoltage planar imaging

<sup>a</sup> The single marker injected prior to polymerisation of the Urografin–glue mixture was visible but re-injection was technically not feasible.

## 7.7 DISCUSSION

This is the first study to demonstrate that Lipiodol™ Ultra can be easily combined with Glubran2 or Histoacryl tissue glue to create discrete injectable fiducial markers within the fluid-filled bladder wall. The combinations are visible on standard imaging modalities used in IGRT. They can be easily delivered using standard endoscopic injection techniques. The other combinations tested were not found to be suitable. Fiducials created with a mixture of Lipiodol™ and Tisseal were not visible on imaging, while Urografin mixtures with each tissue glue had practical limitations in creating more than one fiducial marker given rapid polymerisation.

Several previous studies have demonstrated that Lipiodol™ is safe and effective for use in the bladder to demarcate tumours [753, 754, 757-761]. Success rates with Lipiodol™ alone have been variable, reported between 76 and 100% [753] as summarised in Table 7.2. No toxicity from Lipiodol™ has been reported. Notably, although Chai et al. report 92% of the markers remained in situ at the completion of the radiation course in their 15 patients, a further 16 patients could not be included in the series as the markers could not be registered for image-guided therapy due to splitting or joining [757]. Cyanoacrylic glues such as

Histoacryl and the components of Glubran2 have been used in a range of urologic procedures, including on urethral tissue in animal models, and use in urinary fistulas without toxicity [762]. The use of a mixture of Lipiodol™ and Histoacryl glue has also been previously described for the treatment of persistent anastomotic urine leak after radical prostatectomy without toxicity at 23-week follow-up [763].

Table 7.2 Current published series investigating Lipiodol™ as a marker for image-guided radiotherapy

Study	Patient number	Trial type	Oncological outcome	Adverse effects	Visibility of Lipiodol™ markers on kV planar imaging (%)
Pos et al. 2009 [754]	40	Obs <sup>a</sup>	Difficulty controlling size of markers, with some Lipiodol™ outside bladder wall, thus not feasible to use Lipiodol™ alone as sole reference for delineation. Valuable aid. Tumour would have been missed by radiation in some patients without Lipiodol™ demarcation.	No Lipiodol™ toxicity. Lipiodol™ disappeared over 12 months on CT follow-up.	95 (2 of 40 patients had no Lipiodol™ present on imaging post injection)
Chai et al. 2010 [757]	15	Obs <sup>a</sup>	15 of 32 patients injected with Lipiodol™ markers were included. 17 patients were not included, in 16 because markers had split or joined, in 1 because there was no contrast in the bladder wall. No post-radiation follow-up.	Not recorded	92 at 5 weeks (of included patients)

Study	Patient number	Trial type	Oncological outcome	Adverse effects	Visibility of Lipiodol™ markers on kV planar imaging (%)
Sondergaard et al. 2010 [760]	5	Obs <sup>a</sup>	>50% of treatment fractions required moderate shift to match Lipiodol™ spots. No post-radiation treatment follow-up.	Adverse effects on cystoscopy + injection: 1 patient dysuria, 1 patient mild urinary frequency, both lasting <24 hours	76
Meijer et al. 2012 [759]	20	Obs <sup>a</sup>	Median follow-up 28 months. 9 patients died: 3 died of metastatic disease—no evidence of local relapse; 2 patients died of local muscle invasive relapse and disease progression at 6 and 12 months post treatment; 4 died of MI <sup>c</sup> . Remaining 11 patients had no evidence of disease.	No adverse events from cystoscopy + injection. No G <sup>b</sup> III toxicities, acute G <sup>b</sup> II toxicities ~45%, at 36 months 25%.	100
Baumgarten et al. 2014 [761] Freilich et al. 2014 [758]	5	Obs <sup>a</sup>	Follow-up 18 months. In 2 of 5 patients tumour bed based on Lipiodol™ extended outside planning target volume that would have been treated based on cystoscopy reports alone. 3 no recurrence. 1 alive with metastatic disease, 1 died from metastatic disease.	No adverse events from injection. No treatment-related toxicities/infections.	95
Kliton et al. 2017 [753] [764] (in Hungarian)	3	Obs <sup>a</sup>	Total treatment time was shorted by 4 days. No oncological outcomes reported in English abstract.	No toxicity to injection. 1 patient G <sup>b</sup> II cystitis + proctitis, 1 patient G <sup>b</sup> I cystitis.	100

<sup>a</sup> Obs = observational trial, no randomisation or control group comparison, <sup>b</sup> G = grade as per Radiation Therapy Oncology Group side effects grading recommendation, <sup>c</sup> MI = myocardial infarction

Despite the success in visibility of Lipiodol™ as described in the literature, our clinical experience in using Lipiodol™ alone has been variable. While discrete fiducials have been created, it was often hampered by the significant dispersion of Lipiodol™ through and beyond the bladder wall, limiting its specificity as a fiducial marker. This is reflected in the imaging included in each of the studies listed above that demonstrate good visibility on CT/kV imaging but highlight a lack of specificity in the location of the Lipiodol™ following injection [758]. Consequently, it may not be sufficient as the sole fiducial marker [754]. In addition, wide dispersion of contrast may significantly impact further imaging in these patients, which is commonly required for ongoing follow-up.

Placing a foreign body within an operative site during radiotherapy presents the potential risks of scarring and fistulae formation [605]. These concerns have prompted the consideration of options beyond the conventional gold seeds. Modified gold seeds have been used successfully in the bladder with endoscopic placement for targeting of radiotherapy for treatment of muscle invasive bladder cancer [765]; however, these seeds are not freely available. In contrast, Lipiodol™ and tissue glue (Glubran2 or Histoacryl) may be found in many hospitals, including regional centres. Notably, Lipiodol™ and Histoacryl mixture is a cost-effective combination when compared to most other glues and fiducials.

The major limitation of this study is the evaluation of the fiducial markers at only a single time point immediately following the administration of the contrast–tissue glue combination. It does not address the stability, durability and migration of the marker. However, similar combinations used in other organs such as the upper gastrointestinal tract [766] suggest that these markers are likely to be stable. Further evaluation of the stability

and reliability of Lipiodol™–tissue glue markers through a standard course of radiotherapy is required by appropriate in vivo assessment.

## **7.8 CONCLUSIONS**

This model presents a Lipiodol™–tissue glue combination as a feasible and potentially inexpensive alternative to solid fiducial markers or Lipiodol™ alone to overcome the respective difficulties with each. The technique has the advantages of utilising standard stock available in most hospitals, and endoscopic injection techniques that are in widespread use. Further human trials are required [767], particularly to assess durability through a complete radiation treatment course.

## Chapter 8 EXPLORATORY MODELS COMPARING LIPIODOL™/ ETHIODIZED OIL –GLUE AND GOLD FIDUCIALS FOR POST PROSTATECTOMY & BLADDER RADIOTHERAPY IMAGE- GUIDANCE

---

Daryl Lim Joon<sup>a</sup>, Alexandra Berlangieri<sup>a</sup>, Benjamin Harris<sup>a</sup>, Mark Tacey<sup>a</sup>, Rachel O’Meara<sup>a</sup>,  
Brent Pitt<sup>a</sup>, Angela Viotto<sup>a</sup>, Kerryn Brown<sup>a</sup>, Michal Schneider<sup>b</sup>, Nathan Lawrentschuk<sup>a</sup>,  
Shomick Sengupta<sup>a</sup>, Colleen Berry<sup>a</sup>, Trish Jenkins<sup>a</sup>, Michael Chao<sup>a</sup>, Morikatsu Wada<sup>a</sup>, Farshad  
Foroudi<sup>a</sup>, Vincent Khoo<sup>a,c</sup>

<sup>a</sup> Olivia Newton-John Cancer Centre, Melbourne, Australia

<sup>b</sup> Monash University Melbourne Australia

<sup>c</sup> Royal Marsden NHS Foundation Trust, London, UK

Published: Lim Joon D, Berlangieri A, Harris B, Tacey M, O’Meara R, Pitt B, Viotto A, Brown K,  
Schneider M, Lawrentschuk N, Sengupta S, Berry C, Jenkins T, Chao M, Wada M, Foroudi F,  
Khoo V. Exploratory models comparing ethiodized oil–glue and gold fiducials for bladder  
radiotherapy image-guidance. *Phys Imaging Radiat Oncol.* 2021;17(2021):77–83.

<https://doi.org/10.1016/j.phro.2021.01.008>

## 8.1 PREFACE

Chapter 8 represents a manuscript that has been published in *Physics and Imaging in Radiation Oncology (PhiRO)* in 2021.

The previous studies have aimed at improving radiotherapy precision through imaging and the utilisation of fiducials. The standard gold fiducials were first studied and then compared to an alternative commercially available polymer fiducial. A method using greyscale or computed tomography (CT) number Hounsfield unit (HU) histograms was established for analysing the fiducial and artefact. The purpose of the Lipiodol™–tissue glue fiducial investigations was to develop a novel radiotherapy fiducial and use the CT number HU histogram analytical tool developed in Chapters 5 and 6 to describe its characteristics.

Gold fiducials are commonly used as part of image guidance with prostate radiotherapy. However, they are not frequently utilised in post-prostatectomy radiotherapy, where the vesicourethral anastomosis and bladder base are the primary targets. Gold seeds have been used in the post-prostatectomy setting, but they can be challenging to insert post prostatectomy, may migrate and be expelled from the bladder, and are subject to infection and fistula risk. They also create artefact on imaging, obscuring the major targets including the vesicourethral anastomosis.

Chapter 7 described the detailed procedure of inserting a mixture of Lipiodol™ and tissue glue as a discrete fiducial into a water-filled porcine bladder model, while avoiding premature polymerisation due to the presence of an aqueous solution. This intent was to simulate the insertion of fiducials for post-prostatectomy bladder radiotherapy. The aim of Chapter 8 was to investigate the visibility and CT number HU characteristics of Lipiodol™–

tissue glue fiducials, compared to gold, as bladder fiducials for post-prostatectomy and bladder radiotherapy verification.

## 8.2 CONTEXT

Chapter 7 illustrated the successful delivery of Lipiodol™–liquid glue fiducials into an ex vivo fluid-filled porcine bladder as discrete visible fiducials. Visibility sufficient for verification was confirmed on CT, cone beam CT (CBCT) and kilovoltage (kV) imaging. The verification methodology was improved in Chapter 8, and the fiducial characteristics were further quantified. Chapter 7 mainly described the procedure and the preliminary results. Chapter 8 was designed to report the results in a more comprehensive fashion. Thus, in Chapter 8, to minimize observer bias, the radiation therapists were blinded to the mixtures identities and each other's results for the verification scoring.

Furthermore the methodology from the polymer seeds study was extended to investigate the fiducials' artefact in 3D. In Chapter 8, a standard radiotherapy uniform tissue-equivalent phantom was utilised to analyse the glue fiducials' CT number HU characteristics and artefact compared to the standard gold fiducial, so as to complement the more clinical porcine bladder model. This chapter demonstrates that the glue fiducials have less artefact than gold markers while still being visible.

The exploratory porcine bladder model suggest that contrast glue fiducials make it easier to achieve a discrete fiducial, as the tissue glue limits the dispersion of the Lipiodol. Discrete fiducials are easy to verify and are, therefore, potentially more accurate. However, the installation is more complex. The tissue glue and contrast must be mixed before the

insertion. In addition, one must take care not to allow the glue to polymerize within the scope channel or come into contact with the endoscopic lens. If the glue becomes adherent, then an expensive endoscope may be rendered unusable. Prospective clinical studies are required to assess the utility of glue fiducials in post-prostatectomy and bladder radiotherapy before glue fiducial can be adopted as a standard clinical approach. The study has thus paved the way for clinical investigations in post-prostatectomy radiotherapy patients.

### 8.3 ABSTRACT

**Background and purpose:** Image guidance with fiducials has been shown to improve pelvic radiotherapy outcome. However, bladder fiducials using ethiodised oil (Lipiodol) alone can disperse widely, and gold causes computed tomography (CT) scan metal artefacts. The study's purpose was to investigate the ability to deliver Lipiodol–tissue glue fiducials and compare them to gold for bladder radiotherapy image guidance.

**Materials and methods:** A fluid-filled porcine bladder model was used to assess the ability to cystoscopically inject visible Lipiodol–glue fiducials into the submucosa. We then transferred the bladders into a porcine pelvis for imaging and compared them to gold fiducials using CT, cone beam CT (CBCT) and kilovoltage (kV) planar views. A tissue-equivalent phantom was utilised to analyse the CT number Hounsfield unit (HU) characteristics and artefacts of the glue and gold fiducials. Percentile ranges and normal tissue voxel percentages of the subsequent CT number voxel histogram from a 2cm sphere surrounding the fiducial was used to characterise the artefact.

**Results:** We successfully delivered all Lipiodol glue fiducials into the porcine bladders as discrete fiducials. They were well seen on CT, CBCT and kV imaging. The glue fiducials had lower CT number values, but less CT number spread of the voxel percentile ranges, consistent with the diminished contrast and less artefact than gold. The glue fiducial types had similar CT number characteristics.

**Conclusion:** This study has shown that Lipiodol glue fiducials can be delivered with online visualisation qualities comparable to gold fiducials without metal-related artefacts.

## 8.4 INTRODUCTION

The bladder is a mobile structure that can expand and contract depending on its relative filling volume. Consequently, there has been an increasing interest in using fiducials for bladder image-guided radiotherapy. Gold fiducials are the benchmark for visibility with X-ray imaging and have been used for both bladder tumours and prostate bed radiotherapy [768]. However, they produce a substantial artefact as a result of multiple mechanisms, including beam hardening, scatter, Poisson noise, motion and edge effects [769, 770]. The artefact can interfere with the accurate fiducial definition leading to imprecise image guidance.

Alternatively, ethiodised oil (Lipiodol) has been utilised as a liquid fiducial for bladder tumours, but it can be challenging to achieve a discrete marker due to dispersion [754, 760].

Gastroenterologists routinely use a mixture of Lipiodol and cyanoacrylate tissue glue to treat gastric and oesophageal varices [771, 772]. Lipiodol is an oily X-ray contrast agent that prevents the glue from initially polymerising [771, 773]. The glue rapidly sets once injected into the body and contacts water, for example, in, blood, [771]. We previously have illustrated its utility as a fiducial for oesophageal cancer patients [756]. The tissue glue reduced Lipiodol's dispersion through the oesophagus' wall, increasing the ability to produce a discrete visible fiducial.

While the gastroscopic insertion of Lipiodol and cyanoacrylate glue for the oesophagus is well described, there are no reports of the cystoscopic delivery of tissue glues into a fluid-filled bladder. The cystoscopic insertion of a tissue glue into a watery environment raised concerns that the glue could polymerize prematurely. The glue could obstruct the needle tip, making it difficult to inject into the bladder submucosa. The premature polymerisation may

also glue the cystoscope's lens or channels, permanently damaging an expensive instrument, as has been reported with oesophageal varices [774].

The aim of this study was to investigate the ability to deliver visible discrete Lipiodol–tissue glue fiducials suitable for image guidance, and characterise and compare them in terms of visibility and artefact production to the standard gold fiducials for bladder radiotherapy image guidance.

## **8.5 MATERIALS AND METHODS**

### **8.5.1 Glue fiducials**

The glue fiducials consisted of a mixture of Lipiodol™ Ultra liquid (esterised poppy seed oil, Aspen Medical) with either Histoacryl (monomeric n-butyl-2-cyanoacrylate, B Braun, Germany) (CA) or Glubran2 (n-butyl cyanoacrylate and methacryloxysulpholen monomers, GEM. Italy) (CM), in a 1:1 ratio, respectively.

### **8.5.2 Porcine bladder model: image guidance visibility**

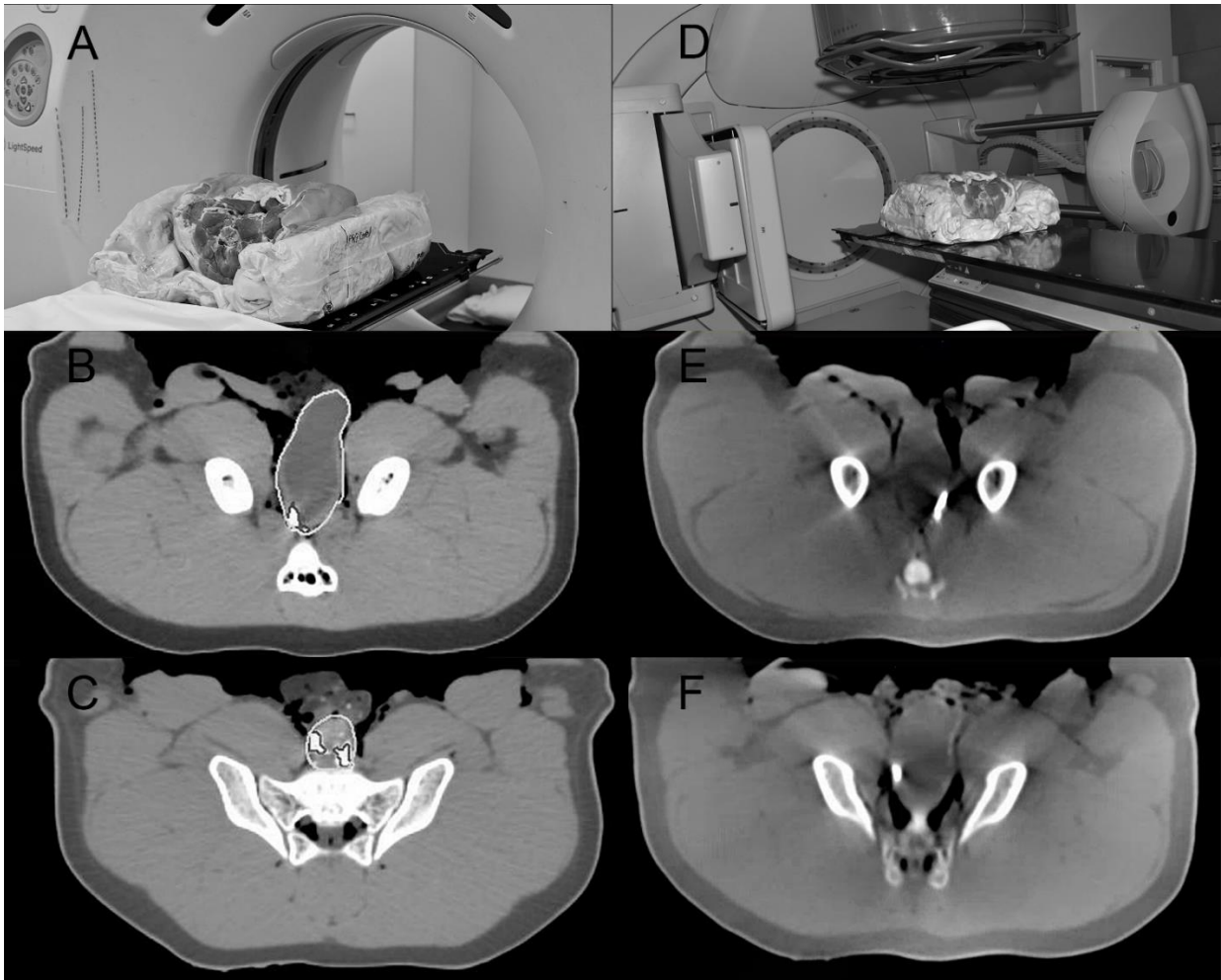
The fiducial insertion utilised a 17fr rigid cystoscope that was initially used to inspect and then fill three ex vivo porcine bladders with saline. Then three sets of three Lipiodol/CA (LC) fiducials, three Lipiodol/CM (LM) fiducials and three gold fiducials were cystoscopically inserted into the three separate porcine bladders. A William's needle (Cook Medical, Australia) was inserted via the scope and used to inject Lipiodol glue combinations submucosally, raising a bleb of 0.1mL. Each set of three discrete fiducials was placed around each bladder's trigone, imitating the demarcation of a small bladder tumour or the

vesicourethral anastomosis following a prostatectomy. Further details of the procedure have been previously described [775].

Following the injection, the cystoscope was removed from the bladder, keeping the needle beyond the scope to avoid the glue occluding the working channel. The glue fiducials were compared with three standard gold fiducials (0.9mm x 3mm, CIVCO Medical Solutions, Kalona, Iowa, USA) in terms of their visibility.

Following the fiducials' insertion, the porcine bladders were transferred sequentially into a porcine pelvis (Figure 8.1). The porcine pelvis was to provide realistic size and tissue densities, including inhomogeneities, for imaging. According to clinical protocols, the pelvis was stabilised and set up in a two-part foam immobilisation device for reproducibility.

The porcine pelvis with the bladder was then imaged using radiotherapy imaging modalities, including computed tomography (CT), cone beam computed tomography (CBCT) (Figure 8.1) and kilovoltage (kV) planar imaging using standard clinical parameters for pelvic radiotherapy.



LC: Lipiodol/ethiodised oil and monomeric n-butyl-2-cyanoacrylate, LM: Lipiodol/ethiodised oil and n-butyl cyanoacrylate and methacryloxysulpholen monomers.

Source: Austin Health

Figure 8.1 Porcine model: pig's bladder and pelvis in two-part foam immobilisation.

A) Computed tomography (CT) simulation. Axial CT image with contoured bladder and fiducial showing visible B) LC fiducial and C) LM fiducial. D) Linac for cone beam CT

The CT simulation was performed on a Lightspeed™ RT CT (GE®, Boston, Massachusetts, USA), with 1.25mm slice width, helical, 0.75 pitch, no gap, 512x512 axial resolution, and 650mm reconstruction diameter.

CBCT was imaged on an Infinity™ linear accelerator (Elekta®, Stockholm, Sweden). The standard abdomen/pelvis scan parameters were used, that is, 41cm diameter field of view (FOV), variable M10/M20 (scan length 12 or 24cm) depending on target size, 120 kV, 25 mA 40ms nominal per frame, 660 frames per scan (360 degrees rotation), 1mm voxel size, 2–3mm viewing slice resolution and axial resolution of 512x512.

2D orthogonal kV planar imaging was performed using anterior-posterior (AP) and lateral views. The Elekta® XVI™ (version 4.5+) kV imaging parameters were 120 kV, 25 (AP) or 32 (lateral) mA, and 40ms nominal per frame; and five frames averaged per image, 25.6x25.6cm imaging area and 0.25mm nominal pixel size (resolution 1024x1024).

Two expert radiation therapists who routinely verify pelvic radiotherapy independently scored the fiducials while blinded to the mixture's identity and each other to measure the fiducial visibility and minimise observer error and bias. The ability to deliver a suitable fiducial set for radiotherapy image verification was scored 0 – not sufficiently visible for verification, or 1 – sufficiently visible for verification for each imaging modality – CT, CBCT and kV planar scans.

### 8.5.3 Phantom model: fiducial and artefact characterisation

A CIRS Torso (tissue-equivalent) phantom was used to characterise the glue fiducials and artefacts. A gold fiducial was used as the standard and embedded centrally in a wax block cylinder measuring 6.3 x 1.0cm for comparison. A wax block cylinder alone was used as a normal tissue control. These wax blocks were constructed and inserted to minimise any air gaps within the phantom.

Further tissue-equivalent, wax block cylinders were constructed for the glue fiducials. Holes for the glue fiducials were drilled into individual blocks that approximated 1) the size of the 0.1mL porcine bladder glue fiducials (i.e. large, 7 x 4mm), and 2) the size of the gold fiducials (i.e. small, 0.9 x 3mm). The holes were moistened for polymerisation and then filled with the glue fiducial. A small Lipiodol alone fiducial control was also created. Each wax cylinder was then sequentially inserted into the CIRS phantom centre and imaged on CT using the same clinical parameters as the porcine model. Two fiducial samples were used for each control, gold and large glue fiducials. Four samples were created for the small glue fiducials, to account for any possible variation due to their small size (Table 8.1).

#### 8.5.4 Fiducial and artefact analysis and statistical description

CT number Hounsfield unit (HU) histograms are increasingly used to analyse human tissue characteristics [776-778]. Consequently, a methodology using CT number histograms derived from clinical tools – MIM Maestro™ version 6.6.13 (MIM Software®, Cleveland, Ohio, USA) (MIM) – was developed to analyse the fiducial artefacts in a three-dimensional manner consistent with modern radiotherapy.

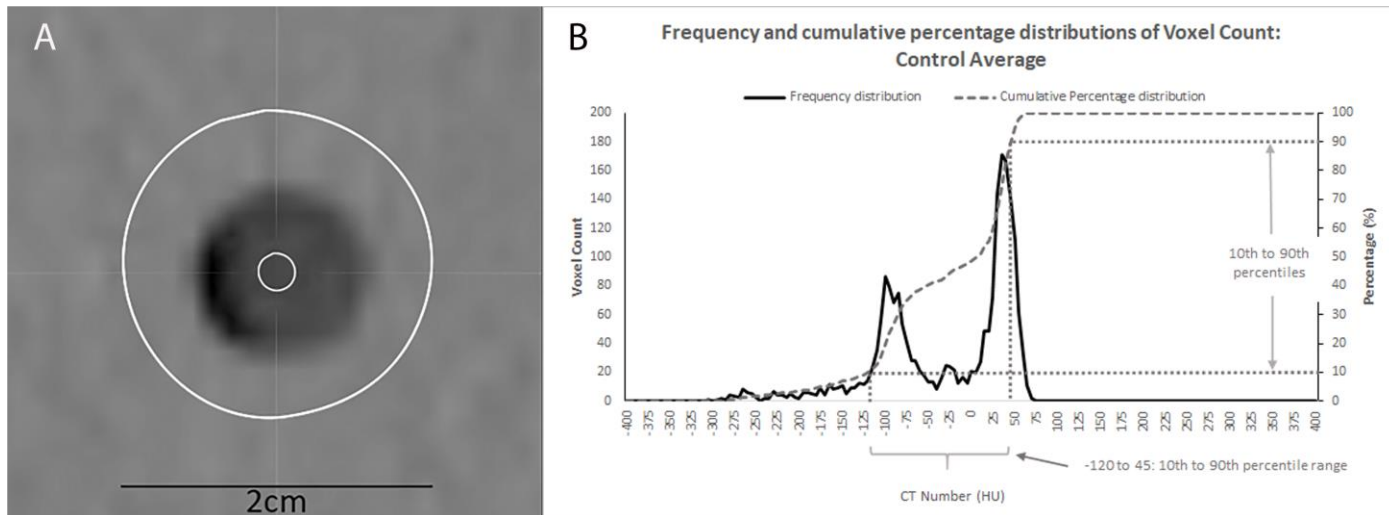
The fiducials were contoured as per clinical protocols using a window level that approximated fiducial size, that is, window level of 4,095 with a width one and gamma [779, 780] of one for the gold fiducials, and level of 600 with a width of 40 and gamma of one for the polymer. Then a 2cm diameter sphere was created around the fiducial contour centre. The high CT number fiducials were subtracted from the sphere using a Boolean function to analyse the artefact's impact on normal tissue. The CT number voxel histogram for the artefact sphere was then exported in bins of 5-HU for analysis. The fiducials' CT number

characteristics were separately investigated as they produced very high CT number signals compared to the artefact.

The spheres contained the phantom, surrounding wax and the relevant fiducial seed's 3D artefact. MIM was used to create histogram plots, presenting the voxels count at each CT number (HU) value to assess the relative differences in CT number variation surrounding each fiducial marker.

Given the non-normal, bi-modal distribution of the voxel count histograms, means and standard deviations were not suitable for describing and comparing the histograms across the fiducial marker types. Therefore, the variation in voxel counts in the spheres (excluding the fiducial) were measured with percentile ranges. An example of the percentiles range is illustrated in Figure 8.2 using the wax control fiducial. Additionally, the normal tissue not hidden by artefact was quantified by the proportion of voxels within the normal tissue CT number ranges of  $\pm 100\text{HU}$  and  $\pm 150\text{HU}$ .

No statistical significance was assigned due to the small sample size for this descriptive study. Data was collected and prepared in Microsoft® Excel (Microsoft®, Redfern, USA). Stata™ version 15.1 (StataCorp®, College Station, Texas, USA) was used to calculate CT number parameters, percentile ranges and proportions.



Source: Austin Health

**Figure 8.2** Phantom model artefact analysis: example of histogram and cumulative percentage distribution of voxel count and calculated percentile range by computed tomography (CT) number Hounsfield unit (HU) for wax control. A) Cross-section through the wax block control inserted in the phantom. The outer contour is the 2cm sphere, while the inner contour denotes the fiducial volume equivalent to the gold or small glue fiducial. B) The corresponding histogram represents the CT number (HU) versus voxel count for the 2cm sphere minus the fiducial volume used to calculate the artefact analysis's percentile ranges.

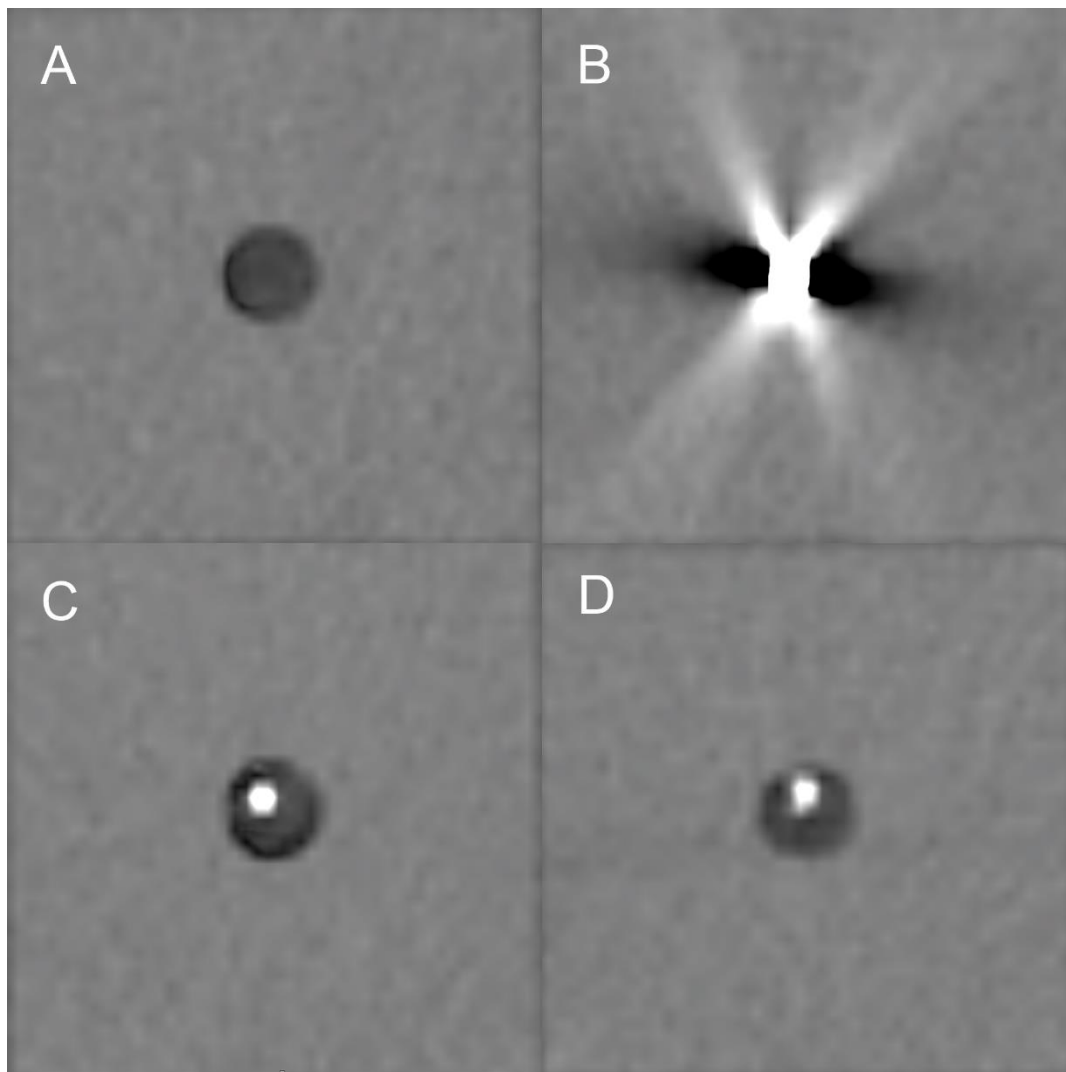
## 8.6 RESULTS

### 8.6.1 Porcine bladder model: fiducial deliverability and visibility

The gold fiducials were well visualised on all imaging modalities. Lipiodol glue combinations could be injected repeatedly into the porcine bladder submucosa, raising consistent multiple small blebs. They were larger than the gold fiducials measuring approximately 7 x 4mm, being overall elliptical in shape. All three fiducials for both LC and LM fiducials could be visualised on CT, CBCT and kV imaging that was adequate for verification. The LC and LM fiducials' appearances were similar on CT and CBCT (Figure 8.1).

### 8.6.2 Phantom model: fiducial characterisation

The fiducials were analysed separately from the surrounding phantom and artefact (Table 8.1). Notably, the fiducials are small relative to the sphere; they occupied only 6 to 38 voxels compared to 1,912 voxels of the sphere. The wax control, gold, Lipiodol alone and small glue fiducials had the same volume and similar voxel count. The wax control had median CT number values 48HU lower than the surrounding phantom but was still within the normal tissue-equivalent range. Therefore, this should not affect the results based on the percentile ranges and percentage of voxels in the normal tissue range. Some wax blocks had incomplete thin rims of air, low CT number voxels adjacent to the phantom interface (Figure 8.3). However, these represented only a small proportion of the sphere and did not affect the results. Lipiodol alone was designed to have the same volume as the small glue fiducials and had comparable CT number characteristics to the glue fiducials (Table 8.1).



LC = Lipiodol/ethiodised oil and monomeric n-butyl-2-cyanoacrylate, LM = Lipiodol/ethiodised oil and n-butyl cyanoacrylate and methacryloxysulpholen monomers, Lipiodol = ethiodised oil

Source: Austin Health

Figure 8.3 Phantom model: computed tomography scan of phantom showing A) Wax control – normal tissue density but less dense than the phantom, B) Gold fiducial and artefact, C) Small LC fiducial, and D) Small LM fiducial. The Lipiodol glue fiducials C) and D) have a minimal artefact.

Table 8.1 Phantom model: comparison of the fiducial and controls in terms of volume, voxel number, and CT number (HU) characteristics. It illustrates that the gold fiducials had a greater CT number (HU) contrast than the small glue fiducials with a comparable volume and voxel number.

<b>Fiducial/Factor</b>	<b>Number of fiducials</b>	<b>Volume cm<sup>3</sup> (average)</b>	<b>Voxel number (average)</b>	<b>Median CT number (HU)</b>	<b>Minimum CT number (HU)</b>	<b>Maximum CT number (HU)</b>
Control (2cm phantom sphere alone)	2	3.85	1,912	24	-220	79
Control (wax)	2	0.02	9	-24	-114	57
Lipiodol alone	2	0.02	9	346	0	1,383
Gold seed	2	0.02	8	6,039	1,229	16,779
Small LC	4	0.02	6	374	50	642
Small LM	4	0.02	6	488	25	835
Large LC	2	0.08	38	717	-261	2,092
Large LM	2	0.07	35	770	-22	2,472

CT = computed tomography, EC = Lipiodol/ethiodised oil and monomeric n-butyl-2-cyanoacrylate, LM = Lipiodol/ethiodised oil and n-butyl cyanoacrylate and methacryloxysulpholen monomers, Lipiodol = ethiodised oil, HU = Hounsfield unit

The gold fiducial was the same size as the small glue fiducials but had a greater contrast with 12 to 16 times greater CT number values than the small Lipiodol fiducials. The glue did not impact the CT number characteristics of the Lipiodol. The differences in median CT number between the glue fiducial and Lipiodol alone was 28–142HU. Both the smaller LC and LM fiducials had similar CT number characteristics, with the difference in their median CT number values being 114HU. The larger LC and LM fiducials were similar, but both exhibited

greater median CT number values than the smaller counterparts but were not as high as gold.

### 8.6.3 Phantom model: fiducial artefact characterisation

The vast majority of the voxels that are represented by the histograms relate to the small wax block surrounded by the 2cm phantom. Both have HU values within the normal tissue range ( $\pm 150$  HU). However, the wax has a lower HU than the phantom, and thus, the histograms are bimodal. The lower HU peak mainly represents the wax, and the high HU peak consists mainly of voxels related to the phantom material.

Sphere voxels were mostly normal tissue density. The bright and dark artefacts result in the HU voxel variation outside the normal tissue range at the extreme high and low HU values, respectively, at the histogram ends, that is, bright radiating or dark shadowing artefact. The greater the spread of the histogram, the less normal tissue is represented as it is obscured by the high or low HU artefact from the fiducials.

The gold fiducial sphere CT number values for the 1st to 99th percentile ranges were 593, 604 and 600HU greater than small LC, LM and Lipiodol alone fiducials, respectively, and 563HU greater than the control (Table 8.2). This suggested a larger number of voxels being present at the extreme ends of the CT number histogram and is representative of an increased artefact for the gold fiducials (Figures 8.3B and 8.4).

Table 8.2 Phantom model: artefact analysis – mean and standard deviations (SD) of percentile ranges of the CT number (HU) versus voxels count histograms and proportion of voxels within normal tissue CT number range for 2cm spheres surrounding the fiducial. It illustrates that the glue fiducials produce fewer artefacts than gold with smaller percentile ranges and a greater percentage of voxels in normal tissue range  $\pm 100$  and  $\pm 150$ HU.

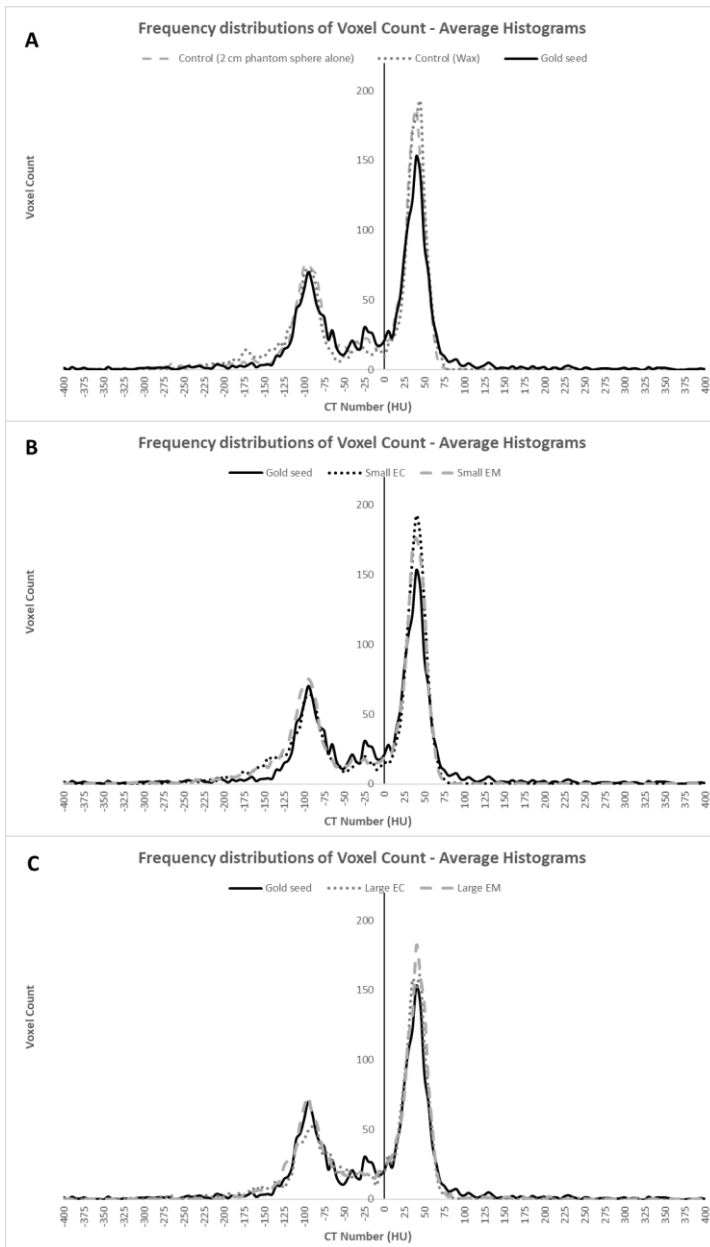
<b>Sphere/ Factor</b>	<b>Number of fiducials spheres</b>	<b>1st to 99th percentile, mean (SD)</b>	<b>5th to 95th percentile, mean (SD)</b>	<b>10th to 90th percentile, mean (SD)</b>	<b>25th to 75th percentile, mean (SD)</b>	<b>Percentage within <math>\pm 100</math>HU, mean (SD)</b>	<b>Percentage within <math>\pm 150</math>HU, mean (SD)</b>
Control (wax)	2	310 (21)	200 (35)	163 (4)	128 (4)	78 (2)	95 (3)
Lipiodol alone	2	273 (11)	215 (14)	175 (7)	133 (4)	75 (3)	92 (1)
Gold	2	873 (110)	270 (57)	173 (11)	128 (4)	74 (1)	91 (2)
Small LC	4	280 (30)	211 (10)	174 (5)	131 (5)	76 (2)	93 (1)
Small LM	4	269 (39)	205 (32)	178 (21)	135 (9)	73 (6)	94 (5)
Large LC	2	360 (35)	203 (4)	165 (0)	123 (4)	80 (1)	94 (0)
Large LM	2	318 (32)	180 (7)	158 (4)	123 (4)	79 (1)	97 (1)

CT = computed tomography, LC = Lipiodol/ethiodised oil and monomeric n-butyl-2-cyanoacrylate, LM = Lipiodol/ethiodised oil and n-butyl cyanoacrylate and methacryloxysulpholen monomers, Lipiodol = Lipiodol/ethiodised oil, HU = Hounsfield unit

Both glue fiducials showed similar CT number values across the percentile ranges, with differences between 1 and 11HU for the small fiducials, and 0 and 42HU for the larger glue fiducials. There were also only small differences from the wax control, indicating that the artefact was minimal (Table 8.2, Figures 8.3C, 8.3D and 8.4). The tissue glue did not affect the fiducials' CT number artefact characteristics, with differences between the small LC and

Lipiodol ranging from 1 to 7HU and 2 to 10HU for the small LM fiducial (Table 8.2). The remaining percentile ranges and percentage of voxels in the designated normal tissue range only showed minor differences with much of the histograms overlaying each other, indicating that the artefacts made up only a small proportion of the 2cm spheres.

Compared to the smaller glue fiducial, the larger glue fiducial's CT number histogram spread was greater for the 1st to 99th percentile range but less than gold. There were only minor variations in values between the LC and LM fiducials for all other values.



LC = Lipiodol/ethiodised oil and monomeric n-butyl-2-cyanoacrylate, LM = Lipiodol/ethiodised oil and n-butyl cyanoacrylate and methacryloxysulpholen monomers

Source: Austin Health

Figure 8.4 Phantom model artefact analysis: average histograms (frequency distribution) of voxel count by CT number Hounsfield Unit (HU) for a 2cm sphere minus the fiducial volume illustrating A) Control (2cm phantom sphere alone), control (wax) and gold fiducial; B) Gold fiducial, small LC and small LM; and C) Gold fiducial, large LC and large LM, i.e. three histograms in each panel.

## 8.7 DISCUSSION

This study has confirmed that glue fiducials can be delivered cystoscopically into a fluid-filled bladder and produce a discrete visible marker with minimal artefact compared to standard gold fiducials, and are thus suitable for image guidance. However, the glue fiducials were larger than the gold markers but had comparable imaging and artefact characteristics to Lipiodol alone.

Fiducials, in an image-guided approach, are critical for targeting in partial bladder radiotherapy to treat the bladder tumour alone or as part of a dose-escalation boost [758, 781]. The bladder can greatly distend, particularly in the cranial-caudal direction. Margins of 2–3cm are required to account for this distension, potentially resulting in increased bowel toxicity [782, 783]. However, studies that use Lipiodol or gold fiducials for partial bladder radiotherapy utilise smaller anisotropic planning target volume (PTV) margins of 5mm to 15mm [602, 754, 758, 760].

Investigations have shown that Lipiodol fiducials effectively define the tumour within the bladder for image guidance [754, 758, 760]. A recent study using cone beam verification has shown that Lipiodol resulted in a higher inter-observer agreement than bladder wall surface matching and decreased PTV margins [784]. However, there was a substantial shape variation of the Lipiodol markers due to bladder filling [784].

While the Lipiodol-only markers can fade, they exhibit a high retention rate and remain visible throughout radiotherapy. However, the ability to use them for radiotherapy verification is variable. In terms of verification with Lipiodol, success rates have been reported to be between 76 and 100% [753]. Chai et al. reported that 92% of the markers

remained in situ after the radiation course in 15 patients. However, a further 16 patients could not be included in the series as the fiducials could not be registered for image-guided therapy due to splitting or joining [757]. Thus, there is a learning curve to achieve Lipiodol markers suitable for radiotherapy verification [760]. Despite success in achieving discrete visible Lipiodol fiducials, our experience when using Lipiodol alone has been inconsistent. Lipiodol dispersion through and beyond the bladder wall into peri-vesical tissue sometimes limited its specificity as a fiducial marker and prompted our investigation of tissue glues.

Side effects of Lipiodol, including an allergic reaction, are uncommon and mostly transient [758]. The studies of Lipiodol bladder markers have not reported any significant toxicity [785]. The Lipiodol and CA combination has been utilised in multiple sites, with infrequent serious side effects [756, 786]. More specifically, CA and CM glues have been used in urological procedures, including in animal urethral tissue models, urinary fistulas [787], and the treatment of persistent anastomotic urine leaks after radical prostatectomy [763].

Gold has also been used as fiducials for partial bladder and post-prostatectomy radiotherapy [597, 602, 768, 788]. Gold is easily visible on X-ray imaging due to its high Z value. However, this subsequently causes bright radiating and dark shadowing metal artefact [785], resulting in the inaccurate fiducial definition that interferes with precise verification. The artefact can also obscure the anatomy causing difficulties in target delineation. Another significant but uncommon risk with the combination of surgery, radiotherapy and foreign body is fistulae [605, 632]. A further issue is the drop-out rate, which is estimated to be 50%, particularly from the tumour area [630, 760, 788]. There have also been technical difficulties inserting gold fiducials into the bladder dome [788].

The caveats of Lipiodol alone and gold fiducial markers have led us to investigate the Lipiodol–glue combinations. Lipiodol and tissue glue (CA or CM) are generally available in most surgical hospitals. The Lipiodol and CA mixture is a less expensive combination [631]. The glue fiducials have good visibility in various imaging modalities, minimal distortion in CT imaging, minimal dose perturbation, and are biocompatible with soft tissue. The widespread use of Lipiodol and tissue glues indicates that they can be safely used in many anatomical sites.

The study did not investigate artefact suppression CT for the gold fiducials [633, 738] or alternative markers, including newer commercially available liquid gel fiducials that have recently been trialled in the bladder, such as BioXmark™ (sucrose acetate isobutyrate [SAIB], iodinated SAIB and ethanol solution) [789] or TraceIT™ (iodinated polyethylene glycol microparticles, or hydrogel) [631]. We have found that glue fiducials and TraceIT™ [631] have their pros and cons. At our centre, the CA and Lipiodol are readily available and less expensive. However, the relative utility of different liquid fiducials can only be resolved in a comparative study that is under consideration.

Interestingly, Lipiodol produces high signal intensity on T1-weighted MRI images and low signal intensity on T2-weighted images [790]. A future interest will be to develop fiducials for MRI, possibly using Lipiodol or another MRI contrast agent with tissue glue. A comparison with TraceIT™ or BioXmark™ would also be appropriate, as both are marketed as being visible on MRI.

The study was an ex vivo and in vitro investigation of glue fiducials where they were imaged immediately after insertion. Issues such as fading, retention, distortion, migration and

dispersion resulting from normal physiological processes during radiotherapy are more appropriately assessed in a clinical study. However, these issues were not evident in our previous gastro-oesophageal patient study [756] or earlier investigations of Lipiodol alone (except dispersion). An in vivo study is planned to address the clinical and imaging aspects, including the fiducials' durability, CBCT, MRI and workflow aspects in a patient population undergoing bladder radiotherapy.

## **8.8 CONCLUSION**

In conclusion, the study has confirmed the potential use of Lipiodol glue fiducials for radiotherapy bladder targeting. They have advantages over gold markers in terms of decreased artefact production and may be more easily deliverable with less dispersion than LIPIODOL alone. The components are readily available, and the Lipiodol Histoacryl mixture is relatively inexpensive. Patient studies are warranted to assess the utility and durability of these fiducials during a radiotherapy course.

## **Acknowledgements**

Radiotherapy Nursing for their support for the procedure and the providers: KARL STORZ Endoscopy Australia Pty Ltd supplied the cystoscopes; William A Cook Australia Pty Ltd supplied the Williams Cystoscopic Injection needles; Guerbet USA supplied the Lipiodol™ ethiodised oil; B.Braun Australia Pty Ltd supplied the Histoacryl; MatrixSurgical supplied the Glubran2 (GEM); Sinclair's Abattoir, Benalla, Victoria, supplied the pig bladders; and Brenta's Butcher, Fairfield, Victoria, supplied the pig pelvis.

## Chapter 9 THESIS DISCUSSION

---

### 9.1 INTRODUCTION

Prostate cancer is a common cancer among men. The advanced state can have a variable and often prolonged and complex natural history. As such, it is a leading cause of cancer-related deaths. Many patients will be diagnosed with locally advanced disease. Patient selection is vital as uncontrolled disease and/or treatment toxicity can result in prolonged morbidity that significantly impacts on quality of life. Radiotherapy can be cost-effective in maintaining the patient's quality of life, but must be delivered appropriately and precisely to maximise treatment efficacy while minimising toxicity.

### 9.2 PROSTATE RADIOTHERAPY AND DOSE ESCALATION

Higher radiation doses [430] and radiotherapy with adjuvant androgen deprivation therapy (ADT) [271, 431-433] have significantly improved the outcome of prostate cancer. Progressive technical developments such as intensity-modulated radiotherapy (IMRT), volumetric modulated arc therapy (VMAT) and imaging techniques, including multi-modality imaging and image-guided radiotherapy (IGRT), continue to improve significantly the precision of radiotherapy so as to exploit the dose-response while minimising dose to organs at risk. IGRT, due to its greater accuracy, has been shown to decrease radiotherapy-related toxicity and possibly improve cancer outcomes [650-652]. This thesis further continues the theme of incremental technical radiotherapy improvements to optimise the treatment of locally advanced prostate cancer and potentially improve patient outcomes.

Surgical treatment – prostatectomy – has been regarded as the gold standard for the treatment of prostate cancer. However, patient selection is essential when deciding between prostatectomy and radiotherapy as treatment with curative intent for prostate cancer [791]. Younger patients with early disease are most often selected for surgery, whereas the older patient with more advanced disease is treated with radiotherapy, due to a trade-off between anaesthetic risks, continence and the possible need for future salvage that are, at least in part, age dependent.

The randomised ProtecT study of low/intermediate-risk prostate cancer has shown that surgery and radiotherapy result in similar outcomes. Both surgery and radiotherapy were associated with a lower incidence of progression and metastasis and possibly dying from prostate cancer compared to active monitoring. Notably, there was no difference between prostatectomy and radiation on these measures [222, 246]. Surgery has greater urinary and sexual side effects, whereas radiotherapy can result in a greater impact on bowel function [246]. There were no differences in general health-related or cancer-related quality of life. The study illustrated that radiotherapy is a reasonable alternative and preferred to surgery in the appropriate patient. It is most often recommended in the older patient and/or more advanced disease. The study did use older radiotherapy techniques, whereas modern precision radiotherapy, IMRT and IGRT, continues to reduce the bowel toxicity.

Therefore, radiotherapy with curative intent has become a well-established treatment for prostate cancer. Depending on the clinical situation, it can be delivered using a number of techniques including external beam radiotherapy (EBRT), EBRT with a high-dose-rate brachytherapy boost, and low-dose-rate brachytherapy monotherapy.

EBRT is the most utilised form of radiotherapy as it does not require any major procedural intervention. Thus, it can be utilised in the elderly and/or patients with comorbidities. Randomised studies have confirmed its utility, by showing it greatly improves prostate cancer-specific mortality and overall mortality/survival with acceptable toxicity when compared to surgery [222, 246] or ADT alone [243, 792].

The indications for radiotherapy to the prostate primary has increased recently to include patients with pelvic nodal disease and even those with low-volume metastatic prostate cancer. The role of definitive local therapy in men with clinically evident lymph nodes has been controversial. However, observational data from a large and comprehensive population-based database and observational studies have supported its use. These studies suggest that initial local therapy to the prostate in men with positive pelvic lymph nodes and at high risk of disseminated prostate cancer may provide selected patients with benefits in terms of local control, prevention of distant metastases and survival [268, 793-796]. It is generally recommended that both neoadjuvant and concurrent ADT be used in such patients, as used in the RTOG 9413 trial [261].

The STAMPEDE study has further supplied prospective non-randomised data that support local radiotherapy for locally advanced prostate cancer with or without pelvic node metastases [245]. The study found that failure-free survival outcomes of nonmetastatic, high-risk prostate cancer patients with newly diagnosed disease were increased by radiotherapy to the prostate with or without pelvic radiotherapy, compared to the standard of care (ADT). These results were confirmed for patients both with and without nodal involvement. The study authors concluded that the data, together with previous studies,

supported the routine use of radiotherapy in patients with positive nonmetastatic prostate cancer.

The concept of radiotherapy to the prostate primary in the setting of metastatic hormone-sensitive prostate cancer (mHSPC) has been tested in three randomised studies [356-358], and recently reviewed by the prospective planned STOPCAP systematic review and meta-analysis [356]. These studies found a highly significant benefit of prostate radiotherapy in biochemical progression and failure-free survival, although there was no significant improvement in survival or progression-free survival for adding prostate radiotherapy to ADT overall. Toxicity results were generally regarded as acceptably low. The benefit was mainly seen with fewer than five metastases. The recommendation was that the addition of local prostate radiotherapy to ADT should be considered in men with mHSPC who have four or fewer bone metastases.

The outcomes for radiotherapy, including biochemical control and lower toxicity, have improved with the utilisation of IMRT and image-guidance techniques. Further technical developments have been seen with a hypofractionated shorter course of radiotherapy that attempts to exploit the low alpha-beta ratio radiobiology of prostate cancer [797] while making it more convenient for the patient. Four large prospective randomised controlled trials have demonstrated that EBRT delivered to the prostate using moderate hypofractionation provides similar early prostate cancer control and similar toxicity to EBRT delivered using conventional fractionation [247]. However, one study did show an increase in toxicity. The majority of patients treated in these studies were low and low-intermediate risk. The CHHiP study noted a steep dose-response with the 57Gy arm producing a worse outcome than 60Gy [492]. Previous studies of dose-response have suggested that high-risk

disease may require higher doses of radiation [443, 798]. However, attempts to dose escalate with hypofractionation have been related to an increase in side effects, as the organs at risk have a similar low alpha-beta ratio and are sensitive to dose per fraction and total dose [496].

Similarly, relatively small prospective studies of ultra-hypofractionated radiotherapy have shown acceptable outcomes and toxicity in mainly low- and low-intermediate-risk prostate cancer. Ongoing randomised studies of ultra-hypofractionation are using mainly one to five fractions. Some also include rectal spacers in an attempt to minimise late rectal effects. Precision radiotherapy, particularly accurate image guidance and possibly spacers, are required to limit severe late toxicity.

The ASCENDE-RT brachytherapy randomised study provides further insight into the interplay of dose escalation, dose-response and toxicity [251]. In this study, the radiation dose was increased with a brachytherapy boost, resulting in a reduced biochemical failure. However, there was a significant increase in acute and late genitourinary toxicity and a trend for worse gastrointestinal side effects [252]. The brachytherapy boost resulted in a significantly greater decline in quality of life on physical and urinary function scales. Thus, improvements in radiotherapy technique may improve disease outcome from further dose escalation but further developments are required to reduce side effects.

Salvage radiotherapy (SRT) for post-prostatectomy prostate-specific antigen (PSA) relapse has been increasingly favoured ahead of immediate adjuvant radiotherapy (ART). While the original randomised studies performed in the adjuvant setting showed an advantage over

surgery alone, there has been a concern about overtreatment and toxicity arising from the use of ART.

The controversy surrounding ART versus SRT has been resolved following a planned meta-analysis of three completed randomised trials. This analysis showed an absolute potential difference of 1% at 5 years in favour of SRT, and thus no advantage for adjuvant treatment. The clinical implementation of SRT for PSA relapse post prostatectomy is consistent with the level 1 evidence. Analysis of radiotherapy doses for SRT indicate a robust dose-response relationship that is similar to that for radiotherapy of intact prostate cancer [512, 518, 523].

Clinical evidence suggests that higher doses improve outcome in terms of biochemical relapse-free survival and disease-free survival [523, 799]. However, the initial analysis reported an increase in late toxicity with dose escalation to the prostate bed [514]. With more sophisticated techniques, including IMRT, the toxicity is acceptable [519], indicating that more conformal dose distributions result in decreased doses to organs at risk.

Investigations of image guidance, including fiducials and rectal spacers, may continue to improve the therapeutic ratio in terms of improved cancer control and reduced toxicity for the patient.

Some of these technical improvements are discussed in Chapter 3, Chapters 5 and 6, and Chapters 7 and 8. Magnetic resonance imaging (MRI) was shown to enhance the accuracy of the target definition, and thus uncertainty margins may be decreased. The margin reduction could potentially reduce doses to organs at risk, while image guidance using fiducials would maintain target coverage and minimise the risk of a geographical miss. Furthermore,

polymer or glue fiducials may provide more accurate delivery of radiotherapy without the interference of artefact, further optimising the therapeutic ratio.

### **9.3 MULTI-MODALITY IMAGING TECHNIQUES FOR RADIOTHERAPY**

VMAT is capable of creating exquisitely tight and conformal dose distributions around a specified or contoured target. Ideally, the target, gross tumour volume and clinical target volume (CTV) are accurately contoured for VMAT planning. Computed tomography (CT) has served as an excellent 3D representation of the patient for radiotherapy planning, as it can be rapidly acquired and is geometrically correct, as well as providing correct electron density values that allow for heterogeneity corrections and accurate dose calculations. However, because of CT's relatively poor soft tissue contrast, it is difficult to distinguish tumour from the prostate or prostate bed, including the vesicourethral anastomosis (VUA).

MRI is increasingly utilised in radiotherapy as more departments install MRI simulators and MRI linear accelerators (linacs). T2-weighted MRI provides an excellent characterisation of soft tissues compared with CT. Furthermore, functional MRI, notably diffusion-weighted imaging, can assist in detecting and defining the actual malignant tumour, both in the intact prostate and in post-prostatectomy situations. Thus, MRI can define both the prostate and the tumour within the prostate [526].

Unlike CT, MRI can visualise the normal prostate zonal anatomy, including the seminal vesicles and capsule [64, 525]. MRI prostate volumes are significantly smaller than CT because less normal tissue is included [528-530]. This increased precision reduces uncertainty and observer variation, particularly at the prostate apex and base [526, 531-

533]. These more accurate and smaller volumes result in a reduced dose to the organs at risk [534].

Chapter 3 further elucidates the use of MRI for post-prostatectomy radiotherapy. Guidelines had suggested that MRI should be better than CT in defining the VUA, the principal target and commonest recurrence site post-prostatectomy, but it was yet to be validated. Chapter 3 confirms and validates that MRI provides a more accurate delineation of the VUA for post-prostatectomy radiotherapy planning.

Guidelines recommend that a CTV margin should extend beyond the VUA to allow for microscopic extension inferiorly, which has been shown in pathological studies to occur with apical involvement or possibly surgical manipulation [699-702]. Chapter 3 illustrates that with the maximum recommended margin of 12mm applied to the CT-defined VUA, almost a quarter of patients that would have less than the minimum recommended margin of 5mm on the MRI-defined VUA. This reduced margin potentially risks a geographic miss.

MRI can also define prostate cancer pathology for radiotherapy targeting. It has a high specificity for the definition of the intra-prostatic lesions including the dominant intra-prostatic lesion (DIL) [535, 536, 800], extracapsular extension [801] and seminal vesicle invasion [174] [537]. These are important considerations as the dominant intra-prostatic lesion (DIL) has been shown to be the most common site of recurrence following radiotherapy, most likely because it represents the site of highest cancer clonogen number [535, 536, 802]. Therefore, the DIL represents an important target for dose escalation. These MRI developments allow increasing precision and individualisation that can lead to further dose escalation and normal tissue sparing strategies by fully utilising the accuracy of IGRT.

Prostate-specific membrane antigen (PSMA) positron emission tomography (PET) has supplanted choline PET for the detection of prostate cancer [803, 804], although choline PET may be useful in those that are not PSMA avid [805]. PSMA PET has high sensitivity and specificity in the detection of prostate cancer [194, 195, 203, 572], and is a useful tool for radiotherapy planning [575-577] [578]. It alters treatment decisions in 26% to 33% of prostate radiotherapy patients [580, 581]. PSMA PET may also assist in the assessment of response following radiotherapy [806]. PET or MRI detects local recurrences in 27% of cases, and it has been shown that dose delivered to the DIL defined by PSMA PET/CT and/or MRI is an independent risk factor for biochemical recurrence [583].

Radiotherapy has mainly used T2-weighted MRI for the structural definition of the prostate anatomy and pathology. Increasingly functional imaging is being used to increase the accuracy and refine the prostate cancer pathology. Functional imaging, including diffusion-weighted MRI [187, 547-550], dynamic contrast-enhanced MRI [547-549, 551] and PET [187, 543], can more reliably identify the DIL. While Chapter 3 focused on defining the post-prostatectomy anatomy, particularly the VUA, multi-modality imaging is increasingly important in defining gross local recurrences for consideration of dose escalation. Multi-parametric MRI (mpMRI), particularly diffusion-weighted imaging, has a high specificity for defining gross tumour recurrence post prostatectomy within the prostate bed [199, 806-808]. While urinary excretion can interfere with the PSMA PET detection of local recurrences post prostatectomy, early phase scans can reduce this effect and can further enhance the MRI detection of gross disease in the prostate bed [807, 809, 810]. Studies of PSMA PET have illustrated that it alters treatment decisions in SRT in 42% to 61% of cases [581, 582]. It

has also been shown to have an impact on the planning of radiotherapy. PSMA PET resulted in modifications of SRT plans in 59% of patients compared to CT alone [579].

Although functional imaging techniques such as diffusion-weighted MRI, dynamic contrast-enhanced MRI and PSMA PET can define the primary or recurrent prostate cancer, they presently have a relatively poor resolution. This low resolution can be partly minimised by co-registering with high-resolution T2-weighted MRI and CT to improve the delineation of the anatomy, DIL or recurrent prostate cancer.

The utilisation of CT heralded the 3D era of prostate radiotherapy with its excellent geometry and dosimetric characteristics. Multi-modality imaging, particularly mpMRI and PET, are increasing the accuracy in defining the appropriate pathological volumes and anatomy. The increased precision of these techniques enhances the targeting and image-guidance precision, which could further improve outcomes by allowing for further dose escalation, and increase organ-at-risk sparing.

#### **9.4 MOTION MANAGEMENT AND IMAGE-GUIDED RADIOTHERAPY**

IMRT, VMAT and multi-modality imaging allow for the design of intricate dose distributions that are precisely shaped around the known cancer targets, the gross tumour volume, clinical target volume (CTV) and planning target volume (PTV), and ideally away from organs at risk. These conformal dose distributions need to be delivered accurately to the patient; otherwise, they risk geometric miss and/or increased toxicity. Image guidance is paramount for the correct daily alignment of the patient and target. The appropriate margins are also required to allow for uncertainties and motion, both between treatments (inter-fractional) and during treatments (intra-fractional).

Prostate motion is secondary to physiological changes including changes in bladder and rectal volume, muscular contractions and respiration [584]. The motion of the prostate is greatest in the anterior-posterior (AP) and superior-inferior (SI) axes, but less laterally. Prostate motion can vary from 1mm to 9mm [585, 586]. Intra-fractional motion is smaller, ranging between 0.86mm and 2mm [588]. Contemporary prostate radiotherapy uses daily pre-treatment online verification, increasingly with cone beam CT (CBCT) and prostate gold fiducials, and soft tissue analysis [589, 735]. The use of IMRT with IGRT using gold fiducial markers has been shown to decrease late gastrointestinal and/or genitourinary toxicity [650-652] and improve prostate cancer outcome [650]. Chapter 4 expanded these themes to use gold fiducials in both the prostate and seminal vesicles to investigate prostate motion and relative seminal vesicle displacement. Chapters 7 and 8 considered an alternative to gold fiducials by investigating polymer fiducials that appear to be well seen on CBCT with less artefact, making verification more efficient and accurate.

The main targets or CTV for post-prostatectomy radiotherapy, typically salvage, relate to the sites of most common recurrence. These sites include the VUA, which is the commonest site of recurrence, followed by the retrovesical space including the posterior bladder, and finally the seminal vesicle bed/remanent to the cut end of the vas deferens [591-596].

Current post-prostatectomy radiotherapy typically uses CBCT for verification. The alignment is most often based on adjacent pelvic bones, but bladder and rectal filling is usually assessed to monitor the bladder/rectum interface. The VUA is difficult to discern because it has the same soft tissue contrast as surrounding tissues. The CTV is also subject to distortion and motion due to changes in relative bowel and bladder filling.

Prostate bed motion is greater in the AP and SI axes than in the left-right (LR) axis. The inter-fractional motion standard deviation has been reported to be about 1.4 to 2.8mm for the LR axis, 4.3 to 5.9mm for the AP axis, and 3.9 to 5.9mm for the SI axis [599, 601]. These shifts are not dissimilar to motion seen with an intact prostate. Therefore, the calculated shifts and difficulty discerning the VUA make the use of fiducial markers for post-prostatectomy radiotherapy a reasonable image-guidance proposition.

The utilisation of surgical clips or inserted fiducials for post-prostatectomy radiotherapy verification has been limited [585, 590, 597-604]. Gold fiducials are favoured as they are stable and easily visualised in the prostate bed [585, 601, 602], whereas surgical clips can sometimes be challenging to match [601, 602]. However, fiducials have not been extensively used due to perceived technical issues such as drop-out rate [630, 760, 788], CT artefact that can interfere with identification of anatomy such as the VUA and cause dose-calculation issues [785], and concern regarding the risk of infection and even fistula, particularly if fiducials are inserted transrectally [605, 632]. Chapter 3 addresses the issues regarding artefact and identification of the VUA with the utilisation of MRI. Chapters 5 and 6 show that the use of polymer seeds with CBCT would negate the issues regarding artefact around the VUA. Chapters 7 and 8 propose a glue fiducial that would potentially be easier to deliver as a liquid fiducial with a minimal artefact in the post-prostatectomy radiotherapy setting.

The seminal vesicles form part of the CTV in the radiotherapy treatment of high-risk prostate cancer, but appear to be subject to greater motion due to variation in bowel filling and, to a lesser extent, bladder volume [617, 619]. Seminal vesicle invasion is a hallmark of very high-risk prostate cancer [436] and is detected in up to 24% of patients at presentation [606, 607]. Most studies of seminal vesicle invasion have shown that the spread extends into the

proximal half or first 1–2cm in 90% of patients. Consequently, guidelines recommend either the proximal half or the proximal 1–2cm [615, 616] of the seminal vesicles should be included in the CTV of patients undergoing radiotherapy for high-risk prostate cancer.

Seminal vesicle displacement is greater than and sometimes independent of that of the prostate, particularly in the AP and SI directions. The estimates of motion, both systematic and random, varies from 1.1 to 1.9mm and 0.4 to 1.4mm, respectively, laterally; 2.8 to 7.3mm and 1.2 to 3.1mm anterior to posterior; and 2.2 to 3.6mm and 0.06 to 2.1mm superior to inferior [617-620]. The subsequent calculated CTV to PTV margins ranged from 4.5mm to 15mm [617-624]. The differences in the studies are partly due to methodology, including that motion of the entire versus proximal seminal vesicle was calculated, and observer contouring variability may have affected results. Estimates of observer contouring variability can be greater than the seminal vesicle motion [727, 728], ranging from 5.4 to 10.7mm [728]. Importantly, this observer variation can be more than the seminal vesicle displacements, and may obscure the correct measurement and direction of the seminal vesicle motion.

Chapter 4 attempted to address these issues of proximal seminal vesicle motion and observer variability by placing gold fiducials in the proximal seminal vesicles. The study confirmed that the proximal seminal vesicle displacement was greater than the prostate motion, with the left seminal vesicle moving more than the right. The greatest shifts in the left seminal vesicle were 2.5mm in the posterior direction and 1.6mm in the superior direction. The study also confirmed and recommended that the PTV margins should be greater in all directions for the proximal seminal vesicles (ranging from 5.2mm to 9.8mm) compared to the prostate (range 4.5mm to 5.6mm).

## 9.5 FIDUCIAL MARKERS FOR PROSTATE CANCER IMAGE-GUIDED RADIOTHERAPY

CBCT is rapidly replacing kilovoltage (kV) imaging for image guidance for prostate radiotherapy. It enables volumetric visualisation of the major organs at risk: the rectum, bowel and bladder. However, gold fiducials are still routinely used so that the prostate can be rapidly aligned for treatment. Optimally, verification to treatment time should be as short as possible to minimise movement by the patient and organs at risk, as well as reducing changes in filling of the bladder and bowel.

Gold fiducials have become the standard marker utilised in radiotherapy. Those used for prostate radiotherapy are approximately 3mm x 1mm and may be scored, knurled, patterned or shaped to minimise migration [625, 629]. They are biologically inert and are easily visualised on X-ray imaging. They are usually inserted transperineally, nowadays under antibiotic cover to minimise infection, using a light general/sedation anaesthetic [641, 642]. Insertion is generally well tolerated with mild side effects that include pain, voiding issues and bleeding [643, 644]. Typically, three gold fiducials are inserted, in the apex, mid-gland and base, to triangulate the prostate position and provide translational and rotational shifts [625, 629]. While three fiducials are considered ideal, two are sufficient if they are inserted in the apex and base. Although gold fiducials are routinely used for radiotherapy of the intact prostate, they are not typically utilised for post-prostatectomy radiotherapy due to technical concerns, such as drop-out rate, and infection and fistula risk, particularly when inserted transrectally. For post-prostatectomy radiotherapy, fiducials can be used to align the VUA, the commonest site of recurrence post surgery and thus pivotal to SRT [699-702]. Further fiducials may also be inserted in the retrovesical space or posterior bladder to mark the second commonest recurrence site.

While image guidance with gold fiducials has improved prostate radiotherapy results, they are not without their caveats. Gold can cause artefacts on CT imaging resulting in a change in tissue density, which leads to inaccurate dosimetry with heterogeneity corrections. The artefact can also interfere with precise radiotherapy verification. Anatomy can be obscured by the artefact, particularly at the prostatic apex or VUA post prostatectomy, resulting in imprecise contouring. Thus, the ideal fiducial should be biocompatible, safe and easy to deliver, with a minimal artefact and negligible migration, and able to be well seen on all radiotherapy imaging modalities [634].

Newer fiducials have been developed to address some of these caveats. To reduce the distortion, some use coils of thinner gold or mixtures of gold particles [634, 635], while others use lower Z but radiopaque materials such as steel, titanium, carbon, ceramic or polymer [625, 636, 637]. Chapters 5 and 6 investigated one such fiducial constructed of a polymer material.

A new phantom was developed for the Chapter 5 study that was tissue-equivalent for both CT and MRI. The preliminary phantom investigation suggested that polymer fiducials could be clearly visualised on CT as a discrete marker with little artefact compared to gold. Both gold and polymer could also be well seen on MRI when imaged in a uniform tissue-equivalent phantom. This visibility suggested that the polymer fiducials could be used for both CT and T2-weighted MRI co-registration as well as radiotherapy verification. The phantom results were confirmed in the patient study for CT and CBCT with the polymer being well visualised. However, the polymer could not be well seen on lateral kV imaging compared to gold, due to its lower contrast resulting in it being obscured by the pelvic bones. Neither gold nor polymer could be seen on T2-weighted MRI due to their low dark

contrast in relation to the prostate tissue's heterogeneity. Chapter 6 suggests that polymer fiducials could be useful for prostate radiotherapy where primarily CT simulation and CBCT verification are used. However, their use with MRI, as with gold, requires further investigation regarding alternative sequences to improve their visibility.

In the post-prostatectomy and bladder radiotherapy setting, injectable liquid fiducials, such as TracelT™ (polyethylene glycol) and BioXmark™ (sucrose acetate isobutyrate), that result in a sticky gel-like fiducial have recently undergone preliminary investigation [631, 789, 811]. Analyses of BioXmark™ in bladder and prostate radiotherapy have shown that it can be successfully delivered as a visible and durable fiducial in 79% of patients. It also had little artefact and could be seen well on CT, CBCT and MRI [789, 811, 812].

We have performed a parallel study to this thesis investigating a commercially available polyethylene glycol liquid fiducial in post-prostatectomy patients [631]. The liquid fiducial was successfully injected in the retrovesical tissue adjacent to the VUA in 45 consecutive patients. These fiducials were used to analyse the prostate bed motion relative to the standard pelvic bone verification. The study showed mean shifts of 2.25mm in the LR direction, 5.89mm in the SI direction and 6.59mm in the AP direction. These shifts would potentially allow tighter PTV margins of 7mm compared to the guideline standard of 10mm with a resultant reduction in dose to the rectum.

Chapters 7 and 8 explored a novel liquid fiducial that would potentially be cost-effective as it uses components already available in surgical units. The glue fiducial is a 1:1 mixture of an oily contrast agent, Lipiodol™, and a tissue glue, either Histoacryl™ or Glubran2™. The oily Lipiodol™ prevents the tissue glue from polymerising while it is injected, whereas water, and

therefore urine or blood, precipitates the glue's setting. Chapter 7 reports on the fiducial's technical delivery, as there were concerns that the adhesive could prematurely polymerise before the fiducial was injected. This chapter illustrated in a porcine bladder model that simulated the clinical and technical process that a visible fiducial could be successfully injected into the submucosa of a water-filled porcine bladder ex vivo without premature polymerisation. The characterisation and visibility of the glue fiducials were compared to gold in the porcine model (in Chapter 7) and a phantom model (in Chapter 8). The glue fiducials injected into the porcine bladder were larger than gold fiducials but were well visualised as verifiable fiducials on CT, CBCT and kV imaging. The glue fiducials had lower Hounsfield unit (HU) values and therefore less contrast than the gold but produced far less metal-related artefact. Potentially, the glue fiducial will be clinically easier to deliver as a discrete fiducial, as Lipiodol™ alone can sometimes diffuse widely. Lipiodol™ -glue fiducial may also be useful on MRI, as it produces high signal intensity on T1-weighted MRI and low signal intensity on T2-weighted images [790].

The use of fiducials remains an integral part of image guidance for prostate radiotherapy. They provide a quick, efficient and accurate method to verify the prostate or prostate bed position. Importantly, fiducials, in combination with image guidance methods such as kV or CBCT, have been shown to reduce toxicity and improve cancer outcome due to the increase in precision of radiotherapy delivery [650-652]. They potentially also allow for further dose escalation or margin reductions. Chapter 4 demonstrated the use of fiducials to track motion and displacement accurately and to calculate more appropriate margins that would avoid potential geographic misses. Chapter 5 and 6 examined the use of an alternative fiducial to the standard gold. It was illustrated that a polymer fiducial has some advantages over gold

as it is well seen on modern radiotherapy imaging, CT and CBCT, with a less obscuring metal artefact. Chapters 7 and 8 explored a new liquid glue fiducial in experimental models that may be easier to deliver, particularly in the post-prostatectomy setting. It was also well seen on CT and verification imaging and had less artefact than gold.

### 9.5.1 MRI linear accelerators

MRI has a growing importance in radiotherapy, with the MRI linac representing a significant advance in radiotherapy precision. The thesis has focused on precision radiotherapy with multi-modality imaging, particularly Chapter 3, with the use of MRI for accurate target delineation and image guidance using fiducials with X-ray imaging, including kV and CBCT. Polymer fiducials were investigated with respect to MRI for image co-registration in Chapter 5, and Chapter 8 proposed a future investigation with Lipiodol™–glue fiducials. Although MRI has been used in radiotherapy to complement CT, CT has generally been regarded as the radiotherapy geometric and dosimetric template for treatment planning and, more recently with CBCT, treatment delivery.

However, the advent of a hybrid linear accelerator with onboard MRI for image guidance, magnetic resonance image guided radiation therapy(MRgRT), may herald a new era of precision for prostate radiotherapy [746]. Due to its greater soft tissue contrast, MRgRT has several advantages. MRgRT would provide direct targeting of the prostate tumour and differentiate it from the surrounding normal tissues. It also permits the real-time characterisation of geometry and motion, and morphology and function of the target cancer as well as normal tissue. It has been proposed that it may be the ultimate online image guidance solution [745].

### 9.5.2 MRI targeting and margins

As previously noted, the better soft tissue contrast of T2-weighted MRI allows for the more precise contouring of the prostate as the zonal anatomy and particularly the capsule can be visualised on MRI but not on CT. The MRI prostate volumes are consistently smaller than volumes estimated by CT, leading to smaller clinical target and planning target volumes [707, 813, 814]. Additionally, the tumour within the prostate and extracapsular extension and seminal vesicle invasion can be seen on MRI, providing a more accurate gross tumour volume for the DIL and CTV [174]. Chapter 3 concluded that MRI provided greater accuracy in defining the VUA for post-prostatectomy radiotherapy and, therefore, more appropriate margins were applied. Consequently, the PTV margins can be smaller as there is less uncertainty, reducing possible overlap with organs at risk. MRgRT allows these targets to be directly aligned prior to radiotherapy delivery, minimising the risk of geographic miss and minimising inaccurate alignment that may increase organ-at-risk doses. There are presently numerable investigations into the appropriate MRI sequences, including functional MRI such as diffusion-weighted MRI, that may help delineate prostate cancer, normal prostate and other normal tissue.

### 9.5.3 Inter-fraction displacement

MRgRT will allow for the very precise pre-treatment online alignment of the prostate and prostate cancer on a daily basis, that is, online adaption to position. Thus, accurate PTV margins can be calculated and adjusted according to the individual patient. Potentially, MRI-compatible and visible fiducials, as investigated in Chapters 5 and 6 and Chapters 7 and 8, may quicken required workflow for adaption to position, although appropriate sequences will require investigation.

However, the prostate can change in shape and volume following treatment. Although the prostate volume generally reduces with ADT and with radiotherapy [815-817], it has been reported that the prostate volume can increase with ultra-hypofractionation or within the first 2 weeks of standard fractionation, presumably due to oedema. The seminal vesicle volume can also change during a course of radiation [817, 818].

There can likewise be changes in normal tissue due to rectal and bladder volume changes, including oedema and swelling. In addition, as reported in Chapter 4, displacement of seminal vesicles during radiotherapy was generally greater and independent of the prostate motion, and thus greater PTV margins are required.

MRgRT would allow for possible offline (or online) adaptive radiotherapy replanning, that is, between treatment fractions, according to the shape and volume of the prostate and seminal vesicles as well as the organs at risk and adjacent soft tissue [745, 819]. Adaption to position is even more likely to be important in hypofractionation and especially ultra-hypofractionation. In these situations, the effect of positional changes could be more dramatic, and precision becomes paramount as only a limited number of fractions are delivered to the tissues sensitive to the dose per fraction, including prostate cancer and organs at risk.

#### 9.5.4 Intra-fraction displacement

Intra-fractional displacement, that is, mainly motion during treatment delivery, of the prostate or prostate bed is generally small and less than 2mm, although it can be larger, mostly due to the passage of flatus [588, 820, 821]. A more significant prostate motion has been noted with real-time monitoring with Calypso™ and with megavoltage (MV) and kV

imaging of stereotactic treatments [588, 822]. A recent study using cine MRI on an MRI linac reported that motion of greater than 2mm was seen in 43% of scans by 5 minutes [823]. MRI-measured intra-fractional movement of the seminal vesicles was found to be greater, ranging between 2.7mm and 7.2mm depending on the time and seminal vesicle side [734]. Sheng et al. found that margins of at least 5mm were required to allow for intra-fraction motion of the seminal vesicles [824].

MRgRT can assess the target volumes and normal tissue during the treatment, thus permitting real-time monitoring. As with stereotactic treatments, treatment could be delayed if the target and normal tissue fell outside a threshold value, avoiding potential geographic miss and unnecessary normal tissue irradiation [745]. A recent study on motion monitoring utilising the MRIdian™ MRgRT system, with a gating boundary of 3mm on the prostate, reported that 2D shifts were required in greater than 20% of fractions [825].

Real-time tracking with MRgRT has led to the investigation of gating techniques. Gating involves only delivering the radiotherapy dose when the target is within defined geographical limits; it therefore dramatically mitigates intra-fractional motion issues. The more time-efficient method would be to track the target, for example, with the multi-leaf collimator. Tracking opens the possibility of real-time inter-fractional adaption. This would produce extremely conformal dose distributions and significantly reduce PTV margins, improving the radiotherapy therapeutic ratio. Real-time adaption would require significant workflow advances, including fast contouring and planning with advances in computer technology and dose calculation algorithms.

### 9.5.5 Response assessment and dose adaption

The geometric advantages of MRI-guided radiotherapy are extremely important in the positional precision of radiotherapy; however, the ability to acquire functional MRI daily would represent a new paradigm of biological adaption. Changes on functional MRI, such as diffusion-weighted imaging, can be used to assess the dose-response of the tumour and possibly the normal tissue. Functional MRI could form the foundation of radiotherapy image-based biomarkers and subsequent radionics algorithms that would enable biological response-based adaption. For example, dose escalation could be used for those with adverse functional MRI parameters, such as those with tumours that are not responding or hypoxic tumours, or radiation de-escalation could be used for those with very responsive tumours, especially if normal tissue toxicity was a concern. These methods have been referred to as biological, image-guided adaptive radiotherapy (BIGART). Differential radiation dose could also be used, based on MRI functional imaging in terms of radiosensitive or radioresistant sub-volumes [745, 746, 826]. Therefore, the initial planning and biological dose adaption throughout the course radiotherapy could be precisely individualised for the patient and their prostate cancer. For such strategies to be accepted, rigorous clinical validation, including prostate cancer and toxicity outcomes, is required.

MRI linacs show an enormous potential to develop a new level of precision for radiotherapy with real-time geometric adaption to position and shape, and potentially biological adaption to radiation sensitivity. However, the machines are first-generation clinical machines with significant caveats [745, 746, 826, 827]. MRI dosimetry is mainly based on synthetic CT and is suitable for prostate pelvis radiotherapy, which has a relatively uniform soft tissue density [826]. However, there are still issues with MRI use where there is significant broad tissue

heterogeneity. Rapid adaptive real-time planning requires sophisticated and robust algorithms and computers with appropriate quality assurance. There are also challenging and potentially complex workflow issues that lead to the patient being on the machine bed for significantly greater durations than with a standard linac. The linac radiotherapy component of the machine also has limitations in terms of technique and slow delivery times. In addition, there are patients in which MRI may be contraindicated such as those with a non-MRI compatible pacemaker, cochlear and other metal implants, claustrophobia or gross obesity.

Consequently, the concepts of this thesis are still very relevant to MRI linacs. The continued and even more widespread use of MRI imaging, as shown in Chapter 3, is paramount, as are studies of motion and adaption strategies as discussed in Chapter 4. The use of MRI-compatible fiducials, as in the studies presented in Chapters 5 to 8, is critically important for developing efficient and effective treatments on the MRI linac, in addition to the many prostate radiotherapy treatments that will continue using the more standard linac. MR linacs in concert with enhancements in technical precision have the potential to further translate into clinical improvements in cancer control and reduction in treatment related side-effects.

## Chapter 10 CONCLUSIONS AND FUTURE DIRECTIONS

---

The demonstration that prostate cancer had a radiotherapy dose-response was one of the main driving forces for radiotherapy's technological revolution. The aim was to escalate the radiation dose to the prostate cancer while minimising rectal toxicity and improving the therapeutic ratio. This aim resulted in progressive developments in the design and planning of increasingly conformal dose distributions by 3D conformal radiotherapy, intensity-modulated radiotherapy and volumetric modulated arc therapy. The increasingly conformal dose distribution was eventually accompanied by ever more precise imaging methods to improve target design and accuracy of delivery. The methods included multi-modality imaging with computed tomography (CT), magnetic resonance imaging (MRI) and positron emission tomography (PET), and image guidance with planar imaging and, more recently, volumetric scans including cone beam CT (CBCT) and fiducial markers. This thesis has focused on methods to incrementally further the precision of prostate radiotherapy by using MRI as part of the multi-modality process, studying motion and displacement to apply appropriate margins better, considering newer commercially available polymer fiducials to minimise artefact, and developing novel liquid fiducials that could be more cost-effective, more efficient and safer to deploy as visible fiducials with less artefact. The improvement in technical precision of radiotherapy can potentially translate clinically into better cancer control and cure as well as reduced toxicity for the patient.

Chapter 3 validates the guideline recommendations that a T2-weighted MRI is critical for the accurate delineation of the vesicourethral anastomosis, the commonest site of recurrence, for post-prostatectomy radiotherapy. It found that MRI was better able to define the vesicourethral anastomosis than the standard CT simulation because of its better soft tissue

contrast. PTV margins could be minimised, therefore safely reducing the dose to organs at risk such as the rectum and penile bulb. We routinely use MRI for prostate cancer salvage radiotherapy, provided it is not contraindicated. Chapter 3 reflects the increasing utilisation of MRI in radiotherapy for greater precision.

Furthermore, multi-parametric MRI and prostate-specific membrane antigen (PSMA) PET are increasingly utilised to investigate prostate cancer patients with a prostate-specific antigen (PSA) relapse. Notably, MRI including diffusion-weighted imaging has been shown to have a greater than 90% sensitivity, specificity and accuracy in detecting gross local recurrence in patients with a PSA relapse post prostatectomy [807]. PET, including PSMA and choline, may further enhance MRI's ability to detect and define a local recurrence post prostatectomy [807, 808] for targeted dose-escalated radiotherapy. MRI-guided radiotherapy would further strengthen this precision in post-prostatectomy radiotherapy as the vesicourethral anastomosis, or local recurrence, could be directly targeted. However, MRI-detectable fiducials may shorten verification to treatment times. Also, MRI, including functional MRI could monitor inter-fraction and intra-fraction motion and response, allowing for adaption to position, shape and response. Studies have been proposed to analyse these concepts.

Appropriate PTV margins are, in part, dependent on the understanding of target motion and displacement. Chapter 4 describes the study of seminal vesicle displacement relative to the prostate by utilising gold fiducials in the prostate and seminal vesicles for patients with high-risk prostate cancer. It concluded that the proximal seminal vesicle displacement is greater than that of the prostate. It recommended that greater margins should be considered for the seminal vesicles compared to the prostate margins. The results have been translated into our clinical practice, and we now standardly use larger margins for the seminal vesicles

relative to the prostate in high-risk patients undergoing radiotherapy. Larger margins are an essential consideration, but caution is required with the organs at risk, particularly with hypofractionation and ultra-hypofractionation in such high-risk patients. Late effects affecting organs at risk, like prostate cancer, may have a low alpha-beta ratio and can be susceptible to the larger dose per fraction. Cine MRI studies of the intra-fraction motion of seminal vesicles have been performed [734]; however, further confirmatory investigations would be appropriate.

Furthermore, the study of prostate and seminal vesicle geometry and motion together with organs at risk during a course of radiotherapy, including inter-fraction and intra-fraction changes, would increase radiotherapy precision. It would provide a better time course for these changes and allow for more precise adaption. The MRI linac with MRI-guided radiotherapy offers the opportunity to perform such analysis.

The polymer fiducial clinical study of Chapter 6 confirmed the preliminary phantom investigation in Chapter 5. The polymer fiducials were well visualised and suitable for verification on CT and CBCT with minimal artefact relative to gold. However, unlike the phantom study, the polymer fiducials could not be well seen on T2-weighted MRI because of the prostate gland's heterogeneity compared to the uniform normal tissue contrast of the phantom. The clinical study also revealed that the polymer seeds could not be imaged on lateral kilovoltage (kV) imaging because they were obscured by the pelvic bones, unlike gold which has a greater CT contrast. The polymer fiducials have been utilised in other centres but are more expensive than gold. The cost-effectiveness in our centre is still being considered. Future studies of the polymer fiducials include the investigation of MRI

sequences to better visualise the fiducial, as MRI availability increases due to MRI simulator installations.

Chapter 7 concluded that a Lipiodol™–glue fiducial could be successfully delivered into the wall of a fluid-filled ex vivo porcine bladder as a discrete and visible fiducial without premature polymerisation. Chapter 8 found that the Lipiodol™–glue fiducial had advantages over gold in terms of producing less artefact and the glue appearing to prevent the dispersion of the Lipiodol™ in this porcine bladder model. The advantages of this combination over commercially available liquid fiducials are that stock of the components is available in most surgical hospitals and the endoscopic injection techniques are in general urological use. However, patient studies are required to assess clinical performance and durability of the fiducial during the entire radiotherapy course. There are also plans to compare and contrast Lipiodol™-glue fiducial with the commercially available TraceIT™ liquid fiducial, as we have completed other studies in this area [631]. The future areas of interest include the utility of the Lipiodol™–glue fiducial with various MRI sequences.

Radiation oncology is at least in part a technology-based speciality, and its development has reflected the rapid advancements in computer, robotic and engineering innovations. These advances have led to increased precision in terms of radiotherapy design, dosimetry and delivery. The result of these advances has been improved outcomes in terms of curability, toxicity and quality of life. This thesis has examined different levels and links in the process, including developmental works with animal models and phantoms in the investigation and analysis of fiducials, to clinical studies of MRI imaging and target motion in patients through their course of radiotherapy. The final aim is that by progressing the precision of treatment, the therapeutic ratio will be improved. However, radiotherapy's technical developments

continue to accelerate with the advent of multi-modality imaging, MRI simulators and magnetic resonance–guided radiotherapy with MRI linacs. Thus, this research will continue investigating concepts derived from the thesis, by evaluating the translation of these concepts in the clinical practice to determine the potential benefit for patient outcomes.

## REFERENCES

- [1] Ferlay J, Soerjomataram I, Dikshit R, Eser S, Mathers C, Rebelo M, et al. Cancer incidence and mortality worldwide: Sources, methods and major patterns in globocan 2012. *Int J Cancer*. 2015;136:E359-86. <https://doi.org/10.1002/ijc.29210>
- [2] Rawla P. Epidemiology of prostate cancer. *World J Oncol*. 2019;10:63-89. <https://doi.org/10.14740/wjon1191>
- [3] Zhou CK, Check DP, Lortet-Tieulent J, Laversanne M, Jemal A, Ferlay J, et al. Prostate cancer incidence in 43 populations worldwide: An analysis of time trends overall and by age group. *Int J Cancer*. 2016;138:1388-400. <https://doi.org/10.1002/ijc.29894>
- [4] Australian Institute of Health and Welfare. Prostate cancer in australia. Cancer series no. 79. Cat. No. Can 76. Canberra: Australian Government 2013.
- [5] Carter BS, Bova GS, Beaty TH, Steinberg GD, Childs B, Isaacs WB, et al. Hereditary prostate cancer: Epidemiologic and clinical features. *J Urol*. 1993;150:797-802. [https://doi.org/10.1016/s0022-5347\(17\)35617-3](https://doi.org/10.1016/s0022-5347(17)35617-3)
- [6] Hemminki K. Familial risk and familial survival in prostate cancer. *World J Urol*. 2012;30:143-8. <https://doi.org/10.1007/s00345-011-0801-1>
- [7] Lloyd T, Hounsome L, Mehay A, Mee S, Verne J, Cooper A. Lifetime risk of being diagnosed with, or dying from, prostate cancer by major ethnic group in england 2008–2010. *BMC Med*. 2015;13:171. <https://doi.org/10.1186/s12916-015-0405-5>
- [8] Bokhorst LP, Roobol MJ. Ethnicity and prostate cancer: The way to solve the screening problem? *BMC Med*. 2015;13:179. <https://doi.org/10.1186/s12916-015-0427-z>
- [9] Tan SH, Petrovics G, Srivastava S. Prostate cancer genomics: Recent advances and the prevailing underrepresentation from racial and ethnic minorities. *Int J Mol Sci*. 2018;19:1255. <https://doi.org/10.3390/ijms19041255>
- [10] Al Olama AA, Kote-Jarai Z, Berndt SI, Conti DV, Schumacher F, Han Y, et al. A meta-analysis of 87,040 individuals identifies 23 new susceptibility loci for prostate cancer. *Nat Genet*. 2014;46:1103-9. <https://doi.org/10.1038/ng.3094>
- [11] Zhen JT, Syed J, Nguyen KA, Leapman MS, Agarwal N, Brierley K, et al. Genetic testing for hereditary prostate cancer: Current status and limitations. *Cancer*. 2018;124:3105-17. <https://doi.org/10.1002/cncr.31316>
- [12] Mateo J, Seed G, Bertan C, Rescigno P, Dolling D, Figueiredo I, et al. Genomics of lethal prostate cancer at diagnosis and castration resistance. *J Clin Invest*. 2020;130:1743-51. <https://doi.org/10.1172/JCI132031>
- [13] Stephan C, Jung K. Advances in biomarkers for pca diagnostics and prognostics-a way towards personalized medicine. *Int J Mol Sci*. 2017;18. <https://doi.org/10.3390/ijms18102193>
- [14] Rebbeck TR. Prostate cancer genetics: Variation by race, ethnicity, and geography. *Semin Radiat Oncol*. 2017;27:3-10. <https://doi.org/10.1016/j.semradi.2016.08.002>
- [15] Martinez-Gonzalez LJ, Pascual Geler M, Robles Fernandez I, Cozar JM, Lorente JA, Alvarez Cubero MJ. Improving the genetic signature of prostate cancer, the somatic mutations. *Urol Oncol*. 2018;36:312 e17- e23. <https://doi.org/10.1016/j.urolonc.2018.03.012>
- [16] Hjelmborg JB, Scheike T, Holst K, Skytthe A, Penney KL, Graff RE, et al. The heritability of prostate cancer in the nordic twin study of cancer. *Cancer Epidemiol Biomarkers Prev*. 2014;23:2303-10. <https://doi.org/10.1158/1055-9965.EPI-13-0568>
- [17] Lin PH, Aronson W, Freedland SJ. Nutrition, dietary interventions and prostate cancer: The latest evidence. *BMC Med*. 2015;13:3. <https://doi.org/10.1186/s12916-014-0234-y>
- [18] Zhao J, Stockwell T, Roemer A, Chikritzhs T. Is alcohol consumption a risk factor for prostate cancer? A systematic review and meta-analysis. *BMC Cancer*. 2016;16:845. <https://doi.org/10.1186/s12885-016-2891-z>

- [19] Key TJ. Nutrition, hormones and prostate cancer risk: Results from the european prospective investigation into cancer and nutrition. *Recent Results Cancer Res.* 2014;202:39-46. [https://doi.org/10.1007/978-3-642-45195-9\\_4](https://doi.org/10.1007/978-3-642-45195-9_4)
- [20] Song Y, Chavarro JE, Cao Y, Qiu W, Mucci L, Sesso HD, et al. Whole milk intake is associated with prostate cancer-specific mortality among u.S. Male physicians. *J Nutr.* 2013;143:189-96. <https://doi.org/10.3945/jn.112.168484>
- [21] Wilson KM, Mucci LA, Drake BF, Preston MA, Stampfer MJ, Giovannucci E, et al. Meat, fish, poultry, and egg intake at diagnosis and risk of prostate cancer progression. *Cancer Prev Res (Phila).* 2016;9:933-41. <https://doi.org/10.1158/1940-6207.CAPR-16-0070>
- [22] Pettersson A, Kasperzyk JL, Kenfield SA, Richman EL, Chan JM, Willett WC, et al. Milk and dairy consumption among men with prostate cancer and risk of metastases and prostate cancer death. *Cancer Epidemiol Biomarkers Prev.* 2012;21:428-36. <https://doi.org/10.1158/1055-9965.EPI-11-1004>
- [23] Lippi G, Mattiuzzi C. Fried food and prostate cancer risk: Systematic review and meta-analysis. *Int J Food Sci Nutr.* 2015;66:587-9. <https://doi.org/10.3109/09637486.2015.1056111>
- [24] Nyame YA, Murphy AB, Bowen DK, Jordan G, Batai K, Dixon M, et al. Associations between serum vitamin d and adverse pathology in men undergoing radical prostatectomy. *J Clin Oncol.* 2016;34:1345-9. <https://doi.org/10.1200/JCO.2015.65.1463>
- [25] Schenk JM, Till CA, Tangen CM, Goodman PJ, Song X, Torkko KC, et al. Serum 25-hydroxyvitamin d concentrations and risk of prostate cancer: Results from the prostate cancer prevention trial. *Cancer Epidemiol Biomarkers Prev.* 2014;23:1484-93. <https://doi.org/10.1158/1055-9965.EPI-13-1340>
- [26] Kristal AR, Till C, Song X, Tangen CM, Goodman PJ, Neuhauser ML, et al. Plasma vitamin d and prostate cancer risk: Results from the selenium and vitamin e cancer prevention trial. *Cancer Epidemiol Biomarkers Prev.* 2014;23:1494-504. <https://doi.org/10.1158/1055-9965.EPI-14-0115>
- [27] Tantamango-Bartley Y, Knutsen SF, Knutsen R, Jacobsen BK, Fan J, Beeson WL, et al. Are strict vegetarians protected against prostate cancer? *Am J Clin Nutr.* 2016;103:153-60. <https://doi.org/10.3945/ajcn.114.106450>
- [28] Ilic D, Misso M. Lycopene for the prevention and treatment of benign prostatic hyperplasia and prostate cancer: A systematic review. *Maturitas.* 2012;72:269-76. <https://doi.org/10.1016/j.maturitas.2012.04.014>
- [29] Zhang M, Wang K, Chen L, Yin B, Song Y. Is phytoestrogen intake associated with decreased risk of prostate cancer? A systematic review of epidemiological studies based on 17,546 cases. *Andrology.* 2016;4:745-56. <https://doi.org/10.1111/andr.12196>
- [30] Esposito K, Chiodini P, Capuano A, Bellastella G, Maiorino MI, Parretta E, et al. Effect of metabolic syndrome and its components on prostate cancer risk: Meta-analysis. *J Endocrinol Invest.* 2013;36:132-9. <https://doi.org/10.1007/BF03346748>
- [31] Elwood PC, Pickering JE, Morgan G, Galante J, Weightman AL, Morris D, et al. Systematic review update of observational studies further supports aspirin role in cancer treatment: Time to share evidence and decision-making with patients? *PLoS One.* 2018;13:e0203957. <https://doi.org/10.1371/journal.pone.0203957>
- [32] Fan LL, Xie CP, Wu YM, Gu XJ, Chen YH, Wang YJ. Aspirin exposure and mortality risk among prostate cancer patients: A systematic review and meta-analysis. *Biomed Res Int.* 2019;2019:9379602. <https://doi.org/10.1155/2019/9379602>
- [33] Huang WY, Daugherty SE, Shiels MS, Purdue MP, Freedman ND, Abnet CC, et al. Aspirin use and mortality in two contemporary US cohorts. *Epidemiology.* 2018;29:126-33. <https://doi.org/10.1097/EDE.0000000000000746>
- [34] Sauer CM, Myran DT, Costentin CE, Zwisler G, Safder T, Papatheodorou S, et al. Effect of long term aspirin use on the incidence of prostate cancer: A systematic review and meta-analysis. *Crit Rev Oncol Hematol.* 2018;132:66-75. <https://doi.org/10.1016/j.critrevonc.2018.09.013>
- [35] Shang Z, Wang X, Yan H, Cui B, Wang Q, Wu J, et al. Intake of non-steroidal anti-inflammatory drugs and the risk of prostate cancer: A meta-analysis. *Front Oncol.* 2018;8:437. <https://doi.org/10.3389/fonc.2018.00437>

- [36] Vidal AC, Howard LE, Moreira DM, Castro-Santamaria R, Andriole GL, Freedland SJ. Aspirin, nsaids, and risk of prostate cancer: Results from the reduce study. *Clin Cancer Res*. 2015;21:756-62. <https://doi.org/10.1158/1078-0432.CCR-14-2235>
- [37] Wang X, Lin YW, Wu J, Zhu Y, Xu XL, Xu X, et al. Meta-analysis of nonsteroidal anti-inflammatory drug intake and prostate cancer risk. *World J Surg Oncol*. 2014;12:304. <https://doi.org/10.1186/1477-7819-12-304>
- [38] Zhou CK, Daugherty SE, Liao LM, Freedman ND, Abnet CC, Pfeiffer R, et al. Do aspirin and other nsaids confer a survival benefit in men diagnosed with prostate cancer? A pooled analysis of nih-aarp and plco cohorts. *Cancer Prev Res (Phila)*. 2017;10:410-20. <https://doi.org/10.1158/1940-6207.CAPR-17-0033>
- [39] Zhou J, Xia S, Li T, Liu R. Could aspirin be a lifesaver for prostate cancer patients in prostate cancer-specific mortality?: An update systematic review and meta-analysis. *BMC Cancer*. 2019;19:1186. <https://doi.org/10.1186/s12885-019-6415-5>
- [40] Huang TB, Yan Y, Guo ZF, Zhang XL, Liu H, Geng J, et al. Aspirin use and the risk of prostate cancer: A meta-analysis of 24 epidemiologic studies. *Int Urol Nephrol*. 2014;46:1715-28. <https://doi.org/10.1007/s11255-014-0703-4>
- [41] Kramer BS, Hagerty KL, Justman S, Somerfield MR, Albertsen PC, Blot WJ, et al. Use of 5-alpha-reductase inhibitors for prostate cancer chemoprevention: American society of clinical oncology/american urological association 2008 clinical practice guideline. *J Clin Oncol*. 2009;27:1502-16. <https://doi.org/10.1200/JCO.2008.16.9599>
- [42] Wu Y, Wang Y, Gu Y, Xia J, Qian Q, Hong Y. Prostate cancer risk and prognostic influence among users of 5-alpha-reductase inhibitors and alpha-blockers: A systematic review and meta-analysis. *Urology*. 2020. <https://doi.org/10.1016/j.urology.2020.05.105>
- [43] Knijnik PG, Brum PW, Cachoeira ET, Paludo AO, Gorgen ARH, Burtet LM, et al. The impact of 5-alpha-reductase inhibitors on mortality in a prostate cancer chemoprevention setting: A meta-analysis. *World J Urol*. 2020. <https://doi.org/10.1007/s00345-020-03202-2>
- [44] Wang L, Lei Y, Gao Y, Cui D, Tang Q, Li R, et al. Association of finasteride with prostate cancer: A systematic review and meta-analysis. *Medicine (Baltimore)*. 2020;99:e19486. <https://doi.org/10.1097/MD.00000000000019486>
- [45] Thompson IM, Jr., Goodman PJ, Tangen CM, Parnes HL, Minasian LM, Godley PA, et al. Long-term survival of participants in the prostate cancer prevention trial. *N Engl J Med*. 2013;369:603-10. <https://doi.org/10.1056/NEJMoa1215932>
- [46] Dawe DE, Mahmud S. Biologic and epidemiologic evidence assessing if statins prevent prostate cancer. *Can J Urol*. 2017;24:9081-8. <https://www.canjurol.com/abstract.php?ArticleID=&version=1.0&PMID=29260632>
- [47] Freedland SJ, Hamilton RJ, Gerber L, Banez LL, Moreira DM, Andriole GL, et al. Statin use and risk of prostate cancer and high-grade prostate cancer: Results from the reduce study. *Prostate Cancer Prostatic Dis*. 2013;16:254-9. <https://doi.org/10.1038/pcan.2013.10>
- [48] Yang H, Pang L, Hu X, Wang W, Xu B, Zhang X, et al. The effect of statins on advanced prostate cancer patients with androgen deprivation therapy or abiraterone/enzalutamide: A systematic review and meta-analysis. *J Clin Pharm Ther*. 2020;45:488-95. <https://doi.org/10.1111/jcpt.13092>
- [49] Tan P, Zhang C, Wei SY, Tang Z, Gao L, Yang L, et al. Effect of statins type on incident prostate cancer risk: A meta-analysis and systematic review. *Asian J Androl*. 2017;19:666-71. <https://doi.org/10.4103/1008-682X.190327>
- [50] Tan P, Wei S, Yang L, Tang Z, Cao D, Liu L, et al. The effect of statins on prostate cancer recurrence and mortality after definitive therapy: A systematic review and meta-analysis. *Sci Rep*. 2016;6:29106. <https://doi.org/10.1038/srep29106>
- [51] Raval AD, Thakker D, Negi H, Vyas A, Kaur H, Salkini MW. Association between statins and clinical outcomes among men with prostate cancer: A systematic review and meta-analysis. *Prostate Cancer Prostatic Dis*. 2016;19:151-62. <https://doi.org/10.1038/pcan.2015.58>

- [52] Zhong S, Zhang X, Chen L, Ma T, Tang J, Zhao J. Statin use and mortality in cancer patients: Systematic review and meta-analysis of observational studies. *Cancer Treat Rev*. 2015;41:554-67. <https://doi.org/10.1016/j.ctrv.2015.04.005>
- [53] Yu O, Eberg M, Benayoun S, Aprikian A, Batist G, Suissa S, et al. Use of statins and the risk of death in patients with prostate cancer. *J Clin Oncol*. 2014;32:5-11. <https://doi.org/10.1200/JCO.2013.49.4757>
- [54] Zaidi S, Gandhi J, Joshi G, Smith NL, Khan SA. The anticancer potential of metformin on prostate cancer. *Prostate Cancer Prostatic Dis*. 2019;22:351-61. <https://doi.org/10.1038/s41391-018-0085-2>
- [55] Wang Y, Liu X, Yan P, Tang J, Chen T, Sun Y, et al. Effect of metformin on the risk of prostate cancer in patients with type 2 diabetes by considering different confounding factors: A meta-analysis of observational studies. *Eur J Cancer Prev*. 2020;29:42-52. <https://doi.org/10.1097/CEJ.0000000000000514>
- [56] Saad F, Caliber M, Doros G, Haider KS, Haider A. Long-term treatment with testosterone undecanoate injections in men with hypogonadism alleviates erectile dysfunction and reduces risk of major adverse cardiovascular events, prostate cancer, and mortality. *Aging Male*. 2020;23:81-92. <https://doi.org/10.1080/13685538.2019.1575354>
- [57] Haider A, Zitzmann M, Doros G, Isbarn H, Hammerer P, Yassin A. Incidence of prostate cancer in hypogonadal men receiving testosterone therapy: Observations from 5-year median followup of 3 registries. *J Urol*. 2015;193:80-6. <https://doi.org/10.1016/j.juro.2014.06.071>
- [58] European Association of Urology. EAU guidelines. Edition presented at the EAU annual congress Amsterdam 2020 (isbn 978-94-92671-07-3) Arnhem, The Netherlands: EAU Guidelines Office; 2020.
- [59] Singh O, Bolla SR. Anatomy, abdomen and pelvis, prostate. In: Statpearls [internet]. Treasure Island, FL 2020.
- [60] McNeal JE. The zonal anatomy of the prostate. *Prostate*. 1981;2:35-49. <https://doi.org/10.1002/pros.2990020105>
- [61] McKay AC, Odeluga N, Jiang J, Sharma S. Anatomy, abdomen and pelvis, seminal vesicle. In: Statpearls [internet]. Treasure Island FL 2020.
- [62] Yacoub JH, Oto A. MR imaging of prostate zonal anatomy. *Radiol Clin North Am*. 2018;56:197-209. <https://doi.org/10.1016/j.rcl.2017.10.003>
- [63] Hricak H, Dooks GC, McNeal JE, Mark AS, Marotti M, Avallone A, et al. MR imaging of the prostate gland: Normal anatomy. *AJR Am J Roentgenol*. 1987;148:51-8. <https://doi.org/10.2214/ajr.148.1.51>
- [64] Sklinda K, Fraczek M, Mruk B, Walecki J. Normal 3T MR anatomy of the prostate gland and surrounding structures. *Adv Med*. 2019;2019:3040859. <https://doi.org/10.1155/2019/3040859>
- [65] Villeirs GM, Verstraete KL, De Neve WJ, De Meerleer GO. Magnetic resonance imaging anatomy of the prostate and periprostatic area: A guide for radiotherapists. *Radiother Oncol*. 2005;76:99-106. <https://doi.org/10.1016/j.radonc.2005.06.015>
- [66] Grignon DJ. Unusual subtypes of prostate cancer. *Mod Pathol*. 2004;17:316-27. <https://doi.org/10.1038/modpathol.3800052>
- [67] Li Y, Mongan J, Behr SC, Sud S, Coakley FV, Simko J, et al. Beyond prostate adenocarcinoma: Expanding the differential diagnosis in prostate pathologic conditions. *Radiographics*. 2016;36:1055-75. <https://doi.org/10.1148/rg.2016150226>
- [68] Sexton WJ, Lance RE, Reyes AO, Pisters PW, Tu SM, Pisters LL. Adult prostate sarcoma: The M.D. Anderson cancer Center experience. *J Urol*. 2001;166:521-5. [https://doi.org/10.1016/s0022-5347\(05\)65974-5](https://doi.org/10.1016/s0022-5347(05)65974-5)
- [69] Sawczuk I, Tannenbaum M, Olsson CA, deVere White R. Primary transitional cell carcinoma of prostatic periurethral ducts. *Urology*. 1985;25:339-43. [https://doi.org/10.1016/0090-4295\(85\)90481-9](https://doi.org/10.1016/0090-4295(85)90481-9)
- [70] Walsh DL, Chang SS. Dilemmas in the treatment of urothelial cancers of the prostate. *Urol Oncol*. 2009;27:352-7. <https://doi.org/10.1016/j.urolonc.2007.12.010>

- [71] Bostwick DG, Mann RB. Malignant lymphomas involving the prostate. A study of 13 cases. *Cancer*. 1985;56:2932-8. [https://doi.org/10.1002/1097-0142\(19851215\)56:12<2932::aid-cncr2820561234>3.0.co;2-h](https://doi.org/10.1002/1097-0142(19851215)56:12<2932::aid-cncr2820561234>3.0.co;2-h)
- [72] Wang C, Jiang P, Li J. Primary lymphomas of the prostate: Two case reports and a review of the literature. *Contemp Oncol (Pozn)*. 2012;16:456-9. <https://doi.org/10.5114/wo.2012.31781>
- [73] Epstein JI, Lieberman PH. Mucinous adenocarcinoma of the prostate gland. *Am J Surg Pathol*. 1985;9:299-308. <https://doi.org/10.1097/0000478-198504000-00006>
- [74] di Sant'Agnese PA. Neuroendocrine differentiation in carcinoma of the prostate. Diagnostic, prognostic, and therapeutic implications. *Cancer*. 1992;70:254-68. [https://doi.org/10.1002/1097-0142\(19920701\)70:1+<254::aid-cncr2820701312>3.0.co;2-e](https://doi.org/10.1002/1097-0142(19920701)70:1+<254::aid-cncr2820701312>3.0.co;2-e)
- [75] di Sant'Agnese PA. Neuroendocrine differentiation in prostatic carcinoma: An update on recent developments. *Ann Oncol*. 2001;12 Suppl 2:S135-40. [https://www.annalsofoncology.org/article/S0923-7534\(19\)54484-2/pdf](https://www.annalsofoncology.org/article/S0923-7534(19)54484-2/pdf)
- [76] Hu J, Han B, Huang J. Morphologic spectrum of neuroendocrine tumors of the prostate: An updated review. *Arch Pathol Lab Med*. 2020;144:320-5. <https://doi.org/10.5858/arpa.2019-0434-RA>
- [77] Sargos P, Ferretti L, Gross-Goupil M, Orre M, Cornelis F, Henriques de Figueiredo B, et al. Characterization of prostate neuroendocrine cancers and therapeutic management: A literature review. *Prostate Cancer Prostatic Dis*. 2014;17:220-6. <https://doi.org/10.1038/pcan.2014.17>
- [78] Tetu B, Ro JY, Ayala AG, Johnson DE, Logothetis CJ, Ordonez NG. Small cell carcinoma of the prostate. Part i. A clinicopathologic study of 20 cases. *Cancer*. 1987;59:1803-9. [https://doi.org/10.1002/1097-0142\(19870515\)59:10<1803::aid-cncr2820591019>3.0.co;2-x](https://doi.org/10.1002/1097-0142(19870515)59:10<1803::aid-cncr2820591019>3.0.co;2-x)
- [79] Tetu B, Ro JY, Ayala AG, Ordonez NG, Logothetis CJ, von Eschenbach AC. Small cell carcinoma of prostate associated with myasthenic (eaton-lambert) syndrome. *Urology*. 1989;33:148-52. [https://doi.org/10.1016/0090-4295\(89\)90017-4](https://doi.org/10.1016/0090-4295(89)90017-4)
- [80] Divatia MK, Ro JY. Intraductal carcinoma of the prostate gland: Recent advances. *Yonsei Med J*. 2016;57:1054-62. <https://doi.org/10.3349/ymj.2016.57.5.1054>
- [81] Epstein JI. Prostatic ductal adenocarcinoma: A mini review. *Med Princ Pract*. 2010;19:82-5. <https://doi.org/10.1159/000252842>
- [82] Epstein JI, Woodruff JM. Adenocarcinoma of the prostate with endometrioid features. A light microscopic and immunohistochemical study of ten cases. *Cancer*. 1986;57:111-9. [https://doi.org/10.1002/1097-0142\(19860101\)57:1<111::aid-cncr2820570123>3.0.co;2-n](https://doi.org/10.1002/1097-0142(19860101)57:1<111::aid-cncr2820570123>3.0.co;2-n)
- [83] Varma M, Delahunt B, Egevad L, Samaratunga H, Kristiansen G. Intraductal carcinoma of the prostate: A critical re-appraisal. *Virchows Arch*. 2019;474:525-34. <https://doi.org/10.1007/s00428-019-02544-6>
- [84] Miura N, Mori K, Mostafaei H, Quhal F, Motlagh RS, Pradere B, et al. The prognostic impact of intraductal carcinoma of the prostate: A systematic review and meta-analysis. *J Urol*. 2020;204:909-17. <https://doi.org/10.1097/JU.0000000000001290>
- [85] Zhang YC, Sun GL, Ma DL, Wei C, Shang HJ, Liu Z, et al. The presence of intraductal carcinoma of the prostate is closely associated with poor prognosis: A systematic review and meta-analysis. *Asian J Androl*. 2020;23:103-8. [https://doi.org/10.4103/aja.aja\\_21\\_20](https://doi.org/10.4103/aja.aja_21_20)
- [86] Gleason DF, Mellinger GT. Prediction of prognosis for prostatic adenocarcinoma by combined histological grading and clinical staging. *J Urol*. 1974;111:58-64. [https://doi.org/10.1016/s0022-5347\(17\)59889-4](https://doi.org/10.1016/s0022-5347(17)59889-4)
- [87] Epstein JI. A new contemporary prostate cancer grading system. *Ann Pathol*. 2015;35:474-6. <https://doi.org/10.1016/j.annpat.2015.09.002>
- [88] Epstein JI, Zelefsky MJ, Sjoberg DD, Nelson JB, Egevad L, Magi-Galluzzi C, et al. A contemporary prostate cancer grading system: A validated alternative to the gleason score. *Eur Urol*. 2016;69:428-35. <https://doi.org/10.1016/j.eururo.2015.06.046>
- [89] Epstein JI. Prostate cancer grading: A decade after the 2005 modified system. *Mod Pathol*. 2018;31 Suppl 1 S47-63. <https://doi.org/10.1038/modpathol.2017.133>
- [90] Epstein JI. Prostate cancer grading: A decade after the 2005 modified system. *Mod Pathol*. 2018;31:S47-63. <https://doi.org/10.1038/modpathol.2017.133>

- [91] Miller DC, Hafez KS, Stewart A, Montie JE, Wei JT. Prostate carcinoma presentation, diagnosis, and staging: An update from the national cancer data base. *Cancer*. 2003;98:1169-78. <https://doi.org/10.1002/cncr.11635>
- [92] Catalona WJ, Richie JP, Ahmann FR, Hudson MA, Scardino PT, Flanigan RC, et al. Comparison of digital rectal examination and serum prostate specific antigen in the early detection of prostate cancer: Results of a multicenter clinical trial of 6,630 men. *J Urol*. 1994;151:1283-90. [https://doi.org/10.1016/s0022-5347\(17\)35233-3](https://doi.org/10.1016/s0022-5347(17)35233-3)
- [93] Richie JP, Catalona WJ, Ahmann FR, Hudson MA, Scardino PT, Flanigan RC, et al. Effect of patient age on early detection of prostate cancer with serum prostate-specific antigen and digital rectal examination. *Urology*. 1993;42:365-74. [https://doi.org/10.1016/0090-4295\(93\)90359-i](https://doi.org/10.1016/0090-4295(93)90359-i)
- [94] Yamamoto T, Ito K, Ohi M, Kubota Y, Suzuki K, Fukabori Y, et al. Diagnostic significance of digital rectal examination and transrectal ultrasonography in men with prostate-specific antigen levels of 4 ng/ml or less. *Urology*. 2001;58:994-8. [https://doi.org/10.1016/s0090-4295\(01\)01409-1](https://doi.org/10.1016/s0090-4295(01)01409-1)
- [95] Kupelian V, Wei JT, O'Leary MP, Kusek JW, Litman HJ, Link CL, et al. Prevalence of lower urinary tract symptoms and effect on quality of life in a racially and ethnically diverse random sample: The boston area community health (bach) survey. *Arch Intern Med*. 2006;166:2381-7. <https://doi.org/10.1001/archinte.166.21.2381>
- [96] Hale N, Choi K, Lohri J. Primary care evaluation and treatment of men with lower urinary tract symptoms. *J Am Osteopath Assoc*. 2014;114:566-71. <https://doi.org/10.7556/jaoa.2014.110>
- [97] Loeb S, Catalona WJ. What is the role of digital rectal examination in men undergoing serial screening of serum psa levels? *Nat Clin Pract Urol*. 2009;6:68-9. <https://doi.org/10.1038/ncpuro1294>
- [98] Coley CM, Barry MJ, Fleming C, Mulley AG. Early detection of prostate cancer. Part i: Prior probability and effectiveness of tests. The american college of physicians. *Ann Intern Med*. 1997;126:394-406. <https://doi.org/10.7326/0003-4819-126-5-199703010-00010>
- [99] Nadler RB, Humphrey PA, Smith DS, Catalona WJ, Ratliff TL. Effect of inflammation and benign prostatic hyperplasia on elevated serum prostate specific antigen levels. *J Urol*. 1995;154:407-13. <https://doi.org/10.1097/00005392-199508000-00023>
- [100] Wolf AM, Wender RC, Etzioni RB, Thompson IM, D'Amico AV, Volk RJ, et al. American cancer society guideline for the early detection of prostate cancer: Update 2010. *CA Cancer J Clin*. 2010;60:70-98. <https://doi.org/10.3322/caac.20066>
- [101] Holmstrom B, Johansson M, Bergh A, Stenman UH, Hallmans G, Stattin P. Prostate specific antigen for early detection of prostate cancer: Longitudinal study. *BMJ*. 2009;339:b3537. <https://doi.org/10.1136/bmj.b3537>
- [102] Thompson IM, Pauler DK, Goodman PJ, Tangen CM, Lucia MS, Parnes HL, et al. Prevalence of prostate cancer among men with a prostate-specific antigen level < or =4.0 ng per milliliter. *N Engl J Med*. 2004;350:2239-46. <https://doi.org/10.1056/NEJMoa031918>
- [103] Dong F, Kattan MW, Steyerberg EW, Jones JS, Stephenson AJ, Schroder FH, et al. Validation of pretreatment nomograms for predicting indolent prostate cancer: Efficacy in contemporary urological practice. *J Urol*. 2008;180:150-4; discussion 4. <https://doi.org/10.1016/j.juro.2008.03.053>
- [104] Carter HB. Prostate cancers in men with low psa levels--must we find them? *N Engl J Med*. 2004;350:2292-4. <https://doi.org/10.1056/NEJMe048003>
- [105] Mottet N, Bellmunt J, Bolla M, Briers E, Cumberbatch MG, De Santis M, et al. EAU-ESTRO-siog guidelines on prostate cancer. Part 1: Screening, diagnosis, and local treatment with curative intent. *Eur Urol*. 2017;71:618-29. <https://doi.org/10.1016/j.eururo.2016.08.003>
- [106] Catalona WJ, Partin AW, Slawin KM, Brawer MK, Flanigan RC, Patel A, et al. Use of the percentage of free prostate-specific antigen to enhance differentiation of prostate cancer from benign prostatic disease: A prospective multicenter clinical trial. *JAMA*. 1998;279:1542-7. <https://doi.org/10.1001/jama.279.19.1542>
- [107] Woodrum DL, Brawer MK, Partin AW, Catalona WJ, Southwick PC. Interpretation of free prostate specific antigen clinical research studies for the detection of prostate cancer. *J Urol*. 1998;159:5-12. [https://doi.org/10.1016/s0022-5347\(01\)63996-x](https://doi.org/10.1016/s0022-5347(01)63996-x)

- [108] Huang Y, Li ZZ, Huang YL, Song HJ, Wang YJ. Value of free/total prostate-specific antigen (f/t psa) ratios for prostate cancer detection in patients with total serum prostate-specific antigen between 4 and 10 ng/ml: A meta-analysis. *Medicine (Baltimore)*. 2018;97:e0249. <https://doi.org/10.1097/MD.00000000000010249>
- [109] Loeb S, Catalona WJ. The prostate health index: A new test for the detection of prostate cancer. *Ther Adv Urol*. 2014;6:74-7. <https://doi.org/10.1177/1756287213513488>
- [110] Bryant RJ, Sjoberg DD, Vickers AJ, Robinson MC, Kumar R, Marsden L, et al. Predicting high-grade cancer at ten-core prostate biopsy using four kallikrein markers measured in blood in the protect study. *J Natl Cancer Inst*. 2015;107:djv095 <https://doi.org/10.1093/jnci/djv095>
- [111] Konety B, Zappala SM, Parekh DJ, Osterhout D, Schock J, Chudler RM, et al. The 4kscore® test reduces prostate biopsy rates in community and academic urology practices. *Rev Urol*. 2015;17:231-40. <https://www.ncbi.nlm.nih.gov/pmc/articles/PMC4735670/>
- [112] Parekh DJ, Punnen S, Sjoberg DD, Asroff SW, Bailen JL, Cochran JS, et al. A multi-institutional prospective trial in the USA confirms that the 4kscore accurately identifies men with high-grade prostate cancer. *Eur Urol*. 2015;68:464-70. <https://doi.org/10.1016/j.eururo.2014.10.021>
- [113] Wang W, Wang M, Wang L, Adams TS, Tian Y, Xu J. Diagnostic ability of %p2psa and prostate health index for aggressive prostate cancer: A meta-analysis. *Sci Rep*. 2014;4:5012. <https://doi.org/10.1038/srep05012>
- [114] Bruzzese D, Mazarella C, Ferro M, Perdon S, Chiodini P, Perruolo G, et al. Prostate health index vs percent free prostate-specific antigen for prostate cancer detection in men with "gray" prostate-specific antigen levels at first biopsy: Systematic review and meta-analysis. *Transl Res*. 2014;164:444-51. <https://doi.org/10.1016/j.trsl.2014.06.006>
- [115] Lughezzani G, Lazzeri M, Haese A, McNicholas T, de la Taille A, Buffi NM, et al. Multicenter european external validation of a prostate health index-based nomogram for predicting prostate cancer at extended biopsy. *Eur Urol*. 2014;66:906-12. <https://doi.org/10.1016/j.eururo.2013.12.005>
- [116] Lazzeri M, Haese A, Abrate A, de la Taille A, Redorta JP, McNicholas T, et al. Clinical performance of serum prostate-specific antigen isoform [-2]proPSA (p2PSA) and its derivatives, %p2PSA and the prostate health index (phi), in men with a family history of prostate cancer: Results from a multicentre european study, the Prometheus project. *BJU Int*. 2013;112:313-21. <https://doi.org/10.1111/bju.12217>
- [117] Voigt JD, Zappala SM, Vaughan ED, Wein AJ. The kallikrein panel for prostate cancer screening: Its economic impact. *Prostate*. 2014;74:250-9. <https://doi.org/10.1002/pros.22746>
- [118] Zappala SM, Scardino PT, Okrongly D, Linder V, Dong Y. Clinical performance of the 4kscore test to predict high-grade prostate cancer at biopsy: A meta-analysis of us and european clinical validation study results. *Rev Urol*. 2017;19:149-55. <https://doi.org/10.3909/riu0776>
- [119] Nordstrom T, Vickers A, Assel M, Lilja H, Gronberg H, Eklund M. Comparison between the four-kallikrein panel and prostate health index for predicting prostate cancer. *Eur Urol*. 2015;68:139-46. <https://doi.org/10.1016/j.eururo.2014.08.010>
- [120] Hessels D, Schalken JA. The use of pca3 in the diagnosis of prostate cancer. *Nat Rev Urol*. 2009;6:255-61. <https://doi.org/10.1038/nrurol.2009.40>
- [121] Duffy MJ. Biomarkers for prostate cancer: Prostate-specific antigen and beyond. *Clin Chem Lab Med*. 2020;58:326-39. <https://doi.org/10.1515/cclm-2019-0693>
- [122] Wei JT, Feng Z, Partin AW, Brown E, Thompson I, Sokoll L, et al. Can urinary pca3 supplement psa in the early detection of prostate cancer? *J Clin Oncol*. 2014;32:4066-72. <https://doi.org/10.1200/JCO.2013.52.8505>
- [123] Scattoni V, Lazzeri M, Lughezzani G, De Luca S, Passera R, Bollito E, et al. Head-to-head comparison of prostate health index and urinary pca3 for predicting cancer at initial or repeat biopsy. *J Urol*. 2013;190:496-501. <https://doi.org/10.1016/j.juro.2013.02.3184>
- [124] Seisen T, Roupert M, Brault D, Leon P, Cancel-Tassin G, Comperat E, et al. Accuracy of the prostate health index versus the urinary prostate cancer antigen 3 score to predict overall and significant prostate cancer at initial biopsy. *Prostate*. 2015;75:103-11. <https://doi.org/10.1002/pros.22898>

- [125] Van Neste L, Hendriks RJ, Dijkstra S, Trooskens G, Cornel EB, Jannink SA, et al. Detection of high-grade prostate cancer using a urinary molecular biomarker-based risk score. *Eur Urol*. 2016;70:740-8. <https://doi.org/10.1016/j.eururo.2016.04.012>
- [126] Bronimann S, Pradere B, Karakiewicz P, Abufaraj M, Briganti A, Shariat SF. An overview of current and emerging diagnostic, staging and prognostic markers for prostate cancer. *Expert Rev Mol Diagn*. 2020;20:841-50 <https://doi.org/10.1080/14737159.2020.1785288>
- [127] Tomlins SA, Rhodes DR, Perner S, Dhanasekaran SM, Mehra R, Sun XW, et al. Recurrent fusion of *tmprss2* and *ets* transcription factor genes in prostate cancer. *Science*. 2005;310:644-8. <https://doi.org/10.1126/science.1117679>
- [128] Pettersson A, Graff RE, Bauer SR, Pitt MJ, Lis RT, Stack EC, et al. The *tmprss2:Erg* rearrangement, *erg* expression, and prostate cancer outcomes: A cohort study and meta-analysis. *Cancer Epidemiol Biomarkers Prev*. 2012;21:1497-509. <https://doi.org/10.1158/1055-9965.EPI-12-0042>
- [129] Tomlins SA, Day JR, Lonigro RJ, Hovelson DH, Siddiqui J, Kunju LP, et al. Urine *tmprss2:Erg* plus *pca3* for individualized prostate cancer risk assessment. *Eur Urol*. 2016;70:45-53. <https://doi.org/10.1016/j.eururo.2015.04.039>
- [130] Leyten GH, Hessels D, Jannink SA, Smit FP, de Jong H, Cornel EB, et al. Prospective multicentre evaluation of *pca3* and *tmprss2-erg* gene fusions as diagnostic and prognostic urinary biomarkers for prostate cancer. *Eur Urol*. 2014;65:534-42. <https://doi.org/10.1016/j.eururo.2012.11.014>
- [131] Partin AW, Van Neste L, Klein EA, Marks LS, Gee JR, Troyer DA, et al. Clinical validation of an epigenetic assay to predict negative histopathological results in repeat prostate biopsies. *J Urol*. 2014;192:1081-7. <https://doi.org/10.1016/j.juro.2014.04.013>
- [132] Stewart GD, Van Neste L, Delvenne P, Delree P, Delga A, McNeill SA, et al. Clinical utility of an epigenetic assay to detect occult prostate cancer in histopathologically negative biopsies: Results of the matloc study. *J Urol*. 2013;189:1110-6. <https://doi.org/10.1016/j.juro.2012.08.219>
- [133] Gaudreau PO, Stagg J, Soulieres D, Saad F. The present and future of biomarkers in prostate cancer: Proteomics, genomics, and immunology advancements. *Biomark Cancer*. 2016;8:15-33. <https://doi.org/10.4137/BIC.S31802>
- [134] Bishoff JT, Freedland SJ, Gerber L, Tennstedt P, Reid J, Welbourn W, et al. Prognostic utility of the cell cycle progression score generated from biopsy in men treated with prostatectomy. *J Urol*. 2014;192:409-14. <https://doi.org/10.1016/j.juro.2014.02.003>
- [135] Freedland SJ, Gerber L, Reid J, Welbourn W, Tikishvili E, Park J, et al. Prognostic utility of cell cycle progression score in men with prostate cancer after primary external beam radiation therapy. *Int J Radiat Oncol Biol Phys*. 2013;86:848-53. <https://doi.org/10.1016/j.ijrobp.2013.04.043>
- [136] Cuzick J, Berney DM, Fisher G, Mesher D, Moller H, Reid JE, et al. Prognostic value of a cell cycle progression signature for prostate cancer death in a conservatively managed needle biopsy cohort. *Br J Cancer*. 2012;106:1095-9. <https://doi.org/10.1038/bjc.2012.39>
- [137] Dalela D, Loppenberg B, Sood A, Sammon J, Abdollah F. Contemporary role of the Decipher® test in prostate cancer management: Current practice and future perspectives. *Rev Urol*. 2016;18:1-9. <https://www.ncbi.nlm.nih.gov/pmc/articles/PMC4859922>
- [138] Marrone M, Potosky AL, Penson D, Freedman AN. A 22 gene-expression assay, Decipher® (genomedx Biosciences) to predict five-year risk of metastatic prostate cancer in men treated with radical prostatectomy. *PLoS Curr*. 2015;7. <https://doi.org/10.1371/currents.eogt.761b81608129ed61b0b48d42c04f92a4>
- [139] Spratt DE, Yousefi K, Deheshi S, Ross AE, Den RB, Schaeffer EM, et al. Individual patient-level meta-analysis of the performance of the Decipher genomic classifier in high-risk men after prostatectomy to predict development of metastatic disease. *J Clin Oncol*. 2017;35:1991-8. <https://doi.org/10.1200/JCO.2016.70.2811>
- [140] Spratt DE, Dai DLY, Den RB, Troncoso P, Yousefi K, Ross AE, et al. Performance of a prostate cancer genomic classifier in predicting metastasis in men with prostate-specific antigen persistence postprostatectomy. *Eur Urol*. 2018;74:107-14. <https://doi.org/10.1016/j.eururo.2017.11.024>

- [141] Michalopoulos SN, Kella N, Payne R, Yohannes P, Singh A, Hettinger C, et al. Influence of a genomic classifier on post-operative treatment decisions in high-risk prostate cancer patients: Results from the pro-act study. *Curr Med Res Opin.* 2014;30:1547-56. <https://doi.org/10.1185/03007995.2014.919908>
- [142] Badani KK, Thompson DJ, Brown G, Holmes D, Kella N, Albala D, et al. Effect of a genomic classifier test on clinical practice decisions for patients with high-risk prostate cancer after surgery. *BJU Int.* 2015;115:419-29. <https://doi.org/10.1111/bju.12789>
- [143] Alford AV, Brito JM, Yadav KK, Yadav SS, Tewari AK, Renzulli J. The use of biomarkers in prostate cancer screening and treatment. *Rev Urol.* 2017;19:221-34. <https://doi.org/10.3909/riu0772>
- [144] Eggener S, Karsh LI, Richardson T, Shindel AW, Lu R, Rosenberg S, et al. A 17-gene panel for prediction of adverse prostate cancer pathologic features: Prospective clinical validation and utility. *Urology.* 2019;126:76-82. <https://doi.org/10.1016/j.urology.2018.11.050>
- [145] Shipitsin M, Small C, Choudhury S, Giladi E, Friedlander S, Nardone J, et al. Identification of proteomic biomarkers predicting prostate cancer aggressiveness and lethality despite biopsy-sampling error. *Br J Cancer.* 2014;111:1201-12. <https://doi.org/10.1038/bjc.2014.396>
- [146] Blume-Jensen P, Berman DM, Rimm DL, Shipitsin M, Putzi M, Nifong TP, et al. Development and clinical validation of an in situ biopsy-based multimarker assay for risk stratification in prostate cancer. *Clin Cancer Res.* 2015;21:2591-600. <https://doi.org/10.1158/1078-0432.CCR-14-2603>
- [147] Counago F, Lopez-Campos F, Diaz-Gavela AA, Almagro E, Fernandez-Pascual E, Henriquez I, et al. Clinical applications of molecular biomarkers in prostate cancer. *Cancers (Basel).* 2020;12:1550 <https://doi.org/10.3390/cancers12061550>
- [148] Jeronimo C, Bastian PJ, Bjartell A, Carbone GM, Catto JW, Clark SJ, et al. Epigenetics in prostate cancer: Biologic and clinical relevance. *Eur Urol.* 2011;60:753-66. <https://doi.org/10.1016/j.eururo.2011.06.035>
- [149] van der Leest M, Cornel E, Israel B, Hendriks R, Padhani AR, Hoogenboom M, et al. Head-to-head comparison of transrectal ultrasound-guided prostate biopsy versus multiparametric prostate resonance imaging with subsequent magnetic resonance-guided biopsy in biopsy-naive men with elevated prostate-specific antigen: A large prospective multicenter clinical study. *Eur Urol.* 2019;75:570-8. <https://doi.org/10.1016/j.eururo.2018.11.023>
- [150] Ahmed HU, El-Shater Bosaily A, Brown LC, Gabe R, Kaplan R, Parmar MK, et al. Diagnostic accuracy of multi-parametric MRI and TRUS biopsy in prostate cancer (promis): A paired validating confirmatory study. *The Lancet.* 2017;389:815-22. [https://doi.org/10.1016/s0140-6736\(16\)32401-1](https://doi.org/10.1016/s0140-6736(16)32401-1)
- [151] Arsov C, Becker N, Rabenalt R, Hiester A, Quentin M, Dietzel F, et al. The use of targeted MR-guided prostate biopsy reduces the risk of gleason upgrading on radical prostatectomy. *J Cancer Res Clin Oncol.* 2015;141:2061-8. <https://doi.org/10.1007/s00432-015-1991-5>
- [152] Evans SM, Patabendi Bandarage V, Kronborg C, Earnest A, Millar J, Clouston D. Gleason group concordance between biopsy and radical prostatectomy specimens: A cohort study from prostate cancer outcome registry - victoria. *Prostate Int.* 2016;4:145-51. <https://doi.org/10.1016/j.pnil.2016.07.004>
- [153] Jones TA, Radtke JP, Hadaschik B, Marks LS. Optimizing safety and accuracy of prostate biopsy. *Curr Opin Urol.* 2016;26:472-80. <https://doi.org/10.1097/MOU.0000000000000310>
- [154] Descotes JL. Diagnosis of prostate cancer. *Asian J Urol.* 2019;6:129-36. <https://doi.org/10.1016/j.ajur.2018.11.007>
- [155] Walker SM, Choyke PL, Turkbey B. What you need to know before reading multiparametric MRI for prostate cancer. *AJR Am J Roentgenol.* 2020;214:1211-9. <https://doi.org/10.2214/AJR.19.22751>
- [156] Stabile A, Giganti F, Rosenkrantz AB, Taneja SS, Villeirs G, Gill IS, et al. Multiparametric MRI for prostate cancer diagnosis: Current status and future directions. *Nat Rev Urol.* 2020;17:41-61. <https://doi.org/10.1038/s41585-019-0212-4>
- [157] Turkbey B, Rosenkrantz AB, Haider MA, Padhani AR, Villeirs G, Macura KJ, et al. Prostate imaging reporting and data system version 2.1: 2019 update of prostate imaging reporting and data system version 2. *Eur Urol.* 2019;76:340-51. <https://doi.org/10.1016/j.eururo.2019.02.033>

- [158] Padhani AR, Weinreb J, Rosenkrantz AB, Villeirs G, Turkbey B, Barentsz J. Prostate imaging-reporting and data system steering committee: Pi-rads v2 status update and future directions. *Eur Urol*. 2019;75:385-96. <https://doi.org/10.1016/j.eururo.2018.05.035>
- [159] Weinreb JC, Barentsz JO, Choyke PL, Cornud F, Haider MA, Macura KJ, et al. Pi-rads prostate imaging - reporting and data system: 2015, version 2. *Eur Urol*. 2016;69:16-40. <https://doi.org/10.1016/j.eururo.2015.08.052>
- [160] Moore CM, Robertson NL, Arsanious N, Middleton T, Villers A, Klotz L, et al. Image-guided prostate biopsy using magnetic resonance imaging-derived targets: A systematic review. *Eur Urol*. 2013;63:125-40. <https://doi.org/10.1016/j.eururo.2012.06.004>
- [161] Robertson NL, Moore CM, Emberton M. Re: Magnetic resonance imaging/ultrasound fusion guided prostate biopsy improves cancer detection following transrectal ultrasound biopsy and correlates with multiparametric magnetic resonance imaging: P. A. Pinto, p. H. Chung, a. R. Rastinehad, a. A. Baccala, jr., j. Kruecker, c. J. Benjamin, s. Xu, p. Yan, s. Kadoury, c. Chua, j. K. Locklin, b. Turkbey, j. H. Shih, s. P. Gates, c. Buckner, g. Bratslavsky, w. M. Linehan, n. D. Glossop, p. L. Choyke and b. J. Wood *J urol* 2011; 186: 1281-1285. *J Urol*. 2012;187:1511-2. <https://doi.org/10.1016/j.juro.2011.12.007>
- [162] Schoots IG, Roobol MJ, Nieboer D, Bangma CH, Steyerberg EW, Hunink MG. Magnetic resonance imaging-targeted biopsy may enhance the diagnostic accuracy of significant prostate cancer detection compared to standard transrectal ultrasound-guided biopsy: A systematic review and meta-analysis. *Eur Urol*. 2015;68:438-50. <https://doi.org/10.1016/j.eururo.2014.11.037>
- [163] Schoots IG, Petrides N, Giganti F, Bokhorst LP, Rannikko A, Klotz L, et al. Magnetic resonance imaging in active surveillance of prostate cancer: A systematic review. *Eur Urol*. 2015;67:627-36. <https://doi.org/10.1016/j.eururo.2014.10.050>
- [164] Tyson MD, Arora SS, Scarpato KR, Barocas D. Magnetic resonance-ultrasound fusion prostate biopsy in the diagnosis of prostate cancer. *Urol Oncol*. 2016;34:326-32. <https://doi.org/10.1016/j.urolonc.2016.03.005>
- [165] Kasivisvanathan V, Rannikko AS, Borghi M, Panebianco V, Mynderse LA, Vaarala MH, et al. MRI-targeted or standard biopsy for prostate-cancer diagnosis. *N Engl J Med*. 2018;378:1767-77. <https://doi.org/10.1056/NEJMoa1801993>
- [166] Pokorny MR, de Rooij M, Duncan E, Schroder FH, Parkinson R, Barentsz JO, et al. Prospective study of diagnostic accuracy comparing prostate cancer detection by transrectal ultrasound-guided biopsy versus magnetic resonance (MR) imaging with subsequent MR-guided biopsy in men without previous prostate biopsies. *Eur Urol*. 2014;66:22-9. <https://doi.org/10.1016/j.eururo.2014.03.002>
- [167] Turpin A, Girard E, Baillet C, Pasquier D, Olivier J, Villers A, et al. Imaging for metastasis in prostate cancer: A review of the literature. *Front Oncol*. 2020;10. <https://doi.org/10.3389/fonc.2020.00055>
- [168] Husband JE. CT/MRI of nodal metastases in pelvic cancer. *Cancer Imaging*. 2002;2:123-9. <https://doi.org/10.1102/1470-7330.2002.0015>
- [169] Hovels AM, Heesakkers RA, Adang EM, Jager GJ, Strum S, Hoogeveen YL, et al. The diagnostic accuracy of CT and MRI in the staging of pelvic lymph nodes in patients with prostate cancer: A meta-analysis. *Clin Radiol*. 2008;63:387-95. <https://doi.org/10.1016/j.crad.2007.05.022>
- [170] Muteganya R, Goldman S, Aoun F, Roumeguere T, Albisinni S. Current imaging techniques for lymph node staging in prostate cancer: A review. *Front Surg*. 2018;5:74. <https://doi.org/10.3389/fsurg.2018.00074>
- [171] Shen G, Deng H, Hu S, Jia Z. Comparison of choline-PET/CT, MRI, SPECT, and bone scintigraphy in the diagnosis of bone metastases in patients with prostate cancer: A meta-analysis. *Skeletal Radiol*. 2014;43:1503-13. <https://doi.org/10.1007/s00256-014-1903-9>
- [172] Langsteger W, Haim S, Knauer M, Waldenberger P, Emmanuel K, Loidl W, et al. Imaging of bone metastases in prostate cancer: An update. *Q J Nucl Med Mol Imaging*. 2012;56:447-58. <https://www.minervamedica.it/en/journals/nuclear-med-molecular-imaging/article.php?cod=R39Y2012N05A0447>

- [173] Cook GJR, Azad G, Padhani AR. Bone imaging in prostate cancer: The evolving roles of nuclear medicine and radiology. *Clinical and Translational Imaging*. 2016;4:439-47. <https://doi.org/10.1007/s40336-016-0196-5>
- [174] Chang JH, Lim Joon D, Nguyen BT, Hiew CY, Esler S, Angus D, et al. MRI scans significantly change target coverage decisions in radical radiotherapy for prostate cancer. *J Med Imaging Radiat Oncol*. 2014;58:237-43. <https://doi.org/10.1111/1754-9485.12107>
- [175] Engelbrecht MR, Jager GJ, Laheij RJ, Verbeek AL, van Lier HJ, Barentsz JO. Local staging of prostate cancer using magnetic resonance imaging: A meta-analysis. *Eur Radiol*. 2002;12:2294-302. <https://doi.org/10.1007/s00330-002-1389-z>
- [176] Ghafoor S, Burger IA, Vargas AH. Multimodality imaging of prostate cancer. *J Nucl Med*. 2019;60:1350-8. <https://doi.org/10.2967/jnumed.119.228320>
- [177] Zacho HD, Nielsen JB, Afshar-Oromieh A, Haberkorn U, deSouza N, De Paepe K, et al. Prospective comparison of (68)ga-PSMA PET/CT, (18)f-sodium fluoride PET/CT and diffusion weighted-MRI at for the detection of bone metastases in biochemically recurrent prostate cancer. *Eur J Nucl Med Mol Imaging*. 2018;45:1884-97. <https://doi.org/10.1007/s00259-018-4058-4>
- [178] Petersen LJ, Zacho HD. PSMA PET for primary lymph node staging of intermediate and high-risk prostate cancer: An expedited systematic review. *Cancer Imaging*. 2020;20:10. <https://doi.org/10.1186/s40644-020-0290-9>
- [179] Petersen LJ, Nielsen JB, Langkilde NC, Petersen A, Afshar-Oromieh A, De Souza NM, et al. (68)ga-PSMA PET/CT compared with MRI/CT and diffusion-weighted MRI for primary lymph node staging prior to definitive radiotherapy in prostate cancer: A prospective diagnostic test accuracy study. *World J Urol*. 2020;38:939-48. <https://doi.org/10.1007/s00345-019-02846-z>
- [180] Chang JH, Lim Joon D, Anderson NJ, Davis I, Lee ST, Gong S, et al. The feasibility of delivering an IMRT boost to the 11C-choline-PET-defined dominant intraprostatic lesion. *Int J Radiat Oncol Biol Phys*. 2009;75(3 Suppl):S323. <https://doi.org/10.1016/j.ijrobp.2009.07.741>
- [181] Chang JH, Lim Joon D, Lee ST, Gong SJ, Anderson NJ, Scott AM, et al. Intensity modulated radiation therapy dose painting for localized prostate cancer using (11)c-choline positron emission tomography scans. *Int J Radiat Oncol Biol Phys*. 2012;83:e691-6. <https://doi.org/10.1016/j.ijrobp.2012.01.087>
- [182] Grubmuller B, Rasul S, Baltzer P, Fajkovic H, D'Andrea D, Berndl F, et al. Response assessment using [(68) ga]ga-PSMA ligand PET in patients undergoing systemic therapy for metastatic castration-resistant prostate cancer. *Prostate*. 2020;80:74-82. <https://doi.org/10.1002/pros.23919>
- [183] Cuccurullo V, Di Stasio GD, Mansi L. Nuclear medicine in prostate cancer: A new era for radiotracers. *World journal of nuclear medicine*. 2018;17:70-8. [https://doi.org/10.4103/wjnm.WJNM\\_54\\_17](https://doi.org/10.4103/wjnm.WJNM_54_17)
- [184] Vargas HA, Wassberg C, Fox JJ, Wibmer A, Goldman DA, Kuk D, et al. Bone metastases in castration-resistant prostate cancer: Associations between morphologic CT patterns, glycolytic activity, and androgen receptor expression on PET and overall survival. *Radiology*. 2014;271:220-9. <https://doi.org/10.1148/radiol.13130625>
- [185] Chang JH, Joon DL, Lee ST, Gong SJ, Scott AM, Davis ID, et al. Histopathological correlation of (11)c-choline PET scans for target volume definition in radical prostate radiotherapy. *Radiother Oncol*. 2011;99:187-92. <https://doi.org/10.1016/j.radonc.2011.03.012>
- [186] Chang JH, Lim Joon D, Davis ID, Lee ST, Hiew CY, Esler S, et al. Comparison of [(11)c]choline positron emission tomography with t2- and diffusion-weighted magnetic resonance imaging for delineating malignant intraprostatic lesions. *Int J Radiat Oncol Biol Phys*. 2015;92:438-45. <https://doi.org/10.1016/j.ijrobp.2015.02.004>
- [187] Chang JH, Lim Joon D, Lee ST, Hiew CY, Esler S, Gong SJ, et al. Diffusion-weighted MRI, 11C-choline PET and 18f-fluorodeoxyglucose PET for predicting the gleason score in prostate carcinoma. *Eur Radiol*. 2014;24:715-22. <https://doi.org/10.1007/s00330-013-3045-1>
- [188] Testa C, Schiavina R, Lodi R, Salizzoni E, Corti B, Farsad M, et al. Prostate cancer: Sextant localization with MR imaging, MR spectroscopy, and 11C-choline PET/CT. *Radiology*. 2007;244:797-806. <https://doi.org/10.1148/radiol.2443061063>

- [189] Van den Bergh L, Koole M, Isebaert S, Joniau S, Deroose CM, Oyen R, et al. Is there an additional value of (11)c-choline PET-CT to t2-weighted MRI images in the localization of intraprostatic tumor nodules? *Int J Radiat Oncol Biol Phys*. 2012;83:1486-92. <https://doi.org/10.1016/j.ijrobp.2011.10.046>
- [190] Evangelista L, Zattoni F, Guttilla A, Saladini G, Zattoni F, Colletti PM, et al. Choline PET or PET/CT and biochemical relapse of prostate cancer: A systematic review and meta-analysis. *Clin Nucl Med*. 2013;38:305-14. <https://doi.org/10.1097/RLU.0b013e3182867f3c>
- [191] Zimmerman ME, Meyer AR, Rowe SP, Gorin MA. Imaging of prostate cancer with positron emission tomography. *Clin Adv Hematol Oncol*. 2019;17:455-63. <https://www.hematologyandoncology.net/files/2019/08/ho0819Zimmerman-1.pdf>
- [192] Maurer T, Eiber M, Schwaiger M, Gschwend JE. Current use of PSMA-PET in prostate cancer management. *Nat Rev Urol*. 2016;13:226-35. <https://doi.org/10.1038/nrurol.2016.26>
- [193] Han S, Woo S, Kim YJ, Suh CH. Impact of (68)ga-PSMA PET on the management of patients with prostate cancer: A systematic review and meta-analysis. *Eur Urol*. 2018;74:179-90. <https://doi.org/10.1016/j.eururo.2018.03.030>
- [194] Hicks RM, Simko JP, Westphalen AC, Nguyen HG, Greene KL, Zhang L, et al. Diagnostic accuracy of (68)ga-PSMA-11 PET/MRI compared with multiparametric MRI in the detection of prostate cancer. *Radiology*. 2018;289:730-7. <https://doi.org/10.1148/radiol.2018180788>
- [195] Muehlethaler UJ, Burger IA, Becker AS, Schawkat K, Hötter AM, Reiner CS, et al. Diagnostic accuracy of multiparametric MRI versus (68)ga-PSMA-11 PET/MRI for extracapsular extension and seminal vesicle invasion in patients with prostate cancer. *Radiology*. 2019;293:350-8. <https://doi.org/10.1148/radiol.2019190687>
- [196] Grubmüller B, Baltzer P, Hartenbach S, D'Andrea D, Helbich TH, Haug AR, et al. PSMA ligand PET/MRI for primary prostate cancer: Staging performance and clinical impact. *Clin Cancer Res*. 2018;24:6300-7. <https://doi.org/10.1158/1078-0432.CCR-18-0768>
- [197] Maurer T, Gschwend JE, Rauscher I, Souvatzoglou M, Haller B, Weirich G, et al. Diagnostic efficacy of (68)gallium-PSMA positron emission tomography compared to conventional imaging for lymph node staging of 130 consecutive patients with intermediate to high risk prostate cancer. *J Urol*. 2016;195:1436-43. <https://doi.org/10.1016/j.juro.2015.12.025>
- [198] Giesel FL, Fiedler H, Stefanova M, Sterzing F, Rius M, Kopka K, et al. PSMA PET/CT with glu-urea-lys-(ahx)-[(68)ga(hbed-cc)] versus 3D CT volumetric lymph node assessment in recurrent prostate cancer. *Eur J Nucl Med Mol Imaging*. 2015;42:1794-800. <https://doi.org/10.1007/s00259-015-3106-6>
- [199] Maurer T, Eiber M, Fanti S, Budäus L, Panebianco V. Imaging for prostate cancer recurrence. *Eur Urol Focus*. 2016;2:139-50. <https://doi.org/10.1016/j.euf.2016.02.006>
- [200] Fendler WP, Calais J, Eiber M, Flavell RR, Mishoe A, Feng FY, et al. Assessment of 68ga-PSMA-11 PET accuracy in localizing recurrent prostate cancer: A prospective single-arm clinical trial. *JAMA Oncol*. 2019;5:856-63. <https://doi.org/10.1001/jamaoncol.2019.0096>
- [201] Treglia G, Annunziata S, Pizzuto DA, Giovanella L, Prior JO, Ceriani L. Detection rate of (18)f-labeled PSMA PET/CT in biochemical recurrent prostate cancer: A systematic review and a meta-analysis. *Cancers (Basel)*. 2019;11:710. <https://doi.org/10.3390/cancers11050710>
- [202] Tan N, Bavadian N, Calais J, Oyoyo U, Kim J, Turkbey IB, et al. Imaging of prostate specific membrane antigen targeted radiotracers for the detection of prostate cancer biochemical recurrence after definitive therapy: A systematic review and meta-analysis. *J Urol*. 2019;202:231-40. <https://doi.org/10.1097/JU.000000000000198>
- [203] Perera M, Papa N, Roberts M, Williams M, Udovicich C, Vela I, et al. Gallium-68 prostate-specific membrane antigen positron emission tomography in advanced prostate cancer—updated diagnostic utility, sensitivity, specificity, and distribution of prostate-specific membrane antigen-avid lesions: A systematic review and meta-analysis. *Eur Urol*. 2020;77:403-17. <https://doi.org/10.1016/j.eururo.2019.01.049>
- [204] Shetty D, Patel D, Le K, Bui C, Mansberg R. Pitfalls in gallium-68 PSMA PET/CT interpretation—a pictorial review. *Tomography (Ann Arbor, Mich)*. 2018;4:182-93. <https://doi.org/10.18383/j.tom.2018.00021>

- [205] de Galiza Barbosa F, Queiroz MA, Nunes RF, Costa LB, Zaniboni EC, Marin JFG, et al. Nonprostatic diseases on PSMA PET imaging: A spectrum of benign and malignant findings. *Cancer Imaging*. 2020;20:23. <https://doi.org/10.1186/s40644-020-00300-7>
- [206] Hofman MS, Hicks RJ, Maurer T, Eiber M. Prostate-specific membrane antigen PET: Clinical utility in prostate cancer, normal patterns, pearls, and pitfalls. *Radiographics*. 2018;38:200-17. <https://doi.org/10.1148/rg.2018170108>
- [207] Barbosa FG, Queiroz MA, Nunes RF, Marin JFG, Buchpiguel CA, Cerri GG. Clinical perspectives of PSMA PET/MRI for prostate cancer. *Clinics (Sao Paulo)*. 2018;73:e586s. <https://doi.org/10.6061/clinics/2018/e586s>
- [208] Jambor I, Kuisma A, Ramadan S, Huovinen R, Sandell M, Kajander S, et al. Prospective evaluation of planar bone scintigraphy, SPECT, SPECT/CT, 18f-naf PET/CT and whole body 1.5t MRI, including dwi, for the detection of bone metastases in high risk breast and prostate cancer patients: Skeleta clinical trial. *Acta Oncol*. 2016;55:59-67. <https://doi.org/10.3109/0284186X.2015.1027411>
- [209] Iagaru A, Mitra E, Dick DW, Gambhir SS. Prospective evaluation of (99m)tc mdp scintigraphy, (18)f naf PET/CT, and (18)f FDG PET/CT for detection of skeletal metastases. *Mol Imaging Biol*. 2012;14:252-9. <https://doi.org/10.1007/s11307-011-0486-2>
- [210] Shen G, Zhang W, Jia Z, Li J, Wang Q, Deng H. Meta-analysis of diagnostic value of 18f-FDG PET or PET/CT for detecting lymph node and distant metastases in patients with nasopharyngeal carcinoma. *Br J Radiol*. 2014;87:20140296. <https://doi.org/10.1259/bjr.20140296>
- [211] Tateishi U, Morita S, Taguri M, Shizukuishi K, Minamimoto R, Kawaguchi M, et al. A meta-analysis of (18)f-fluoride positron emission tomography for assessment of metastatic bone tumor. *Ann Nucl Med*. 2010;24:523-31. <https://doi.org/10.1007/s12149-010-0393-7>
- [212] Sheikhabaehi S, Jones KM, Werner RA, Salas-Fragomeni RA, Marcus CV, Higuchi T, et al. 18f-naf-PET/CT for the detection of bone metastasis in prostate cancer: A meta-analysis of diagnostic accuracy studies. *Annals of Nuclear Medicine*. 2019;33:351-61. <https://doi.org/10.1007/s12149-019-01343-y>
- [213] Zhou J, Gou Z, Wu R, Yuan Y, Yu G, Zhao Y. Comparison of PSMA-PET/CT, choline-PET/CT, naf-PET/CT, MRI, and bone scintigraphy in the diagnosis of bone metastases in patients with prostate cancer: A systematic review and meta-analysis. *Skeletal Radiol*. 2019;48:1915-24. <https://doi.org/10.1007/s00256-019-03230-z>
- [214] Mohler J, Bahnson RR, Boston B, Busby JE, D'Amico A, Eastham JA, et al. NCCN clinical practice guidelines in oncology: Prostate cancer. *J Natl Compr Canc Netw*. 2010;8:162-200. <http://www.ncbi.nlm.nih.gov/pubmed/20141676>
- [215] Mufarrij P, Sankin A, Godoy G, Lepor H. Pathologic outcomes of candidates for active surveillance undergoing radical prostatectomy. *Urology*. 2010;76:689-92. <https://doi.org/10.1016/j.urology.2009.12.075>
- [216] Zlotta AR, Egawa S, Pushkar D, Govorov A, Kimura T, Kido M, et al. Prevalence of prostate cancer on autopsy: Cross-sectional study on unscreened caucasian and asian men. *J Natl Cancer Inst*. 2013;105:1050-8. <https://doi.org/10.1093/jnci/djt151>
- [217] Klotz L. Contemporary approach to active surveillance for favorable risk prostate cancer. *Asian J Urol*. 2019;6:146-52. <https://doi.org/10.1016/j.ajur.2018.12.003>
- [218] Eggener SE, Badani K, Barocas DA, Barrisford GW, Cheng JS, Chin AI, et al. Gleason 6 prostate cancer: Translating biology into population health. *J Urol*. 2015;194:626-34. <https://doi.org/10.1016/j.juro.2015.01.126>
- [219] Bill-Axelsson A, Holmberg L, Garmo H, Rider JR, Taari K, Busch C, et al. Radical prostatectomy or watchful waiting in early prostate cancer. *N Engl J Med*. 2014;370:932-42. <https://doi.org/10.1056/NEJMoa1311593>
- [220] Wilt TJ, Jones KM, Barry MJ, Andriole GL, Culkin D, Wheeler T, et al. Follow-up of prostatectomy versus observation for early prostate cancer. *N Engl J Med*. 2017;377:132-42. <https://doi.org/10.1056/NEJMoa1615869>

- [221] Hamdy FC, Donovan JL, Lane JA, Mason M, Metcalfe C, Holding P, et al. 10-year outcomes after monitoring, surgery, or radiotherapy for localized prostate cancer. *N Engl J Med*. 2016;375:1415-24. <https://doi.org/10.1056/NEJMoa1606220>
- [222] Neal DE, Metcalfe C, Donovan JL, Lane JA, Davis M, Young GJ, et al. Ten-year mortality, disease progression, and treatment-related side effects in men with localised prostate cancer from the protect randomised controlled trial according to treatment received. *Eur Urol*. 2020;77:320-30. <https://doi.org/10.1016/j.eururo.2019.10.030>
- [223] Cooperberg MR, Carroll PR, Klotz L. Active surveillance for prostate cancer: Progress and promise. *J Clin Oncol*. 2011;29:3669-76. <https://doi.org/10.1200/JCO.2011.34.9738>
- [224] Yamamoto T, Musunuru HB, Vesprini D, Zhang L, Ghanem G, Loblaw A, et al. Metastatic prostate cancer in men initially treated with active surveillance. *J Urol*. 2016;195:1409-14. <https://doi.org/10.1016/j.juro.2015.11.075>
- [225] Dall'Era MA, Klotz L. Active surveillance for intermediate-risk prostate cancer. *Prostate Cancer Prostatic Dis*. 2017;20:1-6. <https://doi.org/10.1038/pcan.2016.51>
- [226] Chen RC, Rumble RB, Loblaw DA, Finelli A, Ehdaie B, Cooperberg MR, et al. Active surveillance for the management of localized prostate cancer (cancer care Ontario guideline): American society of clinical oncology clinical practice guideline endorsement. *J Clin Oncol*. 2016;34:2182-90. <https://doi.org/10.1200/jco.2015.65.7759>
- [227] Klotz L, Loblaw A, Sugar L, Moussa M, Berman DM, Van der Kwast T, et al. Active surveillance magnetic resonance imaging study (asist): Results of a randomized multicenter prospective trial. *Eur Urol*. 2019;75:300-9. <https://doi.org/10.1016/j.eururo.2018.06.025>
- [228] Stavrinides V, Giganti F, Trock B, Punwani S, Allen C, Kirkham A, et al. Five-year outcomes of magnetic resonance imaging-based active surveillance for prostate cancer: A large cohort study. *Eur Urol*. 2020;78:443-51. <https://doi.org/10.1016/j.eururo.2020.03.035>
- [229] Merriel SWD, Hetherington L, Seggie A, Castle JT, Cross W, Roobol MJ, et al. Best practice in active surveillance for men with prostate cancer: A prostate cancer UK consensus statement. *BJU Int*. 2019;124:47-54. <https://doi.org/10.1111/bju.14707>
- [230] Nice guidance – prostate cancer: Diagnosis and management. *BJU International*. 2019;124:9-26. <https://doi.org/10.1111/bju.14809>
- [231] Morash C, Tey R, Agbassi C, Klotz L, McGowan T, Srigley J, et al. Active surveillance for the management of localized prostate cancer: Guideline recommendations. *Canadian Urological Association journal = Journal de l'Association des urologues du Canada*. 2015;9:171-8. <https://doi.org/10.5489/cuaj.2806>
- [232] Sanda MG, Cadeddu JA, Kirkby E, Chen RC, Crispino T, Fontanarosa J, et al. Clinically localized prostate cancer: AUA/ASTRO/SUO guideline. Part i: Risk stratification, shared decision making, and care options. *J Urol*. 2018;199:683-90. <https://doi.org/10.1016/j.juro.2017.11.095>
- [233] European Association U. European association of urology pocket guidelines. 2020 edition. Arnhem, The Netherlands: EAU Guidelines Office; 2020.
- [234] Moltzahn F, Karnes J, Gontero P, Kneitz B, Tombal B, Bader P, et al. Predicting prostate cancer-specific outcome after radical prostatectomy among men with very high-risk ct3b/4 pca: A multi-institutional outcome study of 266 patients. *Prostate Cancer Prostatic Dis*. 2015;18:31-7. <https://doi.org/10.1038/pcan.2014.41>
- [235] Wang Z, Ni Y, Chen J, Sun G, Zhang X, Zhao J, et al. The efficacy and safety of radical prostatectomy and radiotherapy in high-risk prostate cancer: A systematic review and meta-analysis. *World Journal of Surgical Oncology*. 2020;18:42. <https://doi.org/10.1186/s12957-020-01824-9>
- [236] Coughlin GD, Yaxley JW, Chambers SK, Occhipinti S, Samaratunga H, Zajdlewicz L, et al. Robot-assisted laparoscopic prostatectomy versus open radical retropubic prostatectomy: 24-month outcomes from a randomised controlled study. *Lancet Oncol*. 2018;19:1051-60. [https://doi.org/10.1016/s1470-2045\(18\)30357-7](https://doi.org/10.1016/s1470-2045(18)30357-7)
- [237] Yaxley JW, Coughlin GD, Chambers SK, Occhipinti S, Samaratunga H, Zajdlewicz L, et al. Robot-assisted laparoscopic prostatectomy versus open radical retropubic prostatectomy: Early outcomes

- from a randomised controlled phase 3 study. *Lancet*. 2016;388:1057-66.  
[https://doi.org/10.1016/S0140-6736\(16\)30592-X](https://doi.org/10.1016/S0140-6736(16)30592-X)
- [238] Mohler JL, Armstrong AJ, Bahnon RR, D'Amico AV, Davis BJ, Eastham JA, et al. Prostate cancer, version 1.2016. *J Natl Compr Canc Netw*. 2016;14:19-30. <https://doi.org/10.6004/jnccn.2016.0004>
- [239] Fossati N, Willemse PM, Van den Broeck T, van den Bergh RCN, Yuan CY, Briers E, et al. The benefits and harms of different extents of lymph node dissection during radical prostatectomy for prostate cancer: A systematic review. *Eur Urol*. 2017;72:84-109.  
<https://doi.org/10.1016/j.eururo.2016.12.003>
- [240] Joung JY, Cho I-C, Lee KH. Role of pelvic lymph node dissection in prostate cancer treatment. *Korean journal of urology*. 2011;52:437-45. <https://doi.org/10.4111/kju.2011.52.7.437>
- [241] Motterle G, Ahmed ME, Andrews JR, Karnes RJ. The role of radical prostatectomy and lymph node dissection in clinically node positive patients. *Front Oncol*. 2019;9:1395.  
<https://doi.org/10.3389/fonc.2019.01395>
- [242] McKay RR, Feng FY, Wang AY, Wallis CJD, Moses KA. Recent advances in the management of high-risk localized prostate cancer: Local therapy, systemic therapy, and biomarkers to guide treatment decisions. *American Society of Clinical Oncology Educational Book*. 2020;40:e241-52.  
[https://doi.org/10.1200/edbk\\_279459](https://doi.org/10.1200/edbk_279459)
- [243] Widmark A, Klepp O, Solberg A, Damber JE, Angelsen A, Fransson P, et al. Endocrine treatment, with or without radiotherapy, in locally advanced prostate cancer (spcg-7/sfuo-3): An open randomised phase iii trial. *Lancet*. 2009;373:301-8. [https://doi.org/10.1016/S0140-6736\(08\)61815-2](https://doi.org/10.1016/S0140-6736(08)61815-2)
- [244] Warde P, Mason M, Ding K, Kirkbride P, Brundage M, Cowan R, et al. Combined androgen deprivation therapy and radiation therapy for locally advanced prostate cancer: A randomised, phase 3 trial. *Lancet*. 2011;378:2104-11. [https://doi.org/10.1016/s0140-6736\(11\)61095-7](https://doi.org/10.1016/s0140-6736(11)61095-7)
- [245] James ND, Spears MR, Clarke NW, Dearnaley DP, Mason MD, Parker CC, et al. Failure-free survival and radiotherapy in patients with newly diagnosed nonmetastatic prostate cancer: Data from patients in the control arm of the STAMPEDE trial. *JAMA Oncol*. 2016;2:348-57.  
<https://doi.org/10.1001/jamaoncol.2015.4350>
- [246] Donovan JL, Hamdy FC, Lane JA, Mason M, Metcalfe C, Walsh E, et al. Patient-reported outcomes after monitoring, surgery, or radiotherapy for prostate cancer. *N Engl J Med*. 2016;375:1425-37. <https://doi.org/10.1056/NEJMoa1606221>
- [247] Morgan SC, Hoffman K, Loblaw DA, Buyyounouski MK, Patton C, Barocas D, et al. Hypofractionated radiation therapy for localized prostate cancer: An ASTRO, asco, and AUA evidence-based guideline. *J Clin Oncol*. 2018;36:1801-097. <https://doi.org/10.1200/jco.18.01097>
- [248] Morgan SC, Hoffman K, Loblaw DA, Buyyounouski MK, Patton C, Barocas D, et al. Hypofractionated radiation therapy for localized prostate cancer: Executive summary of an ASTRO, asco, and AUA evidence-based guideline. *Pract Radiat Oncol*. 2018;8:354-60.  
<https://doi.org/10.1016/j.prro.2018.08.002>
- [249] Khor R, Duchesne G, Tai KH, Foroudi F, Chander S, Van Dyk S, et al. Direct 2-arm comparison shows benefit of high-dose-rate brachytherapy boost vs external beam radiation therapy alone for prostate cancer. *Int J Radiat Oncol Biol Phys*. 2013;85:679-85.  
<https://doi.org/10.1016/j.ijrobp.2012.07.006>
- [250] Hsu IC, Cabrera AR, Weinberg V, Speight J, Gottschalk AR, Roach M, 3rd, et al. Combined modality treatment with high-dose-rate brachytherapy boost for locally advanced prostate cancer. *Brachytherapy*. 2005;4:202-6. <https://doi.org/10.1016/j.brachy.2005.03.005>
- [251] Morris WJ, Tyldesley S, Rodda S, Halperin R, Pai H, McKenzie M, et al. Androgen suppression combined with elective nodal and dose escalated radiation therapy (the ascende-rt trial): An analysis of survival endpoints for a randomized trial comparing a low-dose-rate brachytherapy boost to a dose-escalated external beam boost for high- and intermediate-risk prostate cancer. *Int J Radiat Oncol Biol Phys*. 2017;98:275-85. <https://doi.org/10.1016/j.ijrobp.2016.11.026>
- [252] Rodda S, Tyldesley S, Morris WJ, Keyes M, Halperin R, Pai H, et al. Ascende-rt: An analysis of treatment-related morbidity for a randomized trial comparing a low-dose-rate brachytherapy boost

- with a dose-escalated external beam boost for high- and intermediate-risk prostate cancer. *Int J Radiat Oncol Biol Phys*. 2017;98:286-95. <https://doi.org/10.1016/j.ijrobp.2017.01.008>
- [253] Stish BJ, Davis BJ, Mynderse LA, McLaren RH, Deufel CL, Choo R. Low dose rate prostate brachytherapy. *Transl Androl Urol*. 2018;7:341-56. <https://doi.org/10.21037/tau.2017.12.15>
- [254] Chao MWT, Grimm P, Yaxley J, Jagavkar R, Ng M, Lawrentschuk N. Brachytherapy: State-of-the-art radiotherapy in prostate cancer. *BJU International*. 2015;116:80-8. <https://doi.org/10.1111/bju.13252>
- [255] Peinemann F, Grouven U, Bartel C, Sauerland S, Borchers H, Pinkawa M, et al. Permanent interstitial low-dose-rate brachytherapy for patients with localised prostate cancer: A systematic review of randomised and nonrandomised controlled clinical trials. *Eur Urol*. 2011;60 (7):881-93. <https://doi.org/10.1016/j.eururo.2011.06.044>
- [256] Peinemann F, Grouven U, Hemkens LG, Bartel C, Borchers H, Pinkawa M, et al. Low-dose rate brachytherapy for men with localized prostate cancer. *Cochrane Database Syst Rev*. 2011:CD008871. <https://doi.org/10.1002/14651858.CD008871.pub2>
- [257] Eifler JB, Feng Z, Lin BM, Partin MT, Humphreys EB, Han M, et al. An updated prostate cancer staging nomogram (Partin tables) based on cases from 2006 to 2011. *BJU Int*. 2013;111:22-9. <https://doi.org/10.1111/j.1464-410X.2012.11324.x>
- [258] Roach M, 3rd. Re: The use of prostate specific antigen, clinical stage and gleason score to predict pathological stage in men with localized prostate cancer. *J Urol*. 1993;150:1923-4. [https://doi.org/10.1016/s0022-5347\(17\)35937-2](https://doi.org/10.1016/s0022-5347(17)35937-2)
- [259] Lawton CA, Michalski J, El-Naqa I, Buyyounouski MK, Lee WR, Menard C, et al. RTOG GU radiation oncology specialists reach consensus on pelvic lymph node volumes for high-risk prostate cancer. *Int J Radiat Oncol Biol Phys*. 2009;74:383-7. <https://doi.org/10.1016/j.ijrobp.2008.08.002>
- [260] Harris VA, Staffurth J, Naismith O, Esmail A, Gulliford S, Khoo V, et al. Consensus guidelines and contouring atlas for pelvic node delineation in prostate and pelvic node intensity modulated radiation therapy. *Int J Radiat Oncol Biol Phys*. 2015;92:874-83. <https://doi.org/10.1016/j.ijrobp.2015.03.021>
- [261] Roach M, Moughan J, Lawton CAF, Dicker AP, Zeitzer KL, Gore EM, et al. Sequence of hormonal therapy and radiotherapy field size in unfavourable, localised prostate cancer (NRG/RTOG 9413): Long-term results of a randomised, phase 3 trial. *Lancet Oncol*. 2018;19:1504-15. [https://doi.org/10.1016/s1470-2045\(18\)30528-x](https://doi.org/10.1016/s1470-2045(18)30528-x)
- [262] Tharmalingam H, Tsang Y, Choudhury A, Alonzi R, Wylie J, Ahmed I, et al. External beam radiation therapy (EBRT) and high-dose-rate (HDR) brachytherapy for intermediate and high-risk prostate cancer: The impact of EBRT volume. *Int J Radiat Oncol Biol Phys*. 2020;106:525-33. <https://doi.org/10.1016/j.ijrobp.2019.09.044>
- [263] Link C, Honeck P, Makabe A, Giordano FA, Bolenz C, Schaefer J, et al. Postoperative elective pelvic nodal irradiation compared to prostate bed irradiation in locally advanced prostate cancer - a retrospective analysis of dose-escalated patients. *Radiat Oncol*. 2019;14:96. <https://doi.org/10.1186/s13014-019-1301-5>
- [264] Aizer AA, Yu JB, McKeon AM, Decker RH, Colberg JW, Peschel RE. Whole pelvic radiotherapy versus prostate only radiotherapy in the management of locally advanced or aggressive prostate adenocarcinoma. *Int J Radiat Oncol Biol Phys*. 2009;75:1344-9. <https://doi.org/10.1016/j.ijrobp.2008.12.082>
- [265] Pommier P, Chabaud S, Lagrange JL, Richaud P, Lesaunier F, Le Prise E, et al. Is there a role for pelvic irradiation in localized prostate adenocarcinoma? Preliminary results of GETUG-01. *J Clin Oncol*. 2007;25:5366-73. <https://doi.org/10.1200/JCO.2006.10.5171>
- [266] Amini A, Jones BL, Yeh N, Rusthoven CG, Armstrong H, Kavanagh BD. Survival outcomes of whole-pelvic versus prostate-only radiation therapy for high-risk prostate cancer patients with use of the national cancer data base. *Int J Radiat Oncol Biol Phys*. 2015;93:1052-63. <https://doi.org/10.1016/j.ijrobp.2015.09.006>
- [267] Lieng H, Kneebone A, Hayden AJ, Christie DRH, Davis BJ, Eade TN, et al. Radiotherapy for node-positive prostate cancer: 2019 recommendations of the Australian and New Zealand radiation

- oncology genito-urinary group. *Radiother Oncol.* 2019;140:68-75.  
<https://doi.org/10.1016/j.radonc.2019.05.016>
- [268] Seisen T, Vetterlein MW, Karabon P, Jindal T, Sood A, Nocera L, et al. Efficacy of local treatment in prostate cancer patients with clinically pelvic lymph node-positive disease at initial diagnosis. *Eur Urol.* 2018;73:452-61. <https://doi.org/10.1016/j.eururo.2017.08.011>
- [269] Ventimiglia E, Seisen T, Abdollah F, Briganti A, Fonteyne V, James N, et al. A systematic review of the role of definitive local treatment in patients with clinically lymph node-positive prostate cancer. *Eur Urol Oncol.* 2019;2:294-301. <https://doi.org/10.1016/j.euo.2019.02.001>
- [270] Tosco L, Briganti A, D'Amico A V, Eastham J, Eisenberger M, Gleave M, et al. Systematic review of systemic therapies and therapeutic combinations with local treatments for high-risk localized prostate cancer. *Eur Urol.* 2019;75:44-60. <https://doi.org/10.1016/j.eururo.2018.07.027>
- [271] Shelley MD, Kumar S, Wilt T, Staffurth J, Coles B, Mason MD. A systematic review and meta-analysis of randomised trials of neo-adjuvant hormone therapy for localised and locally advanced prostate carcinoma. *Cancer Treat Rev.* 2009;35:9-17. [https://doi.org/S0305-7372\(08\)00269-7](https://doi.org/S0305-7372(08)00269-7) [pii] 10.1016/j.ctrv.2008.08.002
- [272] Leal F, Figueiredo MA, Sasse AD. Optimal duration of androgen deprivation therapy following radiation therapy in intermediate- or high-risk nonmetastatic prostate cancer: A systematic review and metaanalysis. *Int Braz J Urol.* 2015;41:425-34. <https://doi.org/10.1590/S1677-5538.IBJU.2014.0412>
- [273] Nabid A, Carrier N, Martin AG, Bahary JP, Lemaire C, Vass S, et al. Duration of androgen deprivation therapy in high-risk prostate cancer: A randomized phase iii trial. *Eur Urol.* 2018;74:432-41. <https://doi.org/10.1016/j.eururo.2018.06.018>
- [274] Rosenthal SA, Hu C, Sartor O, Gomella LG, Amin MB, Purdy J, et al. Effect of chemotherapy with docetaxel with androgen suppression and radiotherapy for localized high-risk prostate cancer: The randomized phase iii NRG oncology RTOG 0521 trial. *J Clin Oncol.* 2019;37:1159-68. <https://doi.org/10.1200/JCO.18.02158>
- [275] Fizazi K, Faivre L, Lesaunier F, Delva R, Gravis G, Rolland F, et al. Androgen deprivation therapy plus docetaxel and estramustine versus androgen deprivation therapy alone for high-risk localised prostate cancer (GETUG 12): A phase 3 randomised controlled trial. *Lancet Oncol.* 2015;16:787-94. [https://doi.org/10.1016/S1470-2045\(15\)00011-X](https://doi.org/10.1016/S1470-2045(15)00011-X)
- [276] Kellokumpu-Lehtinen PL, Hjalms-Eriksson M, Thellenberg-Karlsson C, Astrom L, Franzen L, Fransson AS, et al. Docetaxel versus surveillance after radical radiotherapy for intermediate- or high-risk prostate cancer-results from the prospective, randomised, open-label phase iii spcg-13 trial. *Eur Urol.* 2019;76:823-30. <https://doi.org/10.1016/j.eururo.2019.08.010>
- [277] Rosenthal SA, Hunt D, Sartor AO, Pienta KJ, Gomella L, Grignon D, et al. A phase 3 trial of 2 years of androgen suppression and radiation therapy with or without adjuvant chemotherapy for high-risk prostate cancer: Final results of radiation therapy oncology group phase 3 randomized trial NRG oncology RTOG 9902. *Int J Radiat Oncol Biol Phys.* 2015;93:294-302. <https://doi.org/10.1016/j.ijrobp.2015.05.024>
- [278] Bolla M, van Poppel H, Collette L, van Cangh P, Vekemans K, Da Pozzo L, et al. Postoperative radiotherapy after radical prostatectomy: A randomised controlled trial (EORTC trial 22911). *Lancet.* 2005;366:572-8. [https://doi.org/10.1016/S0140-6736\(05\)67101-2](https://doi.org/10.1016/S0140-6736(05)67101-2)
- [279] Bolla M, van Poppel H, Tombal B, Vekemans K, Da Pozzo L, de Reijke TM, et al. Postoperative radiotherapy after radical prostatectomy for high-risk prostate cancer: Long-term results of a randomised controlled trial (EORTC trial 22911). *Lancet.* 2012;380:2018-27. [https://doi.org/10.1016/S0140-6736\(12\)61253-7](https://doi.org/10.1016/S0140-6736(12)61253-7)
- [280] Thompson IM, Jr., Tangen CM, Paradelo J, Lucia MS, Miller G, Troyer D, et al. Adjuvant radiotherapy for pathologically advanced prostate cancer: A randomized clinical trial. *JAMA.* 2006;296:2329-35. <https://doi.org/10.1001/jama.296.19.2329>
- [281] Thompson IM, Tangen CM, Paradelo J, Lucia MS, Miller G, Troyer D, et al. Adjuvant radiotherapy for pathological t3n0m0 prostate cancer significantly reduces risk of metastases and

- improves survival: Long-term followup of a randomized clinical trial. *J Urol*. 2009;181:956-62. <https://doi.org/10.1016/j.juro.2008.11.032>
- [282] Wiegel T, Bartkowiak D, Bottke D, Bronner C, Steiner U, Siegmann A, et al. Adjuvant radiotherapy versus wait-and-see after radical prostatectomy: 10-year follow-up of the aro 96-02/auo ap 09/95 trial. *Eur Urol*. 2014;66:243-50. <https://doi.org/10.1016/j.eururo.2014.03.011>
- [283] Wiegel T, Bottke D, Steiner U, Siegmann A, Golz R, Storkel S, et al. Phase iii postoperative adjuvant radiotherapy after radical prostatectomy compared with radical prostatectomy alone in pt3 prostate cancer with postoperative undetectable prostate-specific antigen: Aro 96-02/auo ap 09/95. *J Clin Oncol*. 2009;27:2924-30. <https://doi.org/10.1200/JCO.2008.18.9563>
- [284] Morgan SC, Waldron TS, Eapen L, Mayhew LA, Winkquist E, Lukka H, et al. Adjuvant radiotherapy following radical prostatectomy for pathologic t3 or margin-positive prostate cancer: A systematic review and meta-analysis. *Radiother Oncol*. 2008;88:1-9. <https://doi.org/10.1016/j.radonc.2008.04.013>
- [285] Stephenson AJ, Scardino PT, Kattan MW, Pisansky TM, Slawin KM, Klein EA, et al. Predicting the outcome of salvage radiation therapy for recurrent prostate cancer after radical prostatectomy. *J Clin Oncol*. 2007;25:2035-41. <https://doi.org/10.1200/JCO.2006.08.9607>
- [286] Stephenson AJ, Shariat SF, Zelefsky MJ, Kattan MW, Butler EB, Teh BS, et al. Salvage radiotherapy for recurrent prostate cancer after radical prostatectomy. *JAMA*. 2004;291:1325-32. <https://doi.org/10.1001/jama.291.11.1325>
- [287] Pearse M, Fraser-Browne C, Davis ID, Duchesne GM, Fisher R, Frydenberg M, et al. A phase iii trial to investigate the timing of radiotherapy for prostate cancer with high-risk features: Background and rationale of the radiotherapy -- adjuvant versus early salvage (raves) trial. *BJU Int*. 2014;113 Suppl 2:7-12. <https://doi.org/10.1111/bju.12623>
- [288] Vale CL, Brihoum M, Chabaud S, Cook A, Fisher D, Forcat S, et al. Adjuvant or salvage radiotherapy for the treatment of localised prostate cancer? A prospectively planned aggregate data meta-analysis. *Annals of Oncology*. 2019;30 Suppl 5 v883. <https://doi.org/10.1093/annonc/mdz394.041>
- [289] Carrie C, Hasbini A, de Laroche G, Richaud P, Guerif S, Latorzeff I, et al. Salvage radiotherapy with or without short-term hormone therapy for rising prostate-specific antigen concentration after radical prostatectomy (GETUG-afu 16): A randomised, multicentre, open-label phase 3 trial. *Lancet Oncol*. 2016;17:747-56. [https://doi.org/10.1016/S1470-2045\(16\)00111-X](https://doi.org/10.1016/S1470-2045(16)00111-X)
- [290] Shipley WU, Seiferheld W, Lukka HR, Major PP, Heney NM, Grignon DJ, et al. Radiation with or without antiandrogen therapy in recurrent prostate cancer. *N Engl J Med*. 2017;376:417-28. <https://doi.org/10.1056/NEJMoa1607529>
- [291] Ahlgren GM, Flodgren P, Tammela TLJ, Kellokumpu-Lehtinen P, Borre M, Angelsen A, et al. Docetaxel versus surveillance after radical prostatectomy for high-risk prostate cancer: Results from the prospective randomised, open-label phase 3 scandinavian prostate cancer group 12 trial. *Eur Urol*. 2018;73:870-6. <https://doi.org/10.1016/j.eururo.2018.01.012>
- [292] Lin DW, Shih MC, Aronson W, Basler J, Beer TM, Brophy M, et al. Veterans affairs cooperative studies program study #553: Chemotherapy after prostatectomy for high-risk prostate carcinoma: A phase iii randomized study. *Eur Urol*. 2020;77:563-72. <https://doi.org/10.1016/j.eururo.2019.12.020>
- [293] Bill-Axelsson A, Holmberg L, Garmo H, Taari K, Busch C, Nordling S, et al. Radical prostatectomy or watchful waiting in prostate cancer - 29-year follow-up. *N Engl J Med*. 2018;379:2319-29. <https://doi.org/10.1056/NEJMoa1807801>
- [294] Huggins C, Hodges CV. Studies on prostatic cancer: I. The effect of castration, of estrogen and of androgen injection on serum phosphatases in metastatic carcinoma of the prostate. [reprint from *cancer res*, 1: 293-297, 1941]. *J Urol*. 2002;168:9-12. [https://doi.org/10.1016/s0022-5347\(05\)64820-3](https://doi.org/10.1016/s0022-5347(05)64820-3)
- [295] Gunner C, Gulamhusein A, Rosario DJ. The modern role of androgen deprivation therapy in the management of localised and locally advanced prostate cancer. *J Clin Urol*. 2016;9:24-9. <https://doi.org/10.1177/2051415816654048>

- [296] Bolton EM, Lynch T. Are all gonadotrophin-releasing hormone agonists equivalent for the treatment of prostate cancer? A systematic review. *BJU Int.* 2018;122:371-83. <https://doi.org/10.1111/bju.14168>
- [297] Brawer MK. Hormonal therapy for prostate cancer. *Rev Urol.* 2006;8 Suppl 2:S35-47. <https://www.ncbi.nlm.nih.gov/pmc/articles/PMC1578721/>
- [298] Klotz L, Boccon-Gibod L, Shore ND, Andreou C, Persson BE, Cantor P, et al. The efficacy and safety of degarelix: A 12-month, comparative, randomized, open-label, parallel-group phase iii study in patients with prostate cancer. *BJU Int.* 2008;102:1531-8. <https://doi.org/10.1111/j.1464-410X.2008.08183.x>
- [299] Tombal B, Miller K, Boccon-Gibod L, Schroder F, Shore N, Crawford ED, et al. Additional analysis of the secondary end point of biochemical recurrence rate in a phase 3 trial (cs21) comparing degarelix 80 mg versus leuprolide in prostate cancer patients segmented by baseline characteristics. *Eur Urol.* 2010;57:836-42. <https://doi.org/10.1016/j.eururo.2009.11.029>
- [300] Mason M, Maldonado Pijoan X, Steidle C, Guerif S, Wiegel T, van der Meulen E, et al. Neoadjuvant androgen deprivation therapy for prostate volume reduction, lower urinary tract symptom relief and quality of life improvement in men with intermediate- to high-risk prostate cancer: A randomised non-inferiority trial of degarelix versus goserelin plus bicalutamide. *Clin Oncol (R Coll Radiol).* 2013;25:190-6. <https://doi.org/10.1016/j.clon.2012.09.010>
- [301] Klotz L, Miller K, Crawford ED, Shore N, Tombal B, Karup C, et al. Disease control outcomes from analysis of pooled individual patient data from five comparative randomised clinical trials of degarelix versus luteinising hormone-releasing hormone agonists. *Eur Urol.* 2014;66:1101-8. <https://doi.org/10.1016/j.eururo.2013.12.063>
- [302] Crook JM, O'Callaghan CJ, Duncan G, Dearnaley DP, Higano CS, Horwitz EM, et al. Intermittent androgen suppression for rising psa level after radiotherapy. *N Engl J Med.* 2012;367:895-903. <https://doi.org/10.1056/NEJMoa1201546>
- [303] Hussain M, Tangen CM, Berry DL, Higano CS, Crawford ED, Liu G, et al. Intermittent versus continuous androgen deprivation in prostate cancer. *The New England journal of medicine.* 2013;368:1314-25. <https://doi.org/10.1056/NEJMoa1212299>
- [304] Hussain M, Tangen C, Higano C, Vogelzang N, Thompson I. Evaluating intermittent androgen-deprivation therapy phase iii clinical trials: The devil is in the details. *J Clin Oncol.* 2016;34:280-5. <https://doi.org/10.1200/JCO.2015.62.8065>
- [305] Mahal BA, Chen MH, Renshaw AA, Loffredo MJ, Kantoff PW, D'Amico AV. Early versus delayed initiation of salvage androgen deprivation therapy and risk of prostate cancer-specific mortality. *J Natl Compr Canc Netw.* 2018;16:727-34. <https://doi.org/10.6004/jnccn.2018.7010>
- [306] Fu AZ, Tsai HT, Haque R, Yood MU, Cassidy-Bushrow AE, Van Den Eeden SK, et al. Mortality and androgen deprivation therapy as salvage treatment for biochemical recurrence after primary therapy for clinically localized prostate cancer. *J Urol.* 2017;197:1448-54. <https://doi.org/10.1016/j.juro.2016.12.086>
- [307] van den Bergh RC, Albertsen PC, Bangma CH, Freedland SJ, Graefen M, Vickers A, et al. Timing of curative treatment for prostate cancer: A systematic review. *Eur Urol.* 2013;64:204-15. <https://doi.org/10.1016/j.eururo.2013.02.024>
- [308] Loblaw DA, Virgo KS, Nam R, Somerfield MR, Ben-Josef E, Mendelson DS, et al. Initial hormonal management of androgen-sensitive metastatic, recurrent, or progressive prostate cancer: 2006 update of an american society of clinical oncology practice guideline. *J Clin Oncol.* 2007;25:1596-605. <https://doi.org/10.1200/JCO.2006.10.1949>
- [309] Duchesne GM, Woo HH, Bassett JK, Bowe SJ, D'Este C, Frydenberg M, et al. Timing of androgen-deprivation therapy in patients with prostate cancer with a rising psa (TROG 03.06 and vcoq pr 01-03 [TOAD]): A randomised, multicentre, non-blinded, phase 3 trial. *Lancet Oncol.* 2016;17:727-37. [https://doi.org/10.1016/S1470-2045\(16\)00107-8](https://doi.org/10.1016/S1470-2045(16)00107-8)
- [310] Garcia-Albeniz X, Chan JM, Paciorek A, Logan RW, Kenfield SA, Cooperberg MR, et al. Immediate versus deferred initiation of androgen deprivation therapy in prostate cancer patients

- with psa-only relapse. An observational follow-up study. *European journal of cancer* (Oxford, England : 1990). 2015;51:817-24. <https://doi.org/10.1016/j.ejca.2015.03.003>
- [311] van den Bergh RC, van Casteren NJ, van den Broeck T, Fordyce ER, Gietzmann WK, Stewart F, et al. Role of hormonal treatment in prostate cancer patients with nonmetastatic disease recurrence after local curative treatment: A systematic review. *Eur Urol*. 2016;69:802-20. <https://doi.org/10.1016/j.eururo.2015.11.023>
- [312] Yang Y, Chen R, Sun T, Zhao L, Liu F, Ren S, et al. Efficacy and safety of combined androgen blockade with antiandrogen for advanced prostate cancer. *Current oncology* (Toronto, Ont). 2019;26:39-47. <https://doi.org/10.3747/co.26.4203>
- [313] Samson DJ, Seidenfeld J, Schmitt B, Hasselblad V, Albertsen PC, Bennett CL, et al. Systematic review and meta-analysis of monotherapy compared with combined androgen blockade for patients with advanced prostate carcinoma. *Cancer*. 2002;95:361-76. <https://doi.org/10.1002/cncr.10647>
- [314] Lukka H, Waldron T, Klotz L, Winkquist E, Trachtenberg J, Genitourinary Cancer Disease Site G, et al. Maximal androgen blockade for the treatment of metastatic prostate cancer—systematic review. *Curr Oncol Rep*. 2006;13:81-93. <http://europepmc.org/abstract/MED/17576447>
- [315] Klotz L. Maximal androgen blockade for advanced prostate cancer. *Best Pract Res Clin Endocrinol Metab*. 2008;22:331-40. <https://doi.org/10.1016/j.beem.2008.01.004>
- [316] Prostate Cancer Trialists' Collaborative Group. Maximum androgen blockade in advanced prostate cancer: An overview of the randomised trials. *Lancet*. 2000;355:1491-8. [https://doi.org/10.1016/S0140-6736\(00\)02163-2](https://doi.org/10.1016/S0140-6736(00)02163-2)
- [317] Takayanagi A, Masumori N, Hashimoto J, Kyoda Y, Yanase M, Tsukamoto T. Effect of delayed maximal androgen blockade therapy for patients with advanced prostate cancer who fail to respond to initial androgen deprivation monotherapy. *Japanese Journal of Clinical Oncology*. 2010;40:1154-8. <https://doi.org/10.1093/jjco/hyq103>
- [318] Klotz L, Drachenberg D, Singal R, Aprikian A, Fradet Y, Kebabdjian M, et al. An open-label, phase 2 trial of bicalutamide dose escalation from 50 mg to 150 mg in men with castration resistance. A canadian urology research consortium study. *Prostate Cancer Prostatic Dis*. 2014;17:320-4. <https://doi.org/10.1038/pcan.2014.24>
- [319] Penson DF, Armstrong AJ, Concepcion R, Agarwal N, Olsson C, Karsh L, et al. Enzalutamide versus bicalutamide in castration-resistant prostate cancer: The strive trial. *J Clin Oncol*. 2016;34:2098-106. <https://doi.org/10.1200/JCO.2015.64.9285>
- [320] Shore ND, Chowdhury S, Villers A, Klotz L, Siemens DR, Phung, et al. Efficacy and safety of enzalutamide versus bicalutamide for patients with metastatic prostate cancer (terrain): A randomised, double-blind, phase 2 study. *Lancet Oncol*. 2016;17:153-63. [https://doi.org/10.1016/S1470-2045\(15\)00518-5](https://doi.org/10.1016/S1470-2045(15)00518-5)
- [321] Tran C, Ouk S, Clegg NJ, Chen Y, Watson PA, Arora V, et al. Development of a second-generation antiandrogen for treatment of advanced prostate cancer. *Science*. 2009;324:787-90. <https://doi.org/10.1126/science.1168175>
- [322] Heidenreich A, Chowdhury S, Klotz L, Siemens DR, Villers A, Ivanescu C, et al. Impact of enzalutamide compared with bicalutamide on quality of life in men with metastatic castration-resistant prostate cancer: Additional analyses from the terrain randomised clinical trial. *Eur Urol*. 2017;71:534-42. <https://doi.org/10.1016/j.eururo.2016.07.027>
- [323] Scher HI, Fizazi K, Saad F, Taplin ME, Sternberg CN, Miller K, et al. Increased survival with enzalutamide in prostate cancer after chemotherapy. *N Engl J Med*. 2012;367:1187-97. <https://doi.org/10.1056/NEJMoa1207506>
- [324] Beer TM, Armstrong AJ, Rathkopf DE, Loriot Y, Sternberg CN, Higano CS, et al. Enzalutamide in metastatic prostate cancer before chemotherapy. *N Engl J Med*. 2014;371:424-33. <https://doi.org/10.1056/NEJMoa1405095>
- [325] Hussain M, Fizazi K, Saad F, Rathenborg P, Shore N, Ferreira U, et al. Enzalutamide in men with nonmetastatic, castration-resistant prostate cancer. *N Engl J Med*. 2018;378:2465-74. <https://doi.org/10.1056/NEJMoa1800536>

- [326] Davis ID, Martin AJ, Stockler MR, Begbie S, Chi KN, Chowdhury S, et al. Enzalutamide with standard first-line therapy in metastatic prostate cancer. *N Engl J Med*. 2019;381:121-31. <https://doi.org/10.1056/NEJMoa1903835>
- [327] Stenzl A, Dunshee C, De Giorgi U, Alekseev B, Iguchi T, Szmulewitz RZ, et al. Effect of enzalutamide plus androgen deprivation therapy on health-related quality of life in patients with metastatic hormone-sensitive prostate cancer: An analysis of the arches randomised, placebo-controlled, phase 3 study. *Eur Urol*. 2020;78:603-14. <https://doi.org/10.1016/j.eururo.2020.03.019>
- [328] Vaishampayan UN, Heilbrun LK, Monk P, Tejwani S, Sonpavde G, Smith D, et al. Randomized trial of enzalutamide versus bicalutamide in combination with androgen deprivation in metastatic hormone sensitive prostate cancer: A prostate cancer clinical trials consortium trial. *Journal of Clinical Oncology*. 2018;36(6 Suppl):190-. [https://doi.org/10.1200/JCO.2018.36.6\\_suppl.190](https://doi.org/10.1200/JCO.2018.36.6_suppl.190)
- [329] Nuhn P, De Bono JS, Fizazi K, Freedland SJ, Grilli M, Kantoff PW, et al. Update on systemic prostate cancer therapies: Management of metastatic castration-resistant prostate cancer in the era of precision oncology. *Eur Urol*. 2019;75:88-99. <https://doi.org/10.1016/j.eururo.2018.03.028>
- [330] de Bono JS, Logothetis CJ, Molina A, Fizazi K, North S, Chu L, et al. Abiraterone and increased survival in metastatic prostate cancer. *The New England journal of medicine*. 2011;364:1995-2005. <https://doi.org/10.1056/NEJMoa1014618>
- [331] Basch E, Autio K, Ryan CJ, Mulders P, Shore N, Kheoh T, et al. Abiraterone acetate plus prednisone versus prednisone alone in chemotherapy-naïve men with metastatic castration-resistant prostate cancer: Patient-reported outcome results of a randomised phase 3 trial. *Lancet Oncol*. 2013;14:1193-9. [https://doi.org/10.1016/S1470-2045\(13\)70424-8](https://doi.org/10.1016/S1470-2045(13)70424-8)
- [332] Ryan CJ, Smith MR, de Bono JS, Molina A, Logothetis CJ, de Souza P, et al. Abiraterone in metastatic prostate cancer without previous chemotherapy. *N Engl J Med*. 2013;368:138-48. <https://doi.org/10.1056/NEJMoa1209096>
- [333] Ryan CJ, Smith MR, Fizazi K, Saad F, Mulders PF, Sternberg CN, et al. Abiraterone acetate plus prednisone versus placebo plus prednisone in chemotherapy-naïve men with metastatic castration-resistant prostate cancer (cou-aa-302): Final overall survival analysis of a randomised, double-blind, placebo-controlled phase 3 study. *Lancet Oncol*. 2015;16:152-60. [https://doi.org/10.1016/S1470-2045\(14\)71205-7](https://doi.org/10.1016/S1470-2045(14)71205-7)
- [334] James ND, de Bono JS, Spears MR, Clarke NW, Mason MD, Dearnaley DP, et al. Abiraterone for prostate cancer not previously treated with hormone therapy. *N Engl J Med*. 2017;377:338-51. <https://doi.org/10.1056/NEJMoa1702900>
- [335] Fizazi K, Tran N, Fein L, Matsubara N, Rodriguez-Antolin A, Alekseev BY, et al. Abiraterone plus prednisone in metastatic, castration-sensitive prostate cancer. *N Engl J Med*. 2017;377:352-60. <https://doi.org/10.1056/NEJMoa1704174>
- [336] Rydzewska LHM, Burdett S, Vale CL, Clarke NW, Fizazi K, Kheoh T, et al. Adding abiraterone to androgen deprivation therapy in men with metastatic hormone-sensitive prostate cancer: A systematic review and meta-analysis. *Eur J Cancer*. 2017;84:88-101. <https://doi.org/10.1016/j.ejca.2017.07.003>
- [337] Zheng X, Zhao X, Xu H, Han X, Xu H, Dong X, et al. Efficacy and safety of abiraterone and enzalutamide for castration-resistant prostate cancer: A systematic review and meta-analysis of randomized controlled trials. *Medicine*. 2019;98:e17748. <https://doi.org/10.1097/MD.00000000000017748>
- [338] Patchell RA, Tibbs PA, Regine WF, Payne R, Saris S, Kryscio RJ, et al. Direct decompressive surgical resection in the treatment of spinal cord compression caused by metastatic cancer: A randomised trial. *Lancet*. 2005;366:643-8. [https://doi.org/10.1016/s0140-6736\(05\)66954-1](https://doi.org/10.1016/s0140-6736(05)66954-1)
- [339] Chen B, Xiao S, Tong X, Xu S, Lin X. Comparison of the therapeutic efficacy of surgery with or without adjuvant radiotherapy versus radiotherapy alone for metastatic spinal cord compression: A meta-analysis. *World Neurosurg*. 2015;83:1066-73. <https://doi.org/10.1016/j.wneu.2014.12.039>
- [340] Maranzano E, Bellavita R, Rossi R, De Angelis V, Frattegiani A, Bagnoli R, et al. Short-course versus split-course radiotherapy in metastatic spinal cord compression: Results of a phase iii,

- randomized, multicenter trial. *J Clin Oncol*. 2005;23:3358-65.  
<https://doi.org/10.1200/JCO.2005.08.193>
- [341] Rades D, Segedin B, Conde-Moreno AJ, Garcia R, Perpar A, Metz M, et al. Radiotherapy with 4 Gy x 5 versus 3 Gy x 10 for metastatic epidural spinal cord compression: Final results of the score-2 trial (aro 2009/01). *J Clin Oncol*. 2016;34:597-602. <https://doi.org/10.1200/JCO.2015.64.0862>
- [342] Francini E, Gray KP, Xie W, Shaw GK, Valenca L, Bernard B, et al. Time of metastatic disease presentation and volume of disease are prognostic for metastatic hormone sensitive prostate cancer (mhspc). *Prostate*. 2018;78:889-95. <https://doi.org/10.1002/pros.23645>
- [343] Gandaglia G, Karakiewicz PI, Briganti A, Passoni NM, Schiffmann J, Trudeau V, et al. Impact of the site of metastases on survival in patients with metastatic prostate cancer. *Eur Urol*. 2015;68:325-34. <https://doi.org/10.1016/j.eururo.2014.07.020>
- [344] Halabi S, Kelly WK, Ma H, Zhou H, Solomon NC, Fizazi K, et al. Meta-analysis evaluating the impact of site of metastasis on overall survival in men with castration-resistant prostate cancer. *J Clin Oncol*. 2016;34:1652-9. <https://doi.org/10.1200/jco.2015.65.7270>
- [345] Hellman S, Weichselbaum RR. Oligometastases. *J Clin Oncol*. 1995;13:8-10.  
<https://doi.org/10.1200/jco.1995.13.1.8>
- [346] Palacios-Eito A, Béjar-Luque A, Rodríguez-Liñán M, García-Cabezas S. Oligometastases in prostate cancer: Ablative treatment. *World journal of clinical oncology*. 2019;10:38-51.  
<https://doi.org/10.5306/wjco.v10.i2.38>
- [347] Ost P, Bossi A, Decaestecker K, De Meerleer G, Giannarini G, Karnes RJ, et al. Metastasis-directed therapy of regional and distant recurrences after curative treatment of prostate cancer: A systematic review of the literature. *Eur Urol*. 2015;67:852-63.  
<https://doi.org/10.1016/j.eururo.2014.09.004>
- [348] Ost P, Jereczek-Fossa BA, Van As N, Zilli T, Muacevic A, Olivier K, et al. Progression-free survival following stereotactic body radiotherapy for oligometastatic prostate cancer treatment-naive recurrence: A multi-institutional analysis. *Eur Urol*. 2016;69:9-12.  
<https://doi.org/10.1016/j.eururo.2015.07.004>
- [349] Muldermans JL, Romak LB, Kwon ED, Park SS, Olivier KR. Stereotactic body radiation therapy for oligometastatic prostate cancer. *Int J Radiat Oncol Biol Phys*. 2016;95:696-702.  
<https://doi.org/10.1016/j.ijrobp.2016.01.032>
- [350] Siva S, Bressel M, Murphy DG, Shaw M, Chander S, Violet J, et al. Stereotactic abative body radiotherapy (SABR) for oligometastatic prostate cancer: A prospective clinical trial. *Eur Urol*. 2018;74:455-62. <https://doi.org/10.1016/j.eururo.2018.06.004>
- [351] Decaestecker K, De Meerleer G, Ameye F, Fonteyne V, Lambert B, Joniau S, et al. Surveillance or metastasis-directed therapy for oligometastatic prostate cancer recurrence (stomp): Study protocol for a randomized phase ii trial. *BMC Cancer*. 2014;14:671. <https://doi.org/10.1186/1471-2407-14-671>
- [352] Palma DA, Olson R, Harrow S, Gaede S, Louie AV, Haasbeek C, et al. Stereotactic ablative radiotherapy versus standard of care palliative treatment in patients with oligometastatic cancers (SABR-comet): A randomised, phase 2, open-label trial. *Lancet*. 2019;393:2051-8.  
[https://doi.org/10.1016/s0140-6736\(18\)32487-5](https://doi.org/10.1016/s0140-6736(18)32487-5)
- [353] Phillips R, Shi WY, Deek M, Radwan N, Lim SJ, Antonarakis ES, et al. Outcomes of observation vs stereotactic ablative radiation for oligometastatic prostate cancer: The oriole phase 2 randomized clinical trial. *JAMA Oncol*. 2020;6:650-9. <https://doi.org/10.1001/jamaoncol.2020.0147>
- [354] Leonel Almeida P, Jorge Pereira B. Local treatment of metastatic prostate cancer: What is the evidence so far? *Prostate Cancer*. 2018;2018:2654572. <https://doi.org/10.1155/2018/2654572>
- [355] Rusthoven CG, Jones BL, Flaig TW, Crawford ED, Koshy M, Sher DJ, et al. Improved survival with prostate radiation in addition to androgen deprivation therapy for men with newly diagnosed metastatic prostate cancer. *J Clin Oncol*. 2016;34:2835-42.  
<https://doi.org/10.1200/JCO.2016.67.4788>

- [356] Burdett S, Boevé LM, Ingleby FC, Fisher DJ, Rydzewska LH, Vale CL, et al. Prostate radiotherapy for metastatic hormone-sensitive prostate cancer: A STOPCAP systematic review and meta-analysis. *Eur Urol*. 2019;76:115-24. <https://doi.org/10.1016/j.eururo.2019.02.003>
- [357] Parker CC, James ND, Brawley CD, Clarke NW, Hoyle AP, Ali A, et al. Radiotherapy to the primary tumour for newly diagnosed, metastatic prostate cancer (STAMPEDE): A randomised controlled phase 3 trial. *Lancet*. 2018;392:2353-66. [https://doi.org/10.1016/S0140-6736\(18\)32486-3](https://doi.org/10.1016/S0140-6736(18)32486-3)
- [358] Boevé LMS, Hulshof M, Vis AN, Zwinderman AH, Twisk JWR, Witjes WPJ, et al. Effect on survival of androgen deprivation therapy alone compared to androgen deprivation therapy combined with concurrent radiation therapy to the prostate in patients with primary bone metastatic prostate cancer in a prospective randomised clinical trial: Data from the horrad trial. *Eur Urol*. 2019;75:410-8. <https://doi.org/10.1016/j.eururo.2018.09.008>
- [359] Tannock IF, de Wit R, Berry WR, Horti J, Pluzanska A, Chi KN, et al. Docetaxel plus prednisone or mitoxantrone plus prednisone for advanced prostate cancer. *N Engl J Med*. 2004;351:1502-12. <https://doi.org/10.1056/NEJMoa040720>
- [360] Petrylak DP, Tangen CM, Hussain MH, Lara PN, Jr., Jones JA, Taplin ME, et al. Docetaxel and estramustine compared with mitoxantrone and prednisone for advanced refractory prostate cancer. *N Engl J Med*. 2004;351:1513-20. <https://doi.org/10.1056/NEJMoa041318>
- [361] Berthold DR, Pond GR, de Wit R, Eisenberger M, Tannock IF. Survival and psa response of patients in the TAX 327 study who crossed over to receive docetaxel after mitoxantrone or vice versa. *Ann Oncol*. 2008;19:1749-53. <https://doi.org/10.1093/annonc/mdn288>
- [362] Berthold DR, Pond GR, Roessner M, de Wit R, Eisenberger M, Tannock AI, et al. Treatment of hormone-refractory prostate cancer with docetaxel or mitoxantrone: Relationships between prostate-specific antigen, pain, and quality of life response and survival in the TAX-327 study. *Clin Cancer Res*. 2008;14:2763-7. <https://doi.org/10.1158/1078-0432.CCR-07-0944>
- [363] Berthold DR, Pond GR, Soban F, de Wit R, Eisenberger M, Tannock IF. Docetaxel plus prednisone or mitoxantrone plus prednisone for advanced prostate cancer: Updated survival in the TAX 327 study. *J Clin Oncol*. 2008;26:242-5. <https://doi.org/10.1200/JCO.2007.12.4008>
- [364] de Bono JS, Oudard S, Ozguroglu M, Hansen S, Machiels JP, Kocak I, et al. Prednisone plus cabazitaxel or mitoxantrone for metastatic castration-resistant prostate cancer progressing after docetaxel treatment: A randomised open-label trial. *Lancet*. 2010;376:1147-54. [https://doi.org/10.1016/s0140-6736\(10\)61389-x](https://doi.org/10.1016/s0140-6736(10)61389-x)
- [365] Gravis G, Fizazi K, Joly F, Oudard S, Priou F, Esterni B, et al. Androgen-deprivation therapy alone or with docetaxel in non-castrate metastatic prostate cancer (GETUG-afu 15): A randomised, open-label, phase 3 trial. *Lancet Oncol*. 2013;14:149-58. [https://doi.org/10.1016/S1470-2045\(12\)70560-0](https://doi.org/10.1016/S1470-2045(12)70560-0)
- [366] Gravis G, Boher JM, Joly F, Soulie M, Albiges L, Priou F, et al. Androgen deprivation therapy (adt) plus docetaxel versus adt alone in metastatic non castrate prostate cancer: Impact of metastatic burden and long-term survival analysis of the randomized phase 3 GETUG-afu15 trial. *Eur Urol*. 2016;70:256-62. <https://doi.org/10.1016/j.eururo.2015.11.005>
- [367] Sweeney CJ, Chen YH, Carducci M, Liu G, Jarrard DF, Eisenberger M, et al. Chemohormonal therapy in metastatic hormone-sensitive prostate cancer. *N Engl J Med*. 2015;373:737-46. <https://doi.org/10.1056/NEJMoa1503747>
- [368] James ND, Sydes MR, Clarke NW, Mason MD, Dearnaley DP, Spears MR, et al. Addition of docetaxel, zoledronic acid, or both to first-line long-term hormone therapy in prostate cancer (STAMPEDE): Survival results from an adaptive, multiarm, multistage, platform randomised controlled trial. *Lancet*. 2016;387:1163-77. [https://doi.org/10.1016/S0140-6736\(15\)01037-5](https://doi.org/10.1016/S0140-6736(15)01037-5)
- [369] Miller RE, Sweeney CJ. Chemotherapy for metastatic castrate-sensitive prostate cancer. *Prostate Cancer Prostatic Dis*. 2016;19:139-44. <https://doi.org/10.1038/pcan.2016.10>
- [370] Clarke NW, Ali A, Ingleby FC, Hoyle A, Amos CL, Attard G, et al. Addition of docetaxel to hormonal therapy in low- and high-burden metastatic hormone sensitive prostate cancer: Long-term survival results from the STAMPEDE trial. *Ann Oncol*. 2019;30:1992-2003. <https://doi.org/10.1093/annonc/mdz396>

- [371] Fizazi K, Jenkins C, Tannock IF. Should docetaxel be standard of care for patients with metastatic hormone-sensitive prostate cancer? Pro and contra. *Ann Oncol*. 2015;26:1660-7. <https://doi.org/10.1093/annonc/mdv245>
- [372] Vale CL, Burdett S, Rydzewska LHM, Albiges L, Clarke NW, Fisher D, et al. Addition of docetaxel or bisphosphonates to standard of care in men with localised or metastatic, hormone-sensitive prostate cancer: A systematic review and meta-analyses of aggregate data. *Lancet Oncol*. 2016;17:243-56. [https://doi.org/10.1016/S1470-2045\(15\)00489-1](https://doi.org/10.1016/S1470-2045(15)00489-1)
- [373] Macherey S, Monsef I, Jahn F, Jordan K, Yuen KK, Heidenreich A, et al. Bisphosphonates for advanced prostate cancer. *Cochrane Database Syst Rev*. 2017;(12):CD006250. <https://doi.org/10.1002/14651858.CD006250.pub2>
- [374] Yuen KK, Shelley M, Sze WM, Wilt T, Mason MD. Bisphosphonates for advanced prostate cancer. *Cochrane Database Syst Rev*. 2006;(4):CD006250. <https://doi.org/10.1002/14651858.CD006250>
- [375] Ford JA, Jones R, Elders A, Mulatero C, Royle P, Sharma P, et al. Denosumab for treatment of bone metastases secondary to solid tumours: Systematic review and network meta-analysis. *Eur J Cancer*. 2013;49:416-30. <https://doi.org/10.1016/j.ejca.2012.07.016>
- [376] Al Farii H, Frazer A, Farahdel L, Alfayyadh F, Turcotte R. Bisphosphonates versus denosumab for prevention of pathological fracture in advanced cancers with bone metastasis: A meta-analysis of randomized controlled trials. *J Am Acad Orthop Surg Glob Res Rev*. 2020;4:e2000045. <https://doi.org/10.5435/JAOSGlobal-D-20-00045>
- [377] Galvano A, Scaturro D, Badalamenti G, Incorvaia L, Rizzo S, Castellana L, et al. Denosumab for bone health in prostate and breast cancer patients receiving endocrine therapy? A systematic review and a meta-analysis of randomized trials. *J Bone Oncol*. 2019;18:100252. <https://doi.org/10.1016/j.jbo.2019.100252>
- [378] Razaq A, Khan S, Hassan J, Malik BH, Razaq M. Comparing the efficacy and safety of denosumab with bisphosphonates in increasing bone mineral density in patients with prostate cancer and breast cancer on antihormonal treatment. *Cureus*. 2019;11:e6401. <https://doi.org/10.7759/cureus.6401>
- [379] Sartor O. Overview of samarium sm 153 lexidronam in the treatment of painful metastatic bone disease. *Rev Urol*. 2004;6 Suppl 10:S3-12. <https://www.ncbi.nlm.nih.gov/pmc/articles/PMC1472939/>
- [380] Sartor O, Reid RH, Hoskin PJ, Quick DP, Ell PJ, Coleman RE, et al. Samarium-153-lexidronam complex for treatment of painful bone metastases in hormone-refractory prostate cancer. *Urology*. 2004;63:940-5. <https://doi.org/10.1016/j.urology.2004.01.034>
- [381] James ND, Bloomfield D, Luscombe C. The changing pattern of management for hormone-refractory, metastatic prostate cancer. *Prostate Cancer Prostatic Dis*. 2006;9:221-9. <https://doi.org/10.1038/sj.pcan.4500880>
- [382] James ND, Pirrie SJ, Pope AM, Barton D, Andronis L, Goranitis I, et al. Clinical outcomes and survival following treatment of metastatic castrate-refractory prostate cancer with docetaxel alone or with strontium-89, zoledronic acid, or both: The trapeze randomized clinical trial. *JAMA Oncol*. 2016;2:493-9. <https://doi.org/10.1001/jamaoncol.2015.5570>
- [383] Bauman G, Charette M, Reid R, Sathya J. Radiopharmaceuticals for the palliation of painful bone metastasis-a systemic review. *Radiother Oncol*. 2005;75:258-70. <https://doi.org/10.1016/j.radonc.2005.03.003>
- [384] D'Angelo G, Sciuto R, Salvatori M, Sperduti I, Mantini G, Maini CL, et al. Targeted "bone-seeking" radiopharmaceuticals for palliative treatment of bone metastases: A systematic review and meta-analysis. *Q J Nucl Med Mol Imaging*. 2012;56:538-43. <https://www.minervamedica.it/en/journals/nuclear-med-molecular-imaging/article.php?cod=R39Y2012N06A0538>
- [385] Terrisse S, Karamouza E, Parker CC, Sartor AO, James ND, Pirrie S, et al. Overall survival in men with bone metastases from castration-resistant prostate cancer treated with bone-targeting radioisotopes: A meta-analysis of individual patient data from randomized clinical trials. *JAMA Oncol*. 2020;6:2016-16 <https://doi.org/10.1001/jamaoncol.2019.4097>

- [386] Parker C, Nilsson S, Heinrich D, Helle SI, O'Sullivan JM, Fossa SD, et al. Alpha emitter radium-223 and survival in metastatic prostate cancer. *N Engl J Med*. 2013;369:213-23. <https://doi.org/10.1056/NEJMoa1213755>
- [387] Parker C, Zhan L, Cislo P, Reuning-Scherer J, Vogelzang NJ, Nilsson S, et al. Effect of radium-223 dichloride (ra-223) on hospitalisation: An analysis from the phase 3 randomised alpharadin in symptomatic prostate cancer patients (ALSYMPCA) trial. *Eur J Cancer*. 2017;71:1-6. <https://doi.org/10.1016/j.ejca.2016.10.020>
- [388] Parker CC, Coleman RE, Sartor O, Vogelzang NJ, Bottomley D, Heinrich D, et al. Three-year safety of radium-223 dichloride in patients with castration-resistant prostate cancer and symptomatic bone metastases from phase 3 randomized alpharadin in symptomatic prostate cancer trial. *Eur Urol*. 2018;73:427-35. <https://doi.org/10.1016/j.eururo.2017.06.021>
- [389] Terrisse S, Karamouza E, Parker CC, Sartor AO, James ND, Pirrie S, et al. Overall survival in men with bone metastases from castration-resistant prostate cancer treated with bone-targeting radioisotopes: A meta-analysis of individual patient data from randomized clinical trials. *JAMA Oncol*. 2019. <https://doi.org/10.1001/jamaoncol.2019.4097>
- [390] Smith M, Parker C, Saad F, Miller K, Tombal B, Ng QS, et al. Addition of radium-223 to abiraterone acetate and prednisone or prednisolone in patients with castration-resistant prostate cancer and bone metastases (era 223): A randomised, double-blind, placebo-controlled, phase 3 trial. *Lancet Oncol*. 2019;20:408-19. [https://doi.org/10.1016/S1470-2045\(18\)30860-X](https://doi.org/10.1016/S1470-2045(18)30860-X)
- [391] Nilsson S, Strang P, Aksnes AK, Franzen L, Olivier P, Pecking A, et al. A randomized, dose-response, multicenter phase ii study of radium-223 chloride for the palliation of painful bone metastases in patients with castration-resistant prostate cancer. *Eur J Cancer*. 2012;48:678-86. <https://doi.org/10.1016/j.ejca.2011.12.023>
- [392] Nilsson S, Franzen L, Parker C, Tyrrell C, Blom R, Tennvall J, et al. Bone-targeted radium-223 in symptomatic, hormone-refractory prostate cancer: A randomised, multicentre, placebo-controlled phase ii study. *Lancet Oncol*. 2007;8:587-94. [https://doi.org/10.1016/S1470-2045\(07\)70147-X](https://doi.org/10.1016/S1470-2045(07)70147-X)
- [393] Kantoff PW, Higano CS, Shore ND, Berger ER, Small EJ, Penson DF, et al. Sipuleucel-t immunotherapy for castration-resistant prostate cancer. *N Engl J Med*. 2010;363:411-22. <https://doi.org/10.1056/NEJMoa1001294>
- [394] Small EJ, Schellhammer PF, Higano CS, Redfern CH, Nemunaitis JJ, Valone FH, et al. Placebo-controlled phase iii trial of immunologic therapy with sipuleucel-t (apc8015) in patients with metastatic, asymptomatic hormone refractory prostate cancer. *J Clin Oncol*. 2006;24:3089-94. <https://doi.org/10.1200/JCO.2005.04.5252>
- [395] Longo DL. New therapies for castration-resistant prostate cancer. *N Engl J Med*. 2010;363:479-81. <https://doi.org/10.1056/NEJMe1006300>
- [396] Higano CS, Schellhammer PF, Small EJ, Burch PA, Nemunaitis J, Yuh L, et al. Integrated data from 2 randomized, double-blind, placebo-controlled, phase 3 trials of active cellular immunotherapy with sipuleucel-t in advanced prostate cancer. *Cancer*. 2009;115:3670-9. <https://doi.org/10.1002/cncr.24429>
- [397] George DJ, Nabhan C, DeVries T, Whitmore JB, Gomella LG. Survival outcomes of sipuleucel-t phase iii studies: Impact of control-arm cross-over to salvage immunotherapy. *Cancer Immunol Res*. 2015;3:1063-9. <https://doi.org/10.1158/2326-6066.CIR-15-0006>
- [398] Holl EK, McNamara MA, Healy P, Anand M, Concepcion RS, Breland CD, et al. Prolonged psa stabilization and overall survival following sipuleucel-t monotherapy in metastatic castration-resistant prostate cancer patients. *Prostate Cancer Prostatic Dis*. 2019;22:588-92. <https://doi.org/10.1038/s41391-019-0144-3>
- [399] Wei XX, Fong L, Small EJ. Prostate cancer immunotherapy with sipuleucel-t: Current standards and future directions. *Expert Rev Vaccines*. 2015;14:1529-41. <https://doi.org/10.1586/14760584.2015.1099437>
- [400] Pritchard CC, Mateo J, Walsh MF, De Sarkar N, Abida W, Beltran H, et al. Inherited DNA-repair gene mutations in men with metastatic prostate cancer. *N Engl J Med*. 2016;375:443-53. <https://doi.org/10.1056/NEJMoa1603144>

- [401] Mateo J, Boysen G, Barbieri CE, Bryant HE, Castro E, Nelson PS, et al. DNA repair in prostate cancer: Biology and clinical implications. *Eur Urol*. 2017;71:417-25. <https://doi.org/10.1016/j.eururo.2016.08.037>
- [402] Abida W, Armenia J, Gopalan A, Brennan R, Walsh M, Barron D, et al. Prospective genomic profiling of prostate cancer across disease states reveals germline and somatic alterations that may affect clinical decision making. *JCO Precis Oncol*. 2017;2017:PO.17.00029. <https://doi.org/10.1200/PO.17.00029>
- [403] Mateo J, Carreira S, Sandhu S, Miranda S, Mossop H, Perez-Lopez R, et al. DNA-repair defects and olaparib in metastatic prostate cancer. *N Engl J Med*. 2015;373:1697-708. <https://doi.org/10.1056/NEJMoa1506859>
- [404] Li K, Luo H, Huang L, Luo H, Zhu X. Microsatellite instability: A review of what the oncologist should know. *Cancer cell international*. 2020;20:16. <https://doi.org/10.1186/s12935-019-1091-8>
- [405] Topalian SL, Hodi FS, Brahmer JR, Gettinger SN, Smith DC, McDermott DF, et al. Safety, activity, and immune correlates of anti-pd-1 antibody in cancer. *N Engl J Med*. 2012;366:2443-54. <https://doi.org/10.1056/NEJMoa1200690>
- [406] Patnaik A, Kang SP, Rasco D, Papadopoulos KP, Ellassais-Schaap J, Beeram M, et al. Phase i study of pembrolizumab (mk-3475; anti-pd-1 monoclonal antibody) in patients with advanced solid tumors. *Clin Cancer Res*. 2015;21:4286-93. <https://doi.org/10.1158/1078-0432.CCR-14-2607>
- [407] Rescigno P, de Bono JS. Immunotherapy for lethal prostate cancer. *Nature Reviews Urology*. 2019;16:69-70. <https://doi.org/10.1038/s41585-018-0121-y>
- [408] Graff JN, Alumkal JJ, Drake CG, Thomas GV, Redmond WL, Farhad M, et al. Early evidence of anti-pd-1 activity in enzalutamide-resistant prostate cancer. *Oncotarget*. 2016;7:52810-7. <https://doi.org/10.18632/oncotarget.10547>
- [409] Le DT, Durham JN, Smith KN, Wang H, Bartlett BR, Aulakh LK, et al. Mismatch repair deficiency predicts response of solid tumors to pd-1 blockade. *Science*. 2017;357:409-13. <https://doi.org/10.1126/science.aan6733>
- [410] Antonarakis ES, Piulats JM, Gross-Goupil M, Goh J, Ojamaa K, Hoimes CJ, et al. Pembrolizumab for treatment-refractory metastatic castration-resistant prostate cancer: Multicohort, open-label phase ii KEYNOTE-199 study. *Journal of Clinical Oncology*. 2020;38:395-405. <https://doi.org/10.1200/jco.19.01638>
- [411] Piper C, Epplen R, van Erps T, Pfister DJKP, Porres D, Heidenreich A. Palliative transurethral resection in men with castration-resistant prostate cancer (CRPC): Minimally invasive procedure with minimal morbidity? *Journal of Clinical Oncology*. 2012;30(5 Suppl):233. [https://doi.org/10.1200/jco.2012.30.5\\_suppl.233](https://doi.org/10.1200/jco.2012.30.5_suppl.233)
- [412] Piper C, Porres D, Pfister D, Heidenreich A. The role of palliative surgery in castration-resistant prostate cancer. *Curr Opin Support Palliat Care*. 2014;8:250-7. <https://doi.org/10.1097/spc.0000000000000078>
- [413] Satkunasingam R, Kim AE, Desai M, Nguyen MM, Quinn DI, Ballas L, et al. Radical prostatectomy or external beam radiation therapy vs no local therapy for survival benefit in metastatic prostate cancer: A SEER-medicare analysis. *J Urol*. 2015;194:378-85. <https://doi.org/10.1016/j.juro.2015.02.084>
- [414] Löppenber B, Dalela D, Karabon P, Sood A, Sammon JD, Meyer CP, et al. The impact of local treatment on overall survival in patients with metastatic prostate cancer on diagnosis: A national cancer data base analysis. *Eur Urol*. 2017;72:14-9. <https://doi.org/10.1016/j.eururo.2016.04.031>
- [415] Leyh-Bannurah SR, Gazdovich S, Budäus L, Zaffuto E, Briganti A, Abdollah F, et al. Local therapy improves survival in metastatic prostate cancer. *Eur Urol*. 2017;72:118-24. <https://doi.org/10.1016/j.eururo.2017.03.020>
- [416] Bianchini D, Lorente D, Rescigno P, Zafeiriou Z, Psychopaida E, O'Sullivan H, et al. Effect on overall survival of locoregional treatment in a cohort of de novo metastatic prostate cancer patients: A single institution retrospective analysis from the royal marsden hospital. *Clin Genitourin Cancer*. 2017;15:e801-7. <https://doi.org/10.1016/j.clgc.2017.04.013>

- [417] Heidenreich A, Pfister D, Porres D. Cytoreductive radical prostatectomy in patients with prostate cancer and low volume skeletal metastases: Results of a feasibility and case-control study. *J Urol*. 2015;193:832-8. <https://doi.org/10.1016/j.juro.2014.09.089>
- [418] Sooriakumaran P. Testing radical prostatectomy in men with prostate cancer and oligometastases to the bone: A randomized controlled feasibility trial. *BJU Int*. 2017;120:E8-20. <https://doi.org/10.1111/bju.13925>
- [419] Hernandez RK, Wade SW, Reich A, Pirolli M, Liede A, Lyman GH. Incidence of bone metastases in patients with solid tumors: Analysis of oncology electronic medical records in the united states. *BMC Cancer*. 2018;18:44. <https://doi.org/10.1186/s12885-017-3922-0>
- [420] Thiagarajan A. Management of bone metastases. *Journal of Xiangya Medicine*. 2019;4:3. <http://jxym.amegroups.com/article/view/4939>
- [421] Dennis K, Vassiliou V, Balboni T, Chow E. Management of bone metastases: Recent advances and current status. *Journal of Radiation Oncology*. 2012;1:201-10. <https://doi.org/10.1007/s13566-012-0058-3>
- [422] Feng H, Wang J, Xu J, Chen W, Zhang Y. The surgical management and treatment of metastatic lesions in the proximal femur: A mini review. *Medicine (Baltimore)*. 2016;95:e3892. <https://doi.org/10.1097/MD.0000000000003892>
- [423] Wood TJ, Racano A, Yeung H, Farrokhyar F, Ghert M, Deheshi BM. Surgical management of bone metastases: Quality of evidence and systematic review. *Ann Surg Oncol*. 2014;21:4081-9. <https://doi.org/10.1245/s10434-014-4002-1>
- [424] Bakar D, Tanenbaum JE, Phan K, Alentado VJ, Steinmetz MP, Benzel EC, et al. Decompression surgery for spinal metastases: A systematic review. *Neurosurg Focus*. 2016;41:E2. <https://doi.org/10.3171/2016.6.FOCUS16166>
- [425] Barzilai O, Fisher CG, Bilsky MH. State of the art treatment of spinal metastatic disease. *Neurosurgery*. 2018;82:757-69. <https://doi.org/10.1093/neuros/nyx567>
- [426] Deng Z, Xu B, Jin J, Zhao J, Xu H. Strategies for management of spinal metastases: A comprehensive review. *Cancer Translational Medicine*. 2015;1:94-100. <https://doi.org/10.4103/2395-3977.159536>
- [427] Rock JP, Ryu S, Shukairy MS, Yin FF, Sharif A, Schreiber F, et al. Postoperative radiosurgery for malignant spinal tumors. *Neurosurgery*. 2006;58:891-8; discussion -8. <https://doi.org/10.1227/01.Neu.0000209913.72761.4f>
- [428] Rades D, Lange M, Veninga T, Stalpers LJ, Bajrovic A, Adamietz IA, et al. Final results of a prospective study comparing the local control of short-course and long-course radiotherapy for metastatic spinal cord compression. *Int J Radiat Oncol Biol Phys*. 2011;79:524-30. <https://doi.org/10.1016/j.ijrobp.2009.10.073>
- [429] Mason MD, Warde PR, Sydes MR, Gospodarowicz MK, Swanson GP, Kirkbride P, et al. Intergroup randomized phase 3 study of androgen deprivation therapy (adt) + radiation therapy (rt) in locally advanced prostate cancer (cap) (ncic-ctg, swog, mrc-UK and int): T94-0110; nct00002633. *Int J Radiat Oncol Biol Phys*. 2010;782(3 Suppl):S2. <https://doi.org/https://doi.org/10.1016/j.ijrobp.2010.07.047>
- [430] Viani GA, Stefano EJ, Afonso SL. Higher-than-conventional radiation doses in localized prostate cancer treatment: A meta-analysis of randomized, controlled trials. *Int J Radiat Oncol Biol Phys*. 2009;74:1405-18. <https://doi.org/10.1016/j.ijrobp.2008.10.091>
- [431] Shelley MD, Kumar S, Coles B, Wilt T, Staffurth J, Mason MD. Adjuvant hormone therapy for localised and locally advanced prostate carcinoma: A systematic review and meta-analysis of randomised trials. *Cancer Treat Rev*. 2009;35:540-6. <https://doi.org/10.1016/j.ctrv.2009.05.001>
- [432] Bria E, Cuppone F, Giannarelli D, Milella M, Ruggeri EM, Sperduti I, et al. Does hormone treatment added to radiotherapy improve outcome in locally advanced prostate cancer?: Meta-analysis of randomized trials. *Cancer*. 2009;115:3446-56. <https://doi.org/10.1002/cncr.24392>
- [433] Bolla M, Van Tienhoven G, Warde P, Dubois JB, Mirimanoff RO, Storme G, et al. External irradiation with or without long-term androgen suppression for prostate cancer with high metastatic

- risk: 10-year results of an EORTC randomised study. *Lancet Oncol.* 2010;11:1066-73. [https://doi.org/10.1016/S1470-2045\(10\)70223-0](https://doi.org/10.1016/S1470-2045(10)70223-0)
- [434] Chang AJ, Autio KA, Roach M, 3rd, Scher HI. High-risk prostate cancer-classification and therapy. *Nat Rev Clin Oncol.* 2014;11:308-23. <https://doi.org/10.1038/nrclinonc.2014.68>
- [435] D'Amico AV, Whittington R, Malkowicz SB, Schultz D, Blank K, Broderick GA, et al. Biochemical outcome after radical prostatectomy, external beam radiation therapy, or interstitial radiation therapy for clinically localized prostate cancer. *JAMA.* 1998;280:969-74. <http://www.ncbi.nlm.nih.gov/pubmed/9749478>
- [436] National Comprehensive Cancer Network. NCCN clinical practice guidelines in oncology-v.1.2010 prostate cancer 2009. Plymouth Meeting, PA.
- [437] Roach M, Lu J, Pilepich MV, Asbell SO, Mohiuddin M, Terry R, et al. Four prognostic groups predict long-term survival from prostate cancer following radiotherapy alone on radiation therapy oncology group clinical trials. *Int J Radiat Oncol Biol Phys.* 2000;47:609-15. [https://doi.org/https://doi.org/10.1016/s0360-3016\(00\)00578-2](https://doi.org/https://doi.org/10.1016/s0360-3016(00)00578-2)
- [438] Huang J, Vicini FA, Williams SG, Ye H, McGrath S, Ghilezan M, et al. Percentage of positive biopsy cores: A better risk stratification model for prostate cancer? *Int J Radiat Oncol Biol Phys.* 2012;83:1141-8. <https://doi.org/10.1016/j.ijrobp.2011.09.043>
- [439] Cooperberg MR, Broering JM, Carroll PR. Risk assessment for prostate cancer metastasis and mortality at the time of diagnosis. *J Natl Cancer Inst.* 2009;101:878-87. <https://doi.org/10.1093/jnci/djp122>
- [440] Kattan MW, Eastham JA, Stapleton AM, Wheeler TM, Scardino PT. A preoperative nomogram for disease recurrence following radical prostatectomy for prostate cancer. *J Natl Cancer Inst.* 1998;90:766-71. <https://doi.org/https://doi.org/10.1093/jnci/90.10.766>
- [441] Kattan MW, Zelefsky MJ, Kupelian PA, Cho D, Scardino PT, Fuks Z, et al. Pretreatment nomogram that predicts 5-year probability of metastasis following three-dimensional conformal radiation therapy for localized prostate cancer. *J Clin Oncol.* 2003;21:4568-71. <https://doi.org/10.1200/JCO.2003.05.046>
- [442] Mohler JL, Antonarakis ES, Armstrong AJ, D'Amico AV, Davis BJ, Dorff T, et al. Prostate cancer, version 2.2019, NCCN clinical practice guidelines in oncology. *J Natl Compr Canc Netw.* 2019;17:479-505. <https://doi.org/10.6004/jnccn.2019.0023>
- [443] Hanks GE, Martz KL, Diamond JJ. The effect of dose on local control of prostate cancer. *Int J Radiat Oncol Biol Phys.* 1988;15:1299-305. [https://doi.org/https://doi.org/10.1016/0360-3016\(88\)90224-6](https://doi.org/https://doi.org/10.1016/0360-3016(88)90224-6)
- [444] Hanks GE. External-beam radiation therapy for clinically localized prostate cancer: Patterns of care studies in the united states. *NCI Monogr.* 1988;(7) 75-84.
- [445] Dearnaley DP, Khoo VS, Norman AR, Meyer L, Nahum A, Tait D, et al. Comparison of radiation side-effects of conformal and conventional radiotherapy in prostate cancer: A randomised trial. *Lancet.* 1999;353:267-72. [https://doi.org/10.1016/S0140-6736\(98\)05180-0](https://doi.org/10.1016/S0140-6736(98)05180-0)
- [446] Pollack A, Zagars GK, Starkschall G, Antolak JA, Lee JJ, Huang U, et al. Prostate cancer radiation dose response: Results of the m. D. Anderson phase iii randomized trial. *Int J Radiat Oncol Biol Phys.* 2002;53:1097-105. [https://doi.org/10.1016/s0360-3016\(02\)02829-8](https://doi.org/10.1016/s0360-3016(02)02829-8)
- [447] Peeters ST, Heemsbergen WD, Koper PC, van Putten WL, Slot A, Dielwart MF, et al. Dose-response in radiotherapy for localized prostate cancer: Results of the Dutch multicenter randomized phase iii trial comparing 68 Gy of radiotherapy with 78 Gy. *J Clin Oncol.* 2006;24:1990-6. <https://doi.org/10.1200/JCO.2005.05.2530>
- [448] Dearnaley DP, Sydes MR, Graham JD, Aird EG, Bottomley D, Cowan RA, et al. Escalated-dose versus standard-dose conformal radiotherapy in prostate cancer: First results from the mrc rt01 randomised controlled trial. *Lancet Oncol.* 2007;8:475-87. [https://doi.org/10.1016/S1470-2045\(07\)70143-2](https://doi.org/10.1016/S1470-2045(07)70143-2)
- [449] Beckendorf V, Guerif S, Le Prise E, Cosset JM, Bougnoux A, Chauvet B, et al. 70 Gy versus 80 Gy in localized prostate cancer: 5-year results of GETUG 06 randomized trial. *Int J Radiat Oncol Biol Phys.* 2011;80:1056-63. <https://doi.org/10.1016/j.ijrobp.2010.03.049>

- [450] Viani GA, da Silva LG, Stefano EJ. High-dose conformal radiotherapy reduces prostate cancer-specific mortality: Results of a meta-analysis. *Int J Radiat Oncol Biol Phys.* 2012;83:e619-25. <https://doi.org/10.1016/j.ijrobp.2012.01.051>
- [451] Jackson A, Skwarchuk MW, Zelefsky MJ, Cowen DM, Venkatraman ES, Levegrun S, et al. Late rectal bleeding after conformal radiotherapy of prostate cancer. II. Volume effects and dose-volume histograms. *Int J Radiat Oncol Biol Phys.* 2001;49:685-98. [https://doi.org/10.1016/s0360-3016\(00\)01414-0](https://doi.org/10.1016/s0360-3016(00)01414-0)
- [452] Kupelian PA, Reddy CA, Carlson TP, Willoughby TR. Dose/volume relationship of late rectal bleeding after external beam radiotherapy for localized prostate cancer: Absolute or relative rectal volume? *Cancer J.* 2002;8:62-6. <https://doi.org/10.1097/00130404-200201000-00011>
- [453] Bentzen SM, Constine LS, Deasy JO, Eisbruch A, Jackson A, Marks LB, et al. Quantitative analyses of normal tissue effects in the clinic (quantec): An introduction to the scientific issues. *Int J Radiat Oncol Biol Phys.* 2010;76(3 Suppl):S3-9. <https://doi.org/10.1016/j.ijrobp.2009.09.040>
- [454] Michalski JM, Gay H, Jackson A, Tucker SL, Deasy JO. Radiation dose-volume effects in radiation-induced rectal injury. *Int J Radiat Oncol Biol Phys.* 2010;76(3 Suppl):S123-9. <https://doi.org/10.1016/j.ijrobp.2009.03.078>
- [455] Viswanathan AN, Yorke ED, Marks LB, Eifel PJ, Shipley WU. Radiation dose-volume effects of the urinary bladder. *Int J Radiat Oncol Biol Phys.* 2010;76(3 Suppl):S116-22. <https://doi.org/10.1016/j.ijrobp.2009.02.090>
- [456] International Commission on Radiation Units and Measurements. ICRU report 50: Prescribing, recording, and reporting photon beam therapy. Bethesda, MD: ICRU; 1993.
- [457] International Commission on Radiation Units and Measurements. ICRU report 62: Prescribing, recording and reporting photon beam therapy (supplement to ICRU report 50) Bethesda, MD: ICRU; 1999.
- [458] International Commission on Radiation Units and Measurements. ICRU report 83: Prescribing, recording, and reporting photon-beam intensity-modulated radiation therapy (IMRT). Bethesda, MD: ICRU; 2010.
- [459] Harrison A, Studenski M, Harvey A, Trabulsi EJ, Xiao Y, Yu Y, et al. Potential for dose escalation in the postprostatectomy setting with intensity-modulated radiation therapy: A dosimetric study using EORTC consensus guidelines for target volume contours. *Pract Radiat Oncol.* 2011;1:105-14. <https://doi.org/10.1016/j.prrro.2010.10.005>
- [460] Luxton G, Hancock SL, Boyer AL. Dosimetry and radiobiologic model comparison of IMRT and 3D conformal radiotherapy in treatment of carcinoma of the prostate. *Int J Radiat Oncol Biol Phys.* 2004;59:267-84. <https://doi.org/10.1016/j.ijrobp.2004.01.024>
- [461] Vaarkamp J, Malde R, Dixit S, Hamilton CS. A comparison of conformal and intensity modulated treatment planning techniques for early prostate cancer. *J Med Imaging Radiat Oncol.* 2009;53:310-7. <https://doi.org/10.1111/j.1754-9485.2009.02078.x>
- [462] Perna L, Fiorino C, Cozzarini C, Broggi S, Cattaneo GM, De Cobelli F, et al. Sparing the penile bulb in the radical irradiation of clinically localised prostate carcinoma: A comparison between MRI and CT prostatic apex definition in 3DCRT, linac-IMRT and helical tomotherapy. *Radiother Oncol.* 2009;93:57-63. <https://doi.org/10.1016/j.radonc.2009.04.004>
- [463] Eade TN, Hanlon AL, Horwitz EM, Buyyounouski MK, Hanks GE, Pollack A. What dose of external-beam radiation is high enough for prostate cancer? *Int J Radiat Oncol Biol Phys.* 2007;68:682-9. <https://doi.org/10.1016/j.ijrobp.2007.01.008>
- [464] Zelefsky MJ, Fuks Z, Happersett L, Lee HJ, Ling CC, Burman CM, et al. Clinical experience with intensity modulated radiation therapy (IMRT) in prostate cancer. *Radiother Oncol.* 2000;55:241-9. [https://doi.org/10.1016/s0167-8140\(99\)00100-0](https://doi.org/10.1016/s0167-8140(99)00100-0)
- [465] Zelefsky MJ, Fuks Z, Hunt M, Lee HJ, Lombardi D, Ling CC, et al. High dose radiation delivered by intensity modulated conformal radiotherapy improves the outcome of localized prostate cancer. *J Urol.* 2001;166:876-81. [https://doi.org/https://doi.org/10.1016/S0022-5347\(05\)65855-7](https://doi.org/https://doi.org/10.1016/S0022-5347(05)65855-7)
- [466] Zelefsky MJ, Yamada Y, Fuks Z, Zhang Z, Hunt M, Cahlon O, et al. Long-term results of conformal radiotherapy for prostate cancer: Impact of dose escalation on biochemical tumor control and

- distant metastases-free survival outcomes. *Int J Radiat Oncol Biol Phys*. 2008;71:1028-33.  
<https://doi.org/10.1016/j.ijrobp.2007.11.066>
- [467] Michalski JM, Moughan J, Purdy J, Bosch W, Bruner DW, Bahary J-P, et al. Effect of standard vs dose-escalated radiation therapy for patients with intermediate-risk prostate cancer: The NRG oncology RTOG 0126 randomized clinical trial. *JAMA oncology*. 2018;4:e180039.  
<https://doi.org/10.1001/jamaoncol.2018.0039>
- [468] Michalski JM, Yan Y, Watkins-Bruner D, Bosch WR, Winter K, Galvin JM, et al. Preliminary toxicity analysis of 3-dimensional conformal radiation therapy versus intensity modulated radiation therapy on the high-dose arm of the radiation therapy oncology group 0126 prostate cancer trial. *Int J Radiat Oncol Biol Phys*. 2013;87:932-8. <https://doi.org/10.1016/j.ijrobp.2013.07.041>
- [469] Alicikus ZA, Yamada Y, Zhang Z, Pei X, Hunt M, Kollmeier M, et al. Ten-year outcomes of high-dose, intensity-modulated radiotherapy for localized prostate cancer. *Cancer*. 2011;117:1429-37.  
<https://doi.org/10.1002/cncr.25467>
- [470] Vora SA, Wong WW, Schild SE, Ezzell GA, Andrews PE, Ferrigni RG, et al. Outcome and toxicity for patients treated with intensity modulated radiation therapy for localized prostate cancer. *J Urol*. 2013;190:521-6. <https://doi.org/10.1016/j.juro.2013.02.012>
- [471] Deutsch I, Zelefsky MJ, Zhang Z, Mo Q, Zaider M, Cohen G, et al. Comparison of psa relapse-free survival in patients treated with ultra-high-dose IMRT versus combination HDR brachytherapy and IMRT. *Brachytherapy*. 2010;9:313-8. <https://doi.org/10.1016/j.brachy.2010.02.196>
- [472] Petrongari MG, Landoni V, Saracino B, Gomellini S, Arcangeli S, Iaccarino G, et al. Dose escalation using ultra-high dose IMRT in intermediate risk prostate cancer without androgen deprivation therapy: Preliminary results of toxicity and biochemical control. *J Exp Clin Cancer Res*. 2013;32:103. <https://doi.org/10.1186/1756-9966-32-103>
- [473] Elliott SP, Adejoro OO, Konety BR, Jarosek SL, Dusenbery KE, Virnig BA. Intensity modulated radiation therapy replaces 3-dimensional conformal radiotherapy as prostate cancer treatment. *J Urol*. 2012;187:1253-8. <https://doi.org/10.1016/j.juro.2011.11.088>
- [474] Bauman G, Rumble RB, Chen J, Loblaw A, Warde P, Members of the IMRT Indications Expert Panel. Intensity-modulated radiotherapy in the treatment of prostate cancer. *Clin Oncol (R Coll Radiol)*. 2012;24:461-73. <https://doi.org/10.1016/j.clon.2012.05.002>
- [475] Al-Mamgani A, Heemsbergen WD, Peeters ST, Lebesque JV. Role of intensity-modulated radiotherapy in reducing toxicity in dose escalation for localized prostate cancer. *Int J Radiat Oncol Biol Phys*. 2009;73:685-91. <https://doi.org/10.1016/j.ijrobp.2008.04.063>
- [476] Yong JH, Beca J, McGowan T, Bremner KE, Warde P, Hoch JS. Cost-effectiveness of intensity-modulated radiotherapy in prostate cancer. *Clin Oncol (R Coll Radiol)*. 2012;24:521-31.  
<https://doi.org/10.1016/j.clon.2012.05.004>
- [477] Zhang P, Happersett L, Hunt M, Jackson A, Zelefsky M, Mageras G. Volumetric modulated arc therapy: Planning and evaluation for prostate cancer cases. *Int J Radiat Oncol Biol Phys*. 2010;76:1456-62. <https://doi.org/10.1016/j.ijrobp.2009.03.033>
- [478] Wolff D, Stielier F, Welzel G, Lorenz F, Abo-Madyan Y, Mai S, et al. Volumetric modulated arc therapy (VMAT) vs. Serial tomotherapy, step-and-shoot IMRT and 3D-conformal rt for treatment of prostate cancer. *Radiother Oncol*. 2009;93:226-33. <https://doi.org/10.1016/j.radonc.2009.08.011>
- [479] Dzierma Y, Bell K, Palm J, Nuesken F, Licht N, Rube C. Marc vs. IMRT radiotherapy of the prostate with flat and flattening-filter-free beam energies. *Radiat Oncol*. 2014;9:250.  
<https://doi.org/10.1186/s13014-014-0250-2>
- [480] Hall WA, Fox TH, Jiang X, Prabhu RS, Rossi PJ, Godette K, et al. Treatment efficiency of volumetric modulated arc therapy in comparison with intensity-modulated radiotherapy in the treatment of prostate cancer. *J Am Coll Radiol*. 2013;10:128-34.  
<https://doi.org/10.1016/j.jacr.2012.06.014>
- [481] Dale RG. The application of the linear-quadratic dose-effect equation to fractionated and protracted radiotherapy. *The British Journal of Radiology*. 1985;58:515-28.  
<https://doi.org/10.1259/0007-1285-58-690-515>

- [482] van Leeuwen CM, Oei AL, Crezee J, Bel A, Franken NAP, Stalpers LJA, et al. The alfa and beta of tumours: A review of parameters of the linear-quadratic model, derived from clinical radiotherapy studies. *Radiat Oncol*. 2018;13:96. <https://doi.org/10.1186/s13014-018-1040-z>
- [483] Miralbell R, Roberts SA, Zubizarreta E, Hendry JH. Dose-fractionation sensitivity of prostate cancer deduced from radiotherapy outcomes of 5,969 patients in seven international institutional datasets:  $A/\beta = 1.4$  (0.9-2.2) Gy. *Int J Radiat Oncol Biol Phys*. 2012;82:e17-24. <https://doi.org/10.1016/j.ijrobp.2010.10.075>
- [484] Brenner DJ, Hall EJ. Fractionation and protraction for radiotherapy of prostate carcinoma. *Int J Radiat Oncol Biol Phys*. 1999;43:1095-101. [https://doi.org/10.1016/s0360-3016\(98\)00438-6](https://doi.org/10.1016/s0360-3016(98)00438-6)
- [485] King CR, Fowler JF. A simple analytic derivation suggests that prostate cancer  $\alpha/\beta$  ratio is low. *Int J Radiat Oncol Biol Phys*. 2001;51:213-4. [https://doi.org/10.1016/s0360-3016\(01\)01651-0](https://doi.org/10.1016/s0360-3016(01)01651-0)
- [486] Brenner DJ, Martinez AA, Edmundson GK, Mitchell C, Thames HD, Armour EP. Direct evidence that prostate tumors show high sensitivity to fractionation (low cancer  $\alpha/\beta$  ratio), similar to late-responding normal tissue. *Int J Radiat Oncol Biol Phys*. 2002;52:6-13. [https://doi.org/10.1016/s0360-3016\(01\)02664-5](https://doi.org/10.1016/s0360-3016(01)02664-5)
- [487] D'Souza WD, Thames HD. Is the  $\alpha/\beta$  ratio for prostate cancer low? *Int J Radiat Oncol Biol Phys*. 2001;51:1-3. [https://doi.org/10.1016/s0360-3016\(01\)01650-9](https://doi.org/10.1016/s0360-3016(01)01650-9)
- [488] Fowler JF, Tomé WA, Fenwick JD, Mehta MP. A challenge to traditional radiation oncology. *Int J Radiat Oncol Biol Phys*. 2004;60:1241-56. <https://doi.org/10.1016/j.ijrobp.2004.07.691>
- [489] Fowler J, Chappell R, Ritter M. Is  $\alpha/\beta$  for prostate tumors really low? *Int J Radiat Oncol Biol Phys*. 2001;50:1021-31. [https://doi.org/10.1016/s0360-3016\(01\)01607-8](https://doi.org/10.1016/s0360-3016(01)01607-8)
- [490] Bentzen SM, Ritter MA. The  $\alpha/\beta$  ratio for prostate cancer: What is it, really? *Radiother Oncol*. 2005;76:1-3. <https://doi.org/10.1016/j.radonc.2005.06.009>
- [491] Vogelius IR, Bentzen SM. Meta-analysis of the alpha/beta ratio for prostate cancer in the presence of an overall time factor: Bad news, good news, or no news? *Int J Radiat Oncol Biol Phys*. 2013;85:89-94. <https://doi.org/10.1016/j.ijrobp.2012.03.004>
- [492] Dearnaley D, Syndikus I, Mossop H, Khoo V, Birtle A, Bloomfield D, et al. Conventional versus hypofractionated high-dose intensity-modulated radiotherapy for prostate cancer: 5-year outcomes of the randomised, non-inferiority, phase 3 CHHiP trial. *The Lancet Oncology*. 2016;17:1047-60. [https://doi.org/10.1016/s1470-2045\(16\)30102-4](https://doi.org/10.1016/s1470-2045(16)30102-4)
- [493] Catton CN, Lukka H, Gu CS, Martin JM, Supiot S, Chung PWM, et al. Randomized trial of a hypofractionated radiation regimen for the treatment of localized prostate cancer. *J Clin Oncol*. 2017;35:1884-90. <https://doi.org/10.1200/JCO.2016.71.7397>
- [494] Lee WR, Dignam JJ, Amin MB, Bruner DW, Low D, Swanson GP, et al. Randomized phase iii noninferiority study comparing two radiotherapy fractionation schedules in patients with low-risk prostate cancer. *J Clin Oncol*. 2016;34:2325-32. <https://doi.org/10.1200/JCO.2016.67.0448>
- [495] Incrocci L, Wortel RC, Alemayehu WG, Aluwini S, Schimmel E, Krol S, et al. Hypofractionated versus conventionally fractionated radiotherapy for patients with localised prostate cancer (HYPRO): Final efficacy results from a randomised, multicentre, open-label, phase 3 trial. *Lancet Oncol*. 2016;17:1061-9. [https://doi.org/10.1016/S1470-2045\(16\)30070-5](https://doi.org/10.1016/S1470-2045(16)30070-5)
- [496] Aluwini S, Pos F, Schimmel E, Krol S, van der Toorn PP, de Jager H, et al. Hypofractionated versus conventionally fractionated radiotherapy for patients with prostate cancer (HYPRO): Late toxicity results from a randomised, non-inferiority, phase 3 trial. *Lancet Oncol*. 2016;17:464-74. [https://doi.org/10.1016/S1470-2045\(15\)00567-7](https://doi.org/10.1016/S1470-2045(15)00567-7)
- [497] Aluwini S, Pos F, Schimmel E, Krol S, van der Toorn PP, de Jager H, et al. Hypofractionated versus conventionally fractionated radiotherapy for patients with prostate cancer (HYPRO): Late toxicity results from a randomised, non-inferiority, phase 3 trial. *The Lancet Oncology*. 2016;17:464-74. [https://doi.org/10.1016/s1470-2045\(15\)00567-7](https://doi.org/10.1016/s1470-2045(15)00567-7)
- [498] de Vries KC, Wortel RC, Oomen-de Hoop E, Heemsbergen WD, Pos FJ, Incrocci L. Hypofractionated versus conventionally fractionated radiation therapy for patients with intermediate- or high-risk, localized, prostate cancer: 7-year outcomes from the randomized,

- multicenter, open-label, phase 3 HYPRO trial. *Int J Radiat Oncol Biol Phys*. 2020;106:108-15. <https://doi.org/10.1016/j.ijrobp.2019.09.007>
- [499] Royce TJ, Lee DH, Keum N, Permpalung N, Chiew CJ, Epstein S, et al. Conventional versus hypofractionated radiation therapy for localized prostate cancer: A meta-analysis of randomized noninferiority trials. *Eur Urol Focus*. 2019;5:577-84. <https://doi.org/10.1016/j.euf.2017.10.011>
- [500] Macias VA, Barrera-Mellado I. Ultra-hypofractionated radiation therapy for unfavourable intermediate-risk and high-risk prostate cancer is safe and effective: 5-year outcomes of a phase ii trial. *BJU International*. 2020;125:215-25. <https://doi.org/10.1111/bju.14925>
- [501] Katz AJ, Santoro M, Diblasio F, Ashley R. Stereotactic body radiotherapy for localized prostate cancer: Disease control and quality of life at 6 years. *Radiat Oncol*. 2013;8:118. <https://doi.org/10.1186/1748-717x-8-118>
- [502] Freeman DE, King CR. Stereotactic body radiotherapy for low-risk prostate cancer: Five-year outcomes. *Radiat Oncol*. 2011;6:3. <https://doi.org/10.1186/1748-717x-6-3>
- [503] Loblaw A, Cheung P, D'Alimonte L, Deabreu A, Mamedov A, Zhang L, et al. Prostate stereotactic ablative body radiotherapy using a standard linear accelerator: Toxicity, biochemical, and pathological outcomes. *Radiother Oncol*. 2013;107:153-8. <https://doi.org/10.1016/j.radonc.2013.03.022>
- [504] Kim DW, Cho LC, Straka C, Christie A, Lotan Y, Pistenmaa D, et al. Predictors of rectal tolerance observed in a dose-escalated phase 1-2 trial of stereotactic body radiation therapy for prostate cancer. *Int J Radiat Oncol Biol Phys*. 2014;89:509-17. <https://doi.org/10.1016/j.ijrobp.2014.03.012>
- [505] Widmark A, Gunnlaugsson A, Beckman L, Thellenberg-Karlsson C, Hoyer M, Lagerlund M, et al. Ultra-hypofractionated versus conventionally fractionated radiotherapy for prostate cancer: 5-year outcomes of the hypo-rt-pc randomised, non-inferiority, phase 3 trial. *Lancet*. 2019;394:385-95. [https://doi.org/10.1016/s0140-6736\(19\)31131-6](https://doi.org/10.1016/s0140-6736(19)31131-6)
- [506] Zilli T, Scorsetti M, Zwahlen D, Franzese C, Forster R, Giaj-Levra N, et al. One shot - single shot radiotherapy for localized prostate cancer: Study protocol of a single arm, multicenter phase i/ii trial. *Radiat Oncol*. 2018;13:166. <https://doi.org/10.1186/s13014-018-1112-0>
- [507] Miralbell R. Stereotactic beam radiotherapy for prostate cancer: Is less, more? *The Lancet Oncology*. 2019;20:1471-2. [https://doi.org/10.1016/s1470-2045\(19\)30652-7](https://doi.org/10.1016/s1470-2045(19)30652-7)
- [508] Parikh NR, Kishan AU. Stereotactic body radiotherapy for prostate cancer. *Am J Mens Health*. 2020;14:1557988320927241. <https://doi.org/10.1177/1557988320927241>
- [509] Alayed Y, Cheung P, Chu W, Chung H, Davidson M, Ravi A, et al. Two stereotactic ablative radiotherapy treatments for localized prostate cancer (2star): Results from a prospective clinical trial. *Radiother Oncol*. 2019;135:86-90. <https://doi.org/10.1016/j.radonc.2019.03.002>
- [510] Jackson WC, Silva J, Hartman HE, Dess RT, Kishan AU, Beeler WH, et al. Stereotactic body radiation therapy for localized prostate cancer: A systematic review and meta-analysis of over 6,000 patients treated on prospective studies. *Int J Radiat Oncol Biol Phys*. 2019;104:778-89. <https://doi.org/10.1016/j.ijrobp.2019.03.051>
- [511] King CR, Kapp DS. Radiotherapy after prostatectomy: Is the evidence for dose escalation out there? *Int J Radiat Oncol Biol Phys*. 2008;71:346-50. <https://doi.org/10.1016/j.ijrobp.2007.10.008>
- [512] Bernard JR, Jr., Buskirk SJ, Heckman MG, Diehl NN, Ko SJ, Macdonald OK, et al. Salvage radiotherapy for rising prostate-specific antigen levels after radical prostatectomy for prostate cancer: Dose-response analysis. *Int J Radiat Oncol Biol Phys*. 2010;76:735-40. <https://doi.org/10.1016/j.ijrobp.2009.02.049>
- [513] King CR, Spiotto MT. Improved outcomes with higher doses for salvage radiotherapy after prostatectomy. *Int J Radiat Oncol Biol Phys*. 2008;71:23-7. <https://doi.org/10.1016/j.ijrobp.2007.09.047>
- [514] Ohri N, Dicker AP, Trabulsi EJ, Showalter TN. Can early implementation of salvage radiotherapy for prostate cancer improve the therapeutic ratio? A systematic review and regression meta-analysis with radiobiological modelling. *Eur J Cancer*. 2012;48:837-44. <https://doi.org/10.1016/j.ejca.2011.08.013>

- [515] Cox JD, Gallagher MJ, Hammond EH, Kaplan RS, Schellhammer PF. Consensus statements on radiation therapy of prostate cancer: Guidelines for prostate re-biopsy after radiation and for radiation therapy with rising prostate-specific antigen levels after radical prostatectomy. American society for therapeutic radiology and oncology consensus panel. *J Clin Oncol*. 1999;17:1155. <https://doi.org/10.1200/jco.1999.17.4.1155>
- [516] Mottet N, Bellmunt J, Bolla M, Joniau S, Mason M, Matveev V, et al. EAU guidelines on prostate cancer. Part ii: Treatment of advanced, relapsing, and castration-resistant prostate cancer. *Eur Urol*. 2011;59:572-83. <https://doi.org/10.1016/j.eururo.2011.01.025>
- [517] Lumen N, Ost P, Van Praet C, De Meerleer G, Villeirs G, Fonteyne V. Developments in external beam radiotherapy for prostate cancer. *Urology*. 2013;82:5-10. <https://doi.org/10.1016/j.urology.2013.03.043>
- [518] Ost P, Lumen N, Goessaert AS, Fonteyne V, De Troyer B, Jacobs F, et al. High-dose salvage intensity-modulated radiotherapy with or without androgen deprivation after radical prostatectomy for rising or persisting prostate-specific antigen: 5-year results. *Eur Urol*. 2011;60:842-9. <https://doi.org/10.1016/j.eururo.2011.04.021>
- [519] Goenka A, Magsanoc JM, Pei X, Schechter M, Kollmeier M, Cox B, et al. Long-term outcomes after high-dose postprostatectomy salvage radiation treatment. *Int J Radiat Oncol Biol Phys*. 2012;84:112-8. <https://doi.org/10.1016/j.ijrobp.2011.10.077>
- [520] Goenka A, Magsanoc JM, Pei X, Schechter M, Kollmeier M, Cox B, et al. Improved toxicity profile following high-dose postprostatectomy salvage radiation therapy with intensity-modulated radiation therapy. *Eur Urol*. 2011;60:1142-8. <https://doi.org/10.1016/j.eururo.2011.08.006>
- [521] Ost P, Fonteyne V, Villeirs G, Lumen N, Oosterlinck W, De Meerleer G. Adjuvant high-dose intensity-modulated radiotherapy after radical prostatectomy for prostate cancer: Clinical results in 104 patients. *Eur Urol*. 2009;56:669-75. <https://doi.org/10.1016/j.eururo.2009.05.041>
- [522] Cozzarini C, Montorsi F, Fiorino C, Alongi F, Bolognesi A, Da Pozzo LF, et al. Need for high radiation dose ( $\geq 70$  Gy) in early postoperative irradiation after radical prostatectomy: A single-institution analysis of 334 high-risk, node-negative patients. *Int J Radiat Oncol Biol Phys*. 2009;75:966-74. <https://doi.org/10.1016/j.ijrobp.2008.12.059>
- [523] King CR. The dose-response of salvage radiotherapy following radical prostatectomy: A systematic review and meta-analysis. *Radiother Oncol*. 2016;121:199-203. <https://doi.org/10.1016/j.radonc.2016.10.026>
- [524] Ghadjar P, Hayoz S, Bernhard J, Zwahlen DR, Holscher T, Gut P, et al. Acute toxicity and quality of life after dose-intensified salvage radiation therapy for biochemically recurrent prostate cancer after prostatectomy: First results of the randomized trial SAKK 09/10. *J Clin Oncol*. 2015;33:4158-66. <https://doi.org/10.1200/JCO.2015.63.3529>
- [525] Khoo VS, Lim Joon DL. New developments in MRI for target volume delineation in radiotherapy. *Br J Radiol*. 2006;79 Spec No 1:S2-15. <https://doi.org/10.1259/bjr/41321492>
- [526] Villeirs GM, De Meerleer GO. Magnetic resonance imaging (MRI) anatomy of the prostate and application of MRI in radiotherapy planning. *Eur J Radiol*. 2007;63:361-8. <https://doi.org/10.1016/j.ejrad.2007.06.030>
- [527] Mullerad M, Hricak H, Kuroiwa K, Pucar D, Chen HN, Kattan MW, et al. Comparison of endorectal magnetic resonance imaging, guided prostate biopsy and digital rectal examination in the preoperative anatomical localization of prostate cancer. *J Urol*. 2005;174:2158-63. <https://doi.org/10.1097/01.ju.0000181224.95276.82>
- [528] Hentschel B, Oehler W, Strauss D, Ulrich A, Malich A. Definition of the CTV prostate in CT and MRI by using CT-MRI image fusion in IMRT planning for prostate cancer. *Strahlenther Onkol*. 2011;187:183-90. <https://doi.org/10.1007/s00066-010-2179-1>
- [529] Roach Mr, Faillace-Akazawa P, Malfatti C, Holland J, Hricak H. Prostate volumes defined by magnetic resonance imaging and computerised tomographic scans for three-dimensional conformal radiotherapy. *Int J Radiat Oncol Biol Phys*. 1996;35:1011-8. [https://doi.org/10.1016/0360-3016\(96\)00232-5](https://doi.org/10.1016/0360-3016(96)00232-5)

- [530] Sannazzari GL, Ragona R, Ruo Redda MG, Giglioli FR, Isolato G, Guarneri A. CT-MRI image fusion for delineation of volumes in three-dimensional conformal radiation therapy in the treatment of localized prostate cancer. *Br J Radiol.* 2002;75:603-7.
- [531] Rasch C, Barillot I, Remeijer PK, Touw A, van Herk M, J. L. Definition of the prostate in CT and MRI: A multi-observer study. *Int J Radiat Oncol Biol Phys.* 1999;43:57-66.
- [532] Khoo EL, Schick K, Plank AW, Poulsen M, Wong WW, Middleton M, et al. Prostate contouring variation: Can it be fixed? *Int J Radiat Oncol Biol Phys.* 2012;82:1923-9. <https://doi.org/10.1016/j.ijrobp.2011.02.050>
- [533] Khoo VS, Lim Joon D. Magnetic resonance imaging. In: Mundt A, Arnold R, editors. *Image guided radiation therapy: A clinical perspective.* City: Peoples Medical Publishing House; 2006.
- [534] Buyyounouski MK, Horwitz EM, Price RA, Hanlon AL, Uzzo RG, Pollack A. Intensity-modulated radiotherapy with MRI simulation to reduce doses received by erectile tissue during prostate cancer treatment. *Int J Radiat Oncol Biol Phys.* 2004;58:743-9. [https://doi.org/10.1016/s0360-3016\(03\)01617-1](https://doi.org/10.1016/s0360-3016(03)01617-1)
- [535] Cellini N, Morganti AG, Mattiucci GC, Valentini V, Leone M, Luzi S, et al. Analysis of intraprostatic failures in patients treated with hormonal therapy and radiotherapy: Implications for conformal therapy planning. *Int J Radiat Oncol Biol Phys.* 2002;53:595-9. <https://doi.org/S0360301602027955> [pii]
- [536] Arrayeh E, Westphalen AC, Kurhanewicz J, Roach M, 3rd, Jung AJ, Carroll PR, et al. Does local recurrence of prostate cancer after radiation therapy occur at the site of primary tumor? Results of a longitudinal MRI and mrsi study. *Int J Radiat Oncol Biol Phys.* 2012;82:e787-93. <https://doi.org/10.1016/j.ijrobp.2011.11.030>
- [537] Nakashima J, Tanimoto A, Imai Y, Mukai M, Horiguchi Y, Nakagawa K, et al. Endorectal MRI for prediction of tumor site, tumor size, and local extension of prostate cancer. *Urology.* 2004;64:101-5. <https://doi.org/10.1016/j.urology.2004.02.036>
- [538] Wang L, Mazaheri Y, Zhang J, Ishill NM, Kuroiwa K, Hricak H. Assessment of biologic aggressiveness of prostate cancer: Correlation of MR signal intensity with gleason grade after radical prostatectomy. *Radiology.* 2008;246:168-76. <https://doi.org/10.1148/radiol.2461070057>
- [539] Zietman AL, Bae K, Slater JD, Shipley WU, Efsthathiou JA, Coen JJ, et al. Randomized trial comparing conventional-dose with high-dose conformal radiation therapy in early-stage adenocarcinoma of the prostate: Long-term results from proton radiation oncology group/american college of radiology 95-09. *J Clin Oncol.* 2010;28:1106-11. <https://doi.org/10.1200/JCO.2009.25.8475>
- [540] Pucar D, Hricak H, Shukla-Dave A, Kuroiwa K, Drobnjak M, Eastham J, et al. Clinically significant prostate cancer local recurrence after radiation therapy occurs at the site of primary tumor: Magnetic resonance imaging and step-section pathology evidence. *Int J Radiat Oncol Biol Phys.* 2007;69:62-9. <https://doi.org/10.1016/j.ijrobp.2007.03.065>
- [541] De Meerleer G, Villeirs G, Bral S, Paelinck L, De Gerssem W, Dekuyper P, et al. The magnetic resonance detected intraprostatic lesion in prostate cancer: Planning and delivery of intensity-modulated radiotherapy. *Radiother Oncol.* 2005;75:325-33. <https://doi.org/10.1016/j.radonc.2005.04.014>
- [542] Housri N, Ning H, Ondos J, Choyke P, Camphausen K, Citrin D, et al. Parameters favorable to intraprostatic radiation dose escalation in men with localized prostate cancer. *Int J Radiat Oncol Biol Phys.* 2011;80:614-20. <https://doi.org/10.1016/j.ijrobp.2010.06.050>
- [543] Pinkawa M, Piroth MD, Holy R, Klotz J, Djukic V, Corral NE, et al. Dose-escalation using intensity-modulated radiotherapy for prostate cancer - evaluation of quality of life with and without (18)f-choline PET-CT detected simultaneous integrated boost. *Radiat Oncol.* 2012;7:14. <https://doi.org/10.1186/1748-717X-7-14>
- [544] Ippolito E, Mantini G, Morganti AG, Mazzeo E, Padula GD, Digesu C, et al. Intensity-modulated radiotherapy with simultaneous integrated boost to dominant intraprostatic lesion: Preliminary report on toxicity. *Am J Clin Oncol.* 2012;35:158-62. <https://doi.org/10.1097/COC.0b013e318209cd8f>
- [545] Fonteyne V, Villeirs G, Speleers B, De Neve W, De Wagter C, Lumen N, et al. Intensity-modulated radiotherapy as primary therapy for prostate cancer: Report on acute toxicity after dose

- escalation with simultaneous integrated boost to intraprostatic lesion. *Int J Radiat Oncol Biol Phys*. 2008;72:799-807. <https://doi.org/10.1016/j.ijrobp.2008.01.040>
- [546] Zelefsky MJ, Reuter VE, Fuks Z, Scardino P, Shippy A. Influence of local tumor control on distant metastases and cancer related mortality after external beam radiotherapy for prostate cancer. *J Urol*. 2008;179:1368-73; discussion 73. [https://doi.org/S0022-5347\(07\)03102-3](https://doi.org/S0022-5347(07)03102-3)
- [547] Khoo VS, Joon DL. New developments in MRI for target volume delineation in radiotherapy. *Br J Radiol*. 2006;79 Spec No 1:S2-15. <https://doi.org/10.1259/bjr/41321492>
- [548] Groenendaal G, Moman MR, Korporaal JG, van Diest PJ, van Vulpen M, Philippens ME, et al. Validation of functional imaging with pathology for tumor delineation in the prostate. *Radiother Oncol*. 2010;94:145-50. <https://doi.org/10.1016/j.radonc.2009.12.034>
- [549] Groenendaal G, van den Berg CA, Korporaal JG, Philippens ME, Luijten PR, van Vulpen M, et al. Simultaneous MRI diffusion and perfusion imaging for tumor delineation in prostate cancer patients. *Radiother Oncol*. 2010;95:185-90. <https://doi.org/10.1016/j.radonc.2010.02.014>
- [550] Rischke HC, Nestle U, Fechter T, Doll C, Volegova-Neher N, Henne K, et al. 3 tesla multiparametric MRI for GTV-definition of dominant intraprostatic lesions in patients with prostate cancer--an interobserver variability study. *Radiat Oncol*. 2013;8:183. <https://doi.org/10.1186/1748-717X-8-183>
- [551] Tan CH, Hobbs BP, Wei W, Kundra V. Dynamic contrast-enhanced MRI for the detection of prostate cancer: Meta-analysis. *AJR Am J Roentgenol*. 2015;204:W439-48. <https://doi.org/10.2214/AJR.14.13373>
- [552] Vargas HA, Akin O, Franiel T, Mazaheri Y, Zheng J, Moskowitz C, et al. Diffusion-weighted endorectal MR imaging at 3 t for prostate cancer: Tumor detection and assessment of aggressiveness. *Radiology*. 2011;259:775-84. <https://doi.org/10.1148/radiol.11102066>
- [553] Murphy G, Haider M, Ghai S, Sreeharsha B. The expanding role of MRI in prostate cancer. *AJR Am J Roentgenol*. 2013;201:1229-38. <https://doi.org/10.2214/ajr.12.10178>
- [554] Kim CK, Park BK, Lee HM, Kwon GY. Value of diffusion-weighted imaging for the prediction of prostate cancer location at 3T using a phased-array coil: Preliminary results. *Invest Radiol*. 2007;42:842-7. <https://doi.org/10.1097/RLI.0b013e3181461d21>
- [555] Sato C, Naganawa S, Nakamura T, Kumada H, Miura S, Takizawa O, et al. Differentiation of noncancerous tissue and cancer lesions by apparent diffusion coefficient values in transition and peripheral zones of the prostate. *J Magn Reson Imaging*. 2005;21:258-62. <https://doi.org/10.1002/jmri.20251>
- [556] Song I, Kim CK, Park BK, Park W. Assessment of response to radiotherapy for prostate cancer: Value of diffusion-weighted MRI at 3 t. *AJR Am J Roentgenol*. 2010;194:W477-82. <https://doi.org/10.2214/AJR.09.3557>
- [557] Franiel T, Hamm B, Hricak H. Dynamic contrast-enhanced magnetic resonance imaging and pharmacokinetic models in prostate cancer. *Eur Radiol*. 2011;21:616-26. <https://doi.org/10.1007/s00330-010-2037-7>
- [558] Barentsz JO, Richenberg J, Clements R, Choyke P, Verma S, Villeirs G, et al. Esur prostate MR guidelines 2012. *Eur Radiol*. 2012;22:746-57. <https://doi.org/10.1007/s00330-011-2377-y>
- [559] Bouchelouche K, Tagawa ST, Goldsmith SJ, Turkbey B, Capala J, Choyke P. PET/CT imaging and radioimmunotherapy of prostate cancer. *Semin Nucl Med*. 2011;41:29-44. <https://doi.org/10.1053/j.semnuclmed.2010.08.005>
- [560] Pinkawa M, Attieh C, Piroth MD, Holy R, Nussen S, Klotz J, et al. Dose-escalation using intensity-modulated radiotherapy for prostate cancer--evaluation of the dose distribution with and without 18f-choline PET-CT detected simultaneous integrated boost. *Radiother Oncol*. 2009;93:213-9. <https://doi.org/10.1016/j.radonc.2009.07.014>
- [561] Seppala J, Seppanen M, Arponen E, Lindholm P, Minn H. Carbon-11 acetate PET/CT based dose escalated IMRT in prostate cancer. *Radiother Oncol*. 2009;93:234-40. <https://doi.org/10.1016/j.radonc.2009.08.010>

- [562] Demirkol MO, Acar O, Ucar B, Ramazanoglu SR, Saglican Y, Esen T. Prostate-specific membrane antigen-based imaging in prostate cancer: Impact on clinical decision making process. *Prostate*. 2015;75:748-57. <https://doi.org/10.1002/pros.22956>
- [563] Mease RC, Foss CA, Pomper MG. PET imaging in prostate cancer: Focus on prostate-specific membrane antigen. *Curr Top Med Chem*. 2013;13:951-62. <http://www.ncbi.nlm.nih.gov/pubmed/23590171>
- [564] Pinkawa M, Eble MJ, Mottaghy FM. PET and PET/CT in radiation treatment planning for prostate cancer. *Expert Rev Anticancer Ther*. 2011;11:1033-9. <https://doi.org/10.1586/era.11.51>
- [565] Leung K. [11C]choline. In *molecular imaging and contrast agent database (micad)* [internet] Bethesda MD2004.
- [566] Farsad M, Schiavina R, Castellucci P, Nanni C, Corti B, Martorana G, et al. Detection and localization of prostate cancer: Correlation of (11)c-choline PET/CT with histopathologic step-section analysis. *J Nucl Med*. 2005;46:1642-9. <https://jnm.snmjournals.org/content/46/10/1642>
- [567] Yamaguchi T, Lee J, Uemura H, Sasaki T, Takahashi N, Oka T, et al. Prostate cancer: A comparative study of 11C-choline PET and MR imaging combined with proton MR spectroscopy. *Eur J Nucl Med Mol Imaging*. 2005;32:742-8. <https://doi.org/10.1007/s00259-004-1755-y>
- [568] Martorana G, Schiavina R, Corti B, Farsad M, Salizzoni E, Brunocilla E, et al. 11C-choline positron emission tomography/computerized tomography for tumor localization of primary prostate cancer in comparison with 12-core biopsy. *J Urol*. 2006;176:954-60; discussion 60. <https://doi.org/10.1016/j.juro.2006.04.015>
- [569] Park H, Meyer CR, Wood D, Khan A, Shah R, Hussain H, et al. Validation of automatic target volume definition as demonstrated for 11C-choline PET/CT of human prostate cancer using multi-modality fusion techniques. *Acad Radiol*. 2010;17:614-23. <https://doi.org/10.1016/j.acra.2010.01.003>
- [570] Schwarzenbock SM, Kurth J, Gocke C, Kuhnt T, Hildebrandt G, Krause BJ. Role of choline PET/CT in guiding target volume delineation for irradiation of prostate cancer. *Eur J Nucl Med Mol Imaging*. 2013;40 Suppl 1:S28-35. <https://doi.org/10.1007/s00259-013-2404-0>
- [571] Piert M, Park H, Khan A, Siddiqui J, Hussain H, Chenevert T, et al. Detection of aggressive primary prostate cancer with 11C-choline PET/CT using multimodality fusion techniques. *J Nucl Med*. 2009;50:1585-93. <https://doi.org/10.2967/jnumed.109.063396>
- [572] Hofman MS, Murphy DG, Williams SG, Nzenza T, Herschtal A, Lourenco RA, et al. A prospective randomized multicentre study of the impact of gallium-68 prostate-specific membrane antigen (PSMA) PET/CT imaging for staging high-risk prostate cancer prior to curative-intent surgery or radiotherapy (proPSMA study): Clinical trial protocol. *BJU Int*. 2018;122:783-93. <https://doi.org/10.1111/bju.14374>
- [573] Abecassis JP, Ghazdar N, Peyromaure M, Giraud P. Prostate imaging: Contribution of PET PSMA and MRI. *Cancer Radiother*. 2020;24:423-8. <https://doi.org/10.1016/j.canrad.2020.06.002>
- [574] Esen T, Kilic M, Seymen H, Acar O, Demirkol MO. Can ga-68 PSMA PET/CT replace conventional imaging modalities for primary lymph node and bone staging of prostate cancer? *Eur Urol Focus*. 2020;6:218-20. <https://doi.org/10.1016/j.euf.2019.05.005>
- [575] Henkenberens C, Von Klot CA, Ross TL, Bengel FM, Wester HJ, Katja H, et al. (68)ga-PSMA ligand PET/CT-based radiotherapy for lymph node relapse of prostate cancer after primary therapy delays initiation of systemic therapy. *Anticancer Res*. 2017;37:1273-9. <https://doi.org/10.21873/anticancer.11444>
- [576] Schmidt-Hegemann NS, Eze C, Li M, Rogowski P, Schaefer C, Stief C, et al. Impact of (68)ga-PSMA PET/CT on the radiotherapeutic approach to prostate cancer in comparison to CT: A retrospective analysis. *J Nucl Med*. 2019;60:963-70. <https://doi.org/10.2967/jnumed.118.220855>
- [577] Schmidt-Hegemann NS, Stief C, Kim TH, Eze C, Kirste S, Strouthos I, et al. Outcome after PSMA PET/CT based salvage radiotherapy in patients with biochemical recurrence after radical prostatectomy: A 2-institutional retrospective analysis. *J Nucl Med*. 2019;60:<https://jnm.snmjournals.org/content/46/10/1642> <https://doi.org/10.2967/jnumed.118.212563>

- [578] Zschaeck S, Wust P, Beck M, Wlodarczyk W, Kaul D, Rogasch J, et al. Intermediate-term outcome after PSMA-PET guided high-dose radiotherapy of recurrent high-risk prostate cancer patients. *Radiat Oncol*. 2017;12:140. <https://doi.org/10.1186/s13014-017-0877-x>
- [579] Bouchelouche K, Choyke PL. Advances in prostate-specific membrane antigen PET of prostate cancer. *Current Opinion in Oncology*. 2018. <https://doi.org/10.1097/cco.0000000000000439>
- [580] Dewes S, Schiller K, Sauter K, Eiber M, Maurer T, Schwaiger M, et al. Integration of (68)ga-PSMA-PET imaging in planning of primary definitive radiotherapy in prostate cancer: A retrospective study. *Radiat Oncol*. 2016;11:73. <https://doi.org/10.1186/s13014-016-0646-2>
- [581] Sterzing F, Kratochwil C, Fiedler H, Katayama S, Habl G, Kopka K, et al. (68)ga-PSMA-11 PET/CT: A new technique with high potential for the radiotherapeutic management of prostate cancer patients. *Eur J Nucl Med Mol Imaging*. 2016;43:34-41. <https://doi.org/10.1007/s00259-015-3188-1>
- [582] Bluemel C, Krebs M, Polat B, Linke F, Eiber M, Samnick S, et al. 68ga-PSMA-PET/CT in patients with biochemical prostate cancer recurrence and negative 18f-choline-PET/CT. *Clin Nucl Med*. 2016;41:515-21. <https://doi.org/10.1097/RLU.0000000000001197>
- [583] Zamboglou C, Klein CM, Thomann B, Fassbender TF, Rischke HC, Kirste S, et al. The dose distribution in dominant intraprostatic tumour lesions defined by multiparametric MRI and PSMA PET/CT correlates with the outcome in patients treated with primary radiation therapy for prostate cancer. *Radiat Oncol*. 2018;13:65. <https://doi.org/10.1186/s13014-018-1014-1>
- [584] Dinkel J, Thieke C, Plathow C, Zamecnik P, Prum H, Huber PE, et al. Respiratory-induced prostate motion: Characterization and quantification in dynamic MRI. *Strahlenther Onkol*. 2011;187:426-32. <https://doi.org/10.1007/s00066-011-2201-2>
- [585] Schiffner DC, Gottschalk AR, Lometti M, Aubin M, Pouliot J, Speight J, et al. Daily electronic portal imaging of implanted gold seed fiducials in patients undergoing radiotherapy after radical prostatectomy. *Int J Radiat Oncol Biol Phys*. 2007;67:610-9. <https://doi.org/10.1016/j.ijrobp.2006.09.042>
- [586] Wu J, Haycocks T, Alasti H, Ottewell G, Middlemiss N, Abdoell M, et al. Positioning errors and prostate motion during conformal prostate radiotherapy using on-line isocentre set-up verification and implanted prostate markers. *Radiother Oncol*. 2001;61:127-33. <https://www.ncbi.nlm.nih.gov/pubmed/11690677>
- [587] McPartlin AJ, Li XA, Kershaw LE, Heide U, Kerkmeijer L, Lawton C, et al. MRI-guided prostate adaptive radiotherapy - a systematic review. *Radiother Oncol*. 2016;119:371-80. <https://doi.org/10.1016/j.radonc.2016.04.014>
- [588] Xie Y, Djajaputra D, King CR, Hossain S, Ma L, Xing L. Intrafractional motion of the prostate during hypofractionated radiotherapy. *Int J Radiat Oncol Biol Phys*. 2008;72:236-46. <https://doi.org/10.1016/j.ijrobp.2008.04.051>
- [589] Chen J, Lee RJ, Handrahan D, Sause WT. Intensity-modulated radiotherapy using implanted fiducial markers with daily portal imaging: Assessment of prostate organ motion. *Int J Radiat Oncol Biol Phys*. 2007;68:912-9. <https://doi.org/10.1016/j.ijrobp.2007.02.024>
- [590] Bell LJ, Cox J, Eade T, Rinks M, Kneebone A. Prostate bed motion may cause geographic miss in post-prostatectomy image-guided intensity-modulated radiotherapy. *J Med Imaging Radiat Oncol*. 2013;57:725-32. <https://doi.org/10.1111/1754-9485.12089>
- [591] Connolly JA, Shinohara K, Presti JC, Jr., Carroll PR. Local recurrence after radical prostatectomy: Characteristics in size, location, and relationship to prostate-specific antigen and surgical margins. *Urology*. 1996;47:225-31. [https://doi.org/10.1016/S0090-4295\(99\)80421-X](https://doi.org/10.1016/S0090-4295(99)80421-X)
- [592] Leventis AK, Shariat SF, Slawin KM. Local recurrence after radical prostatectomy: Correlation of US features with prostatic fossa biopsy findings. *Radiology*. 2001;219:432-9. <https://doi.org/10.1148/radiology.219.2.r01ma20432>
- [593] Scattoni V, Roscigno M, Raber M, Montorsi F, Da Pozzo L, Guazzoni G, et al. Multiple vesico-urethral biopsies following radical prostatectomy: The predictive roles of TRUS, DRE, psa and the pathological stage. *Eur Urol*. 2003;44:407-14. [https://doi.org/10.1016/s0302-2838\(03\)00320-8](https://doi.org/10.1016/s0302-2838(03)00320-8)

- [594] Liauw SL, Pitroda SP, Eggener SE, Stadler WM, Pelizzari CA, Vannier MW, et al. Evaluation of the prostate bed for local recurrence after radical prostatectomy using endorectal magnetic resonance imaging. *Int J Radiat Oncol Biol Phys*. 2013;85:378-84. <https://doi.org/10.1016/j.ijrobp.2012.05.015>
- [595] Miralbell R, Veas H, Lozano J, Khan H, Molla M, Hidalgo A, et al. Endorectal MRI assessment of local relapse after surgery for prostate cancer: A model to define treatment field guidelines for adjuvant radiotherapy in patients at high risk for local failure. *Int J Radiat Oncol Biol Phys*. 2007;67:356-61. <https://doi.org/10.1016/j.ijrobp.2006.08.079>
- [596] Kitajima K, Murphy RC, Nathan MA, Froemming AT, Hagen CE, Takahashi N, et al. Detection of recurrent prostate cancer after radical prostatectomy: Comparison of 11C-choline PET/CT with pelvic multiparametric MR imaging with endorectal coil. *J Nucl Med*. 2014;55:223-32. <https://doi.org/10.2967/jnumed.113.123018>
- [597] Langenhuijsen JF, Donker R, McColl GM, Kiemeny LA, Witjes JA, van Lin EN. Postprostatectomy ultrasound-guided transrectal implantation of gold markers for external beam radiotherapy. Technique and complications rate. *Strahlenther Onkol*. 2013;189:476-81. <https://doi.org/10.1007/s00066-013-0323-4>
- [598] Zhu M, Bharat S, Michalski JM, Gay HA, Hou WH, Parikh PJ. Adaptive radiation therapy for postprostatectomy patients using real-time electromagnetic target motion tracking during external beam radiation therapy. *Int J Radiat Oncol Biol Phys*. 2013;85:1038-44. <https://doi.org/10.1016/j.ijrobp.2012.08.001>
- [599] Huang K, Palma DA, Scott D, McGregor D, Gaede S, Yartsev S, et al. Inter- and intrafraction uncertainty in prostate bed image-guided radiotherapy. *Int J Radiat Oncol Biol Phys*. 2012;84:402-7. <https://doi.org/10.1016/j.ijrobp.2011.12.035>
- [600] Song S, Yenice KM, Kopec M, Liauw SL. Image-guided radiotherapy using surgical clips as fiducial markers after prostatectomy: A report of total setup error, required pTV expansion, and dosimetric implications. *Radiother Oncol*. 2012;103:270-4. <https://doi.org/10.1016/j.radonc.2011.07.024>
- [601] Alander E, Visapaa H, Kouri M, Keyrilainen J, Saarilahti K, Tenhunen M. Gold seed fiducials in analysis of linear and rotational displacement of the prostate bed. *Radiother Oncol*. 2014;110:256-60. <https://doi.org/10.1016/j.radonc.2013.10.037>
- [602] Fortin I, Carrier JF, Beauchemin MC, Beliveau-Nadeau D, Delouya G, Taussky D. Using fiducial markers in the prostate bed in postprostatectomy external beam radiation therapy improves accuracy over surgical clips. *Strahlenther Onkol*. 2014;190:467-71. <https://doi.org/10.1007/s00066-014-0631-3>
- [603] Ost P, De Meerleer G, De Gerssem W, Impens A, De Neve W. Analysis of prostate bed motion using daily cone-beam computed tomography during postprostatectomy radiotherapy. *Int J Radiat Oncol Biol Phys*. 2011;79:188-94. <https://doi.org/10.1016/j.ijrobp.2009.10.029>
- [604] Sandhu A, Sethi R, Rice R, Wang JZ, Marcus L, Salem C, et al. Prostate bed localization with image-guided approach using on-board imaging: Reporting acute toxicity and implications for radiation therapy planning following prostatectomy. *Radiother Oncol*. 2008;88:20-5. <https://doi.org/10.1016/j.radonc.2008.05.009>
- [605] Chao M, Ho H, Chan Y, Tan A, Pham T, Bolton D, et al. Prospective analysis of hydrogel spacer for patients with prostate cancer undergoing radiotherapy. *BJU Int*. 2018;122:427-33. <https://doi.org/10.1111/bju.14192>
- [606] Guillonneau B, Debras B, Veillon B, Bougaran J, Chambon E, Vallancien G. Indications for preoperative seminal vesicle biopsies in staging of clinically localized prostatic cancer. *Eur Urol*. 1997;32:160-5. <https://www.karger.com/Article/Abstract/480851>
- [607] Epstein JI, Carmichael M, Walsh PC. Adenocarcinoma of the prostate invading the seminal vesicle: Definition and relation of tumor volume, grade and margins of resection to prognosis. *J Urol*. 1993;149:1040-5. [https://doi.org/10.1016/s0022-5347\(17\)36291-2](https://doi.org/10.1016/s0022-5347(17)36291-2)
- [608] Partin AW, Mangold LA, Lamm DM, Walsh PC, Epstein JI, Pearson JD. Contemporary update of prostate cancer staging nomograms (Partin tables) for the new millennium. *Urology*. 2001;58:843-8. [https://doi.org/10.1016/s0090-4295\(01\)01441-8](https://doi.org/10.1016/s0090-4295(01)01441-8)

- [609] Parker C, Haycocks T, Bayley A, Alasti H, Warde P, Catton C. A dose-volume histogram analysis of the seminal vesicles in men treated with conformal radiotherapy to 'prostate alone'. *Clin Oncol (R Coll Radiol)*. 2002;14:298-302. <https://doi.org/10.1053/clon.2002.0077>
- [610] Kestin L, Goldstein N, Vicini F, Yan D, Korman H, Martinez A. Treatment of prostate cancer with radiotherapy: Should the entire seminal vesicles be included in the clinical target volume? *Int J Radiat Oncol Biol Phys*. 2002;54:686-97. [https://doi.org/10.1016/s0360-3016\(02\)03011-0](https://doi.org/10.1016/s0360-3016(02)03011-0)
- [611] Korman HJ, Watson RB, Civantos F, Block NL, Soloway MS. Radical prostatectomy: Is complete resection of the seminal vesicles really necessary? *J Urol*. 1996;156:1081-3. [https://doi.org/10.1016/s0022-5347\(01\)65709-4](https://doi.org/10.1016/s0022-5347(01)65709-4)
- [612] Villers AA, McNeal JE, Redwine EA, Freiha FS, Stamey TA. Pathogenesis and biological significance of seminal vesicle invasion in prostatic adenocarcinoma. *J Urol*. 1990;143:1183-7. [https://doi.org/10.1016/s0022-5347\(17\)40220-5](https://doi.org/10.1016/s0022-5347(17)40220-5)
- [613] Bayman NA, Wylie JP. When should the seminal vesicles be included in the target volume in prostate radiotherapy? *Clin Oncol (R Coll Radiol)*. 2007;19:302-7. <https://doi.org/10.1016/j.clon.2007.03.005>
- [614] Epstein JI, Partin AW, Potter SR, Walsh PC. Adenocarcinoma of the prostate invading the seminal vesicle: Prognostic stratification based on pathologic parameters. *Urology*. 2000;56:283-8. [https://doi.org/10.1016/s0090-4295\(00\)00640-3](https://doi.org/10.1016/s0090-4295(00)00640-3)
- [615] Boehmer D, Maingon P, Poortmans P, Baron MH, Miralbell R, Remouchamps V, et al. Guidelines for primary radiotherapy of patients with prostate cancer. *Radiother Oncol*. 2006;79:259-69. <https://doi.org/10.1016/j.radonc.2006.05.012>
- [616] Hayden AJ, Martin JM, Kneebone AB, Lehman M, Wiltshire KL, Skala M, et al. Australian & New Zealand faculty of radiation oncology genito-urinary group: 2010 consensus guidelines for definitive external beam radiotherapy for prostate carcinoma. *J Med Imaging Radiat Oncol*. 2010;54:513-25. <https://doi.org/10.1111/j.1754-9485.2010.02214.x>
- [617] Frank SJ, Dong L, Kudchadker RJ, De Crevoisier R, Lee AK, Cheung R, et al. Quantification of prostate and seminal vesicle interfraction variation during IMRT. *Int J Radiat Oncol Biol Phys*. 2008;71:813-20. <https://doi.org/10.1016/j.ijrobp.2007.10.028>
- [618] Liang J, Wu Q, Yan D. The role of seminal vesicle motion in target margin assessment for online image-guided radiotherapy for prostate cancer. *Int J Radiat Oncol Biol Phys*. 2009;73:935-43. <https://doi.org/10.1016/j.ijrobp.2008.10.019>
- [619] Mak D, Gill S, Paul R, Stillie A, Haworth A, Kron T, et al. Seminal vesicle interfraction displacement and margins in image guided radiotherapy for prostate cancer. *Radiat Oncol*. 2012;7:139. <https://doi.org/10.1186/1748-717X-7-139>
- [620] Smitsmans MH, de Bois J, Sonke JJ, Catton CN, Jaffray DA, Lebesque JV, et al. Residual seminal vesicle displacement in marker-based image-guided radiotherapy for prostate cancer and the impact on margin design. *Int J Radiat Oncol Biol Phys*. 2011;80:590-6. <https://doi.org/10.1016/j.ijrobp.2010.06.026>
- [621] Meijer GJ, de Klerk J, Bzdusek K, van den Berg HA, Janssen R, Kaus MR, et al. What CTV-to-ptv margins should be applied for prostate irradiation? Four-dimensional quantitative assessment using model-based deformable image registration techniques. *Int J Radiat Oncol Biol Phys*. 2008;72:1416-25. <https://doi.org/10.1016/j.ijrobp.2008.03.005>
- [622] Mutanga TF, de Boer HC, van der Wielen GJ, Hoogeman MS, Incrocci L, Heijmen BJ. Margin evaluation in the presence of deformation, rotation, and translation in prostate and entire seminal vesicle irradiation with daily marker-based setup corrections. *Int J Radiat Oncol Biol Phys*. 2011;81:1160-7. <https://doi.org/10.1016/j.ijrobp.2010.09.013>
- [623] O'Daniel JC, Dong L, Zhang L, de Crevoisier R, Wang H, Lee AK, et al. Dosimetric comparison of four target alignment methods for prostate cancer radiotherapy. *Int J Radiat Oncol Biol Phys*. 2006;66:883-91. <https://doi.org/10.1016/j.ijrobp.2006.06.044>
- [624] van der Wielen GJ, Mutanga TF, Incrocci L, Kirkels WJ, Vasquez Osorio EM, Hoogeman MS, et al. Deformation of prostate and seminal vesicles relative to intraprostatic fiducial markers. *Int J Radiat Oncol Biol Phys*. 2008;72:1604-11 e3. <https://doi.org/10.1016/j.ijrobp.2008.07.023>

- [625] Chen Y, O'Connell JJ, Ko CJ, Mayer RR, Belard A, McDonough JE. Fiducial markers in prostate for kV imaging: Quantification of visibility and optimization of imaging conditions. *Phys Med Biol*. 2012;57:155-72. <https://doi.org/10.1088/0031-9155/57/1/155>
- [626] Chung PW, Haycocks T, Brown T, Cambridge Z, Kelly V, Alasti H, et al. On-line asi portal imaging of implanted fiducial markers for the reduction of interfraction error during conformal radiotherapy of prostate carcinoma. *Int J Radiat Oncol Biol Phys*. 2004;60:329-34. <https://doi.org/10.1016/j.ijrobp.2004.03.038>
- [627] Kupelian PA, Lee C, Langen KM, Zeidan OA, Manon RR, Willoughby TR, et al. Evaluation of image-guidance strategies in the treatment of localized prostate cancer. *Int J Radiat Oncol Biol Phys*. 2008;70:1151-7. <https://doi.org/10.1016/j.ijrobp.2007.07.2371>
- [628] Crook JM, Raymond Y, Salhani D, Yang H, Esche B. Prostate motion during standard radiotherapy as assessed by fiducial markers. *Radiother Oncol*. 1995;37:35-42. [https://doi.org/10.1016/0167-8140\(95\)01613-l](https://doi.org/10.1016/0167-8140(95)01613-l)
- [629] Kudchadker RJ, Lee AK, Yu ZH, Johnson JL, Zhang L, Zhang Y, et al. Effectiveness of using fewer implanted fiducial markers for prostate target alignment. *Int J Radiat Oncol Biol Phys*. 2009;74:1283-9. <https://doi.org/10.1016/j.ijrobp.2009.02.033>
- [630] Hulshof MC, van Andel G, Bel A, Gangel P, van de Kamer JB. Intravesical markers for delineation of target volume during external focal irradiation of bladder carcinomas. *Radiother Oncol*. 2007;84:49-51. <https://doi.org/10.1016/j.radonc.2007.05.017>
- [631] Chao M, Ho H, Joon DL, Chan Y, Spencer S, Ng M, et al. The use of tissue fiducial markers in improving the accuracy of post-prostatectomy radiotherapy. *Radiat Oncol J*. 2019;37:43-50. <https://doi.org/10.3857/roj.2018.00556>
- [632] Borchers H, Pinkawa M, Donner A, Wolter TP, Pallua N, Eble MJ, et al. Rectourethral fistula following Idr brachytherapy. *Urol Int*. 2009;82:365-6. <https://doi.org/10.1159/000209374>
- [633] Wei J, Sandison GA, Hsi WC, Ringor M, Lu X. Dosimetric impact of a CT metal artefact suppression algorithm for proton, electron and photon therapies. *Phys Med Biol*. 2006;51:5183-97. <https://doi.org/10.1088/0031-9155/51/20/007>
- [634] Lim YK, Kwak J, Kim DW, Shin D, Yoon M, Park S, et al. Microscopic gold particle-based fiducial markers for proton therapy of prostate cancer. *Int J Radiat Oncol Biol Phys*. 2009;74:1609-16. <https://doi.org/10.1016/j.ijrobp.2009.02.076>
- [635] Gates LL, Gladstone DJ, Kasibhatla MS, Marshall JF, Seigne JD, Hug E, et al. Stability of serrated gold coil markers in prostate localization. *J Appl Clin Med Phys*. 2011;12:3453. <https://doi.org/10.1120/jacmp.v12i3.3453>
- [636] Newhauser W, Fontenot J, Koch N, Dong L, Lee A, Zheng Y, et al. Monte carlo simulations of the dosimetric impact of radiopaque fiducial markers for proton radiotherapy of the prostate. *Phys Med Biol*. 2007;52:2937-52. <https://doi.org/10.1088/0031-9155/52/11/001>
- [637] Handsfield LL, Yue NJ, Zhou J, Chen T, Goyal S. Determination of optimal fiducial marker across image-guided radiation therapy (IGRT) modalities: Visibility and artifact analysis of gold, carbon, and polymer fiducial markers. *J Appl Clin Med Phys*. 2012;13:3976. <https://doi.org/10.1120/jacmp.v13i5.3976>
- [638] Kupelian P, Willoughby T, Mahadevan A, Djemil T, Weinstein G, Jani S, et al. Multi-institutional clinical experience with the calypso system in localization and continuous, real-time monitoring of the prostate gland during external radiotherapy. *Int J Radiat Oncol Biol Phys*. 2007;67:1088-98. <https://doi.org/10.1016/j.ijrobp.2006.10.026>
- [639] Quon H, Loblaw DA, Cheung PC, Holden L, Tang C, Pang G, et al. Intra-fraction motion during extreme hypofractionated radiotherapy of the prostate using pre- and post-treatment imaging. *Clin Oncol (R Coll Radiol)*. 2012;24:640-5. <https://doi.org/10.1016/j.clon.2011.12.001>
- [640] Shchory T, Schifter D, Lichtman R, Neustadter D, Corn BW. Tracking accuracy of a real-time fiducial tracking system for patient positioning and monitoring in radiation therapy. *Int J Radiat Oncol Biol Phys*. 2010;78:1227-34. <https://doi.org/10.1016/j.ijrobp.2010.01.067>
- [641] Shinohara K, Roach M, 3rd. Technique for implantation of fiducial markers in the prostate. *Urology*. 2008;71:196-200. <https://doi.org/10.1016/j.urology.2007.10.011>

- [642] Linden RA, Weiner PR, Gomella LG, Dicker AP, Suh DB, Trabulsi EJ, et al. Technique of outpatient placement of intraprostatic fiducial markers before external beam radiotherapy. *Urology*. 2009;73:881-6. <https://doi.org/10.1016/j.urology.2008.10.071>
- [643] Moman MR, van der Heide UA, Kotte AN, van Moorselaar RJ, Bol GH, Franken SP, et al. Long-term experience with transrectal and transperineal implantations of fiducial gold markers in the prostate for position verification in external beam radiotherapy; feasibility, toxicity and quality of life. *Radiother Oncol*. 2010;96:38-42. <https://doi.org/10.1016/j.radonc.2010.02.027>
- [644] Igdem S, Akpınar H, Alco G, Agacayak F, Turkan S, Okkan S. Implantation of fiducial markers for image guidance in prostate radiotherapy: Patient-reported toxicity. *Br J Radiol*. 2009;82:941-5. <https://doi.org/10.1259/bjr/14201041>
- [645] Langenhuijsen JF, van Lin EN, Kiemeny LA, van der Vight LP, McColl GM, Visser AG, et al. Ultrasound-guided transrectal implantation of gold markers for prostate localization during external beam radiotherapy: Complication rate and risk factors. *Int J Radiat Oncol Biol Phys*. 2007;69:671-6. <https://doi.org/10.1016/j.ijrobp.2007.04.009>
- [646] Deutschmann H, Kametriser G, Steininger P, Scherer P, Scholler H, Gaisberger C, et al. First clinical release of an online, adaptive, aperture-based image-guided radiotherapy strategy in intensity-modulated radiotherapy to correct for inter- and intrafractional rotations of the prostate. *Int J Radiat Oncol Biol Phys*. 2012;83:1624-32. <https://doi.org/10.1016/j.ijrobp.2011.10.009>
- [647] Broggi S, Cozzarini C, Fiorino C, Maggiulli E, Alongi F, Cattaneo GM, et al. Modeling set-up error by daily MVCT for prostate adjuvant treatment delivered in 20 fractions: Implications for the assessment of the optimal correction strategies. *Radiother Oncol*. 2009;93:246-52. <https://doi.org/10.1016/j.radonc.2009.08.029>
- [648] Moseley DJ, White EA, Wiltshire KL, Rosewall T, Sharpe MB, Siewerdsen JH, et al. Comparison of localization performance with implanted fiducial markers and cone-beam computed tomography for on-line image-guided radiotherapy of the prostate. *Int J Radiat Oncol Biol Phys*. 2007;67:942-53. <https://doi.org/10.1016/j.ijrobp.2006.10.039>
- [649] Foster RD, Pistenmaa DA, Solberg TD. A comparison of radiographic techniques and electromagnetic transponders for localization of the prostate. *Radiat Oncol*. 2012;7:101. <https://doi.org/10.1186/1748-717X-7-101>
- [650] Zelefsky MJ, Kollmeier M, Cox B, Fidaleo A, Sperling D, Pei X, et al. Improved clinical outcomes with high-dose image guided radiotherapy compared with non-IGRT for the treatment of clinically localized prostate cancer. *Int J Radiat Oncol Biol Phys*. 2012;84:125-9. <https://doi.org/10.1016/j.ijrobp.2011.11.047>
- [651] Sveistrup J, af Rosenschold PM, Deasy JO, Oh JH, Pommer T, Petersen PM, et al. Improvement in toxicity in high risk prostate cancer patients treated with image-guided intensity-modulated radiotherapy compared to 3D conformal radiotherapy without daily image guidance. *Radiat Oncol*. 2014;9:44. <https://doi.org/10.1186/1748-717X-9-44>
- [652] Kok D, Gill S, Bressel M, Byrne K, Kron T, Fox C, et al. Late toxicity and biochemical control in 554 prostate cancer patients treated with and without dose escalated image guided radiotherapy. *Radiother Oncol*. 2013;107:140-6. <https://doi.org/10.1016/j.radonc.2013.04.007>
- [653] Mc Parland NA. kV-cone beam CT as an IGRT tool in the treatment of early stage prostate cancer: A literature review. *J Med Imaging Radiat Sci*. 2009;40:9-14. <https://doi.org/10.1016/j.jmir.2008.12.002>
- [654] Shi W, Li JG, Zlotecki RA, Yeung A, Newlin H, Palta J, et al. Evaluation of kV cone-beam ct performance for prostate IGRT: A comparison of automatic grey-value alignment to implanted fiducial-marker alignment. *Am J Clin Oncol*. 2011;34:16-21. <https://doi.org/10.1097/COC.0b013e3181d26b1a>
- [655] Stock M, Pasler M, Birkfellner W, Homolka P, Poetter R, Georg D. Image quality and stability of image-guided radiotherapy (IGRT) devices: A comparative study. *Radiother Oncol*. 2009;93:1-7. <https://doi.org/10.1016/j.radonc.2009.07.012>

- [656] Deegan T, Owen R, Holt T, Fielding A, Biggs J, Parfitt M, et al. Assessment of cone beam CT registration for prostate radiation therapy: Fiducial marker and soft tissue methods. *J Med Imaging Radiat Oncol*. 2015;59:91-8. <https://doi.org/10.1111/1754-9485.12197>
- [657] White EA, Brock KK, Jaffray DA, Catton CN. Inter-observer variability of prostate delineation on cone beam computerised tomography images. *Clin Oncol (R Coll Radiol)*. 2009;21:32-8. <https://doi.org/10.1016/j.clon.2008.11.007>
- [658] Lütgendorf-Caucig C, Fotina I, Stock M, Pötter R, Goldner G, Georg D. Feasibility of CBCT-based target and normal structure delineation in prostate cancer radiotherapy: Multi-observer and image multi-modality study. *Radiother Oncol*. 2011;98:154-61. <https://doi.org/10.1016/j.radonc.2010.11.016>
- [659] Tocco BR, Kishan AU, Ma TM, Kerkmeijer LGW, Tree AC. MR-guided radiotherapy for prostate cancer. *Front Oncol*. 2020;10. <https://doi.org/10.3389/fonc.2020.616291>
- [660] Barney BM, Lee RJ, Handrahan D, Welsh KT, Cook JT, Sause WT. Image-guided radiotherapy (IGRT) for prostate cancer comparing kV imaging of fiducial markers with cone beam computed tomography (CBCT). *Int J Radiat Oncol Biol Phys*. 2011;80:301-5. <https://doi.org/10.1016/j.ijrobp.2010.06.007>
- [661] Heemsbergen WD, Hoogeman MS, Witte MG, Peeters ST, Incrocci L, Lebesque JV. Increased risk of biochemical and clinical failure for prostate patients with a large rectum at radiotherapy planning: Results from the Dutch trial of 68 Gy versus 78 Gy. *Int J Radiat Oncol Biol Phys*. 2007;67:1418-24. <https://doi.org/10.1016/j.ijrobp.2006.11.014>
- [662] McNair HA, Wedlake L, Lips IM, Andreyev J, Van Vulpen M, Dearnaley D. A systematic review: Effectiveness of rectal emptying preparation in prostate cancer patients. *Pract Radiat Oncol*. 2014;4:437-47. <https://doi.org/10.1016/j.prro.2014.06.005>
- [663] de Crevoisier R, Tucker SL, Dong L, Mohan R, Cheung R, Cox JD, et al. Increased risk of biochemical and local failure in patients with distended rectum on the planning CT for prostate cancer radiotherapy. *Int J Radiat Oncol Biol Phys*. 2005;62:965-73. <https://doi.org/10.1016/j.ijrobp.2004.11.032>
- [664] Fiorino C, Di Muzio N, Broggi S, Cozzarini C, Maggiulli E, Alongi F, et al. Evidence of limited motion of the prostate by carefully emptying the rectum as assessed by daily MVCT image guidance with helical tomotherapy. *Int J Radiat Oncol Biol Phys*. 2008;71:611-7. <https://doi.org/10.1016/j.ijrobp.2008.01.048>
- [665] Nijkamp J, Pos FJ, Nuver TT, de Jong R, Remeijer P, Sonke JJ, et al. Adaptive radiotherapy for prostate cancer using kilovoltage cone-beam computed tomography: First clinical results. *Int J Radiat Oncol Biol Phys*. 2008;70:75-82. <https://doi.org/10.1016/j.ijrobp.2007.05.046>
- [666] Ogino I, Uemura H, Inoue T, Kubota Y, Nomura K, Okamoto N. Reduction of prostate motion by removal of gas in rectum during radiotherapy. *Int J Radiat Oncol Biol Phys*. 2008;72:456-66. <https://doi.org/10.1016/j.ijrobp.2008.01.004>
- [667] D'Amico AV, Manola J, Loffredo M, Lopes L, Nissen K, O'Farrell DA, et al. A practical method to achieve prostate gland immobilization and target verification for daily treatment. *Int J Radiat Oncol Biol Phys*. 2001;51:1431-6. [https://doi.org/10.1016/s0360-3016\(01\)02663-3](https://doi.org/10.1016/s0360-3016(01)02663-3)
- [668] van Lin EN, Kristinsson J, Philippens ME, de Jong DJ, van der Vight LP, Kaanders JH, et al. Reduced late rectal mucosal changes after prostate three-dimensional conformal radiotherapy with endorectal balloon as observed in repeated endoscopy. *Int J Radiat Oncol Biol Phys*. 2007;67:799-811. <https://doi.org/10.1016/j.ijrobp.2006.09.034>
- [669] Susil RC, McNutt TR, DeWeese TL, Song D. Effects of prostate-rectum separation on rectal dose from external beam radiotherapy. *Int J Radiat Oncol Biol Phys*. 2010;76:1251-8. <https://doi.org/10.1016/j.ijrobp.2009.07.1679>
- [670] Prada PJ, Fernandez J, Martinez AA, de la Rua A, Gonzalez JM, Fernandez JM, et al. Transperineal injection of hyaluronic acid in anterior perirectal fat to decrease rectal toxicity from radiation delivered with intensity modulated brachytherapy or EBRT for prostate cancer patients. *Int J Radiat Oncol Biol Phys*. 2007;69:95-102. <https://doi.org/10.1016/j.ijrobp.2007.02.034>

- [671] Eckert F, Alloussi S, Paulsen F, Bamberg M, Zips D, Spillner P, et al. Prospective evaluation of a hydrogel spacer for rectal separation in dose-escalated intensity-modulated radiotherapy for clinically localized prostate cancer. *BMC Cancer*. 2013;13:27. <https://doi.org/10.1186/1471-2407-13-27>
- [672] Nguyen PL, Devlin PM, Beard CJ, Orio PF, 3rd, O'Leary MP, Wolfsberger LD, et al. High-dose-rate brachytherapy for prostate cancer in a previously radiated patient with polyethylene glycol hydrogel spacing to reduce rectal dose: Case report and review of the literature. *Brachytherapy*. 2013;12:77-83. <https://doi.org/10.1016/j.brachy.2012.03.005>
- [673] Morancy TJ, Winkfield KM, Karasiewicz CA, Kaplan ID. Use of a blood-patch technique to reduce rectal dose during cesium-131 prostate brachytherapy. *International Journal of Radiation Oncology\* Biology\* Physics*. 2008;72(1 Suppl):S331-2. <https://doi.org/10.1016/j.ijrobp.2008.06.1127>
- [674] Noyes WR, Hosford CC, Schultz SE. Human collagen injections to reduce rectal dose during radiotherapy. *Int J Radiat Oncol Biol Phys*. 2012;82:1918-22. <https://doi.org/10.1016/j.ijrobp.2011.02.034>
- [675] Pinkawa M, Piroth MD, Holy R, Escobar-Corral N, Caffaro M, Djukic V, et al. Spacer stability and prostate position variability during radiotherapy for prostate cancer applying a hydrogel to protect the rectal wall. *Radiother Oncol*. 2013;106:220-4. <https://doi.org/10.1016/j.radonc.2012.11.010>
- [676] Ben-Yosef R, Paz A, Levy Y, Alani S, Muncher Y, Shohat S, et al. A novel device for protecting rectum during prostate cancer irradiation: In vivo data on a large mammal model. *J Urol*. 2009;181:1401-6. <https://doi.org/10.1016/j.juro.2008.11.010>
- [677] Gez E, Cytron S, Ben Yosef R, London D, Corn BW, Alani S, et al. Application of an interstitial and biodegradable balloon system for prostate-rectum separation during prostate cancer radiotherapy: A prospective multi-center study. *Radiat Oncol*. 2013;8:96. <https://doi.org/10.1186/1748-717X-8-96>
- [678] Pinkawa M, Corral NE, Caffaro M, Piroth MD, Holy R, Djukic V, et al. Application of a spacer gel to optimize three-dimensional conformal and intensity modulated radiotherapy for prostate cancer. *Radiother Oncol*. 2011;100:436-41. <https://doi.org/10.1016/j.radonc.2011.09.005>
- [679] Hatiboglu G, Pinkawa M, Vallee JP, Hadaschik B, Hohenfellner M. Application technique: Placement of a prostate-rectum spacer in men undergoing prostate radiation therapy. *BJU Int*. 2012;110:E647-52. <https://doi.org/10.1111/j.1464-410X.2012.11373.x>
- [680] Aminsharifi A, Kotamarti S, Silver D, Schulman A. Major complications and adverse events related to the injection of the spaceoar hydrogel system before radiotherapy for prostate cancer: Review of the manufacturer and user facility device experience database. *J Endourol*. 2019;33:868-71. <https://doi.org/10.1089/end.2019.0431>
- [681] Weber DC, Zilli T, Vallee JP, Rouzaud M, Miralbell R, Cozzi L. Intensity modulated proton and photon therapy for early prostate cancer with or without transperineal injection of a polyethylen glycol spacer: A treatment planning comparison study. *Int J Radiat Oncol Biol Phys*. 2012;84:e311-8. <https://doi.org/10.1016/j.ijrobp.2012.03.028>
- [682] Pinkawa M, Berneking V, Schlenter M, Krenkel B, Eble MJ. Quality of life after radiation therapy for prostate cancer with a hydrogel spacer: 5-year results. *Int J Radiat Oncol Biol Phys*. 2017;99:374-7. <https://doi.org/10.1016/j.ijrobp.2017.05.035>
- [683] Pinkawa M, Klotz J, Djukic V, Schubert C, Escobar-Corral N, Caffaro M, et al. Learning curve in the application of a hydrogel spacer to protect the rectal wall during radiotherapy of localized prostate cancer. *Urology*. 2013;82:963-8. <https://doi.org/10.1016/j.urology.2013.07.014>
- [684] Song DY, Herfarth KK, Uhl M, Eble MJ, Pinkawa M, van Triest B, et al. A multi-institutional clinical trial of rectal dose reduction via injected polyethylene-glycol hydrogel during intensity modulated radiation therapy for prostate cancer: Analysis of dosimetric outcomes. *Int J Radiat Oncol Biol Phys*. 2013;87:81-7. <https://doi.org/10.1016/j.ijrobp.2012.12.019>
- [685] Mariados N, Sylvester J, Shah D, Karsh L, Hudes R, Beyer D, et al. Hydrogel spacer prospective multicenter randomized controlled pivotal trial: Dosimetric and clinical effects of perirectal spacer application in men undergoing prostate image guided intensity modulated radiation therapy. *Int J Radiat Oncol Biol Phys*. 2015;92:971-7. <https://doi.org/10.1016/j.ijrobp.2015.04.030>

- [686] Hamstra DA, Mariados N, Sylvester J, Shah D, Karsh L, Hudes R, et al. Continued benefit to rectal separation for prostate radiation therapy: Final results of a phase iii trial. *Int J Radiat Oncol Biol Phys.* 2017;97:976-85. <https://doi.org/10.1016/j.ijrobp.2016.12.024>
- [687] Karsh LI, Gross ET, Pieczonka CM, Aliotta PJ, Skomra CJ, Ponsky LE, et al. Absorbable hydrogel spacer use in prostate radiotherapy: A comprehensive review of phase 3 clinical trial published data. *Urology.* 2018;115:39-44. <https://doi.org/10.1016/j.urology.2017.11.016>
- [688] Chao M, Ong WL, Joon DL, Lawrenstchuk N, Khoo VS, Foroudi F, et al. Post prostatectomy radiotherapy: Can the urologist help to reduce rectal toxicity? *Int J Radiol Radiat Ther.* 2019;6:87-92. <https://doi.org/10.15406/ijrrt.2019.06.00224>
- [689] Lehrich BM, Moyses HM, Ravera J, Yoshida J, Torrey R, Baghdassarian R, et al. Five-year results of post-prostatectomy patients administered a hydrogel rectal spacer implant in conjunction with dose escalated external beam radiation therapy. *Journal of Radiation Oncology.* 2019;8:31-8. <https://doi.org/10.1007/s13566-018-0369-0>
- [690] Pinkawa M, Schubert C, Escobar-Corral N, Holy R, Eble MJ. Application of a hydrogel spacer for postoperative salvage radiotherapy of prostate cancer. *Strahlenther Onkol.* 2015;191:375-9. <https://doi.org/10.1007/s00066-014-0769-z>
- [691] Pinkawa P, Schubert C, Escobar-Corral N, Holy R, Eble M. Application of a hydrogel spacer for postoperative salvage radiotherapy of prostate cancer. *Strahlenther Onkol.* 2014;191. <https://doi.org/10.1007/s00066-014-0769-z>
- [692] Vilotte F, Antoine M, Bobin M, Latorzeff I, Supiot S, Richaud P, et al. Post-prostatectomy image-guided radiotherapy: The invisible target concept. *Front Oncol.* 2017;7:34. <https://doi.org/10.3389/fonc.2017.00034>
- [693] Hernandez D, Salas D, Gimenez D, Buitrago P, Esquena S, Palou J, et al. Pelvic MRI findings in relapsed prostate cancer after radical prostatectomy. *Radiat Oncol.* 2015;10:262. <https://doi.org/10.1186/s13014-015-0574-6>
- [694] Rischke HC, Schafer AO, Nestle U, Volegova-Neher N, Henne K, Benz MR, et al. Detection of local recurrent prostate cancer after radical prostatectomy in terms of salvage radiotherapy using dynamic contrast enhanced-MRI without endorectal coil. *Radiat Oncol.* 2012;7:185. <https://doi.org/10.1186/1748-717X-7-185>
- [695] Bolla M, van Poppel H, Collette L, van Cangh P, Vekemans K, Da Pozzo L, et al. Postoperative radiotherapy after radical prostatectomy: A randomised controlled trial (EORTC trial 22911). *The Lancet.* 2005;366:572-8. [https://doi.org/10.1016/s0140-6736\(05\)67101-2](https://doi.org/10.1016/s0140-6736(05)67101-2)
- [696] King CR. Adjuvant versus salvage radiotherapy for high-risk prostate cancer patients. *Semin Radiat Oncol.* 2013;23:215-21. <https://doi.org/10.1016/j.semradonc.2013.01.009>
- [697] Fossati N, Karnes RJ, Boorjian SA, Moschini M, Morlacco A, Bossi A, et al. Long-term impact of adjuvant versus early salvage radiation therapy in pt3n0 prostate cancer patients treated with radical prostatectomy: Results from a multi-institutional series. *Eur Urol.* 2016;71:886-93 <https://doi.org/10.1016/j.eururo.2016.07.028>
- [698] Pasquier D, Ballereau C. Adjuvant and salvage radiotherapy after prostatectomy for prostate cancer: A literature review. *Int J Radiat Oncol Biol Phys.* 2008;72:972-9. <https://doi.org/10.1016/j.ijrobp.2008.07.026>
- [699] Michalski JM, Lawton C, El Naqa I, Ritter M, O'Meara E, Seider MJ, et al. Development of RTOG consensus guidelines for the definition of the clinical target volume for postoperative conformal radiation therapy for prostate cancer. *Int J Radiat Oncol Biol Phys.* 2010;76:361-8. <https://doi.org/10.1016/j.ijrobp.2009.02.006>
- [700] Poortmans P, Bossi A, Vandeputte K, Bosset M, Miralbell R, Maingon P, et al. Guidelines for target volume definition in post-operative radiotherapy for prostate cancer, on behalf of the EORTC radiation oncology group. *Radiother Oncol.* 2007;84:121-7. <https://doi.org/10.1016/j.radonc.2007.07.017>
- [701] Sidhom MA, Kneebone AB, Lehman M, Wiltshire KL, Millar JL, Mukherjee RK, et al. Post-prostatectomy radiation therapy: Consensus guidelines of the Australian and New Zealand radiation

- oncology genito-urinary group. *Radiother Oncol.* 2008;88:10-9.  
<https://doi.org/10.1016/j.radonc.2008.05.006>
- [702] Wiltshire KL, Brock KK, Haider MA, Zwahlen D, Kong V, Chan E, et al. Anatomic boundaries of the clinical target volume (prostate bed) after radical prostatectomy. *Int J Radiat Oncol Biol Phys.* 2007;69:1090-9. <https://doi.org/10.1016/j.ijrobp.2007.04.068>
- [703] Brendler CB, Walsh PC. The role of radical prostatectomy in the treatment of prostate cancer. *CA Cancer J Clin.* 1992;42:212-22. <https://doi.org/10.3322/canjclin.42.4.212>
- [704] Van Velthoven RF, Ahlering TE, Peltier A, Skarecky DW, Clayman RV. Technique for laparoscopic running urethrovesical anastomosis: The single knot method. *Urology.* 2003;61:699-702.  
<https://www.ncbi.nlm.nih.gov/pubmed/12670546>
- [705] Golabek T, Jarecki P, Jaskulski J, Dudek P, Szopinski T, Chlosta P. Modified technique for laparoscopic running vesicourethral anastomosis. *Wideochir Inne Tech Maloinwazyjne.* 2014;9:357-61. <https://doi.org/10.5114/wiitm.2014.43129>
- [706] Vargas HA, Wassberg C, Akin O, Hricak H. MR imaging of treated prostate cancer. *Radiology.* 2012;262:26-42. <https://doi.org/10.1148/radiol.11101996>
- [707] Khoo V, Lim Joon D. Magnetic resonance imaging. In: Mundt A, Arnold R, editors. *In image guided radiation therapy: A clinical perspective.* Peoples Medical Publishing House 2010.
- [708] Nguyen DP, Giannarini G, Seiler R, Schiller R, Thoeny HC, Thalmann GN, et al. Local recurrence after retropubic radical prostatectomy for prostate cancer does not exclusively occur at the anastomotic site. *BJU Int.* 2013;112:E243-9. <https://doi.org/10.1111/j.1464-410X.2012.11506.x>
- [709] Sella T, Schwartz LH, Swindle PW, Onyebuchi CN, Scardino PT, Scher HI, et al. Suspected local recurrence after radical prostatectomy: Endorectal coil MR imaging. *Radiology.* 2004;231:379-85.  
<https://doi.org/10.1148/radiol.2312030011>
- [710] Bartkowiak D, Bottke D, Wiegel T. Radiotherapy in the management of prostate cancer after radical prostatectomy. *Future Oncol.* 2013;9:669-79. <https://doi.org/10.2217/fon.13.3>
- [711] Meeks JJ, Eastham JA. Radical prostatectomy: Positive surgical margins matter. *Urol Oncol.* 2013;31:974-9. <https://doi.org/10.1016/j.urolonc.2011.12.011>
- [712] Roach M, 3rd, Nam J, Gagliardi G, El Naqa I, Deasy JO, Marks LB. Radiation dose-volume effects and the penile bulb. *Int J Radiat Oncol Biol Phys.* 2010;76(3 Suppl):S130-4.  
<https://doi.org/10.1016/j.ijrobp.2009.04.094>
- [713] Perera M, Papa N, Christidis D, Wetherell D, Hofman MS, Murphy DG, et al. Sensitivity, specificity, and predictors of positive 68ga-prostate-specific membrane antigen positron emission tomography in advanced prostate cancer: A systematic review and meta-analysis. *Eur Urol.* 2016;70:926-37. <https://doi.org/10.1016/j.eururo.2016.06.021>
- [714] Budaus L, Leyh-Bannurah SR, Salomon G, Michl U, Heinzer H, Huland H, et al. Initial experience of (68)ga-PSMA PET/CT imaging in high-risk prostate cancer patients prior to radical prostatectomy. *Eur Urol.* 2016;69:393-6. <https://doi.org/10.1016/j.eururo.2015.06.010>
- [715] Eiber M, Weirich G, Holzapfel K, Souvatzoglou M, Haller B, Rauscher I, et al. Simultaneous 68ga-PSMA hbed-cc PET/MRI improves the localization of primary prostate cancer. *Eur Urol.* 2016;70:829-36. <https://doi.org/10.1016/j.eururo.2015.12.053>
- [716] Kupelian PA, Lee C, Langen KM, Zeidan OA, Mañon RR, Willoughby TR, et al. Evaluation of image-guidance strategies in the treatment of localized prostate cancer. *Int J Radiat Oncol Biol Phys.* 2008;70:1151-7. <https://doi.org/10.1016/j.ijrobp.2007.07.2371>
- [717] Engels B, Soete G, Verellen D, Storme G. Conformal arc radiotherapy for prostate cancer: Increased biochemical failure in patients with distended rectum on the planning computed tomogram despite image guidance by implanted markers. *Int J Radiat Oncol Biol Phys.* 2009;74:388-91. <https://doi.org/10.1016/j.ijrobp.2008.08.007>
- [718] Pierorazio PM, Ross AE, Schaeffer EM, Epstein JI, Han M, Walsh PC, et al. A contemporary analysis of outcomes of adenocarcinoma of the prostate with seminal vesicle invasion (pt3b) after radical prostatectomy. *J Urol.* 2011;185:1691-7. <https://doi.org/10.1016/j.juro.2010.12.059>
- [719] Humphrey PA. Seminal vesicle invasion by adenocarcinoma of the prostate. *J Urol.* 2015;194:1757-8. <https://doi.org/10.1016/j.juro.2015.09.062>

- [720] Mason MD, Parulekar WR, Sydes MR, Brundage M, Kirkbride P, Gospodarowicz M, et al. Final report of the intergroup randomized study of combined androgen-deprivation therapy plus radiotherapy versus androgen-deprivation therapy alone in locally advanced prostate cancer. *J Clin Oncol*. 2015;33:2143-50. <https://doi.org/10.1200/JCO.2014.57.7510>
- [721] Swanson GP, Goldman B, Tangen CM, Chin J, Messing E, Canby-Hagino E, et al. The prognostic impact of seminal vesicle involvement found at prostatectomy and the effects of adjuvant radiation: Data from southwest oncology group 8794. *J Urol*. 2008;180:2453-7;. <https://doi.org/10.1016/j.juro.2008.08.037>
- [722] Beard CJ, Kijewski P, Bussiere M, Gelman R, Gladstone D, Shaffer K, et al. Analysis of prostate and seminal vesicle motion: Implications for treatment planning. *Int J Radiat Oncol Biol Phys*. 1996;34:451-8. [https://doi.org/10.1016/0360-3016\(95\)02081-0](https://doi.org/10.1016/0360-3016(95)02081-0)
- [723] Roeske JC, Forman JD, Mesina CF, He T, Pelizzari CA, Fontenla E, et al. Evaluation of changes in the size and location of the prostate, seminal vesicles, bladder, and rectum during a course of external beam radiation therapy. *Int J Radiat Oncol Biol Phys*. 1995;33:1321-9. [https://doi.org/10.1016/0360-3016\(95\)00225-1](https://doi.org/10.1016/0360-3016(95)00225-1)
- [724] Qi X, Gao XS, Asaumi J, Zhang M, Li HZ, Ma MW, et al. Optimal contouring of seminal vesicle for definitive radiotherapy of localized prostate cancer: Comparison between EORTC prostate cancer radiotherapy guideline, rtog0815 protocol and actual anatomy. *Radiat Oncol*. 2014;9:288. <https://doi.org/10.1186/s13014-014-0288-1>
- [725] Hochberg Y, Benjamini Y. More powerful procedures for multiple significance testing. *Stat Med*. 1990;9:811-8. <https://doi.org/10.1002/sim.4780090710>
- [726] van Herk M. Errors and margins in radiotherapy. *Semin Radiat Oncol*. 2004;14:52-64. <https://doi.org/10.1053/j.semradonc.2003.10.003>
- [727] Fiorino C, Reni M, Bolognesi A, Cattaneo GM, Calandrino R. Intra- and inter-observer variability in contouring prostate and seminal vesicles: Implications for conformal treatment planning. *Radiother Oncol*. 1998;47:285-92. [https://doi.org/10.1016/s0167-8140\(98\)00021-8](https://doi.org/10.1016/s0167-8140(98)00021-8)
- [728] Debois M, Oyen R, Maes F, Verswijvel G, Gatti G, Bosmans H, et al. The contribution of magnetic resonance imaging to the three-dimensional treatment planning of localized prostate cancer. *Int J Radiat Oncol Biol Phys*. 1999;45:857-65. [https://doi.org/10.1016/s0360-3016\(99\)00288-6](https://doi.org/10.1016/s0360-3016(99)00288-6)
- [729] Stenmark MH, Vineberg K, Ten Haken RK, Hamstra DA, Feng M. Dosimetric implications of residual seminal vesicle motion in fiducial-guided intensity-modulated radiotherapy for prostate cancer. *Med Dosim*. 2012;37:240-4. <https://doi.org/10.1016/j.meddos.2011.09.002>
- [730] Gill S, Thomas J, Fox C, Kron T, Thompson A, Chander S, et al. Electronic portal imaging vs kilovoltage imaging in fiducial marker image-guided radiotherapy for prostate cancer: An analysis of set-up uncertainties. *Br J Radiol*. 2012;85:176-82. <https://doi.org/10.1259/bjr/13553326>
- [731] Poggi MM, Gant DA, Sewchand W, Warlick WB. Marker seed migration in prostate localization. *Int J Radiat Oncol Biol Phys*. 2003;56:1248-51. [https://doi.org/10.1016/s0360-3016\(03\)00328-6](https://doi.org/10.1016/s0360-3016(03)00328-6)
- [732] Coronel E, Cazacu IM, Sakuraba A, Luzuriaga Chavez AA, Uberoi A, Geng Y, et al. Eus-guided fiducial placement for GI malignancies: A systematic review and meta-analysis. *Gastrointest Endosc*. 2019;89:659-70 e18. <https://doi.org/10.1016/j.gie.2018.10.047>
- [733] van der Burgt M, Bergsma L, de Vries J, Pos FJ, Kalisvaart R, Heemsbergen W, et al. Impact of tumour invasion on seminal vesicles mobility in radiotherapy of prostate cancer. *Radiother Oncol*. 2015;117:283-7. <https://doi.org/10.1016/j.radonc.2015.09.031>
- [734] Gill S, Dang K, Fox C, Bressel M, Kron T, Bergen N, et al. Seminal vesicle intrafraction motion analysed with cinematic magnetic resonance imaging. *Radiat Oncol*. 2014;9:174. <https://doi.org/10.1186/1748-717X-9-174>
- [735] O'Neill AG, Jain S, Hounsell AR, O'Sullivan JM. Fiducial marker guided prostate radiotherapy: A review. *Br J Radiol*. 2016;89:20160296. <https://doi.org/10.1259/bjr.20160296>
- [736] Parker C. Magnetic resonance imaging in the radiation treatment planning of localized prostate cancer using intra-prostatic fiducial markers for computed tomography co-registration. *Radiotherapy and Oncology*. 2003;66:217-24. [https://doi.org/10.1016/s0167-8140\(02\)00407-3](https://doi.org/10.1016/s0167-8140(02)00407-3)

- [737] Rasch C, Barillot I, Remeijer P, Touw A, van Herk M, Lebesque JV. Definition of the prostate in CT and MRI: A multi-observer study. *Int J Radiat Oncol Biol Phys.* 1999;43:57-66. [https://doi.org/10.1016/s0360-3016\(98\)00351-4](https://doi.org/10.1016/s0360-3016(98)00351-4)
- [738] Chan MF, Cohen GN, Deasy JO. Qualitative evaluation of fiducial markers for radiotherapy imaging. *Technol Cancer Res Treat.* 2015;14:298-304. <https://doi.org/10.1177/1533034614547447>
- [739] Hu Y, Pan S, Zhao X, Guo W, He M, Guo Q. Value and clinical application of orthopedic metal artifact reduction algorithm in CT scans after orthopedic metal implantation. *Korean J Radiol.* 2017;18:526-35. <https://doi.org/10.3348/kjr.2017.18.3.526>
- [740] Baskan O, Erol C, Ozbek H, Paksoy Y. Effect of radiation dose reduction on image quality in adult head CT with noise-suppressing reconstruction system with a 256 slice mdct. *Journal of applied clinical medical physics.* 2015;16:5360-. <https://doi.org/10.1120/jacmp.v16i3.5360>
- [741] Brombal L, Arfelli F, Delogu P, Donato S, Mettivier G, Michielsen K, et al. Image quality comparison between a phase-contrast synchrotron radiation breast CT and a clinical breast CT: A phantom based study. *Sci Rep.* 2019;9:17778. <https://doi.org/10.1038/s41598-019-54131-z>
- [742] Osman SOS, Russell E, King RB, Crowther K, Jain S, McGrath C, et al. Fiducial markers visibility and artefacts in prostate cancer radiotherapy multi-modality imaging. *Radiat Oncol.* 2019;14:237. <https://doi.org/10.1186/s13014-019-1447-1>
- [743] Tanaka O, Komeda H, Hattori M, Hirose S, Yama E, Matsuo M. Comparison of MRI sequences in ideal fiducial maker-based radiotherapy for prostate cancer. *Rep Pract Oncol Radiother.* 2017;22:502-6. <https://doi.org/10.1016/j.rpor.2017.10.002>
- [744] Dinis Fernandes C, Dinh CV, Steggerda MJ, ter Beek LC, Smolic M, van Buuren LD, et al. Prostate fiducial marker detection with the use of multi-parametric magnetic resonance imaging. *Physics and Imaging in Radiation Oncology.* 2017;1:14-20. <https://doi.org/10.1016/j.phro.2017.02.001>
- [745] Hunt A, Hansen VN, Oelfke U, Nill S, Hafeez S. Adaptive radiotherapy enabled by MRI guidance. *Clin Oncol (R Coll Radiol).* 2018;30:711-9. <https://doi.org/10.1016/j.clon.2018.08.001>
- [746] Murray J, Tree AC. Prostate cancer – advantages and disadvantages of MR-guided rt. *Clinical and Translational Radiation Oncology.* 2019;18:68-73. <https://doi.org/10.1016/j.ctro.2019.03.006>
- [747] Chung HT, Xia P, Chan LW, Park-Somers E, Roach M, 3rd. Does image-guided radiotherapy improve toxicity profile in whole pelvic-treated high-risk prostate cancer? Comparison between ig-IMRT and IMRT. *Int J Radiat Oncol Biol Phys.* 2009;73:53-60. <https://doi.org/10.1016/j.ijrobp.2008.03.015>
- [748] Bertelsen AS, Schytte T, Moller PK, Mahmood F, Riis HL, Gottlieb KL, et al. First clinical experiences with a high field 1.5 t MR linac. *Acta Oncol.* 2019;58:1352-7. <https://doi.org/10.1080/0284186X.2019.1627417>
- [749] Kupelian PA, Willoughby TR, Meeks SL, Forbes A, Wagner T, Maach M, et al. Intraprostatic fiducials for localization of the prostate gland: Monitoring intermarker distances during radiation therapy to test for marker stability. *Int J Radiat Oncol Biol Phys.* 2005;62:1291-6. <https://doi.org/10.1016/j.ijrobp.2005.01.005>
- [750] Marks LB, Carroll PR, Dugan TC, Anscher MS. The response of the urinary bladder, urethra, and ureter to radiation and chemotherapy. *Int J Radiat Oncol Biol Phys.* 1995;31:1257-80. [https://doi.org/10.1016/0360-3016\(94\)00431-j](https://doi.org/10.1016/0360-3016(94)00431-j)
- [751] Turner SL, Swindell R, Bowl N, Marrs J, Brookes B, Read G, et al. Bladder movement during radiation therapy for bladder cancer: Implications for treatment planning. *Int J Radiat Oncol Biol Phys.* 1997;39:355-60. [https://doi.org/10.1016/s0360-3016\(97\)00070-9](https://doi.org/10.1016/s0360-3016(97)00070-9)
- [752] Song Y, Yan M, Mueller B, Mychalczak B. Investigation of fiducial marker migration during the treatment of bladder cancer with image-guided radiation therapy. *Clin Oncol.* 2018;3:1481. <http://www.clinicsinoncology.com/full-text/cio-v3-id1481.php>
- [753] Kliton J, Polgár C, Tenke P, Kovács G, Major T, Stelczer G, et al. [image-guided radiotherapy for muscle invasive bladder cancer with intravesical lipiodol injection. A new option for bladder sparing treatment]. *Orv Hetil.* 2017;158:2041-7. <https://doi.org/10.1556/650.2017.30904>

- [754] Pos F, Bex A, Dees-Ribbers HM, Betgen A, van Herk M, Remeijer P. Lipiodol injection for target volume delineation and image guidance during radiotherapy for bladder cancer. *Radiother Oncol*. 2009;93:364-7. <https://doi.org/10.1016/j.radonc.2009.09.003>
- [755] Bhat YM, Banerjee S, Barth BA, Chauhan SS, Gottlieb KT, Konda V, et al. Tissue adhesives: Cyanoacrylate glue and fibrin sealant. *Gastrointest Endosc*. 2013;78:209-15. <https://doi.org/10.1016/j.gie.2013.04.166>
- [756] Chandran S, Vaughan R, Jacob A, Hamilton C, Joon DL, Lim K, et al. A novel endoscopic marker for radiological localization and image-guided radiotherapy in esophageal and gastric cancers (with video). *Gastrointest Endosc*. 2016;83:309-17. <https://doi.org/10.1016/j.gie.2015.06.042>
- [757] Chai X, van Herk M, van de Kamer JB, Remeijer P, Bex A, Betgen A, et al. Behavior of lipiodol markers during image guided radiotherapy of bladder cancer. *Int J Radiat Oncol Biol Phys*. 2010;77:309-14. <https://doi.org/10.1016/j.ijrobp.2009.08.019>
- [758] Freilich JM, Spiess PE, Biagioli MC, Fernandez DC, Shi EJ, Hunt DC, et al. Lipiodol as a fiducial marker for image-guided radiation therapy for bladder cancer. *Int Braz J Urol*. 2014;40:190-7. <https://doi.org/10.1590/S1677-5538.IBJU.2014.02.08>
- [759] Meijer GJ, van der Toorn PP, Bal M, Schuring D, Weterings J, de Wildt M. High precision bladder cancer irradiation by integrating a library planning procedure of 6 prospectively generated SIB IMRT plans with image guidance using lipiodol markers. *Radiother Oncol*. 2012;105:174-9. <https://doi.org/10.1016/j.radonc.2012.08.011>
- [760] Sondergaard J, Olsen KO, Muren LP, Elstrom UV, Grau C, Hoyer M. A study of image-guided radiotherapy of bladder cancer based on lipiodol injection in the bladder wall. *Acta Oncol*. 2010;49:1109-15. <https://doi.org/10.3109/02841861003789491>
- [761] Baumgarten AS, Emtage JB, Wilder RB, Biagioli MC, Gupta S, Spiess PE. Intravesical lipiodol injection technique for image-guided radiation therapy for bladder cancer. *Urology*. 2014;83:946-50. <https://doi.org/10.1016/j.urology.2013.09.058>
- [762] Ayyildiz SN, Ayyildiz A. Cyanoacrylic tissue glues: Biochemical properties and their usage in urology. *Turk J Urol*. 2017;43:14-24. <https://doi.org/10.5152/tud.2017.09465>
- [763] Lim JH, You D, Jeong IG, Park HK, Ahn H, Kim C-S. Cystoscopic injection of n-butyl-2-cyanoacrylate followed by fibrin glue for the treatment of persistent or massive vesicourethral anastomotic urine leak after radical prostatectomy. *International Journal of Urology*. 2013;20:980-5. <https://doi.org/10.1111/iju.12094>
- [764] Kliton J, Polgar C, Tenke P, Kovacs G, Major T, Stelczer G, et al. [image-guided radiotherapy for muscle invasive bladder cancer with intravesical lipiodol injection. A new option for bladder sparing treatment]. *Orv Hetil*. 2017;158:2041-7. <https://doi.org/10.1556/650.2017.30904>
- [765] Garcia MM, Gottschalk AR, Brajtbord J, Konety BR, Meng MV, Roach M, 3rd, et al. Endoscopic gold fiducial marker placement into the bladder wall to optimize radiotherapy targeting for bladder-preserving management of muscle-invasive bladder cancer: Feasibility and initial outcomes. *PLoS One*. 2014;9:e89754-e. <https://doi.org/10.1371/journal.pone.0089754>
- [766] Al-Hillawi L, Wong T, Tritto G, Berry PA. Pitfalls in histoacryl glue injection therapy for oesophageal, gastric and ectopic varices: A review. *World J Gastrointest Surg*. 2016;8:729-34. <https://doi.org/10.4240/wjgs.v8.i11.729>
- [767] Van Bruwaene S, Namdarian B, Challacombe B, Eddy B, Billiet I. Introducing new technology safely into urological practice. *World J Urol*. 2018;36:543-8. <https://doi.org/10.1007/s00345-018-2173-2>
- [768] Shakir SI, Udrescu C, Enachescu C, Rouviere O, Arion S, Caraivan I, et al. Transrectal implantation and stability of gold markers in prostate bed for salvage radiotherapy of macroscopic recurrences. *Phys Med*. 2016;32:1422-7. <https://doi.org/10.1016/j.ejmp.2016.10.009>
- [769] Barrett JF, Keat N. Artifacts in CT: Recognition and avoidance. *Radiographics*. 2004;24:1679-91. <https://doi.org/10.1148/rg.246045065>
- [770] Gjestebj L, De Man B, Jin Y, Paganetti H, Verburg J, Giantsoudi D, et al. Metal artifact reduction in CT: Where are we after four decades? *IEEE Access*. 2016;4:5826-49. <https://doi.org/10.1109/access.2016.2608621>

- [771] Committee AT, Bhat YM, Banerjee S, Barth BA, Chauhan SS, Gottlieb KT, et al. Tissue adhesives: Cyanoacrylate glue and fibrin sealant. *Gastrointest Endosc.* 2013;78:209-15. <https://doi.org/10.1016/j.gie.2013.04.166>
- [772] Weil D, Cervoni JP, Fares N, Rudler M, Bureau C, Plessier A, et al. Management of gastric varices: A french national survey. *Eur J Gastroenterol Hepatol.* 2016;28:576-81. <https://doi.org/10.1097/MEG.0000000000000560>
- [773] Loh DC, Wilson RB. Endoscopic management of refractory gastrointestinal non-variceal bleeding using histoacryl (n-butyl-2-cyanoacrylate) glue. *Gastroenterol Rep (Oxf).* 2016;4:232-6. <https://doi.org/10.1093/gastro/gov019>
- [774] Cheng LF, Wang ZQ, Li CZ, Lin W, Yeo AE, Jin B. Low incidence of complications from endoscopic gastric variceal obturation with butyl cyanoacrylate. *Clin Gastroenterol Hepatol.* 2010;8:760-6. <https://doi.org/10.1016/j.cgh.2010.05.019>
- [775] Duncan C, Joon DL, Lawrentschuk N, Jenkins T, Schneider M, Khoo V, et al. Fiducial markers: Can the urologist do better? *World J Urol.* 2019;37:1281-7. <https://doi.org/10.1007/s00345-018-2515-0>
- [776] Lim HK, Ha HI, Park SY, Lee K. Comparison of the diagnostic performance of CT hounsfield unit histogram analysis and dual-energy x-ray absorptiometry in predicting osteoporosis of the femur. *Eur Radiol.* 2019;29:1831-40. <https://doi.org/10.1007/s00330-018-5728-0>
- [777] Paul J, Yang C, Wu H, Tai A, Dalah E, Zheng C, et al. Early assessment of treatment responses during radiation therapy for lung cancer using quantitative analysis of daily computed tomography. *Int J Radiat Oncol Biol Phys.* 2017;98:463-72. <https://doi.org/10.1016/j.ijrobp.2017.02.032>
- [778] Zhang LX, Xiang JJ, Wei PY, Ding JW, Luo DC, Peng ZY, et al. Diagnostic value of computed tomography (CT) histogram analysis in thyroid benign solitary coarse calcification nodules. *J Zhejiang Univ Sci B.* 2018;19:211-7. <https://doi.org/10.1631/jzus.B1700119>
- [779] Gonzalez RC, Woods RE. In: Some basic intensity transformation functions. *Digital image processing.* 4th ed. New York, NY: Pearson; 2018. p. 139-42.
- [780] Zhou Y, Shi C, Lai B, Jimenez G. Contrast enhancement of medical images using a new version of the world cup optimization algorithm. *Quant Imaging Med Surg.* 2019;9:1528-47. <https://doi.org/10.21037/qims.2019.08.19>
- [781] Muren LP, Redpath AT, McLaren D, Rorvik J, Halvorsen OJ, Hostmark J, et al. A concomitant tumour boost in bladder irradiation: Patient suitability and the potential of intensity-modulated radiotherapy. *Radiother Oncol.* 2006;80:98-105. <https://doi.org/10.1016/j.radonc.2006.06.015>
- [782] Pos F, Remeijer P. Adaptive management of bladder cancer radiotherapy. *Semin Radiat Oncol.* 2010;20:116-20. <https://doi.org/10.1016/j.semradonc.2009.11.005>
- [783] Muren LP, Smaaland R, Dahl O. Organ motion, set-up variation and treatment margins in radical radiotherapy of urinary bladder cancer. *Radiother Oncol.* 2003;69:291-304. [https://doi.org/10.1016/s0167-8140\(03\)00246-9](https://doi.org/10.1016/s0167-8140(03)00246-9)
- [784] Kong V, Kwan M, Chen S, Chung P, Craig T, Rosewall T. Quantification of interobserver variability in image registration using cone beam CT for partial bladder radiotherapy-a comparison between lipiodol and bladder wall surface. *Br J Radiol.* 2019;92:20180413. <https://doi.org/10.1259/bjr.20180413>
- [785] Nolan CP, Forde EJ. A review of the use of fiducial markers for image-guided bladder radiotherapy. *Acta Oncol.* 2016;55:533-8. <https://doi.org/10.3109/0284186X.2015.1110250>
- [786] Machiels M, Voncken FEM, Jin P, van Dieren JM, Bartels-Rutten A, Alderliesten T, et al. A novel liquid fiducial marker in esophageal cancer image guided radiation therapy: Technical feasibility and visibility on imaging. *Pract Radiat Oncol.* 2019;9:e506-15. <https://doi.org/10.1016/j.prro.2019.06.018>
- [787] Ayyildiz SN, Ayyildiz A. Cyanoacrylic tissue glues: Biochemical properties and their usage in urology. *Turk J Urol.* 2017;43:14-24. <https://doi.org/10.5152/tud.2017.09465>
- [788] Mangar S, Thompson A, Miles E, Huddart R, Horwich A, Khoo V. A feasibility study of using gold seeds as fiducial markers for bladder localization during radical radiotherapy. *Br J Radiol.* 2007;80:279-83. <https://doi.org/10.1259/bjr/54321311>

- [789] de Ridder M, Gerbrandy LC, de Reijke TM, Hinnen KA, Hulshof M. Bioxmark® liquid fiducial markers for image-guided radiotherapy in muscle invasive bladder cancer: A safety and performance trial. *Br J Radiol.* 2020;93:20200241. <https://doi.org/10.1259/bjr.20200241>
- [790] De Santis M, Alborino S, Tartoni PL, Torricelli P, Casolo A, Romagnoli R. Effects of lipiodol retention on MRI signal intensity from hepatocellular carcinoma and surrounding liver treated by chemoembolization. *Eur Radiol.* 1997;7:10-6. <https://doi.org/10.1007/s003300050099>
- [791] Moris L, Cumberbatch MG, Van den Broeck T, Gandaglia G, Fossati N, Kelly B, et al. Benefits and risks of primary treatments for high-risk localized and locally advanced prostate cancer: An international multidisciplinary systematic review. *Eur Urol.* 2020;77:614-27. <https://doi.org/10.1016/j.eururo.2020.01.033>
- [792] Warde PR, Catton CN, Huang RYC. Combination of hormone therapy and radiotherapy in treatment of locally advanced prostate cancer—recent developments and update. *Oncology & Hematology Review (US).* 2014;10:48-53. <https://doi.org/10.17925/ohr.2014.10.1.48>
- [793] Abdollah F, Karnes RJ, Suardi N, Cozzarini C, Gandaglia G, Fossati N, et al. Impact of adjuvant radiotherapy on survival of patients with node-positive prostate cancer. *J Clin Oncol.* 2014;32:3939-47. <https://doi.org/10.1200/jco.2013.54.7893>
- [794] Rusthoven CG, Carlson JA, Waxweiler TV, Raben D, Dewitt PE, Crawford ED, et al. The impact of definitive local therapy for lymph node-positive prostate cancer: A population-based study. *Int J Radiat Oncol Biol Phys.* 2014;88:1064-73. <https://doi.org/10.1016/j.ijrobp.2014.01.008>
- [795] Shinde A, Li R, Glaser S, Amini A. Node-positive nonmetastatic prostate cancer: Time to reconsider prognostic staging? *Eur Urol.* 2019;75:355-7. <https://doi.org/10.1016/j.eururo.2018.09.017>
- [796] Abdollah F, Dalela D, Sood A, Keeley J, Alanee S, Briganti A, et al. Impact of adjuvant radiotherapy in node-positive prostate cancer patients: The importance of patient selection. *Eur Urol.* 2018;74:253-6. <https://doi.org/10.1016/j.eururo.2018.04.017>
- [797] Scott SL, Gumerlock PH, Beckett L, Li Y, Goldberg Z. Survival and cell cycle kinetics of human prostate cancer cell lines after single- and multifraction exposures to ionizing radiation. *Int J Radiat Oncol Biol Phys.* 2004;59:219-27. <https://doi.org/10.1016/j.ijrobp.2004.01.027>
- [798] Zelefsky MJ, Pei X, Chou JF, Schechter M, Kollmeier M, Cox B, et al. Dose escalation for prostate cancer radiotherapy: Predictors of long-term biochemical tumor control and distant metastases-free survival outcomes. *Eur Urol.* 2011;60:1133-9. <https://doi.org/10.1016/j.eururo.2011.08.029>
- [799] Cozzarini C, Montorsi F, Fiorino C, Alongi F, Bolognesi A, Da Pozzo LF, et al. Need for high radiation dose (>or=70 Gy) in early postoperative irradiation after radical prostatectomy: A single-institution analysis of 334 high-risk, node-negative patients. *Int J Radiat Oncol Biol Phys.* 2009;75:966-74. <https://doi.org/10.1016/j.ijrobp.2008.12.059>
- [800] Dinh CV, Steenbergen P, Ghobadi G, Heijmink SW, Pos FJ, Haustermans K, et al. Magnetic resonance imaging for prostate cancer radiotherapy. *Phys Med.* 2016;32:446-51. <https://doi.org/10.1016/j.ejmp.2016.01.484>
- [801] Zhang F, Liu CL, Chen Q, Shao SC, Chen SQ. Accuracy of multiparametric magnetic resonance imaging for detecting extracapsular extension in prostate cancer: A systematic review and meta-analysis. *Br J Radiol.* 2019;92:20190480. <https://doi.org/10.1259/bjr.20190480>
- [802] Pucar D, Sella T, Schoder H. The role of imaging in the detection of prostate cancer local recurrence after radiation therapy and surgery. *Curr Opin Urol.* 2008;18:87-97. <https://doi.org/10.1097/MOU.0b013e3282f13ac3>
- [803] Evans JD, Jethwa KR, Ost P, Williams S, Kwon ED, Lowe VJ, et al. Prostate cancer-specific PET radiotracers: A review on the clinical utility in recurrent disease. *Pract Radiat Oncol.* 2018;8:28-39. <https://doi.org/10.1016/j.prro.2017.07.011>
- [804] Schwenck J, Olthof SC, PfannenberG C, Reischl G, Wegener D, Marzec J, et al. Intention-to-treat analysis of (68)Ga-PSMA and (11)C-choline PET/CT versus CT for prostate cancer recurrence after surgery. *J Nucl Med.* 2019;60:1359-65. <https://doi.org/10.2967/jnumed.118.224543>

- [805] Regula N, Kostaras V, Johansson S, Trampal C, Lindstrom E, Lubberink M, et al. Comparison of (68)ga-PSMA-11 PET/CT with (11)c-acetate PET/CT in re-staging of prostate cancer relapse. *Sci Rep*. 2020;10:4993. <https://doi.org/10.1038/s41598-020-61910-6>
- [806] Gaur S, Turkbey B. Prostate MR imaging for posttreatment evaluation and recurrence. *Radiol Clin North Am*. 2018;56:263-75. <https://doi.org/10.1016/j.rcl.2017.10.008>
- [807] Bhargava P, Ravizzini G, Chapin BF, Kundra V. Imaging biochemical recurrence after prostatectomy: Where are we headed? *American Journal of Roentgenology*. 2020;214:1248-58. <https://doi.org/10.2214/ajr.19.21905>
- [808] Sandgren K, Westerlinck P, Jonsson JH, Blomqvist L, Thellenberg Karlsson C, Nyholm T, et al. Imaging for the detection of locoregional recurrences in biochemical progression after radical prostatectomy—a systematic review. *European Urology Focus*. 2019;5:550-60. <https://doi.org/10.1016/j.euf.2017.11.001>
- [809] Evangelista L, Zattoni F, Cassarino G, Artioli P, Cecchin D, dal Moro F, et al. PET/MRI in prostate cancer: A systematic review and meta-analysis. *Eur J Nucl Med Mol Imaging*. 2020: Online ahead of print. <https://doi.org/10.1007/s00259-020-05025-0>
- [810] Barakat A, Yacoub B, Homsy ME, Saad Aldine A, El Hajj A, Haidar MB. Role of early PET/CT imaging with 68ga-PSMA in staging and restaging of prostate cancer. *Scientific Reports*. 2020;10:2705. <https://doi.org/10.1038/s41598-020-59296-6>
- [811] De Roover R, Crijns W, Poels K, Peeters R, Draulans C, Haustermans K, et al. Characterization of a novel liquid fiducial marker for multimodal image guidance in stereotactic body radiotherapy of prostate cancer. *Med Phys*. 2018;45:2205-17. <https://doi.org/10.1002/mp.12860>
- [812] Brown KH, Ghita M, Schettino G, Prise KM, Butterworth KT. Evaluation of a novel liquid fiducial marker, bioxmark®, for small animal image-guided radiotherapy applications. *Cancers (Basel)*. 2020;12:1276. <https://doi.org/10.3390/cancers12051276>
- [813] Lim Joon D, Lim A, Schneider M, Hiew CY, Lawrentschuk N, Sengupta S, et al. Prostate cancer post-prostatectomy radiotherapy: CT vs MRI for vesico-urethral anastomosis target delineation. *Radiother Oncol*. 2017;125:113-7. <https://doi.org/10.1016/j.radonc.2017.08.031>
- [814] Gunnlaugsson A, Persson E, Gustafsson C, Kjellén E, Ambolt P, Engelholm S, et al. Target definition in radiotherapy of prostate cancer using magnetic resonance imaging only workflow. *Physics and Imaging in Radiation Oncology*. 2019;9:89-91. <https://doi.org/10.1016/j.phro.2019.03.004>
- [815] Tomida M, Okudaira K, Kamomae T, Oguchi H, Miyake Y, Yoneda K, et al. Relationship between prostate volume changes and treatment duration of neoadjuvant androgen deprivation during intensity-modulated radiation therapy for Japanese patients with prostate cancer. *Nagoya Journal of Medical Science*. 2016;78:313-21. <https://www.ncbi.nlm.nih.gov/pmc/articles/PMC4995277>
- [816] McPartlin A, Hosni A, McWilliam A, Van Herk M, Kershaw L, Choudhury A. Changes in prostate volume during neo-adjuvant hormone therapy and definitive radiotherapy. *Journal of Clinical Oncology*. 2016;34:e628. [https://doi.org/10.1200/jco.2016.34.2\\_suppl.e628](https://doi.org/10.1200/jco.2016.34.2_suppl.e628)
- [817] Moseley D, White E, Wiltshire K, Haycocks T, Keller H, Siewerdsen J, et al. We-c-j-6c-06: Assessing prostate volume changes during conformal radiotherapy using implanted fiducial markers. *Medical Physics*. 2005;32:2125. <https://doi.org/10.1118/1.1998511>
- [818] Gunnlaugsson A, Kjellén E, Hagberg O, Thellenberg-Karlsson C, Widmark A, Nilsson P. Change in prostate volume during extreme hypo-fractionation analysed with MRI. *Radiat Oncol*. 2014;9:22. <https://doi.org/10.1186/1748-717X-9-22>
- [819] Corradini S, Alongi F, Andratschke N, Belka C, Boldrini L, Cellini F, et al. MR-guidance in clinical reality: Current treatment challenges and future perspectives. *Radiat Oncol*. 2019;14:92. <https://doi.org/10.1186/s13014-019-1308-y>
- [820] Ingrosso G, Miceli R, Ponti E, Lancia A, di Cristino D, de Pasquale F, et al. Interfraction prostate displacement during image-guided radiotherapy using intraprostatic fiducial markers and a cone-beam computed tomography system: A volumetric off-line analysis in relation to the variations of rectal and bladder volumes. *J Cancer Res Ther*. 2019;15:69-75. [https://doi.org/10.4103/jcrt.JCRT\\_463\\_17](https://doi.org/10.4103/jcrt.JCRT_463_17)

- [821] Tong X, Chen X, Li J, Xu Q, Lin MH, Chen L, et al. Intrafractional prostate motion during external beam radiotherapy monitored by a real-time target localization system. *J Appl Clin Med Phys*. 2015;16:5013. <https://doi.org/10.1120/jacmp.v16i2.5013>
- [822] Gorovets D, Burleson S, Jacobs L, Ravindranath B, Tierney K, Kollmeier M, et al. Prostate sbrt with intrafraction motion management using a novel linear accelerator-based mv-kV imaging method. *Pract Radiat Oncol*. 2020;10:e388-96. <https://doi.org/10.1016/j.prr.2020.04.013>
- [823] de Muinck Keizer DM, Kerkmeijer LGW, Willigenburg T, van Lier A, Hartogh MDD, van der Voort van Zyp JRN, et al. Prostate intrafraction motion during the preparation and delivery of MR-guided radiotherapy sessions on a 1.5t MR-linac. *Radiother Oncol*. 2020;151:88-94. <https://doi.org/10.1016/j.radonc.2020.06.044>
- [824] Sheng Y, Li T, Lee WR, Yin FF, Wu QJ. Exploring the margin recipe for online adaptive radiation therapy for intermediate-risk prostate cancer: An intrafractional seminal vesicles motion analysis. *Int J Radiat Oncol Biol Phys*. 2017;98:473-80. <https://doi.org/10.1016/j.ijrobp.2017.02.089>
- [825] Tatar SU, Bruynzeel AME, Lagerwaard FJ, Slotman BJ, Bohoudi O, Palacios MA. Clinical implementation of magnetic resonance imaging guided adaptive radiotherapy for localized prostate cancer. *Physics and Imaging in Radiation Oncology*. 2019;9:69-76. <https://doi.org/10.1016/j.phro.2019.02.002>
- [826] Kurz C, Buizza G, Landry G, Kamp F, Rabe M, Paganelli C, et al. Medical physics challenges in clinical MR-guided radiotherapy. *Radiat Oncol*. 2020;15:93. <https://doi.org/10.1186/s13014-020-01524-4>
- [827] Hehakaya C, Van der Voort van Zyp JR, Lagendijk JJW, Grobbee DE, Verkooijen HM, Moors EHM. Problems and promises of introducing the magnetic resonance imaging linear accelerator into routine care: The case of prostate cancer. *Front Oncol*. 2020;10:1741. <https://doi.org/10.3389/fonc.2020.01741>

## APPENDICES

---

### APPENDIX A: DISSEMINATION OF FINDINGS

2013 June: Olivia Newton-John Cancer Centre Grand Round Invited Speaker: Prostate Intensity Modulated Radiotherapy. Melbourne, Australia.

2014: Cancer Council Victoria – Prostate Cancer Expert Working Group: Invited Discussant. Melbourne, Australia.

2014 June: RANZCR Qld Scientific Meeting Invited Speaker: Pelvic Contouring for Precision Radiotherapy

2015 June: Tolmar- Multi-disciplinary integration and prostate cancer survivorship. Prostate Cancer Symposium Invited Speaker: Prostate Cancer: Precision Radiotherapy. Gold Coast, Australia.

2015 October: Société Internationale d'Urologie (SIU) Meeting: Abstract and Poster Presentation: Novel Fiducials for Imaged Guided Bladder Radiotherapy: A Porcine Study. Melbourne, Australia.

2016 April: Ipsen Astellas Meeting - Contemporary challenges in the management of metastatic and castrate-resistant prostate cancer: Invited Panel Discussant. Melbourne, Australia.

2016 August: Radiation Oncology Registrar Teaching Program: Prostate MRI imaging. Melbourne, Australia.

2017 August: Heidelberg Prostate Cancer (Patient) Interest Group Invited Speaker:

Radiotherapy Advances in Prostate Cancer. Melbourne, Australia

2017 November: Austin Urology Grand Round Invited Speaker: Prostate Cancer

Radiotherapy Update. Melbourne, Australia.

2018 March: Radiation Oncology Teaching Program Invited Speaker: Prostate Cancer

Radiotherapy. Melbourne, Australia.

2018 February: USANZ GU Oncology Masterclass- Advances in Prostate and Renal Cancer

Invited Panel Member. Melbourne Australia

2019 October: Global Prostate Meeting (PROSCA): Abstract and Poster Presentation -

Characterisation of a Novel Glue Fiducial in a Porcine and Phantom Model. Paris, France.

## APPENDIX B: PAPER INCLUDED IN CHAPTER 3 (AS PUBLISHED)

Radiotherapy and Oncology 125 (2017) 113–117



Contents lists available at ScienceDirect

Radiotherapy and Oncology

journal homepage: www.thegreenjournal.com



Prostate cancer radiotherapy

## Prostate cancer post-prostatectomy radiotherapy: CT vs MRI for vesico-urethral anastomosis target delineation



Daryl Lim Joon<sup>a,\*</sup>, Adeline Lim<sup>a</sup>, Michal Schneider<sup>b</sup>, Chee-Yan Hiew<sup>a</sup>, Nathan Lawrentschuk<sup>a</sup>, Shomik Sengupta<sup>a</sup>, Farshad Foroudi<sup>a</sup>, Trish Jenkins<sup>a</sup>, David Angus<sup>a</sup>, Morikatsu Wada<sup>a</sup>, Michael Chao<sup>a</sup>, Vincent Khoo<sup>c</sup>

<sup>a</sup>Olivia Newton John Cancer Centre, Melbourne; <sup>b</sup>Monash University Melbourne, Australia; <sup>c</sup>Royal Marsden NHS Foundation Trust, London, United Kingdom

## ARTICLE INFO

## Article history:

Received 22 May 2017

Received in revised form 15 August 2017

Accepted 16 August 2017

Available online 19 September 2017

## Keywords:

Prostate cancer

Radiotherapy

Prostatectomy

Vesico-urethral anastomosis

Clinical target volume

Computer tomography

Magnetic resonance imaging

## ABSTRACT

**Background:** Vesico-urethral anastomosis (VUA) is critical to the clinical target volume (CTV) in post-prostatectomy radiotherapy (PPRT), as it is the commonest site of recurrence. Typically, this is performed on a CT alone but guidelines recommend MRI.

**Objective:** To evaluate the VUA spatial differences between CT (ctVUA) and MRI (mrVUA) and analyse its impact on the CT defined CTV (ctCTV) as recommended by published guidelines.

**Materials and methods:** We identified 34 patients with a co-registered simulation CT and T2 weighted MRI. The VUA was located on CT and MRI whilst blinded to the opposing scan. The differences were analysed using Wilcoxon's Signed Rank Test. The mrVUA coverage was investigated using three ctCTV margins of 5 mm, 8 mm and 12 mm.

**Results:** Median age was 63 years with 59% having pT3a disease and median Gleason score of 7. The mrVUA was coincident with the ctVUA in 12% and inferior in 88%. Median difference was 5 mm (0–10 mm) ( $P < 0.0001$ ). Only a ctCTV margin of 12 mm would have encompassed all mrVUAs. A ctCTV margin of 8 mm and 5 mm resulted in 12% and 38% cases where the VUA was excluded from the ctCTV.

**Conclusions:** MRI is important for the accurate delineation of VUA for PPRT.

© 2017 Elsevier B.V. All rights reserved. Radiotherapy and Oncology 125 (2017) 113–117

Prostate cancer post-prostatectomy radiotherapy (PPRT) is used as adjuvant treatment for men at high risk of relapse or for the salvage of men who have suffered biochemical prostate specific antigen (PSA) relapse or clinical recurrence [1–6]. However, up to one third of adjuvant patients and two thirds of salvage cases will further relapse following PPRT [7].

Initial investigations to define the site of local recurrence following PSA relapse post prostatectomy used trans-rectal ultrasound guided biopsy alone. They showed that the perianastomotic site or VUA was the most common site of recurrence with the incidence ranging from 56 to 66% [8–10].

It is therefore essential that the VUA be accurately identified prior to PPRT to ensure adequate dosimetric coverage. Precision targeted radiotherapy with intensity modulated radiotherapy (IMRT) and image guided radiotherapy (IGRT) in prostate cancer has been shown to be important for both disease outcome and minimization of toxicity [11–13]. International guidelines and

protocols stress the importance of the VUA [14–17], suggesting that it is critical to the definition of the radiotherapy clinical target volume (CTV) i.e. the volume at high risk of containing residual microscopic disease.

The guidelines recommend that axial CT slices should be used when identifying the VUA [14–17]. They acknowledge that the VUA may be more accurately identified on MRI, as the gold standard reference, [17] because of the superior soft tissue contrast. However, they concede that the utility of MRI has not been fully evaluated [15,17].

The guidelines also recommend an additional caudal CTV margin from the VUA to allow for microscopic extension [14–17]. The suggested geometric margins range from 5 mm to 12 mm. However, unless the VUA is accurately delineated this margin for microscopic disease may be compromised and consequently under-dosed.

The purpose of the study was to evaluate the utility of MRI in the accurate identification of the VUA and the impact on the CTV for PPRT relative to the recommended guidelines. Therefore, the aims of this study are

\* Corresponding author at: Olivia Newton John Cancer Centre, 145 Studley Road, Heidelberg, Victoria 3084, Australia.

E-mail address: daryl.limjoon@austin.org.au (D. Lim Joon).

<http://dx.doi.org/10.1016/j.radonc.2017.08.031>

0167-8140/© 2017 Elsevier B.V. All rights reserved.

- 1) To analyse the spatial differences between MRI and CT in the localization of the VUA.
- 2) To assess the mrVUA relative to the CT based CTV margins (ctCTV) recommended by the published guidelines.

**Materials and methods**

The investigation was approved as a retrospective analysis by the institutional ethics committee. The study cohort consisted of 34 eligible consecutive prostate cancer patients previously treated with post-prostatectomy IMRT/IGRT between December 2011 and October 2013 with uniform CT slice thickness.

*Simulation and imaging*

Patients were positioned supine with an individualized foam Alpha cradle placed on an indexed pelvic board with foot stocks. CT simulation (non-contrast) was performed on a General Electric Radiation Therapy Lightspeed Widebore® helical scanner (General Electric Healthcare, Buckinghamshire, United Kingdom) with a resolution of 512 × 512, pitch 0.75, no gap and a slice thickness of 1.25 mm. The CT origin (Z-axis 0) was centred and tattooed 5 cm superior to base of penis.

The planning MRI was performed on a 1.5 T Siemens Magneto Avanto Syngo MR B17® (Siemens Healthcare, Erlangen, Germany). The MRI sequence utilized for this study was a high-resolution 3D T2 weighted scan with a voxel size of 1 mm. This was reformatted in the axial plane and imported into CMS Focal Sim® (Elekta, Stockholm, Sweden) and co-registered with the simulation CT.

*VUA identification and analysis*

Following a prostatectomy, the bladder is anastomosed to the proximal membranous urethra [18–20]. The membranous urethra is normally closed by the external sphincter, both being contained within the urogenital diaphragm. Subsequently it does not contain urine. Therefore, as the guidelines recommend, the VUA was defined on the axial slice just inferior to the last slice where urine is visible, as the urine defines the bladder on both CT and MRI [14,16,17]. This was confirmed on multi-planar views. Furthermore, on T2 weighted MRI the VUA can be more precisely defined due to ability to visualize the low signal elliptic cylindrical wall of the VUA and proximal membranous urethra in contrast to the very bright signal of urine in the bladder [21].

The CT and MRI were co-registered initially using the entire pelvic bones but then refined to the region of interest that encompasses the urogenital diaphragm and VUA i.e. the bones of the ischiopubic ramus and coccyx.

The department regards the gold standard for delineation of the CTV to be the MRI for the soft tissue components not well visualized on CT i.e. the VUA, membranous urethra & urogenital diaphragm (5–10 mm) and posteriorly the meso-rectal fascia. The CT is used to define the posterior pubis, obturator internus and bladder components of the CTV as these are well seen on CT.

Following co-registration of the CT and MRI, a radiation oncologist delineated the ctVUA on the CT whilst blinded to the MRI. At a later date the same radiation oncologist defined the mrVUA on the co-registered MRI whilst blinded to the CT. All VUAs were reviewed and adjusted by a radiation oncologist and radiologist both of whom were specialized in urology.

The superior–inferior (Z-axis) coordinate i.e. vertical distance from the CT origin was recorded for both the ctVUA and mrVUA. The differences between these VUAs were calculated.

*CTV analysis*

Published guidelines recommend adding an inferior margin to the VUA to allow for microscopic extension beyond the VUA [14–17]. The RTOG guidelines recommend 8–12 mm [14], Princess Margaret Hospital (PMH) recommends 8 mm [17] whereas the Australasian Faculty of Radiation Oncology Genito-Urinary Group (FROGG) guidelines suggest 5–6 mm [16]. The remaining guideline from the EORTC recommends that the relevant CTV include “Centrally: the urethra-vesical anastomosis” and “Caudally: including the apex (15 mm cranially from the penile bulb)” with a 5 mm margin for high risk areas including microscopic extension, incompletely resected ECE and involved margins [15].

*Statistics*

The differences (ctVUA – mrVUA) were calculated for each patient. As the differences relate to the CT discrete slice thickness the median value and range was calculated. A *p*-value of <0.05 was afforded statistical significance between the median differences of the ctVUA and mrVUA using a two-tailed Wilcoxon Signed-Rank Test for paired samples. The mean difference for the patient population was also calculated to compare with the literature. The statistical analysis was performed using Microsoft Excel and Graphpad Prism Version 6.07.

**Results**

*Patient cohort*

The study cohort consisted of 34 patients with a median age was 63 years (range 52–72 years). Nine patients (26%) received adjuvant PPRT to a mean dose of 66 Gy and the remaining 25 (74%) received salvage PPRT for PSA relapse to a mean dose of 70 Gy. The majority had locally advanced disease with almost 60% having extracapsular extension (pT3a), whilst the median Gleason Score was 7. The apical margin was involved in 14 of the 21 patients (56%) with positive surgical margins (Table 1).

In 30 patients (88%) the vector difference between the mrVUA and ctVUA was caudal, (*P* < 0.0001). The ctVUA and mrVUA were coincident in four patients (12%). The median difference was 5 mm with a range of 0–10 mm. The mean difference was 4.82 mm with a standard deviation (SD) of 2.97 mm (Fig. 1). Notably, there were four patients (12%) with a mrVUA that was 10 mm inferior to the ctVUA (Fig. 2).

Comparison of the differences between mrVUA and ctVUA with recommended guidelines for CTV margins is shown in Fig. 3. The mrVUA was encompassed by the ctCTV in all patients when a margin of 12 mm was used. For the 8 mm and 5 mm margins the

**Table 1**  
Prostatectomy pathological characteristics: T stage, Gleason Score and Margin Status.

Prostatectomy Tumour Characteristics (Total patients = 34)		
T Stage	Patients	%
2a	2	5.9%
2b	3	8.8%
2c	5	14.7%
3a	20	58.8%
3b	4	11.8%
Gleason Score		
7	25	73.5%
8	2	5.9%
9	7	20.6%
Surgical Margins		
Positive	21	61.8%
Negative	13	38.2%

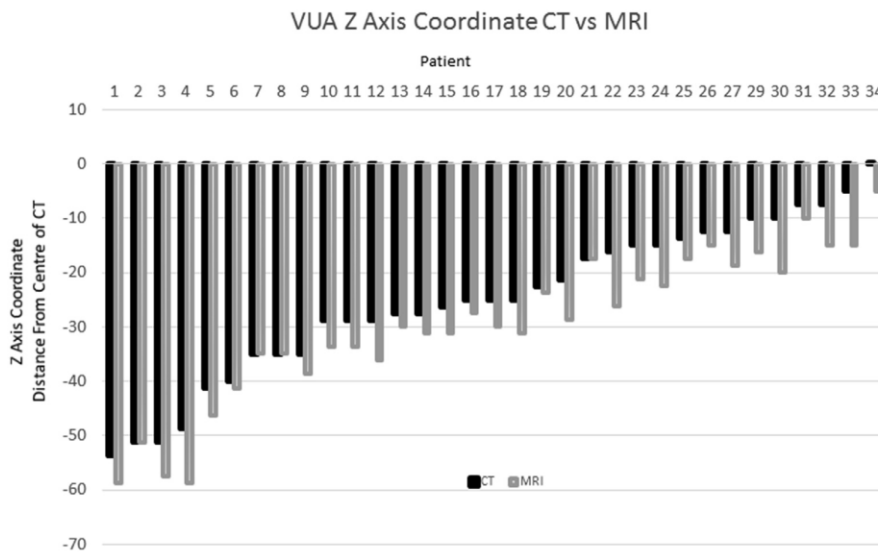


Fig. 1. VUA Z-axis coordinates for 34 patients: CT vs MRI. Z-axis origin (0) is centred and tattooed 5 cm superior to base of penis.

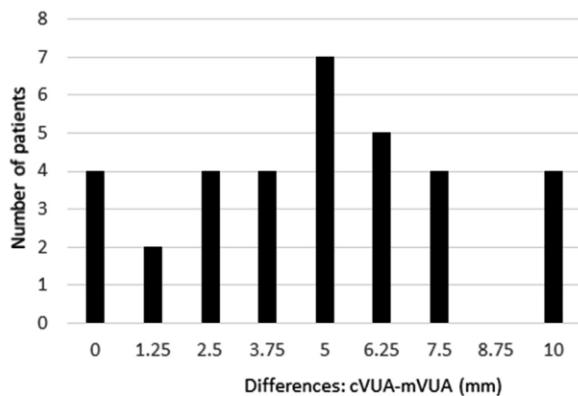


Fig. 2. Differences between the ctVUA and mrVUA based on axial slices of 1.25 mm thickness co-registered CT and MRI respectively.

mrVUA was included within the CTV in 30 (88%) and 21 (62%) patients. Four patients (12%) would have had correct CTV margins as the ctVUA and mrVUA were coincident.

The median (range) mrVUA to ctCTV distance in these patients whose mrVUA was included within the ctCTV was 7 mm (2–12 mm), 3 mm (0.5–8 mm) and 2.5 (1.25–5 mm) mm for the margins of 12 mm, 8 mm and 5 mm respectively.

The mrVUA was caudal and excluded from the ctCTV when using a margin of 8 mm and 5 mm, in four (12%) and 13 (38%) patients respectively. The median distance of the mrVUA from the inferior margin of the ctCTV was of 2 mm (range 2 mm) for the 8 mm margin and 2.5 mm (1.25–5 mm) for the 5 mm margin.

**Discussion**

This study validates the international recommendation for MRI to optimally define the VUA in PPRT, particularly when using non-contrast simulation CT. The MRI defined VUA is more likely to be a truer definition of the VUA because of its markedly better soft tissue contrast. In most patients, the mrVUA was caudal to the ctVUA.

Consequently, the recommended CTV margin was reduced in the majority with the mrVUA compared to ctVUA. Notably, the mrVUA was excluded entirely from the CTV in up to 38%, depending on the CTV margin used.

MRI as compared to CT, improves the target volume delineation in radiotherapy for an intact prostate [22–24]. The present study has similarly confirmed its utility in the post-prostatectomy setting. A non-contrast simulation CT alone only accurately identified the VUA in 12% of patients. Precisely identifying the last CT slice with visible urine can be difficult as it is often a small dot with a grayscale contrast that approaches that of the bladder neck and VUA. In comparison, a T2 weighted MRI, the urine is contrastingly bright compared to the surrounding tissue (Fig. 4).

MRI and more recently multi-parametric MRI (mpMRI) has been used to define the site of recurrence that would suitable for biopsy confirmation and salvage radiotherapy [25,26]. Most MRI studies agree with earlier ultrasound studies that the peri-anastomotic site was the most frequent site of recurrence with an incidence range from 52 to 100% [12–17].

Two contemporary studies, one using MRI [26] and another mpMRI [25] found that the local recurrence occurred at the VUA in 76% and 70% of patients respectively. Interestingly in both studies there were no differences in pathological or clinical variables between the sites of recurrence. Notably, the tumour site and location of the positive surgical margins did not correlate statistically with the site of local recurrence [26].

PMH performed a comprehensive study to derive a consensus definition of the anatomic boundaries of the CTV for PPRT [17]. This included an analysis of 12 patients for the critical VUA localization. They compared CT images with a slice thickness of 2 mm to reference MRI images with a slice thickness of 3 mm. This study found that the mean (±SD) uncertainty in identifying the VUA using CT was 1.8 mm (±2.5). The present study found a larger mean uncertainty when comparing CT to MRI of 4.82 mm (±2.97). The differences maybe a result of the thicker slice images, particularly the MRI and limited patient numbers.

The CTV incorporates the most common sites of local recurrence i.e. the surgical, prostatic and seminal vesicle bed [8,9,27]. This is represented anatomically by the VUA, the bladder base, including posterior bladder suture line, the retro-vesical space

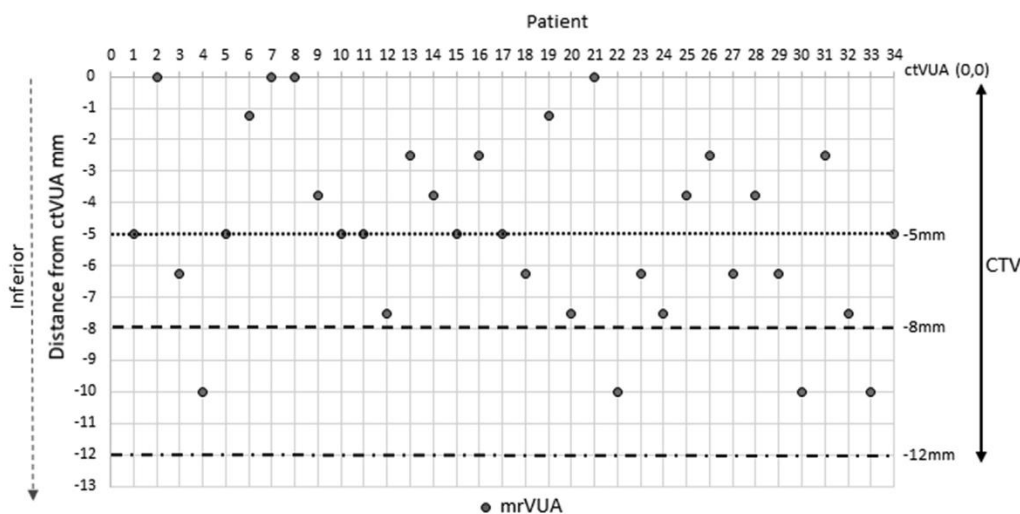


Fig. 3. Vector difference of mrVUA relative to ctVUA for each patient (i.e. ctVUA normalized to 0,0.); illustrating the relationship to the recommended CTV (inferior) margins of 5 mm, 8 mm and 12 mm.

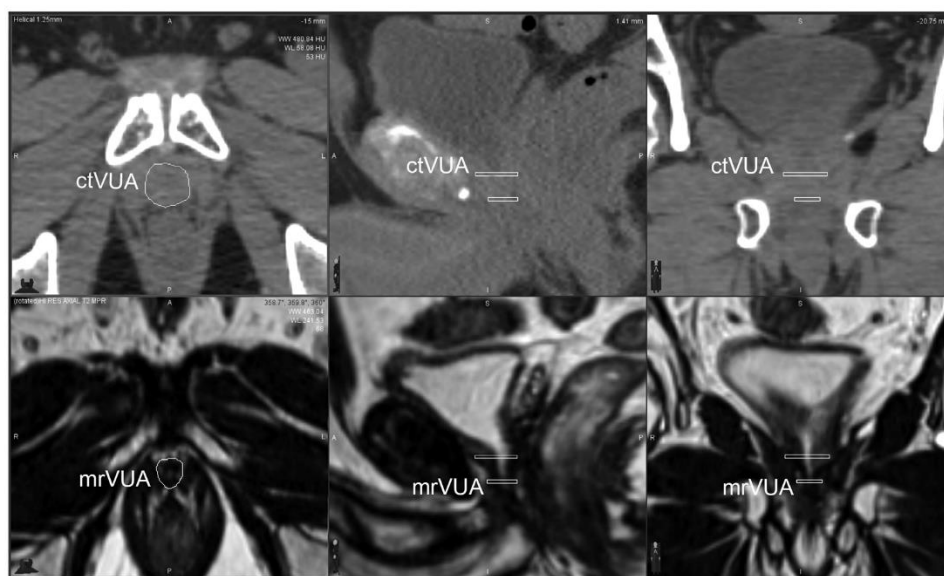


Fig. 4. Multi-planar views of co-registered CT and MRI scans of a single patient showing the mrVUA caudal to the ctVUA.

and the seminal vesicle bed to the cut end of the vas deferens [14-17,26]. The increasing utilization of IMRT in the PPRT permits greater dosimetric conformity around the CTV. Therefore, the correct CTV definition becomes increasingly important in the optimization of local control and the minimization of toxicity. Additionally, it may allow dose escalation to high risk regions to further improve local control [28].

The various guidelines recommend that a CTV margin should be applied to the VUA to allow for microscopic extension inferiorly that may occur with apical involvement or surgical manipulation [14-17]. The present study showed that even if the maximum recommended margin of 12 mm is applied to the ctVUA, there will be still eight patients (24%) that will have less than the minimum recommended margin of 5 mm. If a non-contrast CTV alone is used, then an appropriately larger planning target volume (PTV) or

uncertainty margin needs to be considered to compensate for these uncertainties.

A contrast CT is likely to produce similar results to MRI although it was not investigated in the present study. We have routinely used a non-contrast CT and MRI rather than a contrast CT as the large volume of bladder contrast may lead to dosimetric perturbations necessitating co-registration with a non-contrast CT or alternatively, applying density corrections. The other major caveat is that it could not be used in patients with contrast allergies.

The commonest positive surgical margin is at the prostatic apex. This is a consequence of anatomical factors including broad extent of the dorsal venous plexus, its location under the pubic bone, the proximity of the urethral sphincter and neurovascular bundle and the absence of a complete capsule [29,30]. In the present study, the apical margin was the most common positive

surgical margin, occurring in 71% of patients. Two of the guidelines recommend an additional margin if the apex is involved; the EORTC recommends an additional 5 mm [15] and the RTOG recommends extending to the genito-urinary diaphragm [14]. This additional margin would reduce the dosimetric impact of an inaccurate VUA identification.

Contouring guidelines recommend the superior aspect of the penile bulb as an alternative anatomical marker of the inferior CTV margin. This can be used if the VUA is difficult to identify [14,16]. It ensures that the VUA is encompassed. However, it would increase the penile bulb dose, increasing the risk of erectile dysfunction [31]. QUANTEC recommends keeping the mean dose to 95% of the PB volume to <50 Gy and limiting the penile bulb dose to D95 < 50 Gy and D70 < 70 Gy to minimize the risk of erectile dysfunction [31]. This may be difficult to achieve, particularly with dose escalation, as the CTV would be immediately adjacent to the penile bulb and the planning target volume expansion would overlap this organ at risk.

Limitations of the study include co-registration uncertainty, deformation, inter-observer and intra-observer variation, optimization of window levels and the effect of training. In addition, the VUA location may vary because of internal organ motion secondary to bladder filling. A recent study investigating the prostate bed motion during treatment showed an internal organ motion up to 18 mm in the superior–inferior direction [32]. The other important use of MRI, notably mpMRI is the identification of local recurrences. Notably, MRI with PSMA PET improves the detection of prostate cancer and may better select patients for salvage radiotherapy by detecting the local recurrence and excluding patients with metastatic disease [33–35]. Higher doses of radiotherapy targeting visible local recurrences may be required to optimize local control [28].

## Conclusion

The present study validates the recommendation that a T2 weighted MRI is critical to accurately delineate the VUA for PPRT. If an MRI is not available or contra-indicated, a contrast CT may be an alternative or the PTV margins could be increased to compensate for the delineation uncertainty.

## Conflict of interest

None declared.

## Acknowledgements

Ms Jenny Smith for statistical advice.

## References

- [1] Bolla M, van Poppel H, Collette L, et al. Postoperative radiotherapy after radical prostatectomy: a randomised controlled trial (EORTC trial 22911). *Lancet* 2005;366:572–8.
- [2] King CR. Adjuvant versus salvage radiotherapy for high-risk prostate cancer patients. *Semin Radiat Oncol* 2013;23:215–21.
- [3] Stephenson AJ, Shariat SF, Zelefsky MJ, et al. Salvage radiotherapy for recurrent prostate cancer after radical prostatectomy. *JAMA* 2004;291:1325–32.
- [4] Thompson Jr IM, Tangen CM, Paradelo J, et al. Adjuvant radiotherapy for pathologically advanced prostate cancer: a randomized clinical trial. *JAMA* 2006;296:2329–35.
- [5] Wiegel T, Bartkowiak D, Böttke D, et al. Adjuvant radiotherapy versus wait-and-see after radical prostatectomy: 10-year follow-up of the ARO 96–02/AUO AP 09/95 trial. *Eur Urol* 2014;66:243–50.
- [6] Fossati N, Karnes RJ, Boorjian SA, et al. Long-term impact of adjuvant versus early salvage radiation therapy in pT3N0 prostate cancer patients treated with radical prostatectomy: results from a multi-institutional series. *Eur Urol* 2016.
- [7] Pasquier D, Ballereau C. Adjuvant and salvage radiotherapy after prostatectomy for prostate cancer: a literature review. *Int J Radiat Oncol Biol Phys* 2008;72:972–9.
- [8] Connolly JA, Shinohara K, Presti Jr JC, Carroll PR. Local recurrence after radical prostatectomy: characteristics in size, location, and relationship to prostate-specific antigen and surgical margins. *Urology* 1996;47:225–31.
- [9] Leventis AK, Shariat SF, Slawin KM. Local recurrence after radical prostatectomy: correlation of US features with prostatic fossa biopsy findings. *Radiology* 2001;219:432–9.
- [10] Scattoni V, Roscigno M, Raber M, et al. Multiple vesico-urethral biopsies following radical prostatectomy: the predictive roles of TRUS, DRE, PSA and the pathological stage. *Eur Urol* 2003;44:407–14.
- [11] Zelefsky MJ, Kollmeier M, Cox B, et al. Improved clinical outcomes with high-dose image guided radiotherapy compared with non-IGRT for the treatment of clinically localized prostate cancer. *Int J Radiat Oncol Biol Phys* 2012;84:125–9.
- [12] Sveistrup J, af Rosenschold PM, Deasy JO. Improvement in toxicity in high risk prostate cancer patients treated with image-guided intensity-modulated radiotherapy compared to 3D conformal radiotherapy without daily image guidance. *Radiat Oncol* 2014;9:44.
- [13] Kok D, Gill S, Bressel M, et al. Late toxicity and biochemical control in 554 prostate cancer patients treated with and without dose escalated image guided radiotherapy. *Radiother Oncol* 2013;107:140–6.
- [14] Michalski JM, Lawton C, El Naqa I, et al. Development of RTOG consensus guidelines for the definition of the clinical target volume for postoperative conformal radiation therapy for prostate cancer. *Int J Radiat Oncol Biol Phys* 2010;76:361–8.
- [15] Poortmans P, Bossi A, Vandeputte K, et al. Guidelines for target volume definition in post-operative radiotherapy for prostate cancer, on behalf of the EORTC Radiation Oncology Group. *Radiother Oncol* 2007;84:121–7.
- [16] Sidhom MA, Kneebone AB, Lehman M, et al. Post-prostatectomy radiation therapy: consensus guidelines of the Australian and New Zealand Radiation Oncology Genito-Urinary Group. *Radiother Oncol* 2008;88:10–9.
- [17] Wiltshire KL, Brock KK, Haider MA, et al. Anatomic boundaries of the clinical target volume (prostate bed) after radical prostatectomy. *Int J Radiat Oncol Biol Phys* 2007;69:1090–9.
- [18] Brendler CB, Walsh PC. The role of radical prostatectomy in the treatment of prostate cancer. *CA Cancer J Clin* 1992;42:212–22.
- [19] Van Velthoven RF, Ahlering TE, Peltier A, Skarecky DW, Clayman RV. Technique for laparoscopic running urethrovesical anastomosis: the single knot method. *Urology* 2003;61:699–702.
- [20] Golabek T, Jarecki P, Jaskulski J, Dudek P, Szopinski T, Chlosta P. Modified technique for laparoscopic running vesicourethral anastomosis. *Wideochir Inne Tech Maloinwazyjne* 2014;9:357–61.
- [21] Vargas HA, Wassberg C, Akin O, Hricak H. MR imaging of treated prostate cancer. *Radiology* 2012;262:26–42.
- [22] Chang JH, Lim Joon D, Nguyen BT, et al. MRI scans significantly change target coverage decisions in radical radiotherapy for prostate cancer. *J Med Imaging Radiat Oncol* 2014;58:237–43.
- [23] Khoo V, Lim Joon D. Magnetic Resonance Imaging. In: Mundt A, Arnold R, editors. *Image Guided Radiation Therapy: A Clinical Perspective*. Peoples Medical Publishing House; 2010.
- [24] Khoo VS, Joon DL. New developments in MRI for target volume delineation in radiotherapy. *Br J Radiol* 2006;79 Spec No 1:S2–S15.
- [25] Hernandez D, Salas D, Gimenez D, et al. Pelvic MRI findings in relapsed prostate cancer after radical prostatectomy. *Radiat Oncol* 2015;10:262.
- [26] Nguyen DP, Giannarini G, Seiler R, et al. Local recurrence after retroperitoneal radical prostatectomy for prostate cancer does not exclusively occur at the anastomotic site. *BJU Int* 2013;112:E243–9.
- [27] Sella T, Schwartz LH, Swindle PW, et al. Suspected local recurrence after radical prostatectomy: endorectal coil MR imaging. *Radiology* 2004;231:379–85.
- [28] King CR. The dose-response of salvage radiotherapy following radical prostatectomy: a systematic review and meta-analysis. *Radiother Oncol* 2016;121:199–203.
- [29] Bartkowiak D, Böttke D, Wiegel T. Radiotherapy in the management of prostate cancer after radical prostatectomy. *Future Oncol* 2013;9:669–79.
- [30] Meeks JJ, Eastham JA. Radical prostatectomy: positive surgical margins matter. *Urol Oncol* 2013;31:974–9.
- [31] Roach 3rd M, Nam J, Gagliardi G, El Naqa I, Deasy JO, Marks LB. Radiation dose-volume effects and the penile bulb. *Int J Radiat Oncol Biol Phys* 2010;76: S130–4.
- [32] Bell LJ, Cox J, Eade T, Rinks M, Kneebone A. Prostate bed motion may cause geographic miss in post-prostatectomy image-guided intensity-modulated radiotherapy. *J Med Imaging Radiat Oncol* 2013;57:725–32.
- [33] Perera M, Papa N, Christidis D, et al. Sensitivity, specificity, and predictors of positive 68Ga-Prostate-specific membrane antigen positron emission tomography in advanced prostate cancer: a systematic review and meta-analysis. *Eur Urol* 2016;70:926–37.
- [34] Budaus L, Leyh-Bannurah SR, Salomon G, et al. Initial experience of (68)Ga-PSMA PET/CT imaging in high-risk prostate cancer patients prior to radical prostatectomy. *Eur Urol* 2016;69:393–6.
- [35] Eiber M, Weirich G, Holzapfel K, et al. Simultaneous 68Ga-PSMA HBED-CC PET/MRI improves the localization of primary prostate cancer. *Eur Urol* 2016;70:829–36.



## Proximal seminal vesicle displacement and margins for prostate cancer radiotherapy

Daryl Lim Joon, MBBS, FRANZCR,<sup>1</sup> Michael Chao, MBBS, DMedSc, FRANZCR,<sup>1</sup> Angelina Piccolo, M.Rad.Ther,<sup>1</sup> Michal Schneider, PhD,<sup>2</sup> Nigel Anderson, BAppSc,<sup>1</sup> Monica Handley, BAppSc,<sup>1</sup> Margaret Benci, MHIthSc,<sup>1</sup> Wee Loon Ong, BMedSc, MBBS, MPhil,<sup>1</sup> Karen Daly, BAppSc,<sup>1</sup> Rebecca Morrell, MHIthSc,<sup>1</sup> Kenneth Wan, MRT,<sup>1</sup> Nathan Lawrentschuk, MBBS, PhD, FRACS,<sup>3</sup> Farshad Forouidi, MBBS, DMedSc, MPA, FRANZCR,<sup>1</sup> Trish Jenkins, MPH,<sup>1</sup> David Angus, MBBS, FRACS,<sup>3</sup> Morikatsu Wada, MBBS, FRANZCR,<sup>1</sup> Shomik Sengupta, MBBS, MD, FRACS,<sup>3</sup> & Vincent Khoo, MBBS, MD, FRCR, FRANZCR<sup>1,2,4</sup>

<sup>1</sup>Department of Radiation Oncology, Olivia Newton-John Cancer Wellness and Research Centre, Austin Health, Melbourne, Vic., Australia

<sup>2</sup>Monash University, Melbourne, Vic., Australia

<sup>3</sup>Department of Urology, Austin Health, Melbourne, Vic., Australia

<sup>4</sup>Royal Marsden NHS Foundation Trust, London, UK

### Keywords

Clinical target volume, displacement, fiducial markers, margins, planning target volume, prostate cancer, radiotherapy, radiotherapy planning, seminal vesicles

### Correspondence

Daryl Lim Joon, Olivia Newton John Cancer Centre, 145 Studley Road, Heidelberg, Vic. 3084, Australia. Tel: +61 3 94962800; Fax: +61 3 94962826; E-mail: daryl.limjoon@austin.org.au

Received: 23 August 2020; Accepted: 14 December 2020

*J Med Radiat Sci* 00 (2021) 1–9

doi: 10.1002/jmrs.457

### Abstract

**Introduction:** Guidelines recommend that the proximal seminal vesicles (PrSV) should be included in the clinical target volume for locally advanced prostate cancer patients undergoing radiotherapy. Verification and margins for the prostate may not necessarily account for PrSV displacement. The purpose was to determine the inter-fraction displacement of the PrSV relative to the prostate during radiotherapy. **Methods:** Fiducials were inserted into the prostate, and right and left PrSV (RSV and LSV) in 30 prostate cancer patients. Correctional shifts for the prostate, right and left PrSV and pelvic bones were determined from each patient's 39 daily orthogonal portal images relative to reference digitally reconstructed radiographs. **Results:** There was a significant displacement of the RSV relative to the prostate in all directions: on average 0.38 mm (95% confidence interval (CI) 0.26 to 0.50) to the left, 0.80–0.81 mm (CI 0.68 to 0.93) superiorly and 1.51 mm (CI 1.36 to 1.65) posteriorly. The LSV was significantly displaced superiorly to the prostate 1.09–1.13 mm (CI 0.97 to 1.25) and posteriorly 1.81 mm (CI 1.67 to 1.96), but not laterally (mean 0.06, CI –0.06 to 0.18). The calculated PTV margins (left–right, superior–inferior, posterior–anterior) were 4.9, 5.3–5.6 and 4.8 mm for the prostate, 5.2, 7.1–8.0 and 9.7 mm for the RSV, and 7.2, 7.5–7.6 and 8.6 mm for the LSV. **Conclusion:** There is a significant displacement of the PrSV relative to the prostate during radiotherapy. Greater margins are recommended for the PrSV compared to the prostate.

### Introduction

Seminal vesicle invasion (SVI) occurs in 7–24% of prostate cancer patients at presentation.<sup>1</sup> It is an important poor prognostic factor, indicative of aggressive disease with a high risk of metastases.<sup>1</sup> However, it is not uniformly fatal.<sup>2</sup> Radiotherapy studies have shown an outcome improvement of high-risk patients, including SVI, with dose escalation<sup>3</sup> or androgen deprivation

therapy.<sup>4</sup> The SWOG 8794 subset analysis of post-prostatectomy patients with SVI showed that adjuvant radiotherapy led to a significantly improved recurrence-free survival and a trend to better overall survival.<sup>5</sup>

The risk for SVI in prostate cancer can be estimated using either Partins Tables or Roach's formulae.<sup>6</sup> It is generally recommended that the seminal vesicle (SV) be included in the clinical target volume (CTV) for intermediate to high and very high-risk categories.<sup>6,7</sup>

Inclusion of the SV in the CTV is important so that the SV receives an adequate dose.<sup>8</sup>

Daily online targeting is verified according to the prostate position and does not necessarily account for SV displacement. Studies have illustrated that the SV can move in relation to the prostate.<sup>9–15</sup> Most analysed the motion of the whole SV to the tips. However, prostatectomy pathological analysis has shown that the SVI rarely extends beyond the proximal 2.0–2.5 cm.<sup>16</sup> Guidelines recommend that only the proximal 1–2 cm seminal vesicles (PrSV) should be included in the CTV.<sup>16</sup> Measures of the whole SV motion and margins may not accurately reflect the PrSV.

The present study has minimised observer uncertainties by inserting gold fiducial markers both the prostate and PrSV. This exploratory study aimed to quantify the inter-fraction PrSV displacement relative to the prostate and evaluate the related planning target volume (PTV) margins of the PrSV as recommended in clinical guidelines.

## Methods

### Study cohort

This study was approved by Austin Health Human Research Ethics Committee. The overriding eligibility criteria were men with locally advanced prostate cancer,<sup>7</sup> where the inclusion of the SV in the radiotherapy volume was indicated. Patients were recruited prospectively after signing informed consent. The planned sample size of 25 men was considered sufficient to estimate margins. Some patients were excluded because of incorrectly placed fiducials, and therefore, the protocol was amended and approved by ethics to increase the patient accrual number.

### Gold seed insertion technique

The Northwest Medical Physics Equipment (NMPE) ® Soft Tissue Marker Kit (P/N 887-825) was utilised. Three 3 mm × 1.2 mm gold fiducials were inserted by a single experienced urologist under sedation and antibiotic prophylaxis using trans-rectal ultrasound guidance. The SV fiducials were inserted to define the proximal 2 cm of the SV and confirmed at CT simulation. The five fiducials were positioned as follows: Seed 1 on right prostate base, Seed 2 on left prostate mid-gland, Seed 3 on the right prostate apex, Seed 4 on right seminal vesicle (RSV) and Seed 5 on left seminal vesicle (LSV).

### Image acquisition

CT simulation was performed on a General Electric Radiation Therapy Lightspeed Widebore ® helical

scanner (General Electric Healthcare, Buckinghamshire, United Kingdom) with a resolution of 512 × 512 pixels, pitch 0.75, no gap and a slice thickness of 1.25 mm, two weeks following fiducial insertion. Patients were positioned supine with a custom foam Alpha cradle placed on an indexed pelvic board with foot stocks. A standard bladder and bowel protocol was used to have a comfortably full bladder and empty rectum (Microlax enema). Orthogonal digitally reconstructed radiographs (DRRs) were generated from the CT and used as the reference images for verification. All were treated to a total dose of 78 Gy in 39 fractions using the departmental intensity-modulated radiotherapy (IMRT) protocol on an Elekta ® Synergy linear accelerator (Elekta, Stockholm, Sweden). Daily pre-treatment orthogonal electronic megavoltage portal verification images were performed for each 39 fractions, that is an anterior–posterior image (API) and left lateral image (LLI) with a resolution of 512 x 512 pixels.

### Image verification

Two trained observers (radiation therapists) independently matched the daily verification images with the reference DRRs using Elekta iView® software (Elekta, Stockholm, Sweden) using four different marker matching methods relative to the initial setup. The four matching methods were prostate three seeds (prostate), RSV seed, LSV seed and pelvic bones (Bone) for historical comparison. The observers were blinded to the other observer's matches. The correctional shifts were recorded for each of the four-different marker matches in millimetres for the two images – API and LLI, that is

1. Lateral left–right (LR) and superior–inferior (SI) correctional shifts for the API and
2. Anterior–posterior (AP) and SI shifts for the LLI.

### Statistical methods

The statistician independently checked all the data for data entry errors by comparison with the original handwritten records. No genuine outliers were excluded.

To compare the fiducials, analysis of variance (ANOVA) was performed on the API and LLI separately, adjusting for patients, fractions within patients and observers. If the ANOVA showed significant differences between fiducials ( $P < 0.05$ ), their means were compared using t-tests based on the ANOVA standard error of the difference. As there were no pre-specified hypotheses and six possible pairwise comparisons between the four fiducials, the least significant difference between the means at the 5% level ( $LSD_{0.05}$ ) was adjusted for the number of non-significant comparisons, if any, using the

Hochberg–Benjamini modification of the Bonferroni correction to maintain the overall probability of a false positive conclusion (Type 1 error) at less than 0.05.<sup>17</sup> Ninety-five per cent confidence intervals (CI) for differences between means were calculated as the difference  $\pm$  LSD<sub>0.05</sub>.

To assess the adequacy of PTV margins, the means and standard deviations (SD) for each patient over 39 fractions and two observers were calculated. We then derived the overall mean (group systematic error), the SD of the means (systematic error,  $\Sigma$ ) and the root mean square of the SD (random error,  $\sigma$ ). The margins were calculated according to the formula: Margin =  $2.5\Sigma + 0.7\sigma$ .<sup>18</sup> The PTV margins calculated from the inter-fraction displacements take into account uncertainties including setup, delineation/verification and inter-fraction motion. The formula does not account for the overall mean shift (group systematic error) of the seminal vesicles relative to the prostate. GenStat statistical software, version 18.1, was used for the analysis.

## Results

### Baseline characteristics of the study cohort

The patients were accrued over three years from 7 August 2006 to 15 May 2009. Forty-three patients were enrolled, but 13 were excluded from analysis because at least one seed was incorrectly placed, that is missing, not within the prostate or not in PrSV (eight), had migrated (one), or images were unclear or lost due to power failure (four). The final cohort consisted of 30 men with locally advanced prostate cancer, that is two patients (7%) with NCCN<sup>7</sup> very high risk, 13 (43%) with high risk and 15 (50%) with intermediate-risk prostate cancer. The mean age was 69 years (SD 6.3, range 55–77). The mean PSA was 12 (SD 10.3, range 0.4–54.2). T stages were T1c ( $n = 10$ ), T2 ( $n = 10$ ) and T3 ( $n = 10$ ). All but three had Gleason scores  $\geq 7$ .

The total data set potentially consisted of 18,720 shifts in two dimensions (30 patients  $\times$  39 fractions  $\times$  2 images  $\times$  2 observers  $\times$  4 marker sites). Of these, 190 shifts (1%) were missing. The reasons were image problems: image not taken, lost or poor quality (132 shifts or 0.7%) or observer errors, for example measured the wrong image or not appropriately recorded (58 shifts or 0.3%).

### Comparison of fiducials on the anterior–posterior image

The ANOVA on the shifts for the AP image showed there were highly significant differences between fiducials, both

in the LR and SI directions ( $P < 0.001$ ,  $n = 9250$ ) (Fig. 1). Overall, the prostate, bone and left seminal vesicle shifted to the right, and the right seminal vesicle shifted to the left compared to the initial setup. All fiducials shifted superiorly, with the LSV moving the most.

On average, the RSV and LSV correctional shifts were significantly greater than the prostate in the superior direction, and the RSV shifts were significantly more to the left than the prostate or the LSV. The mean shifts in mm for each verification method (LR, SI) were prostate (0.21, 0.52), RSV (−0.17, 1.33), LSV (0.27, 1.65) and bone (0.36, 0.68). The standard errors of the difference between means for LR and SI directions were 0.050 and 0.062 mm, respectively. The least significant differences ( $P < 0.05$ ) were 0.12 for the LR direction (adjusted for 2 non-significant comparisons) and 0.12 mm for the SI direction (no adjustment required).

The displacement of the RSV relative to the prostate was 0.38 mm to the left (CI 0.26 to 0.50) and 0.80 mm superiorly (CI 0.68 to 0.92). The displacement of the LSV relative to the prostate was 0.06 mm to the right (CI −0.06 to 0.18, not significant) and 1.13 mm superiorly (CI 1.00 to 1.25). The mean shifts of LSV and RSV were significantly different with the LSV mean shift being superior to the RSV by 0.32 mm (CI 0.20 to 0.44). Interestingly the LSV mean shift was to the right, and the RSV shift was to the left indicating that both shifts were towards the midline, that is they are closer together by 0.44 mm (CI 0.32 to 0.56). (Fig. 1)

### Comparison of fiducials on the left lateral image

The analysis of variance showed that there were highly significant differences between the fiducials, both in the AP and SI directions ( $P < 0.001$ ,  $n = 9280$ ) (Fig. 2). The prostate and both RSV and LSV shifted posteriorly, and the bone shifted anteriorly compared to the initial setup. Both SV and bone shifted superiorly, with the LSV moving the most.

The mean shifts in mm for each verification method (AP, SI) were prostate (−0.66, 0.10), RSV (−2.17, 0.91), LSV (−2.48, 1.19) and bone (0.38, 0.53). The standard errors of difference between means for the AP and SI directions were 0.073 and 0.063 mm, respectively. The least significant differences ( $P < 0.05$ ) were 0.14 and 0.12 mm for the AP and SI directions, respectively. All differences were significant ( $P < 0.05$ ), so no adjustments were required for the LSD<sub>0.05</sub>.

The RSV and LSV correctional shifts in the AP and SI directions were significantly greater than the prostate. The displacement of the RSV relative to the prostate was 1.51

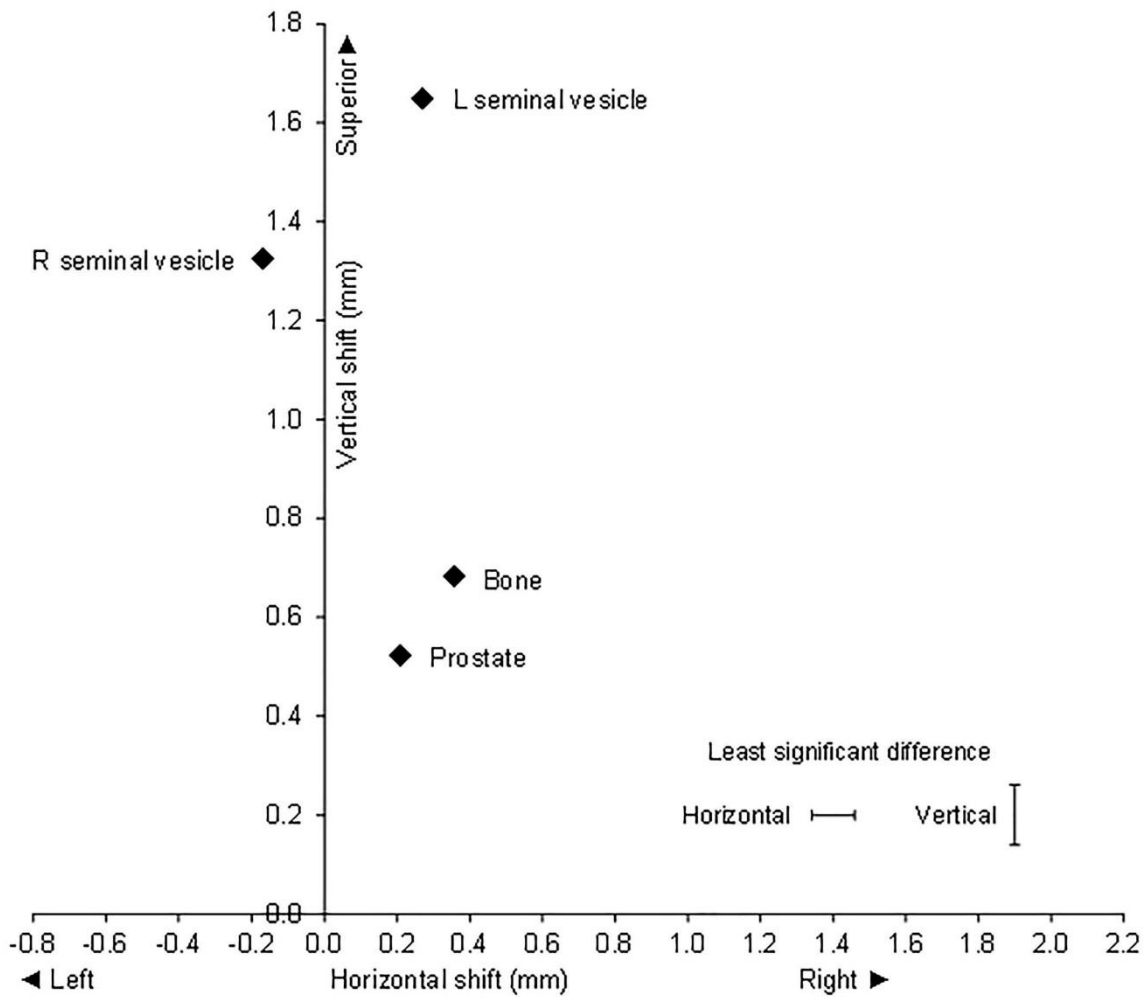


**Figure 1.** Anterior–posterior image: Mean correctional verification shifts with respect to bone and gold seed fiducial in prostate, right seminal vesicle and left seminal vesicle.

mm (CI 1.36 to 1.65) posteriorly and 0.81 mm (CI 0.68 to 0.93) superiorly. The displacement of the LSV relative to the prostate was 1.81 mm (CI 1.67 to 1.96) posteriorly and 1.09 mm (CI 0.97 to 1.22) superiorly. The mean shifts of LSV and RSV were significantly different, the LSV shift being greater than the RSV shift with a displacement of LSV relative to RSV of 0.31 mm (CI 0.16 to 0.45) posteriorly and 0.29 mm (CI 0.16 to 0.41) superiorly (Fig. 2)

**PTV margins**

The CTV to PTV margins of the prostate and PrSV were calculated for both verification images for each axis

(Table 1). The margins for the SV are larger than for the prostate, except in the case of LR shifts for the RSV. The difference in margins between the RSV and prostate were LR 0.3 mm, AP 4.9 mm and SI 1.8–2.4 mm. The differences between the LSV and prostate margins were LR 2.3 mm, AP 3.9 mm and SI 1.9–2.3 mm.

**Discussion**

This exploratory study specifically assessed the motion of the PrSV, rather than the entire SV. Gold fiducials were used to define the prostate as well as the PrSV to approximate a point to point co-registration and minimise observer and verification error.

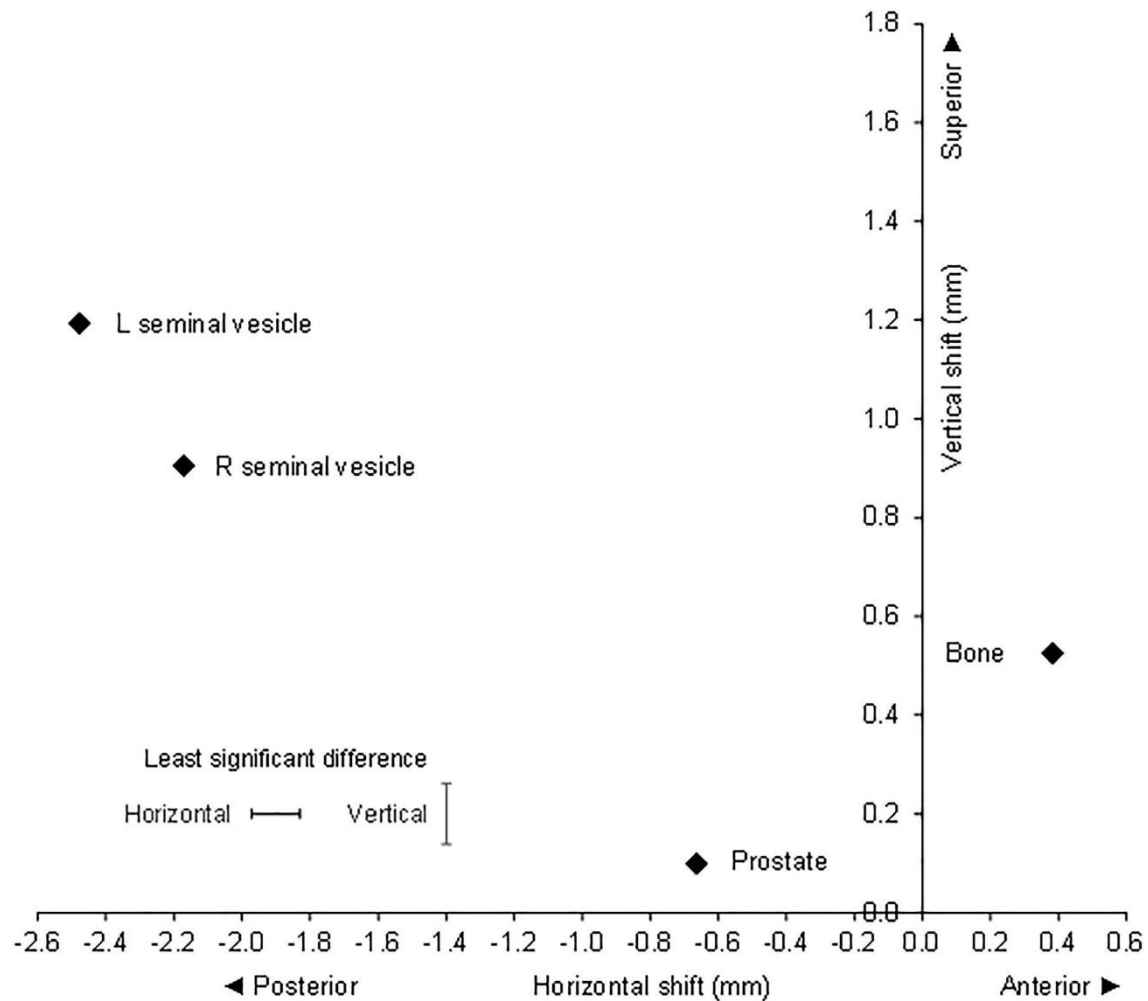


**Figure 2.** Left lateral image: Mean correctional verification shifts with respect to bone and gold seed fiducial in prostate, right seminal vesicle and left seminal vesicle.

This study found significant displacement of the SV relative to prostate verification using gold fiducials and to bone match. We observed significant movement of the RSV relative to LSV. The LSV showed the greatest displacement. This can be expected as the displacement of the SV is mainly due to rectal filling<sup>10,12</sup> which is usually asymmetrical. The calculated margins for both SV were greater than the prostate.

While it is recommended that the PrSV be included in the CTV, studies of SV motion have investigated the entire SV. They have confirmed that the SV move relative to the prostate. The prostate was defined by three fiducials or contoured prostate centroid. The movements, both systematic and random, of the entire SV, were

reported to vary from 1.1 to 1.9 mm and 0.4 to 1.4 mm LR, 2.8 to 7.3 mm and 1.2 to 3.1 mm AP, and 2.2 to 3.6 mm and 0.06 to 2.1 mm SI, respectively. The PTV margins ranged from 4.5 mm to 15 mm.<sup>10-13,15,19-21</sup>

The variation in SV displacement measurements is likely due to differences in methodology in defining the prostate and SVs. Additionally, investigations of SV motion have varied in the verification method, patient number and type and number of scans. Most investigations of SV displacement have contoured the entire SV length +/- prostate on multiple CTs. These studies are subject to a greater observer variability as it is difficult to define the PrSV on CT or cone-beam CT (CBCT). The PrSV is attached to posterior prostate over

**Table 1.** PTV margin calculation based on prostate and seminal vesicle shifts.

Matched On	AP image				+ Superior / – Inferior			
	+ Right / – Left							
	Overall Mean (M)	SD mean Systematic Error ( $\Sigma$ )	RMS SDs Random Error ( $\sigma$ )	Margin (mm)	Overall Mean (M)	SD mean Systematic Error ( $\Sigma$ )	RMS SDs Random Error ( $\sigma$ )	Margin (mm)
Prostate	0.21	1.354	2.162	4.90	0.53	1.315	2.900	5.32
R S V	–0.17	1.372	2.553	5.22	1.33	1.963	3.147	7.11
L S V	0.29	2.103	2.706	7.15	1.65	2.109	3.303	7.58
Bone	0.36	1.503	2.165	5.27	0.69	2.137	2.627	7.18

Matched On	Left lateral image				+ Superior / – Inferior			
	+ Anterior / – Posterior							
	Overall Mean (M)	SD mean Systematic Error ( $\Sigma$ )	RMS SDs Random Error ( $\sigma$ )	Margin (mm)	Overall Mean (M)	SD mean Systematic Error ( $\Sigma$ )	RMS SDs Random Error ( $\sigma$ )	Margin (mm)
Prostate	–0.66	1.110	2.843	4.77	0.10	1.450	2.780	5.57
R S V	–2.20	2.899	3.524	9.71	0.91	2.301	3.191	7.99
L S V	–2.48	2.426	3.685	8.65	1.20	2.098	3.244	7.52
Bone	0.38	2.159	2.439	7.10	0.53	2.270	2.533	7.45

Overall mean (M) = mean of the mean shifts for 30 patients = group systematic error, SD mean ( $\Sigma$ ) = standard deviation of the mean shifts for 30 patients = systematic error, Root Mean Square (RMS) SDs ( $\sigma$ ) = square root of the mean of the squares of the standard deviations for 30 patients = random error, and PTV margin =  $2.5\Sigma + 0.7\sigma$ .

a varied length and is difficult to differentiate as they have similar Hounsfield unit and grey values. Therefore, defining the start of the SV adjacent the prostate and subsequently, its length and position is subject to observer variation. The SV is more easily defined on MRI as they are hyperintense on T2-weighted imaging compared to the prostate.

CT contouring studies of prostate and SV have illustrated this observer variation.<sup>22</sup> A report on the intra-physician variation for prostate contouring calculated a variation of 0.8, 1.1, 1.5 mm for the posterior, anterior and right–left direction with an inter-observer standard deviation of 1.5, 1.4 and 2.0 mm in the posterior, anterior and right–left directions.<sup>22</sup> For the SV, they reported inter-observer variability of 1.5, 2.8 and 2.3 mm in the posterior, anterior and lateral directions and intra-observer variability of 1.2, 1.2 and 1.5 mm, respectively. The largest CT inter-observer variation appears to occur at the prostatic apex.<sup>23</sup> This ranged from 5.4 to 10.7 mm.<sup>23</sup> Importantly, this observer variation is not dissimilar to and sometimes greater than the measure of the SV displacements. The observer uncertainty may cloud the precise measurement and direction of the SV motion.

Other investigators used greyscale matching techniques to calculate changes in SV position relative to the

prostate. A notable study compared entire SV greyscale registration using CBCT, relative to prostate implanted fiducials.<sup>15</sup> They noted significant systematic and random SV displacements of 1.6 mm and 2.0 mm in LR direction and 2.8 mm and 3.1 mm in the AP direction, respectively. They did not find any difference between the RSV and LSV. These measurements are useful for entire SV as they are not subject to contouring errors and relate to a verification method that is used clinically. However, the measurements may be subject to registration errors, especially when dealing with issues such as seminal vesicle deformation.

Another interesting study quantified the PTV margins required to provide the adequate dosimetric margin of the entire SV versus the proximal 1 cm SV.<sup>24</sup> Twenty patients had three CT scans, and the contoured SVs were related to three intra-prostatic fiducials. They illustrated that the SVs move differentially from the prostate with a greater variation and distance. To ensure 95% coverage for 90% of patients, a margin of 8 mm and 5 mm was required for the entire SV and PrSV, respectively. The PrSV margin was the same as the prostate margin. Conversely, our study found that the margin for the PrSV was greater than that of the prostate. The differences may have related to the different lengths of SV used in this study, that is 1 cm versus 2 cm in our study. Other

causes may have related to observer variation with organ delineation and motion assessment technique.

MV imaging was selected for verification as the study protocol, and implementation occurred before and during a rapid departmental transition from MV to KV imaging and then CBCT. KV imaging affords better tissue contrast and CBCT provides volumetric imaging and rotational shifts. However, to maintain consistency with the initial patients, it was decided to continue with MV as the gold fiducials were well visualised, only translational shifts were collected, and a well-performed prospective study by Moseley *et al.* had shown a highly significant correlation of isocentre shifts between MV, KV and CBCT fiducials.<sup>25</sup> Conversely, Gill *et al.* attributed a statistically significant smaller setup error distribution with MV portal imaging compared to KV to the better image quality of KV.<sup>26</sup>

The present study minimised observer uncertainty by using gold fiducials, multiple observers and all verification images. However, the impact of SV deformation or seed migration was not assessed. CT quantification of SV deformation analysis may be difficult as the PrSV origin is difficult to differentiate from the posterior prostate. Thus, it would be ambiguous as to whether the deformation, for example shortening or lengthening, was occurring uniformly or differentially along its length. This could add to uncertainties in contouring and registration studies of SV motion, whereas translational shifts of a fiducial defining the PrSV will at least, in part, reflect the deformation in the calculated margins. MRI may provide a more precise analysis of SV motion and deformation.

Fiducials were inserted into PrSV under ultrasound guidance, and position confirmed at CT simulation. CT and CBCT may have detected gross fiducial migration. However, limited migration would be challenging to differentiate from SV displacement or deformation. Reassuringly, most fiducial studies of prostate and other organs have shown only a very small proportion of fiducials migrate during radiotherapy, and the distance is small.<sup>27,28</sup> Consequently, it is unlikely that fiducial migration would greatly affect the results.

In summary, a gold fiducial inserted into the seminal vesicle defines a fixed anatomical segment of the PrSV. The subsequent shifts reflect motion and deformation that can be followed during the radiotherapy course. The major caveat being possible migration of the fiducial; however, studies of gold fiducials in prostate and other sites have suggested that this infrequent. In comparison contouring matching methodologies are subject to uncertainties in relation to prostate contouring, seminal vesicle contouring or both of approximately one to 10 mm. These methodologies can be affected by

deformation and rotation as the different segments of the PrSV may be contoured even if it is the same length

The clinical scenario of gross SVI, either clinically or MRI, was not addressed. The radiotherapy volume should cover the extent of SVI on MRI and consideration to treat the entire SV would seem appropriate with gross SVI. Margins may need to be greater to cover the entire SV, although a recent study has shown that grossly involved SV is less mobile.<sup>29</sup>

Many of the caveats of this and previous studies of inter-fraction displacement, including migration, deformation and intra-fraction motion would be addressed with MRI volumetric imaging that includes cine (4D) studies.<sup>30</sup> and possibly MRI fiducials. An elegant study of intra-fraction SV displacements that contoured the entire MRI on cine-MRI showed that the SV centroid moved significantly more than the prostate in the superior–inferior direction but not in the anterior–posterior or left–right directions.<sup>30</sup> The displacement increased with time until 10 minutes, after which it plateaued. They concluded that the SV required larger margins in the superior–inferior directions. Furthermore, more sophisticated solutions to PrSV inter-fraction and intra-fraction motion could be investigated with adaptive radiotherapy techniques to account for both position and shape.

## Conclusion

The study confirms that the PrSV displacement is greater than the prostate. While margin expansion is departmental specific, this study has illustrated that larger inter-fraction margins for PrSV should be considered, but careful attention is required regarding the organs at risk, notably the rectum, especially when considering hypofractionated radiotherapy.

## Acknowledgement

The authors would like to thank Carmel Mantle, Laura Spiteri, Drew Smith, Rachael Edmonds, Cathy Jager and Judene Pigou for radiotherapy assistance and Jennifer Smith for statistical analysis. It is acknowledged that the project was a collaborative study between radiotherapy and urology, with Shomik Sengupta acting as the senior surgical author.

## Financial Support/ Funding

No financial support/ funding for this study.

## Conflict of Interest

The author declares no conflict of interest.

### Data Availability Statement

Research data are stored in an institutional repository and will be shared upon request to the corresponding author

### References

- Pierorazio PM, Ross AE, Schaeffer EM, et al. A contemporary analysis of outcomes of adenocarcinoma of the prostate with seminal vesicle invasion (pT3b) after radical prostatectomy. *J Urol* 2011; **185**: 1691–7.
- Humphrey PA. Seminal vesicle invasion by adenocarcinoma of the prostate. *J Urol* 2015; **194**: 1757–8.
- Viani GA, da Silva LG, Stefano EJ. High-dose conformal radiotherapy reduces prostate cancer-specific mortality: results of a meta-analysis. *Int J Radiat Oncol Biol Phys* 2012; **83**: e619–25.
- Mason MD, Parulekar WR, Sydes MR, et al. Final report of the intergroup randomized study of combined androgen-deprivation therapy plus radiotherapy versus androgen-deprivation therapy alone in locally advanced prostate cancer. *J Clin Oncol* 2015; **33**: 2143–50.
- Swanson GP, Goldman B, Tangen CM, et al. The prognostic impact of seminal vesicle involvement found at prostatectomy and the effects of adjuvant radiation: data from Southwest Oncology Group 8794. *J Urol* 2008; **180**: 2453–7.
- Bayman NA, Wylie JP. When should the seminal vesicles be included in the target volume in prostate radiotherapy? *Clin Oncol (R Coll Radiol)* 2007; **19**: 302–7.
- Mohler J, Bahnon RR, Boston B, et al. NCCN clinical practice guidelines in oncology: prostate cancer. *J Natl Compr Canc Netw* 2010; **8**: 162–200.
- Parker C, Haycocks T, Bayley A, Alasti H, Warde P, Catton C. A dose-volume histogram analysis of the seminal vesicles in men treated with conformal radiotherapy to 'prostate alone'. *Clin Oncol (R Coll Radiol)* 2002; **14**: 298–302.
- Beard CJ, Kijewski P, Bussiere M, et al. Analysis of prostate and seminal vesicle motion: implications for treatment planning. *Int J Radiat Oncol Biol Phys* 1996; **34**: 451–8.
- Frank SJ, Dong L, Kudchadker RJ, et al. Quantification of prostate and seminal vesicle interfraction variation during IMRT. *Int J Radiat Oncol Biol Phys* 2008; **71**: 813–20.
- Liang J, Wu Q, Yan D. The role of seminal vesicle motion in target margin assessment for online image-guided radiotherapy for prostate cancer. *Int J Radiat Oncol Biol Phys* 2009; **73**: 935–43.
- Mak D, Gill S, Paul R, et al. Seminal vesicle interfraction displacement and margins in image guided radiotherapy for prostate cancer. *Radiat Oncol* 2012; **7**: 139.
- Mutanga TF, de Boer HC, van der Wielen GJ, Hoogeman MS, Incrocci L, Heijmen BJ. Margin evaluation in the presence of deformation, rotation, and translation in prostate and entire seminal vesicle irradiation with daily marker-based setup corrections. *Int J Radiat Oncol Biol Phys* 2011; **81**: 1160–7.
- Roeske JC, Forman JD, Mesina CF, et al. Evaluation of changes in the size and location of the prostate, seminal vesicles, bladder, and rectum during a course of external beam radiation therapy. *Int J Radiat Oncol Biol Phys* 1995; **33**: 1321–9.
- Smitsmans MH, de Bois J, Sonke JJ, et al. Residual seminal vesicle displacement in marker-based image-guided radiotherapy for prostate cancer and the impact on margin design. *Int J Radiat Oncol Biol Phys* 2011; **80**: 590–6.
- Qi X, Gao XS, Asaumi J, et al. Optimal contouring of seminal vesicle for definitive radiotherapy of localised prostate cancer: comparison between EORTC prostate cancer radiotherapy guideline, RTOG0815 protocol and actual anatomy. *Radiat Oncol* 2014; **9**: 288.
- Hochberg Y, Benjamini Y. More powerful procedures for multiple significance testing. *Stat Med* 1990; **9**: 811–8.
- van Herk M. Errors and margins in radiotherapy. *Semin Radiat Oncol* 2004; **14**: 52–64.
- Meijer GJ, de Klerk J, Bzdusek K, et al. What CTV-to-PTV margins should be applied for prostate irradiation? Four-dimensional quantitative assessment using model-based deformable image registration techniques. *Int J Radiat Oncol Biol Phys* 2008; **72**: 1416–25.
- O'Daniel JC, Dong L, Zhang L, et al. Dosimetric comparison of four target alignment methods for prostate cancer radiotherapy. *Int J Radiat Oncol Biol Phys* 2006; **66**: 883–91.
- van der Wielen GJ, Mutanga TF, Incrocci L, et al. Deformation of prostate and seminal vesicles relative to intraprostatic fiducial markers. *Int J Radiat Oncol Biol Phys* 2008; **72**: 1604–1611.e3.
- Fiorino C, Reni M, Bolognesi A, Cattaneo GM, Calandrino R. Intra- and inter-observer variability in contouring prostate and seminal vesicles: implications for conformal treatment planning. *Radiother Oncol* 1998; **47**: 285–92.
- Debois M, Oyen R, Maes F, et al. The contribution of magnetic resonance imaging to the Three-dimensional treatment planning of localised Prostate cancer. *Int J Radiat Oncol Biol Phys* 1999; **45**: 857–65.
- Stenmark MH, Vineberg K, Ten Haken RK, Hamstra DA, Feng M. Dosimetric implications of residual seminal vesicle motion in fiducial-guided intensity-modulated radiotherapy for prostate cancer. *Med Dosim* 2012; **37**: 240–4.
- Moseley DJ, White EA, Wiltshire KL, et al. Comparison of localisation performance with implanted fiducial markers and cone-beam computed tomography for online image-guided radiotherapy of the prostate. *Int J Radiat Oncol Biol Phys* 2007; **67**: 942–53.

D. Lim Joon *et al.*

Seminal Vesicle Shifts in Prostate Radiotherapy

26. Gill S, Thomas J, Fox C, et al. Electronic portal imaging vs kilovoltage imaging in fiducial marker image-guided radiotherapy for prostate cancer: an analysis of setup uncertainties. *Br J Radiol* 2012; **85**: 176–82.
27. Poggi MM, Gant DA, Sewchand W, Warlick WB. Marker seed migration in prostate localisation. *Int J Radiat Oncol Biol Phys* 2003; **56**: 1248–51.
28. Coronel E, Cazacu IM, Sakuraba A, et al. EUS-guided fiducial placement for GI malignancies: a systematic review and meta-analysis. *Gastrointest Endosc* 2019; **89**: 659–70 e18.
29. van der Burgt M, Bergsma L, de Vries J, et al. Impact of tumour invasion on seminal vesicles mobility in radiotherapy of prostate cancer. *Radiother Oncol* 2015; **117**: 283–7.
30. Gill S, Dang K, Fox C, et al. Seminal vesicle intrafraction motion analysed with cinematic magnetic resonance imaging. *Radiat Oncol* 2014; **9**: 174.

## APPENDIX D: PAPER INCLUDED IN CHAPTER 7 (AS PUBLISHED)

World Journal of Urology  
<https://doi.org/10.1007/s00345-018-2515-0>

INVITED REVIEW



## Fiducial markers: can the urologist do better?

Catriona Duncan<sup>1</sup> · Daryl Lim Joon<sup>2</sup> · Nathan Lawrentschuk<sup>1,3,4</sup> · Trish Jenkins<sup>2</sup> · Michal Schneider<sup>5</sup> · Vincent Khoo<sup>5</sup> · Michael Chao<sup>2</sup> · Marita Lawlor<sup>2</sup> · Rachel O'Meara<sup>2</sup> · Colleen Berry<sup>2</sup> · Angela Viotto<sup>2</sup> · Kerry Brown<sup>2</sup> · Morikatsu Wada<sup>2,3</sup> · Farshad Foroudi<sup>2,3</sup> · Shomik Sengupta<sup>1,6</sup>

Received: 18 March 2018 / Accepted: 29 September 2018  
 © Springer-Verlag GmbH Germany, part of Springer Nature 2018

### Abstract

**Introduction** Radiotherapy to the bladder has a risk of toxicity to pelvic structures, which can be reduced by using fiducial markers for targeting. Injectable contrast offers an alternative marker to gold seeds, which may fall out or exacerbate scarring. Combining contrast agents with tissue glue can minimize dispersion through tissue, enhancing its utility. We evaluated combinations of contrast agents and tissue glue using porcine bladder, for feasibility and utility as fiducial markers to aid image-guided radiotherapy.

**Methods** Different contrast agents (Lipiodol ultra or Urografin) were combined with different tissue glues (Histoacryl, Tisseal or Glubran2). The mixtures were endoscopically injected into porcine bladder submucosa to identify the area of interest with multiple fiducial markers. The porcine bladders were imaged within a phantom porcine pelvis using standard radiation therapy imaging modalities. The feasibility as an injectable fiducial marker and visibility of each fiducial marker on imaging were scored as binary outcomes by two proceduralists and two radiation therapists, respectively.

**Results** Lipiodol–glue combinations were successfully administered as multiple fiducials that were evident on CT and CBCT. Lipiodol with Histoacryl or Glubran2 was visible on kV imaging. The Lipiodol Glubran2 combination was deemed subjectively easiest to use at delivery, and a better fiducial on KV imaging.

**Conclusion** This study demonstrates the feasibility of mixing contrast medium Lipiodol with Histoacryl or Glubran2 tissue glue, which, injected endoscopically, provides discrete and visible fiducial markers to aid image-guided radiotherapy. Although promising, further study is required to assess the durability of these markers through a course of radiotherapy.

**Keywords** Fiducial markers · Prostate cancer · Bladder cancer · Endoscopy · Image-guided radiotherapy · Cone beam computed tomography · Iodized oil · Tissue glue

Catriona Duncan and Daryl Lim Joon contributed equally as first authors.

✉ Shomik Sengupta  
[Shomik.sengupta@monash.edu](mailto:Shomik.sengupta@monash.edu)

<sup>1</sup> Department of Surgery, Austin Health, University of Melbourne, Melbourne, VIC, Australia

<sup>2</sup> Department of Radiation Oncology, Olivia Newtown-John Cancer Centre, Austin Health, Melbourne, VIC, Australia

<sup>3</sup> Olivia Newtown-John Cancer Research Institute, Austin Hospital, Melbourne, VIC, Australia

<sup>4</sup> The Peter MacCallum Cancer Centre, Melbourne, VIC, Australia

<sup>5</sup> Royal Marsden NHS Foundation Trust, London, UK

<sup>6</sup> Eastern Health Clinical School, Monash University, Level 2, 5 Arnold Street, Box Hill, VIC 3128, Australia

### Introduction

Radiotherapy to the bladder is utilized in two common clinical situations. It is often used as adjuvant or salvage therapy following prostatectomy for the management of prostate cancer where the major radiotherapy targets include the vesicourethral anastomosis, posterior bladder and retro-vesical space [1]. It is also used to treat muscle invasive bladder cancer following transurethral resection of bladder tumour (TURBT) in the context of bladder preservation, pre-radical surgery or if radical surgery is not suitable [2]. Efficacy of radiation therapy is directly related to the dose received by the tumour. Similarly, radiation toxicity is directly related to the dosing of normal adjacent tissues. Specifically, bladder toxicity is associated with significant morbidity and is directly related to the proportion of the bladder to receive

Published online: 04 October 2018

Springer

high radiation doses [3]. As such, the aim of modern radiotherapy is to accurately target the area of malignancy to maximize treatment dose while minimizing toxicity [4].

The use of fiducial markers in conjunction with image-guided radiotherapy (IGRT) allows for more accurate dose delivery of radiotherapy to the tumour or target - improving local control, while reducing dose and thus toxicity to the normal bladder and bowel. The requirements of any fiducial marker are visibility on a given imaging modality for use in IGRT, availability and reasonable cost [5]. This concept has been clearly demonstrated with the use of gold fiducial markers and IGRT for radiotherapy to an intact prostate [6]. Several studies have demonstrated that fiducial markers improve targeting of the prostate over use of bony landmarks [5]. Fiducial markers have also been demonstrated to be better than surgical clips for use in image-guided radiotherapy post-prostatectomy [7]. Solid fiducial markers are used in the bladder, but may be subject to migration, dislodgement or foreign body sequelae in the irradiated post-operative field [8]. The degree of migration of solid fiducial markers unrelated to bladder volume change has been documented to be as little as 1 mm over a course of treatment in a single patient [9], but needs further investigation and validation. Injectable contrast offers an alternative to potentially avoid these concerns [10]; however, dispersion of contrast through the bladder wall may impede its use [11].

A mixture of Lipiodol and cyanoacrylate tissue glue has been shown to be a safe and effective treatment of gastric and oesophageal varices [12]. Cyanoacrylate rapidly solidifies in the presence of weak bases such as water and blood. Lipiodol is an oily radiological contrast agent. The oil prevents the cyanoacrylate from polymerization until it contacts water or blood in tissue. It also enables the operator to visualize the process on X-ray imaging. We have previously successfully used a mixture of Lipiodol and cyanoacrylate glue as a fiducial marker for oesophageal cancer [13]. However, the use of glue fiducials has never been described in a water-filled organ such as the bladder.

The aim of the study was to test the technical and procedural aspects of combining and delivering liquid contrast agents with several types of tissue glues in a porcine pelvis bladder model. The objective was to create multiple reproducible discrete glue fiducial markers that could be visualized with standard radiotherapy imaging.

## Materials and methods

Ethics approval was sought but not required according to the institutional HREC, as this study was conducted in vitro on isolated porcine bladder.

Six separate contrast–glue mixtures were tested by combining 2 contrast agents—Lipiodol Ultra liquid (esterized

poppy seed oil, Aspen Medical) or Urografin 76% (amidotrizoate, Bayer Resources) with three different tissue glues: Histoacryl (monomeric *n*-butyl-2-cyanoacrylate, B Braun), Glubran2 (G-NB-2 NBCA-MS co-monomer, Baxter Healthcare) and Tisseal (fibrin sealant, Matrix Surgical), respectively, in a 1:1 ratio. For comparison, porcine bladders with no injection and single agent injection of Histoacryl, Glubran and Tisseal were used as controls. To create the mixtures, 1 ml of contrast agent was drawn up in a 2 ml syringe and 1 ml of tissue glue was drawn up in a separate 1 ml syringe. Mixing was performed using a luer-lock connector by plunging the agents back and forth between the syringes. Once adequately combined, the mixtures were immediately used.

A 17fr rigid cystoscope was used to endoscopically inspect the isolated bladders and fill the bladder with occlusion of the bladder neck against the scope itself by manual pressure to maintain continence. Using a William's needle (Cook Medical, Australia), contrast/glue combinations were injected submucosally to raise a bleb of 0.1 ml of mixture into the submucosal tissue (Fig 1). Injections were placed around the trigone to create discrete markers, to imitate marking out a small bladder tumour or the vesico-urethral anastomosis following a prostatectomy, as demonstrated in Fig. 2. Each individual mixture was tested in a separate bladder specimen.

The contrast/glue combinations were assessed for technical feasibility with regards to mixing and injection procedures on a binary rating system by the investigators carrying out the injections (NL & SS). After the injection was completed, the cystoscope was removed from the bladder with the needle kept beyond the scope to avoid occlusion of the working channel with the glue mixture. Once withdrawn from the bladder, the needle was disengaged from the cystoscope in a retrograde fashion (from the distal end) to protect



**Fig. 1** Endoscopic ex vivo submucosal glue fiducial injection of fluid-filled pigs bladder

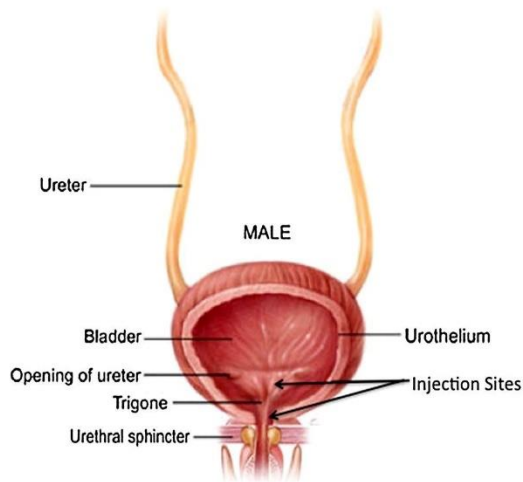


Fig. 2 Contrast/glue injection sites within the porcine bladder



Fig. 3 Verification of lipiodol and glue fiducial marker on computed tomography (CT) and cone beam computed tomography (CBCT)

the scope from the glue mixture passing through the working channel of the cystoscope.

The bladders were then placed in a detached porcine pelvis positioned to imitate a human in a supine position. This also approximates the tissue densities in a human pelvis

undergoing radiotherapy image guidance. The porcine pelvis and contained bladder were then imaged using typical radiotherapy modalities, i.e., cone beam computed tomography (CBCT), computed tomography (CT) and kilovoltage (KV) and megavoltage (MV) planar imaging (Fig. 3). The images were evaluated for visibility of contrast markers. The basis of the fiducial marker utilization during a course of radiotherapy is the accurate registration of the treatment images with the original planned images, so as to accurately deliver the radiation. This targeting and matching process is performed by trained radiation therapists or technicians. Therefore, if the markers were adequate to allow registration by the radiation technicians (consensus opinion of at least two investigators—RO, KB, ML) using standard imaging modalities for IGRT, the contrast–glue combination was considered to be visible on a binary rating system.

## Results

### Combining contrast with glue

Both contrast media were able to be mixed with the tissue glue in all combinations. However, since Urografin set quite quickly when combined with the tissue glue, only limited time was available for injection to be carried out. Ease of mixing was also subjectively better with the Lipiodol Ultra when compared with the Urografin. The rate of polymerization when Lipiodol Ultra was combined with Glubran2 was dependent on the ratio of the agents, with increased time to polymerization as the proportion of Lipiodol Ultra was increased.

### Injection of contrast–glue combination

Urografin combinations could only be injected once as a single marker due to the rapid polymerisation of the mixture, as Urografin is a water-soluble contrast medium.

Lipiodol combinations with Glubran2, Histoacryl and Tisseal could be easily injected repeatedly into the bladder submucosa, raising multiple small blebs. The combination of Lipiodol with Glubran2 was assessed as being technically easiest to inject.

### Imaging of porcine bladders

All markers were assessed with several typical imaging modalities to determine whether the markers were adequately visible to allow registration, recorded as a binary outcome being visible or not visible.

Urografin–glue combinations were each only able to produce a single fiducial that was visible on CT and CBCT, but not visible on KV or MV.

Lipiodol–tissue glue combinations were all able to deliver multiple fiducials that were adequately visualized on CT and CBCT. Lipiodol with either Histoacryl or Glubran produced visible fiducials on KV imaging. Subjectively, the Glubran 2 combination created a better marker. The Lipiodol with Tisseal combination was not visible on imaging. No combination produced sufficient contrast with MV planar imaging. These results are summarized in Table 1.

**Discussion**

This is the first study to demonstrate that Lipiodol Ultra can be easily combined with Glubran2 or Histoacryl tissue glue to create discrete injectable fiducial markers within the fluid-filled bladder wall. The combinations are visible on standard imaging modalities used in IGRT. They can be easily delivered using standard endoscopic injection techniques. The other combinations tested were not found to be suitable. Fiducials created with a mixture of Lipiodol and Tisseal were not visible on imaging, while Urografin mixtures with each tissue glue had practical limitations in creating more than one fiducial marker given rapid polymerization.

Several previous studies have demonstrated that Lipiodol is safe and effective for use in the bladder to demarcate tumours [10, 11, 14–18]. Success rates with Lipiodol alone have been variable, reported between 76 and 100% [10] as summarized in Table 2. No toxicity from Lipiodol has been reported. Notably, although Chai et al. report 92% of the markers remained in situ at the completion of the radiation course in their 15 patients, a further 16 patients could not be included in the series as the markers could not be registered for image-guided therapy due to splitting or joining [16]. Cyanoacrylic glues such as Histoacryl and the components of Glubran2 have been used in a range of urologic procedures including urethral tissue in animal models, and use in urinary fistulas without toxicity

[19]. The use of a mixture of Lipiodol and Histoacryl glue has also been previously described for the treatment of persistent anastomotic urine leak after radical prostatectomy without toxicity at 23-week follow-up [20].

Despite the success in visibility of Lipiodol as described in the literature, our clinical experience in using Lipiodol alone has been variable. While discrete fiducials have been created, it was often hampered by the significant dispersion of Lipiodol through and beyond the bladder wall, limiting its specificity as a fiducial marker. This is reflected in the imaging included in each of the studies listed above that demonstrate good visibility on CT/kV imaging but highlight a lack of specificity in the location of the Lipiodol following injection [14]. Consequently, it may not be sufficient as the sole fiducial marker [11]. In addition, wide dispersion of contrast may significantly impact further imaging in these patients, which is commonly required for ongoing follow-up.

Placing a foreign body within an operative site during radiotherapy presents the potential risks of scarring and fistulae formation [21]. These concerns have prompted the consideration of options beyond the conventional gold seeds. Modified gold seeds have been used successfully in the bladder with endoscopic placement for targeting of radiotherapy for treatment of muscle invasive bladder cancer [22]; however, these seeds are not freely available. In contrast, Lipiodol and tissue glue (Glubran2 or Histoacryl) may be found in many hospitals, including regional centers. Notably, Lipiodol and Histoacryl mixture is a cost-effective combination when compared to most other glues and fiducials.

The major limitation of this study is the evaluation of the fiducial markers at only a single time point immediately following the administration of the contrast–tissue glue combination. It does not address the stability, durability and migration of the marker. However, similar combinations used in other organs such as the upper gastrointestinal tract [23] suggest that these markers are likely to be stable. Further evaluation of the stability and reliability of Lipiodol–tissue glue markers through a standard course of radiotherapy is required by appropriate in vivo assessment.

**Table 1** Injection visibility of Contrast/glue markers with multimodal imaging

Contrast agent	Urografin			Lipiodol		
	Glubran	Histoacryl	Tisseal	Glubran	Histoacryl	Tisseal
Injection feasible	No	No	No	Yes	Yes	Yes
Visible	Yes <sup>a</sup>	Yes <sup>a</sup>	Yes <sup>a</sup>	Yes	Yes	No
	CT, CBCT, KV	CT only	CT and CBCT	CT, CBCT, KV		

CT computed tomography, CBCT cone beam computed tomography, KV kilovoltage planar imaging

<sup>a</sup>The single marker injected prior to polymerization of the Urografin–glue mixture was visible but re-injection was technically not feasible

**Table 2** Current published series investigating as Lipiodol marker for image-guided radiotherapy

Study	Patient number	Trial type	Oncological outcome	Adverse effects	Visibility of Lipiodol markers on kv planar imaging (%)
Pos et al. 2009 [11]	40	Obs <sup>a</sup>	Difficulty controlling size of markers, with some lipiodol outside bladder wall, thus not feasible to use lipiodol alone as sole reference for delineation. Valuable aid, tumour would have been missed by radiation in some patients without lipiodol demarcation	No lipiodol toxicity. Lipiodol disappeared over 12 months on CT follow-up	95 (2 of 40 patients had no Lipiodol present on imaging post-injection)
Chai et al. 2010 [16]	15	Obs <sup>a</sup>	15 of 32 patients injected with lipiodol markers were included. 17 patients were not included, in 16 because markers had split or joined, in 1 because there was no contrast in the bladder wall No post-radiation follow-up	Not recorded	92 at 5 weeks (of included patients)
Sondergaard et al. 2010 [18]	5	Obs <sup>a</sup>	>50% of treatment fractions required moderate shift to match Lipiodol spots No post-radiation treatment follow-up	Adverse effects on cystoscopy + injection: 1 patient dysuria, 1 patient mild urinary frequency, both lasting <24 h	76
Meijer et al. 2012 [17]	20	Obs <sup>a</sup>	Median follow-up 28 months, 9 patients died. 3 died of metastatic disease—no evidence local relapse; 2 patients died of local muscle invasive relapse and disease progression at 6 and 12 months post treatment; 4 died of MI <sup>c</sup> Remaining 11 patients had no evidence of disease	No adverse events from cystoscopy + injection. No G <sup>b</sup> III toxicities, acute G <sup>b</sup> II toxicities ~45%, at 36 months 25%	100
Baumgarten et al. 2014 [15] Freilich et al. 2014 [14]	5	Obs <sup>a</sup>	Follow-up 18 months In 2 of 5 patients tumour bed based on lipiodol extended outside planning target volume that would have been treated based on cystoscopy reports alone 3 no recurrence, 1 alive with metastatic disease, 1 died from metastatic disease Total treatment time was shortened by 4 days. No oncological outcomes reported in English abstract	No adverse events from injection. No treatment related toxicities/infections	95
Klinton et al. 2017 [10] [in Hungarian]	3	Obs <sup>a</sup>		No toxicity to injection. 1 patient G <sup>b</sup> II cystitis + proctitis, 1 patient G <sup>b</sup> I cystitis	100

<sup>a</sup>Obs: observational trial, no randomization or control group comparison

<sup>b</sup>G: grade as per radiation therapy oncology group side effects grading recommendation

<sup>c</sup>MI: myocardial infarction

## Conclusions

This model presents a Lipiodol–tissue glue combination as a feasible and potentially inexpensive alternative to solid fiducial markers or Lipiodol alone to overcome the respective difficulties with each. The technique has the advantages of utilizing standard stock available in most hospitals, and endoscopic injection techniques that are in widespread use. Further human trials are required [24], particularly to assess durability through a complete radiation treatment course.

**Author contributions** CB: data collection or management. KB: data collection or management. MC: protocol/project development. CD: Data analysis, manuscript writing/editing. FF: protocol/project development, data analysis. TJ: protocol/project development. DLJ: protocol/project development, data analysis, manuscript writing/editing. VK: manuscript writing/editing. ML: data collection or management. NL: protocol/project development, manuscript writing/editing. RO: data collection or management. SS: protocol/project development, manuscript writing/editing. AV: data collection or management. MW: protocol/project development.

**Funding** This study was not funded. The Lipiodol Ultra, Histoacryl, Tisseal, and Glubran2 were donated by Aspen, B Braun, Baxter and Matrix Surgical supplies, respectively, for the purpose of this comparison study.

## Compliance with ethical standards

**Conflict of interest** All of the authors declare that they have no conflict of interest.

**Ethics** This article does not contain any experimental studies with human participants or live animals performed by any of the authors. All applicable international, national, and/or institutional guidelines for the care and use of animals were followed. Ethics approval was sought from the institutional ethics committee but deemed redundant by the ethics committee, as porcine bladders were used in isolation.

**Informed consent** No patient data were included in this article.

## References

- Mottet N, Bellmunt J, Briers E, Bolla M, Bourke L, Cornford P, De Santis M, Henry A, Joniau S, Lam T, Mason MD, Van den Poel H, Van den Kwast TH, Rouvière O, Wiegand T (2017) EAU–ESTRO–SIOG guidelines on prostate cancer. European Association of Urology. <https://uroweb.org/guidelines/>. Accessed 28 Feb 2018
- Witjes JAC, Compérat E, Cowan NC, Gakis G, Hernández V, Lebre T, Lorch A, van der Heijden AG, Ribal MJ, Guidelines Associates: Bruins M, Linares Espinós E, Rouanne M, Neuzillet Y, Veskimäe E (2017) Muscle Invasive and Metastatic Bladder Cancer. European Association of Urology. <https://uroweb.org/guidelines/>. Accessed 28 Feb 2018
- Marks LB, Carroll PR, Dugan TC, Anscher MS (1995) The response of the urinary bladder, urethra and ureter to radiation and chemotherapy. *Int J Radiat Oncol Biol Phys* 31:1257–1280
- Turner SL, Swindell R, Bowl N, Marrs J, Brookes B, Read G, Cowan RA (1997) Bladder movement during radiation therapy for bladder cancer: implications for treatment planning. *Int J Radiat Oncol Biol Phys* 39(2):355–360
- O'Neill AGM, Jain S, Hounsfield AR, O'Sullivan J (2016) Fiducial marker guided prostate radiotherapy: a review. *Br J Radiol* 89
- Zelevsky MJ, Kollmeier M, Cox B, Fidaleo A, Sperling D, Pei X, Carver B, Coleman J, Lovelock M, Hunt M (2012) Improved clinical outcomes with high-dose image guided radiotherapy compared with non-IGRT for the treatment of clinically localized prostate cancer. *Int J Radiat Oncol Biol Phys* 84(1):125–129. <https://doi.org/10.1016/j.ijrobp.2011.11.047>
- Fortin I, Carrier J-F, Beauchemin MC, Bêliveau-Nadeau D, Delouya B, Taussky D (2014) Using fiducial markers in the prostate bed in postprostatectomy external beam radiation therapy improves accuracy over surgical clips. *Strahlentherapie Onkologie* 190:467–471. <https://doi.org/10.1007/s00066-014-0631-3>
- Hulskof MC, van Andel G, Bel A, Gangel P, van de Kamer JB (2007) Intravesical markers for delineation of target volume during external focal irradiation of bladder carcinomas. *Radiother Oncol* 84(1):49–51
- Song Y, Yan M, Mueller B, Mychalczak B (2018) Investigation of fiducial marker migration during the treatment of bladder cancer with image-guided radiation therapy. *Clin Oncol (R Coll Radiol)* 3:1481
- Klinton J, Polgar C, Tenke P, Kovacs G, Major T, Stelczer G, Agoston P (2017) Image-guided radiotherapy for muscle invasive bladder cancer with intravesical lipiodol injection. A new option for bladder sparing treatment. *Orvosi Hetilap* 158(51):2041–2047. <https://doi.org/10.1556/650.2017.30904>
- Pos FB, Bex A, Des-Ribbers H (2009) Lipiodol injection for target volume delineation and image guidance during radiotherapy for bladder cancer. *Radiother Oncol* 93:364–367
- Committee AT, Bhat YM, Banerjee S, Barth BA, Chauhan SS, Gottlieb KT, Konda V, Maple JT, Murad FM, Pfau PR, Pleskow DK, Siddiqui UD, Tokar JL, Wang A, Rodriguez SA (2013) Tissue adhesives: cyanoacrylate glue and fibrin sealant. *Gastrointest Endosc* 78(2):209–215. <https://doi.org/10.1016/j.gie.2013.04.166>
- Chandran S, Vaughan R, Jacob A, Hamilton C, Joon DL, Lim K, Tog C, Bhatia K, Aly A, Sweeney T, Efthymiou M (2016) A novel endoscopic marker for radiological localization and image-guided radiotherapy in esophageal and gastric cancers (with video). *Gastrointest Endosc* 83(2):309–317. <https://doi.org/10.1016/j.gie.2015.06.042>
- Freilich JM, Spiess PE, Biagioli MC, Fernandez DC, Shi EJ, Hunt DC, Gupta S, Wilder RB (2014) Lipiodol as a fiducial marker for image-guided radiation therapy for bladder cancer. *Int Braz J Urol* 40(2):190–197. <https://doi.org/10.1590/s1677-5538.lbj.2014.02.08>
- Baumgarten AS, Emtage JB, Wilder RB, Biagioli MC, Gupta S, Spiess PE (2014) Intravesical lipiodol injection technique for image-guided radiation therapy for bladder cancer. *Urology* 83(4):946–950. <https://doi.org/10.1016/j.urology.2013.09.058>
- Chai X, van Herk M, van de Kamer JB, Remeijer P, Bex A, Betgen A, De Reijke TM, Hulshof MC, Pos FJ, Bel A (2010) Behavior of lipiodol markers during image guided radiotherapy of bladder cancer. *Int J Radiat Oncol Biol Phys* 77(1):309–314. <https://doi.org/10.1016/j.ijrobp.2009.08.019>
- Meijer GJ, van der Toorn PP, Bal M, Schuring D, Weterings J, de Wildt M (2012) High precision bladder cancer irradiation by integrating a library planning procedure of 6 prospectively generated SIB IMRT plans with image guidance using lipiodol markers. *Radiother Oncol* 105(2):174–179. <https://doi.org/10.1016/j.radonc.2012.08.011>
- Sondergaard J, Olsen KO, Muren LP, Elstrom UV, Grau C, Hoyer M (2010) A study of image-guided radiotherapy of bladder cancer based on lipiodol injection in the bladder wall. *Acta Oncol* 49(7):1109–1115. <https://doi.org/10.3109/02841861003789491>

19. Ayyıldız SN, Ayyıldız A (2017) Cyanoacrylic tissue glues: biochemical properties and their usage in urology. *Turk J Urol* 43(1):14–24. <https://doi.org/10.5152/tud.2017.09465>
20. Lim JH, You D, Jeong IG, Park HK, Ahn H, Kim C (2013) Cystoscopic injection of *N*-butyl-2-cyanoacrylate followed by fibrin glue for the treatment of persistent or massive vesicourethral anastomotic urine leak after radical prostatectomy. *Int J Urol* 20:980–985. <https://doi.org/10.1111/iju.12094>
21. Chao M, Ho H, Chan Y, Tan A, Pham T, Bolton D, Troy A, Temelcos C, Sengupta S, McMillan K, Cham CW, Liu M, Ding W, Subramanian B, Wasiak J, Lim Joon D, Spencer S, Lawrentschuk N (2018) Prospective analysis of hydrogel spacer for patients with prostate cancer undergoing radiotherapy. *BJU Int*. <https://doi.org/10.1111/bju.14192>
22. Garcia MM, Gottschalk AR, Brajtbord J, Konety B, Meng M, Roach M, Carroll P (2014) Endoscopic gold fiducial marker placement into the bladder wall to optimize radiotherapy targeting for bladder-preserving management of muscle-invasive bladder cancer: feasibility and initial outcome. *PLoS One* 9(3):1–10. <https://doi.org/10.1371/journal.pone.0089754>
23. Al-Hillawi L, Wong T, Tritto G, Berry P (2016) Pitfalls in histocryl glue injection therapy for oesophageal, gastric and ectopic varices: a review. *J Gastrointest Surg* 8(11):729–734. <https://doi.org/10.4240/wjgs.v8.i11.729>
24. Van Bruwaene S, Namdarian B, Challacombe B et al (2018) Introducing new technology safely into urological practice. *World J Urol*. <https://doi.org/10.1007/s00345-018-2173-2>

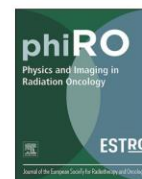
## APPENDIX E: PAPER INCLUDED IN CHAPTER 8 (AS PUBLISHED)

Physics and Imaging in Radiation Oncology 17 (2021) 77–83



Contents lists available at ScienceDirect

## Physics and Imaging in Radiation Oncology

journal homepage: [www.sciencedirect.com/journal/physics-and-imaging-in-radiation-oncology](http://www.sciencedirect.com/journal/physics-and-imaging-in-radiation-oncology)

Original Research Article

## Exploratory models comparing ethiodized oil-glue and gold fiducials for bladder radiotherapy image-guidance



Daryl Lim Joon<sup>a,b</sup>, Alexandra Berlangieri<sup>a</sup>, Benjamin Harris<sup>a</sup>, Mark Tacey<sup>a</sup>, Rachel O'Meara<sup>a</sup>, Brent Pitt<sup>a</sup>, Angela Viotto<sup>a</sup>, Kerry Brown<sup>a</sup>, Michal Schneider<sup>b</sup>, Nathan Lawrentschuk<sup>a</sup>, Shomik Sengupta<sup>a</sup>, Colleen Berry<sup>a</sup>, Trish Jenkins<sup>a</sup>, Michael Chao<sup>a</sup>, Morikatsu Wada<sup>a</sup>, Farshad Foroudi<sup>a</sup>, Vincent Khoo<sup>a,b,c,\*</sup>

<sup>a</sup> Olivia Newton John Cancer Center, Radiation Oncology, 145 Studley Rd, Heidelberg, Victoria 3084, Australia<sup>b</sup> Monash University, Department of Medical Imaging and Radiation Sciences, Faculty of Medicine, Nursing and Health Sciences, Wellington Rd, Clayton, Victoria 3800, Australia<sup>c</sup> Royal Marsden NHS Foundation Trust, 203 Fulham Rd, Chelsea, London SW3 6JJ, United Kingdom

## ARTICLE INFO

## Keywords:

Bladder cancer  
Prostate cancer  
Radiotherapy  
Glue fiducials  
Liquid fiducials  
Image-guided radiotherapy

## ABSTRACT

**Background and purpose:** Image-guidance with fiducials has been shown to improve pelvic radiotherapy outcome. However, bladder fiducials using ethiodized oil (EO) alone can disperse widely, and gold causes Computed Tomography scan (CT) metal artifacts. The study's purpose was to investigate the ability to deliver EO-tissue glue fiducials and compare them to gold for bladder radiotherapy image guidance.

**Materials and methods:** A fluid-filled porcine bladder model was used to assess the ability to cystoscopically inject visible EO glue fiducials into the submucosa. We then transferred the bladders into a porcine pelvis for imaging and compared them to gold fiducials using CT, Cone Beam CT (CBCT), and kilovoltage (KV) planar views. A tissue-equivalent phantom was utilized to analyze the CT number Hounsfield Unit (HU) characteristics and artifacts of the glue and gold fiducials. Percentile ranges and normal tissue voxel percentages of the subsequent CT number voxel histogram from a 2 cm sphere surrounding the fiducial was used to characterize the artifact.

**Results:** We successfully delivered all EO glue fiducials into the porcine bladders as discrete fiducials. They were well seen on CT, CBCT, and KV imaging. The glue fiducials had lower CT number values, but less CT number spread of the voxel percentile ranges consistent with the diminished contrast and less artifact than gold. The glue fiducial types had similar CT number characteristics.

**Conclusion:** This study has shown that EO glue fiducials can be delivered with online visualization qualities comparable to gold fiducials without metal-related artifacts.

## 1. Introduction

The bladder is a mobile structure that can expand and contract depending on its relative filling volume. Subsequently, there has been an increasing interest in using fiducials for bladder image-guided radiotherapy. Gold fiducials are the benchmark for visibility with X-ray imaging and have been used for both bladder tumors and prostate bed radiotherapy [1]. However, they produce a substantial artifact as a

result of multiple mechanisms, including beam hardening, scatter, Poisson noise, motion, and edge effects [2,3]. The artifact can interfere with the accurate fiducial definition leading to imprecise image guidance. Alternatively, ethiodized oil (EO) has been utilized as a liquid fiducial for bladder tumors, but it can be challenging to achieve a discrete marker due to dispersion [4,5].

Gastroenterologists routinely use a mixture of EO and cyanoacrylate tissue glue to treat gastric and oesophageal varices [6,7]. EO is an X-ray

\* Corresponding author at: Royal Marsden NHS Foundation Trust, 203 Fulham Rd, Chelsea, London SW3 6JJ, United Kingdom.

E-mail addresses: [daryl.limjoon@austin.org.au](mailto:daryl.limjoon@austin.org.au) (D. Lim Joon), [alexandra.berlangieri@austin.org.au](mailto:alexandra.berlangieri@austin.org.au) (A. Berlangieri), [benjamin.harris@austin.org.au](mailto:benjamin.harris@austin.org.au) (B. Harris), [mark.tacey@austin.org.au](mailto:mark.tacey@austin.org.au) (M. Tacey), [rachel.omeara@austin.org.au](mailto:rachel.omeara@austin.org.au) (R. O'Meara), [brent.pitt@austin.org.au](mailto:brent.pitt@austin.org.au) (B. Pitt), [angela.viotto@austin.org.au](mailto:angela.viotto@austin.org.au) (A. Viotto), [kerry.brown@austin.org.au](mailto:kerry.brown@austin.org.au) (K. Brown), [michal.schneider@monash.edu](mailto:michal.schneider@monash.edu) (M. Schneider), [colleen.berry@austin.org.au](mailto:colleen.berry@austin.org.au) (C. Berry), [trish.jenkins@austin.org.au](mailto:trish.jenkins@austin.org.au) (T. Jenkins), [michael.chao@austin.org.au](mailto:michael.chao@austin.org.au) (M. Chao), [morikatsu.wada@austin.org.au](mailto:morikatsu.wada@austin.org.au) (M. Wada), [Farshad.Foroudi@austin.org.au](mailto:Farshad.Foroudi@austin.org.au) (F. Foroudi), [vincent.khoo@rmh.nhs.uk](mailto:vincent.khoo@rmh.nhs.uk) (V. Khoo).

<https://doi.org/10.1016/j.phro.2021.01.008>

Received 22 July 2020; Received in revised form 23 January 2021; Accepted 28 January 2021

Available online 6 February 2021

2405-6316/© 2021 The Author(s). Published by Elsevier B.V. on behalf of European Society of Radiotherapy & Oncology. This is an open access article under the

CC BY-NC-ND license (<http://creativecommons.org/licenses/by-nc-nd/4.0/>).

oily contrast agent that prevents the glue from initially polymerizing [6,8]. The glue rapidly sets once injected into the body and contacts water, e.g., blood, [6]. We previously have illustrated its utility as a fiducial for oesophageal cancer patients [9]. The tissue glue reduced EO's dispersion through the esophagus' wall, increasing the ability to produce a discrete visible fiducial.

While the gastroscopic insertion of EO and cyanoacrylate glue for the esophagus is well described, there are no reports of the cystoscopic delivery of tissue glues into a fluid-filled bladder. The cystoscopic insertion of a tissue glue into a watery environment raised concerns that the glue could polymerize prematurely. The glue could obstruct the needle tip, making it difficult to inject into the bladder submucosa. The premature polymerization may also glue the cystoscope's lens or channels, permanently damaging an expensive instrument, as has been reported with oesophageal varices [10].

The aim of this study was to investigate the ability to deliver visible discrete EO-tissue glue fiducials suitable for image guidance and characterize and compare them in terms of visibility and artifact production to the standard gold fiducials for bladder radiotherapy image guidance.

## 2. Material and methods

### 2.1. Glue fiducials

The glue fiducials consisted of a mixture of EO (Lipiodol Ultra liquid, esterized poppy seed oil, Aspen Medical) with either Histoacryl

(monomeric n-butyl-2-cyanoacrylate, B Braun) (CA) or Glubran2 (n-butyl cyanoacrylate and methacryloxysulpholen monomers, GEM) (CM), in a 1:1 ratio, respectively.

### 2.2. Porcine model: image guidance visibility

The fiducial insertion utilized a 17fr rigid cystoscope that was initially used to inspect and then fill three ex-vivo porcine bladders with saline. Then a three sets of three EO/CA (EC) fiducials, three EO/CM (EM) fiducials and three gold fiducials were cystoscopically inserted into the three separate porcine bladders. A William's needle (Cook Medical, Australia) was inserted via the scope and used to inject EO glue combinations submucosally, raising a bleb of 0.1 ml. Each set of three discrete fiducials was placed around each bladder's trigone, imitating the demarcation of a small bladder tumor or the vesicourethral anastomosis following a prostatectomy. Further details of the procedure have been previously described [11].

Following the injection, the cystoscope was removed from the bladder, keeping the needle beyond the scope to avoid the glue occluding the working channel. The glue fiducials were compared with three standard gold fiducials (0.9 mm × 3 mm, CIVCO Medical Solutions, Kalona, Iowa, USA) in terms of their visibility.

Following the fiducials' insertion, the porcine bladders were transferred sequentially into a porcine pelvis (Fig. 1). The porcine pelvis was to provide realistic size and tissue densities, including inhomogeneities for imaging. According to clinical protocols, the pelvis was stabilized

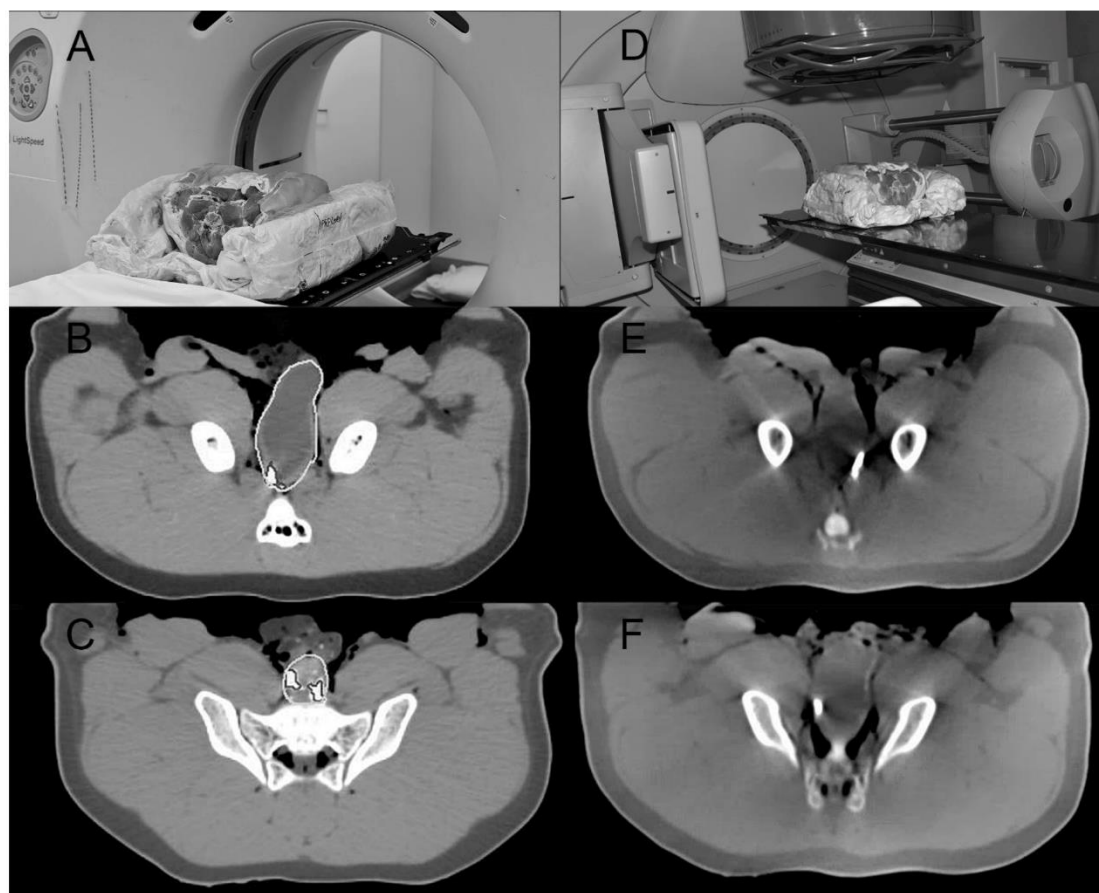


**Fig. 1.** Porcine Model: Pigs bladder & pelvis in two-part foam immobilization. A) CT simulation. Axial CT image with contoured bladder and fiducial showing visible B) EC fiducial and C) EM fiducial. D) Linac for cone-beam CT (CBCT) scan. Axial CBCT image showing a visible E) EC fiducial and F) EM fiducial. Abbreviations: EC: ethiodized oil and monomeric n-butyl-2-cyanoacrylate, EM: ethiodized oil and n-butyl cyanoacrylate and methacryloxysulpholen monomers.

and set up in a two-part foam immobilization device for reproducibility.

The porcine pelvis with the bladder was then imaged using radiotherapy imaging modalities, including computed tomography (CT), cone-beam computed tomography (CBCT) (Fig. 1), and kilovoltage (KV) planar imaging using standard clinical parameters for pelvic radiotherapy.

The CT simulation was performed on a GE Lightspeed RT CT (Boston, Massachusetts, USA) 1.25 mm slice width, helical, 0.75 pitch, no gap, 512x512 axial resolution, 650 mm reconstruction diameter.

CBCT was imaged on an Elekta Infinity linear accelerator (Stockholm, Sweden). The standard abdomen/pelvis scans parameters were used, i.e., 41 cm diameter FOV, variable M10/M20 (scan length 12 or 24 cm) depending on target size, 120 kVp, 25 mA 40 ms nominal per frame, 660 frames per scan (360 degrees rotation), 1 mm voxel size, 2–3 mm viewing slice resolution and axial resolution of 512 × 512.

2D orthogonal KV planar imaging was performed using anterior-posterior (AP) and lateral views. The Elekta XVI (version 4.5+) KV imaging parameters were 120 kVp, 25 (AP) or 32 (lateral) mA, and 40 ms nominal per frame, and five frames averaged per image, 25.6 × 25.6 cm imaging area, 0.25 mm nominal pixel size (Resolution 1024 × 1024).

Two expert radiation therapists who routinely verify pelvic radiotherapy independently scored the fiducials while blinded to the mixture's identity and each other to measure the fiducial visibility and minimize observer error and bias. The ability to deliver a suitable fiducial set for radiotherapy image verification was scored 0, not sufficiently visible for verification, or 1, sufficiently visible for verification for each imaging modality, CT, CBCT, and KV planar scans.

### 2.3. Phantom model: fiducial and artefact characterization

A CIRS Torso (tissue equivalent) phantom was used to characterize the glue fiducials and artifacts. A gold fiducial was used as the standard and embedded centrally in a wax block cylinder measuring 6.3 × 1.0 cm for comparison. A wax block cylinder alone was used as a normal tissue control. These wax blocks were constructed and inserted to minimize any air gaps with the phantom.

Further tissue-equivalent, wax block cylinders were constructed for the glue fiducials. Holes for the glue fiducials were drilled into individual blocks that approximated (1) the size of the 0.1 ml porcine bladder glue fiducials, i.e., large, 7 × 4 mm, and (2) the size of the gold fiducials, i.e., small, 0.9 × 3 mm. The holes were moistened for polymerization and then filled with the glue fiducial. A small EO alone fiducial control was also created. Each wax cylinder was then sequentially inserted into the CIRS phantom center and imaged on CT using the same clinical parameters as the porcine model. Two fiducial samples were used for each control, gold, and large glue fiducials. Four samples were created for the small glue fiducials, to account for any possible variation due to their small size (Table 1).

### 2.4. Fiducial and artefact analysis & statistical description

CT number Hounsfield number (HU) histograms are increasingly used to analyze human tissue characteristics [12–14]. Subsequently, a methodology using CT number histograms derived from clinical tools, i.e., MIM Maestro version 6.6.13 (Cleveland OH, USA) (MIM), was developed to analyze the fiducial artifacts in a three-dimensional manner consistent with modern radiotherapy.

The fiducials were contoured as per clinical protocols using a window level that approximated fiducial size, i.e., window level of 4095 with a width one and gamma [15,16] of one for the gold fiducials and level of 600 with a width of 40 and gamma of one for the polymer. Then a 2 cm diameter sphere was created around the fiducial contour center. The high CT number fiducials were subtracted from the sphere using a Boolean function to analyze the artifact's impact on normal tissue. The CT number voxel histogram for the artifact sphere was then exported in 5 HU bins for analysis. The fiducials' CT number characteristics were separately investigated as they produced very high CT number signals compared to the artifact.

The spheres contained the phantom, surrounding wax, and the relevant fiducial seed's 3D artifact. MIM was used to create histogram plots, presenting the voxels count at each CT number (HU) value to assess the relative differences in CT number variation surrounding each fiducial marker.

Given the non-normal, bi-modal distribution of the voxel count histograms, means and standard deviations were not suitable for describing and comparing the histograms across the fiducial marker type. Therefore, the variation in voxel counts in the spheres (excluding the fiducial) were measured with percentile ranges. An example of the percentiles range is illustrated in Fig. 2 using the wax control fiducial. Additionally, the normal tissue not hidden by artifact was quantified by the proportion of voxels within the normal tissue CT number ranges of +/- 100 HU and +/- 150 HU.

No statistical significance was assigned due to the small sample size for this descriptive study. Data was collected and prepared in Microsoft Excel. Stata version 15.1 (College Station, Texas, USA) was used to calculate CT number parameters, percentile ranges, and proportions.

## 3. Results

### 3.1. Porcine bladder model: fiducial deliverability & visibility

The gold fiducials were well visualized on all imaging modalities. EO glue combinations could be injected repeatedly into the porcine bladder submucosa, raising consistent multiple small blebs. They were larger than the gold fiducials measuring approximately 7 × 4 mm, being overall elliptical in shape. All three fiducials for both EC and EM fiducials could be visualized on CT, CBCT, and KV imaging that was adequate for verification. The EC and EM fiducials' appearances were similar on CT and CBCT (Fig. 1).

**Table 1**

Phantom Model: Comparison of the Fiducial and Controls in terms of volume, voxel number, and CT number Hounsfield Unit (HU) characteristics. It illustrates that the gold fiducials had a greater CT number HU contrast than the small glue fiducials with a comparable volume and voxel number. Abbreviations: EO: ethiodized oil, EC: ethiodized oil and monomeric n-butyl-2-cyanoacrylate, EM: ethiodized oil and n-butyl cyanoacrylate and methacryloxysulpholen monomers.

Fiducial/Factor	Number Of Fiducials	Volume cm <sup>3</sup> (average)	Voxel number (average)	Median CT number (HU)	Min CT number (HU)	Max CT number (HU)
Control (2 cm phantom sphere alone)	2	3.85	1912	24	-220	79
Control (Wax)	2	0.02	9	-24	-114	57
EO alone	2	0.02	9	346	0	1383
Gold	2	0.02	8	6039	1229	16,779
Small EC	4	0.02	6	374	50	642
Small EM	4	0.02	6	488	25	835
Large EC	2	0.08	38	717	-261	2092
Large EM	2	0.07	35	770	-22	2472

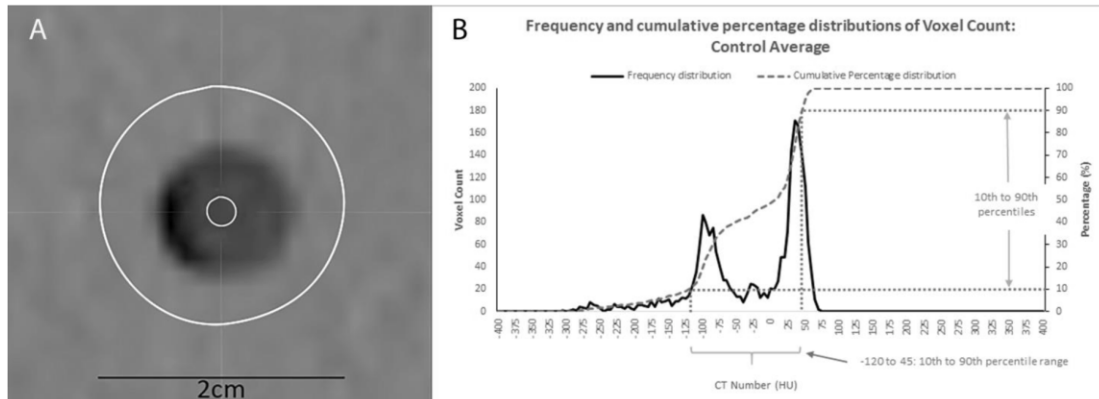


**Fig. 2.** Phantom Model Artefact Analysis: Example of Histogram and Cumulative percentage distribution of voxel count and calculated Percentile Range by CT number Hounsfield Unit (HU) for Wax Control illustrating A) Cross-section through the wax block control inserted in the phantom. The outer contour is the 2 cm sphere, while the inner contour denotes the fiducial volume equivalent to the gold or small glue fiducial. B) The corresponding histogram represents the CT number (HU) versus voxel count for the 2 cm sphere minus the fiducial volume used to calculate the artefact analysis's percentile ranges.

3.2. Phantom fiducial characterization

The fiducials were analyzed separately from the surrounding phantom and artifact (Table 1). Notably, the fiducials are small relative to the sphere; they occupied only 6 to 38 voxels compared to 1912 sphere voxels of the sphere. The wax control, gold, EO alone, and small glue fiducials had the same volume and similar voxel count. The wax control had median CT number values 48 HU lower than the surrounding phantom but was still within the normal tissue-equivalent range. Therefore, this should not affect the results based on the percentile ranges and percentage of voxels in the normal tissue range. Some wax blocks had incomplete thin rims of air, low CT number voxels adjacent to the phantom interface (Fig. 3). However, these represented only a small proportion of the sphere and did affect the results. EO alone was

designed to have the same volume as the small glue fiducials and had comparable CT number characteristics to the glue fiducials (Table 1).

The gold fiducial was the same size as the small glue fiducials but had a greater contrast with 12 to 16 times greater CT number values than the small EO fiducials. The glue did not impact the CT number characteristics of the EO. The differences in median CT number between the glue fiducial and EO alone was 28–142 HU. Both the smaller EC and EM fiducials had similar CT number characteristics, with the differences in their median CT number values being 114 HU. The larger EC and EM fiducials were similar, but both exhibited greater median CT number values than the smaller counterparts but were not as high as gold.

3.3. Phantom fiducial artefact characterization

Sphere voxels were mostly normal tissue density. The bright and dark artifacts result in the HU voxel variation outside the normal tissue range at the extreme high and low HU values, respectively, at the histogram ends, i.e., bright radiating or dark shadowing artifact. The greater spread of the histogram, the less normal tissue is represented as it is obscured by the high or low HU artifact from the fiducials.

The gold fiducial sphere CT number values for the 1st to 99 percentile ranges were 593, 604, and 600 HU greater than small EC, EM, and EO alone fiducials, respectively, and 563 HU greater than the control (Table 2). This suggested a larger number of voxels being present at the extreme ends of the CT number histogram and is representative of an increased artifact for the gold fiducials (Fig. 3B, Fig. 4).

Both glue fiducials showed similar CT number values across the percentile ranges, with differences between 1 and 11HU for the small fiducials and 0 to 42 HU for the larger glue fiducials. There were also only small differences from the wax control, indicating that the artifact was minimal (Table 2, Fig. 3 C & D, Fig. 4). The tissue glue did not affect the fiducials' CT number artifact characteristics, with differences between the small EC and EO ranging from 1 to 7 HU and 2 to 10 HU for the small EM fiducial (Table 2). The remaining percentile ranges and percentage of voxels in the designated normal tissue ranges only showed minor differences, indicating that the artifacts made up only a small proportion of the 2 cm spheres.

Compared to the smaller glue fiducial, the larger glue fiducial's CT number histogram spread was greater for the 1st to 99 percentile range but less than gold. There were only minor variations in values between the EC and EM fiducials for all other values.

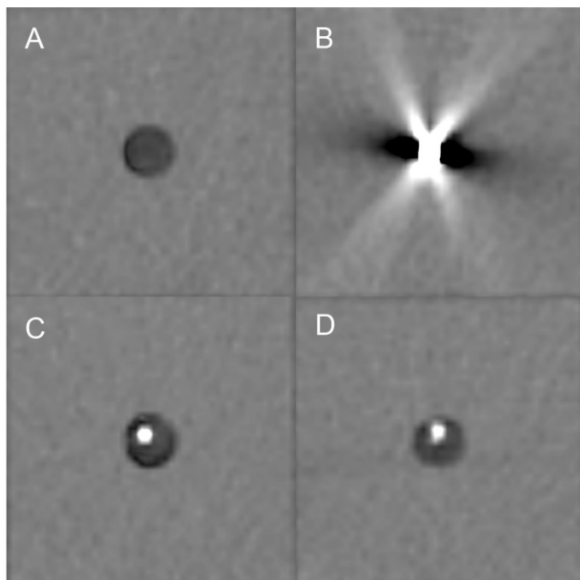


**Fig. 3.** Phantom Model: CT scan of phantom showing A) Wax control – normal tissue density but less dense than the phantom, B) Gold fiducial and artifact, C) Small EC fiducial, and D) Small EM. The EO glue fiducials C) and D) have a minimal artifact. Abbreviations: EC: ethiodized oil and monomeric n-butyl-2-cyanoacrylate, EM: ethiodized oil and n-butyl cyanoacrylate and methacryloxysulpholen monomers, EO: ethiodized oil.

**Table 2**  
Phantom Model: Artefact Analysis – Mean and Standard Deviations (SD) of Percentile ranges of the CT number Hounsfield Unit (HU) versus voxels count histograms and proportion of voxels within normal tissue CT number HU range for 2 cm spheres surrounding the fiducial. It illustrates that the glue fiducials produce fewer artifacts than gold with smaller percentile ranges and a greater percentage of voxels in normal tissue range  $\pm 100$  and  $\pm 150$  HU. Abbreviations: EO: ethiodized oil, EC: ethiodized oil and monomeric n-butyl-2-cyanoacrylate, EM: ethiodized oil and n-butyl cyanoacrylate and methacryloxysulpholen monomers.

Sphere/Factor	Number Of Fiducials Spheres	1st to 99th percentile, mean (SD)	5th to 95th percentile, mean (SD)	10th to 90th percentile, mean (SD)	25th to 75th percentile, mean (SD)	Percentage within $\pm 100$ HU, mean (SD)	Percentage within $\pm 150$ HU, mean (SD)
Control (Wax)	2	310 (21)	200 (35)	163 (4)	128 (4)	78 (2)	95 (3)
EO alone	2	273 (11)	215 (14)	175 (7)	133 (4)	75 (3)	92 (1)
Gold	2	873 (110)	270 (57)	173 (11)	128 (4)	74 (1)	91 (2)
Small EC	4	280 (30)	211 (10)	174 (5)	131 (5)	76 (2)	93 (1)
Small EM	4	269 (39)	205 (32)	178 (21)	135 (9)	73 (6)	94 (5)
Large EC	2	360 (35)	203 (4)	165 (0)	123 (4)	80 (1)	94 (0)
Large EM	2	318 (32)	180 (7)	158 (4)	123 (4)	79 (1)	97 (1)

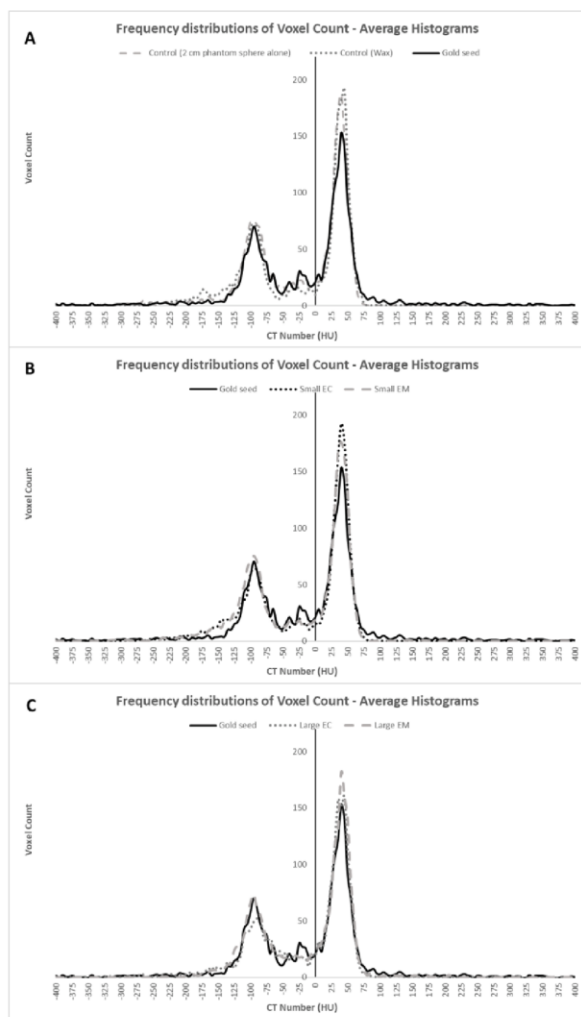


**Fig. 4.** Phantom Model Artefact Analysis: Average Histograms (Frequency Distribution) of voxel count by CT number Hounsfield Unit (HU) for a 2 cm sphere minus the fiducial volume illustrating A) Control (2 cm phantom sphere alone), Control (wax) and Gold fiducial; B) Gold fiducial, Small EC and Small EM; and C) Gold fiducial, Large EC and Large EM. Abbreviations: EC: ethiodized oil and monomeric n-butyl-2-cyanoacrylate, EM: ethiodized oil and n-butyl cyanoacrylate and methacryloxysulpholen monomers.

**4. Discussion**

This study has confirmed that glue fiducials can be delivered cystoscopically into a fluid-filled bladder and produce a discrete visible marker with minimal artifact compared to standard gold fiducials and thus suitable for image guidance. However, the glue fiducials were larger than the gold markers but had comparable imaging and artifact characteristics to EO alone.

Fiducials, in an imaged guided approach, are critical for targeting in partial bladder radiotherapy to treat the bladder tumor alone or as part of a dose-escalation boost [17,18]. The bladder can greatly distend, particularly in the cranial-caudal direction. Margins of two to three cm are required to account for this distension, potentially resulting in increased bowel toxicity [19,20]. However, studies that use EO or gold fiducials for partial bladder radiotherapy utilize smaller anisotropic PTV margins of 5 mm–15 mm [4,5,17,21].

Investigations have shown that EO fiducials effectively define the tumor within the bladder for image guidance [4,5,17]. A recent study using cone-beam verification has shown that EO resulted in a higher interobserver agreement than bladder wall surface matching and decreased PTV margins [22]. However, there was a substantial shape variation of the EO markers due to bladder filling [22].

While the EO only markers can fade, they exhibit a high retention rate and remain visible throughout radiotherapy. However, the ability to use them for radiotherapy verification is variable. In terms of verification with EO, success rates have been reported to be between 76% and 100% [23]. Chai et al. reported that 92% of the markers remained in situ after the radiation course in 15 patients. However, a further 16 patients could not be included in the series as the fiducials could not be registered for image-guided therapy due to splitting or joining [24]. Thus, there is a learning curve to achieve EO markers suitable for radiotherapy verification [5]. Despite success in achieving discrete visible EO fiducials, our experience when using EO alone has been inconsistent. EO dispersion through and beyond the bladder wall into peri-vesical tissue sometimes limited its specificity as a fiducial marker and prompted our investigation of tissue glues.

Side effects of EO, including an allergic reaction, are uncommon and mostly transient [17]. The studies of EO bladder markers have not reported any significant toxicity [25]. The EO and CA combination has been utilized in multiple sites, with infrequent, serious side effects [9,26]. More specifically, CA and CM glues have been used in urological procedures, including animal urethral tissue models, urinary fistulas [27], and the treatment of persistent anastomotic urine leaks after radical prostatectomy [28].

Gold has also been used as fiducials for partial bladder and post-prostatectomy radiotherapy [1,21,29,30]. Gold is easily visible on X-ray imaging due to its high Z value. However, this subsequently causes bright radiating and dark shadowing metal artifact [25], resulting in the inaccurate fiducial definition that interferes with precise verification.

The artifact can also obscure the anatomy causing difficulties in target delineation. Another significant but uncommon risk with the combination of surgery, radiotherapy, and foreign body include fistulae [31,32]. A further issue is the drop-out rate, which is estimated to be 50%, particularly from the tumor area [5,29,33]. There have also been technical difficulties inserting gold fiducials into the bladder dome [29].

The caveats of EO alone and gold fiducials markers have led us to investigate the EO glue combinations. EO and tissue glue (CA or CM) are generally available in most surgical hospitals. EO and CA mixture is a less expensive combination [34]. The glue fiducials have good visibility in various imaging modalities, minimal distortion in CT imaging, minimal dose perturbation, and are biocompatible with soft tissue. The widespread use of EO and tissue glues indicates that they can be safely used in many anatomical sites.

The study did not investigate artifact suppression CT for the gold fiducials [35,36] or alternative markers, including newer commercially available liquid gel fiducials that have recently been trialed in the bladder, such as BioXmark (sucrose acetate isobutyrate (SAIB), iodinated SAIB, and ethanol solution) [37] or TraceIT (iodinated polyethylene glycol microparticles, hydrogel) [34]. We have found that glue fiducials and TraceIT [34] have their pros and cons. At our center, the CA and EO are readily available and less expensive. However, the relative utility of different liquid fiducials can only be resolved in a comparative study that is under consideration.

Interestingly, EO produces high signal intensity on T1-weighted MRI images and low signal intensity on T2-weighted images [38]. A future interest will be to develop fiducials for MRI, possibly using EO or another MRI contrast agent with tissue glue. A comparison with TraceIT or BioXmark would also be appropriate, as both are marketed as being visible on MRI.

The study was an ex vivo and in vitro investigation of glue fiducials where they were imaged immediately after insertion. Issues such as fading, retention, distortion, migration, and dispersion resulting from normal physiological processes during radiotherapy are more appropriately assessed in a clinical study. However, these issues were not evident in our previous gastro-oesophageal patient study [9] or earlier investigations of EO alone (except dispersion). An in vivo study is planned to address the clinical and imaging aspects, including the fiducials' durability, CBCT, MRI, and workflow aspects in a patient population undergoing bladder radiotherapy.

In conclusion, the study has confirmed the potential use of EO glue fiducials for radiotherapy bladder targeting. They have advantages over gold markers in terms of decreased artifact production and maybe more easily deliverable with less dispersion than EO alone. The components are readily available, and the EO Histoacryl mixture is relatively inexpensive. Patient studies are warranted to assess the utility and durability of these fiducials during a radiotherapy course.

#### Declaration of Competing Interest

The authors declare the following financial interests/personal relationships which may be considered as potential competing interests: Providers: KARL STORZ Endoscopy Australia Pty Ltd supplied the cystoscopes, William A. Cook Australia PTY LTD supplied the Williams Cystoscopic Injection needles, Guerbet USA supplied the Lipiodol Ethiodized Oil, B.Braun Australia Pty.Ltd supplied the Histoacryl, MatrixSurgical supplied the Glubran2 (GEM), Sinclair's Abattoir, Benalla Victoria, supplied the pig bladders and Brenta's Butcher, Fairfield Victoria supplied the pigs pelvis.

#### Acknowledgments

Radiotherapy Nursing for their support for the procedure and the providers: KARL STORZ Endoscopy Australia Pty Ltd supplied the cystoscopes, William A. Cook Australia PTY LTD supplied the Williams Cystoscopic Injection needles, Guerbet USA supplied the Lipiodol (EO

Ethiodized Oil), B.Braun Australia Pty. Ltd supplied the Histoacryl, MatrixSurgical supplied the Glubran2 (GEM), Sinclair's Abattoir, Benalla Victoria, supplied the pig bladders and Brenta's Butcher, Fairfield Victoria supplied the pigs pelvis.

#### References

- [1] Shakir SI, Udrescu C, Enachescu C, Rouviere O, Arion S, Caravan I, et al. Transrectal implantation and stability of gold markers in prostate bed for salvage radiotherapy of macroscopic recurrences. *Phys Med* 2016;32:1422–7. <https://doi.org/10.1016/j.ejmp.2016.10.009>.
- [2] Barrett JF, Keat N. Artifacts in CT: recognition and avoidance. *Radiographics* 2004;24:1679–91. <https://doi.org/10.1148/rg.246045065>.
- [3] Gjestebly L, De Man B, Jin Y, Paganetti H, Verburg J, Giantsoudi D, et al. Metal artifact reduction in CT: Where are we after four decades? *IEEE Access* 2016;4:5826–49. <https://doi.org/10.1109/access.2016.2608621>.
- [4] Pos F, Bex A, Dees-Ribbers HM, Betgen A, van Herk M, Remeijer P. Lipiodol injection for target volume delineation and image guidance during radiotherapy for bladder cancer. *Radiother Oncol* 2009;93:364–7. <https://doi.org/10.1016/j.radonc.2009.09.003>.
- [5] Søndergaard J, Olsen KØ, Muren LP, Elstrøm UV, Grau C, Høyer M. A study of image-guided radiotherapy of bladder cancer based on lipiodol injection in the bladder wall. *Acta Oncol* 2010;49:1109–15. <https://doi.org/10.3109/02841861003789491>.
- [6] Committee AT, Bhat YM, Banerjee S, Barth BA, Chauhan SS, Gottlieb KT, et al. Tissue adhesives: cyanoacrylate glue and fibrin sealant. *Gastrointest Endosc* 2013;78:209–15. <https://doi.org/10.1016/j.gie.2013.04.166>.
- [7] Weil D, Cervoni JP, Fares N, Rudler M, Bureau C, Plessier A, et al. Management of gastric varices: a French national survey. *Eur J Gastroenterol Hepatol* 2016;28:576–81. <https://doi.org/10.1097/MEG.0000000000000560>.
- [8] Loh DC, Wilson RB. Endoscopic management of refractory gastrointestinal non-variceal bleeding using Histoacryl (N-butyl-2-cyanoacrylate) glue. *Gastroenterol Rep (Oxf)* 2016;4:232–6. <https://doi.org/10.1093/gastro/gov019>.
- [9] Chandran S, Vaughan R, Jacob A, Hamilton C, Joon DL, Lim K, et al. A novel endoscopic marker for radiological localization and image-guided radiotherapy in esophageal and gastric cancers (with video). *Gastrointest Endosc* 2016;83:309–17. <https://doi.org/10.1016/j.gie.2015.06.042>.
- [10] Cheng LF, Wang ZQ, Li CZ, Lin W, Yeo AE, Jin B. Low incidence of complications from endoscopic gastric variceal obturation with butyl cyanoacrylate. *Clin Gastroenterol Hepatol* 2010;8:760–6. <https://doi.org/10.1016/j.cgh.2010.05.019>.
- [11] Duncan C, Joon DL, Lawrentschuk N, Jenkins T, Schneider M, Khoo V, et al. Fiducial markers: can the urologist do better? *World J Urol* 2019;37:1281–7. <https://doi.org/10.1007/s00345-018-2515-0>.
- [12] Lim HK, Ha HI, Park SY, Lee K. Comparison of the diagnostic performance of CT Hounsfield unit histogram analysis and dual-energy X-ray absorptiometry in predicting osteoporosis of the femur. *Eur Radiol* 2019;29:1831–40. <https://doi.org/10.1007/s00330-018-5728-0>.
- [13] Paul J, Yang C, Wu H, Tai A, Dalah E, Zheng C, et al. Early assessment of treatment responses during radiation therapy for lung cancer using quantitative analysis of daily computed tomography. *Int J Radiat Oncol Biol Phys* 2017;98:463–72. <https://doi.org/10.1016/j.ijrobp.2017.02.032>.
- [14] Zhang LX, Xiang JJ, Wei PY, Ding JW, Luo DC, Peng ZY, et al. Diagnostic value of computed tomography (CT) histogram analysis in thyroid benign solitary coarse calcification nodules. *J Zhejiang Univ Sci B* 2018;19:211–7. <https://doi.org/10.1631/jzus.B1700119>.
- [15] Gonzalez RC, Woods RE. *Some Basic Intensity Transformation Functions*. In: *Digital Image Processing*, 4th Edition. 4 ed: Pearson; 2018. p. 139–42.
- [16] Zhou Y, Shi C, Lai B, Jimenez G. Contrast enhancement of medical images using a new version of the World Cup Optimization algorithm. *Quant Imaging Med Surg* 2019;9:1528–47. <https://doi.org/10.21037/qims.2019.08.19>.
- [17] Freilich JM, Spiess PE, Biagioli MC, Fernandez DC, Shi EJ, Hunt DC, et al. Lipiodol as a fiducial marker for image-guided radiation therapy for bladder cancer. *Int Braz J Urol* 2014;40:190–7. <https://doi.org/10.1590/S1677-5538.IBJU.2014.02.08>.
- [18] Muren LP, Redpath AT, McLaren D, Rorvik J, Halvorsen OJ, Hostmark J, et al. A concomitant tumour boost in bladder irradiation: patient suitability and the potential of intensity-modulated radiotherapy. *Radiother Oncol* 2006;80:98–105. <https://doi.org/10.1016/j.radonc.2006.06.015>.
- [19] Pos F, Remeijer P. Adaptive management of bladder cancer radiotherapy. *Semin Radiat Oncol* 2010;20:116–20. <https://doi.org/10.1016/j.semr.2009.11.005>.
- [20] Muren LP, Smaaland R, Dahl O. Organ motion, set-up variation and treatment margins in radical radiotherapy of urinary bladder cancer. *Radiother Oncol* 2003;69:291–304. [https://doi.org/10.1016/S0167-8140\(03\)00246-9](https://doi.org/10.1016/S0167-8140(03)00246-9).
- [21] Fortin I, Carrier JF, Beauchemin MC, Beliveau-Nadeau D, Delouya G, Taussky D. Using fiducial markers in the prostate bed in postprostatectomy external beam radiation therapy improves accuracy over surgical clips. *Strahlenther Onkol* 2014;190:467–71. <https://doi.org/10.1007/s00066-014-0631-3>.
- [22] Kong V, Kwan M, Chen S, Chung P, Craig T, Rosewall T. Quantification of interobserver variability in image registration using cone beam CT for partial bladder radiotherapy—a comparison between lipiodol and bladder wall surface. *Br J Radiol* 2019;92:20180413. <https://doi.org/10.1259/bjr.20180413>.
- [23] Kliton J, Polgar C, Tenke P, Kovacs G, Major T, Stelzer G, et al. Image-guided radiotherapy for muscle invasive bladder cancer with intravesical lipiodol

- injection. A new option for bladder sparing treatment. *Orv Hetil* 2017;158:2041–7. <https://doi.org/10.1556/650.2017.30904>.
- [24] Chai X, van Herk M, van de Kamer JB, Remeijer P, Bex A, Betgen A, et al. Behavior of lipiodol markers during image guided radiotherapy of bladder cancer. *Int J Radiat Oncol Biol Phys* 2010;77:309–14. <https://doi.org/10.1016/j.ijrobp.2009.08.019>.
- [25] Nolan CP, Forde EJ. A review of the use of fiducial markers for image-guided bladder radiotherapy. *Acta Oncol* 2016;55:533–8. <https://doi.org/10.3109/0284186X.2015.1110250>.
- [26] Machiels M, Voncken FEM, Jin P, van Dieren JM, Bartels-Rutten A, Alderliesten T, et al. A novel liquid fiducial marker in esophageal cancer image guided radiation therapy: technical feasibility and visibility on imaging. *Pract Radiat Oncol* 2019;9:e506–15. <https://doi.org/10.1016/j.proro.2019.06.018>.
- [27] Ayyildiz SN, Ayyildiz A. Cyanoacrylic tissue glues: biochemical properties and their usage in urology. *Turk J Urol* 2017;43:14–24. <https://doi.org/10.5152/tud.2017.09465>.
- [28] Lim JH, You D, Jeong IG, Park HK, Ahn H, Kim CS. Cystoscopic injection of N-butyl-2-cyanoacrylate followed by fibrin glue for the treatment of persistent or massive vesicourethral anastomotic urine leak after radical prostatectomy. *Int J Urol* 2013;20:980–5. <https://doi.org/10.1111/iju.12094>.
- [29] Mangar S, Thompson A, Miles E, Huddart R, Horwich A, Khoo V. A feasibility study of using gold seeds as fiducial markers for bladder localization during radical radiotherapy. *Br J Radiol* 2007;80:279–83. <https://doi.org/10.1259/bjr/54321311>.
- [30] Langenhuijsen JF, Donker R, McColl GM, Kiemeny LA, Witjes JA, van Lin EN. Postprostatectomy ultrasound-guided transrectal implantation of gold markers for external beam radiotherapy. Technique and complications rate. *Strahlenther Onkol* 2013;189:476–81. <https://doi.org/10.1007/s00066-013-0323-4>.
- [31] Borchers H, Pinkawa M, Donner A, Wolter TP, Pallua N, Eble MJ, et al. Rectourethral fistula following LDR brachytherapy. *Urol Int* 2009;82:365–6. <https://doi.org/10.1159/000209374>.
- [32] Chao M, Ho H, Chan Y, Tan A, Pham T, Bolton D, et al. Prospective analysis of hydrogel spacer for patients with prostate cancer undergoing radiotherapy. *BJU Int* 2018;122:427–33. <https://doi.org/10.1111/bju.14192>.
- [33] Hulshof MC, van Andel G, Bel A, Gangel P, van de Kamer JB. Intravesical markers for delineation of target volume during external focal irradiation of bladder carcinomas. *Radiother Oncol* 2007;84:49–51. <https://doi.org/10.1016/j.radonc.2007.05.017>.
- [34] Chao M, Ho H, Joon DL, Chan Y, Spencer S, Ng M, et al. The use of tissue fiducial markers in improving the accuracy of post-prostatectomy radiotherapy. *Radiat Oncol J* 2019;37:43–50. <https://doi.org/10.3857/roj.2018.00556>.
- [35] Wei J, Sandison GA, Hsi WC, Ringor M, Lu X. Dosimetric impact of a CT metal artefact suppression algorithm for proton, electron and photon therapies. *Phys Med Biol* 2006;51:5183–97. <https://doi.org/10.1088/0031-9155/51/20/007>.
- [36] Chan MF, Cohen GN, Deasy JO. Qualitative evaluation of fiducial markers for radiotherapy imaging. *Technol Cancer Res Treat* 2015;14:298–304. <https://doi.org/10.1177/1533034614547447>.
- [37] de Ridder M, Gerbrandy LC, de Reijke TM, Hinnen KA, Hulshof M. BioXmark(R) liquid fiducial markers for image-guided radiotherapy in muscle invasive bladder cancer: a safety and performance trial. *Br J Radiol* 2020;93:20200241. <https://doi.org/10.1259/bjr.20200241>.
- [38] Santis MD, Alborino S, Tartoni PL, Torricelli P, Casolo A, Romagnoli R. Effects of lipiodol retention on MRI signal intensity from hepatocellular carcinoma and surrounding liver treated by chemoembolization. *Eur Radiol* 1997;7:10–6. <https://doi.org/10.1007/s003300050099>.